



UNIVERSITÀ
DEGLI STUDI
FIRENZE

PhD in
Industrial Engineering

Curriculum: Energy and Innovative Industrial and Environmental Technologies

CYCLE XXXIII

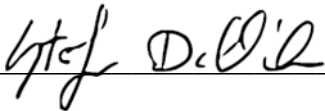
COORDINATOR Prof. Giampaolo Manfrida

Thermochemical biorefineries for the conversion of lignocellulosic biomass: improvements of fast pyrolysis and hydrothermal processes for fuels and chemicals precursors

Academic Discipline (SSD) ING-IND/09

Doctoral Candidate

Dr. Dell'Orco Stefano



Supervisor

Prof. Chiamonti David



Coordinator

Prof. Manfrida Giampaolo

Years 2017/2020

PhD in
Industrial Engineering

Curriculum: Energy and Innovative Industrial and Environmental Technologies

CYCLE XXXIII

**Thermochemical biorefineries for the conversion of
lignocellulosic biomass: improvements of fast
pyrolysis and hydrothermal processes for fuels and
chemicals precursors**

Stefano Dell’Orco

Supervisors:

David Chiaramonti, *Polytechnic of Turin & University of Florence, Italy*, Academic advisor

Kimberly A. Magrini, *National Renewable Energy Laboratory (NREL), United States*, Co-Supervisor

A. Nolan Wilson, *National Renewable Energy Laboratory (NREL), United States*, Co-Supervisor

Calvin Mukarakate, *National Renewable Energy Laboratory (NREL), United States*, Co-Supervisor

Andrea Maria Rizzo, *Renewable Energy Consortium for R&D (RE-CORD), Italy*, Co-Supervisor

Edoardo Miliotti, *Renewable Energy Consortium for R&D (RE-CORD), Italy*, Co-Supervisor

External reviewers:

Lasse Rosendahl, *Department of Energy Technology, Aalborg University, Denmark*

Samir Bensaid, *Department of Chemical Engineering, Politecnico di Torino, Italy*

Years 2017/2020

Declaration

I hereby declare that this submission is my own work, and to the best of my knowledge and belief, it contains no material previously published or written by another person, nor material which to a substantial extent has been accepted for the award of any other degree or diploma at University of Florence or any other educational institution, except where due references are provided in the thesis itself.

Any contribution made to the research by others I have been working with is explicitly acknowledged in the thesis.

Stefano Dell'Orco

October 2020

Abstract

In order to mitigate ongoing effects of the climate change due to the use of fossil sources for the production of fuels and chemicals, strong efforts are necessary for gradually switch to renewable sources, thus improving circular carbon utilization. The transportation sector is one of the major contributors to global green-house gas (GHG) emissions and the CO₂ generation is expected to grow due to increasing demand for transportation driven by growth in world population as well as economies for developing countries. Additionally, the integrated production of fuels and chemicals is nowadays a standard approach in petroleum refinery where 85% of the entire oil barrel is used for fuel production and the remaining 15% to produce chemicals, that account for about 50% of the overall profits. Thermochemical biorefineries for the conversion of lignocellulosic biomass are a promising route to produce precursors for fuels and chemicals for the transportation sector and chemical industry. However, technical challenges still need to be tackled to improve the thermochemical technologies through economically viable approaches for wider industrial applications. In this work, thermochemical conversion-based biorefineries for the valorization of lignocellulosic biomass were investigated to improve the process technologies toward industrial scale-up and commercialization. More in details, studies on the optimization of the thermochemical conversion process, pathway for co-products extraction and scale-up/commercialization routes were addressed for fast pyrolysis (FP) and hydrothermal liquefaction (HTL) biorefineries.

In collaboration with the U.S. National Renewable Energy Laboratory (NREL), fast pyrolysis biorefinery for the conversion of lignocellulosic feedstock (e.g. forest residues) has been investigated through advanced approaches for process optimization and co-products extraction as well as the integration of bio-intermediates into existing petroleum infrastructures. Fast pyrolysis (FP) or catalytic fast pyrolysis (CFP) is a suitable process for the conversion of dry lignocellulosic sources through a thermal and catalytic cracking of the molecular structures. The process take place in absence of oxygen where the solid matrix composing the lignocellulosic biomass (cellulose, hemicellulose and lignin) is thermally cracked to form lighter compounds in form of vapors that are quickly condensed in order to maximize the liquid bio-oil percentage. Therefore, FP/CFP are efficient processes that leads to the production of high yields of liquid bio-oil (up to 80 wt.%). Raw bio-oil from FP has high oxygen content and high acidity as well as chemical instability from these properties that make it incompatible to be directly used as conventional fuels substitute or in blends. Thus, vapor or liquid upgrading is needed to improve the overall bio-oil quality and reduce the costs of final upgrading to fuel hydrocarbons. In this work, experimental studies have been carried out on micro-scale equipment and pilot plant, showing the possibility of preconditioning the FP vapors through a catalytic hot gas filter (CHGF) in order to partially deoxygenates the organic streams forming aromatic hydrocarbons, increasing the presence of valuable phenolics compounds as well as reducing the presence of unwanted corrosive compounds (such as carboxylic acids). Furthermore, the controlled fractional condensation of the partially upgraded vapors was used to validate the upgrading efficacy and to propose a separation pathway that has the potential of roughly concentrate interesting fraction for biorefinery co-products extraction. Thus, potential co-products pathway can be achieved through compounds separation directly from the vapor phase (e.g. through fractional condensation) or from the liquid phase (e.g. distillation or liquid-liquid extraction). In this regard, bio-based co-products from CFP biorefinery have been investigated, extracting organic molecules from pyrolysis liquid streams that can be used as bio-derived active ingredients in insecticides formulations. Fractions of CFP oil were obtained by vacuum distillation and then tested to evaluate the insecticidal activity. A correlation study between the dosage and the insect mortality allowed to

individuate the most active compounds. The results showed that compounds with longer alkyl chain in the substituted group of phenol have higher effect on insect mortality and therefore alkylphenols with 3 to 5 carbon in the alkyl chain were selected as the most suitable species for this application. After the experimental campaign, a techno-economic analysis (TEA) as well as a life cycle analysis (LCA) were carried out to validate the plant economic advantages and the environmental benefits in term of energy demand and GHG emissions. An existing CFP plant model was modified in order to include an extraction step comprising two distillation columns. Different simulations have been carried out varying the amount of CFP oil used for the extraction of co-products in order to obtain a correlation between minimum product selling price (MPSP), defined as the plant gate selling price of the product that makes the net present value of the project equal to zero, and the product yield. In addition, starting from the biorefinery model outputs, a life cycle inventory (LCI) has been extrapolated and used as input for the evaluation of the GHG emissions and energy demand of the bio-based insecticides supply chain. The results were compared to the supply chain of traditional insecticides (Pyrethroids and Organo-phosphates) showing large benefits in term of overall CO₂ emissions and energy demand when active ingredients are produced from lignocellulosic biorefineries. In addition, in order to improve the growth and commercialization of the FP/CFP technology, and at the same time accelerate the insertion of renewable carbon into the transportation fuels sector, a potential approach would be the integration of biorefineries into existing petroleum refineries through co-processing. Previous studies demonstrated the possibility of introducing FP/CFP bio-intermediates into refinery units, such as fluid catalytic cracker (FCC) or hydrotreaters (HT) without modifying the existing infrastructure. However, the accurate quantification of biogenic carbon ending up in gasoline, diesel, and jet fuels is a key barrier that still needs addressing, as refineries use this measurement to demonstrate compliance to local, state and government regulatory mandates. In this part of the work, the individuation of the limitation of traditional biogenic carbon accounting techniques have been investigated, proposing some new advanced approaches for the implementation of analytical methods directly at refinery sites. Traditional biogenic carbon tracking methods include mass and energy balances or ¹⁴C analysis through accelerated mass spectrometry (AMS) or liquid scintillation counting (LSC). However, the overall balances are not precise due to potential small differences in yields when co-processing; on the other hand, traditional ¹⁴C techniques are precise, reliable and robust but they are expensive and time-consuming with few facilities available around the world, thus they cannot be implemented directly in-line in refineries. Potential alternatives such as ¹⁴C optical analysis and ¹³C/¹²C ratio analysis have been selected as the most promising approaches to develop advanced in-line analytical instruments to be applied on refinery units.

The other biorefinery concept investigated in this work is based on hydrothermal liquefaction (HTL) for the valorization of wet lignocellulosic residual streams. The work has been carried out in collaboration with the RECORD consortium of the University of Florence, studying the hydrothermal liquefaction of lignin-rich stream derived from lignocellulosic ethanol biorefineries. More in details, the HTL biorefinery has been studied through experimental campaigns for process optimization, potential co-product recovery pathways, as well as scale-up perspectives (i.e. model and pilot plant design and commissioning). In contrast to FP or CFP biorefinery, where the thermochemical reactions require very low moisture content, HTL is a suitable process for organic-rich wet streams, in form of slurries. This interesting characteristic makes the technology suitable for several industrial and domestic organic waste streams, such as paper pulp, food residues, sewage sludge and lignin-rich co-products from lignocellulosic ethanol biorefineries. The advantage is that a dewatering step can be bypassed since the liquefaction happens in presence of water at near critical or critical state (i.e. 374 °C and 22,064 MPa). In these conditions, the feedstock first undergoes to an initial degradation into water soluble organics, with water and carbon dioxide as

byproducts. Then, repolymerization reactions occurs by different recombination and condensation mechanisms to form water-insoluble liquid organic compounds (biocrude) and water-insoluble solid organic/inorganic compounds (biochar or hydrochar). Among suitable feedstocks, lignin-rich stream from lignocellulosic ethanol biorefineries is a potential candidate for a valorization through hydrothermal processing due to an expected high availability in the mid-long term. Hydrothermal liquefaction offers large opportunities for this wet feedstock but implies several technical challenges that still needs to be deeply tackled. The first part of this study was mainly focused on the HTL overall process characterization through an experimental campaign using batch micro reactors to observe how the operative conditions affected the biocrude yield. Among the parameters evaluated during the experimental tests, high temperature and the use of catalytic additives were found to be the most effective approaches to maximize the biocrude yield. Then, the identification of the main compounds in the biocrude light fractions and dissolved in the aqueous phase have been evaluated, observing how the process conditions influenced the detectable-monomers generation. In addition, since part of the original carbon always remains trapped in the residual aqueous phase a pathway for compounds recovery through liquid-liquid extraction (LLE) followed by adsorption over a polymeric resin was proposed. The backbone idea is to recover valuable monomers that can enter the market as bio-based commodity chemicals (e.g. phenol or acetic acid) or to be used as precursors for materials manufacturing (e.g. precursors for polymers). LLE recovery was experimentally tested processing HTL aqueous phase with four different organic solvents, evaluating the fraction of mass extracted and the selectivity towards some oxygenated aromatic species. Moreover, the raffinate aqueous phase post-LLE was processed over a polymeric resin to adsorb the remaining valuable acidic species. The potential chemicals production in EU and USA trough these approaches was estimated from the experimental data as baseline and the current and future lignin availability data. In order to evaluate the benefit of the aqueous phase valorization, a TEA model has been implemented to compare the introduction of an aqueous phase recirculation coupled with a LLE unit to reduce the costs associated with traditional wastewater treatments. First a HTL plant model have been realized designing every part of the plant for a capacity of 180.000 tonnes/year of lignin. Then, a modification has been implemented introducing the aqueous phase recycle into the process and the LLE for the recovery of commodity chemicals. The minimum biocrude selling price (MBSP) was calculated in both configurations obtaining positive economic benefits of recirculating the aqueous phase and extracting organic mixtures for the chemical industry. In addition, since the technology needs to be investigated at larger scale in perspective of industrial applications, a continuous HTL pilot plant was designed, built and tested to convert 1-2 l/h of lignin slurries at 350°C and 250 bar.

To sum up, improvements of fast pyrolysis and hydrothermal liquefaction lignocellulosic biorefineries have been investigated through theoretical and experimental studies, highlighting benefits of specific processes modifications to maximize the main products quality and evaluate co-products extraction routes to improve the overall plant economy. Moreover, pathways for industrial scale-up and commercialization have been individuated or experimentally tested, highlighting technical challenges that needs to be tackled for future broader industrial implementations of the technologies.

Acknowledgements

This long and intense PhD journey is ending, unfortunately in weird and challenging times. However, I feel lucky to have had many who helped me along the way on my personal growth and career development. I think they really deserve to be well acknowledged, since without their presence it would have been another story.

First of all, I am deeply grateful to Prof. David Chiaramonti for giving me the opportunity of pursuing this challenging doctoral program and to be part of his RE-CORD research team. Also, I really want to thank him for trusting me and allowing me to spend time abroad to expand and improve the level of this research.

I am extremely grateful to Dr. Andrea Maria Rizzo and Dr. Edoardo Miliotti from RE-CORD for being great supervisors, colleagues and friends, supporting my ideas and helping me on keeping a straight and goal-oriented path on our research topics. I would also like to extend my gratitude to all the other RE-CORD team members (Marco, Ramin, Giulia, Lore, Silvia, Dani, Salva, Stefano, Arturo... and all the others that I am not mentioning for brevity) that makes a wonderful, colorful and creative research group with their great skills on scientific, technical and human aspects.

My deep gratitude goes also to Dr. Kim Magrini for kindly accepting me in her research groups at NREL, she is an amazing group leader and she has been a great mentor on scientific matters as well as a pillar for my personal development.

Moreover, a huge thanks goes to Dr. Nolan Wilson and Dr. Calvin Mukarakate who helped me in many phases of this work with their impressive technical and scientific knowledges as well as their great mentorship skills. They trained me to always think as a scientist and they opened my mind on many different and new topics, helping me to obtain a broader vision on biorefineries and related aspects. Of course, I would also like to express my sincere gratitude all the other NRELIans (Mike, Brady, Chai, Jessica, Kelly, Anne, Kristiina, Abhijit, Joe, Rebecca, Danny, I probably forgot someone!) that helped in different ways and made me realize the importance of being surrounded by awesome persons to achieve great and outstanding results. I could have not asked for more!.. By the way, Colorado is just a perfect place and I feel so lucky to have spent part of my life there.

I would like to extend my sincere thanks to the reviewers and the committee members for generously offering their time for evaluation my work, giving thoughtful feedback.

Finally, I would love to deeply thank my whole family for always offering me their priceless support and help to evolve and build a life and a career that I simply love. If I am who I am, it is thanks to their job.

Last but not least, Giulia. I profoundly want to acknowledge her for being my biggest supporter, even if this required sometimes huge sacrifices, especially when distance and stressful times were upon us. However she was always pushing and encouraging me to do my best. I surely would not be the person I am without her. Thanks!

Summary

| | |
|--|-----------|
| Declaration | 4 |
| Abstract | 5 |
| Acknowledgements | 8 |
| List of Figures | 12 |
| List of Tables..... | 17 |
| Glossary | 19 |
| 1 - Introduction: thermochemical biorefineries concept and challenges | 20 |
| 1.1 - Fast pyrolysis and catalytic fast pyrolysis of lignocellulosic biomass | 24 |
| 1.2 - Hydrothermal liquefaction of organic-rich wet streams..... | 27 |
| 2 - Fast pyrolysis biorefinery for bio-intermediates generation, co-products extraction and petroleum refineries integration..... | 30 |
| 2.1 - Preconditioning of Fast Pyrolysis Vapors through Catalytic Hot-Gas Filtration and Fractional Condensation | 32 |
| 2.1.1 - Introduction | 32 |
| 2.1.2 - Materials and methods..... | 33 |
| 2.1.3 - Results and discussions | 38 |
| 2.1.4 - Conclusion..... | 50 |
| 2.2 - Co-products from catalytic fast pyrolysis biorefinery: bio-based insecticides from bio-oil fractions | 51 |
| 2.2.1 - Introduction | 51 |
| 2.2.2 - Material and Methods..... | 53 |
| 2.2.3 - Results and Discussion..... | 55 |
| 2.2.4 - Conclusion and future development..... | 65 |
| 2.3 - Pathway for commercialization of fast pyrolysis bio-intermediates: co-processing of bio-oils and petroleum-derived feeds in existing refineries and the need of advanced analytical techniques for biogenic carbon tracking..... | 68 |

| | |
|---|----|
| 2.3.1 - Introduction | 68 |
| 2.3.2 - Co-processing in refinery: the case of fluid catalytic cracking units | 71 |
| 2.3.3 - Microscale studies on biogenic carbon tracking and incorporation..... | 73 |
| 2.3.4 - Established methods for measuring biogenic carbon | 76 |
| 2.3.5 - Advanced analytical techniques for online carbon tracking in petrochemical refineries | 80 |
| 2.3.6 - Refinery benefits for on-line biogenic carbon analyzers..... | 83 |
| 2.4 - Conclusions | 87 |

3 - Hydrothermal liquefaction and depolymerization of lignin-rich streams derived from lignocellulosic ethanol biorefineries: process optimization and scale-up pathway90

| | |
|--|-----|
| 3.1 - Process characterization through batch micro-scale experiments: influence of reaction conditions on overall yields | 93 |
| 3.1.1 - Introduction | 93 |
| 3.1.2 - Materials and methods..... | 94 |
| 3.1.3 - Results and discussions | 98 |
| 3.1.4 - Conclusions | 110 |
| 3.2 - Influence of reaction conditions and catalytic additives on the organic monomers yields in biocrude and aqueous phase | 112 |
| 3.2.1 - Introduction | 112 |
| 3.2.2 - Materials and methods..... | 113 |
| 3.2.3 - Results and discussions | 117 |
| 3.2.4 - Conclusion..... | 132 |
| 3.3 - Co-products from lignin hydrothermal liquefaction biorefinery: a potential pathway for extraction of chemical precursors from residual aqueous phase | 134 |
| 3.3.1 - Introduction | 134 |
| 3.3.2 - Material and methods | 136 |
| 3.3.3 - Results and discussion..... | 138 |
| 3.3.4 - Conclusion..... | 157 |
| 3.4 - Process scale up: HTL pilot plant design and commissioning | 159 |
| 3.4.1 - Introduction | 159 |

| | |
|--|------------|
| 3.4.2 - Plant description | 162 |
| 3.4.3 - Design | 163 |
| 3.4.4 - Commissioning with lignin-rich stream as feedstock..... | 168 |
| 3.4.5 - Conclusion..... | 171 |
| 3.5 - Conclusions | 172 |
| 4 - Conclusions and future developments | 175 |
| Appendix A – Analytical methods for catalytic hot gas filtration studies..... | 179 |
| Appendix A1 – Molecular Beam Mass Spectrometer | 179 |
| Appendix A2 – Other analytical methods | 179 |
| Appendix B – Further details and analysis on HTL lab-scale investigations | 181 |
| Appendix B1 – Biocrude extraction procedures and analytical methods..... | 181 |
| Appendix B2 – Further results on the effects of reaction conditions to biocrude yields | 183 |
| Appendix B3 – Total organic carbon correction | 186 |
| Appendix B4 – Biocrude elemental analysis..... | 186 |
| Appendix B5 – Biocrude molecular weight | 188 |
| Appendix B6 – Monomers detection in HTL-derived liquids..... | 189 |
| Appendix C – Techno-economic analysis of a demo-scale HTL plant | 192 |
| Appendix C1 – HTL model | 193 |
| Appendix C2 – HTL TEA data | 210 |
| Appendix C3 – Minimum Biocrude Selling Price..... | 217 |
| References..... | 218 |

List of Figures

| | |
|--|----|
| Figure 1. Total anthropogenic GHG emissions (GtCO ₂ eq / yr) by economic sectors in 2010; direct CO ₂ emissions per sector and indirect CO ₂ emission shares from electricity and heat production. AFOLU means Agriculture, Forestry and Other Land Use and includes emissions from forest fires, peat fires and peat decay. Data from IPCC 2014 ⁵ | 20 |
| Figure 2. Thermochemical lignocellulosic biorefinery conceptual scheme | 21 |
| Figure 3. Potential products from lignin (adapted from de Jong et al. ⁹) | 23 |
| Figure 4. Schematic summary of the thesis work | 23 |
| Figure 5. Lignocellulosic biorefinery scheme based on fast pyrolysis thermochemical conversion process with potential integration in petroleum refineries | 24 |
| Figure 6. Lignocellulosic biorefinery scheme based on HTL as thermochemical conversion process | 28 |
| Figure 7. General NREL fast pyrolysis (FP) and catalytic fast pyrolysis (CFP) biorefinery scheme, including potential downstream pathways. | 30 |
| Figure 8. Catalytic hot gas filtration (CHGF) coupled with fractional condensation of fast pyrolysis vapors. Image adapted from Peterson et al. ⁸⁶ | 33 |
| Figure 9. Lab scale pulsed-flow experimental setup comprising of a horizontal quartz reactor system coupled to a molecular beam mass spectrometer (MBMS) for real-time analysis of vapors products. | 34 |
| Figure 10. Catalytic hot-gas filter (CHGF) and Davison Circulating Riser (DCR) systems coupled to a small pilot scale pyrolyzer reactor system. The pilot-scale pyrolyzer system includes: biomass feed system, fluidized bed pyrolyzer, char cyclones + catch-pots, hot-gas filter (HGF) unit, slipstreams to the CHGF and DCR systems, and a scrubber product quench system for raw pyrolysis oil product with liquid phase separation and collection systems. The biomass feed system employs a feed hopper drive (1), biomass metering drive (2), and biomass conveying drive (3). The CHGF system is comprised of the CHGF unit operation (shown as inset) housed in a furnace (not shown), CHGF flow control valve, molecular beam mass spectrometer (MBMS) slipstream, and fractional condensation train (FCT). The FCT includes: passive-cool condenser, electrostatic precipitator (ESP), aqueous condenser, and coalescing filter, each with an associated product knockout. The system effluent train is equipped with a backpressure regulator (117 kPa (5 PSIG) setpoint), volumetric flow meter (dry test meter), and gas bag sampling system. Effluent is exhausted to local exhaust ventilation (LEV). *The MBMS system utilized a slipstream via a flow-by plate and was used for real-time analysis of products. | 36 |
| Figure 11. P&ID of fractional condensation train. | 37 |
| Figure 12. Mass spectra for pulsed-flow lab scale experiments for (A) partial upgrading of pine pyrolysis vapors with 15 wt.% molybdenum heteropolyacid on titania (15 wt.% Mo-HPA/TiO ₂) using a WHSV of 2.0 h ⁻¹ and 50 vol% H ₂ , (B) partial upgrading of pine pyrolysis vapors using 15 wt.% tungsten heteropolyacid on titania (15 wt.% W-HPA/TiO ₂), WHSV of 2.0 h ⁻¹ and 50 vol% H ₂ , (C) pine pyrolysis vapors using TiO ₂ , WHSV of 2.0 h ⁻¹ without H ₂ , and (D) pure pine pyrolysis vapors (control) at a flowrate equivalent to WHSV of 2.0 h ⁻¹ without H ₂ . All experiments conducted at 400°C. The m/z values 78, 91, 106, 120, 128, 142, 156, 170, and 184 correspond to benzene, toluene, xylenes, trimethylbenzenes, naphthalene, mono-, di-, tri-, and tetra-methyl-naphthalenes, respectively. The m/z values 124, 138, 150, 164, and 180 correspond to primary vapor products: guaiacol, methyl-guaiacol, 4-vinyl-guaiacol, isoeugenol, and coniferyl alcohol. Various alkylated isomers are | |

not distinguishable based on MBMS spectra and were denoted as the methylated derivatives. (*m/z = 43 is a carbohydrate fragment and m/z = 44 is carbon dioxide.) 39

Figure 13. Mass spectra for pulsed-flow lab scale experiments for partial upgrading of pine pyrolysis vapors with 15 wt.% molybdenum heteropolyacid on titania (15 wt.% Mo-HPA/TiO₂) using a WHSV of 2.0 h⁻¹ and varying the amount of H₂ from 0 to 10 and 50 vol%. All experiments conducted at 400°C. The m/z values 78, 91, 106, 120, 128, 142, 156, 170, and 184 correspond to benzene, toluene, xylenes, trimethylbenzenes, naphthalene, mono-, di-, tri-, and tetra-methyl-naphthalenes, respectively. The m/z values 124, 138, 150, 164, and 180 correspond to primary vapor products: guaiacol, methyl-guaiacol, 4-vinyl-guaiacol, isoeugenol, and coniferyl alcohol. Various alkylated isomers are not distinguishable based on MBMS spectra and were denoted as the methylated derivatives. (*m/z = 43 is a carbohydrate fragment and m/z = 44 is carbon dioxide.) 40

Figure 14. Mass spectra for pulsed-flow lab scale experiments for (A) partial upgrading of pine pyrolysis vapors with 15 wt.% molybdenum heteropolyacid on titania (15 wt.% Mo-HPA/TiO₂) using a WHSV of 2.0 h⁻¹ and 50 vol% H₂. From the bottom to the top, biomass-to-catalyst ratio was increased from 0.12 to 1.5. All experiments conducted at 400°C. The m/z values 78, 91, 106, 120, 128, 142, 156, 170, and 184 correspond to benzene, toluene, xylenes, trimethylbenzenes, naphthalene, mono-, di-, tri-, and tetra-methyl-naphthalenes, respectively. The m/z values 124, 138, 150, 164, and 180 correspond to primary vapor products: guaiacol, methyl-guaiacol, 4-vinyl-guaiacol, isoeugenol, and coniferyl alcohol. Various alkylated isomers are not distinguishable based on MBMS spectra and were denoted as the methylated derivatives. (*m/z = 43 is a carbohydrate fragment and m/z = 44 is carbon dioxide.) 41

Figure 15. Mass spectra for simultaneous reduction in weight-hourly space velocity (WHSV) and increase in H₂ concentration for (A) partial upgrading of pine pyrolysis vapors with 10 wt.% molybdenum heteropolyacid on titania (10 wt.% Mo-HPA/TiO₂) using a WHSV of 0.25 h⁻¹ and 80 vol% H₂, (B) partial upgrading of pine pyrolysis vapors using 10 wt.% Mo-HPA/TiO₂, WHSV of 0.5 h⁻¹ and 60 vol% H₂, (C) partial upgrading of pine pyrolysis vapors using 10 wt.% Mo-HPA/TiO₂, WHSV of 1.0 h⁻¹ and 40 vol% H₂, and (D) pure pine pyrolysis vapors (control) at a flowrate equivalent to WHSV of 1.0 h⁻¹ and 40 vol% H₂. Carbon dioxide signals (m/z = 44) were similar across spectra and were omitted to reduce the ordinate scale. All experiments conducted at 400°C. The m/z values 78, 91, 106, 120, and 134 correspond to benzene, toluene, xylenes, tri-, and tetramethylbenzenes, respectively. The m/z values 124, 138, 150, 164, and 180 correspond to primary vapor products: guaiacol, methyl-guaiacol, 4-vinyl-guaiacol, isoeugenol, and coniferyl alcohol. (*m/z = 43 is a carbohydrate fragment.) 42

Figure 16. Composition of condensed organic oil product, as determined by GC-MS, for pine pyrolysis vapors partially upgraded via catalytic hot-gas filtration (CHGF) using a molybdenum heteropolyacid on titania (15 wt.% Mo-HPA/TiO₂) catalyst. From left to right: empty filter (control) with WHSV 1.0 h⁻¹ and 40 vol % H₂, filter + TiO₂ with WHSV 1.0 h⁻¹ and 40 vol % H₂, filter +15 wt.% Mo-HPA/TiO₂ with WHSV 1.0 h⁻¹ and 40 vol % H₂. All experiments were conducted at 400 °C. 45

Figure 17. Spotted Wing Drosophila mortality in function of CFP oil fraction and dose concentration 56

Figure 18. Composition of CFP oil fraction and linear coefficient of dose concentration vs mortality correlation 57

Figure 19: Correlation between dose and mortality of compounds in CFP distilled fractions: blue dots (130-180°C), red dots (185-230°C) and green dots (230-250°C) 58

| | |
|---|-----|
| Figure 20. Modelled process and MPSP analysis for the extraction of alkylphenols (C3-C5) mixtures for bio-based insecticides: general model process flow (A), distillation columns for extraction of compounds from light fraction of CFP oil (B) and MPSP variation correlated to product yields and purity. | 59 |
| Figure 21. Supply Chain GHG emissions (A) and energy consumption (B) of bio-based active ingredients from CFP co-products at different purity and yields compared to fossil-based commercial active ingredients insecticides | 61 |
| Figure 22. Bio-based insecticidal active ingredient production varying CFP plant size with co-products directly in place on the CFP plant. *NREL FY19 model baseline | 62 |
| Figure 23. Composition of CFP oil fractions for future investigations on smaller temperature range cuts and higher temperature limit (i.e. 270°C). | 66 |
| Figure 24. General scheme of co-processing of fossil and renewable sources in existing petroleum refineries | 69 |
| Figure 25. Products yields derived from selected studies on co-processing of VGO and pyrolysis oils. [1] Wang et al. (2016) ⁵⁹ , [2, 3, 4] Wang et al. (2018) ⁶⁰ , [5] Fogassy et al. (2012) ⁶¹ , [6, 7] Pinho et al. (2015) ⁶² , [8] Pinho et al. (2017) ⁶³ . | 72 |
| Figure 26. Ion signals of products from co-processing of VGO and ¹³ C oak followed by catalyst oxidative regeneration in the py-MBMS using (A) E-Cat and (B) CP758. Reaction conditions: VGO, 30 mg; oak, 30 mg; per pulse catalyst, 500 mg; temperature, 550 °C. | 75 |
| Figure 27. Ion signals of products from catalytic upgrading of A) VGO over E-cat and B) ¹³ C oak over E-cat followed by catalyst regeneration in the py-MBMS. Reaction conditions: VGO 30mg, oak 30mg, per pulse catalyst 500mg, temperature 550 °C | 75 |
| Figure 28. Co-Processing of pyrolysis oil and VGO - Biogenic carbon and incorporation in total-liquid for literature data, error bars refers to absolute precision stated in ASTM-D6866 Method B (± 3 wt.%) ²⁴⁰ and in Haverly et al. (0.26 wt.%) ²⁶⁵ ; [1] Wang et al. (2016) ⁵⁹ , [2, 3, 4] Wang et al. (2018) ⁶⁰ , [5] Fogassy et al. (2012) ⁶¹ , [6, 7] Pinho et al. (2015) ⁶² , [8] Pinho et al. (2017) ⁶³ . | 78 |
| Figure 29. Biomass availability forecast comprising forest and agricultural residues, accordingly to Langholtz et al. ²⁹⁶ (A); (right) $\delta^{13}\text{C}$ ranges, comparison of petroleum sources with C ₃ and C ₄ biomasses, data from Peters et al. ²⁸⁰ , Kohn et al. ²⁹² and O'Leary et al. ²⁹³ (B) | 82 |
| Figure 30. Example showing how refiners can utilize on-line analyzers to maximize overall refinery economics with co-processing | 84 |
| Figure 31. Simplified schematic showing insertion points for different bio-oils in existing refineries and possible positions for coupling biogenic carbon analyzer to accurately measure renewable fuels in finished fuels. | 86 |
| Figure 32. Scheme of a lignocellulosic ethanol biorefineries and lignin-rich stream (LRS) extraction | 91 |
| Figure 33. Scheme of Procedure 1 (a) and 2 (b) for products collection. | 95 |
| Figure 34. Products collected from a typical hydrothermal liquefaction (HTL) experiment in the micro-batch reactors: light biocrude or BC1 (a), heavy biocrude or BC2 (b), aqueous phase with water-soluble organics (WSO) (c) and solid residue (d). | 96 |
| Figure 35. Effect of the collection procedure on biocrude 1 composition by GC-MS analysis (a) and on aqueous phase composition by HPLC analysis (b). The experiment was performed at 350 °C, 10 min, 10%. | 99 |
| Figure 36. Dry-basis mass yields under different reaction conditions. | 101 |
| Figure 37. Normal plot of the standardized effects for BC1 yield. | 102 |

| | |
|--|-----|
| Figure 38. Normal plot of the standardized effects for BC2 yield. | 103 |
| Figure 39. Normal plot of the standardized effects for total biocrude yield. | 103 |
| Figure 40. Effect of increased temperature and reaction time on products yield; error bars represent absolute standard deviation. | 104 |
| Figure 41. Van Krevelen diagram of lignin-rich stream (feedstock), BC1, BC2 and solid residue (char). | 105 |
| Figure 42. Higher heating value of light, heavy and total biocrude from the experiments carried out at 10% biomass-to-water mass ratio. | 106 |
| Figure 43. Carbon distribution among HTL products. | 107 |
| Figure 44. Infrared spectra of the LRS and light and heavy fraction of biocrude from the experiment carried out at 370 °C, 5 min, 20%; (a) entire spectra, (b) particular. | 108 |
| Figure 45. Weight-average molecular weight at different reaction conditions: (a) biocrude 1, (b) biocrude 2, (c) total biocrude. Error bars represent the absolute standard deviation. | 109 |
| Figure 46. Stacked molecular weight distribution of BC1 (left) and BC2 (right) from experiments carried out at 10wt.% (a–b) and 20wt.% (c–d). | 110 |
| Figure 47. Graphical scheme of lignin depolymerization with catalytic additive | 112 |
| Figure 48. Extraction procedure for hydrothermal liquefaction (HTL) products recovery (Procedure 1). | 115 |
| Figure 49. Water-soluble compounds in LRS liquid fraction of the slurry: yield on feed at 10 wt.% of B/W | 119 |
| Figure 50. Typical GC-MS chromatogram for BC1 fraction obtained at 350 °C, 10 min, 10% biomass to water ratio. 1. Acetic acid, 2. Propanoic acid, 3. 1,2-Cyclopenten-1-one, 2-methyl-, 4. Phenol, 5. Phenol, 2-methoxy-, 6. Phenol, 2-methoxy-4-methyl-, 7. 1,2-Benzenediol, 8. 1,2-Benzenediol, 3-methoxy-, 9. Phenol, 4-ethyl-2-methoxy-, 10. Phenol, 2,6-dimethoxy-, 11. Phenol, 2,6-dimethoxy-4-methyl-, 12. Benzene, 1,2,3-trimethoxy-5-methyl-, 13. Homosyringaldehyde, 14. Syringylacetone, 15. o-Terphenyl (Internal Standard). | 120 |
| Figure 51. Typical partial HPLC chromatogram for water-soluble organics (WSO) in aqueous phase (AP) fraction obtained at 350 °C, 10 min, 10% biomass to water ratio. 1. Succinic acid, 2. Glycolic acid, 3. Lactic acid, 4. Glycerol, 5. Glutaric acid, 6. Acetic acid, 7. Methanol. | 121 |
| Figure 52. ¹ H NMR spectra for DEE-soluble biocrude (BC1) and DMK-soluble biocrude (BC2) from test at 370 °C and 5 min. | 122 |
| Figure 53. Effect of reaction temperature on yields of quantified compounds for uncatalyzed HTL tests: (a) phenolics, (b) acids and alcohols, (c) phenolic carbonyls and cyclopentenones. When no graph column is depicted, the concentration was below quantification limits. | 123 |
| Figure 54. (a) Effect of reaction temperature on yields of specific acids and alcohols species; (b) difference plot for acids degradation versus formation compared to the initial acids content in the lignin-rich streams (LRS) slurry for uncatalyzed HTL tests. | 124 |
| Figure 55. Effect of residence time on yields of quantified compounds for uncatalyzed HTL tests: (a) phenolics, (b) acids and alcohols, (c) phenolic carbonyls and cyclopentenones. When no graph column is depicted, the concentration was below quantification limits. | 125 |
| Figure 56. Effect of base catalyzed reaction, increasing KOH to LRS ratio from 2 wt. % to 4 wt. %: average molecular weight of BC1, BC2, and total biocrude. Error bars represent absolute standard deviation. | 128 |

| | |
|--|-----|
| Figure 57. Effect of base catalyzed reactions increasing KOH to LRS ratio from 2 wt. % to 4 wt. % on yields of quantified compounds: (a) phenolics, (b) acids, and alcohols, (c) phenolic carbonyls and cyclopentenones. When no graph column is depicted, the concentration was below quantification limits. | 129 |
| Figure 58. Effect of CO ₂ acid catalyzed reaction compared to base catalyzed and blank tests on yields of quantified compounds: (a) phenolics, (b) acids and alcohols, (c) phenolic carbonyls, and cyclopentenones. When no graph column is depicted, the concentration was below quantification limits. | 131 |
| Figure 59. Influence of collection procedures on organic compounds distribution among BC1 and AP fractions. Tests performed at 350 °C, 10 min, 10 wt. % B/W in absence of catalysts. | 132 |
| Figure 60. Scheme of HTL aqueous phase valorization strategy. | 135 |
| Figure 61. Characterization of LRS-HTL residual aqueous phase on wet (left bar) and dry (right bar) basis. | 138 |
| Figure 62. Partition coefficient (A) and fraction extracted (B) with four different solvents LLE. With EtAc acids and alcohols were not quantified due to HPLC peak coverage by the solvent itself. | 139 |
| Figure 63. Phenolics selectivity (left) and effect of concentration of phenolic in the extract (right) | 140 |
| Figure 64. Carbon balance for the overall HTL process with LLE integration (data obtained with BuAc extraction) | 141 |
| Figure 65. Loading curve for the organic acids and glycerol of the post-LLE raffinate (left) and elution curve desorbed from the resin using ethanol (right). | 142 |
| Figure 66. Scheme of the HTL with AP recirculation and LLE integration for the extraction of organic compounds | 150 |
| Figure 67. Model mass flows for HTL-LLE integration; AP/solvent ratio of 5:1 | 152 |
| Figure 68. Electrical and thermal power of the LLE section. | 153 |
| Figure 69. Influence of aqueous phase recycle and LLE integration on MBSP: base case in absence of aqueous phase valorization (left) and with recycle coupled with LLE (right) | 156 |
| Figure 70. Simplified flow chart (a) and picture of the HTL pilot plant (b) | 163 |
| Figure 71. Pressure values showing leakage in the filter's lines during the BRR testing | 167 |
| Figure 72. Pressure decrease during piston switch (a); pressure increase after anticipated closure of inlet valve (b) (the switch is occurring every two minutes); pressure fluctuation after PID implementation (c). | 168 |
| Figure 73. Block diagram of the extraction procedure used for products recovery (left) and pictures of the recovered products (right). | 170 |

List of Tables

| | |
|---|-----|
| Table 1. Characterization of pulsed-flow (PF) and continuous-flow (CF) unreacted and reacted TiO ₂ control and Mo-HPA/TiO ₂ materials with and without H ₂ | 44 |
| Table 2. GC-MS characterization of organic oil product from catalytic hot-gas filtration..... | 46 |
| Table 3. GC-MS characterization of aqueous product from catalytic hot-gas filtration..... | 46 |
| Table 4. Mass distribution of chemical classes between the condenser and the cold trap of the fractional condensation train..... | 48 |
| Table 5. Mass balance results for catalytic hot-gas filter (CHGF) experiments with the ESP second stage condenser (FCT-ESP-01) at 70°C and 170°C. Experiments were conducted using 10 wt.% molybdenum heteropolyacid on titania (10 wt.% Mo-HPA/TiO ₂) with a weight-hourly space velocity (WHSV) of 1.0 h ⁻¹ and 40 vol% H ₂ | 49 |
| Table 6. Results from Addition of Steam to Oak CFP Using ZSM-5 Performed on the py-MBMS System..... | 76 |
| Table 7. Biogenic carbon content measured by ¹⁴ C radiocarbon analysis, with AMS (accordingly to ASTM D6866-12 – method b)..... | 79 |
| Table 8. Operating parameters of the design of the experiments (DOE)..... | 94 |
| Table 9. Characterization of the lignin-rich stream (w.b.: wet basis; d.b.: dry basis)..... | 98 |
| Table 10. Lignin and sugars content in LRS. | 98 |
| Table 11. Effect of the collection procedure on measured yields of products—experiment performed at 350 °C, 10 min, 10%. Absolute standard deviation is given in brackets. | 100 |
| Table 12. Yields of the HTL products from all investigated reaction conditions. Absolute standard deviation is reported in brackets. | 117 |
| Table 13. Lignin and sugars content in LRS. | 118 |
| Table 14. pH values of feed and products with and without KOH. Test performed at 350 °C, 5 min, and 10 wt. % biomass to water ratio (B/W)..... | 126 |
| Table 15. Effect of base catalyzed reaction increasing KOH to LRS ratio from 2 wt. % to 4 wt. % at 300–350–370 °C, 5 min and 10 wt. % B/W: mass yields of light biocrude (BC1), heavy biocrude (BC2), solid residues (SR), Gas, and water-soluble organics (WSO) + loss. Absolute standard deviation is reported in brackets. | 127 |
| Table 16. Total organic carbon (TOC) concentration of WSO, influence of KOH at 300–350–370 °C. Compared to carbon concentration calculated by HPLC detected compounds. Test performed at 5 min and 10 wt. % B/W. | 127 |
| Table 17. Effect of CO ₂ acid catalyzed reaction compared to base catalyzed and control test at 300 °C, 5 min and 10 wt. % B/W: mass yields of BC1, BC2, SR, Gas, and WSO + loss. Absolute standard deviation is reported in brackets..... | 130 |
| Table 18. Solvents data for LLE..... | 136 |
| Table 19. Total organic carbon, water content and ph of HTL-LRS aqueous phase..... | 138 |
| Table 20. Solvent selection results from Prat et al. CHEM21 guide scores ⁴²¹ | 140 |
| Table 21: Results summary of PVP adsorption of organic compounds in raffinate post-LLE..... | 143 |
| Table 22. Cellulosic ethanol and LRS availability in EU (2017-2030) and US (2019-2030)..... | 144 |
| Table 23. Targeted molecules extracted from HTL AP through LLE and resin adsorption: EU data 2017-2030..... | 144 |
| Table 24. Targeted molecules extracted from HTL AP through LLE and resin adsorption: US data 2019-2030..... | 145 |

| | |
|--|-----|
| Table 25. Experimental data of fraction extracted and calculated mass flow of organic components in raffinate and extract. | 152 |
| Table 26. Mass flows of the chemicals coming out of the refining step..... | 153 |
| Table 27. Electrical power installed and electricity consumption per year for each pump. | 154 |
| Table 28. Equipment cost of the LLE integration. | 155 |
| Table 29. Operating costs of the HTL plant with LLE integration..... | 155 |
| Table 30. Prices of the chemicals considered in the economic analysis..... | 155 |
| Table 31. Annual mass flow and revenue of the chemicals coming out of the refining step..... | 156 |
| Table 32. Recent continuous HTL pilot plant (CSTR – Continuous stirred tank reactor; PFR – Plug-flow reactor; BPR – Back-pressure regulator). | 161 |
| Table 33. HTL continuous unit design specifications | 164 |
| Table 34. Reaction conditions for the test with lignin-rich stream..... | 168 |
| Table 35. Average, maximum and minimum temperature measured along the system during the whole test. | 169 |
| Table 36. Average, maximum and minimum temperature measured along the system during the sample collection. | 169 |
| Table 37. Flow rate, medium velocity and residence time during the feeding. | 170 |
| Table 38. HTL continuous product yields. | 171 |

Glossary

AMS – Accelerator Mass Spectrometry
BTX – Benzene, Toluene and Xylene
BuAc – Butyl acetate
BV – Bed Volume
CFP – Catalytic Fast Pyrolysis
CHGF – Catalytic Hot-Gas Filtration
CRDS – Cavity Ring-Down Spectroscopy
DCR – Davison Circulating Riser
DEE – Diethyl Ether
DMK – dimethyl ketone (acetone)
DOE – Design of Experiments or US Department of Energy
EFSA – European Food Safety Authority
EPA – Environmental Protection Agency
EtAc – Ethyl acetate
FC – Fractional Condensation
FCC – Fluid Catalytic Cracker
FCT – Fractional Condensation Train
FP – Fast Pyrolysis
GHG – Greenhouse gas
GGE – gallon of gasoline equivalent
HC – Hydrocracker
HCO – Heavy cycle oil
HDO – Hydrodeoxygenation
HPA – Heteropolyacids
HT – Hydrotreater
HTL – Hydrothermal Liquefaction
ICOGS – Intracavity Optogalvanic Spectroscopy
ICP-AES – Inductively Coupled Plasma Atomic Emission Spectroscopy
IPM – Integrated pest management
IRMS – Isotope Ratio Mass Spectrometry
ISCC – International Sustainability and Carbon Certification
kTA – kilotonnes per annum
LCA – Life cycle assessment
LCO – Light cycle oil
LLE – Liquid-Liquid Extraction
LPG – Liquefied petroleum gas
LRS – Lignin-rich streams
LSC – liquid scintillation counting
MBMS – Molecular beam mass spectrometer
MIBK – Methyl isobutyl ketone
MPSP – Minimum Product Selling Price
MRTB – Micro-Reactor Test Bench
NREL – National Renewable Energy Laboratory
pMC – percentage of Modern Carbon
PVP – poly(4-vinylpyridine)
RED II – Renewable Energy Directive II
SCAR – Saturated-Absorption Cavity Ring-Down
SCCM – Standard Cubic Centimeters per Minute
TEA – Technoeconomic Analysis
TOS – time-on-stream
TPD – Temperature programmed desorption
VGO – Vacuum Gas Oil
WHSV – Weight hourly space velocity
WSO – Water-soluble organics

1 - Introduction: thermochemical biorefineries concept and challenges

Potential shortage of fossil resource and GHG reduction constraints are underlining the need of a switch from a linear economy towards a circular bio-based economy.^{1,2} Climate change mitigation targets need strong effort towards a decarbonized economy, reducing the dependence on fossil sources. Nowadays, most of CO₂ emitted in the atmosphere comes from electrical energy/heat production followed by agriculture, forestry and other land use (AFOLU) and industry and transport sectors (Figure 1). Thus, in order to mitigate the ongoing effects of the climate change, the efforts need to be focused on those sensitive subjects. For these reasons, in the last years the EU and other countries have introduced several regulations and guidelines to promote the development of bio-based economies introducing renewable sources into the existing industrial markets, such as the production of biofuels for the transport sector. In the EU the recast Renewable Energy Directive 2018/2001 (RED II) sets an increased 14 % target for the share of renewable fuels in transport by 2030. In addition, the EU in 2020 launched a set of initiatives with the name of European Green Deal. With this strategy, the EU wants to tackle climate and environmental-related challenges towards a green-based economy, with the aim of zeroing the GHG emission by 2050. While in US, the federal Clean Air Act (CAA) (42 U.S.C. 7401 et seq.) introduced regulations for all of sources of air pollutions, therefore defining the Environmental Protection Agency (EPA) responsibilities for improving and protecting the air quality, limiting the GHG emissions. EPA, through the Renewable Fuel Standard Program is boosting the introduction of 36 billion gallons (about 136 billion liters) of renewable fuel, extending the volume required yearly until the 2022.^{3,4}

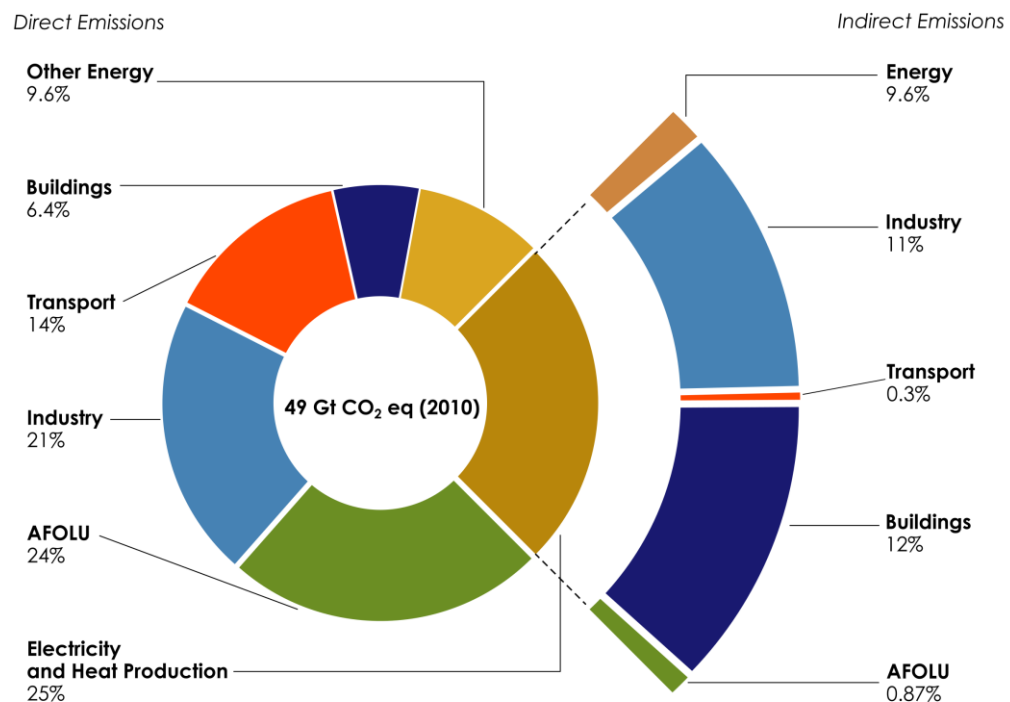


Figure 1. Total anthropogenic GHG emissions (GtCO₂eq / yr) by economic sectors in 2010; direct CO₂ emissions per sector and indirect CO₂ emission shares from electricity and heat production. AFOLU means Agriculture, Forestry and Other Land Use and includes emissions from forest fires, peat fires and peat decay. Data from IPCC 2014⁵

Biofuels for transport sector and bioproducts for the chemical industry have been highlighted to play a fundamental role to face these challenges in the mid and long term, by introducing renewable sources into traditional fossil-based markets, thus reducing the impact in term of carbon dioxide emissions. Especially in the perspective of an environmentally, economically and socially sustainable circular global economy, residual biomass from agricultural lands, forests or industry has the potential to cover the need of renewable substitution of traditional chemicals and fuels. Moreover, the deployment of valorization pathways of biomass in rural areas will economically and socially stimulate regional developments.

Among different types of naturally available biomasses, lignocellulosic biomass or industrial residual streams have the peculiarity of not competing with the food production chain, therefore not influencing the food market. This important characteristic classifies lignocellulosic biomass as feedstock for “second generation biofuel” in comparison with the first generation of biofuels that implied the use of edible matrix, such as corn or vegetable oils.

The integrated production of fuels and chemicals is nowadays a standard approach in petroleum refinery, where 85% of the entire oil barrel is used for fuel production and the remaining 15% to produce chemicals. However, from an economical point of view, the production of chemicals account for 50% of the overall profits.⁶

Therefore, a similar approach is possible in an integrated lignocellulosic biorefinery concept, where biomass can be converted into both fuels and chemicals precursors. In general, the term biorefining has been defined by the International Energy Agency as "sustainable processing of biomass into a spectrum of marketable products (food, feed, materials, chemicals) and energy (fuels, power, heat)"⁷. In this perspective, thermochemical conversion platforms with the extraction of co-products along with biofuels, will improve the overall plant economics reducing the biofuels costs of about 30%^{8,9}, therefore increasing the competitiveness of biomass thermochemical conversion technologies. Besides, in this way carbon valorization would be maximized to aim for “zero waste” and therefore implementing a more efficient use and conversion of biomass.¹⁰ In addition, transport and industry sector are responsible of 14% and 21% of the global CO₂ emissions⁵, as showed in Figure 1. Hence, switching towards a more sustainable and low-GHG impact refinery processes, based on renewable biomass valorization might, be the most promising way to mitigate the climate change.

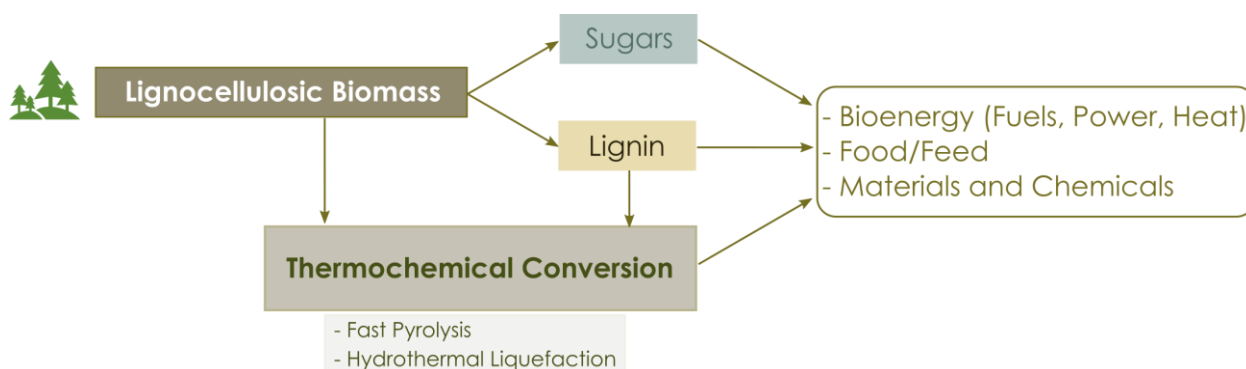


Figure 2. Thermochemical lignocellulosic biorefinery conceptual scheme

Thermochemical biorefineries for the conversion of lignocellulosic biomass are considered an interesting approach for the production of a broad spectrum of precursors for fuels or materials and chemicals, as conceptually summarized in the scheme in Figure 2. The lignocellulosic feedstock can undergo a separation between sugars (cellulose and

hemicellulose) and lignin through pretreatment such as steam explosion, organosolv process or ionic liquid fractionation^{11–14}; the isolated sugars can then be converted, through enzymatic hydrolysis and fermentation, to form alcohols for energy purposes (e.g. ethanol for transportation fuel) or be used in the food/feed supply chain. The remaining lignin can be directly combusted for energy and heat production¹⁵ as well as be used unmodified in materials manufacturing (e.g. composites or fibers).¹⁶ In addition, lignin can be transformed through thermochemical processes, such as hydrothermal liquefaction, to generate organic mixture to be used as precursor for biofuels and chemicals. Moreover, once the lignin matrix is deconstructed there is the possibility to extract molecules for other markets such as chemicals, agrochemicals and materials, as well as food and feed additives.

Another route that does not require the lignocellulosic biomass pre-fractionation is through a direct thermochemical conversion of the whole biomass. Fast pyrolysis is an example where cellulose, hemicellulose and lignin are converted together to generate an organic vapors mixture that can be condensed into a liquid stream called bio-oil. In this case the biomass matrix is totally converted into lighter substances that can be used for energy purposes (upgraded to fuel or combusted to heat and electrical power generation) or be extracted and transformed for chemicals and materials markets as well as for food or feed supply chains.

Through the development of biorefineries, sustainable and cost-effective processing of renewable feedstock to a broad range of bio-based products can be achieved. Compared to fuel market, the industrial chemicals market comprises of a large amount of diverse and complex products. Commonly in the petrochemical sector, high value-added products such as polymers, specialty chemicals, and active ingredients are manufactured from lower-value petroleum feedstocks.⁶ Bio-derived products may compete with petroleum-based chemicals as drop-in replacements or new and unique end-products that can be manufactured as replacement of traditional fossil-based materials. Drop-in replacements include commodity chemicals (e.g. phenol, cresols, acetic acid) while other more complex molecules can drive the fabrication of polymers building blocks or active substances for other purposes (e.g. molecules for pesticides).

Lignin is one of the main constituents of lignocellulosic biomass, making up to 15–35 wt. % of the total organic matter weight, carrying also the highest specific energy content compared to cellulose and hemicellulose^{17–19}. The global amount of lignin estimated on the Earth's surface is 300 billion tonnes and annually increases by around 20 billion tonnes²⁰. Thermochemical conversion always leads to the generation of a mixture of oxygenated compounds through the thermal and catalytic deconstruction of biomass building blocks, such as lignin and cellulose. In this regard, oxygenated aromatic chemicals (phenols, methoxyphenols and alkylphenols) derived from lignin are rising large interests due to the fact that at present these compounds are being produced from fossil-based molecules derived from coal or petroleum. Besides, lignin can potentially generate a broad range of chemicals and materials precursors due to its unique aromatic nature, as depicted in Figure 3.⁹ In spite of the long-standing belief that “you can make anything out of lignin, except money”, large interests are rising toward the deconstruction of the aromatic matrix, and the separation of macro fractions or single monomers has been the subject of investigation by several authors.^{21–25}, showing that “yes, there are ways to make money from lignin”, as Graichen et al.²⁶ summarized. The main challenges are related to the separation of the whole lignin matrix from the feedstock or the extraction of the lignin fragments from end-products of conversion processes (e.g. phenols from fast pyrolysis or hydrothermal liquefaction).

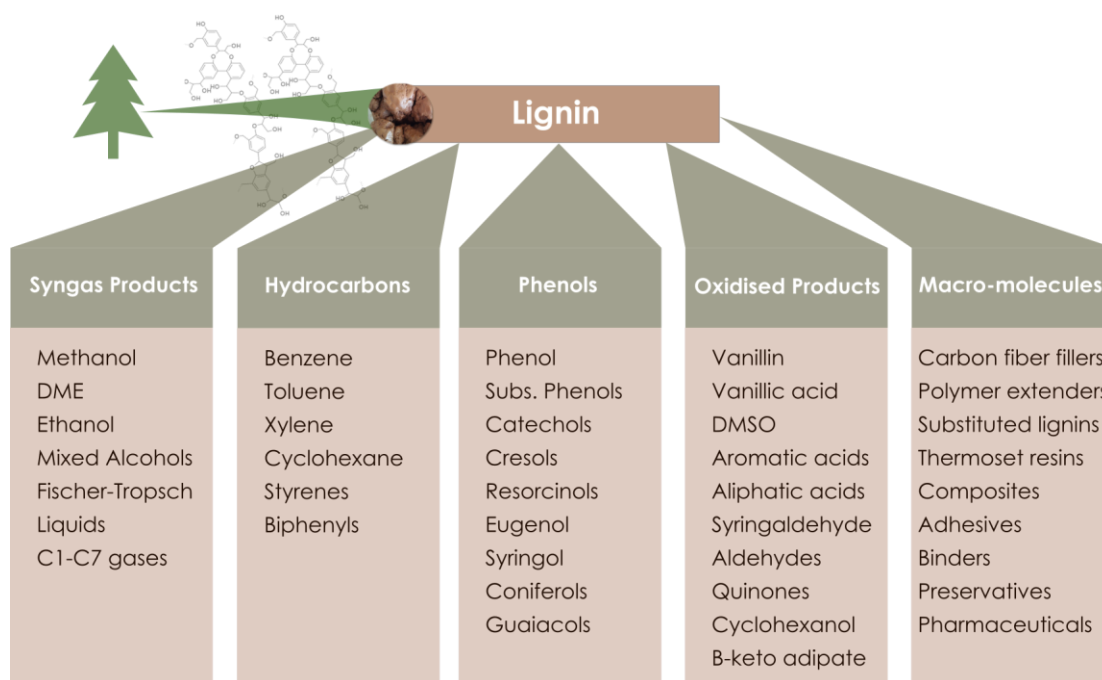


Figure 3. Potential products from lignin (adapted from de Jong et al.⁹)

In this work two different types of biorefineries for the valorization of lignocellulosic biomass have been investigated, both employing a thermochemical conversion step as primary biomass deconstruction process. In both the cases, the work followed a three-tiers approach, as depicted in Figure 4, encompassing: 1) studies on the optimization of the thermochemical conversion process, 2) pathways for co-products extraction and 3) scale-up/commercialization routes.

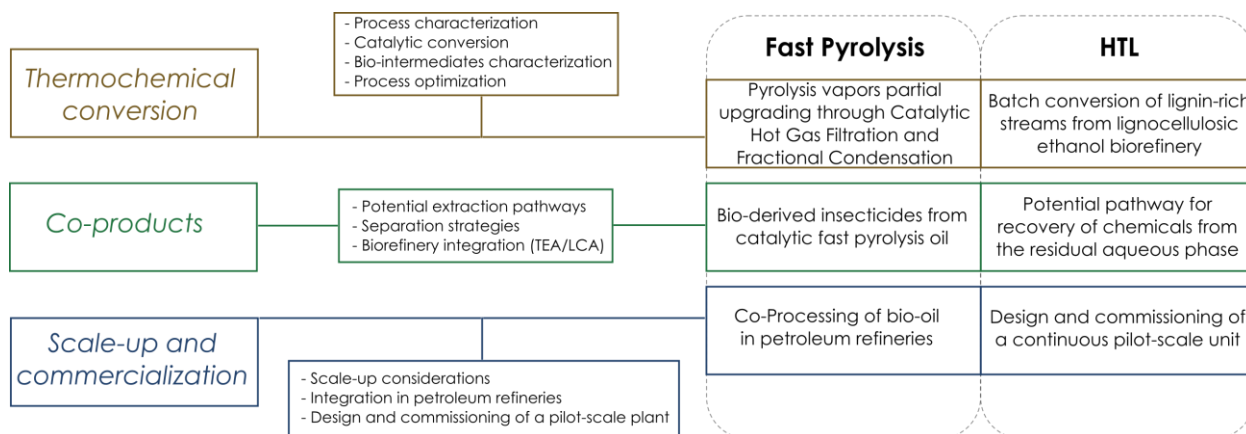


Figure 4. Schematic summary of the thesis work

Fast pyrolysis biorefinery for the conversion of lignocellulosic feedstock (e.g. forest residues) has been investigated through advanced approaches for process optimization and co-products extraction as well as the integration of bio-intermediates into existing petroleum infrastructures; the work was carried out in collaboration with the U.S. National Renewable Energy Laboratory (NREL). The second biorefining approach leveraged the hydrothermal liquefaction of

lignin-rich stream, derived from lignocellulosic ethanol process, focusing on the process characterization and co-product recovery, as well as the design and commissioning of a continuous pilot-scale unit. This latter activity was carried out at the Renewable Energy Consortium for R&D (RE-CORD), a not for profit research organization based in Florence and participated by the University of Florence.

1.1 - Fast pyrolysis and catalytic fast pyrolysis of lignocellulosic biomass

Fast pyrolysis (FP) and catalytic fast pyrolysis (CFP) is a suitable process for the conversion of dry lignocellulosic sources through a thermal and catalytic cracking of their molecular structures. The process takes place in absence of oxygen, where the solid matrix composing the lignocellulosic biomass (cellulose, hemicellulose and lignin) is thermally cracked to form lighter compounds in form of vapors that are quickly condensed in order to maximize recovery of the liquid product, i.e. the bio-oil. Other FP by-products are a solid (biochar) and a mixture of non-condensable gases (such as CO and CO₂). FP is an efficient process that leads to the production of high yields of liquid bio-oil (up to 80 wt.%)²⁷. Raw bio-oil has high oxygen and water content, high acidity as well as poor chemical stability, making its direct use as fuels substitute or in blends not straightforward. Thus, vapor- or liquid-phase upgrading is needed to improve the overall bio-oil quality and unlock the production of fuel hydrocarbons.

Figure 5 depicts an example of FP/CFP lignocellulosic biorefinery: upgraded or raw pyrolysis vapors can be directly quenched to form bio-oil as bio-intermediate liquid product. While potential co-products pathway can be achieved through compound separation directly from the vapor phase (e.g. through fractional condensation) or from the liquid phase (e.g. distillation for CFP bio-oils, liquid-liquid extraction or other fractionation techniques for FP and CPF liquids). Several strategies for the process optimization have been studied in the last century by many researchers, implying *in situ* or *ex situ* catalytic upgrading as potential strategy for the deoxygenation of the organic vapor mixture towards the formation of hydrocarbons for fuel production.^{10,28-30} In general, the liquid bio-oil from fast pyrolysis (FP) or catalytic fast pyrolysis (CFP) always needs further upgrading steps prior to obtain a complete deoxygenation towards the generation of hydrocarbons and thus be used as drop-in fuel. Hydrotreatment (or hydrodeoxygenation – HDO) as well as co-processing in petroleum refineries are possible routes already demonstrated by other works.³¹⁻³³

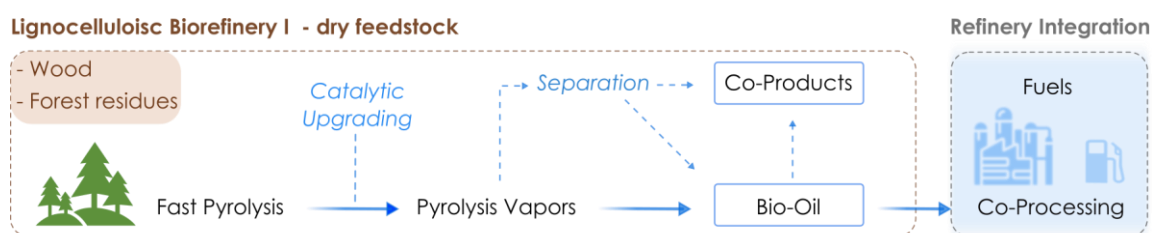


Figure 5. Lignocellulosic biorefinery scheme based on fast pyrolysis thermochemical conversion process with potential integration in petroleum refineries

Different approaches or strategies have been investigated in order to improve the bio-oil quality, reducing the costs of the final treatments for advanced biofuels production. One of the main focus is the removal of reactive oxygen and

corrosive acids through the transformation of the vapor mixture into more valuable compounds, e.g. via decarboxylation and ketonization of carboxylic acids. In addition, char and alkali content in the bio-oil should be limited to improve the stability and aging issues and hot gas filtration (at the reaction conditions of about 500°C) has been demonstrated has an interesting solution in this respect.^{34–36}

Regarding the co-products pathways from fast pyrolysis biorefineries, several strategies have been proposed, such as the extraction of precursors for polymers or other bio-based materials (e.g. phenolic resins from phenols), as well as the extraction of commodities chemicals (e.g. pure phenols and cresols).^{37–39} Other interesting applications are represented by the substitution of fossil-based agricultural chemicals, especially pesticides. The Food and Agricultural Organization of the United Nations (FAO) projects food demand needs to be subjected to about 70% of increment by 2050 due to an expected large increment in the world population that will reach 9.7 billion people.^{40–42} The use of pesticides (including herbicides, insecticides and fungicides) provide a net benefit in term of crops production yields, but still face major sustainability and environmental challenges. Consequently, the global proliferation of pesticides has also resulted in reduction to air and water quality, increases to GHG emissions, and detriment to beneficial insects (e.g. bees). Pesticides, specifically insecticides, impact water quality when they are transported to ground water reservoirs and streams where the insecticides or degradation products can bioaccumulated and persist.⁴³ Conventional pesticides are enduring additional pressures beyond tightening regulations as well as pests resistance due to massive during the last century. Therefore, in the near future, renewable and sustainable chemicals such as bio-based pesticides will be necessary to meet the food supply projections by 2050 and mitigate the environmental impact of conventional synthetic agrochemicals towards a more sustainable pest management in a green-economy perspective. Particularly interesting is the extraction of pesticides active ingredients from bio-oil mixtures. Liquid fractions derived from pyrolysis of lignocellulosic biomass have already been demonstrated to have pesticidal and insecticidal activity. Pesticides are always formulated with two fractions: active and inert ingredients. Active ingredients are the ones that have the repellent or mortal effects on pests while inert does not participate in the pest control mechanisms. Potentially, active ingredients can be extracted from pyrolysis liquids, as other literature studies shows.^{44–51} More in detail, in other previous works carried out by Canadian research groups, liquid fractions derived from pyrolysis of lignocellulosic biomass has been demonstrated to have pesticidal and insecticidal activity. Bedmutha et al.⁴⁶ investigated the effect of pyrolysis oil from coffee grounds, modifying the oil compositing by varying the reaction temperature between 400–600°C and separating the oil in different fractions; their results showed a marked insecticidal activity of phenols. Hossain et al.⁴⁸ studied the toxicity of pyrolysis liquids derived from lignin, cellulose and hemicellulose individually and in mixtures; they concluded that lignin fractions have the strongest pesticide activity. Similar results were obtained by Booker et al.⁵² where bio-oil from tobacco leaves showed high pesticide activity. To sum up, their work showed that the active pesticide effect is mostly due to lignin-derived compounds mixture, especially phenols. In addition, a study from Saini et al.⁵³ investigated the insecticidal property of alkyl-substituted guaiacols finding that the presence of a methyl group at 4-position of guaiacol increase the insecticidal activity. Further studies are strongly needed in order to identify the active molecules and proposes new bio-based pesticides formulations for substituting traditional agrochemicals that are often fossil-based (e.g. organophosphates).

In order to stimulate the growth and commercialization of large-scale fast pyrolysis biorefineries, supporting policies and incentives schemes are needed for them to hit the market and allow their integration into existing refineries. The insertion of bio-intermediates from FP or CFP into existing petroleum refinery infrastructures can drive the integration of renewable sources into the existing transportation sector, stimulating the growth of this technology and

simultaneously promoting the manufacturing of bio-based products. Modern petroleum refineries are a complex and interconnected set of multiple chemical processing units, where crude oil is transformed and refined in more useful products transport sector (gasoline, diesel, jet-fuel, naphtha, LPG) or other tradable commodities (e.g. lubricants, asphalt base, heating oil); due to the extensive slate of products, investigations have been carried out in the last years to identify the more suitable point of insertion for biogenic carbon into the refinery, and how the process could be optimized.^{33,54} Petroleum refineries could potentially dedicate whole upgrading sections to bio-intermediates, such as hydrotreaters, but the existing capacity is currently at least one order of magnitude larger compared to the actual throughput of fast pyrolysis bio-oil in existing facilities.⁵⁵ Hydrotreating and hydrocracking facilities typically process around 100,000 barrels of fuel per day, while commercial pyrolysis facilities are usually designed to be about 30 times smaller at around 3,000 barrels per day, in order to benefit from economies of scale while limiting the size to avoid transporting biomass over excessively long distances.⁵⁶ Consequently, co-processing of bio-oils and fossil-derived feeds seems the most logical approach for a quicker integration of renewable feed into the fuel for transportation sector, as it will have the least impact on existing refining facilities, while additional FPBO production capacity is being built.^{57,58} Laboratory and pilot scale studies have evaluated the feasibility of co-processing bio-derived liquids (such as pyrolysis oils) with VGO in an FCC with feed blends in the range 5:95 – 20:80 weight ratio.⁵⁹⁻⁶⁵ A recent review reported challenges and opportunities for co-processing FP, CFP, and hydrotreated FP (HT-FP) oils with vacuum gas oil (VGO) in an FCC and concluded this technology is viable after minor reactor modifications.³³ Several reports cited in that review demonstrated that coprocessing bio-oils in an FCC led to increased yields of CO, CO₂, coke, and heavy cycle oil compared to VGO alone, indicating that biogenic carbon fed into the process does not necessarily end up in fuels produced. Thus, it is critical to determine the destination of biogenic carbon during co-processing to evaluate true GHG impacts on transportation fuels, in order to allocate the portion of renewable share of the products entering the market and thus receiving economic incentives from local policies. In addition, studies on catalysts and reaction mechanisms pointed the attention towards the mechanisms of biogenic carbon incorporation into the final products for the process optimization.^{61,66,67} Hence, a proper evaluation of the biogenic carbon is needed to help spreading the technology and control the real amount of renewable carbon ending up into the fuels, thus being able to evaluate the reduced impact in term of GHG emissions.

In this study several aspects about these topics have been investigated and presented in Chapter 2. In paragraph 2.1 experimental studies, carried out on micro-scale equipment and pilot plant, showed the possibility of preconditioning the pyrolysis vapors through a catalytic hot gas filter (CHGF), in order to partially deoxygenates the organic streams and yielding aromatic hydrocarbons, increasing the presence of valuable phenolics compounds (e.g. alkylphenols) as well as reducing the presence of unwanted corrosive compounds (such as carboxylic acids). Furthermore, the controlled fractional condensation of the partially upgraded vapors was used to validate the upgrading efficacy and to propose a separation pathway that has the potential of roughly concentrate interesting fraction for biorefinery co-products extraction. Paragraph 2.2 describes an example of bio-based co-product from CFP biorefinery, that is the extraction of molecules that can be used as bio-derived active ingredients in insecticides. In this case, the experimental distillation of CFP bio-oil was used to separate fractions and the insecticidal activity was tested by a project partner. Then, through statistical data analysis, it was possible to identify target molecules and apply a techno-economic analysis (TEA) as well as a life cycle analysis (LCA) to validate the plant economic advantages and the environmental benefits in term of energy demand and GHG emissions. The last paragraph of section 2 concludes the discussion with

a perspective on co-processing of bio-intermediates into existing refinery as a promising route for commercialization of fast pyrolysis bio-intermediates, pointing the attention toward the need of advanced analytical techniques for the biogenic carbon measurement in the final products. Moreover, some aspects of the biogenic carbon fate have been experimentally investigated focusing on how the presence of oxygenated species negatively impacts the co-processing of pyrolysis compounds together with petroleum feeds (vacuum gas oil – VGO) in a simulated fluid catalytic cracking (FCC) unit. This work has been carried out during two international exchange periods in the NREL laboratories and facilities specialized on pyrolysis technologies, where lab- and pilot scale pyrolysis units were operated for the optimization of the conversion process and co-processing studies, performing studies on catalysts and reaction products through specific analytical techniques (i.e. molecular beam mass spectrometer, GC-MS/FID, Karl Fischer titration, BET and TPD), while batch distillation units were used for the separation of pyrolysis oil fractions to be tested as bio-based insecticides and analyzed through GC-MS/FID analytical apparatus.

1.2 - Hydrothermal liquefaction of organic-rich wet streams

The other biorefinery concept investigated in this work is based on hydrothermal liquefaction (HTL) for the valorization of wet lignocellulosic residual streams. In contrast to FP or CFP biorefinery, where the thermochemical reactions require very low moisture content, HTL is a suitable process for organic-rich wet streams, in form of slurries. This interesting characteristic makes the technology viable for several industrial and domestic organic waste streams, such as paper pulp, food residues, sewage sludge and lignin-rich co-products from lignocellulosic ethanol biorefineries. The advantage is that a dewatering step can be bypassed since the liquefaction happens in presence of water at near critical or critical state (i.e. 374 °C and 22,064 MPa). In these conditions, the feedstock first undergoes to an initial degradation (timescale < minutes) by a combination of solvolysis, hydrolysis, dehydration and decarboxylation into water soluble organics and with water and carbon dioxide as (main) byproducts. Then, repolymerization reactions occurs (timescale ~ minutes) by different recombination and condensation mechanisms, originating water-insoluble organic compounds (the liquid biocrude), and water-insoluble organic/inorganic compounds (the solid biochar or hydrochar).^{68,69} Among the suitable feedstocks, lignin-rich stream from lignocellulosic ethanol biorefineries is a potential candidate for a valorization through hydrothermal processing due to an anticipated significant availability in the mid-long term, as additional lignocellulosic ethanol capacity is being built. As an example, Clariant, a Swiss-based company, is building in Romanian a commercial-scale plant for the production of 50000 tons per year of cellulosic ethanol from agricultural residues.⁷⁰

The uses of lignocellulosic biomass for ethanol production always requires a separation of sugars from lignin through thermophysical pretreatments (e.g. steam explosion) and further hydrolysis and fermentation of the generated sugars. Lignin remains as co-product in large water residual streams and, accordingly to various lignocellulosic ethanol production scenarios, the exploitation of residual lignin for fuels and products manufacturing can unlock additional economic and environmental benefits to the biorefinery. For example, one of the future scenario foresees a ramp up in Europe from one ethanol plant producing at commercial scale in 2017 to 46 plants in 2030.⁷¹ This study considers a central scenario that foresees an increment in the ethanol production capacity from 31 million liters in 2017 to 2.75 billion of liters in 2030, while a more ambitious scenario predicts a capacity of 3.8 billion liters in 2030. In US, the ethanol capacity in 2019 has been estimated to be about 51 billion of liters but mainly from other biomass sources, such as corn, while cellulosic biomass as feedstock represents only the 0.5% of the total, thus about 253 million of

liters. However, studies and prediction from the US Department of Energy set a potential goal for 2030 of 60-75 billion of gallons (220-270 billion of liters) of cellulosic ethanol. All biological process (such as enzymatic hydrolysis followed by fermentation) converts polysaccharides (cellulose and hemicellulose) into bioethanol resulting also in the formation of a large residual lignin stream (LRS) of about 25-35 wt.% of the total biomass.⁷² Moreover, the process produces a large amount of CO₂, estimated as about the same mass of ethanol) and, as first approximation based on available data, the LRS is about twice the mass of ethanol produced by the process.^{73,74} Therefore, due to the large volumes available in the foreseeable future, valorization of lignin-rich streams will be a mandatory step for the lignocellulosic ethanol biorefineries to improve and expand the products portfolio and maximize the economics. Hydrothermal liquefaction offers large opportunities for this wet feedstock, but several technical challenges still needs to be overcome to unlock the full potential of lignin conversion into marketable products by means of HTL. In this work, an overall study of this conversion pathway has been undertaken from the process point of view, as well as in view of potential co-products recovery pathways to improve the overall LRS-HTL economy. Even though HTL is a known process since many years, a very limited number of industrial and commercial example have been developed, especially on lignin as feedstock. The technological readiness level of the HTL process still lags behind FP/CFP, where industrial facilities have already hit the market (e.g. BTG⁷⁵ in the EU or Ensyn⁷⁶ in North and South America). The only example of industrial development of HTL technology is Steeper Energy⁷⁷ (marketed under the trade name Hydrofraction[®]) that after few years of pilot-scale studies is currently trying to scale-up the process on a demonstrative scale. However, the conversion of lignin in valuable biocrudes or chemical precursors still represents a technological and economical challenge. In perspective of industrial scale-up, the HTL can be integrated in a biorefinery concept in order to produce biocrude as main stream and co-products to improve the plant economics and valorize residual streams, as depicted in Figure 6.

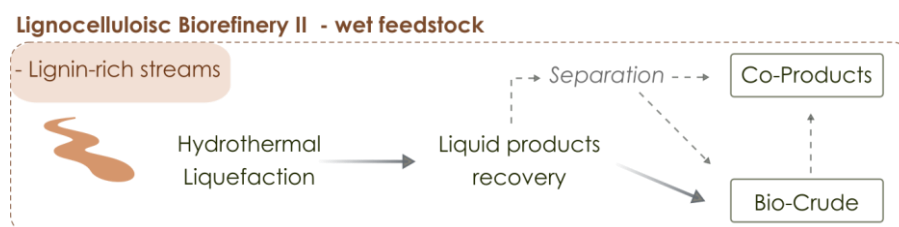


Figure 6. Lignocellulosic biorefinery scheme based on HTL as thermochemical conversion process

Co-products can be obtained through fractionation of biocrude as well as extraction of compounds from the residual aqueous phase, which accounts for 20-40 wt.% of the feedstock carbon, although with a concentration of 1-3 wt.%.⁷⁸ The latter seems to be a promising route because it contains mainly light water-soluble monomers that can have high value in the chemicals market. In such an approach, through a fractional product recovery it is possible to separate the aqueous phase from the biocrude and residual solids, ultimately recovering chemicals precursors from the aqueous stream.

In this work several aspects about HTL of lignin have been investigated and presented in Chapter 3. The first part of this study, described in paragraph 3.1 - was mainly focused on the HTL overall process characterization through an experimental campaign using batch micro reactors to observe how the operative conditions affected the biocrude yield.

Then, in paragraph 3.2, it is reported the study on the identification of the main organic compounds in the biocrude light fraction and dissolved in the aqueous phase, observing how the process conditions influenced the monomers generation, and in which way it is possible to maximize the lignin depolymerization rate through the use of catalytic additives. In addition, since part of the original carbon always remains trapped in the residual aqueous phase, a pathway for compounds recovery through liquid-liquid extraction (LLE) followed by resins adsorption was proposed, and results are reported in paragraph 3.3. The rationale is to recover valuable monomers that can either enter the market as bio-based commodity chemicals (e.g. phenol or acetic acid), or be used as precursors for materials manufacturing (e.g. precursors of polymers). In order to evaluate the benefit of the aqueous phase valorization, a TEA model has been developed, to compare the introduction of a LLE unit and reduce the costs associated with traditional wastewater treatments, with benefits also on the overall carbon efficiency. The minimum biocrude selling price (MBSP) in absence of wastewater treatment was calculated and compared to the one obtained with LLE and residual aqueous phase recirculation, finding clear economic benefits as well as introducing the possibility of separating molecules for the chemical market. Finally, since the technology needs to be investigated at larger scale, paragraph 3.4 reports on the design and tests of a continuous HTL pilot plant with a capacity 1-2 l/h of lignin slurries at subcritical conditions (350°C and 250 bar). The main mechanical and operative issues were identified, and some solutions were proposed, however further and longer investigation are needed in order to optimize the conversion and product recovery.

This part of the work has been carried out in the RE-CORD laboratories, where micro-reactors units were used for characterizing and optimizing the hydrothermal liquefaction of lignin. Moreover, micro-scale tests were performed for the extraction of chemicals from the residual aqueous phase through LLE and resin adsorption. Several analytical techniques (i.e. GC-MS, HPLC, GPC, TOC, CHNS, Karl Fischer titration) were used to investigate these processes and observe the conversion and extraction performances. Additionally, the continuous HTL pilot plant has been assembled and commissioned in the RE-CORD experimental area where preliminary tests were also performed.

2 - Fast pyrolysis biorefinery for bio-intermediates generation, co-products extraction and petroleum refineries integration

As previously introduced, an option for the conversion of dry lignocellulosic biomass is represented by fast pyrolysis (FP) biorefineries. Lignocellulosic biomass, such as forest residues, are converted into valuable liquid products through pyrolysis reactions, where the biomass constituents are thermally cracked in absence of oxygen to form lighter molecules that can be rapidly quenched in a liquid fraction. The process always involves a drying step to reduce the amount of water trapped in the feedstock, in order to limit the energy consumption, enhancing the heating rate.

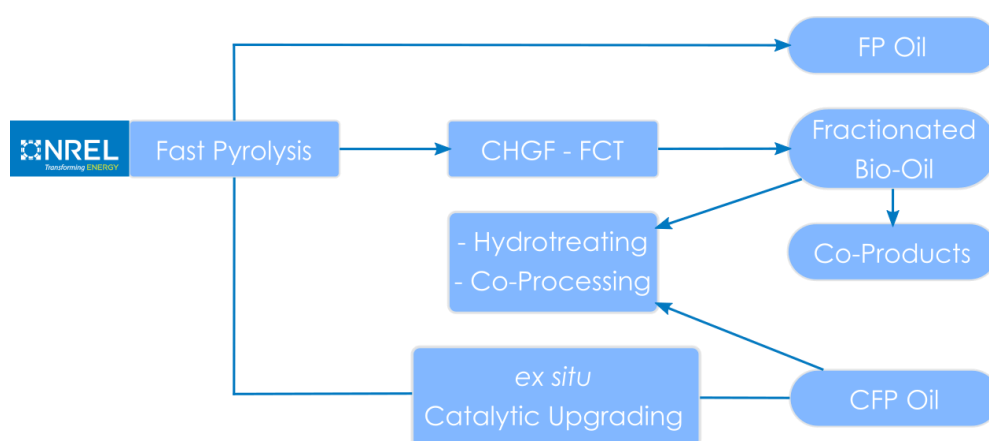


Figure 7. General NREL fast pyrolysis (FP) and catalytic fast pyrolysis (CFP) biorefinery scheme, including potential downstream pathways.

A general fast pyrolysis biorefinery scheme and downstream pathways studied by NREL in the last decades is depicted in Figure 7. Unless burning the FP oil directly for thermal energy generation, upgrading steps are always necessary to improve the oil quality, varying the composition towards fuel and chemicals precursors. Catalytic fast pyrolysis (CFP) of biomass is an interesting approach that has the potential to produce valuable end-products and intermediates for the production of renewable liquid fuels and chemicals. This conversion process integrates rapid thermal depolymerization of biomass with catalytic upgrading to yield desirable products.^{79–85}

Moreover, preconditioning the pyrolysis vapors prior to CFP represents a new approach in order to tune the composition towards higher value molecules as well as reducing the complexity of downstream processes, such as co-processing in petroleum refineries or extraction of chemicals as co-products. Preconditioning strategies (e.g., partial deoxygenation) have the capacity to chemically convert specific components of biomass-derived pyrolysis vapors to more amenable compounds for downstream upgrading, separations and refinery integration steps.

In this work, carried out in the NREL labs, microscale studies have been carried out to evaluate the effect of heteropolyacids (HPA) as catalysts material in a fixed bed reactor to partially deoxygenates batches of pyrolysis vapors in a catalytic hot gas filter (CHGF). In addition, the experimental campaign was scaled up to a continuous system coupled with a fractional condensation train (FCT) to demonstrate the efficacy of the CHGF unit operation as well as to investigate the possibility of tuning the oil fractions composition for further downstream processes (e.g. co-products extraction). Here, fractions were collected and analyzed to determine the degree of deoxygenation achieved by CHGF.

This new approach proposed utilizes partial deoxygenation and fractional condensation in tandem to control the composition of biomass-derived product for downstream upgrading processes. More details of this study can be found in Peterson et al.⁸⁶, where part of the work has been published.

Regarding downstream process, some approaches have been considered in this work. Especially for co-products generation, FCT seems to be a valuable technology for a first separation step. During the condensation stages, different molecules are condensed at different dew points and thus it is possible to roughly separate target cuts. However, in order to obtain chemical precursors further separation and purification steps are necessary. An interesting co-products route studied in this work was represented by the extraction of molecules to be used as bio-derived pesticides in the agricultural sector. Inside of a NREL collaboration with an entomology research group of the Michigan State University (MSU), the insecticidal activity of bio-oil fractions was evaluated. Once target molecules have been individuated through data analysis and correlations, a techno-economic analysis (TEA) have been carried out to address how the minimum product selling price (MPSP) is affected by varying the yield and the purity of the product. In addition to this, a LCA study showed that the overall GHG emissions of producing bio-derived insecticides is reduced, compared with standard synthetic pesticide supply chain.

Another interesting and emerging downstream process is the co-processing of pyrolysis oils into petroleum refinery units for fuel production. This technology is an advanced approach that will permit a faster spread of insertion of renewable fuels into the market in the mid-term, therefore enhancing the commercialization of CFP biorefinery technology. An example of refinery point of insertion is represented by fluid catalytic cracking (FCC) units for the production of gasoline and LPG from vacuum gas oil (VGO). Several studies showed how, a more severe upgrading of bio-oil would positively affect the fuels yields as well as the biogenic carbon incorporation, as described below. Regarding the biogenic carbon incorporation, not many studies have tackled the chemistry of the process as well as the biogenic carbon detection in the final products. In this work, a review of the technology has been carried out pointing the attention to the analytical approaches traditionally used to measure the renewable carbon content in the final products. Furthermore, modern and perspective methods have been summarized and proposed as inline refinery measurement in order to enhance the process control and optimization. Another aspect investigated for the biogenic carbon incorporation is the effect of the oxygenated compounds on the formation of coke as well as the chemistry of the carbon incorporation into final hydrocarbons. This has been experimentally addressed pyrolyzing in microscale setups labelled ¹³C biomass together with VGO over specific catalysts. This work focus specifically on the coke origin analyzing the post-combustion gases through a molecular beam mass spectrometer (MBMS), while more details on the biogenic carbon incorporation can be found in Mukarakate et al.⁶⁶

2.1 - Preconditioning of Fast Pyrolysis Vapors through Catalytic Hot-Gas Filtration and Fractional Condensation

2.1.1 - Introduction

Significant advances in heterogeneous catalysis for bio-oil upgrading via CFP have been made but there is a continuing need for new catalytic processes and chemistries in order for CFP to be successfully deployed⁸⁷. One of the main challenges associated with CFP is catalyst deactivation due to coke formation, which ultimately leads to biogenic carbon loss.⁸⁷⁻⁸⁹ The formation of coke is strongly influenced by feed composition. Char and residual alkali metals (particulate matter) are known to catalyze polymerization reactions in both vapors and condensed oils, accelerating coke formation and bio-oil instability, respectively.^{34,87,90-93} Recently, the importance of removing the char and alkali metals from biomass-derived fast pyrolysis vapors was highlighted by demonstrating that hot-gas filtration (HGF) was able to produce a bio-oil with substantially improved properties (i.e., greatly reduced particulate matter including alkali metals).³⁴⁻³⁶ Additionally, a significant portion of the biomass-derived pyrolysis vapors have reactive oxygen moieties such as acid carbonyls (e.g., acetic acid), which tend to negatively impact CFP due to their corrosive properties. These corrosive acids promote coking reactions (leading to carbon loss) and poor bio-oil stability with respect to storage.^{90,92,94-96} Catalytic deoxygenation reactions for the conversion of corrosive acids to more desirable products have been identified in CFP (e.g., decarboxylation). The ketonization of carboxylic acids is a feasible reaction pathway for upgrading biomass-derived pyrolysis vapors and suppressing the formation of corrosive acids while achieving additional carbon-carbon coupling chemistry (i.e., compounds with higher heating values).⁹⁵⁻⁹⁷ It is important to note that decarboxylation and ketonization reactions tend to remove oxygen from carboxylic acids as CO₂.^{96,98} This loss of carbon ultimately lowers the carbon efficiency of the conversion of biomass to liquid fuel products. For maximizing fuel yield and quality, hydrodeoxygenation is the preferred reaction route since oxygen is eliminated as water and carbon is retained.⁹⁹ Hydrodeoxygenation (HDO) further presents an opportunity for incorporating hydrogen into end-products prior to hydrotreating, thereby mitigating downstream hydrotreating severity. In order to expand the types of potential catalysts to achieve the desired chemistry, it may be necessary to precondition the vapors with advanced separation processes before downstream catalytic upgrading

Efforts have been made to integrate catalytic components into hot-gas filter elements used in biomass gasification and gas reforming processes.¹⁰⁰⁻¹⁰⁶ These efforts utilized metal-impregnated (e.g., nickel, ruthenium) ceramic filter elements, with or without mixed-metal oxides (e.g., alumina, zirconia, CaO) incorporated, to both remove particulates and reform tars and light hydrocarbons to synthesis gas (H₂ + CO). Our approach here is to apply hot-gas filtration with an integrated catalytic component to biomass pyrolysis vapors. Denoted as catalytic hot-gas filtration (CHGF), this approach was taken to capture char and alkali metals while simultaneously performing partial deoxygenation and alkylation (i.e., carbon-carbon coupling) on pyrolysis vapors prior to ex situ CFP upgrading. The effect of reaction conditions on the concentration of partially upgraded product vapors was studied. This single unit operation has the potential to extend catalyst lifetime, enable efficient downstream processing, and provide low CapEx oil stabilization, while preserving carbon for downstream CFP upgrading and allowing for the production of carbon-carbon coupled species for tailoring the fuel end-product properties. The use of CHGF within CFP may also present an opportunity

for process intensification by eliminating a cyclone separator used to remove entrained solids in fast pyrolysis vapors.¹⁰¹

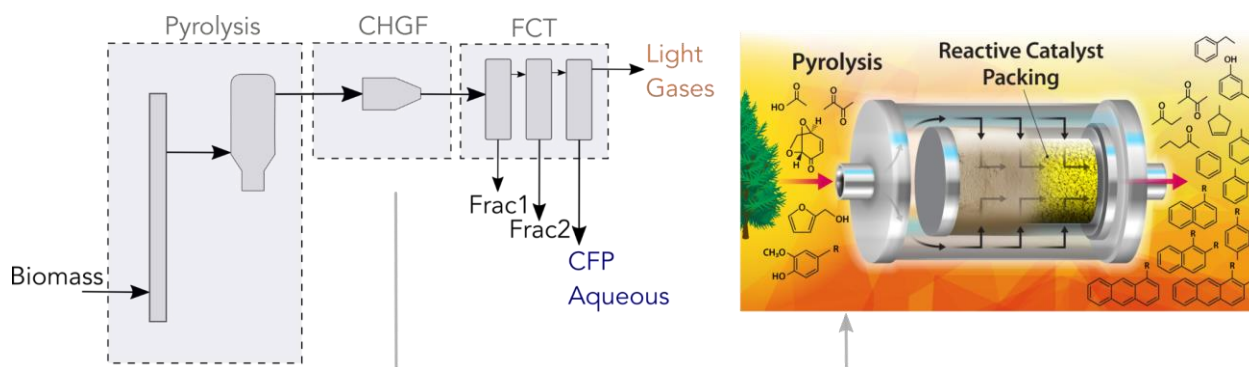


Figure 8. Catalytic hot gas filtration (CHGF) coupled with fractional condensation of fast pyrolysis vapors. Image adapted from Peterson et al.⁸⁶

In addition to partial deoxygenation and alkali removal, as previously mentioned, in this work a fractional condensation unit was coupled to the CHGF in order to separate unwanted compounds from the oil fraction (such as heavies, acids and water), as depicted in Figure 8. Fractional condensation of biomass pyrolysis vapors has been previously utilized to alter the composition of the condensed phase by removing water, fouling agents, and value-added chemicals.^{107–113} Fractional condensation permits additional tailoring of vapors for downstream upgrading through the removal of reactive and high molecular weight components that contribute to catalyst fouling and oil instability. Moreover, the selective removal of value-added components, such as polymer precursors (e.g., phenols, alkylphenols, methoxyphenols, cyclopentenones), by fractional condensation presents an opportunity for offsetting capital costs within a CFP and/or hydrotreating process.^{114,115}

2.1.2 - Materials and methods

Biomass and Catalyst Materials

Loblolly pine biomass feedstock was supplied by Idaho National Laboratory for all experiments. The feedstock was provided in nominal size <2 mm with subsequent knife-milling to <1 mm prior to being used. Carbon, hydrogen, and nitrogen (CHN) and proximate analysis indicated the composition of the pine on a dry basis to be 51.0 wt.% carbon, 6.2 wt.% hydrogen, 0.1 wt.% nitrogen, 42.6 wt.% oxygen (by difference), and 0.4 wt.% ash. The pine was further characterized as 42 wt.% cellulose, 21 wt.% hemicellulose, and 30 wt.% lignin.

Titania-supported molybdenum and tungsten heteropolyacid catalyst materials (Mo-HPA/TiO₂ and W-HPA/TiO₂, respectively) were prepared using standard techniques. Titania (Alfa Aesar, anatase, #44429) was ground and sieved to a particle size of 1.4–2.0 mm. The catalysts were prepared via incipient wetness impregnation of the TiO₂ support using an aqueous solution containing either 10 wt.% phosphomolybdic acid hydrate (Sigma-Aldrich, #221856) or phosphotungstic acid (Sigma-Aldrich, #P4006). The resulting samples were dried at 120°C for 18 h. These materials possess the well-characterized Keggin-type structure within the class of heteropolyacids (HPAs) and are also referred to as polyoxometalates when in their conjugate anion form.¹¹⁶ The HPA structure consists of a metal oxide framework surrounding a central heteroatom, in this case phosphorus. The metal oxide framework is comprised of twelve octahedrally coordinated metal clusters (e.g., molybdenum or tungsten) bonded together through oxygen atoms with

oxygen linkages to the central heteroatom. These HPA materials were selected based on their HDO and alkylation activity towards pyrolysis model compounds.¹¹⁷ Similar activity was promoted with molybdenum oxide supported catalysts^{118–121} and it was determined that the redox properties of molybdenum oxide influenced the reaction selectivity.^{120,122,123} Due to the unique redox properties of molybdenum oxide, a reducible support material (i.e., TiO₂) was leveraged in an attempt to further stabilize and tune the activity of the Mo-HPA via a charge-transfer mechanism between the TiO₂ support and HPA.¹²⁴

Pulsed-Flow Lab Scale Experiments for Catalyst Screening

Initial Mo-HPA/TiO₂ and W-HPA/TiO₂ catalyst screening experiments were accomplished via a pulsed-flow lab scale horizontal quartz reactor system coupled to a molecular beam mass spectrometer (MBMS) for real-time analysis of products (Figure 9). The reactor employed an annular flow tubular packed-bed geometry (i.e., axial flow path) with 12.7 mm internal diameter and has been used also elsewhere for the catalyst screening experiments in previous investigations.^{28,125} Pulsed-flow biomass feeding was used for ease of operation at lab scale. Loblolly pine was pyrolyzed at 500°C in a 0.4 slm inner flow of He or H₂/He mixture and the resulting vapors subsequently upgraded at 400°C over 0.5 g of catalyst, suspended with quartz wool. The flow in the inner tube is after diluted with 4 slm of Ar from the outer tube before the MBMS sampling channel in order to minimize secondary reactions. Resulting upgraded vapors were swept into the MBMS for analysis. Biomass increments of 30 mg were added via quartz boats to give a cumulative biomass-to-catalyst ratio of 1.5 (25 boats) and vapor weight-hourly space velocity (WHSV) of ~ 2 h⁻¹. The MBMS have already been used as an effective analytical method for real-time analysis of biomass pyrolysis and vapor phase upgrading.^{126–128} Literature regarding the thermocatalytic conversion of lignin model phenolics (e.g., anisole and 4-propylguaiacol) over a Mo-HPA/TiO₂ catalyst suggested that H₂ was necessary to promote HDO and alkylation reactions via Lewis and Brønsted acidic site activation.¹¹⁷ Therefore, experiments were conducted with 10 vol% and 50 vol% H₂ (balance He). The reaction temperature (400°C) was chosen based on the thermal stability of the HPA and TiO₂.^{129–131} Elevated temperatures (>500°C) induce a phase transition from anatase-to-rutile, where anatase is the preferred phase. Additionally, pyrolysis vapors tend to condense below 400°C. All catalyst experiments were tested against corresponding control experiments using only the TiO₂ support. Pulsed-flow lab scale experimental results were used to guide the continuous-flow experiments described in the following section.

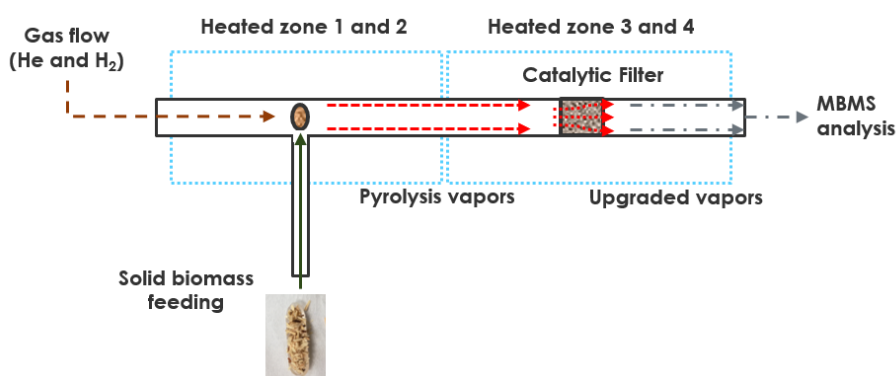


Figure 9. Lab scale pulsed-flow experimental setup comprising of a horizontal quartz reactor system coupled to a molecular beam mass spectrometer (MBMS) for real-time analysis of vapors products.

Continuous-Flow Experiments using a Small Pilot-Scale Pyrolyzer and Catalytic Hot-Gas Filtration

As depicted in Figure 10, a custom small pilot-scale fluidized bed pyrolyzer system was employed to pyrolyze biomass at a rate of 1.2 kg/h at 500°C in a nitrogen (N₂) carrier gas fed at a rate of 1.8 kg/h with ~0.4 kg/h of additional N₂ purges and operated at 220 kPa (20 PSIG) backpressure (backpressure regulator at the Scrubber outlet not shown in Figure 10). Acknowledging that the biomass feedrate is on the low-end of pilot-scale, we considered the system to be a small pilot-scale but may also term it as pilot-scale for brevity. The pyrolyzer consisted of a 5.3 cm internal diameter fluidized bed reactor employing an olivine bed material as a heat transfer media. The system uses a series of two cyclones downstream of the pyrolyzer followed by HGF for char and alkali removal. Subsequently, clean hot-gas filtered pyrolysis vapors could be quenched and condensed in a scrubber or sent to a Davison Circulating Riser (DCR) system as a slipstream for vapor-phase upgrading via CFP.¹³² For our study, a pyrolysis vapor slipstream post-HGF was utilized to transfer vapors to a second, smaller, filtration unit operation. This secondary filter setup functioned as a continuous-flow apparatus for CHGF. Experiments employing a pre-HGF slipstream were initially conducted but significant clogging occurred in the transfer line due to char fines entrainment and subsequent deposition.

In addition, complete removal of char and ash using the small pilot-scale HGF was demonstrated and detailed below in the Results and Discussion section. The removal of these components will protect downstream catalyst beds regardless if the catalyst bed is internal to the immediate filter (small pilot-scale HGF) or secondary filter downstream (CHGF). Therefore, utilizing a slipstream post- HGF was suitable for evaluating CHGF. Both the HGF and CHGF unit operations utilized ceramic DiaSchumalith® filter elements (filtration grade, 0.3 µm) comprised of a silicon carbide inner-core with a mullite (aluminosilicate mineral) outer layer. The cyclones, HGF, and transfer lines were heated to 450°C, 430°C, and 400-450°C, respectively.

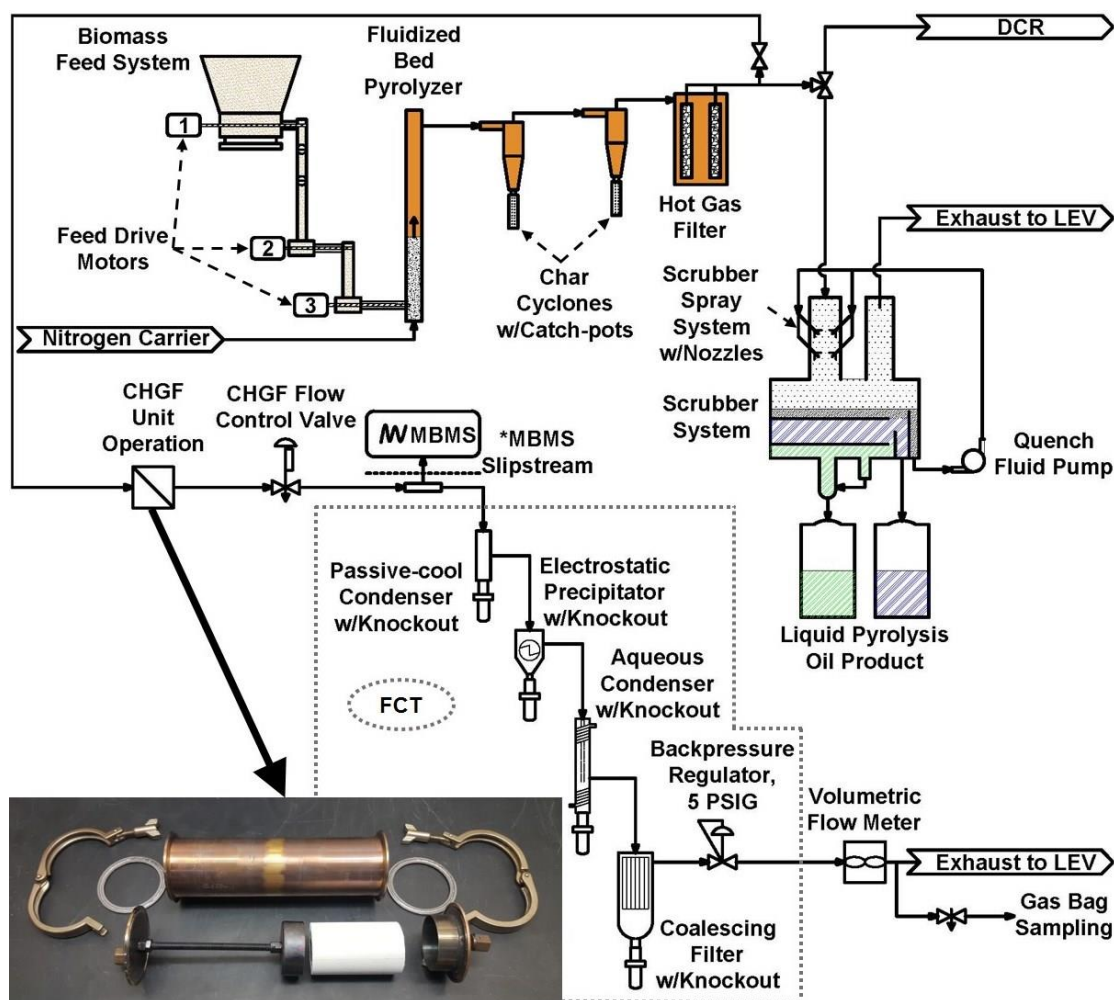


Figure 10. Catalytic hot-gas filter (CHGF) and Davison Circulating Riser (DCR) systems coupled to a small pilot scale pyrolyzer reactor system. The pilot-scale pyrolyzer system includes: biomass feed system, fluidized bed pyrolyzer, char cyclones + catch-pots, hot-gas filter (HGF) unit, slipstreams to the CHGF and DCR systems, and a scrubber product quench system for raw pyrolysis oil product with liquid phase separation and collection systems. The biomass feed system employs a feed hopper drive (1), biomass metering drive (2), and biomass conveying drive (3). The CHGF system is comprised of the CHGF unit operation (shown as inset) housed in a furnace (not shown), CHGF flow control valve, molecular beam spectrometer (MBMS) slipstream, and fractional condensation train (FCT). The FCT includes: passive-cool condenser, electrostatic precipitator (ESP), aqueous condenser, and coalescing filter, each with an associated product knockout. The system effluent train is equipped with a backpressure regulator (117 kPa (5 PSIG) setpoint), volumetric flow meter (dry test meter), and gas bag sampling system. Effluent is exhausted to local exhaust ventilation (LEV). *The MBMS system utilized a slipstream via a flow-by plate and was used for real-time analysis of products.

CHGF was accomplished by the addition of catalyst materials within the core of the filter elements of the slipstream filtration unit operation (Figure 10, see inset). In packing the elements with catalyst material, a decoupling of HGF from partial deoxygenation and chemical conditioning was accomplished, allowing for char and alkali removal prior to partial catalytic upgrading in a single unit operation. Additionally, the CHGF filtration apparatus was coupled to an MBMS for real-time analysis of products followed by a fractional condensation train (FCT) for controlled condensation of liquid products. The FCT (shown in Figure 10 and detailed in Figure 11) was comprised of a passive-cool condenser, temperature-controlled electrostatic precipitator (ESP) with condenser, aqueous condenser, and coalescing filter; all with associated product knockouts. The ESP condenser was operated between 70-170°C with the aqueous condenser at -15°C and coalescing filter at ambient temperature. Mass flowrate through the CHGF system was controlled using an air-to-close proportioning control valve (CHGF flow control valve). The MBMS and FCT

systems were operated at 117 kPa (5 PSIG) with the CHGF operating at 220 kPa (~20 PSIG); ~6.9-13.8 kPa (~1-2 PSI) differential across CHGF unit operation with pyrolyzer marginally above 220 kPa (20 PSIG). The volumetric flowrate of the vapor-stripped effluent from the coupled MBMS-FCT system was measured by a dry test meter. Residual non-condensable gases were captured for off-line analysis via a gas bag sampling system on the MBMS-FCT system effluent.

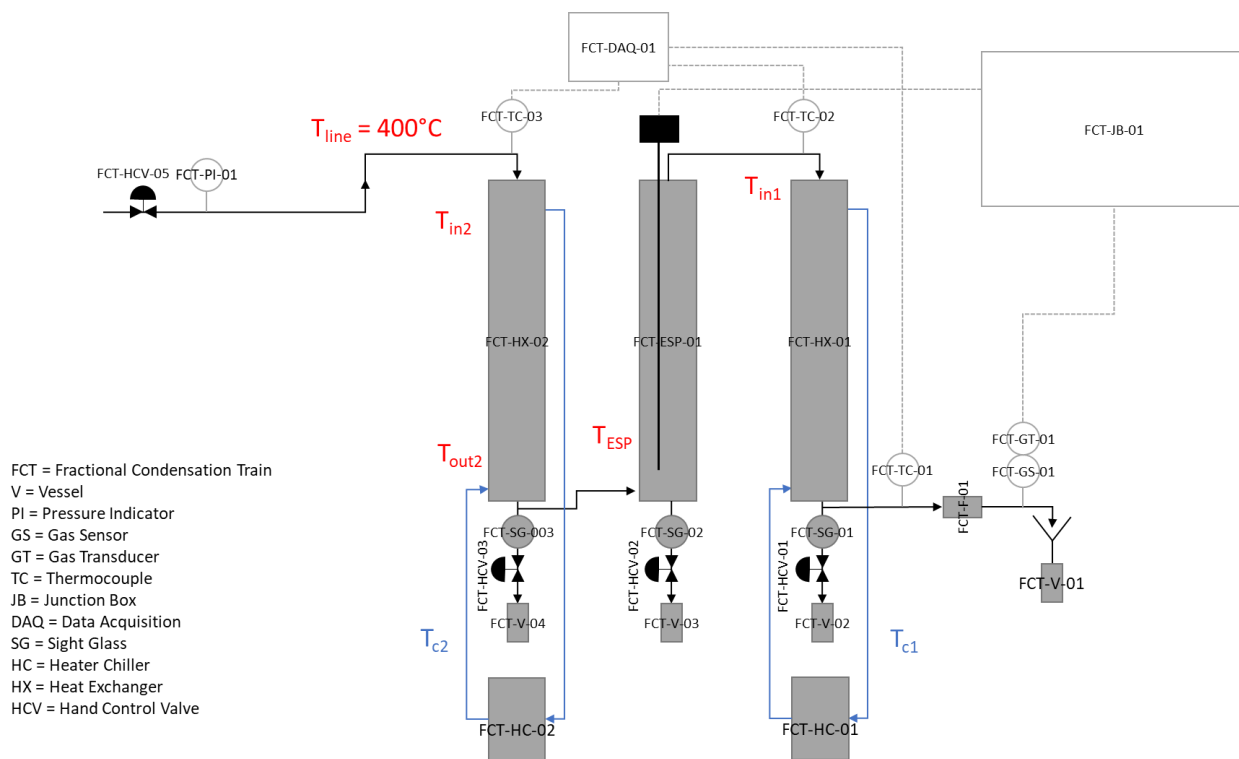


Figure 11. P&ID of fractional condensation train.

The continuous-flow CHGF system was comprised of a housing equipped with a mount for securing 102 mm lengths of 60 mm diameter ceramic DiaSchumalith® filter elements. Filters were mounted in the housing and the filter unit installed in a heated furnace in line with the slipstream transfer line. The flow path was directed from the outside of the filter and inward radially through the filter and into the packed catalyst bed. All CHGF experiments were conducted at 400°C with a time-on-stream (TOS) of 60 min using 40 g of Mo-HPA/TiO₂ catalyst. A series of control experiments were conducted prior to upgrading experiments: (1) empty filter housing, (2) filter housing with ceramic filter, and (3) filter housing with ceramic filter packed with TiO₂, all in 40 vol% H₂. The filter elements were then packed with Mo-HPA/TiO₂ catalyst for upgrading experiments. The series of controls followed by catalyst testing allowed for the tracking of incremental changes in the vapor composition throughout the experimental hierarchy of no filter, filter, TiO₂-packed filter, and catalyst-packed filter. Only the Mo-HPA/TiO₂ catalyst material described above was investigated in the continuous-flow catalyst test experiments as the W-HPA/TiO₂ proved to be ineffective based on the pulsed-flow lab scale results (discussed below). Both WHSV and H₂ concentration sweep experiments were conducted with the Mo-HPA/TiO₂ catalyst to investigate the impact of each parameter on activity. Initial testing of the Mo-HPA/TiO₂ at a pyrolysis vapor WHSV of ~2 h⁻¹ with 40 vol% H₂ showed diminished activity compared to the lab scale results obtained at the same WHSV and 50 vol% H₂. Consequently, pyrolysis vapor WHSV was swept from 1–0.25 h⁻¹ while the H₂ concentration was swept from 40-80 vol%. These parameter sweeps were conducted both independently and simultaneously to determine their individual and combined effects.

Subsequent to the sweep experiments, a triplicate set of Mo-HPA/TiO₂ experiments was conducted to assess reproducibility and mass balance closure. Because the goal was to implement a partial deoxygenation step between pyrolysis and downstream upgrading, the replicate experiments were conducted at the less severe conditions using WHSV of 1 h⁻¹, 40 vol% H₂ at 400°C, and 60 min TOS. In addition, Mo-HPA/TiO₂ regeneration experiments were conducted using H₂. This protocol (in situ regeneration) entailed flowing 100 vol% H₂ at a flowrate of 300 SCCM over the catalyst at 400°C for 5 h. The regeneration time was based on the complete removal of the hydrogen-induced desorbed species as monitored via MBMS. Post-regeneration, the catalyst was re-evaluated using the same conditions as those used in the replicate experiments above.

Real-time analysis of products was accomplished via the MBMS slipstream on the CHGF setup. Condensed liquid product from the FCT was quantified gravimetrically and analyzed via GC-MS and Karl Fischer titration while non-condensable gases were analyzed via a GC-FID equipped with a Polyarc® universal carbon detector (Activated Research Company). The Polyarc® employs a catalytic methanation reaction to convert all GC-separated species into methane prior to FID analysis (i.e., normalizes response factors to 1) to provide for a uniform carbon quantification (i.e., carbon number). The total mass of non-condensable products was determined from the average molecular weight of the product gas, the molar concentration of carbon detected from the Polyarc® and the total volumetric flow through the CHGF system. The average molecular weight of the product gas was determined from the weight fractions and molecular weights of the quantified species. Quenched pyrolysis oil product from the pilot-scale pyrolyzer was analyzed for alkali metals content via ICP-AES. Mass balances were completed around the replicate experiments by comparing the gravimetric yields of condensable FCT fractions and non-condensable products to those obtained for the filter housing with filter control. The degree of char and alkali removal was assessed gravimetrically through a char and ash balance surrounding the pilot-scale pyrolyzer and associated HGF system. Both the TiO₂ control and Mo-HPA/TiO₂ materials were analyzed, pre- and post-reaction, for metals composition (ICP-AES), surface area (BET), acid site density (NH₃ TPD, combined Brønsted and Lewis acidity), and coke deposition (gravimetrically) to assess reaction-induced changes as they relate to morphology and deactivation. Prior to ICP-AES, BET and TPD analysis, both pre- and post-reaction catalyst materials were calcined in air. The calcination protocol entailed heating in air using a muffle furnace to 550°C at 3°C/min, holding for 4 h, and then passively cooling to ambient temperature. Further details regarding the analytical methods employed are provided in the Appendix A.

2.1.3 - Results and discussions

Pulsed-Flow Biomass Pyrolysis Vapors: Catalyst Screening Studies

Initial lab scale screening of Mo-HPA/TiO₂ and W-HPA/TiO₂ catalyst materials without hydrogen using a WHSV of pyrolysis vapors of 2 h⁻¹ showed limited activity towards pyrolysis vapor deoxygenation or alkylation with rapid deactivation. Both materials produced large amounts of carbon dioxide (m/z = 44) at the expense of primary pyrolysis vapors without any clear changes in oxygenate composition, suggesting thermal and/or catalytic cracking as the primary mechanism for carbon loss. Upon the addition of 50 vol% hydrogen, Mo-HPA/TiO₂ showed a marked increase in activity and stability, while the W-HPA/TiO₂ catalyst showed little improvement. Comparison of catalytic

activity between the Mo-HPA/TiO₂ and W-HPA/TiO₂ materials is shown in Figure 12. Due to the inactivity of the W-HPA/TiO₂ material compared to the control tests, continued screening experiments focused on Mo-HPA/TiO₂.

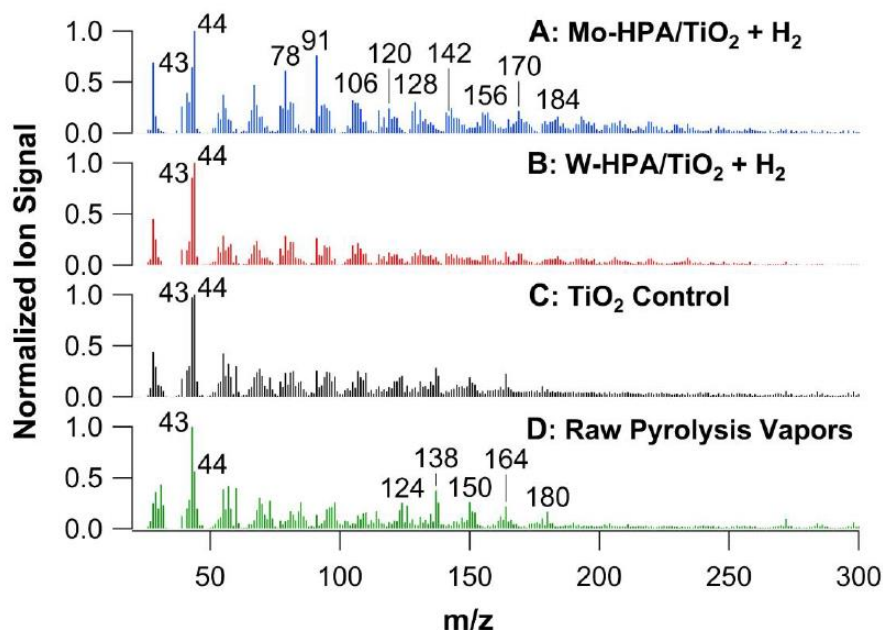


Figure 12. Mass spectra for pulsed-flow lab scale experiments for (A) partial upgrading of pine pyrolysis vapors with 15 wt.% molybdenum heteropolyacid on titania (15 wt.% Mo-HPA/TiO₂) using a WHSV of 2.0 h⁻¹ and 50 vol% H₂, (B) partial upgrading of pine pyrolysis vapors using 15 wt.% tungsten heteropolyacid on titania (15 wt.% W-HPA/TiO₂), WHSV of 2.0 h⁻¹ and 50 vol% H₂, (C) pine pyrolysis vapors using TiO₂, WHSV of 2.0 h⁻¹ without H₂, and (D) pure pine pyrolysis vapors (control) at a flowrate equivalent to WHSV of 2.0 h⁻¹ without H₂. All experiments conducted at 400°C. The m/z values 78, 91, 106, 120, 128, 142, 156, 170, and 184 correspond to benzene, toluene, xylenes, trimethylbenzenes, naphthalene, mono-, di-, tri-, and tetra-methyl-naphthalenes, respectively. The m/z values 124, 138, 150, 164, and 180 correspond to primary vapor products: guaiacol, methyl-guaiacol, 4-vinyl-guaiacol, isoeugenol, and coniferyl alcohol. Various alkylated isomers are not distinguishable based on MBMS spectra and were denoted as the methylated derivatives. (*m/z = 43 is a carbohydrate fragment and m/z = 44 is carbon dioxide.)

As depicted in Figure 12 and Figure 13, the Mo-HPA/TiO₂ catalyst exhibited both HDO activity, as evidenced by benzene (m/z 78), toluene (m/z 91), xylene (m/z 106) production, and alkylation activity based on the appearance of polyalkyl benzenes, naphthalene, anthracene, and their respective alkylated derivatives (methyl and dimethyl). In addition, higher order alkylated hydrocarbons (m/z > 200) were observed. Both HDO and alkylation activity appeared to be proportional to the hydrogen concentration as shown in Figure 13 where the MBMS signal intensity of aromatic and alkylated aromatic hydrocarbons increases when 50 vol.% of H₂ was mixed with the He. These findings coincide well with those of Anderson et al. for lignin model phenolic compounds.¹³³ Here, similar HDO and alkylation reactions were promoted when using a polyoxometalate catalyst (conjugate anion of a heteropolyacid) with anisole and 4-propylguaiacol model compounds in a hydrogen-rich environment.

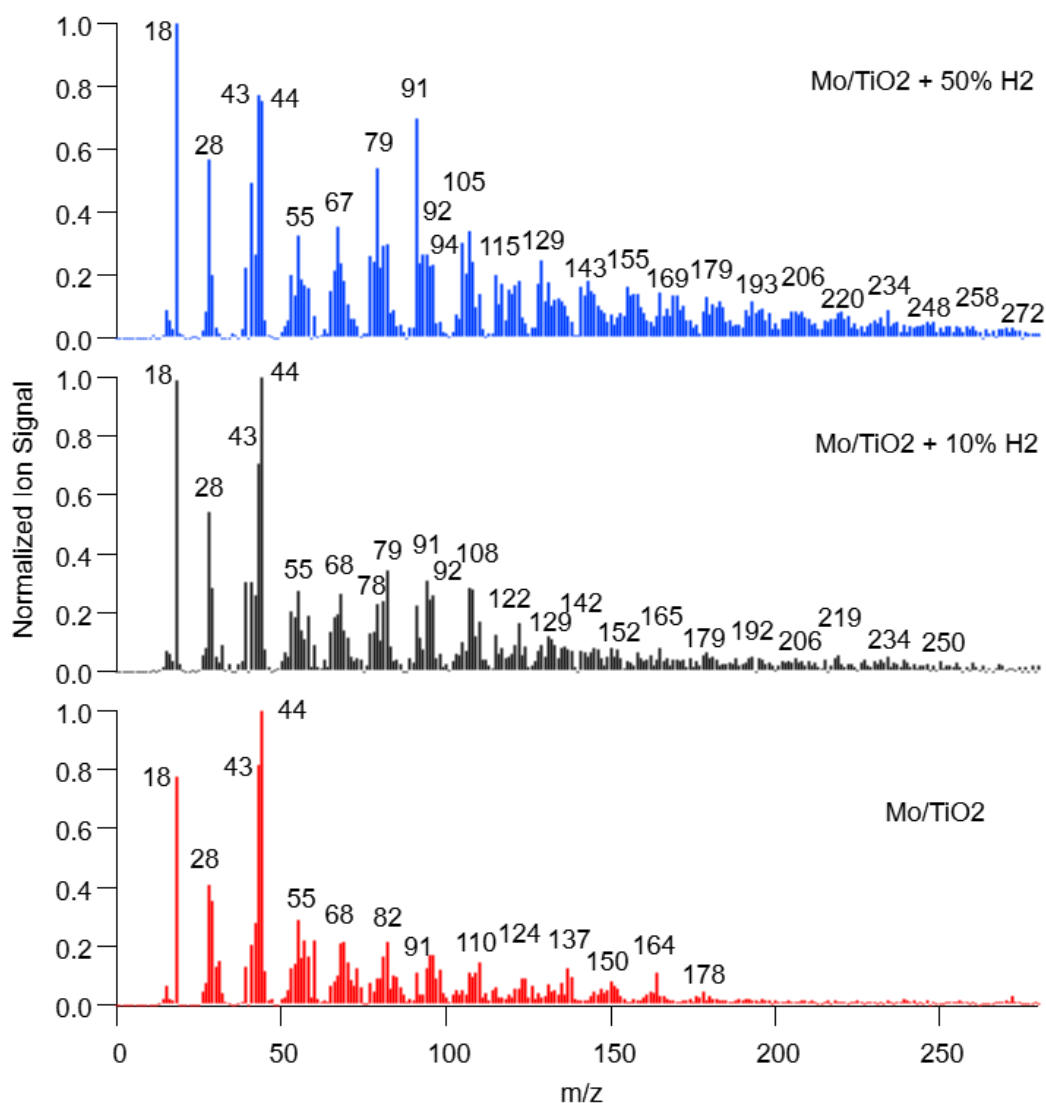


Figure 13. Mass spectra for pulsed-flow lab scale experiments for partial upgrading of pine pyrolysis vapors with 15 wt.% molybdenum heteropolyacid on titania (15 wt.% Mo-HPA/TiO₂) using a WHSV of 2.0 h⁻¹ and varying the amount of H₂ from 0 to 10 and 50 vol%. All experiments conducted at 400°C. The m/z values 78, 91, 106, 120, 128, 142, 156, 170, and 184 correspond to benzene, toluene, xylenes, trimethylbenzenes, naphthalene, mono-, di-, tri-, and tetra-methyl-naphthalenes, respectively. The m/z values 124, 138, 150, 164, and 180 correspond to primary vapor products: guaiacol, methyl-guaiacol, 4-vinyl-guaiacol, isoeugenol, and coniferyl alcohol. Various alkylated isomers are not distinguishable based on MBMS spectra and were denoted as the methylated derivatives. (*m/z = 43 is a carbohydrate fragment and m/z = 44 is carbon dioxide.)

Stability experiments for Mo-HPA/TiO₂ (50 vol% H₂) over a cumulative biomass-to-catalyst ratio of 1.5 indicated that little to no deactivation occurred. In fact, the deoxygenated and alkylated products appeared to increase with TOS. These results are shown in Figure 14, where the mass spectra for biomass-to-catalysts of 1.5 still presents characteristics peaks of deoxygenated compounds such as single and double ring aromatics hydrocarbons and alkylated aromatics hydrocarbons.

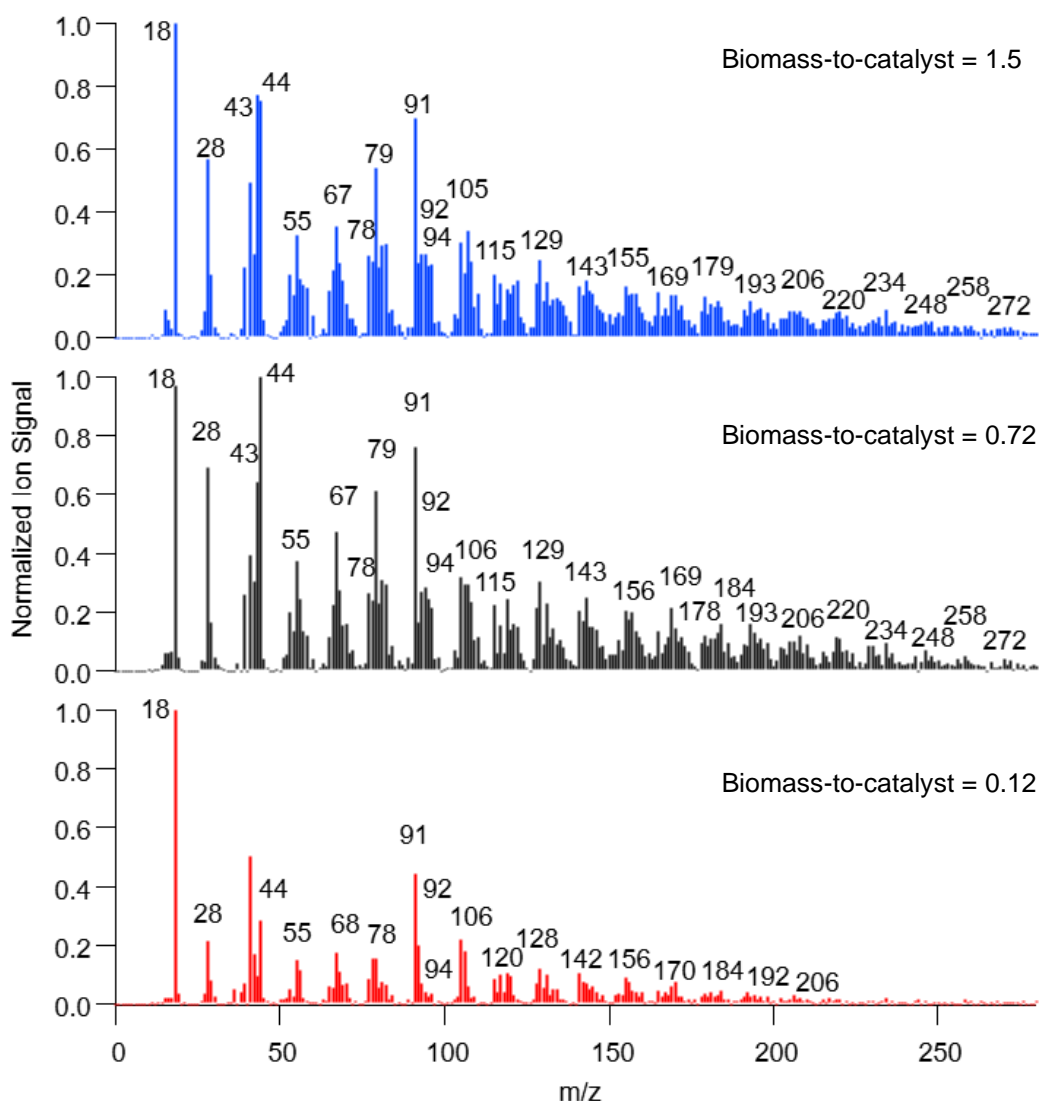


Figure 14. Mass spectra for pulsed-flow lab scale experiments for (A) partial upgrading of pine pyrolysis vapors with 15 wt.% molybdenum heteropolyacid on titania (15 wt.% Mo-HPA/TiO₂) using a WHSV of 2.0 h⁻¹ and 50 vol% H₂. From the bottom to the top, biomass-to-catalyst ratio was increased from 0.12 to 1.5. All experiments conducted at 400°C. The m/z values 78, 91, 106, 120, 128, 142, 156, 170, and 184 correspond to benzene, toluene, xylenes, trimethylbenzenes, naphthalene, mono-, di-, tri-, and tetra-methyl-naphthalenes, respectively. The m/z values 124, 138, 150, 164, and 180 correspond to primary vapor products: guaiacol, methyl-guaiacol, 4-vinyl-guaiacol, isoeugenol, and coniferyl alcohol. Various alkylated isomers are not distinguishable based on MBMS spectra and were denoted as the methylated derivatives. (* $m/z = 43$ is a carbohydrate fragment and $m/z = 44$ is carbon dioxide.)

To sum up, the Mo-HPA/TiO₂ in presence of H₂ showed the potential to be implemented as catalytic filter to partially upgrade fast pyrolysis vapors, maximizing the deoxygenation compared to other HPA tested (i.e. W-HPA/TiO₂). Another important characteristic for fixed bed catalytic filter is the stability over time and the microscale studies demonstrated that in presence of 50 vol.% H₂ the HDO and alkylation was still presents increasing the amount of pyrolysis vapors passing through the catalyst. For this reason, it was selected for the experimental campaign on the pilot scale reactor using the same operative conditions of the microscale tests.

Continuous-Flow Biomass Pyrolysis Vapors: Integration of a Catalytic Component with Hot-Gas Filtration

Here some of the main results of the continuous experimental campaign on the pilot scale pyrolyzer will be presented but more details can be found in Peterson et al.⁸⁶

Continuous-flow pyrolysis vapor experiments using Mo-HPA/TiO₂ with the CHGF system employing the same operating conditions as used in the pulsed-flow studies (i.e., 400°C, WHSV of ~2 h⁻¹, 40 vol% H₂) showed lower activity. Since hydrogen was constantly flowing during the biomass pulses, catalyst deactivation in pulsed-flow experiments may have been mitigated. Additionally, the difference in flow dynamics between the pulsed- and continuous-flow experiments (i.e., axial versus radial flow path, respectively) may have contributed to the diminished activity. As shown in Figure 15, a marked improvement in HDO and alkylation activity emerged after decreasing the WHSV to 1 h⁻¹. A progressively higher activity was observed after lowering the WHSV to 0.25 h⁻¹. Activity was also enhanced by increasing the H₂ concentration at a constant WHSV of 1 h⁻¹. Simultaneously decreasing the WHSV of the pyrolysis vapors over the catalyst and increasing the hydrogen concentration resulted in a cumulative effect where activity was further enhanced compared to the independent changes in the two parameters.

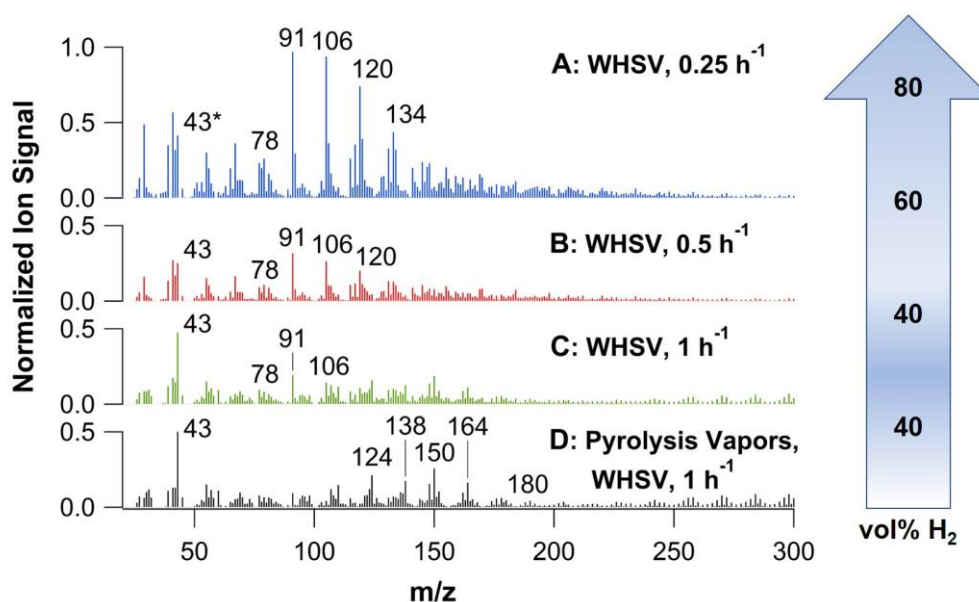


Figure 15. Mass spectra for simultaneous reduction in weight-hourly space velocity (WHSV) and increase in H₂ concentration for (A) partial upgrading of pine pyrolysis vapors with 10 wt.% molybdenum heteropolyacid on titania (10 wt.% Mo-HPA/TiO₂) using a WHSV of 0.25 h⁻¹ and 80 vol% H₂, (B) partial upgrading of pine pyrolysis vapors using 10 wt.% Mo-HPA/TiO₂, WHSV of 0.5 h⁻¹ and 60 vol% H₂, (C) partial upgrading of pine pyrolysis vapors using 10 wt.% Mo-HPA/TiO₂, WHSV of 1.0 h⁻¹ and 40 vol% H₂, and (D) pure pine pyrolysis vapors (control) at a flowrate equivalent to WHSV of 1.0 h⁻¹ and 40 vol% H₂. Carbon dioxide signals (m/z = 44) were similar across spectra and were omitted to reduce the ordinate scale. All experiments conducted at 400°C. The m/z values 78, 91, 106, 120, and 134 correspond to benzene, toluene, xylenes, tri-, and tetramethylbenzenes, respectively. The m/z values 124, 138, 150, 164, and 180 correspond to primary vapor products: guaiacol, methyl-guaiacol, 4-vinyl-guaiacol, isoeugenol, and coniferyl alcohol. (*m/z = 43 is a carbohydrate fragment.)

These results are summarized in a series of MBMS spectra shown in Figure 15; (A) partial upgrading of pine pyrolysis vapors with 10 wt.% Mo-HPA/TiO₂, WHSV of 0.25 h⁻¹ and 80 vol% H₂, (B) partial upgrading of pine pyrolysis vapors using 10 wt.% Mo-HPA/TiO₂, WHSV of 0.5 h⁻¹ and 60 vol% H₂, (C) partial upgrading of pine pyrolysis vapors using 10 wt.% Mo-HPA/TiO₂, WHSV of 1.0 h⁻¹ and 40 vol% H₂, and (D) pure pine pyrolysis vapors (control) at a flowrate equivalent to WHSV of 1.0 h⁻¹ and 40 vol% H₂. In decreasing WHSV and increasing H₂, enhanced HDO

and alkylation activity were observed with the progressive appearance of benzene (m/z 78), toluene (m/z 91), xylene (m/z 106), and further methylated benzene derivatives (m/z 120 and 134) at the expense of lignin-derived pine pyrolysis compounds (primary vapor products: m/z 124, 138, 150, 164, and 180) produced in the pure pine pyrolysis vapors control (D). Carbon dioxide signals (m/z = 44) were similar across spectra and were omitted to reduce the ordinate scale. These products coincide well with Anderson et al. where methylated benzene derivatives up to pentamethyl benzene and alkylated phenolics were observed for anisole conversion over a titania-supported molybdenum polyoxometalate at 320°C.¹³³ Further replicate experiments at less severe conditions, reducing the percentage of H₂ in the flow, confirmed the production of benzene, toluene and xylene (BTX) with minor alkylation activity thus still achieving a partial upgrading. Moreover, stability of the catalyst over time was evaluated when Mo-HPA/TiO₂ was

Another important observation is that Mo-HPA/TiO₂ system was stable under H₂ with no significant indication of deactivation after 1 h of continuous-flow time of stream, as evidenced by a continuous increase in the trends of hydrocarbons compounds. More details on the catalysts experimental evaluation on pilot-scale pyrolysis plant can be found in Peterson et al.¹³⁴

Pre- and Post-Reaction Catalyst Characterization

The proposed hydrogen-based mitigation of coke-induced deactivation is further supported by the reduction in coke on the reacted catalyst in the presence of H₂ as shown in Table 1 for the Mo-HPA/TiO₂ catalyst used in pulsed-flow screening experiments. The coke was reduced from 13.4 wt.% to 8.5 wt.% with the addition of H₂. Moreover, in hydrogen, a potentiating effect is exhibited for the Mo-HPA/TiO₂ as coke was further reduced on the catalyst relative to the titania support for the materials used in the continuous-flow experiments. Here, coke was reduced from 7.2 wt.% to 3.5 wt.% with the addition of the Mo-HPA on the titania in H₂. In both instances, it is believed that hydrogen activation on either the TiO₂ and/or Mo-HPA/TiO₂ occurs followed by reaction with surface-adsorbed intermediate species; resulting hydrogenated products more readily desorb from the catalyst surface, thereby preventing further surface reactions that form coke. Coproduction of steam may further contribute to coke reduction in a similar fashion. This indicates that Mo-HPA promotes H₂ activation in addition to TiO₂, with a synergy potentially experienced between the two materials.²⁹ A summary of additional pre- and post-reaction catalyst characterization results for molybdenum and phosphorus content, surface area, and acid site density are shown in Table 1. The Mo-HPA loading on the titania support was determined based on the molybdenum content of the samples and the known weight fraction of molybdenum of the Mo-HPA (i.e., H₃PMo₁₂O₄₀). The molybdenum and phosphorus content, and therefore the Mo-HPA content, of the catalysts remained unchanged upon reaction. The BET surface area increased upon deposition of the Mo-HPA material on the titania support while it remained unchanged upon reaction for both titania and Mo-HPA/TiO₂ materials. The increased surface area upon addition of Mo-HPA is expected due to the surface area enhancement imparted by the dispersed nanostructured Mo-HPA deposits on the low porosity titania support. The acid site density (combination of Brønsted and Lewis acid sites) of the Mo-HPA impregnated titania support was approximately 100 μmol/g greater than the native titania support. Upon reaction, the acid site density slightly increased for both the support and the Mo-HPA/TiO₂. The reducible nature of and subsequent oxygen deficient site formation on titania is believed to be responsible for this increase in acidity.¹²⁴ The stability of these catalyst properties was expected since minimal deactivation was observed during the time-on-stream experiments. These data are in

agreement with lignin-derived model compound studies where a reacted molybdenum-based HPA catalyst maintained its Keggin-type structure and did not appreciably deactivate appreciably.¹¹⁷

Table 1. Characterization of pulsed-flow (PF) and continuous-flow (CF) unreacted and reacted TiO₂ control and Mo-HPA/TiO₂ materials with and without H₂.

| Catalyst ID | | ICP-AES, Mo [wt.%] | ICP-AES, P [wt.%] | Mo-HPA Loading [wt.%] | BET Surface Area [m ² /g] | NH ₃ TPD [μmol/g] | Catalyst Coke [wt.%] |
|---------------------------------|------------------------------|--------------------|-------------------|-----------------------|--------------------------------------|------------------------------|----------------------|
| Mo-HPA/TiO ₂ (PF) | Reacted w/out H ₂ | - | - | - | - | - | 13.4 |
| | Reacted w/ H ₂ | - | - | - | - | - | 8.5 |
| TiO ₂ (Control) (CF) | Unreacted w/ H ₂ | - | - | - | 55 | 365 | - |
| | Reacted (CF) | - | - | - | 67 | 412 | 7.2 |
| Mo-HPA/TiO ₂ (CF) | Unreacted w/ H ₂ | 9.1 | 0.4 | 14.4 | 97 | 480 | - |
| | Reacted (CF) | 9.2 | 0.4 | 14.6 | 101 | 497 | 3.5 |
| Mo-HPA/TiO ₂ (CF) | Unreacted w/ H ₂ | 9.2 | 0.4 | 14.6 | 94 | 432 | - |
| | Regen. (CF) | 9.2 | 0.4 | 14.6 | 96 | 481 | 3.2 |

As described in the publication¹³⁴, the whole filtration system, comprising the cyclones plus the two steps of hot gas filtration, is also able to trap most of the char and ashes entrained by the vapors stream exiting the pyrolyzer. Since char and alkali metals have been shown to promote aging of condensed oils through accelerated polymerization reactions,^{34,87,90,92,93,135} the ability to remove these materials via cyclonic action coupled with hot- gas filtration is significant. Because the majority of the char and ash was captured in the first cyclone, it is proposed that the second cyclone can be eliminated (Figure 1). According to Dutta et al., the impact of HGF may lead to a capital savings if one of the two cyclones after the fast pyrolysis reactor is eliminated.¹³⁶

Fractional Condensation of CHGF Vapor Products and System Mass Balance.

Fractional condensation is a strategy for separating liquid product from vapor phase product conversion streams in a controlled, sequential process. The strategy can be used to separate selected compounds from the organic oil product (ketones, acids, aldehydes), remove heavy oligomeric material, concentrate organic matter, separate the aqueous phase, and isolate coproducts by process control.¹³⁷ Oil stability, and therefore oil quality, depends on the ability of reactive oxygen moieties (e.g., acid carbonyls) within the oil to promote aging reactions during storage. The complex mechanisms and pathways associated with oil aging reactions have been described in other studies.^{90,94,138–141} Since carbonyl compounds (e.g., aldehydes and ketones) and organic acids (e.g., acetic acid) are the main contributors to oil instability of fast pyrolysis oil,^{90,140} an FCT (staged condensation process) was coupled with the CHGF unit operation

to reduce the content and distribution of these aging compounds within the organic liquid product. The hot-gas filtered pyrolysis vapors were condensed in the FCT (shown schematically in Figure 10 and Figure 11) with both qualitative and quantitative analysis conducted on the liquid product samples. The impact of Mo-HPA/TiO₂ catalytic activity on pyrolysis vapor composition is shown in the GC-MS analysis of the condensed oil product as indicated in Figure 16. Figure 16 represents the quantity of GC-detectable compounds per condition, where the increase in GC-detectable compounds when using a catalyst is consistent with upgrading and the concurrent reduction in primary vapors. The change in GC-detectable compounds as a function of upgrading accounts for the lower detectable yield shown in Figure 16 for the filter alone (noncatalytic) since the heavy, nonupgraded species were not detected by the GC method. It is important to note that the group of compounds labeled “Unknown” refers to those compounds that were detected but not identified by the GC method employed. A summary of the oil compositions of CHGF vapors for filter, filter + TiO₂, and filter + Mo-HPA/TiO₂ is provided in Table 2.

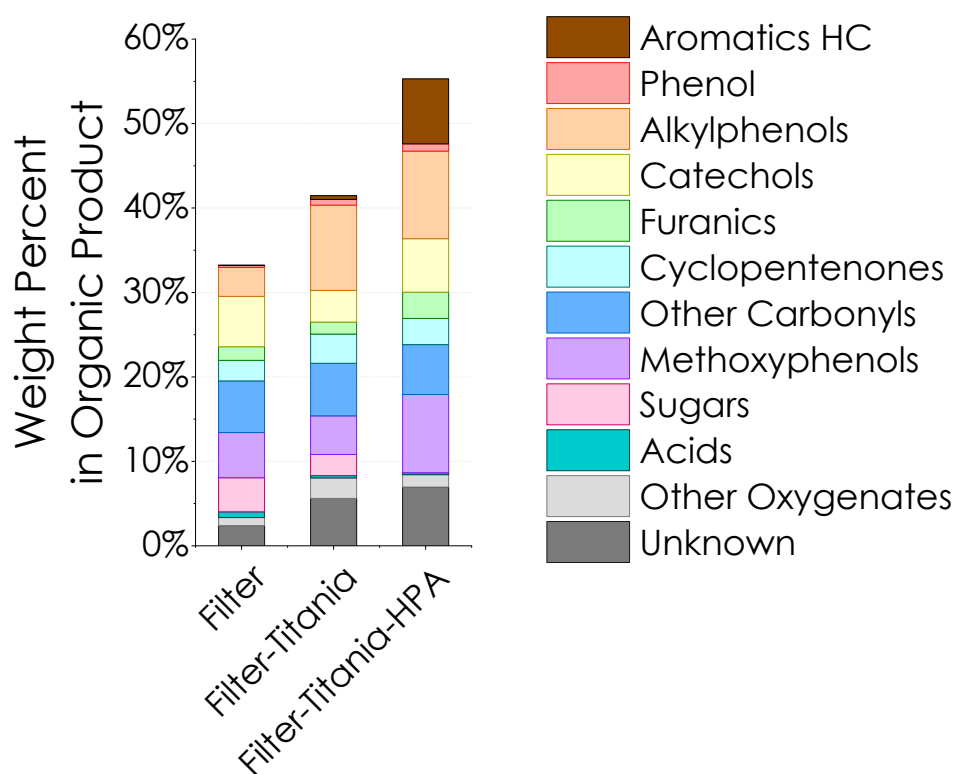


Figure 16. Composition of condensed organic oil product, as determined by GC-MS, for pine pyrolysis vapors partially upgraded via catalytic hot-gas filtration (CHGF) using a molybdenum heteropolyacid on titania (15 wt.% Mo-HPA/TiO₂) catalyst. From left to right: empty filter (control) with WHSV 1.0 h⁻¹ and 40 vol % H₂, filter + TiO₂ with WHSV 1.0 h⁻¹ and 40 vol % H₂, filter +15 wt.% Mo-HPA/TiO₂ with WHSV 1.0 h⁻¹ and 40 vol % H₂. All experiments were conducted at 400 °C.

Table 2. GC-MS characterization of organic oil product from catalytic hot-gas filtration

| | Chemical Class | Blank Filter | Filter + TiO ₂ | Filter + Mo-HPA/TiO ₂ |
|----------------------------------|------------------------------|-------------------|---------------------------|----------------------------------|
| | | w/ H ₂ | w/ H ₂ | w/ H ₂ |
| Weight Percent in Product [wt.%] | Aromatic Hydrocarbons | 0.06 | 0.45 | 7.70 |
| | Phenol | 0.22 | 0.68 | 0.85 |
| | Alkylphenols | 3.43 | 10.10 | 10.37 |
| | Catechols | 5.96 | 3.75 | 6.33 |
| | Furanics | 1.62 | 1.41 | 3.11 |
| | Cyclopentenones | 2.43 | 3.46 | 3.10 |
| | Other Carbonyls | 6.12 | 6.21 | 5.91 |
| | Methoxyphenols | 5.34 | 4.58 | 9.26 |
| | Sugars | 4.05 | 2.51 | 0.00 |
| | Carboxylic acids | 0.68 | 0.28 | 0.24 |
| | Other Oxygenates | 0.96 | 2.41 | 1.47 |
| | Unknown | 2.39 | 5.62 | 6.95 |
| | Total | 33.26 | 41.46 | 55.29 |

Table 3. GC-MS characterization of aqueous product from catalytic hot-gas filtration

| | Chemical Class | Blank Filter | Filter + TiO ₂ | Filter + Mo-HPA/TiO ₂ |
|----------------------------------|------------------------------|-------------------|---------------------------|----------------------------------|
| | | w/ H ₂ | w/ H ₂ | w/ H ₂ |
| Weight Percent in Product [wt.%] | Aromatic Hydrocarbons | 0.02 | 0.00 | 0.11 |
| | Phenol | 0.10 | 0.13 | 0.07 |
| | Alkylphenols | 0.29 | 0.30 | 0.15 |
| | Catechols | 0.14 | 0.00 | 0.81 |
| | Furanics | 1.06 | 0.86 | 0.81 |
| | Cyclopentenones | 1.03 | 0.75 | 0.34 |
| | Other Carbonyls | 2.70 | 1.42 | 0.89 |
| | Methoxyphenols | 0.39 | 0.16 | 0.34 |
| | Sugars | 0.14 | 0.00 | 0.29 |
| | Carboxylic acids | 6.04 | 4.23 | 2.30 |
| | Other Oxygenates | 0.11 | 0.00 | 0.12 |
| | Unknown | 1.04 | 0.33 | 0.50 |
| | Total | 13.06 | 8.18 | 6.73 |

When the filter was packed with the TiO₂, an increase in the percentage of alkylphenols from 3 to 10 wt.% relative to the filter was observed, and this effect was maintained upon the addition of the Mo-HPA (Figure 16). Minor increases in phenol and cyclopentenones were observed using TiO₂. The production of phenol and alkylphenols from biomass using TiO₂ has been reported in the literature.^{142,143} While alkylated phenols production was catalyzed by the TiO₂ support, aromatic hydrocarbons and methoxyphenols were further enhanced through the addition of the Mo-HPA to

the support (Figure 16). The aromatic hydrocarbon class depicted in the plot comprises 1-ring, 2-ring, and 3-ring aromatic hydrocarbons and alkyl benzenes. These results confirm the real-time MBMS data, which also showed an enhancement of aromatic hydrocarbons and alkylation of aromatic rings along with the production of phenolic compounds. The presence of these upgraded products validates the results obtained in the pulsed-flow lab scale experiments and the scaled-up, continuous-flow system. In addition to hydrocarbons, alkylated phenols and methoxyphenols are chemical classes of interest as value-added chemicals since they are or can be converted to polymer precursors (e.g., phenol, cresols, and xylenols) via further upgrading processes like catalytic hydrodeoxygenation.^{144,145} In addition, cyclopentenones and other carbonyls (e.g., aromatic aldehydes or ketones) marginally decreased in the condensed oil and increased in the gas phase (gas bag analysis) with the catalyst addition. The Mo-HPA/TiO₂ in the presence of hydrogen promotes the conversion of acids as demonstrated by the compositional analysis. GC-MS results show a reduction of ~4 wt.% in the collected aqueous phase relative to a blank filter and a ~2 wt.% reduction relative to the catalyst support. These results are presented in Table 3.

To further investigate staged condensation of pyrolysis vapors partially upgraded using Mo-HPA/TiO₂, the distribution in mass fractions for several main compound classes (methoxyphenols, ketones and acids) was tracked across different condensation conditions. The product distribution between the fractions depends on vapor pressure, composition, and temperature of the pyrolysis mixture. Moreover, thermodynamic interactions between oxygenated compounds, heat-transfer characteristics of the condenser (tube-in-shell in this case), and residence time of vapor mixture in the heat exchanger can have strong effects on the selective condensation efficiency as mentioned in other works.¹⁴⁶ Throughout the CHGF-FCT experiments, only a smaller percentage of heavy sugars (i.e. levoglucosan) was captured in the first passive-cooled condenser shown in Figure 10 and Figure 11. The class-selective staged condensation was achieved by varying the ESP condensation stage temperature (heat exchanger + ESP) from low (70 °C) to high (170 °C) while keeping the third condensation stage (cold trap) temperature constant at -15 °C. The tube-in-shell heat exchanger used in the third stage cold trap was designed to condense the compounds in the oil according to their dew point, while the ESP stage actively removes entrained aerosols electrostatically and thermally. At 70 °C, the majority of the organic phase was condensed in the ESP second stage while the majority of the aqueous phase was condensed in the third stage cold trap. At the condensation temperature of 170 °C, only sugars (e.g., levoglucosan) were collected in the ESP stage and the oil phase was condensed together with the aqueous fraction contained in the cold trap. In the latter case, the aqueous phase was decanted from this composite oil-aqueous product and the resulting separated oil and aqueous phases were quantified gravimetrically and characterized independently. Fugitive vapors that were not captured in the third stage cold trap were subsequently captured in the coalescing filter as an organic phase. The oil captured in the coalescing filter accounted for <5 wt.% of the total product recovered. The organic phase collected in the second ESP condenser at 70 °C was nearly free of water (1.6 wt.% water) as determined by Karl Fischer titration. Coupling CHGF with fractional condensation improved the ability to collect light organic components (<300 °C boiling point). A 42% decrease in heavies (pyrolytic lignin) collected in the heat exchanger (FCT-V-04, in Figure 11) and a 67% increase in light organics (FCT-V-03, in Figure 11) with the ESP condensation stage operated at 70 °C were observed. Separation of the heavy components of pyrolysis vapors is a significant challenge, and the reduction in the heavy component demonstrates the benefit of combining the two-unit operations to access chemicals and fuels from pyrolysis vapors. Normalized mass distributions between the ESP condenser and the cold trap of selected classes are provided in Table 4.

Table 4. Mass distribution of chemical classes between the condenser and the cold trap of the fractional condensation train

| Chemical Class | Condenser Temperature | Condenser Product | Cold Trap Product |
|------------------|-----------------------|-------------------|-------------------|
| | (°C) | (wt.%) | (wt.%) |
| Methoxyphenols | 70 | 94 | 6 |
| | 170 | 0 | 100 |
| Ketones | 70 | 33 | 67 |
| | 170 | 0 | 100 |
| Cyclopentenones | 70 | 59 | 41 |
| | 170 | 0 | 100 |
| Carboxylic Acids | 70 | 5 | 95 |
| | 170 | 0 | 100 |

These results show the ability to shift compounds between liquid products based on temperature. At 70 °C, in the ESP condensation stage (second), the methoxyphenols were condensed primarily in the oil fraction while upon increasing the temperature to 170°C they were allowed to remain as vapor through the second stage until being condensed in the cold trap. Here, the aqueous and organic phases condensed together as a phase-separated composite. Methoxyphenols have a higher dew point where vapor saturation is reached at higher temperatures (>250 °C), and therefore at 70 °C, the condenser is able to remove them effectively.

As shown in Table 4, slightly different behavior was observed for the ketones when condensed at 70 °C. The total mass of cyclopentenones generated during pyrolysis tended to be distributed evenly between the ESP condenser stage and cold trap. The cyclopentenone compound class has a broad range of boiling points (and therefore dew points) which contribute to the distribution between the two stages. Hence, saturation in the ESP condensing stage could not be achieved for all compounds within the cyclopentenone class. For example, 2-cyclopenten-1-one, 2-hydroxy-3-methyl- has a normal boiling temperature of 253 °C and is completely condensed into the first fraction at 70 °C, while 2-cyclopenten- 1-one has a lower normal boiling point (135 °C) and tended to condense within the cold trap. The same reasoning can be applied to the remaining ketones detected with compositional variations in distribution arising from differing dew points among the various ketones. When the condensation temperature was controlled to 170 °C, all the cyclopentenones and the other ketones present in the vapors were completely condensed in the cold trap. The organic acids, including acetic acid, represented ~5 wt.% of the mass collected in the ESP condensation stage at 70 °C. Because these compounds possess low dew points, they remained as vapor at 70 °C and were therefore collected in the cold trap within the aqueous phase. This resulted in a deacidified oil phase in the ESP condensation stage. These results show the difficulty in removing any specific class of compounds in high purity using a simple separation and are in accordance with Rover et al.¹⁴⁷ However, the ability to remove crude fractions of unwanted compounds (e.g., acids) from the organic product through the combined use of partial upgrading via CHGF coupled to fractional condensation was demonstrated and has the potential to enhance oil stability and mitigate downstream CFP and/or hydrotreating catalyst deactivation. The product distributions obtained for the FCT experiments conducted with CHGF using Mo-HPA/TiO₂ suggest that an average temperature between the two evaluated temperatures (70–170 °C) may be sufficient to isolate the majority of the ketones from the oil, aside from trace-amounts of cyclopentenones. The results further indicate that, for temperatures below 170 °C, the majority of the methoxyphenols can be retained in the organic oil phase within the ESP stage while simultaneously isolating the majority of the acids in the aqueous phase

within the cold trap. Controlling product condensation in this fashion allows for the ability to densify, deacidify, and dewater the organic oil phase while concentrating alkylphenols within the same phase. Alternatively, at the higher ESP stage temperature of 170 °C where all upgraded product condensed in the downstream cold trap, the acids and carbonyls partitioned between the oil and aqueous phases; partitioning of reactive carbonyls into the aqueous phase constitutes another means for enhancing oil stability and catalyst lifetime in downstream processes since these species promote aging reactions in the condensed oil phase and catalyst coking reactions in the vapor phase.^{141,148} In addition, the heavier aromatic hydrocarbons, alkylphenols, methoxyphenols, and polyalkylated benzenes generated during the upgrading using Mo-HPA/TiO₂ were collected completely in the condensed oil phase within the ESP stage at 70 °C. This demonstrates our intended separation control toward targeted alkylphenols and methoxyphenols as value-added chemicals. Additional stages within the FCT may prove useful in enhancing separations control over targeted cyclopentenones. The efficiency of the FCT in capturing product was assessed via mass balance using Mo-HPA/TiO₂ CHGF replicates (WHSV of 1 h⁻¹, 40 vol % H₂) with the FCT ESP stage at 170 °C. These data are shown in Table 5 in conjunction with mass balance data for when the FCT ESP stage was at 70 °C.

Table 5. Mass balance results for catalytic hot-gas filter (CHGF) experiments with the ESP second stage condenser (FCT-ESP-01) at 70°C and 170°C. Experiments were conducted using 10 wt.% molybdenum heteropolyacid on titania (10 wt.% Mo-HPA/TiO₂) with a weight-hourly space velocity (WHSV) of 1.0 h⁻¹ and 40 vol% H₂.

| Product Type | | Second Stage @ 70°C (wt.%) | Second Stage @ 170°C (wt.%) |
|------------------------------------|---------------|----------------------------------|-----------------------------------|
| Liquids Product | Aqueous | 30.20 | 33.50 |
| | Oil | 22.00 | 15.10 |
| | Subtotal | 52.20 | 48.60 |
| Gaseous Product | Total | 44.60 | 45.20 |
| Solids Product | Catalyst Coke | 3.5 | 3.5 |
| Mass Balance Closure (Total) | | 100.3 | 97.30 |

The mass balance closure for the Mo-HPA/TiO₂ replicate experiments was 97.3 ± 3.3 wt.% with 45.2 wt.% residing as gaseous product, 3.5 wt.% lost to catalyst coke, 33.5 wt.% aqueous product, and 15.1 wt.% as organic oil product. In comparison, the filter + TiO₂ control exhibited a mass balance closure of 96.6 wt % with 48.0 wt % residing as gaseous product, 7.2 wt % lost to catalyst coke, 15.9 wt % aqueous product, and 25.5 wt % organic oil product. The filter control without packing yielded a mass closure of 92.0 wt % with 43.1 wt % gaseous product, nondetectable coke loss, 24.4 wt % aqueous phase, and 24.1 wt % organic oil product. The gas yields were high due to thermal cracking of pyrolysis vapors in the small pilot-scale pyrolyzer system prior to their delivery to the CHGF unit. The pyrolyzer was not optimized for pyrolysis vapor quality prior to experiments. It is anticipated that an optimized pyrolyzer would improve vapor quality by reducing the light gas yield while concomitantly increasing the viable upgradable vapor yield. A reduction in the oil product yield in the Mo-HPA/TiO₂ can be attributed to much of the upgraded product being volatile and not efficiently condensed in the FCT. Partial deoxygenation also removes oxygen as water, evidenced by the increase in aqueous phase when using catalyst. Previous work indicated a negative

correlation to oil yield and degree of deoxygenation.³¹ It should be noted that the mass balances were comparable for the two ESP stage temperatures investigated (70 and 170 °C).

2.1.4 - Conclusion

Catalytic hot-gas filtration (CHGF) was successfully used to condition biomass fast pyrolysis vapors provided by a continuous-flow small pilot-scale pyrolyzer unit by integrating a catalytic component based on a heteropolyacid into a hot-gas-filtration (HGF) unit. This CHGF process in combination with a cyclone system produced clean (i.e., no particulates and low alkali metals) and partially upgraded fast pyrolysis vapors for either fractional condensation or downstream catalytic upgrading. Produced vapors contained increased quantities of aromatic and alkylated hydrocarbons. Both hydrodeoxygenation and alkylation reactions were essential in the partial conversion of the pine-derived oxygenates. In the combined process, the removal of alkali metals stabilizes associated pyrolysis and upgraded oils, while the partial deoxygenation (i.e., removal of reactive oxygen moieties) enhances CFP by reducing coke formation and promoting improved oil stability. The efficient capturing of char and alkali particulate at the HGF indicates that a single cyclone for entrained solids removal will suffice, thereby allowing for the elimination of the second cyclone typically employed in ex situ CFP. The coupling of the catalytic preconditioning of pyrolysis vapors via CHGF with the controlled condensation demonstrated an additional means to enhance oil stability while preserving carbon for downstream upgrading and production of carbon-carbon coupled species for tailoring fuel end-product properties. Controlled condensation provided phase separation between organic oil and aqueous products. Controlled condensation additionally allowed for the targeted condensation of heavy aromatic hydrocarbons, alkylphenols, and methoxyphenols within the oil phase and reactive acid carbonyls within the aqueous phase. On the contrary, the distribution of ketones spanned both the oil and aqueous phases, suggesting that additional FCT stages would be necessary for improving their separation. This chemical tailoring of either vapor phase or condensed phase product composition is a viable option for enhancing downstream upgrading within CFP and/or hydrotreating via foulant removal. Value-added product separation using FCT represents an additional enhancement to the upgrading process; polymer precursors or other chemicals, such as bio-derived pesticides discussed in the next chapter, have the potential to offset process capital costs. The CHGF and FCT unit operations together offer a low CapEx approach for enhancing oil stability, product composition, and overall efficiency within CFP processing of biomass fast pyrolysis vapors to selected fuels and chemicals. In addition, tuning the oil compositions and separating organic fractions through FC of pyrolysis vapors can be implemented also for the production of co-products precursors as presented in the next section.

2.2 - Co-products from catalytic fast pyrolysis biorefinery: bio-based insecticides from bio-oil fractions

2.2.1 - Introduction

The previous chapter presented a potential route to partially upgrade the bio-intermediate fast pyrolysis oil tuning the composition with a controlled fractional condensation unit. Promising conclusions were obtained in term of catalyst and organic fractions composition, especially increasing the phenol alkylation as well as reducing the acidity and improving the stability partially removing the ketones content. Moreover, the fractionation results are important in biorefinery perspective for the production of co-products in an integrated biorefinery concept. Co-products can help to reduce the fuel production costs by valorizing other bio-derived compounds at a higher value. Example of biorefinery integration approaches have been studied in the last decades.^{38,39,149–154} The extraction of value-added products from biomass sources is dependent on the process and the feedstock and in this section the discussion is focused on catalytic fast pyrolysis (CFP) of lignocellulosic biomass. In general, several valorization routes have been proposed to extract and separate molecules from pyrolysis aqueous or organic streams^{9,38,39}. In this work we focused on the extraction of bio-based compounds to be used as in agriculture as pesticides.

Bio-based pesticides will be necessary to meet food supply projections by 2050 and these pesticides can reduce the environmental impacts in pest mitigation along the agricultural supply. Food and Agricultural Organization of the United Nations (FAO) projects food demand needs to be subjected to about 70% of increment by 2050.^{40–42} This is due to a significant grow in the world's population that will reach 9.7 billion by 2050, 10.8 billion by 2080, and 11.2 billion by 2100. As an example, global cereal demand is expected to reach 3.5-5.5 billion of tonnes by 2050 from 2.1 billion of tonnes in 2005. Thus, strategies to minimize the impact of agricultural sector are needed in a mid and long-term period. Agricultural production has been prioritized over sustainability, which puts food security at odds with long term sustainability.¹⁵⁵ Pesticides, which includes herbicides, insecticides, fungicides, and rodenticides, provide a net benefit but still face major sustainability and environmental challenges. Between 1990 and 2015 food production and crop yields increased by 70% and 27%, respectively, however, these gains also corresponded with a 78% increase in global pesticide use.¹⁵⁶ The gains in production and yield can be partially contributed to pesticides as weeds alone can reduce crop yields by 40%.¹⁵⁷ The benefits of pesticides go beyond production to include reduced land use which offsets water consumption and mitigates climate change, disease management in both plant and animals, and price stabilization through increased and consistent supply.¹⁵⁸ Unfortunately, the global proliferation of pesticides has also resulted in reduction to air and water quality, increases to GHG emissions, and detriment to beneficial insects. Pesticides, specifically insecticides, impact water quality when they are transported to ground water reservoirs and streams where the insecticides or degradation products can bioaccumulated and persist.⁴³ Half-lives in the environment for organochlorines, many of which are now band, range from months to over 100 years so the exposure risks such as reproductive failure, impairment to the nervous systems, and cancer-causing mutations are likely to exist long past initial use.¹⁵⁹ The energy input to produce insecticides contributes to GHG emissions and has been estimated to range from 6 to 16% of the total energy consumption of arable crops.¹⁶⁰ Agricultural and food sector are both victim and perpetrator to climate change: on one hand they are responsible of 10% of the total global GHG emissions¹⁶¹ due to the use of chemical fertilizers, pesticides and animal wastes, while on the other hand these GHG emissions have a strong effect on global warming and consequently impacting yields and rural livelihoods.⁴⁰ Among these, pesticide

are often considered as GHG contributor mostly during the manufacturing process and not in the crops uses, which includes the formulation, packaging and transportation. A correct estimation of overall GHG emissions associated with pesticides is complex and other studies propose emissions factor of 25 to 94 kg of carbon dioxide equivalent per kg of product.^{160,162} Additional pressures within the agrochemical sector, such as public concern about the use of synthetic petroleum-based chemicals as pesticides and more severe regulations to limit the impact on the environment and humans, are requiring greener solution. Pollinators play a critical role in ecosystems and provided €153 billion (\$123 billion USD, 2005) in ecological services to the global economy. The combined pressure of insecticides with other colony risk factors, such as parasites and pathogens, are resulting in substantial annual colony losses, 40% loss in 2015 within the United States.¹⁶³⁻¹⁶⁵ In 2018 the European Commission ban three major neonicotinoids insecticides due to honeybee and pollinator harm, while in the US, five neonicotinoids are currently under review from the EPA and a final decision is expected in 2021.^{166,167} Conventional insecticides are enduring additional pressures beyond tightening regulations. In addition, resistance has been observed from sublethal doses of pyrethroids during cis- and trans-generational exposures to the insecticides.^{168,169} The WHO has mobilized a concerted effort to deal with the health concerns from exposure to highly hazardous pesticides via unintentional or self-inflicted poisoning, which disproportionately affect low- and middle-income countries and account 1 in 5 suicides globally.^{170,171} New insecticides are needed that do not have negative ecological impacts, are sustainable in the long term, and reduced risks to human health.¹⁷² The revision of the current regulations towards more stringent restriction for the use of fossil-derived chemical as pesticide, together with increasing demand for agriculture products with lower environmental and safety impact, are boosting interest towards bio-based natural products. In 2019, only 5-6% of the total global pesticide market is represented by biopesticides and about 17% of the market is represented by insecticides, both bio- and fossil-derived. Hence, representing a relatively low percentage, considering that the overall global pesticides market reached a value of nearly \$84.5 billion in 2019 and it is expected to grow rapidly stretching to \$130.7 billion by 2023.¹⁷³⁻¹⁷⁵ Pesticides are always formulated with two components, the active and inert ingredients, and the active ingredients can be potentially extracted from pyrolysis liquids as other previous studies showed.⁴⁴⁻⁵¹ Particularly interesting, a work by Canadian research groups showed that liquid fractions derived from pyrolysis of lignocellulosic biomass have pesticidal and insecticidal activity. Bedmutha et al.⁴⁶ investigated the effect of pyrolysis oil from coffee grounds, modifying the oil composition by varying the reaction temperature between 400-600°C and separating the oil in different fractions; their results showed a marked insecticidal activity of phenols. Hossain et al.⁴⁸ studied the toxicity of pyrolysis liquids derived from lignin, cellulose and hemicellulose individually and in mixtures; they concluded that lignin fractions have the strongest pesticide activity. Similar results were obtained by Booker et al.⁵² where bio-oil from tobacco leaves showed high pesticide activity. In addition, a study from Saini et al.⁵³ investigated the insecticidal property of alkyl-substituted guaiacols finding that the presence of a methyl group at 4-position of guaiacol increase the insecticidal activity. In this context, eugenol (Phenol, 2-methoxy-4-(2-propenyl)-), has a well-established insecticidal activity demonstrated by other research studies^{53,176} and it is already approved as active ingredient by EPA in USA and in Europe as low risk pesticide.^{177,178} Eugenol can be formed by lignin depolymerization and it is also contained in several essential oils extracted from plants that are commonly used as insecticide.^{179,180} To sum up, their work showed that the active pesticide effect is mostly due to lignin-derived phenolic compounds.

Biorefining is a viable strategy for simultaneously replacing conventional fuels and accessing novel oxygenated chemicals. CFP is an emerging technology to access bio-derived compounds through thermochemical conversion processes of lignocellulosic resources where the constituents of the natural matrix are depolymerized and recovered

in form of concentrated liquid organic streams.^{32,181,182} Extraction, separation, and concentration of natural substances from pyrolysis liquids that can be used as active ingredients becomes a key challenge for enabling these bioinsecticides. There is still a lack of literature regarding the production and use of thermochemically derived chemicals as bio-based renewable pesticides, especially regarding separation technologies. Among separation technologies, fractional condensation and distillation or a combination of both for concentrating organic compounds classes in specific cuts, have the potential to be implemented as fundamental step for co-products extraction. Distillation has been previously demonstrated as a potential way to fractionate bio-based mixtures from the organic streams of fast pyrolysis but issues related to reactivity have been observed: mostly condensation reactions that leads to the formation of water and high residue yield due to polymerization.⁴⁴ The distillation behavior and oil processability is strictly dependent on the chemical composition of the oil, and therefore, upgraded oils are more stable during vacuum distillation.^{183,184} Fractional condensation of pyrolysis vapors have been investigated, also in this work, as potential alternative for a first rough compositional conditioner which can reduce process energy and stabilize the liquid product streams through separation of reactive components. In order to obtain high purity of target molecules one separation step is typically insufficient. Potentially a coupling of a first fractional condensation step followed by high-purity distillation steps is a more suitable way to extract and generate chemicals precursors.

In this work fundamental research has been carried out to highlight the advantages of extracting and separating thermochemically biomass-derived target molecules to be used as bio-derived insecticides. In order to evaluate which group of molecules have higher insecticidal activity, a fractionation of catalytic fast pyrolysis organic streams have been carried out through experimental batch-mode vacuum distillation of oil. The distillate fractions have been further tested in a bioassay to address the activity as natural-based insecticide towards *Spotted Wing Drosophila*. A techno-economic analysis (TEA) has been carried out by modifying an existing NREL proprietary CFP model.¹⁰ Throughout the TEA analysis it was possible to extrapolate information about the minimum product selling price (MPSP) trend as a function of yield and product purity. In addition, interesting results have been obtained from Life Cycle Assessment (LCA) on GHG emissions and supply chain energy demand associated with the production of bio-derived insecticides, which are benchmarked against LCA metrics for traditional pesticides (such as Organophosphates or Pyrethroids).

2.2.2 - Material and Methods

CFP oil production and distillation set-up

The PtTiO₂ oil was produced on NREL's 2-inch Fixed Bed Reactor (2FBR) where pyrolysis vapors were upgraded across a fixed bed of the platinum catalyst as described elsewhere¹⁸⁵. Fractions of CFP oil were obtained through batch mode vacuum distillation at 30 torr, performed on a 800-SB-A (B/R Instruments) spinning band distillation column. The distillations were carried out with a Teflon band, simulating 30 theoretical trays loading 100-500 ml of CFP oil into a round-bottom flask externally heated and insulated, connected to the bottom of the column. The vapors temperature profile was acquired through a M690 PC Interface (B/R Instruments), while the atmospheric equivalent temperature (AET) was calculated using BR AET Utility 1.0 software. Fractions were collected at selected AET ranges.

GC MS-FID

Analysis of the fractions was performed using a GC MS-FID (Agilent Technologies 7890A, 5975c GC-MS, and GC-FID with a DB-5 column) coupled to a polyarc® catalytic micro-reactor (Activated Research Company) installed upstream of the FID detector. MS detector was used to identify the compounds in the CFP oil fractions while polyarc® and FID were used for quantification of species *via* external standard of cyclopentanone, p-xylene and 2-methyl naphthalene. The polyarc® reactor converts all the organic compounds to methane prior to their detection by the FID, and the concentration of a species in the sample is proportional to the GC peak area divided by the number of carbons in the compound. Acetone was used as analytical solvent. Peaks integration was performed using Agilent's Enhanced Chemstation software through the Chemstation Integrator for area determination and NIST library 2017 for spectrum comparison and compounds identification. The resulting peaks areas were analyzed with Python 3.6, using libraries chemspipy- 1.0.5 and pyvalence-0.0.2.

Insecticidal Assays

Insecticidal activity tests were performed by an entomology research group of the Michigan State University as part of a collaboration with NREL. Here briefly reported the insecticidal bioassays setup. Adult spotted-wing drosophila, *Drosophila suzukii* (Matsumura as a model insect for evaluating the direct and residual insecticidal activity of three pyrolysis fractions). *Drosophila suzukii* is a serious pest of high value fruit crops in the America's, Europe and Asia.¹⁸⁶⁻¹⁹⁰ Following a preliminary range-finding experiment 80 mg/ml, 60 mg/ml, 40 mg/ml, 20 mg/ml 10 mg/ml and 0 mg/ml of each fraction with the balance of material made up of 70% acetone. Six replicates were performed for each dose/application condition. Insects were sourced from laboratory colonies established from wild flies caught in 2018 and reared on a standard corn meal *Drosophila* diet¹⁹¹. For each dose/replicate 5 males and 5 females were knocked out with CO₂ and stored at room temperature before use in trials. Insecticide applications were made to test subjects directly or to 9 cm petri dishes used in residual contact trials. For each replicate, 1.5 ml of the appropriate dose was loaded into a Potter spray tower (Burkard Manufacturing Co Ltd Hertfordshire, UK) and applied to flies on a 9cm petri dish (direct mortality) or to a petri dish to which flies were added after dishes were dried in a fume hood for approximately 1 hour (residual mortality). The Potter spray tower was rinsed with 2ml of 95% acetone between each concentration. Flies in the residual mortality trial were provide with 1 ml of fly diet and left in the treated arena for the duration of the study. Fly mortality and morbidity were evaluated at 0, 2, 8, 24 h after direct application or placement into the treated dish. Flies were scored dead or moribund if flies showed no signs of movement or moved legs without locomotion when agitated with a small brush, respectively.

Techno economic analysis (TEA)

In order to evaluate the economic impact of the co-products extraction a TEA model has been adopted for the distillation of organic mixtures to be used as bio-derived insecticides. The CFP NREL Aspen Plus® model (FY19 version) is described and detailed elsewhere.¹⁹² Briefly, the model comprises a CFP plant with *ex-situ* upgrading of pyrolysis vapors and a throughput of 2000 dry tonnes per day of lignocellulosic biomass. In this study, only a portion of the plant that fractionally condenses upgraded vapors into two bio-oil streams has been considered without any further upgrading for fuel production (such as hydrotreating), therefore the economic analysis has been carried out considering the CFP oil as main product. Two distillation columns to separate the targeted insecticide mixtures from the lighter CFP oil stream were added to the process model. The Dortmund-UNIFAC¹⁹³ model was used for modeling the separation train. The bottom fractions of both distillation units are then mixed back into the main CFP oil line and

sent for hydroprocessing to hydrocarbon fuel. Five different simulations, each varying the flowrate of the co-product stream were carried out to evaluate the yield and purity of the insecticide mixtures, which were previously identified during the insecticidal assays. The feed stream used for modeling included the insecticidal species in experimentally measured proportions. The purity has been defined by considering several compounds and isomers of the same class identified as active insecticides in the experimental campaign. The economic analysis was completed using the same dataset for the capital and fixed operating expenditures as presented in Dutta et al.¹⁹², and utilizing the derived CFP-oil production cost from the model and the proportion of it going towards an insecticides coproduct designated as the raw material cost for insecticides production. Note that the portions sent back for hydroprocessing is assumed to be processable just like the whole stream prior to the separation of insecticidal compounds. The economic analysis was used for the calculation of the minimum biocrude selling price (MPSP) of the bio-based insecticide active ingredient mixture, which represents the minimum price to sell the product to cover capital and operating expenditures to produce the co-product after separating the insecticides from CFP-oil. The MPSP was calculated using discounted cash flow rate of return analysis, and 2016 dollars were used as the basis for the economic calculations.¹⁹²

Supply chain analysis through life cycle assessment (LCA)

In order to assess the energy consumption and the carbon dioxide emissions of producing bio-based mixture for the insecticides market the Materials Flows through Industry (MFI) supply chain analysis tool^{194,195} was used. Moreover, a comparison with traditional fossil-based active ingredients (Organo-Phosphates or Pyrethroids) have been carried out in order to estimate the energy and GHG impact of bio-based products from CFP biorefineries. The comparative analysis of conventional and bioinsecticide supply chains relies on life cycle inventories of material and energy inputs to the final production process as well as manufacturing processes for the intermediate (upstream) inputs. For the bioinsecticide processes, the technoeconomic models developed in this work provide the inventories, while for the conventional insecticides, inventory data was sourced from the ecoinvent database¹⁹⁶. For a more complete discussion of the MFI tool methodology, see Hanes and Carpenter¹⁹⁴. The overall GHG impact has been estimated in term of carbon dioxide equivalent per kg of product (kgCO₂e/kg) in order to compare the emissions based upon the global warming potential. The overall GHG emissions included the ones generated from the process fuel, the electricity generation and the transportation for the production process. The energy consumption was extrapolated considering the energy demand of the process fuel, the fuel used for the electricity production and the electricity from renewable sources. In addition, the energy contribution of the fuel used for transportation and the chemical energy contained in the feedstock were considered.

2.2.3 - Results and Discussion

Insecticidal activity of CFP oil fractions and correlations for active compounds identification

Previous studies highlighted some issues when fast pyrolysis bio-oil was fractionated through distillation, due to the high reactivity of some compounds in the organic mixture that leads to water generation through condensation and dehydration reactions as well as polymerization due to slow heating rate.^{197,198} However, fractional distillation is a possible route considering two factors needs to improve the process viability: first, bio-oil composition can be strongly improved and stabilized when a catalytic step is employed during fast pyrolysis and, on the other hand, the compound reactivity can be sufficiently limited distilling under vacuum conditions, thus keeping a lower temperature level.^{183,184}

In a biorefinery scale-up perspective, another step of fractionation can be employed to better optimize the whole separation process while minimizing the energy consumption. Instead of one single step of pyrolysis vapors condensation, catalytic upgraded pyrolysis vapors can be condensed in a fractional condensation unit able to already separate two or more fractions of interest and removing water in the last condensation step.^{86,113,199}

In this study was chosen to fractionate PtTiO₂ upgraded bio-oil because it shows the best properties in term of physico-chemical composition and thus reducing the reactivity issues during distillation.¹⁸⁵

A batch experimental distillation campaign has been carried out to fractionate the whole bio-oil into main classes of compounds based on boiling points and the results of a five-step fractional distillation is depicted in Figure 18A. Some of the phenolic compounds have been classified accordingly to the carbon number of the alkyl functional group.

The first cut was extracted in a temperature range of 110-115°C and it is composed mainly by water plus a small percentage of light carboxylic acids (mainly acetic and propanoic acid), cresols and cyclopentanone. Increasing the pot temperature to 130°C most of the acids were separated in the second cut, in good agreement with the theoretical boiling point of acetic acid (118°C). While the third fraction (130-185°C) was mainly composed by cyclopentenones (2-Cyclopenten-1-one and 2-Cyclopenten-1-one, 2-methyl) as well as acids, ketones, cyclic ketones and methoxyphenols. Increasing the temperature to 230°C most of the lighter phenol and 1 or 2 carbon alkyl-phenols (e.g. m/p-Cresol or dimethylphenols) have been extracted and concentrated. In addition, this fraction contains also methoxyphenols (e.g. phenol, 2-methoxy) and other alkyl-substituted methoxyphenols. Then the temperature was increased further, reaching 250°C to collect the last fraction, comprising heavier alkyl-phenols, with 3,4,5 carbon in the substituted group as well as methoxyphenols. The overall mass balance was never 100 wt.% and it was possible to identify and quantify about 60 wt.% for the fraction 130-185°C and 185-230°C, while the percentage decreased to about 50 wt.% for the last fraction 230-250°C. This is due to the complexity of the mixtures that still contains dozens of molecules as well as heavier fractions (e.g. dimers and trimers) that are not well analyzed by the GC system.

The last three CFP oil fractions were tested on *Spotted Wing Drosophila* bioassay to evaluate the effect as insecticide. Two different tests were carried out considering 24h of direct contact and 24h of residual contact. Figure 17 shows the dose response curves for each fraction tested and the dose of bio-oil fraction was increased from 0 to 80 mg/mL.

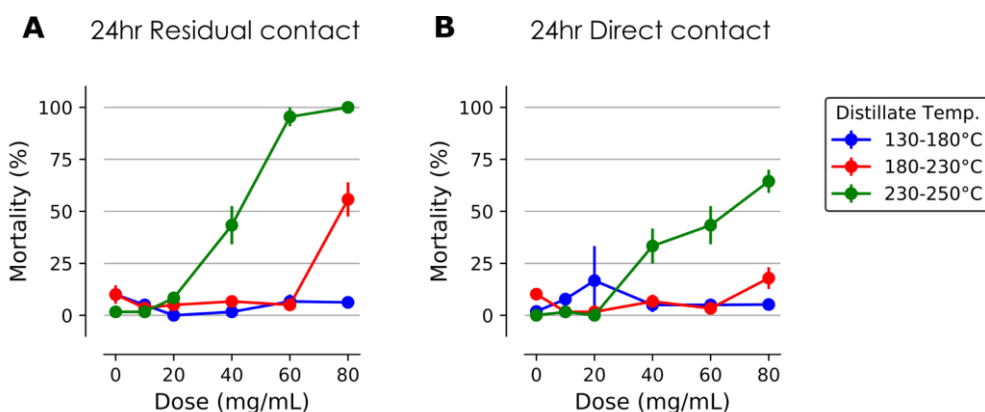


Figure 17. Spotted Wing *Drosophila* mortality in function of CFP oil fraction and dose concentration

Increasing the organic dose concentration, the insects' mortality increased for both 185-230°C and 230-250°C but no effect was measured by the first cut 130-185°C. Moreover, the last cut showed higher effect at lower dose concentration, resulting in an enhanced mortality in both, direct and residual contact. Separation through distillation

reduces the number of molecules presents in the organic mixture and the observed effects induces primary conclusion on the insecticidal effects of groups of molecules. However, further studies on model compounds are needed to correctly address a molecule or a group of molecules as active ingredient for pesticide. This study was further focused on searching and extracting information related to the compounds responsible of the mortality in order to identify target substances that can potentially be addressed as bio-based active ingredients.

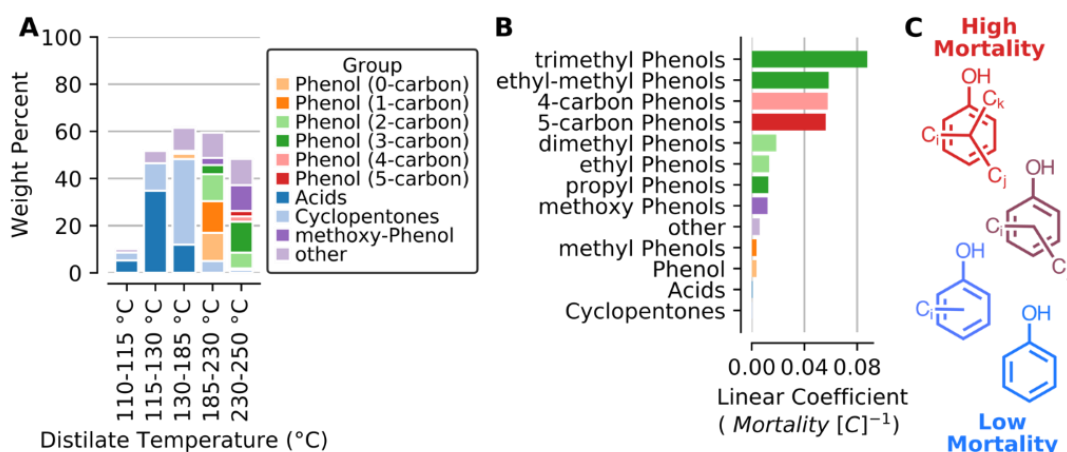


Figure 18. Composition of CFP oil fraction and linear coefficient of dose concentration vs mortality correlation

Data analysis was carried out correlating the concentration of the compounds in the fractions to the insect mortality (Figure 17A, and Figure 18A). Correlation curves for each compound class were obtained and the resulting scatter plots are depicted in Figure 19, while the resulting linear coefficients of the correlation slopes is showed in the bar plot in Figure 18B. Even though some substances did not show a good correlation it was possible to obtain interesting information. The third fraction (130-185°C) is mainly composed by carboxylic acids and cyclopentenones and the low mortality of the mixture seems to be confirmed by the low absolute value of the slope linear coefficient. On the other hand, the other two fractions, that have shown pesticide activity, contains a broad range of phenolics substances. As can be noticed by the bar plot in Figure 18B it is clear that substituted phenols have higher effect than simple phenol. Moreover, the correlations data shows that the mortality is correlated to the carbon number in the alkyl functional groups. From phenol to cresols and xylenols and then to heavier alkyl groups (such as trimethyl-phenol or 4-5 alkyl-chains groups) the linear coefficient of the correlation slope substantially increased. As a preliminary conclusion, the carbon number in the alkyl functional group was observed as the most influent characteristic toward the insecticidal activity.

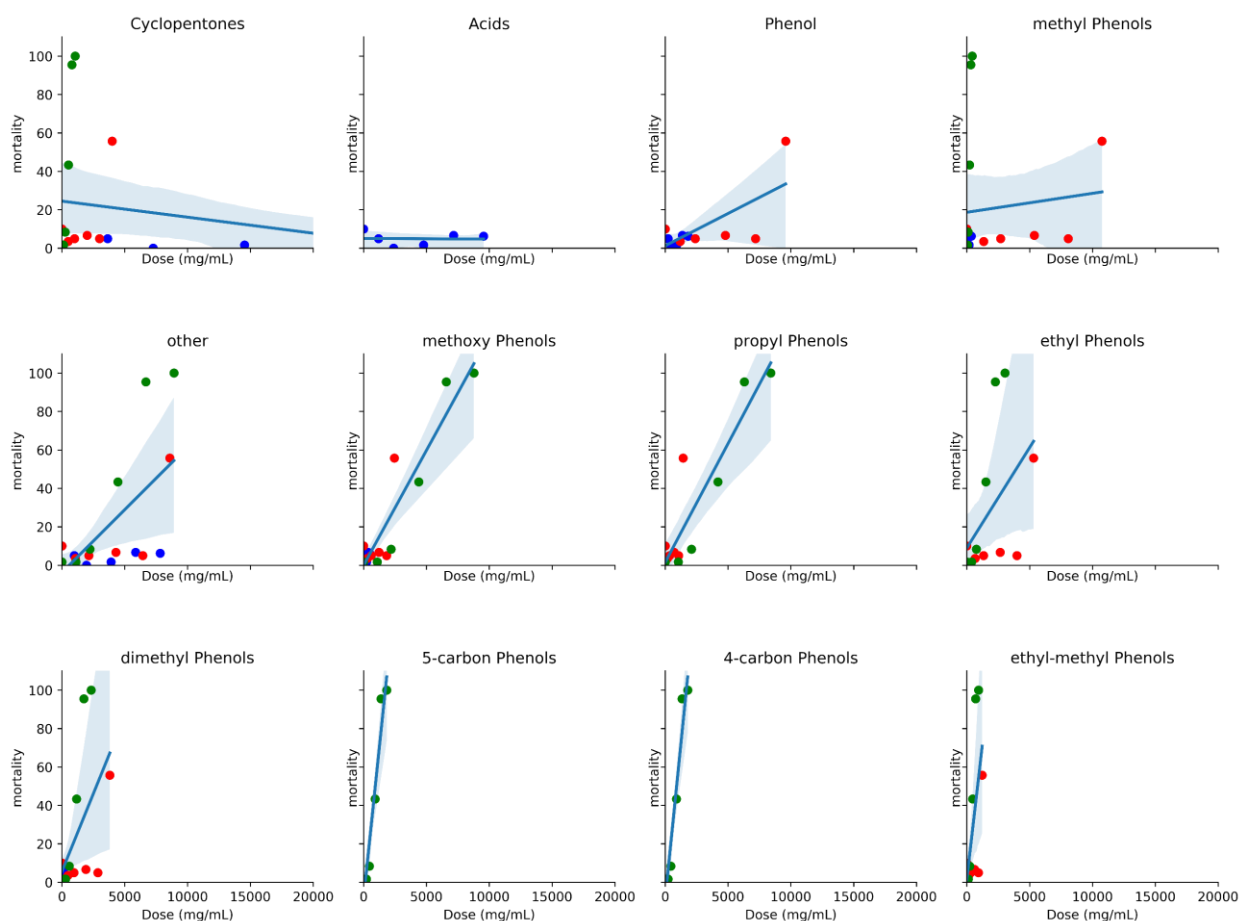


Figure 19: Correlation between dose and mortality of compounds in CFP distilled fractions: blue dots (130-180°C), red dots (185-230°C) and green dots (230-250°C)

These promising results also confirmed that lignin monomeric fragments have the highest efficiency towards insects' mortality and can be taken in consideration as active ingredients for bio-based pesticides. The fact that heavier phenolics molecules are more suitable for this application have been confirmed by other authors in studies on the effect of alkylation of compounds such as eugenol.^{53,176,200}

Techno Economic Analysis: impact of product purity and yield to the MPSP

The experimental campaign on bioassays and the further data analysis highlighted the effective insecticidal activity of alkylphenols with 3 to 5 carbon in the substituted group. Therefore, a CFP plant Aspen Plus® model described in previous studies^{10,192}, was modified in order to include an extraction step for these compound class. Figure 20A and Figure 20B depict the general model concept. Briefly, after the pyrolysis reactions and catalytic upgrading, the organic vapors are further condensed in a fractional condenser that separates roughly heavies from light compounds. In this model, the light fraction, containing most of the target species, was sent to a two-step distillation unit. The first distillation column separates the lighter phenols such as phenol and cresols that are sent back to the whole CFP oil stream. While the bottom part, rich in heavier compounds, is sent to another distillation column for the separation of the targeted phenols (C3-C5) (Figure 20B). The remaining heavy-residual fraction from the bottom of the second distillation column is back mixed with the whole CFP oil stream.

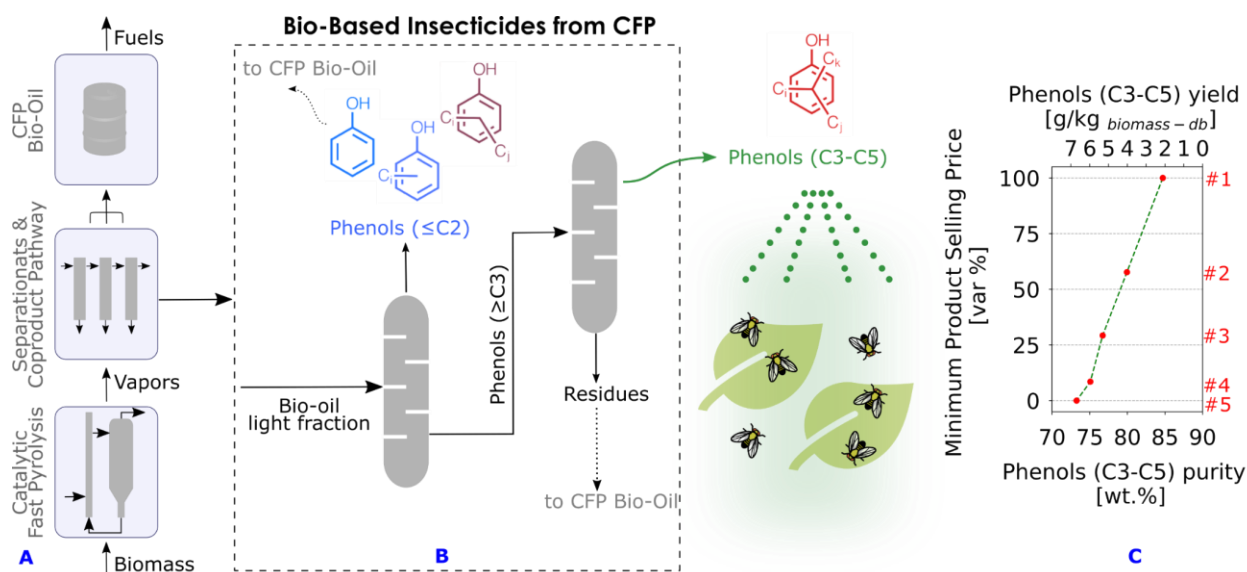


Figure 20. Modelled process and MPSP analysis for the extraction of alkylphenols (C3-C5) mixtures for bio-based insecticides: general model process flow (A), distillation columns for extraction of compounds from light fraction of CFP oil (B) and MPSP variation correlated to product yields and purity.

Five different simulations have been carried out varying the amount of CFP oil used for the extraction of co-products. This flow rate was varied between 430 kg/h and 820 kg/h over a total CFP oil flow of 17911 kg/h. The base case was defined as the lowest mass flow rate (#1 in Figure 20C) and the distillation columns were designed to optimize the purity of the extracted mixture. Increasing the co-products mass flow rate (from point #1 to #5 in Figure 20C), the yield of the co-products stream increases from 2 g/kg of biomass to 7 g/kg of biomass, while the purity of alkylphenols (C3-C5) decreases from 85% to about 72%. This is the expected consequence of the fact that part of lighter alkylphenols are not extracted in the first column and are then recovered together with the target compounds in the second distillation section, reducing the product purity.

Regarding the MPSP calculation, an important assumption has been made: the CFP oil value remained unvaried removing a fraction of the organic from the stream for alkylphenols extraction. This approximation considers that the mass flow rate extracted in form of alkylphenols with 3 to 5 carbon in the alkyl chain is only a small fraction (2 to 5 wt.%) of the main CFP oil stream. The MPSP, reported in the ordinate of the plot in Figure 20C, was found inversely proportional to the flow rate and thus minimized at high yield and low purity, however always in the range of common values for phenols (1-4 \$/kg³⁸). The model output suggests that the economical optimum is not aligned with the product purity. Improving the purity means increasing the concentration of the proposed active molecules for insecticides and thus, a lower product concentration in the final product formulation. Lower purity corresponds to higher yields at a reduced MPSP. However, at the same time, higher purity means a smaller number of compounds that needs to be registered as pesticide for regulatory scopes and potentially reduce the cost of toxicity tests. All of these considerations need to be further addressed for commercialization purposes, in order to minimize also the indirect costs associated with the whole pesticide manufacturing process and registration.

Supply chain GHG emissions and energy demand for bio-based active ingredients from CFP biorefineries.

Starting from the CFP Aspen Plus® model outputs, a life cycle inventory (LCI) has been extrapolated and used as input in the MFI tool for the evaluation of the GHG emissions and energy demand of the bio-based insecticides supply chain. The LCI is the same contained in Dutta et al.¹⁹² (2020 Co-HP Projection) without the section relative to the petroleum refinery hydrotreating, and it has been modified introducing the co-products bio-derived insecticides streams for the same five different conditions previously showed. The bio-based thermochemical co-products has been compared to traditional active ingredients commonly produced for insecticides. Pyrethroids are the commercial synthetic version of pyrethrins previously developed and used as pesticides from the extracts of flowers (e.g. *Chrysanthemum cinerariaefolium*).²⁰¹ Pyrethroids are broad-spectrum of traditional insecticides, effective against a wide range of flying, crawling, chewing, and sucking insects, that can be found in household insecticides, as grain protectants, and to control pests on edible products just prior to harvest.²⁰² The commercial production of synthetic pyrethroids started with around 1950 and the classic pyrethroids are esters of cyclopropane carboxylic acids with alkenylmethyl cyclopentenolone alcohols.²⁰³ Even though pyrethroids are biodegradable and photo sensible, the two main concerns about these substances are related to toxicity in aquatic environment²⁰¹ as well as the use of ozone depletion substances such as bromochloro methane (BCM) for the production of cyclopropanes or chlorofluorocarbon (CFC-113a) used for the manufacturing of Lambda-cyhalothrin^{204,205}, that is a registered agrochemical pyrethroid insecticide. Organophosphates are another class of common insecticides extensively used in agriculture, homes, gardens and veterinary applications. Although their high insecticidal activity, several of these substances are considered as highly toxic and have been discontinued (e.g. parathion or chlorpyrifos).²⁰⁶ Organophosphates are usually produced by esterification between phosphoric acid and alcohol.²⁰⁷ Although the demonstrated insecticidal activity, these compounds and their by-product might have high environmental issues as contaminant in the soil, leading to loss of fertility as well as soil acidification, nitrate leaching, resistance of weed species as well as the consequent loss of biodiversity.²⁰⁸ Among several organophosphates-based commercial products, malathion is an approved substances in many developed countries, including EU and US.^{209,210}, due to its low toxicity to mammals and birds as well as a shorter life in aquatic environments and soil (less than a week). In this section a comparison of bio-based alkylphenols mixture has been made, focusing on the energy and GHG emission of the overall supply chain, further investigations are needed to address the toxicity on humans and not-targeted compounds, of these bioderived insecticides.

Figure 21 shows the results in term of overall GHG emissions in kgCO₂e/kg of product, in order to compare the emissions based upon the global warming potential. The highest GHG emissions were estimated for the pyrethroids, with about 42 kgCO₂e/kg, followed by organophosphates (15 kgCO₂e/kg). On the other hand, the CFP bio-derived insecticides resulted in a lower GHG emissions level with a minimum of 5.1 kgCO₂e/kg when larger production was modelled (#5 in Figure 21A and Figure 20C). Observing the single contribution of process fuel, the organo-phosphate compounds production has a lower impact compared to pyrethroid, while about same level of 2.7 kgCO₂e/kg can be obtained with the bio-based products at the highest production rate (#5 in Figure 21A and Figure 20C). Regarding the emissions associated with the electricity generation, high contribution are noticeable for traditional insecticide manufacturing (4.1 kgCO₂e/kg for organophosphates and 6.4 kgCO₂e/kg pyrethroids), while for the products of CFP biorefinery only negative contribution are present. This is due to the fact that a CFP biorefinery produce an excess of electricity as co-products (about 20 MW in the FY19 model¹⁹²) that reflects as negative contribution in the overall

GHG balance. Emissions due to transportation have lower impact but still higher in case of traditional pesticides compared to bio-based thermochemical insecticides.

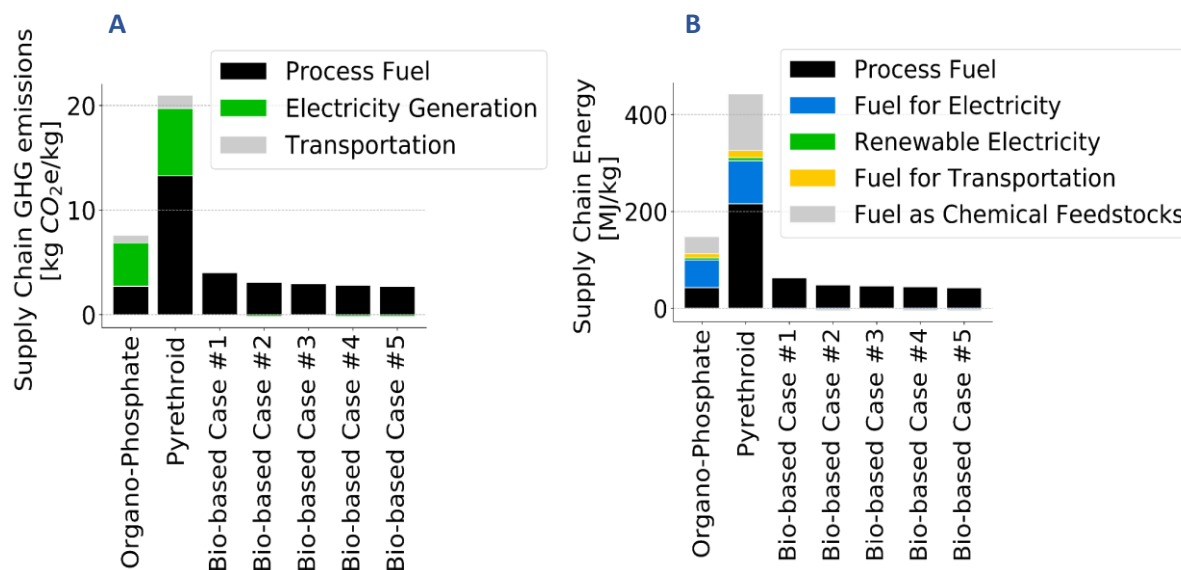


Figure 21. Supply Chain GHG emissions (A) and energy consumption (B) of bio-based active ingredients from CFP co-products at different purity and yields compared to fossil-based commercial active ingredients insecticides

The energy consumption of the supply chain can be observed in Figure 21B, and it reflects the GHG emissions distribution. Pyrethroids account for the highest energy demand, with a total of 886 MJ/kg of product, distributed as process fuel (216 MJ/kg), fuel as chemical feedstock (117 MJ/kg), fuel for electricity (88 MJ/kg), fuel for transportation (74.7 MJ/kg) and renewable electricity (6.5 MJ/kg). While lower specific energy is needed for the production of organophosphates, with a total of 296 MJ/kg and highest contribution of fuel for electricity (57 MJ/kg), followed by fuel for process (42 MJ/kg), fuel as chemical feedstock (35 MJ/kg) and lower values for transportation (8.6 MJ/kg) and renewable electricity (4.2 MJ/kg). Looking at the biorefinery data, the energy required is mostly associated with the process fuel, accounting for values between 42 MJ/kg and 62 MJ/kg, depending of the product yield and purity. Also, in this analysis, the electrical energy required is taken directly from the excess of electrical power of the biorefinery (that is implicitly renewable) and a negative contribution of the “fuel as chemical feedstocks” that comes from the production of acetone as by-product in the CFP model. This means that for the amount of acetone produced by the bio-insecticide process, there is a credit in energy/GHG impacts equal to the supply chain level impacts and the MFI estimates from the production of that same amount of acetone from conventional sources. The contribution of transportation fuel is also very low (less than 1.0 MJ/kg). Therefore, the substitution of traditional insecticidal products with bio-based mixtures derived from thermochemical CFP biorefineries clearly shows benefits in term of energy consumption and consequent GHG emissions. This also confirm that the switch toward a circular green economy is possible with positive environmental impact in term of global warming limitations.

Biorefinery size considerations

Bio-based active ingredients from CFP of lignocellulosic biomass has been demonstrated as a viable route for substituting traditional agrochemicals. The TEA model results in term of yield, purity and MPSP and the subsequent LCA study were obtained considering the NREL FY19 model based on a CFP plant with a capacity of 2000 tonnes

of dry lignocellulosic biomass as feedstock. This size was estimated in US as the best compromise to minimize the minimum fuel selling price (MFSP) of a CFP plant after several previous studies. For each different flow-rates investigated in this work (conditions #1 to #5 in Figure 20C) a different total phenolic mixture production can be obtained, ranging from 2.6 to 4.3 kTA, as depicted in Figure 22. According to a FAO statistic, the global pesticide demand in 2017 was about 4114 kTA¹⁵⁶, then considering that insecticides represent about 17% of this market^{173–175}, the total demand of insecticides is about 700 kTA. The production from a single 2000 tonnes per day CFP plant would produce about 0.6% of the total insecticides demand, thus a very low market saturation is foreseeable in the future. As a consequence, positive and smooth growth is expected, especially where green policies are reinforced.

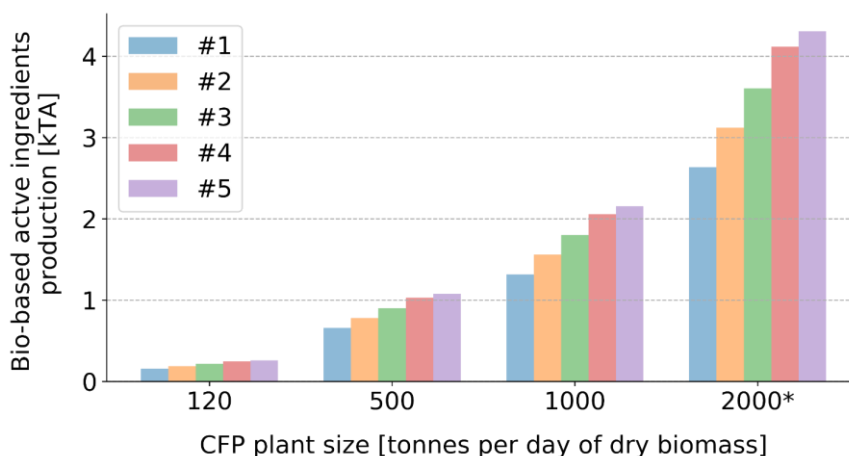


Figure 22. Bio-based insecticidal active ingredient production varying CFP plant size with co-products directly in place on the CFP plant. *NREL FY19 model baseline

In different places around the globe discussions and model are ongoing, to evaluate the best biorefinery plant size. The central issue is the centralization or decentralization of fast pyrolysis biorefineries, with cost differences mainly related to the feedstock transportation to the conversion plant as well as the economy of scale.^{211,212} The economy of a higher capacity centralized plant will be positively impacted economy of scale, however biomass availability and transportation of feedstock for long distances has to be taken in consideration also for the environmental impact of traditional road transport. While decentralized solutions, where CFP oil is produced and then sent to a central further refining unit (e.g. co-processing in existing petroleum refineries), would have higher operative plant costs but offering reduced costs of feedstock transportation as well as an energy densification and the consequent reduction of specific GHG emissions. In addition, decentralized solutions would have a different impact on our society, generating employments in rural areas and consequently spreading the population outside of already over-populated cities around the world. There is no definition of a specific capacity for a centralized/decentralized classification due to different geographical distributions of biomass as well as the choice of the feedstock. When decentralized are adopted, two options for the extraction of bio-based insecticidal active ingredients as co-products are possible: one is to separate the target molecules from the CFP oil directly on sites and the other is to separate them on the centralized refining unit together with bio-oil upgrading. The first solution would produce a lower volume of final products per plant as depicted in Figure 22. Moreover, larger costs associated with smaller distillation columns can be expected. In alternative, a better solution can be the co-products extraction on centralized units, shipping the produced bio-oil to higher size distillation columns. Decentralized facilities producing CFP oil will be even more attractive when co-

hydroprocessing is considered due to economic advantages of this process at larger scale. Comparing the active ingredients volumes from a 2000 dry tonnes per day to the one derived from a smaller 120 dry tonnes per day, about 17 decentralized CFP plants are necessary to reach a similar volume of products. The 2000 dry tonnes per day conceptual refinery is considered as standard benchmark size in US after some previous studies²¹³, however lower size is expected for first installations. To sum up, the optimal condition should be selected depending on geographical and biomass availability aspects, as well as through detailed economic and environmental investigations on the impact of the different approaches.

Regulatory Environment for the introduction of new pesticides formulations into the market

After showing that extracting active ingredients as co-products of CFP biorefineries is economically feasible with less environmental impact than commonly used active ingredients, it is important to clarify the complexity of the introduction of new active ingredients and insecticide formulation into the market. The overall process requires large investment and timespan of several years. In this regard, it is also important to mention how regulatory frameworks are defined, especially in developed countries such as EU and USA. The pathway of commercialization of a new pesticide depends strictly on national and local policies. Each country around the world has its own regulatory process with some similarity, especially regarding the toxicity evaluation. The obvious consequence is that national market can be developed where favorable policies are leading to higher and faster developments of bio-based pesticides, while in other countries with more restricted regulations the development of new greener pesticides formulations remains restrained, thus limiting the synthetic fossil-based pesticide substitution. These not homogeneous regulations and directives between countries also limit the international market expansion of both pesticides and crops-derived products. However, it is important to consider that the active ingredients present in the pesticides always needs to have minimum toxicity to humans or not-targeted animal species, as well as low retention in the soil and water for environment protection. Thus, less restrictive regulations do not directly imply less compliances with environmental and health rules. On this topic, bio-based molecules, such as the ones extracted from fast pyrolysis liquids, can potentially have several advantages in term of toxicity and biodegradability compared to complex fossil-based synthetic ingredients and consequently be more easily approved as substitute in the pesticide market.

Regarding two specific regulatory frameworks, US and EU have significative differences especially for bio-derived active ingredients. In US, EPA classifies Biopesticides three classes of compounds: naturally occurring substances that control pests (biochemical pesticides), microorganisms that control pests (microbial pesticides), and pesticidal substances produced by plants containing added genetic material (plant-incorporated protectants) or PIPs.²¹⁴ Biochemical pesticides are considered naturally occurring substances with a non-toxic mode of actions regarding the pest control, while microbial pesticides includes fungus, bacteria or viruses as active ingredients. The last class of PIPs are pesticidal substances directly produced by the plants from genetic material previously added to the plant.²¹⁵ In US pesticides (both synthetic and bio) needs to be registered and approved by EPA before being commercialized as specified in Pesticide Registration Improvement Act of 2003 (PRIA) that amended previous federal laws (e.g. Federal Insecticide, Fungicide, and Rodenticide Act – FIFRA). The EPA registration process include the examination of the active and inactive ingredients and the site/crop where the pesticide will be used.

Moreover, EPA examines the amount, frequency and timing of pesticide use as well as storage and disposable practices. Most important, the EPA evaluate through a low-risk assessment, the hazard of the formulation to humans, wildlife, fish and plants including non-targeted organisms as well as the contamination of soil and water. Hence, prior

to start the evaluation process EPA requires toxicology and ecotoxicology analysis including studies on animals.^{173,216} The Biopesticides and Pollution Prevention Division (BPPD) is responsible for the risk assessment regarding biopesticides. In addition, EPA defined some criteria to include ingredients in a “minimum-risk” category for substances that represents little risk to health and environment exempting that from regulations under FIFRA. Several natural extract or molecules falls under this category such as some essential oils and Eugenol.²¹⁷

Regarding the other inert ingredients present in pesticides formulations, EPA specifies substances that are allowed to us in food or non-food crops as well as fragrance ingredients. The compounds defined in the fragrance list can be used for nonfood crops. In this regard, many phenolic substances such as alkylated phenols or methoxyphenols are already approved for fragrance use.

On the contrary, EU does not differentiate biopesticides as a regulatory category and biopesticides, as well as synthetic pesticides active ingredients and products compositions are regulated case-by-case.²¹⁸ Regardless the nature of the substances, new pesticides formulations must follow the EU Reg. No. 1107/2009 and from 2014, through the Sustainable Use Directive, other restrictions were implemented forbidding the use of many more chemical active ingredients as well as pushing toward an improved integrated pest management (IPM) involving more ecological and efficient use of soil for crops.²¹⁹ Additionally, EU Reg. No. 540/2011 contains the list of all the active substances already approved in EU countries, while the standardized analytical evaluations about the toxicological, ecotoxicological requirements as well as the fate on the environment and the residual amount on food sources are regulated under EU Reg. 283/2013 and EU Reg. 284/2013 for the plant protective products and active substances respectively. The labelling information for final products formulation entering the market are published in the EU Reg. 547/2011. Moreover, the EU regulations expressly requires the grade of purity of the active substances. Impurities are considered relevant and significant when the concentration in the formulation is higher than 1 g/kg. This may reflect on the grade of purity required by the separation strategies proposed in this work. Moreover, the organic mixtures extracted from CFP oil may contains different isomers under the same class, and EU regulations requires to report the ratio or the ratio range of the content of isomers as well as the relative biological activity of each isomer. EU regulations impart restrictions forbidding the use of many chemical active ingredients and push towards integrated pest management (IPM) that involve more ecological and efficient use of soil for crops. (Integrated Pest Management (IPM)| Food Safety). The organism that verify the safety of the active substances in EU countries is the European Food Safety Authority (EFSA) that is responsible of the peer review process for the approvals and registration of active substances used in plant protection products, evaluating the applications dossiers for new registration or re-evaluations of active substances and PPPs²²⁰. EFSA has not any regulatory functions but is only in charge of the risk assessment. This is one of the main differences with US system, where EPA has the control over the whole process with legal powers, while EFSA delivers only scientific evaluation on the health and environmental risks^{221–223}. The approval process for active substances in EU follows a complex procedure where the applicant submits an approval proposal to an EU country called *Rapporteur Member State (RMS)* that verifies the admissibility of the proposals as well as prepare a draft assessment report. EFSA review the application and further decisions have to pass through the Standing Committee for Food Chain and Animal Health that votes on approval or non-approval of the substances. The last two steps involve the adoption of the decision by the EU Commission followed by the publication on the EU Official Journal. The EU guidelines suggests a period of minimum 2.5 to 3.5 years between the date of the admissibility of the application to the final decisions and publications. Therefore, EU approvals are comparatively longer than the US, but recently the EU Commission is introducing a new regulation for low-risk substances to

promote sustainable plant protection, low-risk solutions and efficient risk mitigation and consequently improve the biopesticide market, together with a strengthened expertise in Member States for the assessment of applications for biopesticides through training initiatives called Better Training for Safer Food (BTSF)¹⁶⁶. Further changes may be introduced through legislation, driven by the European Green Deal, that aim to zero net GHG emissions in the EU by 2050. The EU commission explicitly states that strategic plans are to adopt strategies to drastically reduce the use and risk of chemical pesticides, targeting a reduction of 50% by 2030 and pushing towards a goal of 25% of organic farming.²²⁴ The use of natural substances is the global backbone of the organic farming in order to limit the overall health and environmental impact of agriculture. The extraction of bio-derived agrochemicals from thermochemical biorefineries can represent a potential strategy also in organic farming perspectives. Regulations in EU and USA already includes a series of natural substances already allowed to be used in organic farming, such as plant essential oils (Annex II - Regulation (EC) No 889/2008 and EPA - The National List of Allowed and Prohibited Substances (National List) contained in 7 CFR part 205). Therefore, the possibility of introducing substances derived from biomass sources through CFP in organic farming should be addressed, considering the general lower impact on environment and health hazard of the target species highlighted in this study. For both US and EU markets, biobased pesticides may play a significant role in future pest management systems which will be dependent on navigating the evolving regulatory landscape.

2.2.4 - Conclusion and future development

The work conducted on the evaluation of co-products from CFP biorefineries to be used as agrochemicals insecticides showed some significant advancement in term of substitution of traditional pesticide manufacturing. Fractions of organic mixtures were obtained through distillation of CFP oil, up to 250°C. The distillation cuts obtained in the temperature ranges at 130-185°C, 185-230°C and 230-250°C were used in bioassays to investigate the potential activity as insecticide toward specific pests (*spotted winged drosophila*). Direct and indirect 24h contact tests showed that the highest insect mortality activity at the lowest dose was achieved with the fraction 230-250°C, followed by the fraction 185-230 that showed activity only at higher dose. Looking at the fractions compositions, the cut at 130-180°C included mostly light carboxylic acids (i.e. acetic acid) and cyclopentenones, while the 185-230°C cut contains high percentage of phenol and cresols (about 20 wt.%) as well as heavier alkyl phenols with 2 carbon in the functional groups (another 10wt.%). The fraction 230-250°C instead, was composed by mainly heavier phenolic species, including alkylphenols with 3 or more carbon in the substituted group as well as methoxyphenols (e.g. guaiacol and alkylated guaiacols). Therefore, it was hypothesized that phenolic species are responsible of such activity, being the only class comprising the 230-250°C and partially the 185-230°C cut with lighter phenolics. The investigation continued through a data analysis used for extrapolating correlations between each compound dose and the mortality of the fraction. The results showed that the highest linear coefficient of the correlating slopes was obtained for alkylphenols with 3 to 5 carbon in the functional group, thus confirming the hypothesis that the functional group is probably the main leader in the insecticidal mortality mechanism, as previously suggested by other works. Once identified that phenols (C3-C5) have the highest potential to be used as insecticide, a technoeconomic analysis was carried out to estimate the minimum product selling price (MPSP) and its variation with mixture purity and yield. The minimum value was obtained at the highest yield (7g/kg of biomass) and lowest purity (72 wt.%). However, the lower mixture purity potentially leads to a lower activity at the same dose, meaning that higher concentration would be

needed in the product formulation. The final optimization can be done only after more detailed model compound studies on the effect of the proposed active molecules as well as the co-operation effects of model compound mixtures. Nevertheless, the effect of every other compound here considered as impurity needs to be addressed singularly in order to define if these “other” molecules can be considered as inert ingredient (e.g. fragrance additives). Moreover, the mixture purification will need further investigation in order to narrow down the distillation temperature range and better evaluate the samples composition as regard to the undetected portion. Further CFP oil distillations have been already carried out to increase the number fractions reaching higher temperature and evaluate the insecticidal activity of heavy compounds (such as 250-270°C fraction in Figure 23) and further investigations are needed on the insect bioassay.

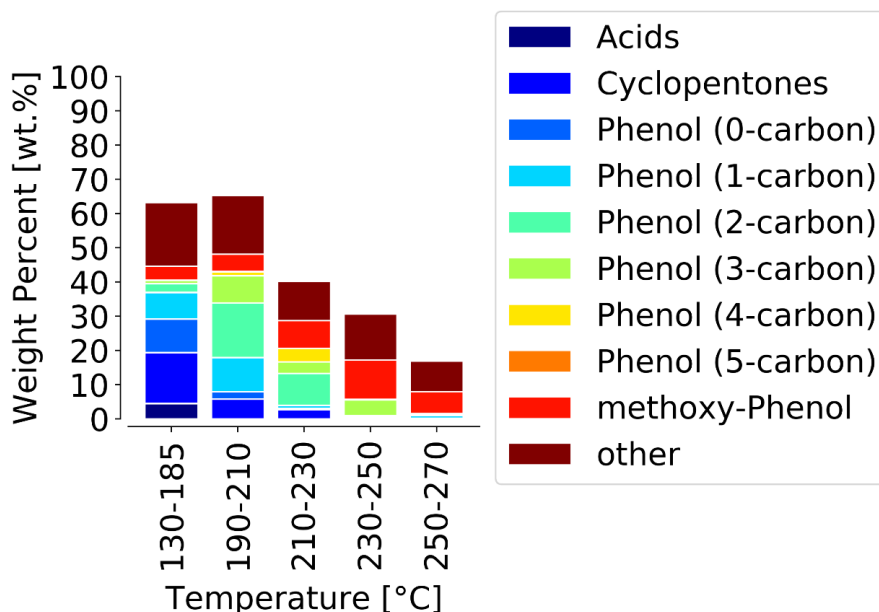


Figure 23. Composition of CFP oil fractions for future investigations on smaller temperature range cuts and higher temperature limit (i.e. 270°C).

After the identification of the active species and the TEA, a LCA study was carried out to evaluate the environmental impact of the production of such phenolic mixtures in a CFP biorefinery compared to traditional active ingredients used in insecticides manufacturing. The results clearly showed that a lower energy consumption and a consequent lower GHG emissions per kilogram of product can be obtained with bio-based active ingredient extracted as CFP co-products. Moreover, the model showed negative GHG contributions due to the excess of electrical power available at the biorefinery. Even though the agricultural impact on the global CO₂ emissions is about 10% and the pesticide only a fraction of it, the switch toward the use of lignocellulosic biorefinery co-products will show large benefits on the regard of global warming. Most of all the extraction of bio-based natural substances from lignocellulosic sources, has potential benefits on the environmental impact substituting pollutant substances with naturally derived molecules. Obviously, further investigations are needed on the regard of the toxicity and side-effects of each compound. In this context, the regulatory frameworks in both EU and US requires a specific evaluation of the toxicity towards humans, animals and the environment (as groundwater or soil pollutant), making the registration process long and expensive. However, new regulations and drivers towards a bio-based economy (such as EU Green Deal) will potentially open the way for a faster technological development of such manufacturing processes, always with a severe control on the compounds' toxicity and hazards. Moreover, once identified an exact product composition, the production costs may

be reduced with a broader spreading of biorefineries around the world and therefore higher feedstock availability. In order to expand the CFP biorefinery commercial applications, a potential way for a near-term growth is represented by the integration with existing petroleum refineries through co-processing of CFP oil with fossil sources for fuel production. The next chapter will be focused on this, especially pointing the attention on one of the main technological barriers represented by the analytical evaluation of the biogenic renewable carbon in the final products.

2.3 - Pathway for commercialization of fast pyrolysis bio-intermediates: co-processing of bio-oils and petroleum-derived feeds in existing refineries and the need of advanced analytical techniques for biogenic carbon tracking

2.3.1 - Introduction

In the previous chapters, some potential routes for improving pyrolysis biorefineries for the conversion of dry lignocellulosic biomass into bio-intermediates have been addressed, evaluating potential route for pyrolysis vapors pre-treatment and fractional condensation to improve bio-oil quality. Moreover, co-production of bio-derived insecticides in a CFP biorefinery concept has been investigated through experimental and theoretical process modelling, considering a large-scale biorefinery. In order to improve the growth and commercialization of the CFP technology, and at the same time accelerate the insertion of renewable sources into the transportation fuels sector, a potential approach would be the integration of biorefineries into existing petroleum refineries through co-processing. In the last decades, studies on co-processing of bio-derived intermediates, such as bio-oil from fast pyrolysis, demonstrated the possibility of introducing renewable carbon into the existing fossil fuels infrastructures. In this section, co-processing of bio-oils into refineries will be presented starting from a general background, then highlighting the case of co-refining pyrolysis oils and vacuum gas oil (VGO) into Fluid Catalytic Cracking (FCC) units for the production of gasoline and LPG. Moreover, the main issue during co-processing is measuring the amount of biogenic carbon that ends up in the final liquid products as well as understanding how the renewable carbon is incorporated in the final molecules. The importance of this tracking is also related to the evaluation of side effects of introducing oxygenated compounds into processes that are optimized to deal with mainly hydrocarbons (e.g. coke enhancement, CO and CO₂ generation). Thus, micro-scale studies were carried out to address the biogenic carbon incorporation into final products as well as the into coke and CO₂. In addition, traditional biogenic carbon analytical methods will be discussed showing the evident limitations and proposing potential solutions in perspective of in-line refinery biogenic carbon measurement.

The transportation sector is one of the major contributors to the global anthropogenic GHG emissions that have an adverse impact on climate change and global warming. The CO₂ emissions from this sector are expected to grow due to increasing demand for transportation driven by growth in world population as well as economies for developing countries. Federal, state, and local governments are enacting policies and incentives to limit CO₂ emissions from the transportation sector. In the U.S., Congress created the renewable fuel standard (RFS) program to increase the share of renewable fuel to 36 billion gallons by 2022.²²⁵ Individual states in the U.S. enacted additional mandates such as the low carbon fuel standards (LCFS) and/or alternative fuel standards to help reduce carbon intensity from transportation fuels.²²⁶ The Airlines for America (A4A) set an ambitious goal of cutting CO₂ emissions in half by 2050.²²⁷ In Europe, the Renewable Energy Directive II (RED II) mandated that renewable fuels should increase to 14% of the total transport fuels by 2030.²²⁸ Thus, multiple efforts are underway to increase the share of renewable sources for transportation fuels to meet the increasing regulatory mandates.

Co-processing bio-derived liquids with petroleum-derived feedstocks in existing refineries is a cost-effective near-term approach for introducing renewable carbon in the transportation sector. Moreover, this approach utilizes existing infrastructure, which could simplify the potential technology implementation at a larger scale. The co-processing technology, in Figure 24, shows how it can generate products with a proportion of renewable carbon. The accurate quantification of biogenic carbon ending up in gasoline, diesel, and jet fuels is a key barrier that still needs addressing as refineries use this measurement to demonstrate compliance to local, state and government regulatory mandates.

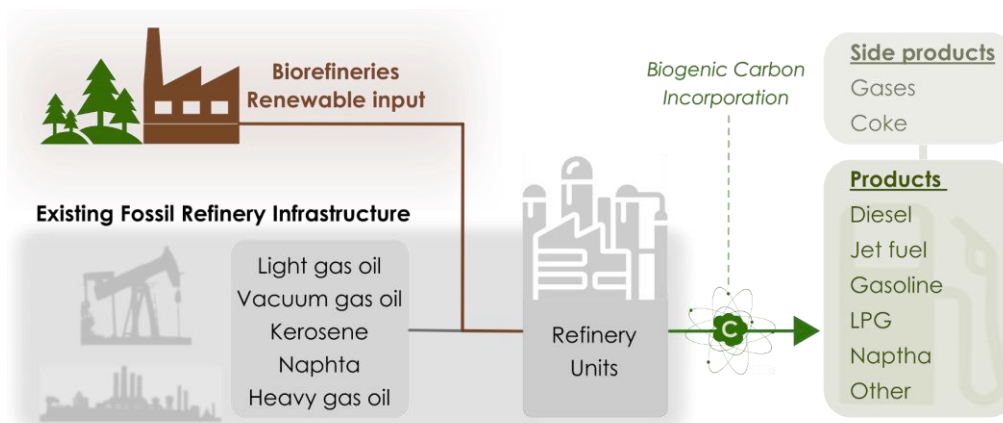


Figure 24. General scheme of co-processing of fossil and renewable sources in existing petroleum refineries

During the last decades, technologies for the conversion of biomass have been investigated to produce bio-derived molecules suitable for fuels. Among several renewable sources, lignocellulosic biomass presents unusual characteristics that make it suitable for advanced biofuel production while avoiding conflicts with food crops. Moreover, it is the most abundant biomass on earth with an estimated annual total global production of 182 billion tonnes of which 7 billion tonnes are currently harvested for energetic purposes.²²⁹ A viable option for converting lignocellulosic biomass into liquid fuels is represented by thermochemical conversion processes, such as fast pyrolysis (FP).^{27,32} Among different approaches, FP is an efficient process that leads to the production of high yields of liquid bio-oil (up to 80 wt.%) through the deconstruction of the lignocellulosic biomass matrix.²⁷ Raw bio-oil has high oxygen content and high acidity as well as chemical instability from these properties that make it incompatible to be directly used as conventional fuels substitute or in blends. Thus, vapor or liquid upgrading is needed to improve the overall quality. Different approaches have been investigated and among them, *ex situ* or *in situ* catalytic fast pyrolysis (CFP) as well as hydrotreating (HT) have shown the most promising results.^{31,99,134,185,230–234} Although petroleum refineries could potentially dedicate whole upgrading sections, such as hydrotreaters, to bio-intermediates the capacity of existing hydrotreaters is approximately an order of magnitude larger than the actual commercial production of bio-oils in a fast pyrolysis plant.⁵⁵ The FP bio-oil volume could grow substantially with further development and product demand; however, existing refinery infrastructure would be more economically utilized with a mixed feedstock of biogenic and fossil carbon sources.

Petrochemical refinery design configurations vary widely, and many are highly complex. Identifying suitable insertion points for the bio-derived liquids is key to the successful implementation of the co-processing approach. Bio-derived liquids have different compositions and oxygen contents. For example, FP bio-oils contain 36-55wt.% oxygen, have carboxylic acid (CAN) contents of 40-100 mg KOH/g, a total acid number (TAN) in the range 100-200 mg KOH/g

and about 5 mmol/g of reactive carbonyls, while catalytic fast pyrolysis (CFP) and/or hydrotreated (HT) oils have 1-25wt.% oxygen contents, <1-50 mg KOH/g CAN, up to 10-200 mg KOH/g TAN and 0-2.5 mmol/g of reactive carbonyls.^{141,151,197,235-238} As a result, FP oils and CFP/HT oils should be upgraded to hydrocarbon fuels using different operating conditions and, therefore, co-processed in refineries using different unit operations. Previous reports identified hydrotreaters/hydrocrackers (HT/HC) or fluid catalytic crackers (FCC) as suitable insertion points for bio-derived liquids.^{55,239,240} A recent review reported challenges and opportunities for co-processing FP oil, CFP oils, and FP-HT oils with vacuum gas oil (VGO) in an FCC and concluded that this technology is viable after minor reactor modifications.³³

The key challenge that needs addressing to meet regulatory mandates is being able to accurately measure the amount of biogenic carbon ending up in fuels. Further, studies on catalysts and reaction mechanisms have focused on the pathways of biogenic carbon incorporation into the final products emphasizing the importance of this tracking.^{61,66,67} In addition, in the last decades, the global bioeconomy on bio-products has grown considerably due to positive policies such as the U.S. Department of Agriculture (USDA) BioPreferred program launched in the U.S.²⁴¹ or the EU Bioeconomy Strategy.²⁴² Therefore, the production of bio-derived materials as well as fuel blendstocks has already highlighted the need for accurate bio-based content evaluation methods for certification purposes.^{243,244} In these applications, the biogenic carbon content is evaluated through carbon isotope analyses to differentiate between fossil and modern carbon.²⁴⁵⁻²⁴⁸ These techniques as well as simpler mass, carbon, and energy balances have been also used in refinery co-processing studies to account for biogenic carbon incorporation into liquid products.²⁴⁹ The interpretation of results from the simpler techniques are intuitive for co-processing operations (e.g. hydrotreaters and hydrocrackers) but with several limitations. Biogenic carbon incorporation can be calculated by difference from historical carbon efficiencies for hydrocarbon streams; differences in carbon efficiencies during co-processing can be attributed to contributions from the biogenic feed material. However, the calculations become more complex for more complicated operations such as FCC units. Carbon fed into an FCC unit can either show up as fuel and gas products from the reactor, or as products from the combustion of coke deposits on the catalyst in the regenerator. A simple calculation attributing the product yield difference to biogenic material is not accurate, due to potential impact of the introduction of bio-intermediates liquids that contains biogenic carbon and high amount of oxygen as well. The oxygenated biogenic feedstocks have different reaction mechanisms for product and coke formation compared to hydrocarbon feedstocks and thus have different product yield profiles that vary even within biogenic feedstocks with different oxygen contents. Moreover, the presence of oxygenated species may cause changings in the reaction mechanisms of petroleum compounds as well as impact the operating conditions of the unit, thus the baseline yield measurement for the petroleum stream only may be no longer valid. Even though the yield difference approach is valid if one takes a wholistic view regarding the overall product yield changes, the results could lead to different answers compared to the actual measurements of biogenic carbon in the products. Therefore, analytical post-reaction measurements will be simpler in such overall yield-based systems but will still need to be designed and deployed for continuous mass balance/yields validation of calculations and to help account for shifts associated with feed composition and operating conditions.

Among the direct measurement techniques, analysis of radiocarbon ¹⁴C has been adopted as an ASTM International standard (ASTM D6866-20²⁵⁰) and the methods described have been approved by certain regulatory agencies such as the USDA and the Environmental Protection Agency (EPA) in the United States for verifying biobased content²⁵¹. Even though the traditional radiocarbon analysis techniques described in the ASTM D6866-20, “Accelerated Mass

Spectrometry (AMS, Method B) and Liquid Scintillation Counting (LSC, Method C),” are well-established and fairly robust methods for several applications, they show some limitations in terms of costs, complexity, and analysis time. As a result, there are a limited number of laboratories capable of performing these techniques, primarily universities and research facilities. The current state-of-the-art analytical techniques are largely unsuitable for real-time process monitoring directly in a petroleum refinery or in-field analysis of fuel products. To assist in process optimization for renewable carbon utilization and accelerate adoption of co-processing of renewable feedstocks, targeted efforts are needed to develop on-line/in-field deployable measurements of biogenic carbon directly in refinery sites.

This perspective section reviews current analytical techniques used for quantifying renewable fuel components in finished fuels produced by co-processing, discusses short-comings, pain-points, and opportunities for developing advanced rapid on-line analytical methods. We will first review state of the art methods used for biogenic carbon measurements and then propose potential solutions for in-line refinery measurements when co-processing, individuating also the most appropriate measurement zones in refineries. This work has also been published as a perspective scientific article.²⁵²

2.3.2 - Co-processing in refinery: the case of fluid catalytic cracking units

Petroleum refineries have the potential to accept renewable bio-intermediate liquids in three main units: HT, HC and FCC.^{239,240} Hydrotreaters are employed in petroleum refineries to eliminate heteroatoms (primarily sulfur) through catalytic reactions at high hydrogen pressure and high temperature. Hydrocrackers instead are used to reduce the molecular weights of the compounds while consuming hydrogen, with similar catalytic reactions but at more severe conditions and with specific bifunctional catalysts.²⁵³ FCCs also reduce molecular weights of heavier hydrocarbon streams, but without the need for hydrogen injection. An FCC as a point of insertion may be more attractive than HT or HC since no hydrogen is required in the process, but lower carbon efficiencies compared to HT and HC can offset those benefits. Deoxygenation of the biogenic feed for hydrocarbon production occurs via the production of CO and CO₂ and light dry gases (C1–C2 hydrocarbons) in an FCC either in the reactor or via the combustion of biogenic coke (that also contains biogenic oxygen) in the regenerator; this results in the loss of carbon as gaseous products⁶¹. Corresponding adjustments in FCC reactor conditions (e.g. temperature) may help drive more of the hydrocarbon feedstock towards desirable products. However, we don’t account for the overall gain when directly measuring biogenic carbon in the fuel products; efficiencies may be optimized if there is an incentive to account for the overall gain for the FCC reactor/regenerator duo, which also has benefits from an environmental standpoint. Catalyst optimization can potentially maximize the conversion of bio-derived oxygenated molecules reducing the formation of unwanted products (e.g. coke or non-condensable gases).^{66,254} FCC units can tolerate higher feed oxygen content compared to HT and can adapt more easily to feedstock variability compared to hydrotreaters, therefore, it seems a preferable first approach for co-processing of bio-oil in refineries.^{65,255} The choice of the insertion point is also related to local market considerations: FCC units produce gasoline range hydrocarbons as the main output while hydrocrackers (HCs) primarily produce diesel and kerosene range products; hence the selection of fuel type may be connected to a particular fuel market’s demand.²⁵⁶ In the U.S., the Department of Energy estimated that 8 billion gallons of bio-derived fuels can be produced in the existing 110 domestic currently active FCC units; therefore, it is possible to foresee utilization of this technology in the mid-term.²⁵⁷

A fair amount of experimental studies have been carried out in the past decades at both laboratory and pilot scale to address the potential of co-processing of lignocellulosic pyrolysis oil with vacuum gasoil (VGO) in an FCC⁵⁹⁻⁶⁵ while a more limited number of studies have investigated the possibility of co-hydroprocessing lignocellulosic bio-derived molecules and lipids in refinery units²⁵⁸. Stefanidis et al.³³, in a recent review article, detailed yields for FCC co-processing of three different types of pyrolysis oils: FP, CFP and hydrodeoxygenated (HDO) oils. Here, some results from previous studies have been selected. In addition to process output yields, these investigations measured the renewable carbon content in the products, which will be discussed further in the next paragraphs. The conversion of VGO in FCC units produces gasoline-range hydrocarbons as the main product, reaching about 50% of the total gasoline production in a refinery. In addition, other hydrocarbon mixtures are generated during the reactions, such as Liquefied Petroleum Gas (LPG), Light Cycle Oil (LCO), Heavy Cycle Oil (HCO or bottom) as well as coke and a mixture of light hydrocarbons.^{259,260} In general, FP and CFP oils as well as HDO oils have been demonstrated as suitable feedstocks for co-processing at 5-20 wt.% blends with VGO in FCC units for the production of liquefied petroleum gas (LPG), gasoline, and light-cycle oil (LCO) with slightly enhanced yields compared to baseline pure VGO processing, depending on the type of bio-oil treated.^{33,65}

Co-feeding bio-intermediates in an FCC produced largely similar product distributions but also some undesirable outputs due to higher oxygen content. Product distributions were found to vary based on the bio-oil type or blend percentage. Figure 25 shows product mass yields of the selected FCC co-processing studies with overall feed conversion in the range of 66-71%, defined as the sum of the yields in gases, LPG, gasoline and coke.

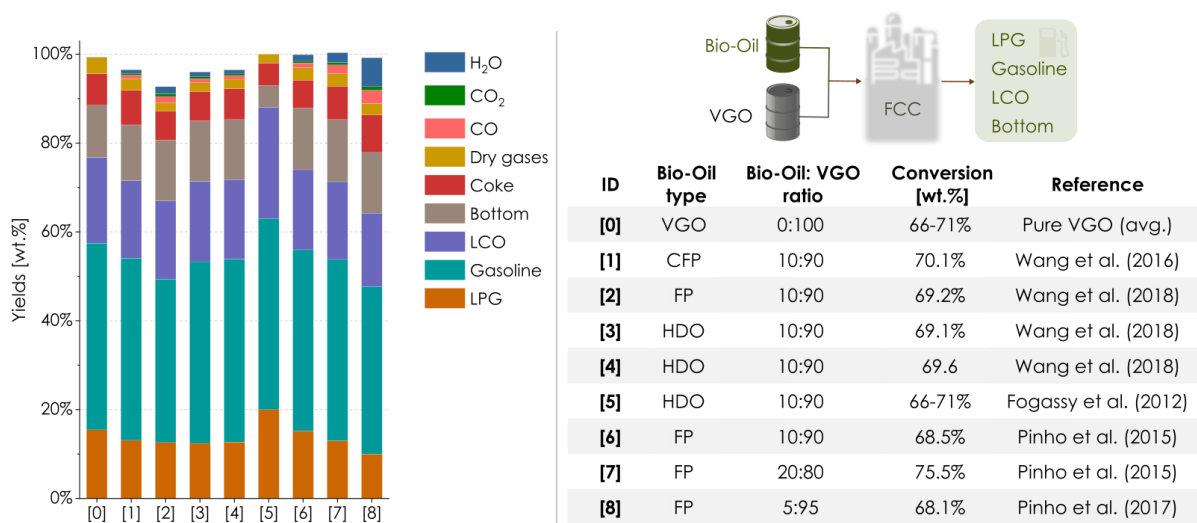


Figure 25. Products yields derived from selected studies on co-processing of VGO and pyrolysis oils. [1] Wang et al. (2016)⁵⁹, [2, 3, 4] Wang et al. (2018)⁶⁰, [5] Fogassy et al. (2012)⁶¹, [6, 7] Pinho et al. (2015)⁶², [8] Pinho et al. (2017)⁶³.

In two separate studies, Wang et al.^{59,60} investigated the conversion of VGO co-processed with FP, CFP and two types of HDO oil in a pilot-scale riser reactor using a bio-oil to VGO ratio of 10:90. The authors found a decrement in the gasoline yield when FP was co-fed, while higher gasoline yields were obtained with CFP or HDO oils. No substantial differences were identified in the other products. For all renewable feedstocks tested, a higher amount of CO and CO₂ was observed due to decarboxylation and decarbonylation of oxygenated species. Fogassy et al.^{61,261} reported similar gasoline yields when co-processing HDO/VGO blends, but higher LPG and LCO production, while a reduced

percentage of HCO was recovered. The experiments by Fogassy et al. were carried out in lab-scale fixed bed quartz reactors. Pinho et al.^{62,63} carried out FCC pilot-scale investigations reporting product yields when the ratio of FP/VGO was varied. Increasing the ratio from 5:95 to 10:90 and 20:80, the gasoline yields remained stable but a decrement in the LPG formation was observed as well as higher coke formation. In contrast to this, Wang et al. reported a reduction in the coke formation rate when FP or HDO oils were co-processed compared to baseline of pure VGO conversion⁶⁰. These studies demonstrated that higher percentages of oxygenated compounds lead to larger amounts of CO, CO₂ and H₂O. To sum up, partial upgrading of bio-oils (e.g. CFP or HDO) leads to slightly higher total yields of liquid products while coke formation remained at similar levels compared to FP co-processing as also found by Lindfors et al.⁶⁴. The effect of introducing bio-derived oxygenated compounds within refinery units, such as an FCC, can impact the composition and distribution of products. To enhance renewable carbon utilization, it is therefore important to track and understand how renewable carbon is incorporated into the final products as well as to evaluate the total amount which is lost as CO and CO₂. In one study⁶⁶, biogenic carbon incorporation was evaluated in a microscale reactor by cofeeding ¹³C labeled biomass pyrolysis vapors with VGO over two catalysts, one designed and optimized for FCC (E-Cat) and the other for catalytic fast pyrolysis (JM CP758). The results showed that the biogenic carbon was incorporated into alkenes and aromatic hydrocarbons and not in linear alkenes, while cycloalkanes contained biogenic carbon only when E-Cat was used. Another important result was that all the CO₂ generated during the reactions was composed of biogenic carbon as was the coke formed on the catalyst. From a refinery scale-up perspective, biogenic carbon tracking can be used to analyze and optimize renewable carbon incorporation, especially regarding the amount in value-added products. Hence, biogenic carbon analysis directly in refinery units would facilitate process design improvements as well as enhance understanding of reaction pathways for optimizing catalyst formulations for co-refining. Most importantly, it would be possible to consistently track the renewable share in the fuel products in compliance with the U.S. RINs system to get credit for introducing fuels from renewable sources into the market.^{262,263}

2.3.3 - Microscale studies on biogenic carbon tracking and incorporation

In another work⁶⁶, microscale studies were carried out to investigate the biogenic carbon incorporation testing ¹³C labeled oak biomass pyrolysis vapors together with VGO over two catalysts (E-Cat and JM-CP758). These experiments were conducted in a micro- pyrolyzer equipped with a GC-MS/FID system and a quartz annular reactor coupled to an online molecular beam mass spectrometer (MBMS). The results showed that the biogenic carbon is incorporated into alkenes and aromatic hydrocarbons and not in linear alkenes, while cycloalkanes incorporated biogenic carbon only when E-Cat was used as catalyst. More details on GC-MS evaluation of biogenic carbon incorporation into the hydrocarbons products can be found in a previously published paper (Mukarakate et al.⁶⁶). Another important result, that will be presented here in this section, was that all the CO₂ generated during the reactions was composed only by biogenic carbon as well as the coke formed on the catalyst. Even though bio-oils and not biomass will be the actual feedstock co- processed in refineries, this study provide insight into the fate of biogenic carbon and oxygenates and their impact on co- processing bio-oils with petroleum feeds in an FCC.

Material and methods

^{13}C -labeled oak was obtained from IsoLife BV 97%; VGO was provided by British Petroleum (BP); E-Cat was provided by Equilibrium Catalysts Inc.; and CP758, a ZSM-5-based catalyst, was provided by Johnson Matthey. CP758 was subjected to several reaction and regeneration cycles in a Davison circulating riser (DCR) reactor, upgrading biomass vapors until the effluent compositions were constant. The equilibrated form of CP758 zeolite was used in this work.

Horizontal Pyrolizer-MBMS

This reactor system was used to evaluate coke deposits on the catalysts during co-processing oak particles and VGO. The detailed description and application of the horizontal pyrolizer–MBMS (py–MBMS) in studying catalyst coking during catalytic upgrading of biomass was extensively discussed in other studies.^{264,265} Moreover the system has been already presented in Figure 9. Briefly, this system consists of a horizontal quartz annular flow tube reactor coupled with an MBMS. The tube reactor is housed in a four-zone furnace set to 550 °C. Three quartz boats each containing a mixture of 60 mg of VGO and biomass were introduced to the inner tube. The produced vapors and gases were carried by an inner helium flow of 0.4 slm (standard liter per minute) through a 1.5 g fixed bed containing 0.5 g of catalyst mixed with 1 g of inert coarse material to prevent excessive pressure drop across the bed. Helium (4 slm) flowed from the outer tube at the end of the reactor to dilute the cracked products, in order to prevent secondary reactions and meet the flow demands of the MBMS sampling orifice. In addition, 0.04 slm of argon mixed with the helium carrier gas provided a tracer gas to correct drift in the signal resulting from flow changes through the molecular beam inlet. The MBMS monitored real-time signals of the products. After adding three boats of the VGO–biomass mixture, oxygen was added to regenerate the catalyst and monitor the signature of CO_2 evolved during this process. Control experiments were separately conducted with neat VGO and oak to measure CO_2 . The co-processing experiments were then repeated, without regenerating the catalyst to collect spent samples for coke quantification by thermogravimetric analysis (TGA). The amount of residual coke deposited on the catalyst generated from the py–MBMS experiment was measured in a TGA Setaram (TN688, SETSYS Evolution) analyzer. The spent catalysts were heated in air at 20 °C min^{-1} from 25 to 780 °C. Two distinct mass loss peaks were observed with the mass loss from 250 to 650 °C attributed to coke, while that below 250 °C was associated with water and weakly adsorbed species.

Results and discussion

Reports show that co-processing bio-oils and VGO results in increased coke deposits on the catalyst.^{62,64} In order to identify and demonstrate the source of coke deposition, a series of py–MBMS experiments were conducted in which several VGO- ^{13}C oak mixtures were sequentially cracked over a fixed bed containing E-Cat at 550 °C and, after upgrading the mixture, oxygen was added to regenerate the coked catalyst.

Figure 26A shows ion signals for selected species generated during sequential catalytic cracking followed by oxidation of the spent catalyst. As shown, the first three pulses contain species separated into m/z 45, 44, and 32, and these are assigned to mixtures of hydrocarbon fragment ions (alkanes and alkenes) plus CO_2 (deoxygenation of biomass oxygenates). Oxygen was added after 9 min to burn off coke deposited on the catalyst. A signal at m/z 45 ($^{13}\text{CO}_2$) and not 44 ($^{12}\text{CO}_2$) increased rapidly (at about 9 min in Figure 26A) and then decreased gradually indicating that the carbon removed from the catalyst was essentially 100% biogenic. Additional evidence is provided when two similar experiments were conducted separately with VGO and ^{13}C oak. Figure 27B shows that a peak at m/z 45 is produced during regeneration of spent E-Cat after catalytic upgrading of ^{13}C oak. There was no peak observed during

regeneration of spent E-Cat after catalytic cracking of VGO, even after loading almost twice the amount of VGO as oak (Figure 27A). Experiments conducted with non-labeled oak showed a peak at m/z 44 during catalyst regeneration.

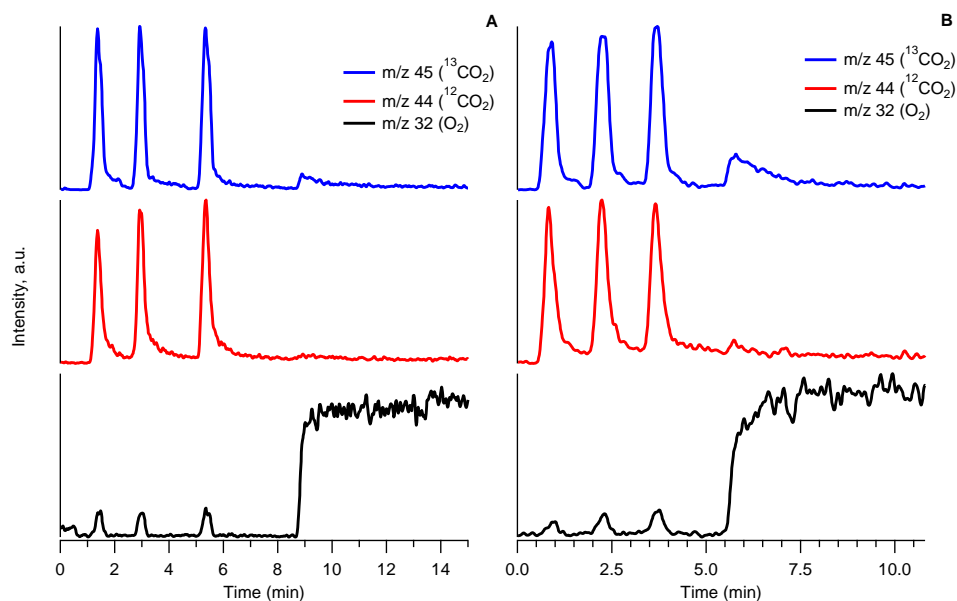


Figure 26. Ion signals of products from co-processing of VGO and ^{13}C oak followed by catalyst oxidative regeneration in the py-MBMS using (A) E-Cat and (B) CP758. Reaction conditions: VGO, 30 mg; oak, 30 mg; per pulse catalyst, 500 mg; temperature, $550\text{ }^{\circ}\text{C}$.

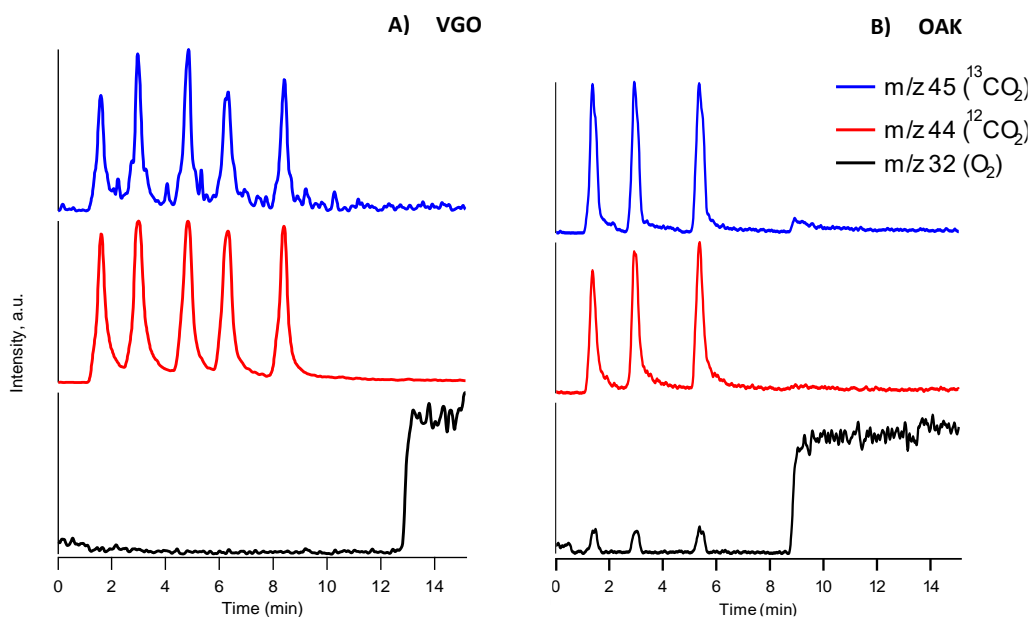


Figure 27. Ion signals of products from catalytic upgrading of A) VGO over E-cat and B) ^{13}C oak over E-cat followed by catalyst regeneration in the py-MBMS. Reaction conditions: VGO 30mg, oak 30mg, per pulse catalyst 500mg, temperature $550\text{ }^{\circ}\text{C}$

Figure 26B, from a similar experiment with CP758, also shows an intense peak at m/z 45 during catalyst regeneration, indicating that coke formed from this catalyst was mostly biogenic; a small peak observed at m/z 44 suggests that coke was also formed from ^{12}C constituent. Collectively, these data suggest that coke on E-Cat is formed on the surface of the catalyst. Coke on CP758 was formed in the micropores leading to contribution from the ^{12}C component and, as reported in numerous studies, from condensation of lignin and sugar oligomers on the catalyst surface.²⁶⁴ The experiments with both catalysts were repeated in order to quantify coke deposits using thermogravimetric analysis.

Table 6. Results from Addition of Steam to Oak CFP Using ZSM-5 Performed on the py-MBMS System

| Sample | Water mass loss [mg] | coke mass loss [mg] | % Coke on dry Coke free basis |
|--------|----------------------|---------------------|-------------------------------------|
| CP758 | 0.13 | 0.29 | 0.67 |
| E-cat | 0.045 | 0.35 | 0.60 |

Table 6 shows that the amount of coke deposited on CP758 was slightly higher than that on E-Cat. Thus, biomass-derived molecules are responsible for coke buildup during co-processing experiments.

The results of this study are a clear example of how the tracking of biogenic carbon can have an impact on the process optimization in a refinery process. Traditional methods of biogenic carbon tracking through ^{14}C measurement have been used for decades on many applications that requires a differentiation between renewable and fossil sources. However, they still have limited applications and issues on being used for refinery scopes. In the next sections a review of the traditional methods as well as a perspective development of new analytical technologies will be presented and discussed showing guidelines for the optimized integration between biorefineries and petroleum refineries.

2.3.4 - Established methods for measuring biogenic carbon

Regardless of the refinery insertion point, as previously mentioned, biogenic carbon tracking plays a fundamental role for the quantification of the renewable content in the final fuel products for both process optimization and regulatory compliance purposes. Accounting of biogenic carbon in liquid products in accordance with a regulatory framework is essential in order to validate credits for introducing renewable fuel volumes into the transportation market. Traditional tracking techniques can involve different approaches included in the International Sustainability and Carbon Certification Guidance (ISCC 203-01).²⁶⁶ Some basic approaches for the evaluation of the renewable share involve the comparison between mass yields during co-processing and the baseline with only fossil feedstocks as well as carbon yields or energy yields. One approach is based on the measurement of overall mass yields while another and more detailed is based on carbon yields, accounting also the gases production, such as CO and CO₂. While the approach based on the energy content considers that bio-intermediates have lower heating value (LHV) due to the presence of oxygen compared to fossil-derived feedstocks, then calculating proportionally the percentage of biogenic energetic share in the final products.^{249,267} These indirect approaches have evident advantages in terms of implementation without any additional investments and simplicity, as mass balances are a fundamental concept of

process design engineering. However, such basic calculations cannot be easily generalized due to the fact that co-processing product yields are highly feedstock and process dependent. Therefore, baseline scenarios need to be remeasured as feedstocks change. Furthermore, there can be slight yield differences from baseline data, making it challenging to assign a precise yield to the renewable feedstock. Besides, from a research and optimization point of view, these methods do not give information on the reaction pathways that are useful to both process and catalyst development. Moreover, the introduction of oxygenated compounds may change the reaction pathways and mechanism, interacting with the fossil feed and the catalyst, thus making the baseline case not valid anymore. Alternatively, renewable carbon in final products can be evaluated through more accurate post-reaction physical measurements. These techniques involve the measurement of carbon isotopes, ^{12}C , ^{13}C and ^{14}C , and their ratios. Radiocarbon dating is a concept that has been utilized for decades. The atmosphere contains stable ^{12}C and ^{13}C isotopes together with a much smaller fraction of unstable ^{14}C (natural abundance in parts per trillion), all in the form of carbon dioxide. Carbon dioxide is continuously consumed by plants during photosynthesis, and therefore similar atmospheric distribution of carbon isotopes is present in living entities. After the death of a plant, carbon is no longer taken up as CO_2 and the amount of ^{14}C begins to decrease relative to living matter. The rate of radioactive decay is a constant (half-life of $5,720 \pm 47$ years for ^{14}C ²⁶⁸), thus it is possible to date organic materials up to a certain age at which radiocarbon is no longer detectable (ca. 50,000 years). Fossil sources, being hundreds of millions of years old do not contain any measurable ^{14}C and therefore the biogenic content of any mixture of fossil and modern carbon sources can be correlated to the ^{14}C content.^{268,269}

Post-reaction carbon isotopes measurements techniques

In the last decades, several methods of measuring carbon isotopes have been developed to determine the amount of bio-based carbon in solid, liquid, and gaseous samples in a broad range of applications. Regarding materials and fuels, ASTM International adopted the standard ASTM D6866 in 2004 and updated it in February 2020 (ASTM D6866-20).²⁷⁰ This standard includes two analytical methods: accelerator mass spectrometry (AMS) and liquid scintillation counting (LSC). In the United States, EPA under the Renewable Fuel Standard Program (RFS) has approved the use of this standard to evaluate the bio-derived portion in the final fuels.²⁵¹

Accelerator Mass Spectrometry (AMS)

AMS consists of an ultra-sensitive instrument for measuring naturally occurring radio nuclides. The atoms contained in the samples are ionized, accelerated, and separated to be counted in a Faraday collector. AMS directly counts the amount of ^{14}C , ^{13}C and ^{12}C in a given sample, determining the ^{14}C to ^{12}C ratio directly. Prior to the carbon isotopes analysis, samples are usually converted to solid graphite via oxidation into CO_2 in a pure oxygen environment, followed by a reduction to CO on a zinc catalyst and a further reduction to graphite on an iron catalyst. Graphite and reference samples are then placed into the analyzer equipment and fired with cesium ions to generate negatively charged carbon ions. The resultant ions, after passing through a focusing device, are sent into the accelerator where they undergo a voltage difference of 2 million volts. The negatively ionized atoms lose electrons in a stripper and become positively charged atoms. Thus, triple positively charged carbon ions are further accelerated and sent to a mass analyzer where a magnetic field deflects the flow of atoms measuring deflection differences due to different mass of the atoms and therefore counting them.^{61,250,271,272} AMS measures $^{14}\text{C}/^{12}\text{C}$ and also $^{13}\text{C}/^{12}\text{C}$ ratios comparing the results to a modern standard as reference (NIST SRM 4990C). The results can be expressed as percentage of

modern carbon (pMC) representing the amount of ^{14}C relative to the standard.²⁵⁰ A correction is applied using the measurement of the stable isotopes $^{13}\text{C}/^{12}\text{C}$ ratio. The reason is related to the fact the different plant types incorporate atmospheric CO_2 in slightly different ways thus affecting the ^{14}C results. The correction is based on the comparison of $^{13}\text{C}/^{12}\text{C}$ ratios to the standard reference (usually called $\delta^{13}\text{C}$ correction).²⁷³

Past studies on co-feeding VGO with pyrolysis oils have measured biogenic carbon content using this AMS method⁵⁹⁻⁶³ and the results are summarized in Table 7. One challenge of this test method is the stated precision, which indicates an absolute uncertainty up to $\pm 3\%$, thus leading to broader ranges of calculated biogenic carbon incorporation in the products.²⁵⁰ For biogenic carbon content below 10 wt.%, this uncertainty strongly affects the results. D6866 states that the instrumental error can be within 0.1-0.5 % but an interlaboratory evaluation suggested $\pm 3\%$ as the potential absolute error. This statement seems to be confirmed by a limited number of studies^{274,275} but the real uncertainty of this measurement in the context of liquid fuels is still unclear. An ASTM research report for the ILS which determined this precision is not available for this test method; therefore, it is unclear exactly how this value was calculated. Indeed, a more recent study by Haverly et al.²⁷⁶ investigated D6866 precision by analyzing samples containing both fossil and biogenic carbon in four different laboratories. The results showed that the absolute measurement error was much lower, indicating a confidence interval of ± 0.26 wt.% as well as a detection limit of 0.40 wt.%. This study indicates much more reliable evaluations using this analytical technique than would be assumed from the stated precision. This precision value is highly important for biogenic carbon tracking in co-processing due to the low overall biogenic content in the co-fed refinery products. In fact, the uncertainty in this measurement (if it were $\pm 3\%$) could lead to drastic miscalculation in the actual biogenic carbon incorporation, resulting in erroneous conclusions about process efficacy or the renewable share in fuels. To emphasize this, the error bars depicted in Figure 28 show the biogenic carbon measurement uncertainty calculated using the stated precision of D6866 and that derived by Haverly et al. applied to studies on co-processing in an FCC. It is evident that ± 3 wt.% would lead to broad ranges of uncertainty, inversely proportional to the amount of biogenic carbon in the sample. Indeed, the more recent Haverly et al. investigation found that the uncertainty is likely much lower, thus confirming the high precision and low limit of detection of the AMS method.

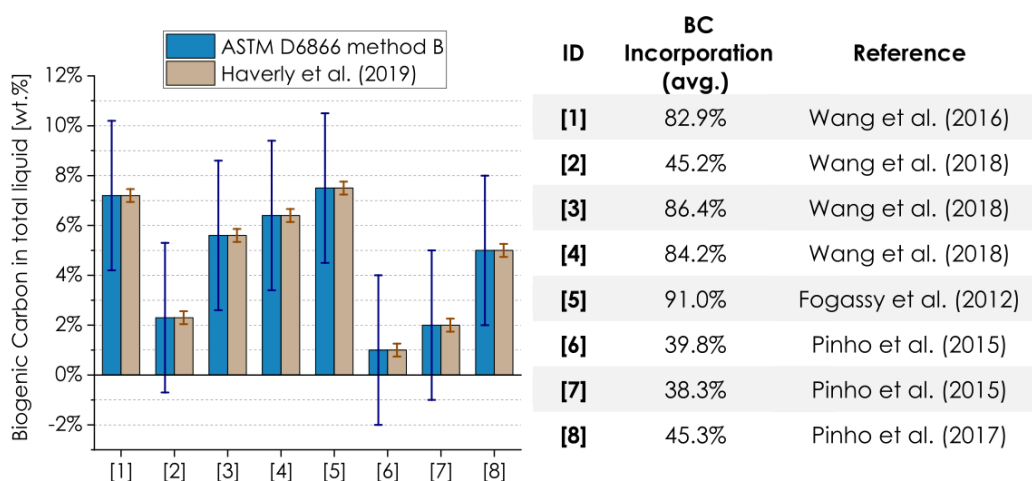


Figure 28. Co-Processing of pyrolysis oil and VGO - Biogenic carbon and incorporation in total-liquid for literature data, error bars refers to absolute precision stated in ASTM-D6866 Method B (± 3 wt.%)²⁵⁰ and in Haverly et al. (0.26 wt.%)²⁷⁶; [1] Wang et al. (2016)⁵⁹, [2, 3, 4] Wang et al. (2018)⁶⁰, [5] Fogassy et al. (2012)⁶¹, [6, 7] Pinho et al. (2015)⁶², [8] Pinho et al. (2017)⁶³.

Most of the previous investigations on co-processing of pyrolysis oil and VGO in FCC units utilized D6866 Method B (AMS) for biogenic carbon tracking. Table 7 summarizes the results measured in these studies indicating the percentage of biogenic carbon in each FCC product. The percentage in each liquid product is always below 10wt.% thus highlighting the high-precision requirement for the analytical techniques. Consequently, the evaluation of biogenic carbon incorporation become can be hard to properly assess using through the D6866 stated absolute error, leading to wrong conclusions about the renewable share in the products. For example, at 1% biogenic carbon content, the stated precision is 3x the measured value

An interesting result of these studies is a dependency on the bio-oil type. Upgrading pyrolysis vapors or oils through CFP or HT leads to higher biogenic carbon incorporation when co-processed with VGO in the FCC as shown by Wang et al. in his two studies^{59,60} with three different bio-oils as feedstock (FP, CFP and HDO). These results show that CFP and HDO oils seems to be the most suitable feedstock for co-processing in FCC, leading to higher renewable carbon incorporation in the liquid products compared to FP. In addition, Wang et al.⁶⁰, co-processed two different HDO oils, one mildly treated (HDO 1) and the other from a further hydrodeoxygenation of HDO 1 (HDO 2), and the biogenic carbon measurements shows an increment when HDO2 was used as feedstock.

Table 7. Biogenic carbon content measured by ¹⁴C radiocarbon analysis, with AMS (accordingly to ASTM D6866-12 – method b)

| FCC product | Total liquid | LPG | Gasoline | LCO | Bottom | Coke | Dry gases | Bio-Oil-VGO ratio [wt.%] | Type of pyrolysis oil | References |
|--------------------------------|--------------|-----|----------|---------|---------|------|-----------|--------------------------|-----------------------|-------------------------------------|
| Biogenic carbon content [wt.%] | 7.2-7.3 | - | 7.0-7.1 | 7.3-7.4 | 7.6-7.7 | - | - | 10:90 | CFP | Wang et al. (2016) ⁵⁹ |
| | 2.3 | | 2 | 2.5 | 2.6 | - | - | 10:90 | FP | Wang et al. (2018) ⁶⁰ |
| | 5.6 | | 5.3 | 5.9 | 6.2 | - | - | 10:90 | HDO 1 | |
| | 6.4 | | 6.1 | 6.3 | 6.8 | - | - | 10:90 | HDO 2 | |
| | 7.5 | - | 7.2 | - | - | 15.8 | 11.94 | 10:90 | HDO | Fogassy et al. (2012) ⁶¹ |
| | 1 | - | - | - | - | - | - | 5:95 | FP | Pinho et al. (2017) ⁶³ |
| | 2 | - | - | - | - | - | - | 10:90 | FP | Pinho et al. (2015) ⁶² |
| 5 | - | 3-5 | 5 | 6 | - | - | 20:80 | FP | | |

Liquid Scintillation Counting (LSC)

The second method, described in the ASTM D6866 - Method C, involves the isotope determination using a technique called Liquid Scintillation Counting (LSC). The standard method only describes the sub-method that involves benzene synthesis but other two alternatives have been studied and applied on mixtures containing biogenic carbon: carbon dioxide absorption and direct counting. The LSC-benzene technique includes a complex and time-consuming benzene synthesis that increases the overall cost of the analysis. Briefly, the sample is first combusted under pure O₂ to form CO₂ and then reacted with molten lithium preheated at 700°C, producing Li₂C₂. Further hydrolysis with distilled or de-ionized water leads to the formation of acetylene gas (C₂H₂) that is further catalyzed to benzene. The standard LSC method consists of counting a cocktail of benzene samples mixed with a scintillation cocktail and analyzed in a counter. The LSC counter apparatus needs to be optimized using a standard reference (NIST SRM-4990B).^{250,272,277} In an alternative technique, the CO₂ after sample oxidation can be absorbed in a cocktail prior to scintillation counting but this method is less accurate although less expensive than the LSC-benzene method.^{278,279} Another interesting and relatively simple option, only suitable for liquid samples, is the direct counting without any sample preparation. In this technique, the ¹⁴C signal is directly detected in the liquid mixed with the scintillation cocktail.^{280–282} Despite the simplicity of the method, which requires much less time for sample preparation, the precision can be fairly low, due to quenching properties related to different colors of the liquid that lead to loss of counts. Baseline corrections and calibration need to be properly addressed to reduce the error window and improve the reliability of the analysis. Additionally, a study from Norton et al.²⁸³ showed that increasing the counting time, increased the precision (0.2wt.% absolute for 2% of biogenic content), comparable with AMS by Haverly et al. and LSC-benzene. In the transportation fuels sector, the use of direct LSC has been investigated by other authors^{281,284,285} to determine the biogenic content in a wide range of fuel blends with ethanol, gasoline, diesel, HVO, FAME^{282,284} but obtaining better results a higher content of biogenic materials and consequently less impact from method absolute precision. In the case of FCC co-processing outputs, biogenic content is typically at relatively low percentages (< 10 wt.%) and applying this technique requires high precisions suggested by Norton et al, thus increasing the time and costs of the analysis.

2.3.5 - Advanced analytical techniques for online carbon tracking in petrochemical refineries

AMS and LSC radiocarbon methods described in the previous section are well established as analytical approaches to differentiate carbon from renewable and fossil sources. However, there are several aspects that make these techniques complex and expensive both in terms of equipment costs and analysis time, thus limiting the applicability for use in refinery sites. In order to directly measure biogenic carbon during processing, new techniques will need to be developed.

First, as previously introduced, the analytical apparatus would ideally be implementable on-line in reactor units, where samples batches or products streams³³; therefore, the precision and accuracy of an applicable technique should be maximized for biogenic carbon ranges of about 10 wt.% or less, as well as the detection limit should be minimized at similar level or below Haverly et al. AMS (0.40 wt.%). Another consideration is the overall analysis time, including all the steps for samples preparation. Reducing or eliminating these steps is one of the fundamental objectives for the development of new technological approaches, because they represent one of the bottlenecks for AMS or LSC-benzene analysis. Moreover, although AMS is widely considered the standard for the highest precision, the method

requires large, highly sophisticated and expensive analytical facilities with high operating costs. Recently, some efforts have been made to make AMS more economical and reduce the equipment size²⁸⁶⁻²⁹⁰. Some analytical alternatives have shown potential to address the challenges and be employed in co-refining applications.

$\delta^{13}\text{C}$ - Isotope Ratio Mass Spectrometry

. Measurement of $^{13}\text{C}/^{12}\text{C}$ isotope ratio is expressed in the form of $\delta^{13}\text{C}$ through the equation provided below:

$$\delta^{13}\text{C} = \left(\frac{\left(\frac{^{13}\text{C}}{^{12}\text{C}} \right)_{\text{sample}}}{\left(\frac{^{13}\text{C}}{^{12}\text{C}} \right)_{\text{standard}}} - 1 \right) \cdot 1000$$

The amount of ^{13}C depends mainly on organic source and geographical origin. Minute differences in isotope ratios can be used to determine region of origin as well as modern vs fossil carbon source.^{291,292} Generally, classes of materials, such as plants and petroleum products have different average $\delta^{13}\text{C}$ values. Measuring $\delta^{13}\text{C}$ values of a mixture's components, such as VGO and a specific BDL, can be used to develop a mixing model that can be used to determine the percentage of each in the mixture as well as their products from co-processing. This measurement can be carried out by much simpler equipment than AMS, such as an elemental analyzer gas-source isotope ratio mass spectrometer (EA-IRMS or IRMS), nuclear magnetic resonance spectroscopy (NMR),²⁹³ or cavity ring down spectroscopy (CRDS).²⁹⁴ IRMS can potentially be used as a standalone system to differentiate carbon sources.²⁹⁵ Potential advantages of IRMS are lower cost than AMS and faster analysis time than LSC. $^{13}\text{C}/^{12}\text{C}$ ratio has been used to measure renewable carbon content in biodiesel blends with petroleum-derived diesel.^{296,297} A recent report²⁹⁸ used this method to measure biogenic carbon during co-processing in a pilot scale FCC. Promising results were obtained in terms of precision and detection limit. The precision obtained with this method was $\pm 0.013\%$, and the uncertainty decreased with greater difference in isotopic ratios between petroleum and BDL feeds. While the biogenic carbon detection limit observed was approximately 0.3% when a 4‰ difference in $\delta^{13}\text{C}$ was measured between bio-oil and petroleum feeds, it increased when this difference was reduced due to similar $\delta^{13}\text{C}$ signal between the feedstocks. Biogenic carbon contents from this study were compared with D6866 Method B, showing strong correlation ($R^2 = 0.998$). A limitation stated by the authors is overlapping $\delta^{13}\text{C}$ values between some modern carbon sources and petroleum feedstocks. Stable carbon isotope ratios in plants are related to photosynthetic pathways for carbon fixation and plants are categorized in two families: C_3 plants such as trees, rice, soybean, cotton and cold-season grass or C_4 plants such as corn stover, switchgrass, warm-season grass, miscanthus, sugarcane.²⁹⁹⁻³⁰² $\delta^{13}\text{C}$ of petroleum sources have been reported in the range -34 to -24 ‰ depending on the source, while the values for C_3 and C_4 are in the range -30 to -22 ‰ and -18 to -13 ‰, respectively.^{291,298,303-305} As shown in Figure 29B, the range of $\delta^{13}\text{C}$ values for C_3 plants largely overlaps with that of petroleum fossil sources (e.g. VGO) while for C_4 plants the range of values is clearly separated from fossil sources. As described by the authors²⁹⁸, the method measures $\delta^{13}\text{C}$ of each single blend unit (bio-oil and VGO), estimating the fractionation in the co-processing unit. Then the $\delta^{13}\text{C}$ of the end products is measured calculating the blending level through a mixing model. In co-processing of BDL, it would be easier to differentiate the $\delta^{13}\text{C}$ of the biogenic portion when C_4 plants are used as biomass sources, while with C_3 plants, a tolerable isotopic difference is needed (i.e. about 4-5 ‰) with current measurement precision. It should be noted that the $\delta^{13}\text{C}$ method depends on the individual sources and while the range of possible isotopic values for C_3 plants and

VGO overlaps, it has the potential for differentiating small blending levels from VGO as demonstrated in a recent report.³⁰⁶ This method could succeed in refineries, especially with BDL mainly from agricultural residues such as the ones specified.

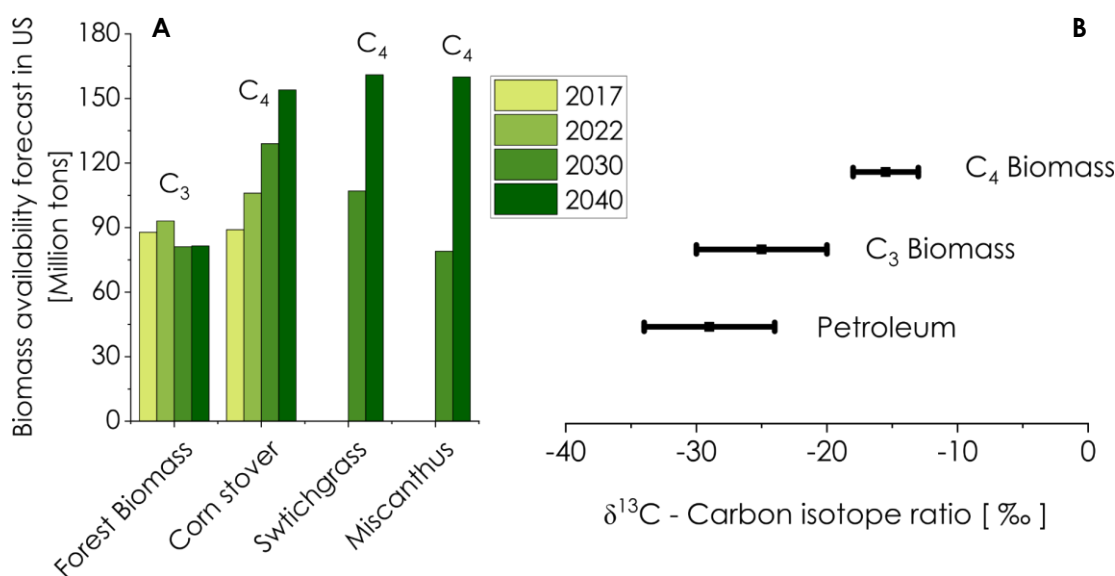


Figure 29. Biomass availability forecast comprising forest and agricultural residues, accordingly to Langholtz et al.³⁰⁷ (A); (right) $\delta^{13}\text{C}$ ranges, comparison of petroleum sources with C₃ and C₄ biomasses, data from Peters et al.²⁹¹, Kohn et al.³⁰³ and O'Leary et al.³⁰⁴ (B)

Observing future forecasts of U.S. biomass availability for energy purposes (Figure 29A), some C₄ plants (agricultural residues of corn stover, switchgrass and miscanthus) would reach higher amounts than C₃ biomass by 2040. However, woody biomass (C₃) are the most researched feedstocks for FP and CFP because they are less difficult to feed into reactors, produce high bio-oil yields, and have low inorganic content compared to agricultural (C₄) plants.^{237,308} Despite potential advantages of $\delta^{13}\text{C}$ as a method for tracking renewable carbon in co-processing, widespread adoption would be straightforward only in the scenario of using C₄ derived BDLs. With C₃ type, in some cases, petroleum feeds would be indistinguishable from BDL in terms of $\delta^{13}\text{C}$, limiting application flexibility.

Optical and laser techniques for ¹⁴C detection

Among prospective candidates, optical and laser techniques for ¹⁴C detection and quantification have been proposed as advanced techniques.^{309,310} In general, the optical detection of carbon isotopes such as ¹⁴C has shown some issues, especially when high precision and low limits of detection are required. The reason is the susceptibility of a spectroscopy detector to physical interference from background signals thus requiring a chemical or physical sample preparation to improve precision. Some of these methods require a complete combustion of the sample to form CO₂. Nevertheless, the ¹⁴C content can be directly detected without any other further chemical modification steps. Researchers in several laboratories have studied solutions to improve the precision of optical technologies addressing different approaches. Galli et al.³¹¹ in 2011 demonstrated optical ¹⁴C detection based on saturated-absorption cavity ring-down (SCAR) spectroscopy³¹²⁻³¹⁴. More recent studies demonstrated the possibility of achieving precision closer to that of AMS³¹⁵. Problems and limitations reported for SCAR spectroscopy for radiocarbon tracking are mainly

related to the complex and non-linear nature of the analysis.³¹⁶⁻³¹⁸ Other studies have demonstrated significant improvement in precision using mid-infrared $^{14}\text{C}_{16}\text{O}_2$ spectrometers based on cavity ring-down spectroscopy (CRDS) on several applications.³¹⁸⁻³²⁰ McCartt et al.³²⁰ tested the possibility of using CRDS in place of AMS, obtaining fairly accurate measurements of ^{14}C , even in the presence of interferences in biological sample for biomedical applications. This work identified interferences, such as other CO_2 isotopes or nitrous oxides that limited spectrometer sensitivity and the study highlighted that a pMC fraction of > 1 would be ideal to achieve significant accuracy. Further investigations from Fleisher et al.²⁹⁴, using a laser-based mid-infrared CRDS method, showed the possibility of detecting ^{14}C in samples with pMC < 1 . Genoud et al.³²¹ applied mid-infrared CRDS together with an advanced sampling system to analyze atmospheric $^{14}\text{CO}_2$ in an in-line set-up. With this system the authors were able to differentiate between the ^{14}C contained directly in form of $^{14}\text{CO}_2$ and the one derived from the combustion of $^{14}\text{CH}_4$. The sampling unit included a first cryogenic separation of the CO_2 contained in the air that is concentrated and further sent to the CRDS detector. The analysis is carried out in a continuous way, cyclically separating pure CO_2 while the previous samples is being analyzed in the CRDS. Other biogenic carbonic contained in CH_4 is analyzed by catalytically converting $^{14}\text{CH}_4$ into $^{14}\text{CO}_2$. In order to determine the portion of ^{14}C in the form of CO_2 or CH_4 , two measurements with and without the catalytic conversion were carried out. Another optical ^{14}C detection method, intracavity optogalvanic spectroscopy (ICOGS), was first proposed by Murnick et al.³²² in 2008 laying the foundations for potential applications in several fields that require very low detection limits for replacing AMS with a simpler, less expensive and faster technique. This method works with a fixed frequency stabilized $^{14}\text{CO}_2$ laser and combines four different techniques previously studied: laser assisted ratio analyzer (LARA), optogalvanic spectroscopy, optical impedance spectroscopy and laser intracavity absorption spectroscopy³²³. Although another study³²⁴ in 2014 was able to replicate the first results, issues have been found by other authors around the repeatability of the results and the absorption background due to $^{13}\text{CO}_2$ and $^{12}\text{CO}_2$ ^{323,325-327}. According to Murnick et al.³¹⁰, a precision of 1% is achievable for ICOGS with few minutes of analysis although calibration can be challenging. The main advantage of SCAR, CRDS and ICOGS optical techniques for ^{14}C detection is the possibility of real-time analysis. Samples need to be oxidized to obtain a CO_2 gas flow that can be further directed to the optical isotope spectrometer; thus, direct on-line measurement of refinery unit outputs.

2.3.6 - Refinery benefits for on-line biogenic carbon analyzers

The major objectives of refiners considering alternative feedstocks like pyrolysis-derived bio-oils are to (1) maintain safe and reliable operations throughout the refinery, (2) maximize refinery profitability with feedstock processing margins and applicable policy incentives, and (3) strategically improve the refinery's overall environmental sustainability profile. While other aspects of DOE-funded research, focus on process analysis and associated risk identification and minimization for reliable refinery operations with co-processing, new on-line analyzers would further contribute to operational risk mitigation and contribute significantly in improving refiner's ability to both quantify and monitor renewable carbon in fuels and optimize overall refinery profitability.

On-line refinery stream analyzers would be integrated into a refinery's distributed control system (DCS), where operating personnel are interacting continuously with the control system for process monitoring to facilitate response to changing process trends, alarms, upset conditions, etc. On-line biogenic carbon analyzer data can contribute to advanced notifications for abnormal trends and/or operating range exceedances. For example, on-line renewable

carbon content in a process stream decreased in absence of other operational changes like a feedstock change (i.e. different VGO composition), this may indicate that bio-oil flow issues like plugging, overcracking or coking are occurring. Refiners can utilize on-line analyzers in this way to reduce risk of operational upsets while co-processing. Therefore, on-line techniques for determining the fraction of biogenic carbon in the product streams are highly desirable. Currently, on-line analytics are integral to refinery operations for compliance with regulations, maintenance of smooth operation, and enabling rapid product distribution adjustments. The EPA requires the measurement of carbon dioxide, methane, and nitrous oxide emissions (40 CFR (Code of Federal Regulations) 98, subpart Y) as well as sulfur emissions (40 CFR 60, Subpart Ja), all of which can be performed with on-line process mass spectrometry.³²⁸ On-line distillation analyzers are used to monitor product quality.³²⁹ Non-dispersive infrared (NDIR) analyzers are commonly used throughout refineries for process monitoring.³³⁰ Due to peak overlap, they are coupled with multivariate statistical analysis, such as PLS, PCA, and MCR.³³¹ Therefore, due to the fact that other refinery on-line analytical tools are already in place, on-line biogenic carbon measurement could be a practical route to analyzing the renewable carbon fraction in products from co-processing and could help drive co-processing of renewable intermediate organic streams into the fuel production chain.

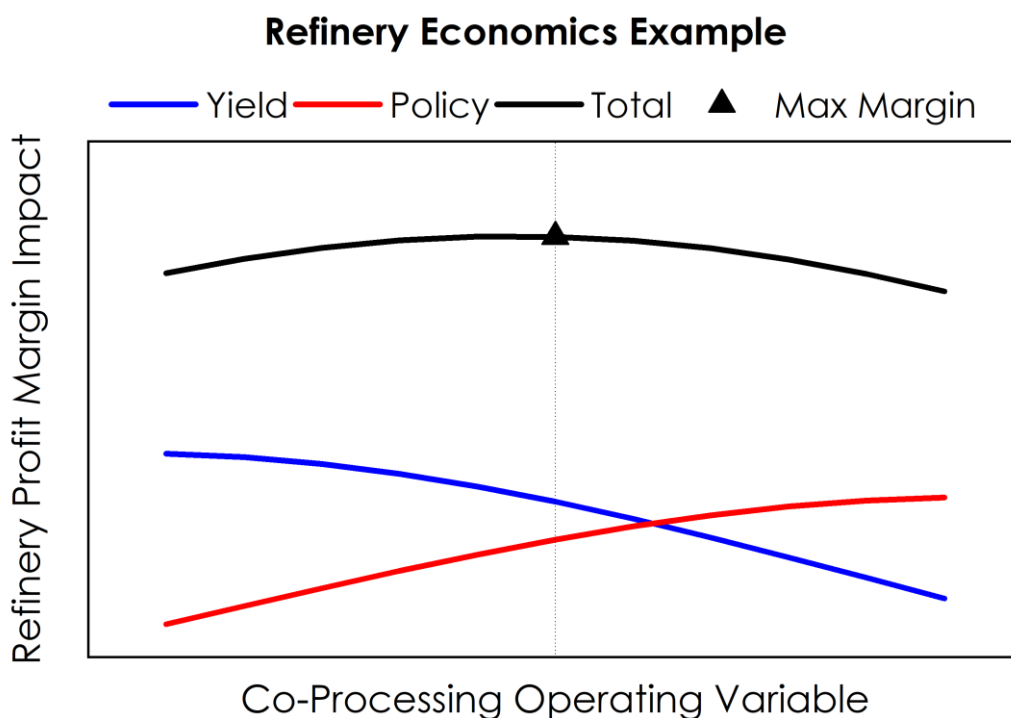


Figure 30. Example showing how refiners can utilize on-line analyzers to maximize overall refinery economics with co-processing

In addition, today's refineries have sufficient instrumentation to perform detailed mass balance-based, yield calculations and quantify product yield impacts resulting from changes in unit operations including new feedstocks. However, current refinery control and instrumentation systems lack the means to measure renewable carbon contents accurately, reliably, and quickly. Renewable carbon contents would be required inputs for bio-fuel product allocation

calculations applied for quantifying applicable policy incentives. With the data provided by on-line biogenic carbon analyzers, refiners would have the capability to optimize refinery economics for co-processing scenarios by considering margin impacts from yields, measured and calculated by existing refinery instrumentation, and from policy credits, measure and calculated with biogenic carbon data. Figure 30 shows a simple example of a how a refinery might assess both yield (blue line) and potential policy credits from co-processing biomass-derived feedstocks (red line) to maximize total profitability (black line and triangular data point). Without reliable means to quantify biogenic carbon, a major component of the optimization data is missing.

The data reported through the DCS is also saved in a data historian for future investigations, data analysis and reporting. With the data reported and historized, the refinery technical and environmental teams can easily access and apply it for certification or compliance-related reports. This data can also be combined with the rest of the historical plant data and integrated in refinery analysis tools like process simulations and optimization models. With these tools, refiners can further evaluate biogenic carbon distribution and utilization in the refinery. Ultimately, with tools like on-line biogenic analyzers, refiners can quantify and track progress in reducing overall facility carbon intensity.

In initial commercial phases of co-processing, it is likely that bio-oil concentrations in refinery unit feedstocks to be less than 5wt.% to minimize risk to reliable operations and considering the bio-oil availability³³. This means that quantifying the biogenic carbon in gasoline, diesel, and jet fuel blend pools collected from all refinery unit operations will require extremely sensitive analytical tools due to increased dilution from petroleum derived finished fuels. There are also strong drivers for accurate on-line analytical methods that can be installed on the product streams of refinery unit operations in which co-processing of bio-derived liquids is conducted. The co-processing examples for straight-run diesel oil hydroprocessing and fluid catalytic cracking (FCC) in Figure 31 highlight streams where on-line biogenic carbon analyzers could be installed. Refiners would likely prioritize installation of analyzers for quantifying biogenic carbon in fuel blendstocks like “Diesel” from the hydrotreater and “Naphtha” and “Light Cycle Oil” from the FCC. In addition, refiners may also consider adding analyzers to petrochemical products like propylene “Olefins” if incentives for renewable plastics evolve from future policy.

Based on current co-processing work, it is likely that catalytic fast pyrolysis oils or heavily upgraded oils would be co-processed in hydroprocessing units and heavier bio-oils like fast pyrolysis oil would be co-processed in fluid catalytic cracking (FCC) or residuum FCC (RFCC) units. In refinery unit operations where on-line analyzers are installed on unit product streams, a slip stream of each product can be combusted to generate $^{12}\text{CO}_2$, $^{13}\text{CO}_2$ and $^{14}\text{CO}_2$. The ratio of the isotopes can be used to calculate biogenic carbon incorporated in the refinery intermediate stream and, by volumetric blending calculations, in the finished fuel products.

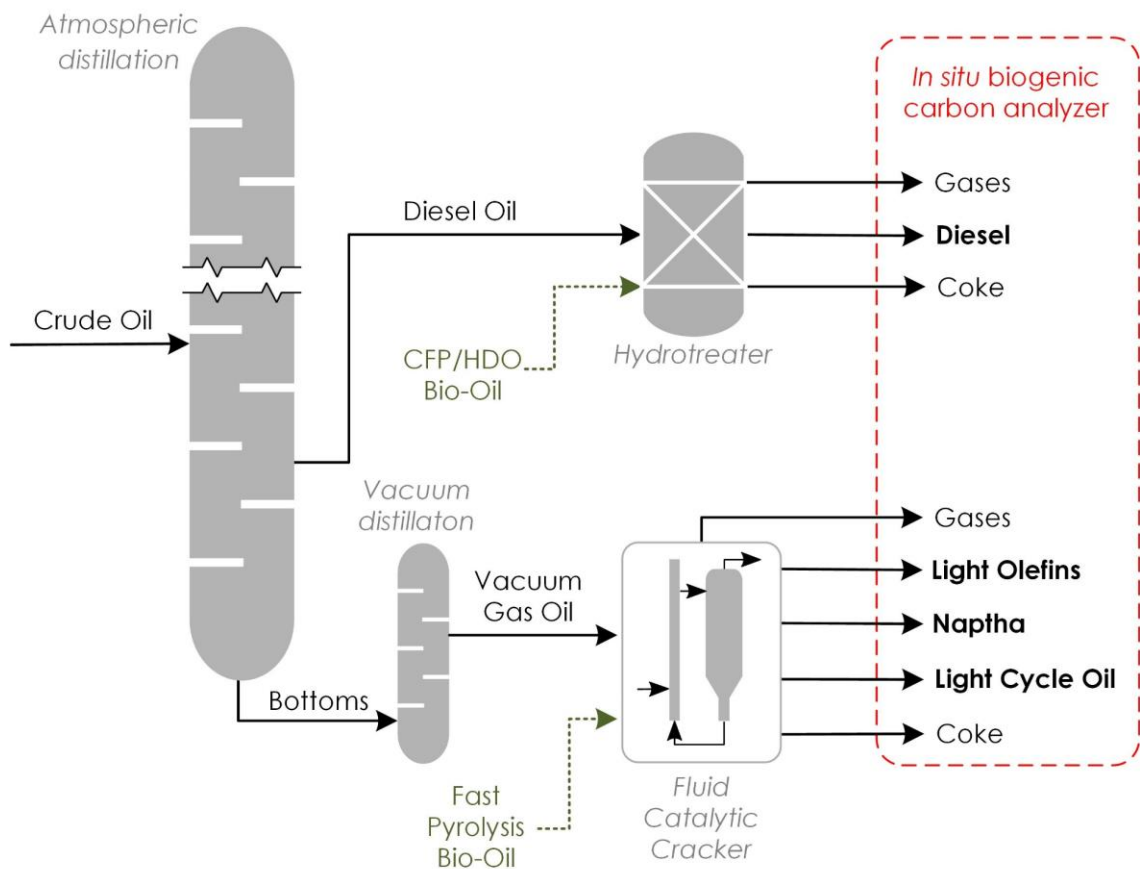


Figure 31. Simplified schematic showing insertion points for different bio-oils in existing refineries and possible positions for coupling biogenic carbon analyzer to accurately measure renewable fuels in finished fuels.

On-line analyzers are nothing new for refineries who routinely utilize them for safety, process control, process optimization, product quality control, and continuous monitoring of major emissions sources. An optimal on-line biogenic carbon analyzer should be inexpensive, accurate, reliable, easy to maintain and enables rapid analytical results. Reliable and accurate devices for measuring renewable carbon contents in blended finished products would address a major and technology gap associated with concern co-processing bio-intermediates in existing refining infrastructure.

2.4 - Conclusions

The conversion of lignocellulosic biomass in FP and CFP have already been demonstrated as one of the most promising route for the conversion of renewable source into bio-intermediates for the production of fuels and chemicals.^{10,27,38,39,182,185,332} In this work an interesting approach have been investigated for the pre-conditioning of fast pyrolysis vapors through catalytic hot-gas filtration (CHGF) to improve downstream processes (e.g. *ex-situ* CFP) and the quality of the condensed bio-oil. Heteropolyacids catalysts based on molybdenum and tungsten on titania support (Mo-HPA/TiO₂ and W-HPA/TiO₂, respectively) were tested in a packed-bed catalytic reactor using a pulsed-flow small scale reactor and then in a continuous pilot system. The results from both micro and pilot scale suggested an enhanced catalytic activity in presence of H₂, towards the generation aromatic and alkylated hydrocarbons (e.g. BTX) as well as alkylated phenols. Thus, leading to a partial deoxygenation and vapors stabilization for downstream processes due to the reduction of acidic species in the mixtures. Moreover, CHGF was tested in tandem with staged condensation unit (FCT) in order to validate the upgrading results and to characterize a potential downstream process for chemicals precursors extraction (aromatics hydrocarbons, phenols and alkylphenols). Separation of organic fraction from aqueous stream was achieved concentrating heavy aromatic hydrocarbons, alkylphenols, and methoxyphenols within the oil phase and separating part of the ketones and acids, known to be responsible of oil aging and instability. The fractional condensation has been proved to be an effective method for a first separation of chemical species also in the perspective of co-products precursors extraction in an integrated biorefinery concept. Bio-derived co-products have the potential of reducing the fuel costs as well as introducing into the market bioproducts from renewable sources towards a green and circular economy, preserving the environment due to an overall GHG reduction. As an example of potential co-product from CFP biorefinery, in this work the extraction of molecules from fast pyrolysis organic streams was investigated for the production of bio-based insecticides. Fractions of PtTiO₂-CFP oil were distilled and tested in insects' bioassay to observe the insecticidal activity. Data analysis was carried out in order to correlate the insect mortality and specific molecules concentration. Other works suggests that lignin fractions have higher pest control activity compared to lighter compounds^{46,49,52} and in this work we proposes that alkyl substitution is one of the main parameters that enhances the insecticidal activity. Further model compounds studies are needed to validate these results, however other studies already suggested that alkylated phenols have higher effects compared to simple phenol or methoxyphenols. In addition, as a partial confirmation, the results suggests that lighter alkyl phenols (such as cresols) have limited activity compared to heavier alkyl substituted phenols (with three or more carbons in the alkyl chain). Hence, a vapors precondition step with heteropolyacids (e.g. Mo-HPA/TiO₂), due to the generation of higher alkylphenols content, could also be a potential route for the generation of bio-derived molecules that can be used as insecticides. Interestingly, fractional condensation can be employed as a first rough separation of these species followed by a distillation to improve the product purity at the expenses of a reduced yields. In this context a NREL proprietary Aspen Plus® model, comprising a fractional condensation unit, was modified adding a downstream separation step for a technoeconomic analysis (TEA) and a life-cycle assessment (LCA), considering alkylphenols with 3-5 carbons in the functional group as target insecticide compounds. A sensitivity analysis has been carried out varying the flow rate of CFP oil used for the co-products stream, observing how the purity and yield are affected, as well as the variation of the minimum product selling price.

Even though, bio-derived compounds or compounds-mixture showed insecticidal activity, the pathway for the commercialization includes a complex and long regulatory framework to be respected in order to be compliant at the

local environmental and safety requirements. US regulations (under the EPA) seems to be more favorable compared to the more branched EU framework, especially regarding bio-derived active substances. In both cases the regulations require several expensive health and environment tests prior to be admitted in the market, therefore consistently increasing the overall costs that will affect the potential final selling price.

As previously mentioned, the main goal of a biorefinery is to produce fuels as main product combined with co-products to maximize the carbon valorization and reducing the overall costs. In order to stimulate the commercialization of fast pyrolysis technologies favorable policies are needed as well as other solutions to be applied in the near term. Regarding the fuels chain, a modern and advanced approach to integrate renewable sources into the existing transport fuel market is represented by co-processing of bio-intermediates (such as bio-oil) into existing petroleum refinery. The objective is to minimize the existing infrastructures modification and at the same time maximize the biogenic carbon incorporation into the final products. In this context, several constraints limit the process optimization and the eventual technology spread. On one hand, understanding how the renewable carbon, mostly contained in oxygenated species, affects the overall co-refining process is an important step especially regarding catalysts optimization. On the other hand, tracking the biogenic carbon is fundamental for measures the renewable share in the final products, in order to receive governmental credits for introducing renewable advanced fuels into the market. In this work a background of co-processing technologies has been presented, highlighting fluid catalytic cracking units (FCC) as one of the most promising refinery points of insertion for FP, CFP or HDO oils. A summary of past studies has been presented, showing interesting results in term of fuel products yields as well as observing how the introduction of oxygenated species (e.g. phenols) increase the generation of coke and incondensable gases (CO and CO₂). Hence, microscale studies with labelled ¹³C biomass co-processed with vacuum gas oil (VGO) were carried out in order to investigate how the carbon get incorporated into final molecules and the origin of coke. MBMS investigations showed that coke generated over two different catalysts (one specific for CFP and one already used in FCC) is mainly caused by the presence of biomass-derived compounds. In addition to this experimental study, part of the work was focused on understanding how the up-to-date biogenic carbon tracking methods limits the technology advancements. For this reason, a review of the traditional techniques for biogenic carbon tracking using radiocarbon dating have been summarized. Among traditional biogenic carbon tracking, analysis on ¹⁴C contained in co-processing products is a technique that permits to differentiate biogenic from fossil source. The reason is that petroleum-derived materials, being millions of years old, does not contains any percentage of unstable radioisotopes ¹⁴C. However, traditional methods represent a bottleneck regarding administrative renewable carbon evaluation or process optimization in refinery units. The main problem is that ¹⁴C facilities (e.g. AMS) are not available everywhere and the analysis is time consuming and expensive as well. Therefore, strong efforts are needed in order to be able to track biogenic carbon directly inline in refinery units. Unfortunately, some modern and advanced techniques, such as optical and laser ¹⁴C measurements, still have challenges to face in order to achieve precisions of traditional methods. However, these approaches are promising due to the relative simplicity of the equipment compared to AMS or LSC facilities and can be easily adopted inline on refinery outputs, measuring directly ¹⁴C contained in previously oxidized form as ¹⁴CO₂. Another approach is based on stable carbon isotopes ¹³C where, measuring $\delta^{13}\text{C}$ through IRMS, is possible to differentiate different carbon origin. The problem is that this technique is possible only when a certain type of biomass is used as original bio-source for the production of bio-intermediates. C4 biomass-type (such as residual corn-stover, switchgrass and miscanthus) originated $\delta^{13}\text{C}$ that does not overlap with petroleum values. On the contrary, C3 biomasses (such as most of the trees and forests residues) have $\delta^{13}\text{C}$ that overlap with petroleum signal,

making it impossible to differentiate the two origins. Even though the availability of Some C4 biomasses will considerably increase in the future, fast pyrolysis of agricultural residues is still facing challenging compared to forests biomass and the spreading of this method is still uncertain.

3 - Hydrothermal liquefaction and depolymerization of lignin-rich streams derived from lignocellulosic ethanol biorefineries: process optimization and scale-up pathway

As introduced previously, many thermochemical conversion processes like pyrolysis or gasification normally require biomass with a moisture content under certain limit and an energy-consuming drying step is needed before feeding the reactors. Some domestic, industrial or agricultural residues and wastes (e.g. sewage sludge, food-industry residues, lignin-rich streams such as paper pulps or lignocellulosic ethanol biorefinery residues) can have a very high moisture content (even more than 50 wt.%) and the dewatering step can have a high impact on the overall process economy. Thus, an interesting approach to treat these organic streams is represented by hydrothermal liquefaction (HTL). In short, the HTL technology involves the conversion of biomass or organic wastes in an aqueous medium, near the critical temperature of water. Under these conditions, biomass first undergoes to an initial degradation (timescale <minutes) by a combination of solvolysis, hydrolysis, dehydration and decarboxylation into water soluble organics and with water and carbon dioxide as (main) byproducts. Then, repolymerization reactions occurs (timescale ~minutes) by different recombination and condensation mechanisms water-insoluble liquid organic compounds (biocrude) and water-insoluble solid organic/inorganic compounds (biochar).^{68,69} Among HTL suitable feedstocks, lignin-rich streams from lignocellulosic ethanol biorefineries is a potential candidate for a valorization through hydrothermal processing (Figure 32). Lignin is one of the main constituents of lignocellulosic biomass, and making up to 15–35 wt. % of the total organic matter weight, carrying also the highest specific energy content compared to cellulose and hemicellulose^{17–19}. The global amount of lignin estimated in the Earth's surface is 300 billion tonnes and annually increases by around 20 billion tonnes.²⁰ Lignin separation from cellulose and hemicellulose takes place extensively in the second generation lignocellulosic ethanol biorefineries and pulp and papers industry.³³³ As depicted in Figure 32, in ethanol biorefineries the lignin co-products is recovered at the end of the whole process, filtering the alcohol produced from the fermentation of the previously separated sugars. In order to estimate the potential of lignin from lignocellulosic ethanol biorefinery, an European study from E4 Tech ⁷¹ investigated scenarios for the growth of biorefinery industry under a favorable supporting policy as the one foreseen by the Directive (EU) 2018/2001 of the European Parliament and of the Council of 11 December 2018 on the promotion of the use of energy from renewable sources (in short Renewable Energy Directive - RED II). Future scenario foresees a ramp up in Europe from one plant producing at commercial scale in 2017 to 46 plants in 2030. From 2022 to 2025, 3–4 new plants per year across Europe are expected, but from 2025 to 2030, this rate should increase to an average of 6–7 new plants commencing production annually. Consequently, the amount of lignin co-product will considerably increase, rising the interests on its conversion pathways to chemicals or fuels precursors, reducing CO₂ emissions and the need for fossil resources. For these reasons, the economic viability of future biorefineries will mostly depend on efficient conversion of each biomass constituent, transforming both cellulose/hemicellulose and lignin into value-added compounds.

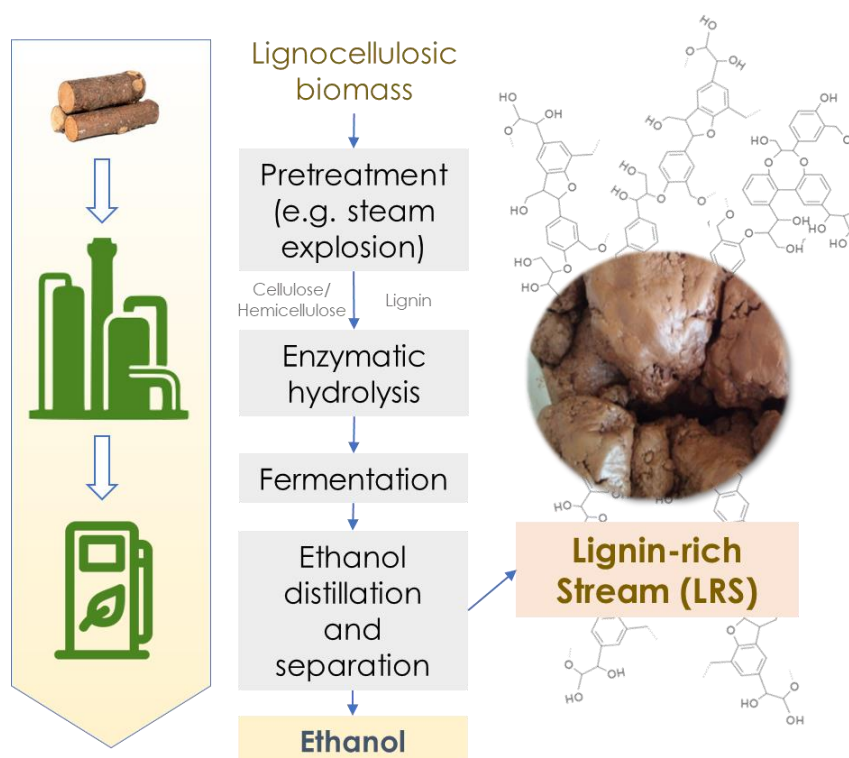


Figure 32. Scheme of a lignocellulosic ethanol biorefineries and lignin-rich stream (LRS) extraction

The current use of the LRS in industrial complexes is still limited to combustion for heat and power generation. However, being lignin the most abundant renewable source of aromatics in nature, its valorization is a very attractive opportunity in a circular economy perspective. Therefore, several research works addressed the economic valorization of lignin-rich streams from lignocellulosic ethanol production, either as chemical or as fuel, highlighting the challenges and importance of co-product valorization to achieve commercial competitiveness of these processes.^{334,335} The economic relevance of lignin co-products valorization clearly emerged since the initial modelling studies of the process⁷³ and it was later confirmed by experimental data from a pilot, demo and first-of-a-kind plants. For decades the pulp industry has been converting lignocellulosic materials into valuable fibers and products.³³⁶ Second-generation biomass conversion technologies are nowadays able to produce renewable chemicals and biofuels only from the cellulose and hemicellulose fraction at commercial scale. However, due to its aromatic structure, lignin has unique properties that makes this material a highly interesting biopolymer for further processing³³⁷. Lignin-rich streams (LRS) from lignocellulosic ethanol contain high amount of water (60–70 wt. %)³³⁸ making the material suitable for hydrothermal liquefaction (HTL) as first-step for product valorization. Among other thermochemical conversion strategies, HTL is a process recommended for wet biomass: the reactions are generally carried out in water at 280–370 °C and between 10 and 25 MPa. At these conditions, the water is in its subcritical state and the dielectric constant of water decreases; thus, behaving like a non-polar organic solvent breaking structural links of the biomass matrix. In these physical conditions it also has enhanced acidity donating protons to molecules, impacting the decomposition process³³⁹. The main HTL reaction products are biocrude, char, water-soluble substances, and gas (mostly CO₂). Efforts have already been made to convert lignin feedstocks into valuable products through liquefaction.

In this section several aspects of the hydrothermal conversion of LRS have been investigated, from process investigation, to potential pathways for co-products extraction and process scale-up for. First, through microscale studies, carried out in lab-scale high-pressure reactors, it was possible to observe how the process conditions (temperature, pressure and time) statistically influenced the overall mass yields. Then, a more detailed investigation on the compositions of the HTL products have been analyzed to understand how the process configuration influenced the detectable liquid organic and aqueous fractions. Moreover, the effect of catalytic additives, such as supercritical carbon dioxide (sCO₂) and KOH, have been addressed to improve the liquid products yields and quality. Most of the results obtained during these investigations have been published in two manuscripts: Miliotti et al.³⁴⁰ and Dell'Orco et al.³⁴¹

In a biorefinery perspective and process integration, as previously discussed for fast pyrolysis, it is important to generate co-products in order to reduce the overall OpEX costs. HTL, as other thermochemical processes, produces solid residues (biochar) and a significant amount of residual aqueous stream with water-soluble organics trapped during the conversion. Thus, the work has been further focused on a specific separation strategy for the recovery of organic compounds from the aqueous phase. Liquid-liquid extraction (LLE) through organic solvents has been addressed for the extraction of aromatic phenolic monomers as well as the separation of an acid-rich residual solution through adsorption on polymeric membranes. Regarding the implementation of a LLE unit at industrial scale, a simplified HTL model have been modified and a techno-economic analysis has been carried out in order to evaluate the impact of the recovery of chemicals in a integrated biorefinery concept.

Regarding the pathway for a scale-up and commercialization of the technology, a key step is represented by the demonstration of the process at larger scale in a continuous set-up. Thus, the operative data obtained by the lab micro-scale experimental campaign were used as baseline for a design of continuous pilot scale plant able to process 1 kg h⁻¹ of slurry (published in Rizzo et al.³⁴²). The units have been assembled and commissioned and a preliminary test for the conversion of biorefinery lignin has been carried out to individuate operative and safety issues.

3.1 - Process characterization through batch micro-scale experiments: influence of reaction conditions on overall yields

3.1.1 - Introduction

Among the different processes and technologies that deal with lignin depolymerization³³⁷, hydrothermal liquefaction (HTL) is a noteworthy thermochemical process that can convert lignocellulosic biomass mostly into a liquid fraction by using solely hot compressed water, or mixtures of water, co-solvents and chemicals^{343,344}. HTL is a wet process, which does not require feedstock drying, as it is instead necessary for other thermochemical processes like fast pyrolysis. Therefore, the high water-content, rather a constant composition, and the continuous availability at the industrial site of the lignin-rich co-product makes it a promising candidate for processing under hydrothermal liquefaction conditions into a liquid biocrude as main bio-intermediate product that can further be converted into fuel after further upgrading steps (e.g. hydrotreating). The valorization of the residual lignin would significantly improve the overall ethanol biorefinery carbon efficiency and economic performances, opening new business opportunities.

In previous studies, several authors carried out fundamental investigations on HTL of lignin using model compounds, as Vanillin, Monobenzene and 2-2'-biphenol³⁴⁵. They showed that ether bonds are more reactive under hydrothermal conditions than C-C bonds. Thus, the liquid yield reduces from monobenzene (almost complete conversion) to vanillin to 2-2'-biphenol (minimum conversion). Both fragmentation and condensation reactions occur on phenolic compounds in a hydrothermal environment, probably in competition, depending on the specific conditions. During hydrothermal liquefaction of lignin, α - and β -aryl ether hydrolysis, C—C bonds cleavage, alkylation, deoxygenation and repolymerization reactions take place simultaneously, whereas typically the aromatic structure is not affected by hydrothermal reactions. High molecular weight compounds from lignin HTL come from the partial depolymerization of the initial lignin from selective ether bonds splits but also from alkylation of the aromatic structures.

HTL conversion of lignin stream is often carried out at 350–400 °C, 22 MPa and 10 min residence time³⁴⁶. The process generates an energy-dense biocrude as the main fraction, along with gaseous products, solids, and an aqueous-phase byproduct. The biocrude yields can reach typically around 40–50 wt.%, with catechol, phenols, and methoxyphenols as main constituents. Similar results are obtained in the hydrothermal treatment of Kraft pine and organosolv lignin³⁴⁷. Most of the known HTL studies addressed lignin from pulp and paper or high-purity model compounds^{345–350}, both of them structurally different from lignin-rich stream originated from lignocellulosic ethanol biorefineries, which is still an unexploited material.

This part of the work investigates the conversion of a lignin-rich stream from industrial-scale lignocellulosic ethanol into a biocrude suitable for further processing and upgrading into fuels and chemicals. Several tests have been carried out in order to evaluate the statistical influence of the process parameters on the products yields. In addition, a special focus was given to the development and implementation of an extraction method in combination with the batch HTL micro-reactors system used in this research.

3.1.2 - Materials and methods

Feedstock: Lignin-Rich Stream

The lignin-rich stream (LRS) was obtained after ethanol distillation and mechanical separation of water from a demo lignocellulosic ethanol plant fed with poplar. The feedstock was dried in an oven for 48 h at 75 °C, knife-milled and then sieved to 0.25 mm; the LRS arrived as a moist agglomerated powder. After drying these agglomerates were size-reduced by milling. The characterization of this feedstock is given in the results and discussion section.

Experimental Equipment and Procedure

Batch hydrothermal liquefaction experiments were carried out in a custom-made micro-reactor test bench (MRTB), described in a previous publication by the authors³⁵¹. The reactor consists of an AISI 316 ¾" (outer diameter) tube with a length of 300 mm (~43 mL of internal volume). In order to prepare batch experiments, dried feedstock was dispersed in ultrapure water (0.055 $\mu\text{S cm}^{-1}$) to attain the desired biomass-to-water mass ratio. The mass of slurry loaded into the reactor was 33 g for each test. Prior to each experiment, a leakage test was performed with argon pressurized at 8 MPa. Then, three purging cycles with nitrogen (0.5 MPa) were carried out in order to remove air and ensure an inert atmosphere in the reactor. An initial pressure of 3 MPa was set using argon, then the reactor was immersed into a fluidized sand bath. Counting of residence time started when the inner reactor temperature reached 2 °C below the set reaction temperature: as the design residence time was completed, the reactor was rapidly cooled by immersion in a water bath. After nearly 20 min, the pressure was gradually released, the reactor opened and disconnected from the test bench.

A full factorial experimental plan with three factors and two levels was adopted, and the influence of temperature, time, the biomass-to-water mass ratio (B/W) and their interactions on the biocrude yield was assessed by means of an analysis of variance (ANOVA) on the experimental results. Each experiment was replicated between two to three times. In Table 8, the factors and the related low and high levels are reported. Besides the experiments planned, higher temperature (370 °C) and longer residence time (15–20 min) were also investigated in order to find the maximum yield of light biocrude.

Table 8. Operating parameters of the design of the experiments (DOE).

| Factor | Low level | High level |
|--------------------------------|-----------|------------|
| Temperature (°C) | 300 | 350 |
| Time (min) | 5 | 10 |
| B/W (-) wt.% d.b. ¹ | 10 | 20 |

¹d.b.: dry basis

In the present study, a light and a heavy fraction of the biocrude, named biocrude 1 (BC1) and biocrude 2 (BC2), respectively, were recovered with a two-steps solvent extraction method. The selection of the solvent for the recovery of the light fraction (diethyl ether, in short DEE) was based on a comparison with dichloromethane (GC-MS analysis). The solvent for the extraction of the heavy fraction (acetone, in short DMK) was based on the literature (see Appendix B1 for detailed results and references). Two different collection procedures were first developed and then evaluated, named Procedure 1 and Procedure 2, whose block diagrams are shown in Figure 33. In regards Procedure 1, once the reactor is disconnected from the test bench, it is rinsed with DEE and its content is vacuum-filtered over a Whatman glass microfiber filter (1 μm). Water and water-soluble organics (WSO) are then recovered by gravity separation,

while biocrude 1 is obtained after rotary evaporation of DEE at reduced pressure. The reactor and the solids are then rinsed with DMK; then, the DMK and the DMK-solubles are subjected to rotary evaporation at reduced pressure for the collection of biocrude 2, while the solid residue (SR) is oven-dried at 105 °C overnight. Procedure 2 differs only in the first step, where water and WSO are collected prior to solvent extraction. The products obtained from the experiments defined in the DOE were collected according to Procedure 1.

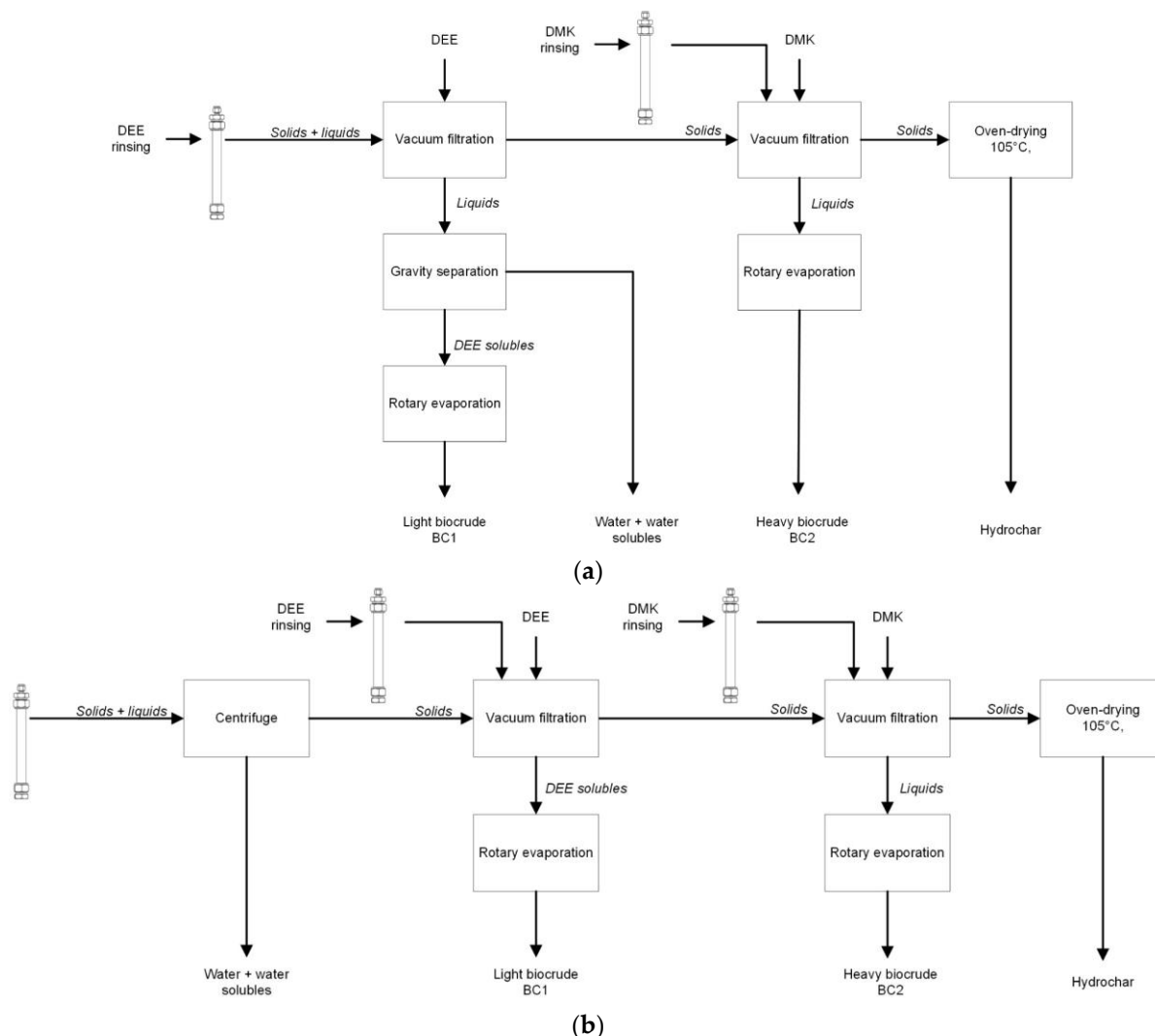


Figure 33. Scheme of Procedure 1 (a) and 2 (b) for products collection.

The mass yield and the carbon yield of the HTL products were evaluated according to the equations below:

$$\text{Mass yield} = \frac{\text{mass of product}}{\text{dry mass of LRS}} \cdot 100$$

$$\text{Carbon yield} = \frac{\text{carbon mass in the product}}{\text{carbon mass in the LRS (d. b.)}} \cdot 100$$

The gas yield was estimated assuming the produced gas fraction as composed entirely by CO₂, and ideal gas behavior, while the unrecovered products and the WSO fraction, which were not detected in HPLC, were determined by difference. The assumption of considering the gas phase made up entirely of carbon dioxide is legitimated, under a reasonable degree of approximation, by the fact that decarboxylation is one of the main reaction involved in hydrothermal liquefaction, leading to the formation of a CO₂-rich gas.^{68,352} The products obtained from a typical

experiment are shown in Figure 34. BC1 is a viscous brown liquid, while BC2 was recovered as a powder or as a very viscous black liquid, as similarly experienced by the research group of Xu (Ahmad et al.³⁵³, Cheng et al.³⁵⁴) in their experiments on hydrothermal depolymerization of lignin.



Figure 34. Products collected from a typical hydrothermal liquefaction (HTL) experiment in the micro-batch reactors: light biocrude or BC1 (a), heavy biocrude or BC2 (b), aqueous phase with water-soluble organics (WSO) (c) and solid residue (d).

Analytical Methods and Chemicals

Prior to feedstock characterization, the LRS was dried at 75 °C for 48 h and milled in a knife mill (RETSCH SM 300) equipped with a 0.25 mm sieve. The drying process was carried out at low temperature in order to minimize the devolatilization of the organic matrix. Moisture, ash content and volatile matter were determined in a Leco TGA 701 instrument according to UNI EN 13040, UNI EN 14775 and UNI EN 15148, respectively. Fixed carbon was calculated by difference. The content of carbon, hydrogen, nitrogen (CHN) was determined through a Leco TruSpec according to UNI EN 15104, while the sulphur content of the feedstock was analyzed by means of a TruSpec S Add-On Module, according to ASTM D4239. The oxygen content was evaluated by difference, considering C, H, N, S and ash content. For the biocrude samples, the sulphur content was neglected in the evaluation of oxygen. Higher heating value (HHV) was measured according to UNI EN 14918 by means of a Leco AC500 isoperibol calorimeter. The HHV of the biocrudes was also estimated with the Channiwala and Parikh equation³⁵⁵, due to the small available amount of samples. The validity of the latter correlation was assessed by a comparison with the measurement of the HHV of two light and heavy biocrude samples. Details are reported in Appendix 2D. The determination of the pH of the LRS was performed according to DIN ISO 10390.

The lignin content of the LRS was evaluated by a combination of three NREL procedures:

- The LRS was subjected to Soxhlet extraction with water and then ethanol in order to obtain the water-soluble and ethanol-soluble extractives (NREL procedure TP-510-42619³⁵⁶)
- The remaining solid residue was subjected to acidic hydrolysis for the evaluation of the acid soluble, acid insoluble lignin and structural sugars (cellulose and hemicellulose) by UV-VIS spectrophotometer and HPLC (NREL procedure TP-510-42618³⁵⁷)
- The ash content of the acid insoluble lignin was measured in order to determine the correct value of the latter (NREL procedure TP-510-42622³⁵⁸)

Infrared analyses were carried out with a Fourier transform infrared spectrophotometer (FT-IR, Affinity-1, Shimadzu), equipped with a Specac's Golden Gate ATR.

The evaluation of the apparent molar mass (polystyrene equivalent) of the BC1 and BC2 was determined by gel permeation chromatography (GPC). The samples were firstly dissolved in tetrahydrofuran (THF), left overnight and then passed through a 0.45 μm syringe filter. Afterwards, 100 μL of sample was injected in an HPLC apparatus (Shimadzu LC 20 AT Prominence) connected to a refractive index detector (RID) and equipped with two in-series columns (Agilent, PL gel 5 μm 100 \AA 300x7.5 mm) and a guard column (Agilent, PL gel 5 μm 50x7.5 mm). The analyses were performed at 40 $^{\circ}\text{C}$ with 1 mL min^{-1} of THF as eluent. Linear polystyrene standards (Agilent) with a molecular weight ranging from 370 to 9960 g mol^{-1} were used for calibration.

Qualitative and quantitative analysis of the organic compounds in the light biocrude samples were performed by GC-MS: 2 μL of BC1:isopropanol solution (0.1 g:10 mL) was injected in a GC 2010 with a GCMS-QP2010 mass spectrometer (Shimadzu) equipped with a ZB-5 MS Phenomenex column (30 m length, internal diameter 0.25 mm, film diameter 0.25 μm). The temperature was held at 40 $^{\circ}\text{C}$ for 10 min and then increased to 200 $^{\circ}\text{C}$ (heating rate 8 $^{\circ}\text{C min}^{-1}$, holding time 10 min) and 280 $^{\circ}\text{C}$ (heating rate 10 $^{\circ}\text{C min}^{-1}$, holding time 30 min). The qualitative analysis was performed comparing the mass spectra to the NIST 17 library after a previous 4-point calibration with the main compounds observed in the prior qualitative screening, using *o*-terphenyl as an internal standard.

The concentration of the WSO in the aqueous phase was evaluated by HPLC (LC-20 AT Prominence Shimadzu) equipped with a refractive index detector, a Hi-Plex H column 300x7.7 mm (Agilent) and a guard column PL Hi-Plex H 50x7.7 mm (Agilent), operating at 40 $^{\circ}\text{C}$ with a flow of 0.6 mL min^{-1} with 0.005 M sulfuric acid as mobile phase. Twenty-five microliter of each aqueous sample was injected after a 0.2 μm syringe filtration. The quantitative analysis was accomplished after a 5-point calibration following the NREL 42623 guidelines³⁵⁹. In addition, a Karl Fischer titration (848 Titrino Plus, Metrohm) was performed following ASTM E203-08 to determine the WSO yields.

The total organic carbon (TOC) of the aqueous phase was determined by a Merck TOC test kit and a Shimadzu UV-1800 spectrophotometer (605 nm). Samples were heated in a Merck TR320 thermoreactor for 2 h at 120 $^{\circ}\text{C}$ and then allowed to cool for 1 h in a test tube rack at room temperature. As DEE is slightly soluble in water, the TOC measurement of the aqueous samples collected with Procedure 1 was corrected with the method reported in Appendix B3 .

All solvents and reagents required for this work were purchased from Carlo Erba and Sigma Aldrich: they were used as received without any further purification. All chemicals were ACS reagent grade. Water for HPLC and THF for GPC were HPLC grade. Ultrapure water (0.055 $\mu\text{S cm}^{-1}$) for HTL experiments was produced with a TKA Microlab ultrapure water system. Analytical standards for GC and HPLC were $\geq 98\%$ purity. Chemical standards for HHV and CHNS calibrations were purchased from Leco. All gases were purchased from Rivoira. Argon, air, nitrogen and oxygen were supplied with a 99.999% purity, whilst helium was at 99.9995%.

The statistical analysis for the determination of significant operating parameter was carried out with the software Minitab (Minitab Inc.), by considering a significance level of 5%.

3.1.3 - Results and discussions

Feedstock Characterization

Table 9 reports the properties of the feedstock. As it was obtained after mechanical dewatering, the LRS still has a high moisture content, nearly 70 wt.% (w.b.), while its ash content is relatively low, as the fermentation feedstock was a hardwood (poplar) and not a herbaceous biomass, for instance. The lignin content is nearly 54 wt.% (d.b.).

Table 9. Characterization of the lignin-rich stream (w.b.: wet basis; d.b.: dry basis).

| Parameter | Value |
|---|-------|
| Moisture (wt.%) w.b | 69.7 |
| Ash (wt.%) d.b | 2.6 |
| Volatile matter (wt.%) d.b. | 71.0 |
| Fixed Carbon (wt.%) d.b | 26.4 |
| Higher Heating Value (MJ kg ⁻¹) | 22.9 |
| C (wt.%) d.b | 54.2 |
| H (wt.%) d.b | 5.9 |
| N (wt.%) d.b | 1.0 |
| S (wt.%) d.b | 0.2 |
| O (wt.%) d.b | 36.1 |
| Lignin content (wt.%) d.b | 53.9 |
| pH (-) | 4.4 |

The detailed results from the analysis of the lignin content are reported in Table 10: 52.51% of the lignin contained in the feedstock was acid insoluble. After the Soxhlet extraction of the extractives, the residual lignin, cellulose and hemicellulose were approximately ash-free; the low amount of ashes from the LRS were concentrated in the extractives due to leaching during the extraction process. A lower amount of residual cellulose and hemicellulose (structural sugars) was detected. The data are in good agreement with similar feedstock from enzymatic hydrolysis of lignocellulosic biomass investigated by Jensen et al.³⁶⁰

Table 10. Lignin and sugars content in LRS.

| Parameter | Value [-] wt. % (d.a.f.) |
|-----------------------|--------------------------|
| Acid insoluble lignin | 52.7 ± 4.99 |
| Acid soluble lignin | 0.253 ± 0.0216 |
| Total lignin | 53.0 ± 5.02 |
| Structural sugars | 35.8 ± 0.314 |
| Glucan | 30.7 ± 0.484 |
| XMG* | 4.94 ± 0.170 |
| Arabinan | 0.163 ± 0.0287 |

* Xylan, Mannan, Galactan

Comparison of Extraction Procedures

Given the lab-scale size of the experimental apparatus, the recovery of the HTL products is a challenging task, as some can be retained in the reactor wall after the experiments. In order to collect the largest amount of biocrude from these small reactors, a solvent extraction procedure was developed; it is technically not possible to separate the biocrude and the aqueous phase gravimetrically. This would instead be the preferred solution in case of large scale continuous processes and the same approach should be considered also in lab-scale experiments, as reported also by Castello, Pedersen and Rosendahl.³⁴⁴

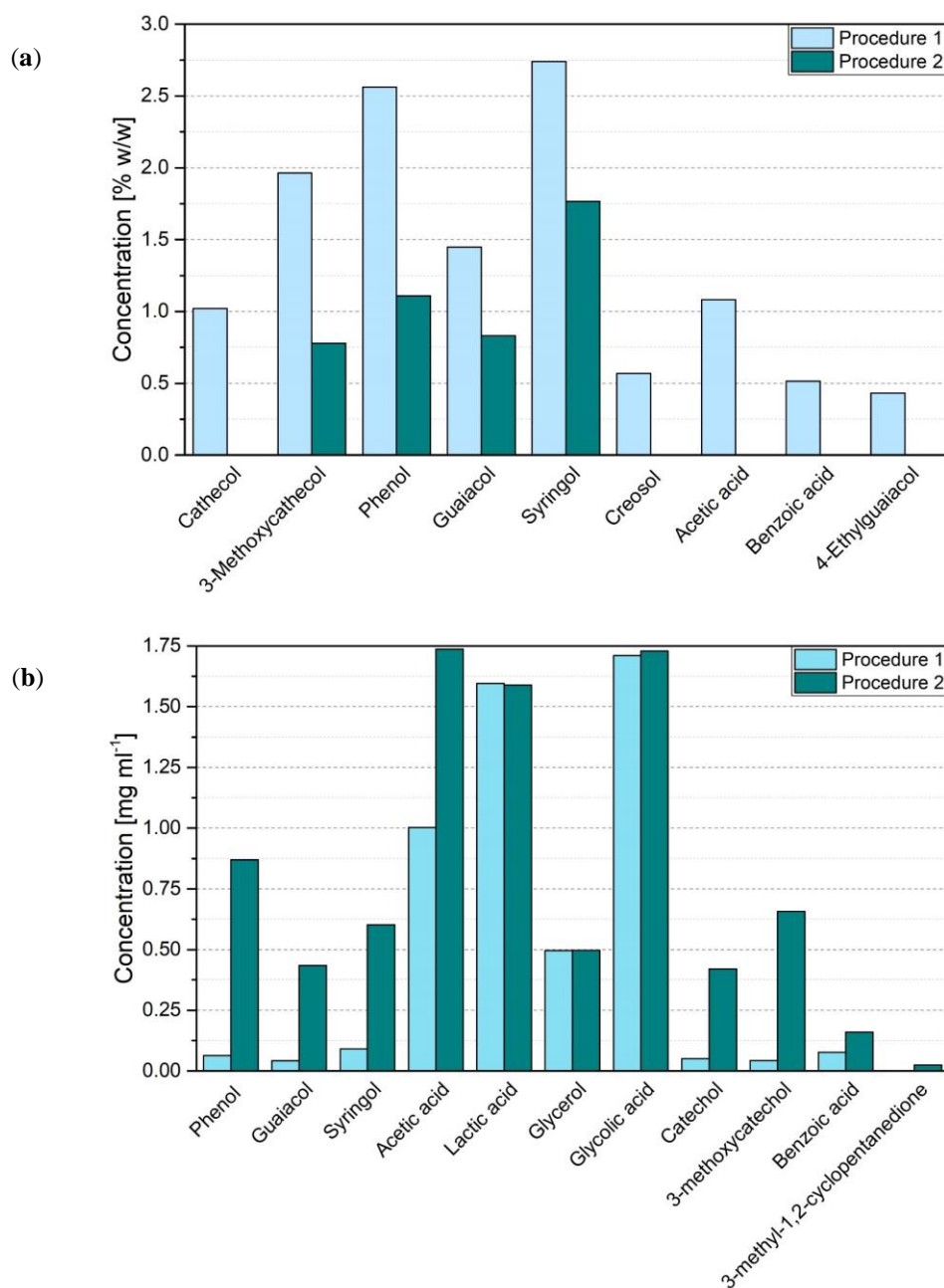


Figure 35. Effect of the collection procedure on biocrude 1 composition by GC-MS analysis (a) and on aqueous phase composition by HPLC analysis (b). The experiment was performed at 350 °C, 10 min, 10%.

Figure 35 reports the effects of the collection procedure on the composition of the light biocrude fraction (biocrude 1) and on the aqueous phase obtained from an experiment performed at 350 °C, 10 min, 10%. It is clearly visible that by using Procedure 1, the light biocrude has a higher amount of organics and, in particular, catechol, creosol, acetic acid, benzoic acid and 4-ethylguaiacol are under the detection limit in the case of Procedure 2. Accordingly, in the aqueous phase, the situation is reversed: a greater concentration of organics is obtained in the sample collected through the Procedure 2; this is true for all the calibrated compounds, except for lactic acid, glycerol and glycolic acid, whose concentrations are comparable. In addition, Table 11 shows the difference in products yield between the two collection procedures: a higher amount of BC1 and a lower amount of WSO are recovered by means of Procedure 1. This behavior is explained by the fact that in Procedure 1 water is not removed prior to DEE extraction of BC1 and therefore water-soluble organics are in part recovered in the light biocrude. From now on, the results showed in this study were based on this latter collection procedure, which was adopted because it allowed for a larger recovery of organics in the biocrude. However, it should be kept in mind that Procedure 2 would be more suitable for a direct comparison with a scaled-up/continuous process, where the biocrude would be gravimetrically separated from the water.

Table 11. Effect of the collection procedure on measured yields of products—experiment performed at 350 °C, 10 min, 10%. Absolute standard deviation is given in brackets.

| Product | Yield (wt.%) d.b. | |
|---------------|-------------------|-------------|
| | Procedure 1 | Procedure 2 |
| Biocrude 1 | 29.31 (0.01) | 23.1 (1.7) |
| Biocrude 2 | 22.5 (6.4) | 17.1 (0.7) |
| Solid residue | 11.8 (0.2) | 12.7 (0.9) |
| WSO | 12.2 (n.d.) | 20.5 (n.d.) |
| Gas | 5.5 (0.9) | 5.5 (1.4) |

n.d.: not determined

Yields and Influence of Operating Parameters

Figure 36 shows the yield of the HTL products, which were obtained at the operating conditions selected according to the experimental plan. The unidentified WSO were evaluated by difference and take into account also the losses due to the collection procedure.

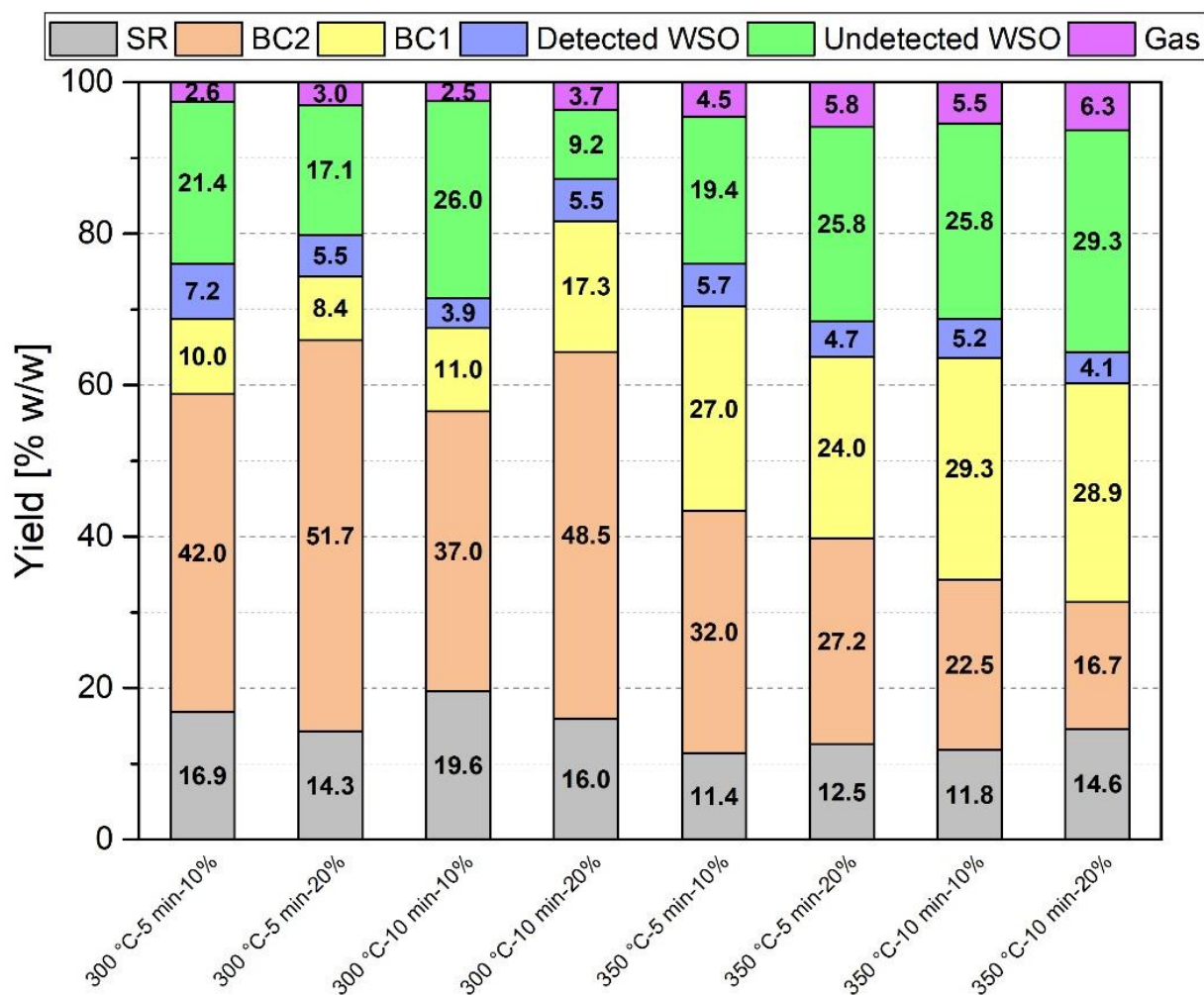


Figure 36. Dry-basis mass yields under different reaction conditions.

A high yield of total biocrude was obtained, ranging from 44.1% to 65.7wt.%, with the amount of light and heavy fraction changing with reaction conditions. In general, by increasing the reaction temperature, an increase in the yield of BC1 and a decrease in that of BC2 are observed, while the solid residue is approximately constant throughout all operating conditions, being char yields between 11.4% and 19.6wt.%. The maximum total biocrude yield was achieved at 300 °C, 10 min, 20% but nearly 74% of it was composed by BC2. At 350 °C, 10 min, 10%, the total biocrude yield was 51.8wt.% and the maximum BC1 yield was obtained (29.3wt.%). The yields of the detected WSO and of the gas products were lower and the latter experienced an increase at 350 °C, as a higher temperature is known to enhance gasification reactions ³⁶¹. It is known from the literature ⁶⁸ that the hydrothermal liquefaction of lignin is more likely to produce a rather high amount of solid product and therefore the use of alkali catalysts, such as KOH, K₂CO₃ or NaOH ^{361,362}, and capping agents as phenol or boric acid ^{350,362–364} have been suggested to limit the char formation hampering polymerization, as well as different reaction medium than just water, as ethanol, methanol or water-mixture thereof ^{354,365,366}. For instance, Arturi et al. ³⁶⁴ investigated the effect of phenol in the HTL of Kraft pine lignin with K₂CO₃ and, in the temperature range of 280–350 °C, at a concentration of 3.2%–3.6wt.% of phenol obtained comparable solid yields to the present study, where no additives were adopted and with the use of a similar solvent extraction procedure.

A statistical analysis was also performed in order to assess the influence of process parameters (temperature, time, B/W) and their interaction on BC1, BC2 and total biocrude yield. The significance level for this model was chosen to

be 0.05 (95% confidence level). A Pareto plot ³⁶⁷ is reported in Figure 37, Figure 38, Figure 39 to visually highlight the absolute values of the main factors and the effect of interaction between the three parameters. The reference line in the chart indicates the limit between significance. The Pareto plot is useful to discriminate which process parameters can be neglected and which ones have an importance in the hydrothermal conversion process. However, to have a deeper understating of the positive and negative effects, the main effects plot and the interactions plot are reported in Appendix B2 (Figure B2.1, Figure B2.2 and Figure B2.3), showing how positively or negatively each parameter or combination thereof affects the biocrude yield.

It can be noticed from Figure 37 that temperature (A) had the greatest effect on BC1 yield, but also the residence time (B) is statistically significant at 95% confidence level, being both above the mentioned reference line. On the contrary, the ratio B/W (C), as well as the combination of factors, can be considered as not significant for the yield of BC1. This validates the fact that the temperature and partially the residence time drive the reactions pathways that lead to the formation of lighter intermediates that forms the BC1, as already shown in other works.³⁶⁴

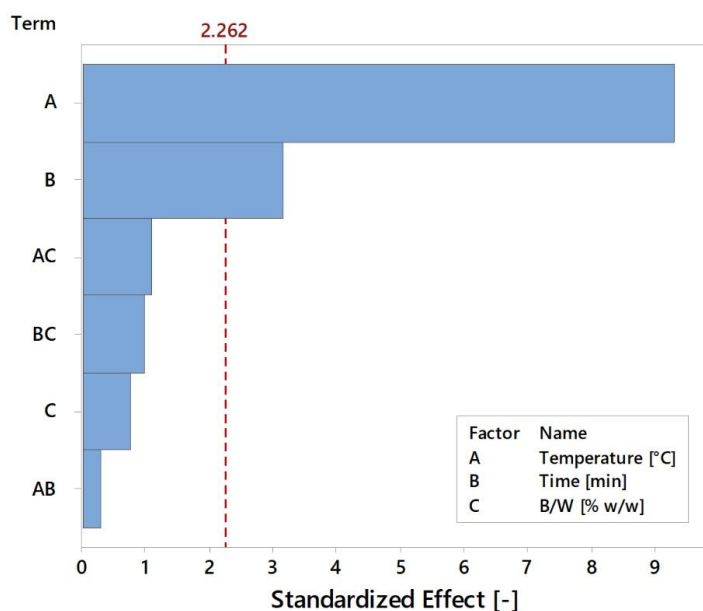


Figure 37. Normal plot of the standardized effects for BC1 yield.

Figure 38 depicts the Pareto chart reporting the absolute standardized effect of the factors for the BC2 yield. In this case, beyond temperature and time that remains important in the generation of BC2 heavy branched molecules, the combined interaction between temperature and B/W becomes significant. This means that a relative variation in the solid material introduced in the slurry, combined with a variation of the reaction temperature, has more influence in the reaction mechanisms that produce BC2 rather than varying the B/W alone.

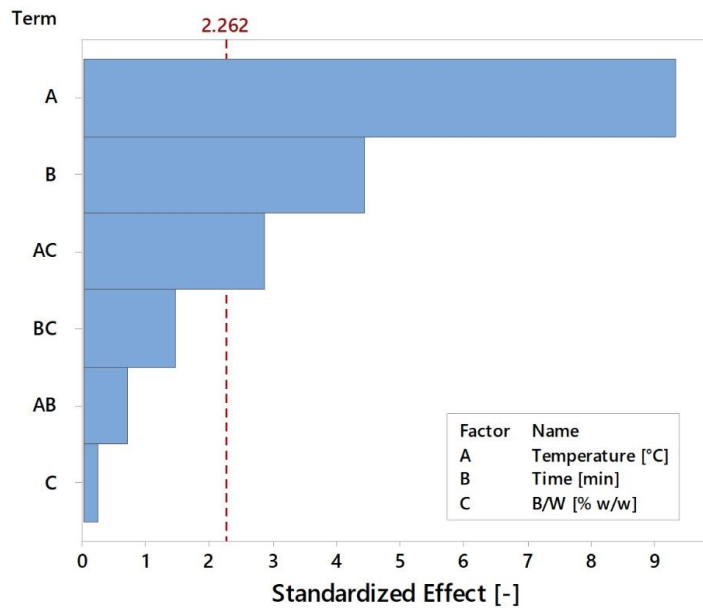


Figure 38. Normal plot of the standardized effects for BC2 yield.

Interestingly, concerning the total biocrude yield (Figure 39), the most significant factor is the interaction between temperature and B/W, followed by temperature. In this case, time is not significant, suggesting that, in order to detect a statistically significant effect, longer residence time should be investigated. This effect demonstrates that increasing (or decreasing) the biomass content together with a variation in the reaction temperature drive the degradation reactions that form the biocrude (e.g., phenols, methoxyphenols and longer oxygenated aromatics chains). In general, this means that, if the objective is to optimize the process in terms of total biocrude yield without considering its quality, both factors have to be jointly taken into account.

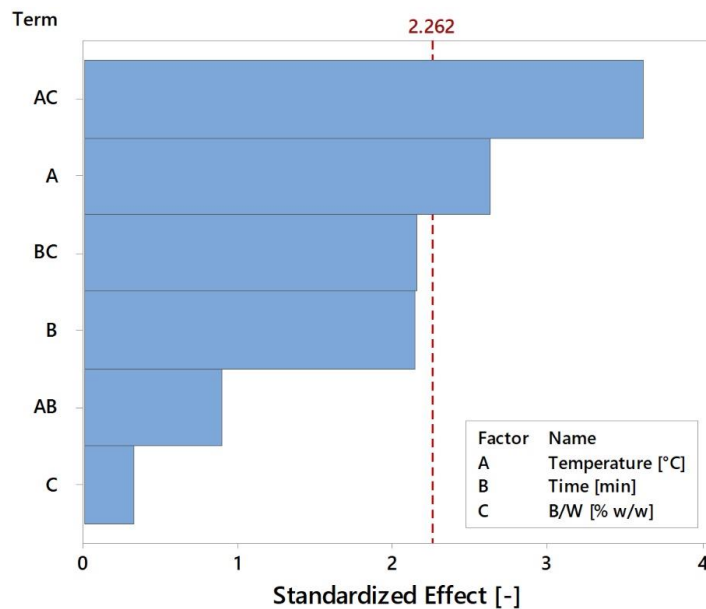


Figure 39. Normal plot of the standardized effects for total biocrude yield.

In addition to the experiments of the DOE, four other reaction conditions were tested in duplicates, by increasing temperature to 370 °C and time to 15 and 20 min, collecting the products with Procedure 1. Figure 40 reports the solid residue and biocrudes yields from the experiments carried out at a B/W of 10wt.%. At 370 °C, 5 min, 10% an increase in the yield of the light biocrude and a decrease in that of the heavy one is achieved; BC2 yield decreases with residence time, while BC1 yield reaches the maximum value of 41.7wt.% at 15 min.

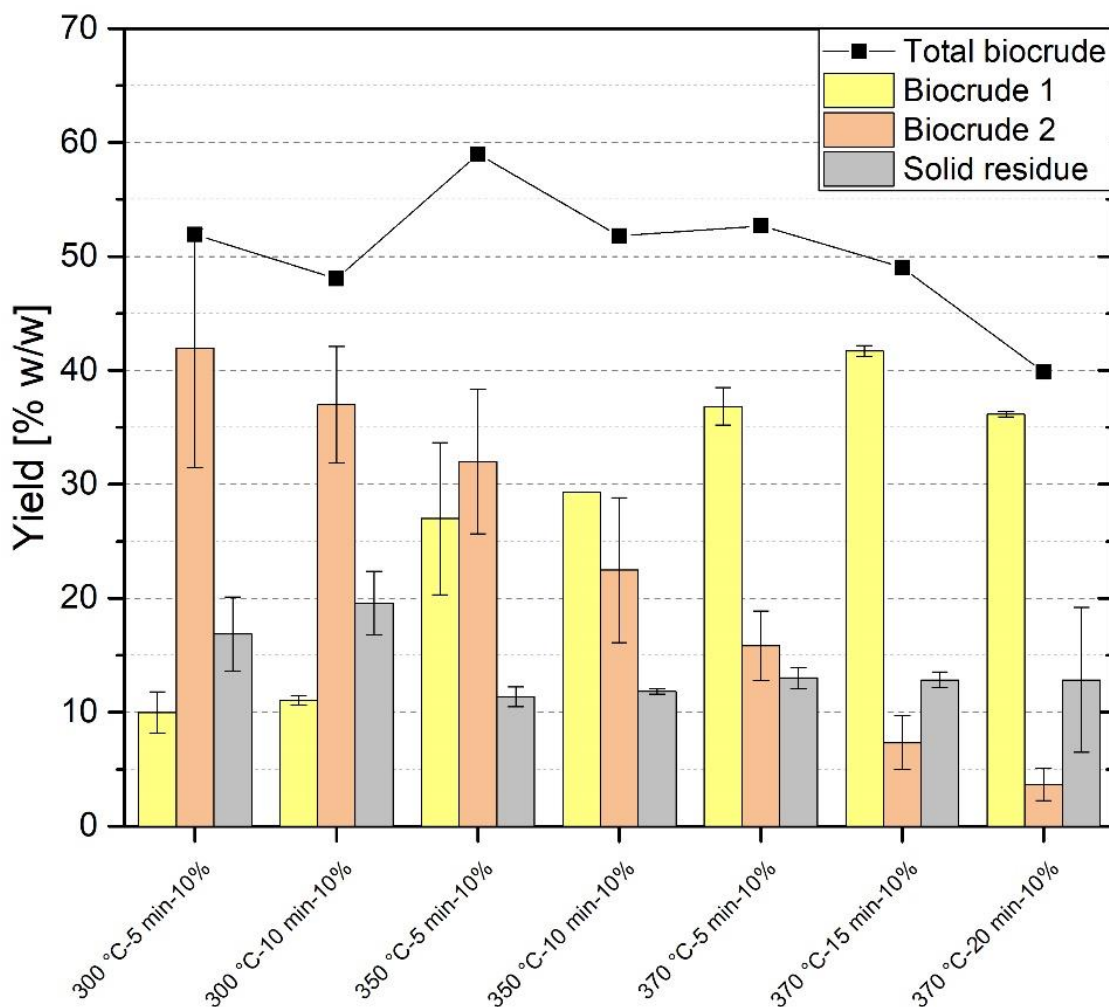


Figure 40. Effect of increased temperature and reaction time on products yield; error bars represent absolute standard deviation.

Although Castello, Pedersen and Rosendahl³⁴⁴ recently reported that favorable HTL conditions can be obtained also at supercritical condition, it is known that the HTL temperature range where the biocrude is maximized lies between 300 and 350 °C^{69,343}. At lower temperatures, partial conversion occurs, whereas at higher values the production shifts towards gases and char. In the present study, the maximum total biocrude yield was obtained at 350 °C, but the peak of its light fraction was achieved at 370 °C, indicating that higher temperatures are needed in order to optimize the conversion of this particular lignin-rich material.

Elemental Analysis and Higher Heating Value

With respect to the elemental analysis of the LRS (Table 9), both light and heavy biocrude reported an increase in the C and H content and a decrease in O and ash concentration, confirming the energy densification effect of the process. The as-received elemental analysis of biocrude 1 and 2 is reported in Appendix B4 (Table B4.1 and Table B4.2). In

general, a lower C content and a higher H and O content characterize the light biocrude fraction. These values are in line with literature: Arturi et al.³⁶⁴ performed batch HTL of Kraft lignin at 300 °C, 15 min, 6% lignin concentration with the addition of 1.6% of K₂CO₃ and obtained a biocrude with 69.9% and 23.6wt.% (d.b.) of carbon and oxygen content, respectively. The feedstock, the two biocrudes and the solid residues CHO compositions are given in the van Krevelen diagram of Figure 41. The light biocrudes have a wider range of H/C and O/C molar ratios with changing reaction conditions, while the heavy biocrudes are less dispersed, having an H/C comprised between 1.10 and 1.25 and an O/C between 0.25 and 0.30. The solid residues are the products that mostly differ from the LRS, having O/C ratios similar to BC2 but lower H/C. The H/C and O/C values of the BC2 obtained in this study are in line with those reported in the review of Ramirez, Brown and Rainey³⁶⁸, concerning HTL of lignocellulosic biomass. The decrease in the O/C and the increase in the H/C ratio of BC1 with respect to the feedstock suggest that the production of light biocrude was mainly due to decarboxylation rather than dehydration, which, on the contrary, was more evident for the production of BC2 and the solid residues.

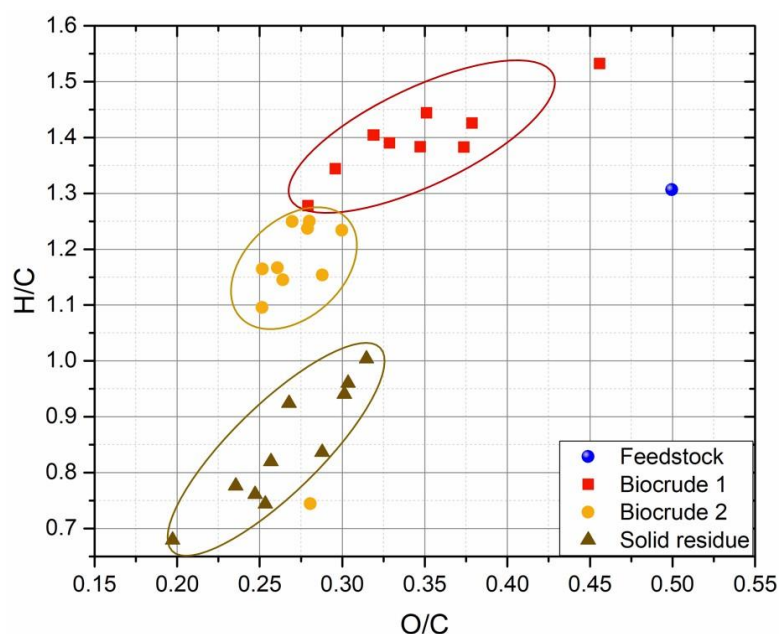


Figure 41. Van Krevelen diagram of lignin-rich stream (feedstock), BC1, BC2 and solid residue (char).

A significant energy densification effect was achieved through the HTL treatment: the higher heating values of the biocrudes ranged between 24.9 and 29.5 MJ kg⁻¹ (see Table B4.4 in Appendix B4). Although rather similar values were observed, HHVs of heavy biocrudes were generally higher than those of light ones. The HHV of the total biocrude was determined as a yield-based weight-average from that of BC1 and BC2. The maximum increase with respect to the feedstock (27%) was achieved at 350 °C, 5 min, 10%, the same operating condition, which produced the maximum amount of total biocrude at a B/W of 10%. When BC1 and BC2 are considered separately, their yields and energy densifications, in terms of calorific value, have contrasting trends. Indeed, the yield of BC1 increases with severity, while that of BC2 decreases. The opposite is shown for the HHV: that of BC1 nearly decreases, while that of BC2 increases with severity (Figure 42). However, considering the total biocrude as the sum of BC1 and BC2, both yield and HHV reach a maximum at the same condition, i.e., 350 °C, 5 min, 10%, as the HHV of total biocrude is evaluated as a yield-based weight-average from that of BC1 and BC2.

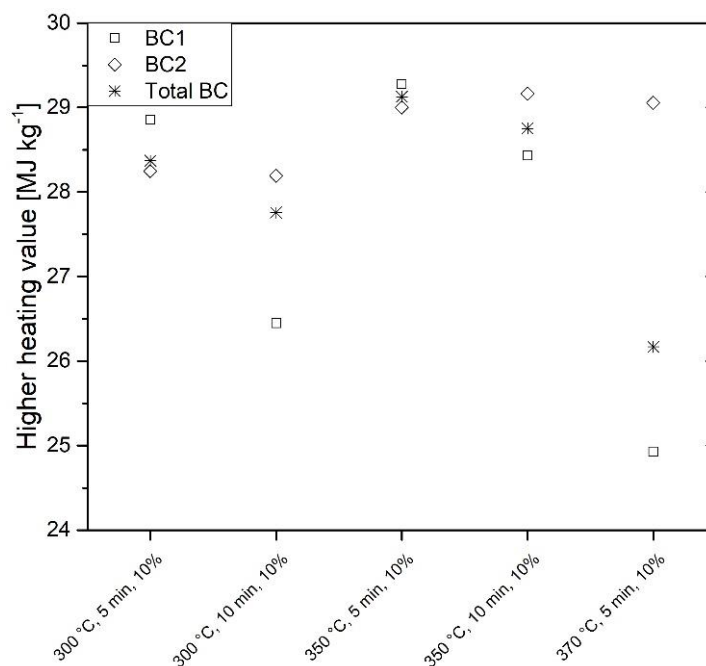


Figure 42. Higher heating value of light, heavy and total biocrude from the experiments carried out at 10% biomass-to-water mass ratio.

Carbon Balance

Figure 43 shows the carbon balance from the experiments set in the DOE and those carried out at 370 °C, 5 min, 10% and 20%. The balance was reasonably close, ranging from 83% to 108%, with an average value of 92%. The reasons behind this slight underestimated, or in one case, overestimated closure has to be addressed to the approximation of gas composition and to the propagation of errors through products collection and analysis. The majority of the carbon from the lignin-rich stream is retained in the biocrude (from 53.8% to 77.6%). At a low temperature, in general, it is mainly recovered in the heavy biocrude (from 40.9% to 62.3%), while at higher values, especially at 370 °C, it is largely retained in BC1. The carbon ending in the solid residue is not negligible, ranging from 13.0% to 23.6%, indicating that this product can still represent a valuable resource. The percentage of the feedstock carbon retained in the gas phase is the lowest among all products, which is estimated to lay between 1.0% and 3.1%, while a percentage range of 4.6%–11.3% is trapped in the aqueous phase in form of WSO.

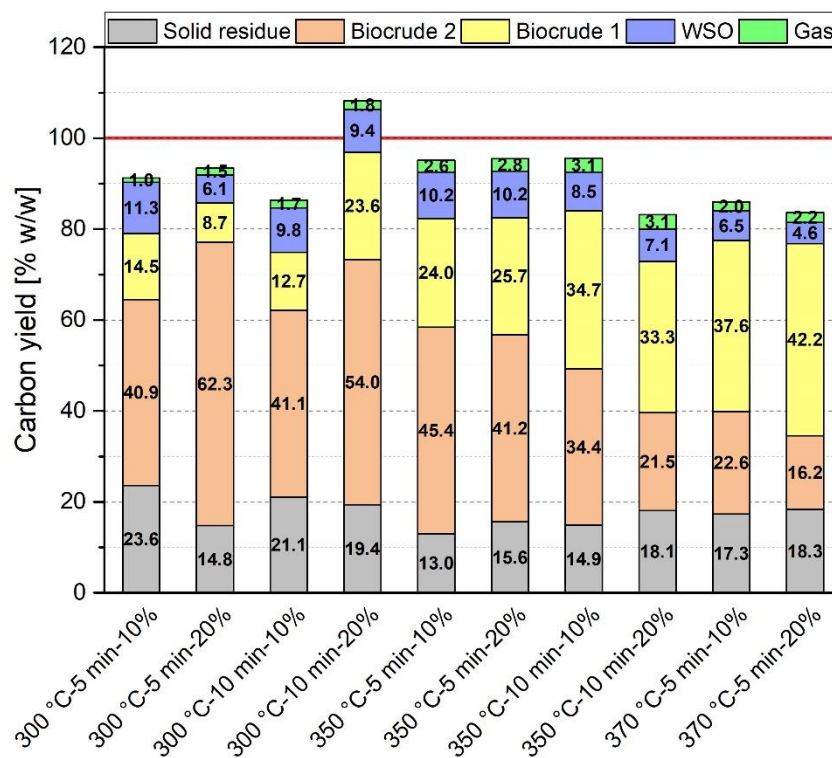


Figure 43. Carbon distribution among HTL products.

FTIR Analysis

FTIR spectra of the LRS, BC1 and BC2 were qualitatively analyzed in order to evaluate functional moieties modifications after the HTL treatment (Figure 44). If compared with the feedstock, biocrudes exhibit a decrease in intensity at $1000\text{--}1070\text{ cm}^{-1}$, along with the loss of a peak at 1056 cm^{-1} . This is probably due to breaking the $\beta\text{--O--4}$ or/and $\alpha\text{--O--4}$ ether bonds of lignin, as also confirmed by other studies^{353,369,370}, suggesting that the feedstock underwent to hydrolysis depolymerization^{345,353}. The macromolecular lignin backbone is in fact preferentially fragmented by ether bonds, which can be more easily broken than the C-C linkages through hydrolysis reactions³⁴⁵. The two biocrudes show only slight differences. The presence of a relevant peak in the BC2 spectrum around 1700 cm^{-1} , typical of $\nu\text{C=O}$ ^{353,369–372}, is presumably related to the presence of acetone residues, confirmed by the peaks around 1360 and 1419 cm^{-1} . The peaks in the region of aromatics, typical of the lignin structure, around 1600 , 1515 and 1460 cm^{-1} ^{369,370}, are always present in the three samples, suggesting that the lignin aromatic rings were, in general, preserved during HTL. An enhancement of the intensity around $1250\text{--}1200\text{ cm}^{-1}$ is probably related to guaiacols and mainly syringols³⁷³, first products of lignin depolymerization³⁴⁵.

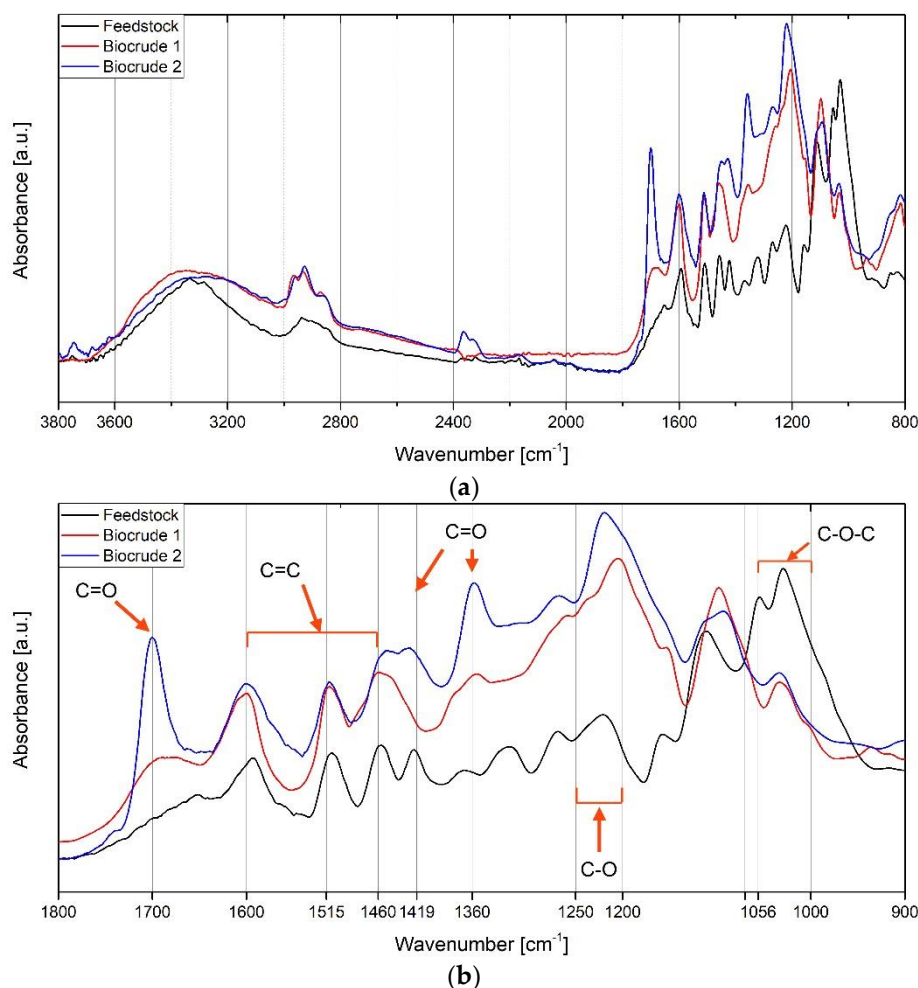


Figure 44. Infrared spectra of the LRS and light and heavy fraction of biocrude from the experiment carried out at 370 °C, 5 min, 20%; (a) entire spectra, (b) particular.

Molecular Weight Analysis

In order to gain further insight on differences between the light and the heavy biocrude, their molecular weight (or molar mass) was evaluated by gel permeation chromatography (GPC). The weight-average molecular weight (M_w), the number-average molecular weight (M_n) and the polydispersity index ($PDI = M_w/M_n$) are reported in Appendix B5 (Table B5.1). In addition, it was attempted to determine the average molecular weight of the lignin-rich stream, but only ~10% of this was soluble in THF (ambient temperature) and therefore this value was not estimated. Differently, the biocrude samples were completely THF-soluble and, as expected, the molar masses of the light biocrudes were far lower than the ones of the BC2. The former is comprised between 390 and 490 g mol^{-1} , while the latter range between 1030 and 1400 g mol^{-1} . The values of M_w at 10% and 20% B/W for BC1, BC2 and total biocrude are shown in Figure 45. The M_w of the total biocrude was determined as a yield-based weight-average from that of BC1 and BC2. Concerning BC1, a higher B/W, in general, produces a higher molar mass. An increase with residence time is shown at 300 °C, while an opposite behavior is reported at 350 °C. A maximum is reached at 350 °C, 5 min, both at 10% and 20wt.% of B/W, though the latter is subjected to high standard deviation, and the minimum values are reached at 370 °C (400 and 391 g mol^{-1} , respectively). Despite the complex trend of the molecular weight of BC2, the M_w of the total biocrude clearly decreases with temperature and time, changing from 1146 to 565 g mol^{-1} , indicating that a higher extent of depolymerization occurred at harsher reaction conditions.

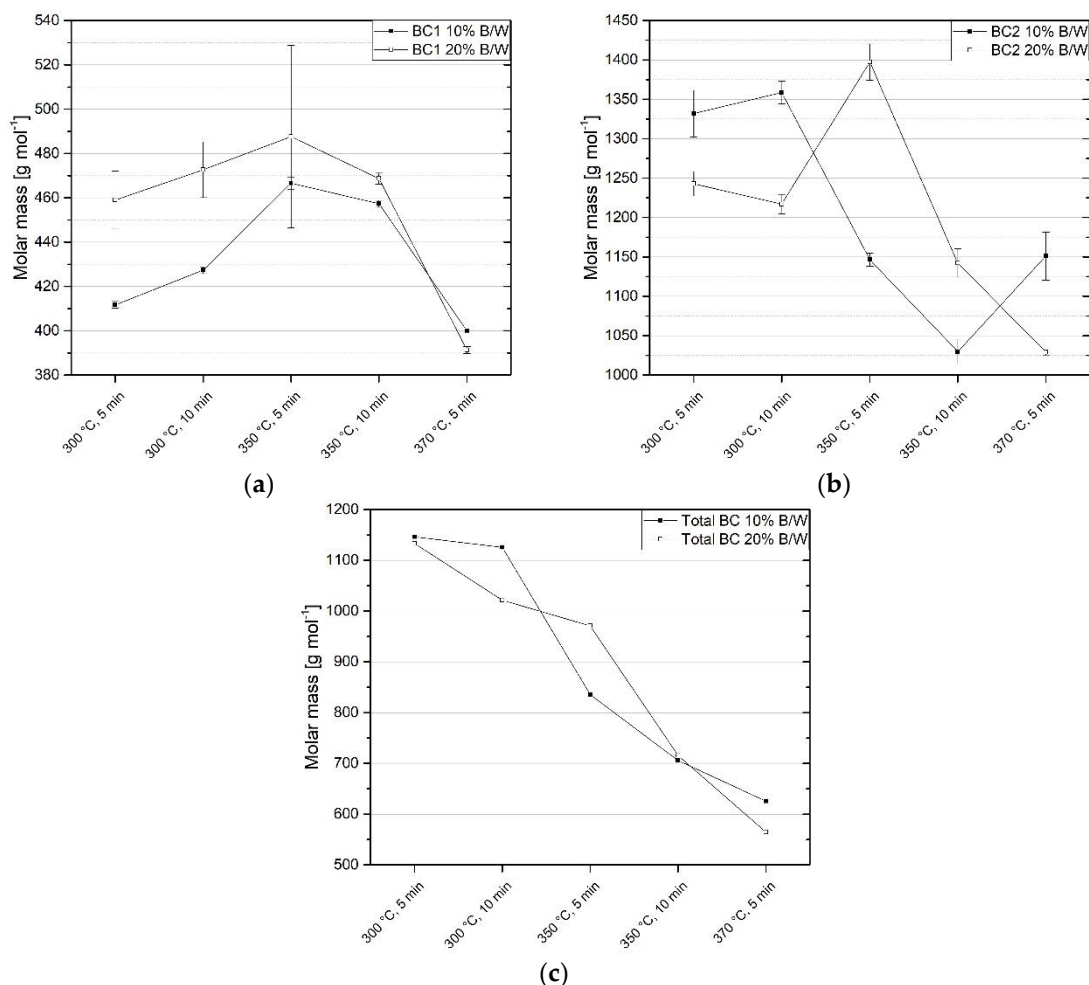


Figure 45. Weight-average molecular weight at different reaction conditions: (a) biocrude 1, (b) biocrude 2, (c) total biocrude. Error bars represent the absolute standard deviation.

Furthermore, it is interesting to look at the effect of reaction conditions on the molar mass distributions (Figure 46). The shape of the distribution is only slightly altered by changing residence time at fixed temperature and B/W but greatly changes with temperature, suggesting the latter to be a more influencing parameter, at least at the investigated reaction conditions. Concerning the light biocrude, at 300 °C and 10%, there is a contribution of low weight compounds (between 40 and 100 g mol⁻¹), which disappears at 350 °C and reappears, even with a slightly different shape, at 370 °C, confirming the presence of a maximum. On the contrary, the molar masses of the heavy biocrudes are more homogeneous, as confirmed by the lower PDI. Considering the BC1 samples obtained at a B/W of 20%, at 300 °C they still exhibit a low-molecular-weight peak, but, in this case, it is narrower and shifted towards higher values, precisely between 100 and 200 g mol⁻¹. The shapes of the distributions of samples at 350 and 370 °C are more similar to the ones of the 10% case. The distributions of BC2 are comparable to those obtained at 10%, only a more marked hump between 500 and 600 g mol⁻¹ is present in the samples obtained at 300 °C.

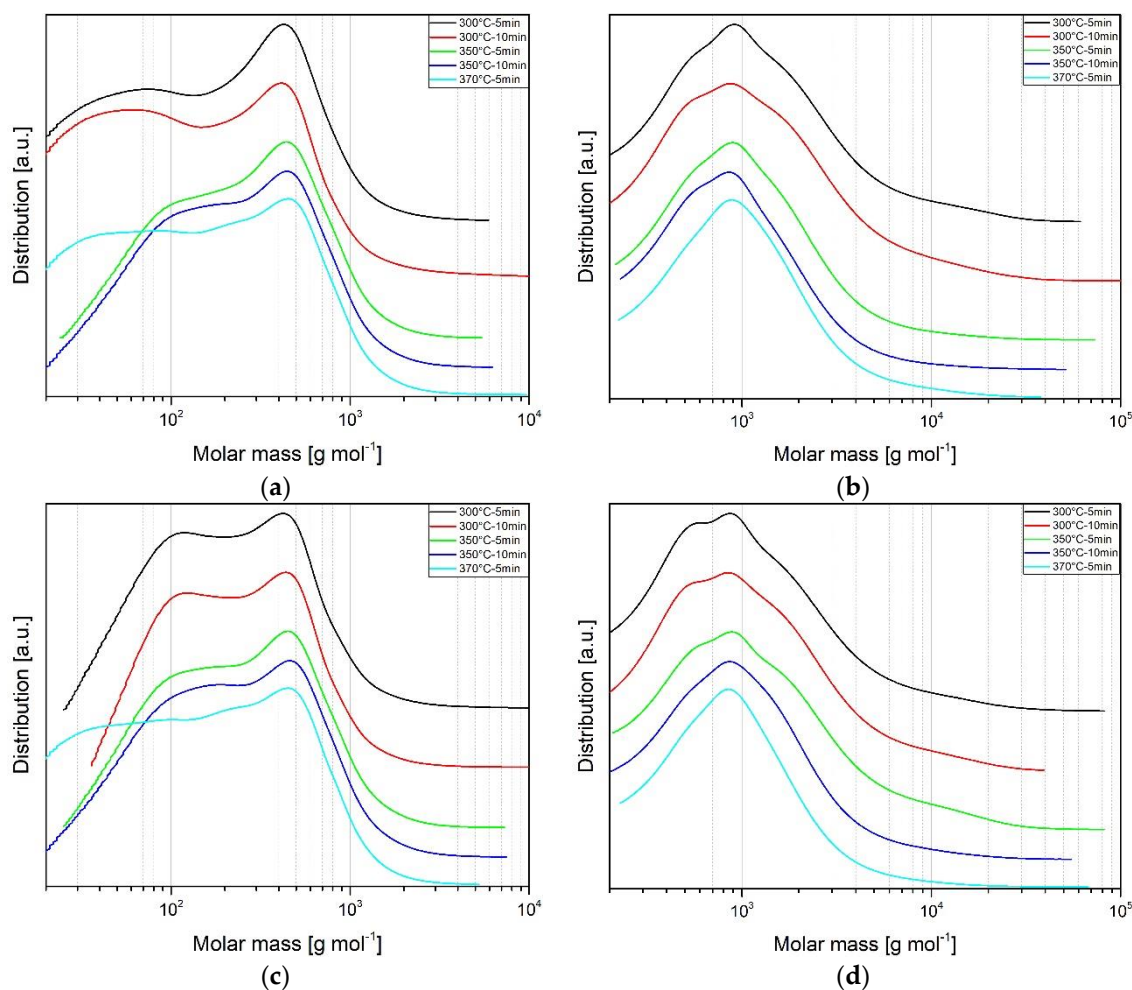


Figure 46. Stacked molecular weight distribution of BC1 (left) and BC2 (right) from experiments carried out at 10wt.% (a–b) and 20wt.% (c–d).

These findings, along with the FTIR results, show that LRS was effectively depolymerized during the HTL treatment, even if without any alkali catalyst or capping agent and with far lower residence time than commonly reported in lignin depolymerization experiments, where the reaction time is generally extended up to several tens of minutes or hours^{353,354,363,374}.

3.1.4 - Conclusions

In this work, hydrothermal liquefaction of lignin-rich stream (LRS) from a demo-scale lignocellulosic ethanol plant was investigated without the use of any catalyst or capping agent, recovering two biocrude fractions, a light (BC1) and a heavy one (BC2). Batch lab-scale experiments were carried out and two different collection procedures were developed and compared in terms of yields, biocrude and aqueous phase composition. When performing lab-scale experiments, the use of extraction solvents is somehow mandatory, due to technical limitations related to the small size of reactors, and it was demonstrated here that the collection procedure directly affects yields and products composition. Thus, particular attention should be given when comparing the results from different studies. Indeed, if the aqueous phase is not separated prior to biocrude extraction, a larger amount of biocrude is recovered. On the other hand, removing the process water before biocrude recovery allows for a more suitable comparison with an industrial/continuous process, where the biocrude will be reasonably separated from the water by gravity. Moreover,

it was statistically demonstrated that, at the investigated reaction conditions, the most significant factor influencing light, heavy and total biocrudes yield was the reaction temperature. Residence time was significant only as regards the yield of BC1 and BC2, while the biomass-to-water mass ratio (B/W) significantly affected only the BC2 and total biocrude yields by its interaction with temperature. The maximum total biocrude yield (65.7wt.%) was achieved at 300 °C, 10 min, 20% while the maximum yield of the light fraction (41.7wt.%) was achieved at 370 °C, 15 min, 10%. These results suggest that the conversion process can be optimized in different ways, depending on the characteristics or on the amount of the biocrude to be obtained. Another interesting result in biorefinery perspective is that the HTL process increased the feedstock energy density up to 27%. The elemental analysis suggests that the light biocrude was mainly produced by decarboxylation reactions rather than dehydration, which was more evident for BC2 and the solid residue. The carbon balance indicated that only a low amount of carbon from the LRS ended up in the aqueous phase as water-soluble organics and its major part was retained in the biocrude (up to 77.6%). At low temperatures, carbon is particularly concentrated in the heavy fraction, while at higher temperatures it moved to the light one (up to 42.2%). The FTIR analysis showed that the lignin aromatic structure was preserved in the two biocrudes, showing that the feedstock was mainly subjected to hydrolysis depolymerization. Indeed, the analysis of the molecular weight confirmed this statement, indicating that a consistent fractionation occurred, especially favored by high temperatures. The HTL experiments herein reported effectively depolymerized the lignin matrix, preserved the aromatic structure of the feedstock and made available phenolic compounds that are valuable precursors of fuel and chemicals, for further separation, purification and processing. It was therefore shown that LRS has the potential of being a source for valuable chemical intermediates and hydrothermal liquefaction can represent a promising technology for the conversion of this high-moist co-product.

3.2 - Influence of reaction conditions and catalytic additives on the organic monomers yields in biocrude and aqueous phase

3.2.1 - Introduction

The second part of the work was focused on the identifications and quantifications of light compounds in the biocrude and aqueous phase derived from lignin hydrothermal depolymerization. The main goal was to observe how the composition is affected by varying the process operative conditions as well as the study of the effect of catalytic additives to improve the depolymerization treatment, as schematically depicted in Figure 47.

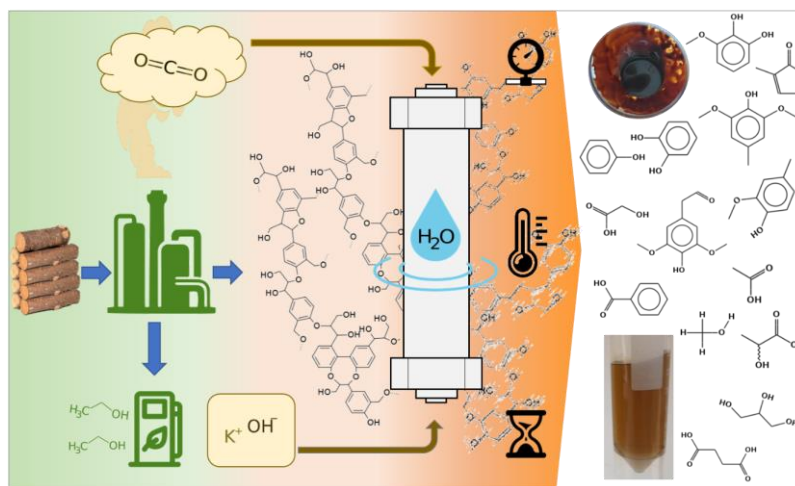


Figure 47. Graphical scheme of lignin depolymerization with catalytic additive

Lignin from paper and pulp industries (Kraft lignin) have been depolymerized by Yuan et al.³⁷⁵ at 220–300 °C in a water-ethanol medium with NaOH as catalyst and phenol as capping agent, observing a decrement in the products molecular weight distribution, optimized at 260 °C and 3 h of residence time. On the other hand, Nguyen et al.³⁴⁸ studied the effect of higher temperature (290–370 °C) on Kraft lignin liquefaction in subcritical water using ZrO_2/K_2CO_3 as catalysts and phenol as the co-solvent, characterizing the composition of the aqueous phase and the biocrude at different temperature levels and catalyst load. Regarding lignin from lignocellulosic ethanol, the conversion into valuable products through HTL has been investigated by other authors in the past. Jensen et al.³⁶⁰ investigated the conversion of enzymatic hydrolysis lignin, focusing in how plant species and pretreatment severity affect the HTL product composition and lignin depolymerization. Katahira et al.³⁷⁶ investigated base catalyzed lignin depolymerization from five different feedstocks, evaluating product composition after 40 min of reaction time, varying reaction temperature (270–300–330 °C) and amount of alkaline additive. Nielsen et al.³⁷⁷, studied batch liquefaction of lignin from enzymatic hydrolysis in supercritical ethanol by varying reaction temperature (250–450 °C), reaction time (0–8 h), and solvent:lignin ratio (0–40 g in 100 ml), in absence of catalysts.

In addition, the effect of KOH was evaluated, highlighting how the liquefaction conversion is influenced. A variation of initial pH, with the addition of KOH, have already been demonstrated as an effective method to optimize the depolymerization of Kraft lignin by Belkheiri et al.³⁷⁸. In this study, its effect has been evaluated on a different type of lignin that was found to generate a higher acidity in the aqueous product, thus finding always a low pH in the

residual aqueous phase regardless of the initial amount of KOH. On the other hand, the effect of an acid reaction environment has been tested with the use of supercritical CO₂ (sCO₂). Indeed, concentrated carbon dioxide is always produced in large amount during sugars fermentation: theoretically, 1 mol of glucose yields 2 mol of ethanol and 2 mol of CO₂, and the worldwide carbon dioxide emission due to first and second generation ethanol fermentation plants was estimated to be 49.8 Mt.^{379,380} Some efforts have been made to capture and store CO₂ in order to further reduce the carbon footprint of the technology through bio-energy with carbon capture and storage (BECCS) technologies as, differently to fossil fuels, the CO₂ produced in ethanol plants came from renewable sources and its capture would determine a net atmospheric carbon removal.^{379,381} Furthermore, the use of CO₂ at its supercritical state has been extensively investigated as selective solvent for phenolic compounds separation and extraction.^{382–385} Moreover, Numan-AI-Mobin³⁸⁶ converted alkali lignin using a mixture of subcritical water and supercritical carbon dioxide, varying temperature (250, 300, and 350 °C) and water-to-sCO₂ ratio (1:5, 1:2, 1:1, and 2:1) showing an enhanced yield of specific phenolic compounds and suggesting a conversion mechanism driven by the heterogeneous acid catalytic activity of the dissolved CO₂. In another study, Chan et al.³⁸⁷ studied the effect of supercritical carbon dioxide on the liquefaction of palm kernel shell, suggesting an improved biocrude yield at lower temperature due to the higher CO₂ dissolution in water enhancing the protons availability in the water medium. In the present work, the measured products yield and the selectivity towards phenolic species have been evaluated at 300 °C, comparing the results to the ones observed in uncatalyzed and base catalyzed reactions.

In a perspective of industrial applications, HTL should ideally target high yield, minimization of reaction time and the increasing in solid load of the processed slurry. For these reasons, in a previously published manuscript³⁴⁰, the authors suggested how the HTL conditions can be tuned to optimize the process in term of biocrude mass yield testing in a batch-reactor unit, short residence time (5–10 min) and two level of solid load (10–20 wt. % of dry biomass to water ratio, B/W). In addition, the B/W ratio influence to the process was found to be not statistically significant in regards to the light biocrude mass yield and in this work, it was chosen to analyze the results from experiments with 10 wt. % B/W. These previous results suggested different ways for process optimization, affecting the characteristics and the amount of produced biocrude. Thus, to further improve the understanding of HTL-based conversion of lignin-rich stream, the present work intends to add specific know-how on the influence of several reaction conditions in subcritical water such as temperature, residence time, base or acid catalyzed reactions, focusing on the monomeric composition of the liquid products. A critical characterization of the HTL products is here presented, showing how valuable monomers from the LRS conversion can be optimized in terms of yield and how the reaction conditions affect the depolymerization process and products.

3.2.2 - Materials and methods

Feedstock Characterization

Lignin-rich material was obtained from an industrial demo-scale lignocellulosic ethanol plant after ethanol distillation and water mechanical separation. The original biomass feedstock used in the ethanol biorefinery was hardwood, specifically poplar. Carbon, hydrogen, nitrogen, and sulfur (CHN-S) content was quantified using a Leco (St. Joseph, Michigan, USA) TruSpec (UNI EN 15104, ASTM D4239) and oxygen was obtained by difference. LRS moisture, ash content and volatile matter were determined in a Leco TGA 701 (UNI EN 13040, UNI EN 14775, UNI EN 15148) and fixed carbon was calculated by difference. The feedstock was further characterized after mixing solid particles of

lignin with water for the slurry preparation, quantifying the water-soluble compounds in a LC-20 AT Prominence (Shimadzu, Kyoto, Japan) prior to the hydrothermal reactions. The HPLC apparatus is equipped with a refractive index detector, a Hi-Plex H column 300 x 7.7 mm and a guard column PL Hi-Plex H 50 x 7.7 mm (Agilent, Santa Clara, California, USA), operating at 55 °C with a flow of 0.6 mL min⁻¹ with 0.005 M sulfuric acid as mobile phase. Moreover the percentage of lignin and structural sugars were determined accordingly to the NREL/TP-510-42618 procedure.³⁵⁹

Microreactors Test Bench for Screening Reaction Conditions

Biocrude and aqueous phase samples from hydrothermal liquefaction were obtained in a custom-made Micro-Reactor Test Bench (MRTB) described in the previous paragraph (pag. 94). In brief, prior to experiments a slurry sample was prepared stirring dried feedstock in ultrapure water (0.055 µS cm⁻¹) at the desired biomass-to-water mass ratio. For each test, 33 g of slurry were inserted into a 43 mL stainless steel reactor. A leakage test was performed with argon pressurized at 8 MPa before purging the system with nitrogen (0.5 MPa). An initial pressure of 3 MPa was set using argon and the reactor was afterwards immersed into a fluidized sand bath previously heated at the requested temperature. Evaluation of residence time started when the temperature in the reactor reached 2 °C below the set temperature, the reactor was then rapidly cooled by immersion into a water bath.

Two biocrude fractions were always recovered at the end of each test by separating them from the residual aqueous phase through a double-step diethyl-ether (#32203-M Merck/Sigma-Aldrich) and acetone (#32201-M Merck/Sigma-Aldrich) extraction procedure (Procedure 1), carried out at ambient temperature. First, the reactor was washed with diethyl-ether (DEE), vacuum filtering the content over a Whatman glass microfiber filter (1 µm). Water and water-soluble organics (WSO) were then recovered by gravity separation, while DEE-soluble fraction (lighter biocrude, BC1) was obtained after rotary evaporation of DEE at reduced pressure. Finally, the reactor walls and the solids were washed with acetone (DMK) recovering a second biocrude fraction (BC2) and separating the solid residues (SR). A scheme representing the solvent extraction is depicted in Figure 48. Furthermore, a second and different procedure (Procedure 2) was also tested to evaluate the influence of the extraction method on compounds distribution. Here the aqueous phase was recovered before the solvent extraction step.

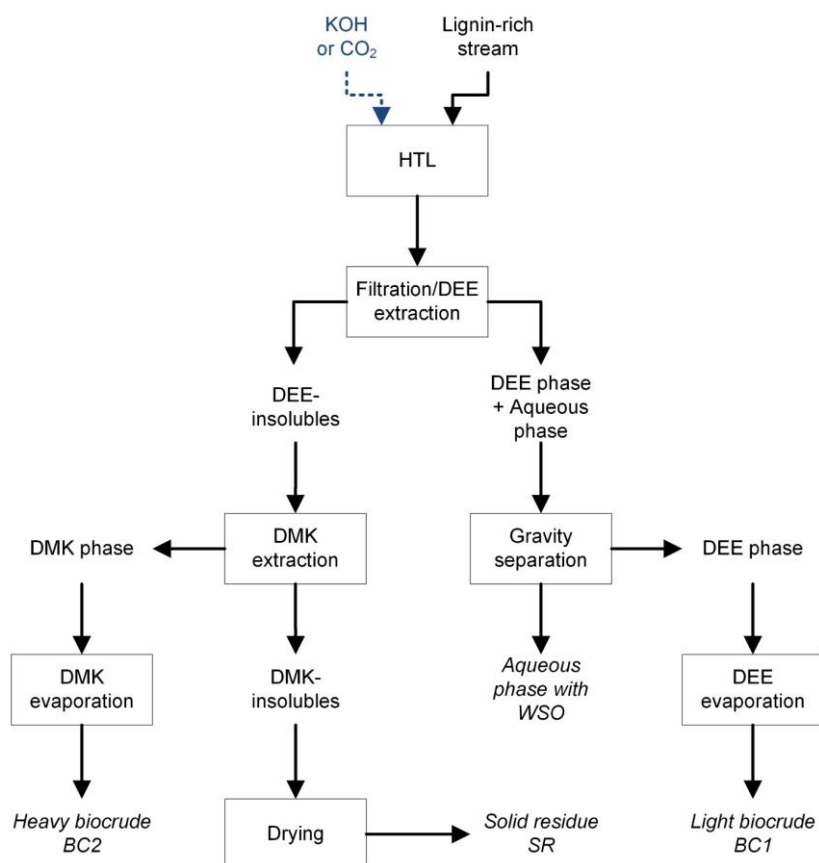


Figure 48. Extraction procedure for hydrothermal liquefaction (HTL) products recovery (Procedure 1).

For the additional tests with CO_2 , an overall molar ratio of 2.68% $\text{molCO}_2/\text{molH}_2\text{O}$ was inserted in the reactor at 3 MPa and 25 °C, substituting the Ar used for the uncatalyzed reactions and, at this initial condition, 1.83% $\text{molCO}_2/\text{molH}_2\text{O}$ were dissolved into water.

Hydrothermal Reaction Conditions

The experimental campaign was first carried out by varying the reaction severity through temperature and residence time regulations. The ranges of reaction parameters were chosen within typical industrially viable limits. Residence time ranged respectively from 5 to 10 min and 10 wt. % of B/W, while three values were investigated for reaction temperature, 300–350–370 °C. The effect of base catalyzed reactions at 300 and 350 °C was also evaluated by adding KOH in a percentage of 2 wt. % and 4 wt. % relative to dry lignin sample. Hydrothermal reactions were also tested in the presence of an acid environment using supercritical CO_2 at 300 °C and the effect evaluated in comparison with KOH and in absence of catalysts.

Characterization of Liquid Products

Each hydrothermal liquefaction experiment was replicated at least two times. The aqueous phase (AP) was analyzed by quantifying the WSO content in HPLC. Before the injection, aqueous samples (25 μL) were first filtered through a 0.2 μm pore size syringe filters and quantitative analysis was carried out after a five levels calibration for each compound. Moreover, total organic carbon (TOC) analyses were carried out on aqueous phases samples by a TOC Cell Test Spectroquant® 14879 (Merck) test kit and a Shimadzu UV-1800 spectrophotometer (605 nm). A Merck

TR320 thermoreactor was used to heat the samples for 2 h at 120 °C and then cooled for 1 h in a test tube rack until reaching room temperature. The correction due to DEE contamination is reported in authors' previous work ³⁴⁰. Qualitative and quantitative analysis of BC1 samples were carried out into a GC-MS apparatus: 0.1 g of BC1 samples were first dissolved in 10 ml of isopropanol and 2 µL of the solution were injected in a GC 2010 with a GCMS-QP2010 mass spectrometer (Shimadzu, Kyoto, Japan). The gas chromatograph was equipped with ZB-5 MS column (Phenomenex, Torrance, California, USA): 30 m length, 0.25 mm internal diameter and 0.25 µm film diameter. The temperature was initially set at 40 °C for 10 min, increased first to 200 °C (heating rate 8 °C min⁻¹, holding time 10 min) and then to 280 °C (heating rate 10 °C min⁻¹, holding time 30 min). Spectral interpretation was performed with NIST 17 database and the quantification was carried out through a 4-point calibration using o-terphenyl as internal standard. A complete list of calibrated compounds for GC-MS and HPLC quantification is given in Table B6.1 in Appendix B6. In both the adopted analytical methods, the compounds detected below 25 % of the lowest calibration point concentration were considered as below limit of quantification and not taken in account. In addition, a comparison between the molecular weight (polystyrene equivalent) of the light and heavy biocrudes obtained by KOH-catalyzed reactions were evaluated by gel permeation chromatography (GPC). Tetrahydrofuran (THF) was used to dissolve biocrude samples, leaving the solution overnight. The solution was syringe-filtered at 0.45 µm and 100 µL were injected in an HPLC apparatus (Shimadzu LC 20 AT Prominence) with two in-series columns (Agilent, PL gel 5 µm 100 Å 300 x 7.5 mm), a guard column (Agilent, PL gel 5 µm 50 x 7.5 mm) a refractive index detector. The flow of the eluent (THF, 1 mL min⁻¹) was kept at 40 °C. Calibration was carried out with linear polystyrene standards (Agilent, 370–9960 g mol⁻¹).

The quantitative results were further referred to the dry feedstock mass, calculating the yields according to the equations below:

$$Y_x = Y_{BC1,x} + Y_{WSO,x}$$

$$Y_{BC1,x} = \frac{C_{GC,x} \cdot v_{GC}}{m_{l,db}} \cdot 100 ; Y_{WSO,x} = \frac{C_{HPLC,x} \cdot v_{HPLC}}{m_{l,db}} \cdot 100$$

Where Y_x is the total yield of a x compound as sum of yields in BC1 ($Y_{BC1,x}$) and water soluble organics (WSO) in the aqueous phase ($Y_{WSO,x}$). While $C_{GC,x}$ and $C_{HPLC,x}$ are the concentrations in µg mL⁻¹ obtained in GC-MS and HPLC multiplied for the respective volumes of each phase (v_{GC} and v_{HPLC}). $m_{l,db}$ represents the mass of feedstock in dry basis employed in each experiment.

NMR analyses were carried out on BC1 and BC2 samples. Moreover, ¹H NMR spectra were recorded with a INOVA NMR 400 (Varian, Palo Alto, California, USA) using dimethylsulfoxide-d₆ as solvent. Spectra were referenced to tetramethyl-silane. Solvent suppression was employed to record the spectra.

3.2.3 - Results and discussions

The hydrothermal conversion of LRS resulted in the generation of five main products: DEE-soluble biocrude (BC1), DMK-soluble biocrude (BC2), aqueous phase (AP) with water-soluble organics (WSO), char or solid residue (SR) and gases. The solvent extraction procedure was employed to maximize the recovery of biocrude fractions. In another work³⁴⁰ the authors reported the results of the uncatalyzed experimental campaign only in terms of yields, elemental analysis and molecular weight: here, a detailed characterization of BC1 and AP was carried out to observe how the mechanism of lignin depolymerization is influenced by reaction conditions.

A detailed list of the resulting overall mass yields is presented in Table 12, including the tests with KOH and sCO₂ as additives. The analyzed compounds in BCs and AP were grouped in these chemical classes: Phenol (considered as a single compound), Methoxyphenols, Dimethoxyphenols, Catechols, Methoxycatechols, Phenolic Ketones, Phenolic Aldehydes, Acids, and Alcohols.

Table 12. Yields of the HTL products from all investigated reaction conditions. Absolute standard deviation is reported in brackets.

| Exp. Conditions | Catalyst | BC1 | BC2 | SR | Gas | WSO + loss* |
|--------------------------------|------------------|----------------|---------------|--------------|----------------|---------------|
| 300°C 5 min 10 wt.% B/W | - | 9.8% (1.6%) | 38.8% (11.5%) | 16.5% (3.0%) | 2.4% (0.7%) | 32.6% (10.5%) |
| 300°C 10 min 10 wt.% B/W | - | 11.0% (0.3%) | 33.0% (7.7%) | 19.5% (2.0%) | 1.5% (1.9%) | 34.9% (9.8%) |
| 350°C 5 min 10 wt.% B/W | - | 27.0% (6.7%) | 32.0% (6.4%) | 11.4% (0.9%) | 4.5% (0.8%) | 23.8% (5.4%) |
| 350°C 10 min 10 wt.% B/W | - | 29.3% (0.0%) | 22.5% (6.4%) | 11.8% (0.2%) | 5.5% (1.4%) | 30.9% (7.0%) |
| 370°C 5 min 10 wt.% B/W | - | 36.8% (1.7%) | 15.8% (3.1%) | 13.0% (0.9%) | 4.0% (0.1%) | 30.3% (2.3%) |
| 300°C 5 min 10 wt.% B/W | 2 wt.% KOH | 18.8% (0.7%) | 36.5% (2.6%) | 13.5% (0.7%) | 2.2% (n.d.) | 29.0% (2.6%) |
| 350°C 5 min 10 wt.% B/W | 2 wt.% KOH | 37.0% (1.4%) | 17.0% (0.5%) | 10.2% (0.7%) | 4.4% (0.6%) | 31.3% (1.1%) |
| 370°C 5 min 10 wt.% B/W | 2 wt.% KOH | 39.2% (0.5%) | 9.7% (1.9%) | 12.3% (0.0%) | 4.3% (0.1%) | 34.5% (2.0%) |
| 350°C 5 min 10 wt.% B/W | 4 wt.% KOH | 35.5% (2.1%) | 17.7% (1.4%) | 9.3% (0.5%) | 2.2% (0.3%) | 35.4% (0.6%) |
| 300°C 5 min 10 wt.% B/W | sCO ₂ | 15.5% (5.0%) | 38.1% (8.2%) | 16.2% (0.7%) | 3.3% (n.d.) | 26.9% (2.56%) |

* calculated by difference, n.d.: not determined

Lignin-Rich Stream Characterization

The lignin-rich feedstock was received in form of wet agglomerated particles with 69.7 wt. % of moisture content; therefore, it was dried, knife-milled, and sieved to < 0.25 mm prior to be used in the experiments. Carbon, hydrogen, nitrogen, and sulfur (CHN-S) and proximate analysis indicated the dry based composition to be 54.2 wt. % carbon, 5.9 wt. % hydrogen, 1.0 wt. % nitrogen, 0.2 wt. % sulfur, 36.1 wt. % oxygen (by difference), and 2.6 wt. % ash. Volatile matter and fixed carbon resulted to be respectively 71.0 wt. % d.b. and 26.4 wt. % d.b. The lignin content of the feedstock, together with its residual structural sugars is reported in Table 13 and the data are in good agreement with similar feedstock from enzymatic hydrolysis of lignocellulosic biomass investigated by Jensen et al.³⁶⁰. These data were already reported in the previous paragraph.

Table 13. Lignin and sugars content in LRS.

| Parameter | Value [-] wt. % (d.a.f.) |
|-----------------------|--------------------------|
| Acid insoluble lignin | 52.7 ± 4.99 |
| Acid soluble lignin | 0.253 ± 0.0216 |
| Total lignin | 53.0 ± 5.02 |
| Structural sugars | 35.8 ± 0.314 |
| Glucan | 30.7 ± 0.484 |
| XMG* | 4.94 ± 0.170 |
| Arabinan | 0.163 ± 0.0287 |

* Xylan, Mannan, Galactan

The slurry of LRS in water was prepared at 10 wt. % of biomass to water ratio (B/W). The initial aqueous fraction of lignin-rich slurry was analyzed in HPLC to characterize the water-soluble content prior to the hydrothermal reactions, discriminating the compounds that were soluble at ambient conditions from those produced during the hydrothermal treatment. The total water-soluble HPLC-detectable content was about 4–5 wt. % (d.b.). The results, depicted in Figure 49, showed the presence of a small percentage of dissolved sugars such as glucose and xylose-mannose-galactose (XMG) as well as glycerol, acetic and lactic acid. Lactic acid was the most abundant compound, deriving from bacterial contamination in the fermentation process. Indeed, lactic acid bacteria, which produces also acetic acid, can survive to typical fermentation conditions and represent the most common bacterial species found in ethanol facilities³⁸⁸. On the other hand, glycerol is known to be one byproduct of bioethanol production performed by yeasts, such as *Saccharomyces cerevisiae*, under aerobic and anaerobic growth condition.³⁸⁹

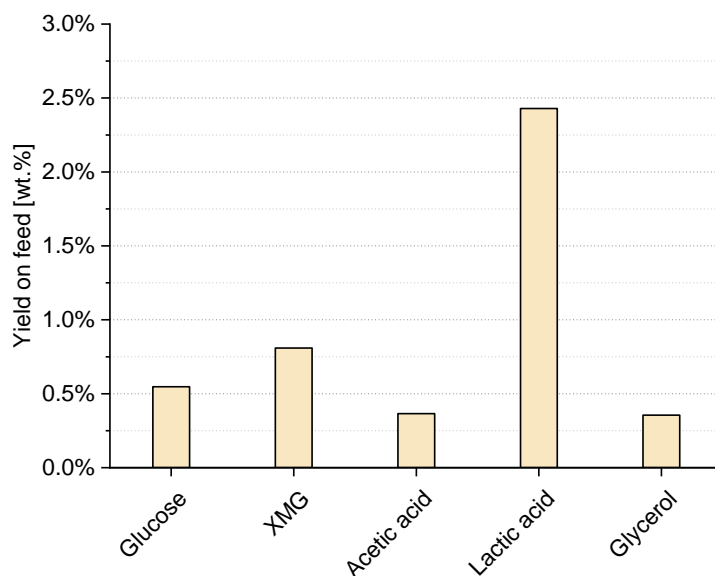


Figure 49. Water-soluble compounds in LRS liquid fraction of the slurry: yield on feed at 10 wt.% of B/W

Analysis of HTL Products

Typical chromatograms from GC-MS of BC1 and HPLC of AP are shown Figure 50 and Figure 51, respectively, showing also chemical structures of the most present compounds. Moreover, Table B6.2 in Appendix B6 provides a complete light biocrude qualitative characterization with classes subdivisions for the same sample. HPLC chromatogram in Figure 51 depicts only the fraction of chromatogram containing organic acids and alcohols; however, this method was used to quantify also some phenolic compounds retained in the AP (Phenol; Phenol, 2-methoxy-; Phenol, 2,6-dimethoxy-; Phenol, 2-methoxy-4-methyl-; 1,2 Benzenediol and 1,2-Benzenediol, 3-methoxy-).

The degradation of the main biomass constituents under hydrothermal conditions have been extensively studied and reviewed^{68,352}. The lignin three-dimensional matrix results from the interaction of three main aromatic structures (monolignols) named coniferyl, sinapyl, and p-coumaryl alcohols, which yielded aromatics constituents: guaiacyl (G), syringyl (S), and p-hydroxyphenyl (H) units. These monolignols are linked together in the polymeric structure through many different bonds such as ether (β -O-4, α -O-4, and 4-O-5) and C-C (β - β , β -5, and β -1) bonds^{390,391}. During hydrothermal conversion reactions, the chemical bonds of the branched aromatic polymeric structure of lignin are broken to form phenolic monomers such as phenol, methoxyphenols, alkylphenols, dimethoxyphenols, catechols, methoxycatechols, phenolic aldehydes, and phenolic ketones.^{348,364,392} In previous studies, it was observed that the ether bonds are more easily broken than C-C bonds, and this is the main depolymerization mechanism occurring in absence of catalyzed reactions.³⁴⁵ The results from the present study confirmed that the reaction products from hydrothermal conversion maintains the aromatic rings, while the substituent groups have different trends depending on reaction conditions. Indeed, in absence of catalysts, the main reaction occurring in aqueous environment at subcritical condition is known to be hydrolysis. Moreover, also, fragmentation and repolymerization occur during the liquefaction reaction mechanisms. Primary depolymerization products found in BC1 were Phenol, 2-methoxy (guaiacol) and Phenol, 2,6-dimethoxy- (syringol) coming from the thermal cleavage of guaiacyl and syringyl units as identified in peaks 5 and 10 in the GC-MS chromatogram in Figure 50. In addition, model compounds studies^{393,394} showed that secondary reactions lead to the formation of catechol (peak 7), methoxycatechol (peak 8) and phenol

(peak 4) through demethylation and demethoxylation giving rise to the methanol content in the AP, as detected through HPLC (Figure 51). Other lignin degradation products, which were detected by GC-MS are phenolic aldehydes and ketones, especially: Syringaldehyde (Benzaldehyde,4-hydroxy-3,5-dimethoxy-), Vanillin (Benzaldehyde,4-hydroxy-3-methoxy-), Acetovanillone (Ethanone,1-(3-hydroxy-4-methoxyphenyl)-), and Acetosyringone (Ethanone, 1-(4-hydroxy-3,5-dimethoxyphenyl)-). Due to the polarity of most of these compounds, a fraction of the oxygenated aromatic substances (mostly phenol, guaiacol, and syringol) was also found trapped in AP after the solvent extraction procedure.

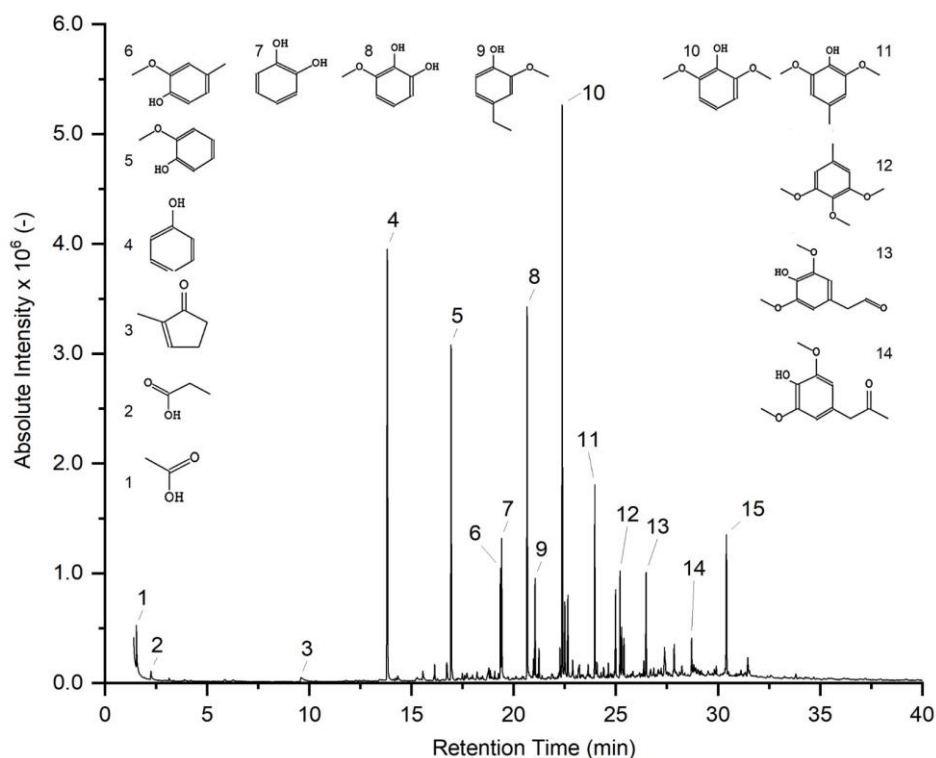


Figure 50. Typical GC-MS chromatogram for BC1 fraction obtained at 350 °C, 10 min, 10% biomass to water ratio. **1.** Acetic acid, **2.** Propanoic acid, **3.** 1,2-Cyclopenten-1-one, 2-methyl-, **4.** Phenol, **5.** Phenol, 2-methoxy-, **6.** Phenol, 2-methoxy-4-methyl-, **7.** 1,2-Benzenediol, **8.** 1,2-Benzenediol, 3-methoxy-, **9.** Phenol, 4-ethyl-2-methoxy-, **10.** Phenol, 2,6-dimethoxy-, **11.** Phenol, 2,6-dimethoxy-4-methyl-, **12.** Benzene, 1,2,3-trimethoxy-5-methyl-, **13.** Homosyringaldehyde, **14.** Syringylacetone, **15.** o-Terphenyl (Internal Standard).

The polysaccharides contained in the feedstock adopted for lignocellulosic ethanol production were already subject to depolymerization during hydrolytic pretreatment in the ethanol production process (steam explosion and enzymatic hydrolysis), right before fermentation.^{73,395} In HTL, cellulose, hemicellulose, and derived sugars (e.g., glucose or fructose) are mainly converted into organic acids, alcohols and ketones during hydrolysis reaction.^{396–398} As known, acid and alcohols have higher affinity with water and therefore were mostly found in the aqueous phase, as reported in the HPLC chromatogram of the residual aqueous phase in Figure 51. Acetic acid and formic acids are formed by degradation of glucose in alkaline and neutral conversion. Even though acetic and lactic acid can potentially be produced during hydrothermal reactions, they were also already found in the feedstock slurry thus meaning that they were mainly produced and dissolved in water during ethanol fermentation in the upstream production plant and not only during hydrothermal reactions.^{73,399} It was also confirmed that reaction of sugars in hydrothermal media leads to the generation of cyclic ketones (e.g. cyclopentenones) and their alkylated forms, as already proposed in literature.⁴⁰⁰

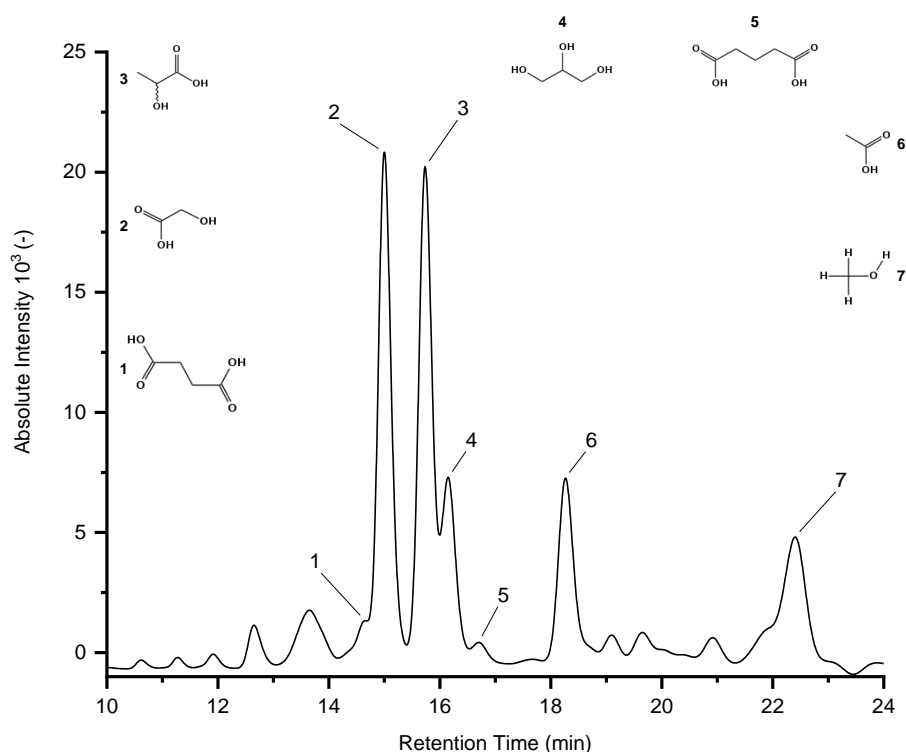


Figure 51. Typical partial HPLC chromatogram for water-soluble organics (WSO) in aqueous phase (AP) fraction obtained at 350 °C, 10 min, 10% biomass to water ratio. **1.** Succinic acid, **2.** Glycolic acid, **3.** Lactic acid, **4.** Glycerol, **5.** Glutaric acid, **6.** Acetic acid, **7.** Methanol.

It was not possible to analyze heavy molecular weight compounds comprised in BC2 using GC-MS or HPLC. The heavier fraction still contains oligolignols generated in the first depolymerization steps as well as repolymerization of lignin fractions.⁴⁰¹ Thus, we were unable to characterize the composition of BC2 with these analytical techniques, but representative infra-red spectra and molecular weight-average distributions of BC1 and BC2 were already given in a previous work³⁴⁰, showing similarities with the lignin feedstock and demonstrating the higher average molecular weight of BC2, ranging from 1030 to 1400 g mol⁻¹. Therefore, BC2 was supposed to be completely composed by lignin-oligomers not converted to lighter compounds (e.g., phenolic monomers). Here, to further characterize the biocrudes, ¹H NMR analysis was carried out on BC1 and BC2 derived from reaction at 370 °C and 5 min of residence time, comparing the resulting spectra with literature data. ¹H NMR spectra reported in Figure 52 show typical depolymerized lignin signals in light and heavy biocrude fractions.^{354,375,402-404} The signals in the 8–10 ppm region, ascribable to phenolic OH^{402,403}, are slightly visible only in BC1 and probably due to the cleavage of the β -O-4 bonds. The region between 6–8 ppm indicates the aromatic protons and unsaturated aliphatic bonds (C=C) signals typical of the lignin oligomers and primary lignin monomeric units, confirming the aromatic ring and β -double bonds preservation in both BC1 and BC2 samples^{402,404}. Both biocrude fractions also denote the presence of peaks in chemical-shift range 3-4 ppm related to methoxy groups ($-\text{OCH}_3$) as confirmed by literature data^{405,406}. The 1.5–3 ppm protons are typically assigned to $-\text{CH}_3$ and $-\text{CH}_2-$ bonded to aromatic structures⁴⁰⁷ and signals are visible in both fractions. In the 0.5–1.5 ppm region, aliphatic protons typical of methyl and methylene groups are more defined in BC2, suggesting an ineffective hydrolysis of C-C lignin bonds^{345,405}. To sum up, ¹H NMR confirmed the incomplete depolymerization of lignin structures and no conspicuous differences were found in the functional groups of the two biocrudes due to the similar nature of the structural oligolignols constituents.

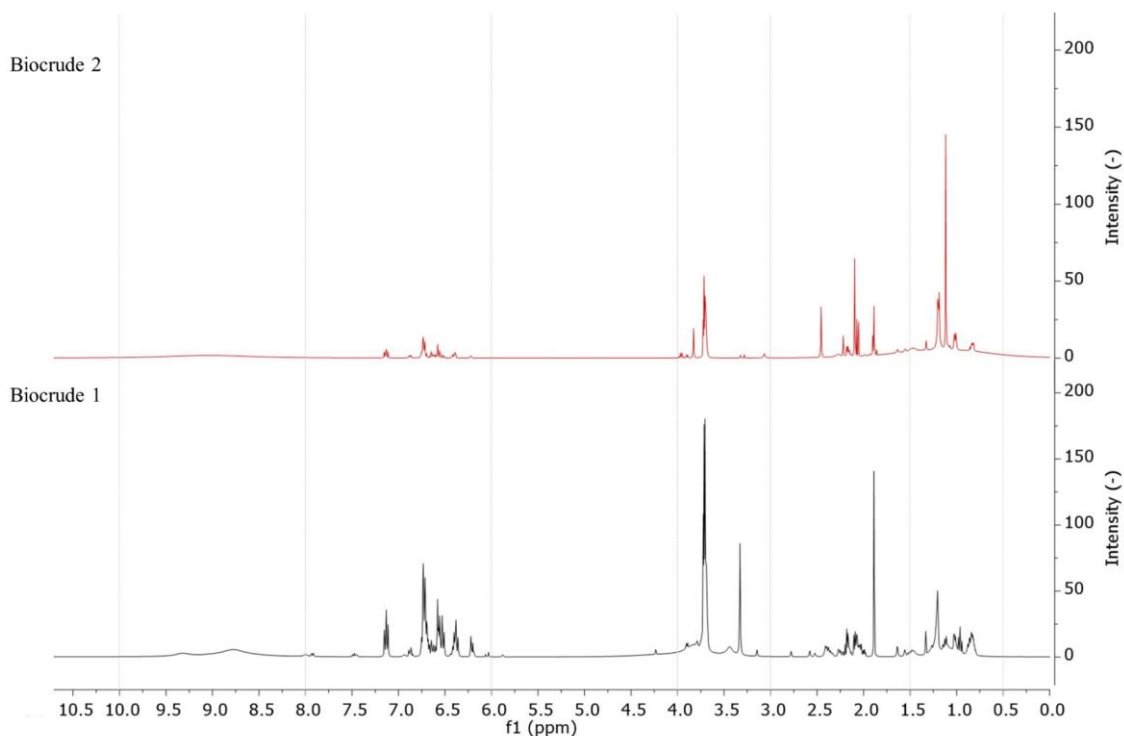


Figure 52. ^1H NMR spectra for DEE-soluble biocrude (BC1) and DMK-soluble biocrude (BC2) from test at 370 °C and 5 min.

In the next sections, the trend of detected monomeric LRS-derived fractions in function of the reaction conditions will be analyzed to further characterize the hydrothermal depolymerization process.

Hydrothermal Liquefaction in Absence of Catalysts: Influence of Temperature and Time

The results from hydrothermal liquefaction of lignin-rich streams shows an effective depolymerization into more valuable products, even in absence of catalyzed reaction. These results have been used to optimize the process conditions prior to test the effect of catalytic additives.

The effect of temperature in non-catalytic condition was evaluated carrying out HTL tests at 300–350–370 °C with 5 minutes of residence time and 10 wt. % of B/W. Yields of compounds versus dry feedstock, evaluated according to Eq.3.2.1, are shown in Figure 53. First, higher temperatures enhance the production of aromatic monomers from lignin. Catechols content linearly increased and their methoxylated forms were almost absent at low temperature, appearing only at 350 °C. Similar trends were observed for methoxyphenols, dimethoxyphenols, and phenol. However, a lower or absent increment-rate at temperature between 350–370 °C was noticed. Moreover, the yield of phenolic carbonyls zeroed passing from 300 °C to 350 °C, suggesting the high reactivity of the carbonyl substituent that leads to the formation of simpler monomers. The same effect was observed for cyclopentenones.

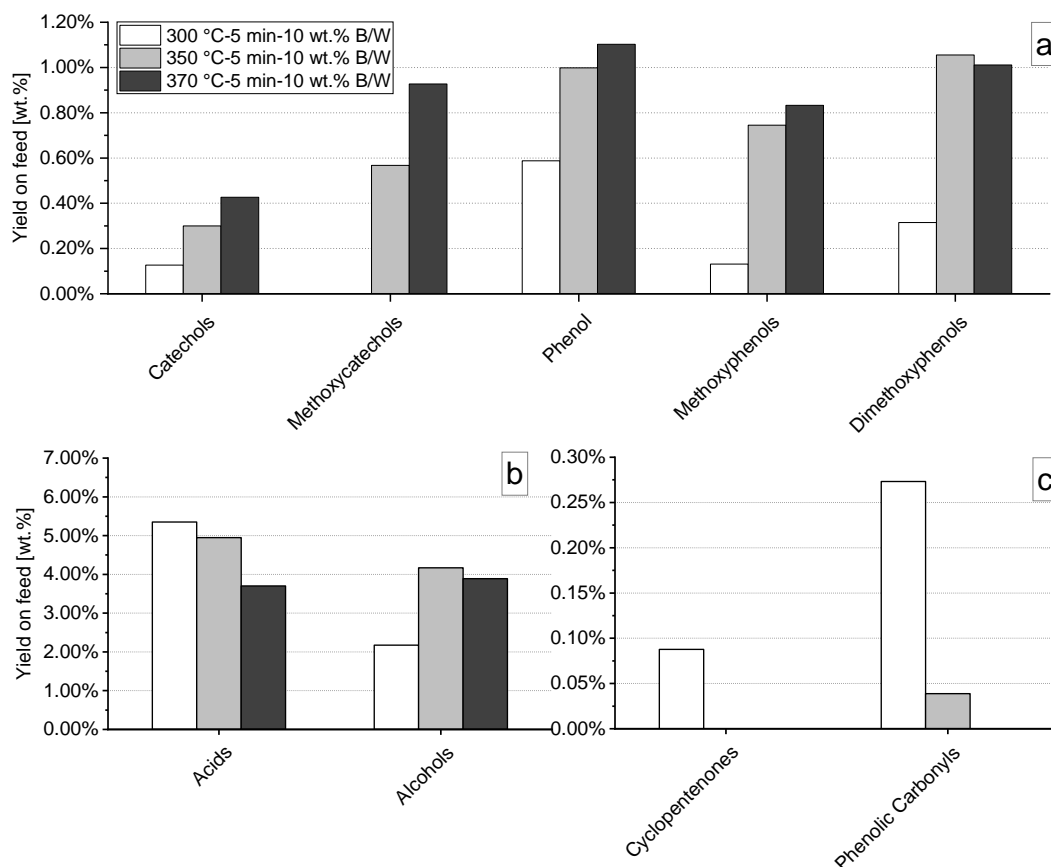


Figure 53. Effect of reaction temperature on yields of quantified compounds for uncatalyzed HTL tests: (a) phenolics, (b) acids and alcohols, (c) phenolic carbonyls and cyclopentenones. When no graph column is depicted, the concentration was below quantification limits.

It was also observed that an increment in the reaction temperature caused a considerably high decrement in the acids yield, from 6 wt. % at 300 °C to less than 4 wt. % at 370 °C. This is mainly due to the degradation of lactic acid while acetic and glycolic acid formation remained more stable, as depicted in Figure 54a. In addition, the difference plot in Figure 54b shows a comparison between the acids already contained in the initial slurry at ambient conditions and the acids content after the reaction. Glycolic acid was always generated during liquefaction reactions as it was not identified in the initial slurry. Acetic acid instead was partially produced, while lactic acid was always cracked during the conversion process and it was not generated during the reactions. The rate of lactic acid degradation increased at higher temperature and, as other authors suggests⁴⁰⁸, the fragmentation reaction forms mainly light gases like CO, CO₂, and CH₄. The gas yield was theoretically evaluated from initial and final reactor pressure, by assuming only CO₂ as gaseous specie and by considering the ideal gas law; results are reported in Table S2. Benzoic acid has a similar trend as phenolic carbonyls compounds, and its presence in the resulting liquids was reduced at higher temperature (Figure 54a). The analysis on the AP showed that the alcohols produced are mainly methanol and glycerol. Methanol content seemed to be highly influenced by the temperature (Figure 54a) while glycerol, already presents in the LRS slurry, was cracked during the reactions (Figure 54b). As explained before, the effect of higher temperature in the reaction zone promotes the depolymerization of the lignin structures, including the loss of the methoxy group from the fragmentation of the methoxyphenols and dimethoxyphenols. The availability of free methoxy substituents in the subcritical environment gives rise to the formation of methanol through demethylation reactions. This mechanism is enhanced by temperature: an increase in reaction temperature leads to higher rate of formation of free radicals from

lignin cracking, as the formation of methoxyphenolic compounds raised together with the enhanced cracking into catechols and phenol. To sum up, the reaction temperature had a strong effect on BC1 monomers and WSO yield, especially in the range 300–350 °C. Moreover, even though moving close to critical condition, i.e., 370 °C, could have a positive effect on depolymerization and WSO reduction (see mass yields in Table S2), the overall process costs would increase in a scale-up perspective. For this reason, a temperature of 350 °C was selected in the following experiments, where the influence of residence time was evaluated.

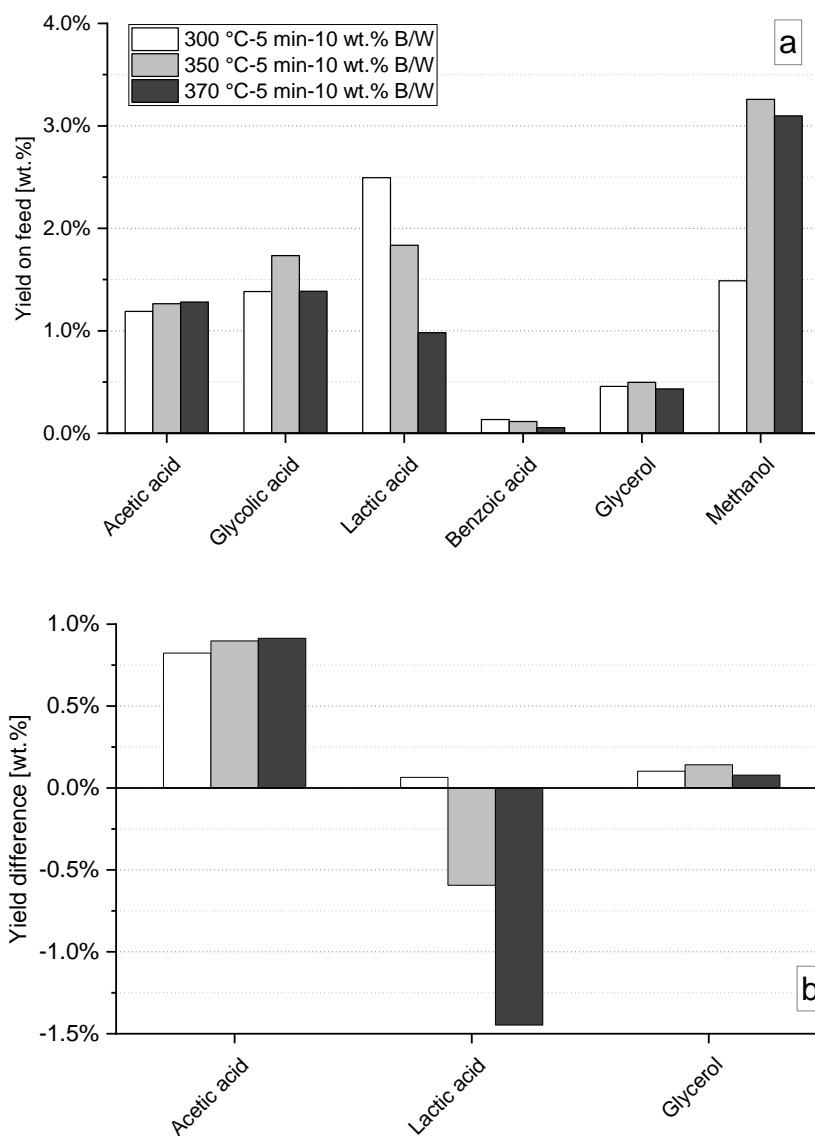


Figure 54. (a) Effect of reaction temperature on yields of specific acids and alcohols species; (b) difference plot for acids degradation versus formation compared to the initial acids content in the lignin-rich streams (LRS) slurry for uncatalyzed HTL tests.

The reaction mechanisms of the HTL process also depends on the residence time of the feedstock at the reaction condition with water at subcritical state. The latter is indeed a very important parameter and should be kept as low as possible, as in a continuous scaled-up perspective, it influences the size of the reactor and, consequently, the throughput of the plant. Moreover, other studies^{409,410} already reported that an increment in the residence time would favor condensation and repolymerization reactions increasing the yield of heavy biocrude and solid residues. Thus, a

fast cooling step is needed to quench the reactions and partially avoids further polymerization of lignin intermediates. Therefore, in agreement with literature, we decided to investigate rather short residence times, from 5 to 10 minutes at 350 °C (Figure 55). As also found by other authors^{349,411}, during HTL reactions in subcritical water, methoxylated phenols cleavage rate increases with reaction time, leading to a higher amount of catechols in the product (e.g., 1,2 Benzenediol from Phenol, 2-methoxy-). In agreement with them, in this work, a small increment in the yields of catechols and methoxycatechols was observed together with a reduction of methoxyphenols yields in the range 5–10 minutes. Phenol yield was reduced at higher time due to the fact that catechols formation is always the preferred reaction route from methoxyphenols cleavage in subcritical water conditions, meaning that phenols undergo to substitution reactions more rapidly than catechols⁴¹². Regarding the acids content in the liquid products, a higher residence time slightly reduced the overall yield due to the enhanced cracking rate, leading to the formation of light gases, as confirmed by the gas yield increase from 4.5 to 5.5 wt. % (see Table S2. This is due to the enhanced cracking of lactic acid from the feed and to the degradation of the produced acetic and glycolic acids. The generation of alcohols remained constants, probably due to an equilibrium between the cleavage of alcohols functional group from lignin cracking and the consequent enhanced volatilization. The phenolic carbonyls completely crack with higher reaction time, meaning that a complete hydrolysis of the carbonyl substituent groups is achieved in the investigated residence time.

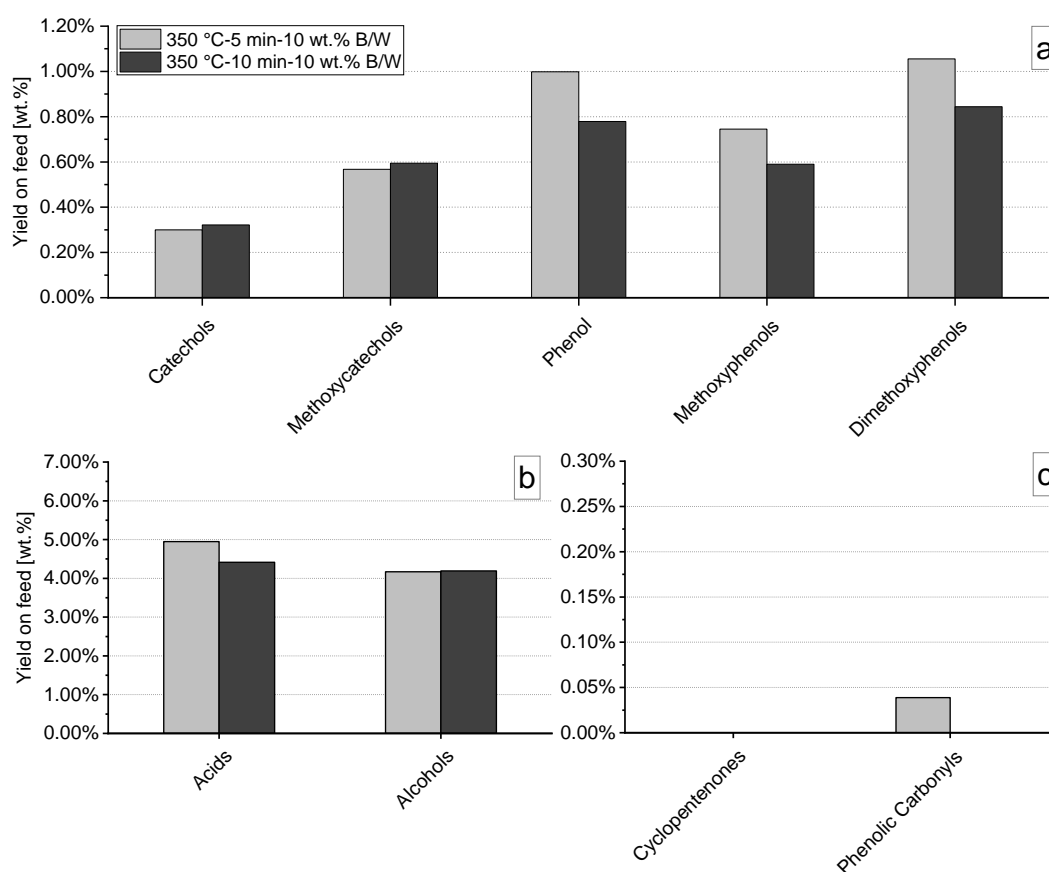


Figure 55. Effect of residence time on yields of quantified compounds for uncatalyzed HTL tests: (a) phenolics, (b) acids and alcohols, (c) phenolic carbonyls and cyclopentenones. When no graph column is depicted, the concentration was below quantification limits.

Influence of Catalytic Additives in the Process

The effect of additives with catalytic effect was evaluated as a method to improve the liquefaction process. First, base catalyzed reactions were carried out by varying the reaction temperature and comparing the results to those obtained in absence of alkaline hydroxides catalysts. In addition, the catalytic effect of supercritical carbon dioxide (sCO₂) was tested comparing the effect at lower reaction temperature, substituting the Ar inside of the tubular reactor.

Effect of pH Control Using Strong Basis

Base catalyzed depolymerization was realized adding KOH in the slurry mixture, at 2 and 4 wt. % of KOH to LRS ratio dry basis, obtaining an initial slurry pH of 8.0 and 10.0 respectively, doubling the baseline value as reported in Table 14.

Table 14. pH values of feed and products with and without KOH. Test performed at 350 °C, 5 min, and 10 wt. % biomass to water ratio (B/W).

| Stream | pH of Control | pH @ 2 wt. % KOH | pH @ 4 wt. % KOH |
|--------|---------------|------------------|------------------|
| feed | 4.6 | 8.0 | 10.0 |
| AP | 4.4 | 5.1 | 5.8 |

When reactions occurred in alkaline condition, the overall biocrude mass yield (BC1 + BC2), measured by weighting each resulting phase, increased at lower temperature (300 °C) from 48.8 wt. % to 55.3 wt. % when 2 wt. % of KOH was used, as summarized in Table 15. On the contrary, increasing the reaction temperature to 350 °C the total biocrude mass yield was reduced from 59.0 wt. % in absence of KOH to 54.0 wt. % and 53.2 wt. % when 2 wt. % and 4 wt. % of KOH were tested respectively. A further increment in the temperature (370 °C) confirmed the same trend. However, high initial pH had an overall positive effect increasing on lighter biocrude fraction (BC1) resulting in higher mass yields at each temperature tested. On the other hand, heavier BC2 yield was always reduced, especially in the range 350–370 °C. Hence, although the total biocrude yield was found decreased in basic conditions, higher amount of lighter lignin-derived compound was measured. Moreover the WSO content in the residual AP increased when final higher pH was achieved, in agreement with Belkheiri et al.³⁷⁸. TOC analysis (corrected subtracting the carbon contained in the water-dissolved DEE), reported in Table 4 shows an increment in the concentration of soluble organics in residual AP. At 350 °C the carbon concentration of WSO varied from 6648 to 8823 and 10,981 mg l⁻¹ increasing the initial slurry pH from 4.6 to 8 and 10 respectively. Similar effects were observed also at 370 °C. Moreover, as can be deduced from Table 16, the WSO carbon concentration, calculated from HPLC detectable data, diverge from the TOC value when higher depolymerization rate is reached, (i.e., at higher temperature and in alkaline conditions) and this is probably due to the higher concentration of undetected oligomeric compounds.

Table 15. Effect of base catalyzed reaction increasing KOH to LRS ratio from 2 wt. % to 4 wt. % at 300–350–370 °C, 5 min and 10 wt. % B/W: mass yields of light biocrude (BC1), heavy biocrude (BC2), solid residues (SR), Gas, and water-soluble organics (WSO) + loss. Absolute standard deviation is reported in brackets.

| Temp. [°C] | KOH [%] | BC1 | BC2 | SR | Gas | WSO + Loss* |
|------------|---------|--------------|---------------|--------------|-------------|---------------|
| 300 | - | 9.8% (1.6%) | 38.8% (11.5%) | 16.5% (3.0%) | 2.4% (0.7%) | 32.6% (10.5%) |
| | 2 | 18.8% (0.7%) | 36.5% (2.6%) | 13.5% (0.7%) | 2.2% (n.d.) | 29.0% (2.6%) |
| 350 | - | 27.0% (6.7%) | 32.0% (6.4%) | 11.4% (0.9%) | 4.5% (0.8%) | 23.8% (5.4%) |
| | 2 | 37.0% (1.4%) | 17.0% (0.5%) | 10.2% (0.7%) | 4.4% (0.6%) | 31.3% (1.1%) |
| | 4 | 35.5% (2.1%) | 17.7% (1.4%) | 9.3% (0.5%) | 2.2% (0.3%) | 35.4% (0.6%) |
| 370 | - | 36.8% (1.7%) | 15.8% (3.1%) | 13.0% (0.9%) | 4.0% (0.1%) | 30.3% (2.3%) |
| | 2 | 39.2% (0.5%) | 9.7% (1.9%) | 12.3% (0.0%) | 4.3% (0.1%) | 34.5% (2.0%) |

* calculated by difference, n.d.: not determined.

Table 16. Total organic carbon (TOC) concentration of WSO, influence of KOH at 300–350–370 °C. Compared to carbon concentration calculated by HPLC detected compounds. Test performed at 5 min and 10 wt. % B/W.

| Temp. [°C] | KOH [wt. %] | TOC – Concentration [mg l ⁻¹] | C – HPLC Detected WSO Concentration [mg l ⁻¹] |
|------------|-------------|---|---|
| 300 | - | 4741 | 3405 |
| | 2 | 5310 | 3859 |
| 350 | - | 6648 | 3186 |
| | 2 | 8823 | 3337 |
| | 4 | 10,981 | 4707 |
| 370 | - | 5937 | 5608 |
| | 2 | 8692 | 4513 |

Molecular weight (or molar mass) was evaluated by gel permeation chromatography (GPC) and the average results for BC1, BC2 and the total biocrude (BC tot) were compared with KOH-catalyzed tests at 300 °C and 350 °C (Figure 56). The Mw of the total biocrude was determined as a yield-based weight-average from that of BC1 and BC2. The strong alkaline environment improved BC1 yield over BC2, consequently the resulting BC2 molecular mass increases. These results are in accordance with the fact that the increased rate of depolymerization leads to higher quantity of BC1 leaving in BC2 only heavier compounds. A confirmation can be found observing the total biocrude molecular mass (line in Figure 56) that it is always reduced when KOH is used. Therefore, an increment in the amount of KOH from 2 wt. % to 4 wt. % resulted in a higher depolymerization rate as confirmed by lower BC2 yields, plus a reduction of the total biocrude average molecular weight.

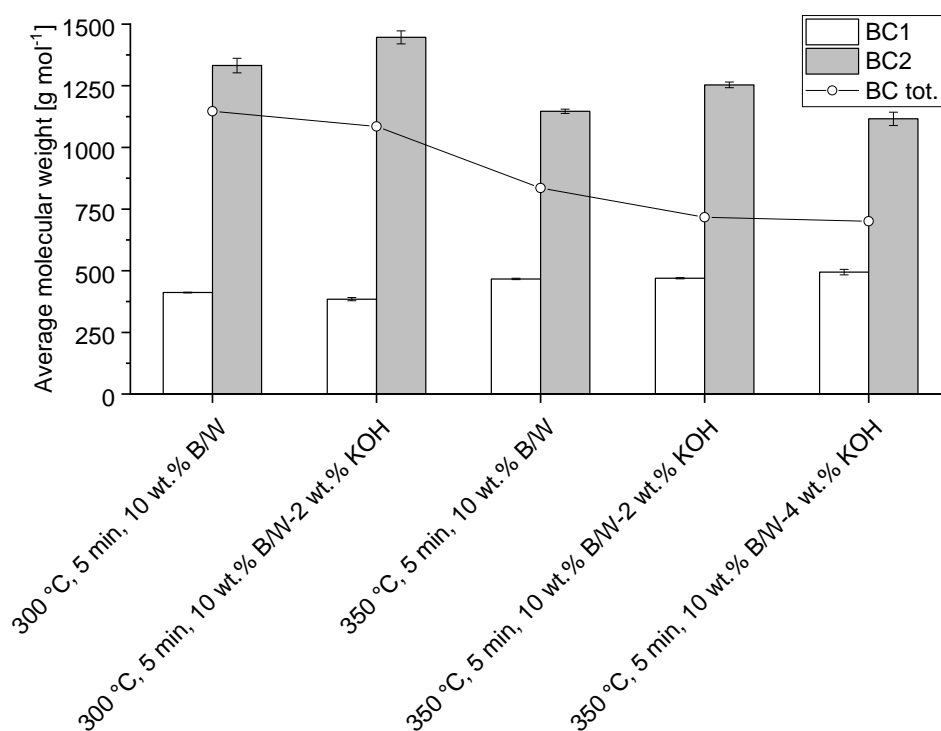


Figure 56. Effect of base catalyzed reaction, increasing KOH to LRS ratio from 2 wt. % to 4 wt. %: average molecular weight of BC1, BC2, and total biocrude. Error bars represent absolute standard deviation.

Looking at the monomeric compounds production, the results in term of yield of detected compounds are summarized in Figure 57 at constant reaction temperature (350 °C), time (5 min) and B/W (10 wt. %). Increasing the pH of the initial slurry solution from 4.6 to 8.0, corresponding to an increment from no KOH to 2 wt. % of KOH to LRS ratio, a slight enhancement in the formation of phenolics species was observed, especially the methoxylated forms (i.e. methoxyphenols and dimethoxyphenols). Phenol yields were slightly increased with 2 wt. % of KOH but decreased again adding more KOH in the slurry. Regarding the catechols, the yield remained almost constant increasing the pH of the slurry but methoxycatechols yield was enhanced. The average acids yield was not significantly affected by the basic environment. Indeed, an increase of pH negatively affected the cracking of lactic acid, thus increasing its yield from 1.84 wt. % to 2.60 wt. % while the generation of glycolic acid was inhibited from 1.73 wt. % to 1.22 wt. % when initial slurry pH was 4.6 and 10.0 respectively. Alcohols production increases by adding higher amount of KOH, due to the already discussed effect on the overall enhanced depolymerization rate. In other words, the increment in BC1 yields can be correlated to the formation of a higher amount of methanol due to the demethylation and demethylation of the methoxy groups during the cleavage of the lignin methoxyaromatic building blocks. As regards to phenolic carbonyls species, the presence of base catalyzed reaction reduced the presence of this compound class below instruments calibration limits, meaning that the carbonyl branches were cracked to form other phenolic monomers (e.g., methoxyphenols) during catalyzed hydrolysis reactions.

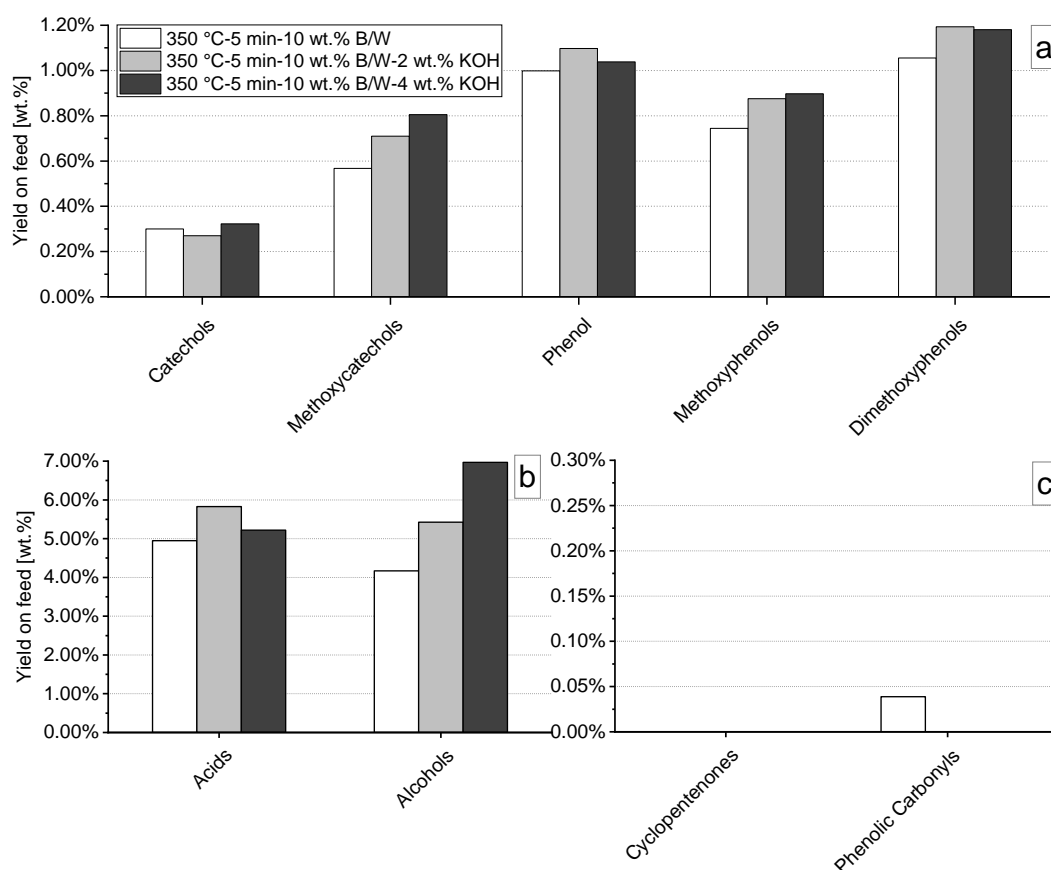


Figure 57. Effect of base catalyzed reactions increasing KOH to LRS ratio from 2 wt. % to 4 wt. % on yields of quantified compounds: (a) phenolics, (b) acids, and alcohols, (c) phenolic carbonyls and cyclopentenones. When no graph column is depicted, the concentration was below quantification limits.

Effect of Supercritical CO₂

The effect of supercritical CO₂ was tested in a biphasic mixture together with subcritical water in order to investigate the selectivity of specific monomers during the depolymerization of the biorefinery lignin-rich material. Other previous literature works demonstrated that sCO₂ can be used to enhance the selectivity towards the formation of specific phenolic compounds such as guaiacol during the depolymerization of alkali lignin⁴¹³. Carbon dioxide become supercritical above 31.1 °C and 7.39 MPa and its catalytic effect was evaluated in an HTL experiment carried out at 300 °C, 5 min residence time and 10 wt. % B/W. As in the reference experiment, with inert Ar atmosphere, the reactor was initially pressurized at 3 MPa, but the maximum obtained pressure (8 MPa) was lower of about 5 MPa, denoting higher dissolution rate of CO₂ compared to Ar. At the considered reaction temperature the percentages of dissolved moles of CO₂ increased, reaching a theoretical value of 2.9 molCO₂/molH₂O as other author suggests⁴¹³⁻⁴¹⁵. In this work the effect of CO₂ was evaluated in comparison to the results obtained in absence of catalysts and with KOH base catalyzed depolymerization. The results showed that, compared to the uncatalyzed case, the light biocrude yield increased, but the other mass yields were only slightly affected by the presence of supercritical carbon dioxide, meaning that the overall depolymerization rate is not influenced by the presence of sCO₂, as summarized in Table 17.

Table 17. Effect of CO₂ acid catalyzed reaction compared to base catalyzed and control test at 300 °C, 5 min and 10 wt. % B/W: mass yields of BC1, BC2, SR, Gas, and WSO + loss. Absolute standard deviation is reported in brackets

| Temp. [°C] | Catalyst | BC1 | BC2 | SR | Gas | WSO + Loss* |
|------------|------------------|-----------------|-----------------|-----------------|----------------|-----------------|
| 300 | - | 9.8% (1.6%) | 38.8% (11.5%) | 16.5% (3.0%) | 2.4% (0.7%) | 32.6% (10.5%) |
| 300 | 2 wt. % KOH | 18.8% (0.7%) | 36.5% (2.6%) | 13.5% (0.7%) | 2.2% (n.d.) | 29.0% (2.6%) |
| 300 | sCO ₂ | 15.5% (5.0%) | 38.1% (8.2%) | 16.2% (0.7%) | 3.3% (n.d.) | 26.9% (2.56%) |

* calculated by difference, n.d.: not determined.

Even though the mass of depolymerized material was almost constant, the synergetic effect of sCO₂ together with subcritical water was highlighted by an enhanced generation of phenol, methoxyphenols and dimethoxyphenols compared to the results in absence of catalysts, as reported in Figure 58. Similar catalytic effect has been explained by Numan-Al-Mobin et al.³⁸⁶, observing that sCO₂ in hydrothermal medium acts like acid homogeneous catalyst promoting the selectivity towards phenolic compounds. Compared to other homogeneous catalysts, the use of fluids at supercritical state with catalytic effects, like carbon dioxide, reduces the mass transportation limitations due to diffusivity and lower density that permits a higher penetration in the feedstock's pores. As a result, in our study, the phenolics yields obtained with supercritical carbon dioxide at 300 °C (1.10 wt. %) was comparable to the yields achieved in absence of catalyst or with 2 wt. % of KOH at higher reaction temperature (350 °C). Catechols and methoxycatechols yields were not affected by the presence of sCO₂, confirming the catalytic selectivity towards monohydroxy benzenes species (e.g., phenol, methoxyphenols and dimethoxyphenols), as also confirmed by the larger presence of phenolic carbonyls (mostly vanillin and syringaldehyde) in the liquid products. However, the methanol yield remained unvaried, therefore demethylation was not enhanced by the presence of sCO₂, confirming a stable depolymerization efficiency at 300 °C compared to the control test. In addition, a higher yield of cyclopentenones (e.g. 1,2-Cyclopentanedione, 3-methyl-) was observed when sCO₂ was injected in the process, this is probably due to an effective repolymerization or cracking inhibition of also sugars-derived compounds.

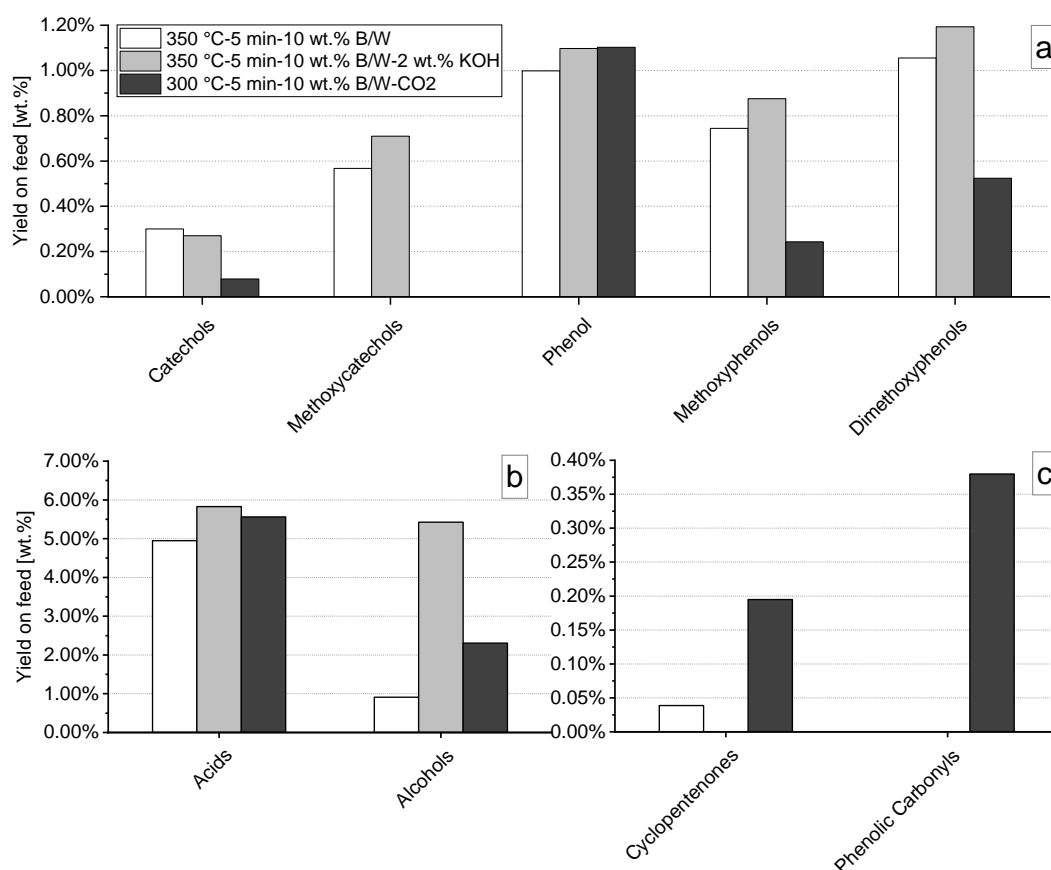


Figure 58. Effect of CO₂ acid catalyzed reaction compared to base catalyzed and blank tests on yields of quantified compounds: (a) phenolics, (b) acids and alcohols, (c) phenolic carbonyls, and cyclopentenones. When no graph column is depicted, the concentration was below quantification limits.

Compound Distribution among HTL Fractions: Influence of Biocrude Extraction Procedures

In the previous sections a detailed discussion on the depolymerization of LRS in subcritical water, with and without the use of heterogeneous catalysts, has been presented without considering how the detected compounds are distributed among the resulting fractions. It is important to note that the products collection procedure have a strong effect on the detectable organic content of both BC1 and AP, due to differences in the sample composition analyzed. Complex chemical and thermodynamic equilibrium reactions are involved during the solvent extraction due to the presence of a multitude of different organic compounds in the aqueous, oily and solid HTL products. The use of a procedure rather than the other can have more than one justification. In this lab-scale work, Procedure 1 (described in Figure 48) was chosen to maximize the organic collection in the biocrude but, at larger scale, there could be the possibility to directly separate the oily fraction from the aqueous solution only with physical techniques (e.g., centrifugation or gravimetric separation). For this reason, a different test at the same HTL conditions (350 °C, 10 min, 10 wt. % B/W, no catalysts) was carried out recovering the aqueous solution directly after the reaction removing the DEE-extraction step on the aqueous phase (Procedure 2). The whole data set discussed before was obtained using the Procedure 1. With this method, the solvent (DEE) was directly put in contact with the HTL liquid and solid products, therefore maximizing the organic extraction in the BC1. As depicted in Figure 59, substantial differences in the product distribution have been identified when the aqueous solution was collected prior to the DEE extraction

(Procedure 2). In this case, the solvent was not able to recover part of the organics in the biocrude, leaving some molecules in the AP as WSO.

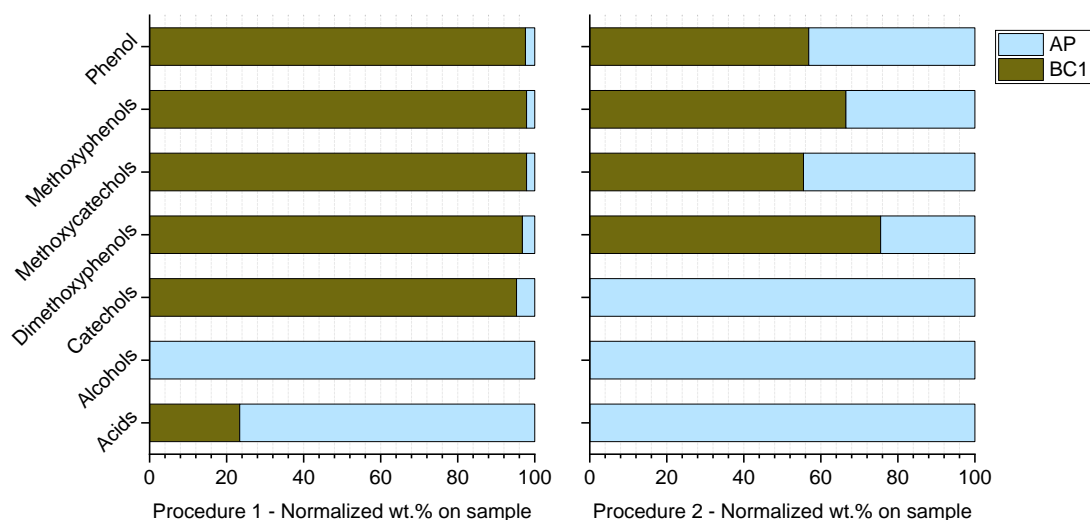


Figure 59. Influence of collection procedures on organic compounds distribution among BC1 and AP fractions. Tests performed at 350 °C, 10 min, 10 wt. % B/W in absence of catalysts.

As regards the normalized distributions in Figure 59, the collection of phenolics in the BC1 is highly reduced (about 20–30 %) when Procedure 2 was tested. Same results were observed for the methoxycatechols, whereas the catechols (mostly 1,2 benzenediol) remained totally trapped in the AP without getting recovered as DEE-soluble. Part of the carboxylic acids were recovered as DEE-soluble with Procedure 1 (mostly acetic acid) but when the aqueous phase was recovered directly after the reactions, the whole acid content remained in the AP, given the high affinity with water. On the other hand, the collection methodology did not have any effect on the alcohols distribution since the solvent was not able to extract these compounds. Thus, the collection procedure must be carefully considered for adequate comparisons of results as well as for the implementation of these types of procedures in an industrial scale-up perspective. Moreover, the implication of different extraction procedures will impact on possible downstream aqueous phase valorization steps such as aqueous phase reforming⁴¹⁶ or other valorization routes for chemicals extraction.^{35,38}

3.2.4 - Conclusion

Lignin-rich streams (LRS) from a demo-scale lignocellulosic ethanol plant was successfully depolymerized in subcritical water varying three main process parameters, such as temperature, time, as well as introducing KOH and sCO₂ as catalysts for process optimization. Even though temperature was found to be the most influent parameter increasing the LRS depolymerization efficacy at the experimental conditions investigated in this work, the effect of time and B/W was evaluated in order to observe differences in the detected monomeric products yields into BC1 and AP. Regarding residence time, 5 minutes were sufficient for lignin and sugars cleavage in subcritical water, while the increase to 10 minutes eventually promoted substitution and repolymerization reactions, leading to a reduction in methoxyphenols contents while keeping constant the catechols content. Temperature was demonstrated to play a fundamental role in the hydrothermal reaction mechanisms, and a T increase from 300 to 370 °C caused an enhanced

phenolic monomer content in BC1 and AP, together with a reduction of AP acids content. However, increasing the temperature closer to water critical point (374 °C, 22 MPa) will also increase the CAPEX of a scaled plant, due to higher equipment costs related to materials resistance at these severe operation conditions, however at sufficiently high pH of the liquid medium the corrosion effects on metals will be reduced. Thus, the use of an alkaline slurry solution is a preferable route at higher temperature ⁴¹⁷. Moreover, the use of KOH as alkaline homogeneous catalyst resulted in an improved overall LRS depolymerization, as observed by the enhanced overall BC1 mass yield and WSO content as well as a reduction in the average molecular weight of the total BC. On the other hand, the presence of KOH did not enhance the formation of phenolic monomers, but the higher yield of methanol in the aqueous solution confirmed the positive effect on lignin structure cleavage. CO₂ as acid catalyst showed interesting phenolics-selective properties at his supercritical state, when tested in a biphasic solvent mixture with subcritical water. Comparing acid (sCO₂) to base catalyzed depolymerization (with KOH), similar phenolic yields were generated at low temperature (300 °C). The phenolics fraction produced with sCO₂ was also comparable to the one obtained at 350 °C with and without KOH. Therefore, although the introduction of sCO₂ as acid catalyst into the process had not significant effects on the overall BC yields, it showed an enhanced selectivity on the formation of phenol and methoxyphenols monomers in the products at lower temperature compared to the uncatalyzed control test. Moreover, the influence of the collection procedure has been presented and discussed in order to demonstrate the different composition of BC1 and AP when a physical separation step is interposed before a chemical solvent extraction.

3.3 - Co-products from lignin hydrothermal liquefaction biorefinery: a potential pathway for extraction of chemical precursors from residual aqueous phase

3.3.1 - Introduction

In the previous paragraphs of this chapter, the hydrothermal liquefaction of lignin-rich stream has been addressed in term of process characterization and optimization as well as investigating the post-reactions monomers content in the aqueous phase and biocrude, through a lab-scale experimental campaign. In this section a potential pathway for the extraction and valorization of compounds from the residual HTL aqueous phase (AP) will be proposed and discussed. Despite the potential of HTL for the conversion of wet feedstock into valuable organic biocrude, a bottleneck for the development at larger scale, limiting the whole process economic, is the production of a large amount of residual aqueous phase (AP). During the previously described depolymerization reactions, water-soluble lignin monomers are generated, and a fraction remains dissolved in the water medium. Since the biocrude is the main product, most of the attention have been placed to the biocrude optimization, while a limited number of studies focused on the use and valorization of the aqueous phase. However, about 20–40 wt.% of the initial carbon contained in the feedstock ends up in light water-soluble monomers, with a concentration of 1–3 wt.%.⁷⁸ This represents a significant carbon loss that hinders the industrial scale-up of the technology. Previous investigations proposed some strategies for the utilization of the residual aqueous phase. The state-of-the-art proposes the AP valorization through anaerobic digestion for the production of biomethane for energy production.⁴¹⁸ However, the high presence of carboxylic acids in the AP may represents an issue due to inhibition of the anaerobic digestion process efficiency, as described by other studies.^{419,420} Another approach, proposed by Davidson et al.⁴²¹ is the catalytic upgrading of the carboxylic acid towards fuel molecules through condensed phase ketonization (CPK) or steam reforming for the generation of H₂. The direct catalytic conversion includes several challenges, especially regarding the catalyst deactivation due to coke formation.⁴²² However, they were able to demonstrate the feasibility and effectiveness of these approaches in term of modelled Minimum Fuel Selling Price (MFSP), showing how the CPK, generating higher value compounds is able to improve the economic even in presence of higher operative costs. A similar approach has been investigated by Pipitone et al.⁴¹⁶, focusing on the H₂ generation through aqueous phase reforming on a Pt/C catalyst, where they found the influence of phenolic species on the rapid deactivation of the catalyst.

Another strategy consists in recycling the aqueous phase into the hydrothermal liquefaction reactor. Previous studies have focused on how the organic content in the AP influences the biocrude yields when reintegrated into the process. Biller et al.⁴²³ showed how the biocrude yields are positively affected by the AP recycling, especially when alkali metal oxides are used as catalysts (K₂CO₃) in the process. As a consequence of the organics recycling into the system, the concentration of water-soluble compounds increases each cycle. Moreover, in this case, further downstream extraction and valorization of such molecules can be carried out with higher efficiency positively impacting the economy of the potential process integration.

In this work, first a complete AP characterization has been carried out through chromatographic analytical methods (GC-MS and HPLC) in order to identify the main chemical groups in the solution, and thus define the target molecules for the separation strategy. As a result, a high weight percentage of carboxylic acid (i.e. acetic acid, lactic acid, glycolic acid and propionic acid) followed by methanol and a mixture of phenolics monomers (i.e. phenol, catechol, methoxy

substituted phenols and phenolic carbonyls) were found dissolved in the aqueous medium. After the identification of the substances present in the aqueous solution, a proposed pathway for the valorization of the HTL AP has been addressed and experimentally tested following the scheme proposed in Figure 60. The proposed valorization strategy includes a liquid-liquid extraction (LLE) step with organic solvents as extraction medium to selectively separate the phenolic mixture that can be further purified to separate single components or back-mixed in the biocrude product to increase the yield. At the same time, the raffinate phase, still containing valuable organic compounds, can be further treated to extract molecules for the chemical industry and in this study the dewatering through resin adsorption has been addressed.

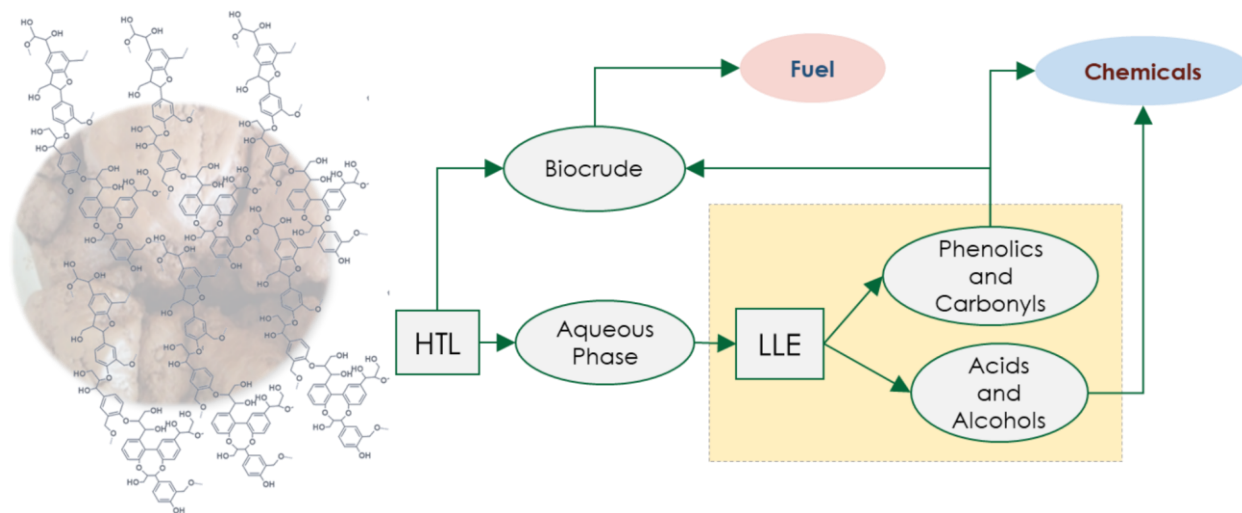


Figure 60. Scheme of HTL aqueous phase valorization strategy.

The extraction of water-soluble compounds from HTL AP has been investigated out through a liquid-liquid extraction method, evaluated in term of solvent performances as well as compounds selectivity. The liquid-liquid extraction (LLE) is a process already utilized in the petrochemical industry since the beginning of the last century in numerous applications ranging from petroleum to pharmaceutical and nuclear industry as well as .⁴²⁴ The LLE is a method to separate compounds of a homogeneous solution by means of a unequal distribution between two immiscible liquids. Typically, one phase is an aqueous solution while the other is an organic solvent and the extraction is driven by transfer of mass from the aqueous phase into the second immiscible liquid phase through mixing.^{424,425} Therefore, the method can be implemented as a extraction and purification method for aqueous solutions derived by biorefinery processes, such as the recovery of phenolics or carboxylic acids contained in aqueous phases from thermochemical conversion of biomass.^{38,39,426}

In addition, since the LLE alone is not able to recover the total amount of water-soluble compounds, further separation is needed. In this study, the raffinate aqueous phase still containing valuable carboxylic acids (e.g. lactic and glycolic acids) have been further treated through a polymeric resin adsorption. The adsorption over resins is a separation technique already used in the chemical and waste industry especially for wastewater purification and it is also suitable for recovering substances in dilute concentration. The adsorption is carried out through ion-exchange between the target molecules and the resin structure, selectively trapping compounds that can be further washed out through an eluent. The eluent needs to have low boiling point and low toxicity in order to facilitate the downstream separation. Among several polymeric options, poly(4-vinylpyridine) resin (PVP) have already been demonstrated as an effective

resin for the recovery of carboxylic acids in several applications, including the valorization of the fermentation broths derived from ethanol production.^{427,428} In addition, Wilson et al.³⁹ demonstrated the use of PVP as recovery strategies also for phenolic species. Furthermore, a list of target molecules with potential pathways and application in the chemical industry as commodity or building block for high value materials will be presented and discussed, estimating a total productivity based on lignin availability and recovery yields.

Finally, the economic impact of the integration of a LLE unit into a HTL process has been investigated through a simplified techno-economic analysis (TEA), observing how the recovery of phenolic species affects the minimum biocrude selling price (MBSP), previously calculated in absence of wastewater valorization.

3.3.2 - Material and methods

Hydrothermal liquefaction tests

Hydrothermal liquefaction tests were carried out in a 160 ml stainless steel stirred reactor (Parr instrument company, model 4564). In a typical run, 7 g of lignin were mixed with 70 g ultrapure water ($0.055 \mu\text{S cm}^{-1}$) obtaining a slurry with solid/water ratio of 10 wt.%. The reactor was then purged with nitrogen and an initial pressure of 0.6 MPa was set. The reactor was afterwards heated at 350°C through an electrical heater and the reaction temperature was maintained for 10 minutes. Residence time evaluation started when the temperature in the vessel reached 5 °C below the set temperature, then the reactor was rapidly cooled by immersing into a water bath. The system was afterwards depressurized, and the reactor opened to collect the products. The aqueous phase was directly collected and centrifuged to remove all the solid particles.

Phenolic extraction through liquid-liquid extraction

Liquid-liquid extraction (LLE) solvent screening experiments were carried out in triplicate with four different solvents (Diethyl ether, Ethyl Acetate, Butyl Acetate, Methyl Isobutyl Ketone). 4 ml of AP were weighted in a 10 ml glass flasks and 4 or 2 ml to respectively reach 1:1 and 2:1 AP/Solvent ratio. The corrected mass and volume ratios were back-calculated weighting the amount of solvent used for each replicate. The two-phase solution was then mixed for 5 minutes at room temperature. Table 18 summarized the main data for the selected solvents, such as the energetic parameters (vaporization enthalpy and boiling point) and safety data (flash point) as well as the solubility in water.

Table 18. Solvents data for LLE

| ID | Name | ΔH_{vap} [kJ/kg] | T _{boil} [°C] | Flash Point [°C] | Solubility in H ₂ O [g/l] |
|------|------------------------|--------------------------|------------------------|------------------|--------------------------------------|
| DEE | Diethyl ether | 28 | 34.5 | -45 | 60.5 |
| EtAc | Ethyl Acetate | 33 | 77 | -4 | 83 |
| BuAc | Butyl Acetate | 41 | 126 | 22 | 6.8 |
| MIBK | Methyl Isobutyl ketone | 40.5 | 117 | 13 | 19.1 |

Raffinate aqueous phase dewatering through PVP resin

Raffinate acids-rich aqueous phase post-LLE was dewatered adsorbing the organic molecules in a poly(4-vinylpyridine) 25 % cross-linked with divinylbenzene resin (Reillex 425, Merck #547697) targeting the maximization of lactic and glycolic acid extraction. The loading capacity of the target acids was determined by generating breakthrough curves. These tests were carried out with 10g of dry PVP resin which corresponds to 16 ml of wet bed volume (BV). The resin was first washed with 5 BV ethanol (EtOH) for 20 min, then the ethanol was filtered off and the resin was afterward rinsed in 10-15 BV of DI UHP water. The resin slurry was poured into a 25 ml buret with a metering stopcock. The PVP was allowed to settle into the column supporting the beads on a glass wool porous support. Then, 30 ml of BuAc Raffinate AP was added on the top of the column and drained out at 0.5-1 ml/min as suggested by other authors^{39,427}. Samples were collected every 3 ml and analyzed to quantify the acids/alcohols residual content as described below. Breakthrough point was determined as the average level between the first detectable data measured and the previous point. The loading capacity (LC) was afterward determined through the following the equation:

$$LC = \frac{V_{eff,BP} \times C_{in}}{m_{PVP}}$$

Were, $V_{eff,BP}$ is the total volume at the breakthrough, C_{in} is the initial concentration of the species and m_{PVP} is the mass of dry resin packed in the column. The elution curves were obtained in order to estimate the amount of solvent necessary to recover and remove completely the target species from the resin bed. For these experiments, 10 g of dry PVP were added in a 25 ml buret as the previous tests. The resin was then loaded with the calculated volume of BuAc Raffinate AP up to the loading capacity. Then, 2-3 BV of EtOH was used to elute the compounds from the column material. Eluent samples were taken every 3 ml and the minimum volume was determined when the first elution fraction yield to a concentration of the target acid below 0.01 g/l and 0.04 g/l for lactic and glycolic acid respectively.

Analytical methods

The HTL aqueous phase (AP) as well as post-LLE raffinate and PVP effluents were analyzed quantifying the carboxylic acids and alcohols content in a HPLC (LC-20 AT Prominence Shimadzu) equipped with a refractive index detector, a Hi-Plex H column 300 x 7.7 mm (Agilent) and a guard column PL Hi-Plex H 50 x 7.7 mm (Agilent), operating at 40°C with a flow of 0.6 mL/min with 0.005 M sulfuric acid as mobile phase. Aqueous sample (25 µl) was injected after a 0.2 µm syringe filtration. The quantitative analysis was accomplished after a 5-point calibration. Moreover, phenolic content of HTL AP and post-LLE extracts was analyzed in GC-MS, GC 2010 with a GCMS-QP2010 mass spectrometer (Shimadzu) equipped with a ZB-5 MS Phenomenex column (30 m length, internal diameter 0.25 mm, film diameter 0.25 µm) for qualitative and quantitative analysis of phenolic content. Temperature was held at 40 °C for 10 min and then increased to 200 °C (heating rate 8 °C min⁻¹, holding time 10 min) and 280 °C (heating rate 10 °C min⁻¹, holding time 30 min). Aqueous HTL AP was diluted 1:1 in isopropanol. The qualitative analysis was performed comparing the mass spectra to the NIST 17 library and quantification was carried out after a previous 4 points TIC calibration using o-terphenyl as internal standard. The phenolic content in the raffinate and the acid/alcohol content in the extract were calculated by mass difference. TOC analyses were carried out by a Merck TOC test kit and a Shimadzu UV-1800 spectrophotometer (605 nm). Samples were heated in a Merck TR320 thermoreactor for 2 h at 120 °C and then allowed to cool for 1 h in a test tube rack at room temperature. Karl Fischer titration (848 Titrino Plus, Metrohm) was performed to determine the organic concentration of the aqueous phase.

3.3.3 - Results and discussion

Aqueous phase characterization

A summarized characterization of the residual aqueous phase from hydrothermal liquefaction of LRS is shown in Figure 61. Moreover, Table 19 shows the TOC, KF and ICP results as well as the measured pH of the aqueous stream. As can be seen, the water content of the aqueous phase was 97.7 ± 1.09 wt.% and the total organic carbon (TOC) was 9.73 ± 0.780 g l⁻¹.

Table 19. Total organic carbon, water content and ph of HTL-LRS aqueous phase

| Analysis | Value | Units |
|-----------------------------|------------------|-------------------|
| Total organic carbon | 9.73 ± 0.780 | g l ⁻¹ |
| Water Content | 97.7 ± 1.09 | wt.% |
| KF Titration | | |
| pH | 4.27 | - |

Two different methods were applied for the organic content analysis, as suggested by other authors^{422,429}: one value was obtained by multiplying for a factor of 2.3 (in the range 1.7–2.5^{430,431}) the TOC measurement and the other by difference from the Karl Fisher water measurement considering the amount of inorganic elements detected with the ICP. Resulting in a total mass balance closure in the range 80-84 wt.% after the GC-MS and HPLC compound quantification. The remaining 16-20 wt.% were considered unknown/unidentified compounds. Observing the dry basis quantification in Figure 61 (right bar), alcohols (mostly methanol) were the most abundant compound class reaching 36 wt.% of the total organics. The other detected and quantified chemical groups were carboxylic acids (28 wt.%), methoxyphenols (8 wt.%), methoxycatechols (5 wt.%), phenol (4 wt.%) and other carbonyls such as phenolic ketones (1 wt.%).

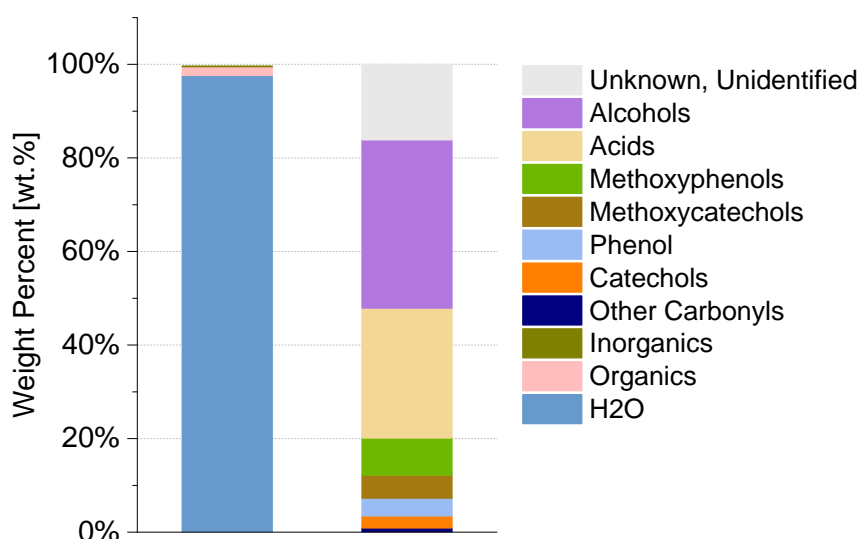


Figure 61. Characterization of LRS-HTL residual aqueous phase on wet (left bar) and dry (right bar) basis.

Liquid-liquid extraction for organics separation from aqueous phase

The liquid-liquid extraction was carried out with four different organic solvents to evaluate the potential of extracting organic compounds from HTL residual aqueous phase. The results from the lab-scale experiments are reported in Figure 62 in term of partition coefficient (K_d) and mass fraction extracted.

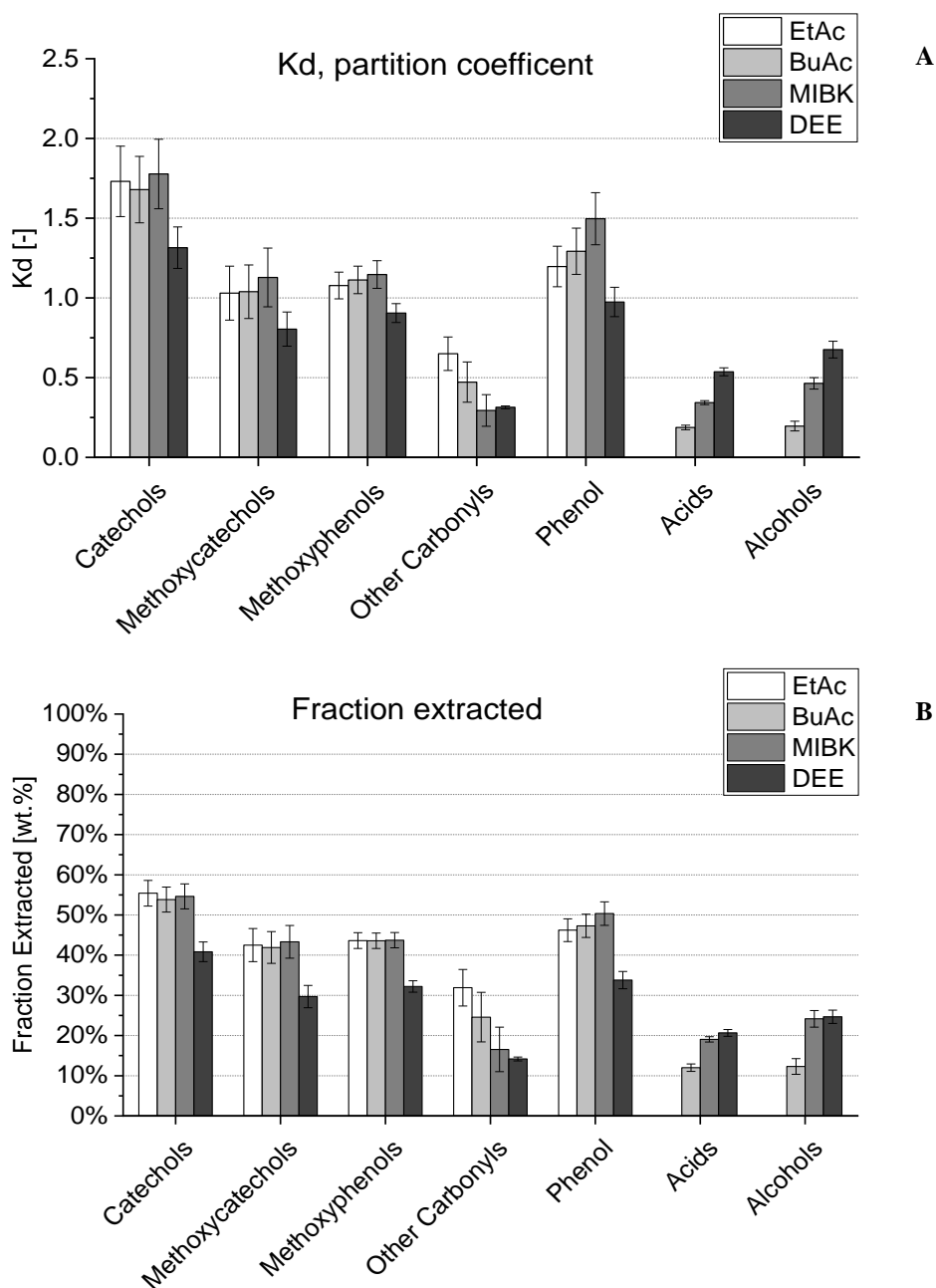


Figure 62. Partition coefficient (A) and fraction extracted (B) with four different solvents LLE. With EtAc acids and alcohols were not quantified due to HPLC peak coverage by the solvent itself.

The K_d represents how a specific class is fractionated between the extract and raffinate phase and is calculated as the ratio of concentration in the extract over the concentration in the raffinate. When $K_d > 1$, the concentration is higher in the extract and consequently is a good indication of higher affinity of that species with the solvent employed. Most

of the phenolics compounds have higher partition coefficient when EtAc, BuAc or MIBK was used as solvent, while with DEE the extraction was slightly inhibited. Same conclusion can be extrapolated observing the fraction extracted, that represents the effective mass extracted from the initial mass in the aqueous feed of the group considered. Higher extraction of phenolics was obtained with EtAc, BuAc and MIBK while DEE shows an enhanced extraction of acids and alcohols. As direct consequence, EtAc, BuAc and MIBK showed higher selectivity towards phenolics extraction compared to DEE, as depicted in

Figure 63. It can be noticed that among the solvents tested, BuAc showed the highest selectivity compared to the other solvents.

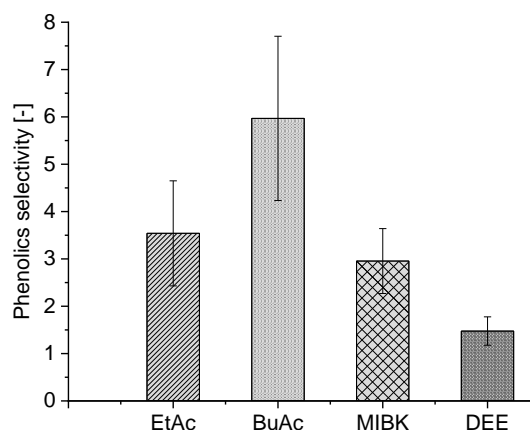


Figure 63. Phenolics selectivity (left) and effect of concentration of phenolic in the extract (right)

Improving the selectivity is an important achievement in term of selective separation of some molecules groups over other improving the overall separation process, and potentially reducing the economic impact of further separation and purification steps.

To sum up, EtAc, BuAc and MIBK can be considered as the most appropriate solvents for this application. The choice among them depends mostly on the downstream purification steps. EtAc have a low boiling point and can be easily extracted from the residual raffinate during distillation while BuAc and MIBK, having a boiling point higher than water needs to be extracted following different approaches (molecular sieves or resin adsorption).

The selection of the correct organic solvent to be used in a potential industrial scale up needs to be carried out taking in account also the safety, health and environment concerns. Prat et al⁴³² in 2015 defined a comprehensive selection guide of common solvents ranking the solvents on safety, health and environment criteria. Table 20 summarizes the results for the solvents tested in this work.

Table 20. Solvent selection results from Prat et al. CHEM21 guide scores ⁴³²

| ID | Safety score | Healthy score | Env. Score | Ranking |
|------|--------------|---------------|------------|------------------|
| DEE | 10 | 3 | 7 | Highly Hazardous |
| EtAc | 5 | 3 | 3 | Recommended |
| BuAc | 4 | 2 | 3 | Recommended |
| MIBK | 4 | 2 | 3 | Recommended |

It can be noticed that diethyl ether, even though the toxicity on humans is very limited, is considered highly hazardous and not recommended due to high safety risks associated with the low boiling and flash point as well as a low vaporization heat that increases explosion risks. While the other solvents tested are considered preferable and the only concern remains the flammability in air/oxygen environments. However, since the boiling and flash point are relatively high, they can be more easily controlled, drastically reducing potential accident. Among these three, ethyl acetate needs a little higher attention since the flash point is still low (-4°C), with risks associated with the flammability of the vapor phase even at ambient temperature.

Carbon and mass balance

To further investigate the potential benefits of compounds extraction and separation through LLE, a carbon balance has been carried out. Figure 64 shows a Sankey diagram with the carbon yields for each step of the HTL process, including the carbon ending in the extract and raffinate when BuAc was used as extraction medium. The major fraction of carbon ends up in the biocrude (52 wt.%) while 16 wt.%, 3 wt.% and 17 wt.% of the initial carbon was found respectively in solids, carbon dioxide and general losses (including carbon on the reactor walls and undetected). In addition, 12 wt.% of the original carbon was trapped in the aqueous phase when no AP recirculation is in place. Interestingly, as previously showed in Figure 61, the carbon in the residual AP is in form of stable, light and valuable monomers (aromatic or aliphatic) thus opening potential route for extraction of commodity chemicals or building blocks. After a 1:1 BuAc extraction, 3 wt.% of the initial carbon was recovered mostly in form of phenolic mixture with traces of acids and alcohols, while most of the carbon still remains in the raffinate phase (9 wt.%) in form of carboxylic acids and methanol. Therefore, further carbon recovery from the raffinate phase needs to be addressed in order to maximize the economy of the separation process.

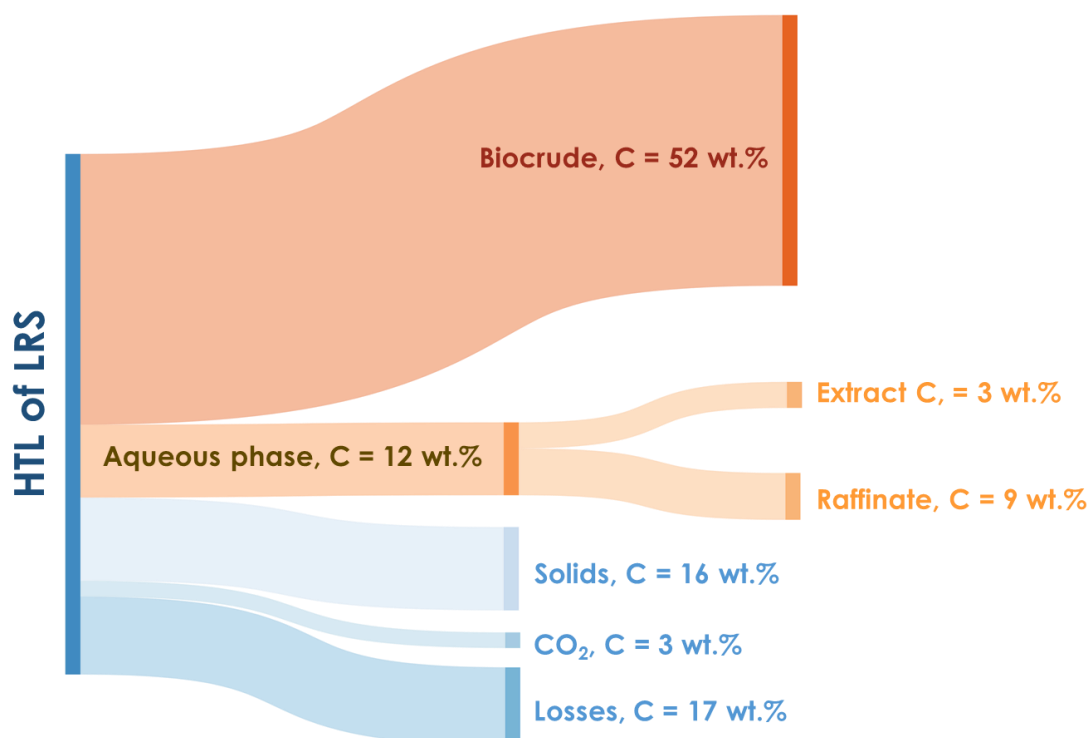


Figure 64. Carbon balance for the overall HTL process with LLE integration (data obtained with BuAc extraction)

Separation of carboxylic acids in water-rich raffinate-phase through PVP resins adsorption

The complete separation of compounds from aqueous phase cannot be carried out in a single step and it needs further processes to enhance the overall extraction of dissolved substances. The residual aqueous phase comprising the raffinate post-LLE still contains a percentage of valuable organic compounds for potential further applications in the chemical industry. Most of all, the aqueous raffinate contains a fair percentage of carboxylic acids that still represents a high carbon loss as described in the previous section. On this work, it was decided to test the recovery of carboxylic acids from the aqueous raffinate through ionic resin adsorption. A polymeric poly(4-vinylpyridine) (PVP) resin was selected as dewatering techniques and tested in a lab-scale setup. The PVP resin have been loaded to generate the loading profile for each species contained in the raffinate. Thus, a breakthrough point has been identified targeting the maximization of lactic and glycolic adsorption due to the high concentration and value.

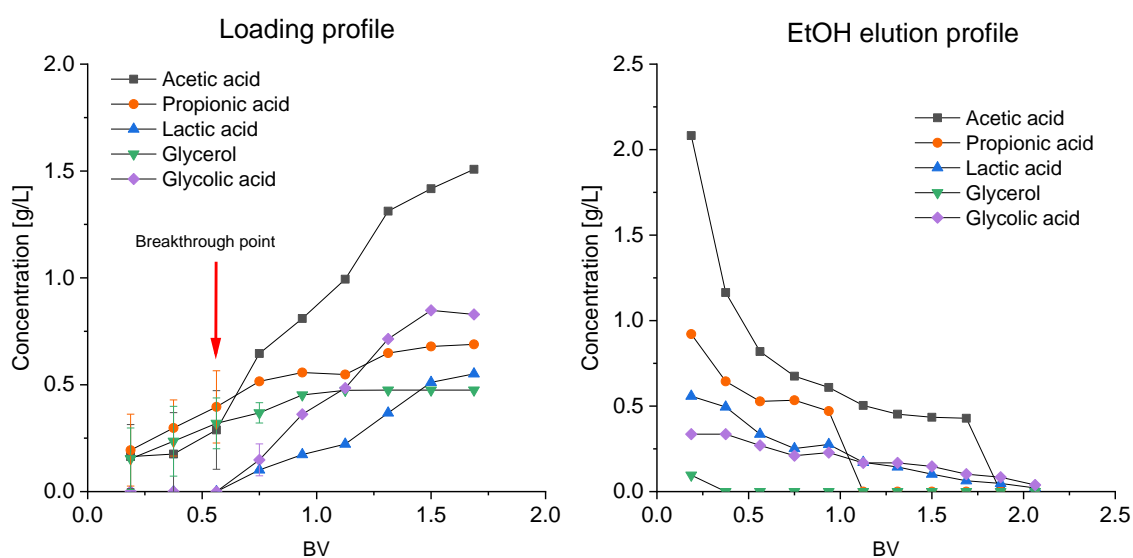


Figure 65. Loading curve for the organic acids and glycerol of the post-LLE raffinate (left) and elution curve desorbed from the resin using ethanol (right).

The breakthrough point has been found to be at 0.56 BV and consequently an optimal amount of 10 ml of raffinate for 10 g of resin was identified. After loading again the resin with raffinate phase, the elution profiles was generated by flushing the resin with ethanol (EtOH). The results suggest that the maximum products recovery was reached when 2.1 BV (~33 ml) of EtOH is used as eluent on 10g of PVP resin. Table 21 summarizes the experimental results. Regarding the loading capacity, expressed as the compound mass over the adsorption resin mass, the highest value was observed with glycolic acid and methanol, followed by lactic acid, acetic acid, propionic acid and glycerol. In term of percentage, lactic and glycolic acid were adsorbed completely over the resin surface, while a slightly lower efficacy on the acetic acid trapping was observed. In addition, limited affinity of PVP resin to the adsorption of glycerol and propionic acid was observed. Regarding methanol, it was noticed that even though the loading capacity was high, the effective capture was not achieved. However, methanol quantification was also subjected to issues on the repeatability due to the volatile nature and the correct procedure needs to be re-addressed, potentially keeping the setup at lower and controlled temperature.

Once the elution fluid (EtOH) was poured over the resin until 2.1 BV, almost all the acetic acid and propionic acid was recovered, followed by lactic acid (86%), glycolic acid (48%) and glycerol (21%). This indicate that higher amount of ethanol is needed to extract all the trapped amount of lactic and glycolic acids.

To sum up, the overall recovery, defined as the percentage of the initial mass transferred to the elution fluid (calculated as the product of the loading and elution efficacy) shows that, in these conditions, high recovery of lactic acid (86%), followed by acetic acid (76%), propionic acid (55%) and glycolic acid (48%), while a very low percentage of glycerol was extracted from the raffinate feed.

Table 21: Results summary of PVP adsorption of organic compounds in raffinate post-LLE

| TARGET | Initial Concentration [mg/mL] | Loading Capacity [mg/g_PVP] | PVP resin loading efficacy at BT [wt. %] | Final concentration in EtOH [mg/mL] | EtOH elution recovery efficacy [wt. %] | Overall Recovery [wt.%] |
|----------------|----------------------------------|--------------------------------|---|--|---|----------------------------|
| Acetic acid | 1.67 | 0.251 | 76% | 0.562 | ~100% | 76% |
| Propionic acid | 0.958 | 0.144 | 55% | 0.242 | ~100% | 55% |
| Lactic acid | 0.801 | 0.841 | ~100% | 0.219 | 86% | 86% |
| Glycerol | 0.475 | 0.071 | 29% | 0.009 | 21% | 6% |
| Glycolic acid | 1.24 | 1.306 | ~100% | 0.192 | 48% | 48% |
| Methanol | 6.89 | 1.034 | 36% | - | - | - |

Production of co-products from lignin HTL biorefineries: target of compounds and future production predictions

The commercial impact of the recovered monomers from the HTL aqueous phase depends on the lignin availability, and therefore on the deployment of the lignocellulosic ethanol biorefinery around the world. In a previous study⁴³³ two different scenarios have been evaluated for the development and spreading of cellulosic ethanol around EU. A central scenario foresees an increment in the production capacity from 31 million liters in 2017 to 2.75 billion of liters in 2030, while a more ambitious scenario predicts a capacity of 3.8 billion liters in 2030. The authors suggest that both scenarios are possible depending on the supportive policies applied during the years, and the more ambitious prediction does not represent an industrial technological upper limit, but a faster growth of the technology due to positive incentives. In this work, the central scenario has been selected as reference, to calculate the co-products capacity and the prediction at 2030, in a more conservative political environment. While in US, the ethanol capacity in 2019 has been estimated to be about 51 billion of liters but mainly from other biomass sources, such as corn, while cellulosic biomass as feedstock represents only the 0.5%⁴³⁴ of the total, thus about 253 million of liters. However, studies and prediction from the US DOE set a potential goal for 2030 of 60-75 billion of gallons (220-270 billion of liters) of cellulosic ethanol⁴³⁵. All biological process (such as enzymatic hydrolysis followed by fermentation) converts polysaccharides (cellulose and hemicellulose) into bioethanol resulting also in the formation of a large residual lignin stream (LRS) of about 25-35 wt.% of the total biomass.⁷² Moreover, the process produces a large amount of CO₂, estimated as about the same mass of ethanol) and, as first approximation based on available data, the LRS stream is about two times in mass the amount of ethanol produced by the process.^{73,74} As a result, the amount of lignin available in EU and US has been calculated in two different scenarios: one the amount nowadays available (2017 for EU and 2019 for US) and the other the prediction at 2030, as summarized in Table 22.

Table 22. Cellulosic ethanol and LRS availability in EU (2017-2030) and US (2019-2030)

| | unit | EU | | US | |
|-----------------------|----------------------------|----------|----------|----------|----------|
| | | 2017 | 2030 | 2019 | 2030 |
| Ethanol | Liters per annum | 3.10E+07 | 2.75E+09 | 2.53E+08 | 2.27E+11 |
| Residual Lignin (LRS) | kilotonnes per annum (kTA) | 49 | 4340 | 400 | 358403 |

As previously described, through LLE and resin adsorption is possible to recover a mixture of bio-derived light monomers (both phenolic and acids) that can be further purified and enter the market as commodity chemicals or building blocks for materials manufacturing. In this work the compound purification has not been tested experimentally, thus a conservative estimation has been applied on the LLE and PVP resulting yields. Therefore, the overall yield on feed for each compound has been calculated as 10% of the experimental separation yield previously measured. This estimation has been carried out in order to include in the evaluation further separation steps such as distillations and further treatments (e.g. crystallization of phenolics). Table 23 and Table 24 summarize the resulting production data for each compound targeted for EU and US respectively, showing also the prediction at 2030. Comparing the production results to the global market sizes, it is possible to define how this process can impact the market.

Table 23. Targeted molecules extracted from HTL AP through LLE and resin adsorption: EU data 2017-2030

| Class | Compound name | Separation yield on feed [wt.%] | Yield on feed* [wt.%] | EU Production 2017 [kTA] | EU Production 2030 [kTA] | Global market size [kTA] | Price** [\$ /kg] |
|--------------------|-----------------------------|---------------------------------|-----------------------|--------------------------|--------------------------|--------------------------|------------------------------|
| Phenolics † | 1,2-Benzenediol | 0.25% | 0.025% | 0.037 | 3.3 | 44 ⁴³⁶ | 4.0 ³⁸ |
| | 1,2-Benzenediol, 3-methoxy- | 0.54% | 0.054% | 0.079 | 7.0 | - | 2.0 |
| | Phenol, 2,6-dimethoxy- | 0.47% | 0.047% | 0.068 | 6.1 | 40 ²¹ | 2.0 ²¹ |
| | Phenol, 2-methoxy- | 0.26% | 0.026% | 0.038 | 3.4 | | |
| | Phenol | 0.46% | 0.046% | 0.068 | 6.0 | 11400 ³⁸ | 1.1 ³⁸ |
| Carboxylic acids ‡ | Acetic acid | 1.2% | 0.12% | 0.172 | 15.2 | 18000 ⁴³⁷ | 0.5 ⁴³⁸ |
| | Propionic acid | 0.57% | 0.057% | 0.084 | 7.4 | 350 ⁴³⁹ | 1.1 ⁴³⁹ |
| | Lactic acid | 0.72% | 0.072% | 0.106 | 9.4 | 300 ⁴⁴⁰ | 0.55-1.54 ^{441,442} |
| | Glycolic acid | 0.60% | 0.060% | 0.088 | 7.8 | 80 ⁴⁴³ | - |

* Estimation of compound purification efficiency of 10 %

** Values updated at June 2020 through Producer Price Index by Commodity for Chemicals and Allied Products: Industrial Chemicals⁴⁴⁴

† Recovered through LLE of the HTL AP

‡ Recovered through PVP adsorption of raffinate phase from LLE

Table 24. Targeted molecules extracted from HTL AP through LLE and resin adsorption: US data 2019-2030

| Class | Compound name | Separation yield on feed [wt.%] | Yield on feed* [wt.%] | US Production 2019 [kTA] | US Production 2030 [kTA] | Market size [kTA] | Price** [\$/kg] |
|--------------------|-----------------------------|---------------------------------|-----------------------|--------------------------|--------------------------|----------------------|------------------------------|
| Phenolics † | 1,2-Benzenediol | 0.25% | 0.02% | 0.30 | 269 | 44 ⁴³⁶ | 4.0 ³⁸ |
| | 1,2-Benzenediol, 3-methoxy- | 0.54% | 0.05% | 0.64 | 576 | - | - |
| | Phenol, 2,6-dimethoxy- | 0.47% | 0.06% | 0.56 | 502 | 40 ²¹ | 2.0 ²¹ |
| | Phenol, 2-methoxy- | 0.26% | 0.03% | 0.31 | 279 | | |
| | Phenol | 0.46% | 0.05% | 0.56 | 500 | 11400 ³⁸ | 1.1 ³⁸ |
| Carboxylic acids ‡ | Acetic acid | 1.17% | 0.12% | 1.41 | 1259 | 18000 ⁴³⁷ | 0.5 ⁴³⁸ |
| | Propionic acid | 0.57% | 0.06% | 0.68 | 614 | 350 ⁴³⁹ | 1.1 ⁴³⁹ |
| | Lactic acid | 0.72% | 0.07% | 0.86 | 775 | 600 ⁴⁴⁵ | 0.55-1.54 ^{441,442} |
| | Glycolic acid | 0.60% | 0.06% | 0.72 | 644 | 80 ⁴⁴³ | - |

* Estimation of compound purification efficiency as 10 % of the measured yields

** Values updated at June 2020 through Producer Price Index by Commodity for Chemicals and Allied Products: Industrial Chemicals⁴⁴⁴

† Recovered through LLE of the HTL AP

‡ Recovered through PVP adsorption of raffinate phase from LLE

Phenol

Phenol is a commodity chemical nowadays synthesized from fossil benzene, and it can be further used for production of resins (i.e. epoxy or phenolic resins) that are used in electronics components manufacturing⁴⁴⁶ as well as used as flame retardant materials⁴⁴⁷, wood adhesives and laminates⁴⁴⁸, foaming polymers⁴⁴⁹. The market size is about 11400 kilotonnes per annum and the industrial price of 1.1 \$/kg. The present and future production from HTL AP in both US and EU shows that a very low percentage of the market could be potentially covered, even in a positive future growth, but surely can contribute to the substitution of fossil derivatives together with other biomass conversion processes (e.g. fast pyrolysis).

Catechol

Catechol (1,2 Benzenediol) is an interesting crystalline compound that currently is industrially produced through hydroxylation of phenol, hydrolysis of 2- chlorophenol or dehydrogenation of 1,2-Cyclohexanediol, thus from fossil sources. It is mainly used as building block for several chemicals in the pharmaceutical sector or in the pesticides

production. Other uses include food and fragrances or as polymerization inhibitors as well as corrosion inhibitor in the electronics industry. In general, about 50% of the total catechol production is used as raw material for pesticides (especially insecticides such as Propoxur), 35-40% in perfumes and drugs and 10-15% for polymerization inhibitors and other chemicals.^{450,451} Moreover, catechol has been studied as building block for the synthesis of high performance polymers such as Poly(ether ether ketone) (“o-PEEK”).^{452,453} HTL of LRS produced a fair amount of catechol in biocrude and AP, and it can be recovered through LLE of the AP, resulting in about 0.25 wt.% of the initial lignin. Estimating the purification steps, a European production of 0.012 kTA (2017) and a forecast of 3.3 kTA can be expected, thus representing about 7.5% of the global market. While in US, according to the production in 2030, the amount of catechol that can be recovered from this process will exceed the current market size thus completely covering the market demand. A complete market saturation is not positive in the perspective of introducing products in the market and therefore research should focus on finding other applications for this compound). In addition, the catechol market value is fairly high with 4 \$/kg, representing an interesting business opportunity.

3-Methoxycatechol

Another compound contained in the HTL AP and further extracted through LLE is the 1,2-Benzenediol, 3-methoxy- (or 3-methoxycatechol). This molecule is composed by a catechol with the addition of a methoxy group in position 3 and no existing data has been found regarding the market, but in first approximation the market price can be considered similar to the catechol. However, the interesting structure makes this molecule a potential building block for polymers such as PEEK, in similar potential pathways of catechol. The only one caveat that needs to be addressed is how the presence of the methoxy group would affect the polymer performances. The amount available from HTL AP valorization can potentially reach 7 kTA in EU and 576 kTA in US in 2030, thus further investigations are strongly needed to implement the utilization of this compounds for several applications.

Guaiacol and Syringol

Regarding the methoxyphenols extracted, the main compounds quantified in the LLE-extract were Phenol, 2,6-dimethoxy- (Syringol) and Phenol, 2-methoxy- (Guaiacol) derived from the cleavage of the lignin syringyl (S) and guaiacyl (G) aromatics units. These compounds are mainly used as a precursor of flavorants and aromas in the food industry (e.g. synthetic smoke flavorings), and guaiacol is also used in medicine as expectorant, antiseptic, and local anesthetic.^{454,455} The market size for both is about 40 kTA with a market value of about 2.0 \$/kg. Guaiacol can also be produced by methylation of catechol, while syringol is mainly obtained from biomass conversion (e.g. pyrolysis). Observing the EU 2030 prediction, through the valorization of HTL AP is possible to reach a production of 6.1 and 3.4 kTA respectively for syringol and guaiacol. While the US production also in this case will exceed the market demand opening the way for new applications as bio-based material precursors. In this context, these compounds may represent an interesting and important platform for the manufacturing of bio-based materials. Previous studies proposed the synthesis of new polymer guaiacol-based for application as antibacterial polymer, benzoxazine resins.⁴⁵⁶⁻⁴⁵⁸ In addition, another work from Koelewijn et al.⁴⁵⁹ demonstrated the possibility of producing bisphenols from lignin, especially from alkylated guaiacols (e.g. 4-propylguaiacol). Regarding the syringol, a study by Holmberg et al.⁴⁶⁰, demonstrated the synthesis of syringyl methacrylate for further production of high-performance polymers. The authors found that polymers synthesized with syringyl methacrylate had good thermal stability, high glass transition

temperature (ranging from 114°C to 205°C) and deformation resistances, thus confirming the potential use of syringol as bio-based source for new materials and additives.

Acetic acid

Acetic acid is one of the simplest carboxylic acids and it is used for a vast range of applications as commodity chemical. It is present in a percentage 5-20 wt.% in vinegar in the food industry as well as used for the production of plastics, photographic film and adhesives. Moreover, it is used for the production of polyvinyl acetate for wood glue, as well as many synthetic fibres and fabrics (e.g. nylon). It is also used as cleaning agent in households and in medicine as an antiseptic due to the excellent antibacterial properties.^{461,462} The large market applications results in an annual production of 18000 kilotonnes that is mainly produced by carbonylation of methanol or bacterial fermentation of sugars (mainly for the food industry that requires biological origin).⁴⁶³

HTL of LRS produce a fair amount of acid acetic that is trapped in the aqueous phase and, after a first LLE extraction can be recovered from the raffinate phase through polymeric resin adsorption as previously indicated. From the lignin available today is possible to recover about 0.172 kTA and 1.41 kTA in EU and US respectively, but with a projection at 2030, the amount can reach 15.2 kTA and 1259 kTA in EU and US in 2030.

Propionic acid

Propionic acid is used in the manufacturing of cellulose esters, plastic dispersions, and herbicides. In addition, it is also used in the pharmaceutical industry and in flavors and fragrances. Moreover, it has fungicidal and bactericidal action and it is used as food and feed preservative, for example it can be found in bakery product and cheese to protect them from bacteria and mold. Propionic acid is industrially produced by two different processes, carbonylation of ethylene and oxidation of propionaldehyde, therefore from petroleum sources. Another way to produce propionic acid from renewable sources is represented by fermentation of sugars. The extraction from HTL AP can represent an alternative way of industrial production from renewable sources. Observing the production estimation, the amount that can be currently produced in EU and US is less than 1% of the global market, but accordingly to the projection the potential production will exceed the current demand.

Lactic acid

Lactic acid is a natural carboxylic acid with a long and broad history of applications in several industries, from food and pharmaceutical to textile, and chemical.⁴⁶⁴ In the last decades, the demand for lactic acid and consequently the market size has increased considerably because of its use as precursor for the manufacturing of polylactic acid (PLA)^{464,465}, reaching an annual production of 600 kTA⁴⁴⁵. PLA is a biodegradable and biocompatible polymer that found applications in a multitude of applications: from packaging and fibers to foams⁴⁶⁵ and applications in biomedical devices⁴⁶⁶. Lactic acid can be produced in two ways: fermentation or chemical synthesis. Production by the fermentation involves the conversion of sugars (e.g. glucose or sucrose) in presence of organism, such as *Lactobacillus*⁴⁶⁵, in anaerobic conditions. While synthetic lactic acid is produced from petrochemical sources, acetaldehyde and hydrogen cyanide reacts to produce lactonitrile that is further processed to form pure lactic acid.⁴⁶⁷ Larger interested is attributed to the microbial fermentation process due to the use of renewable source and the possibility to produce pure isomers (L(+)- or D(-)-lactic acid), as well as low energy consumption, and mild conditions required during the conversion.⁴⁶⁷ Moreover, lactic acid can be produced from non-food sources through the

fermentation of the separated and hydrolyzed sugars from lignocellulosic biomass.⁴⁶⁸ As a matter of fact, during the cellulosic ethanol production a percentage of lactic acid is always generated in the fermentation broth.⁴⁶⁹ In this work, we already demonstrated that the lactic acid content observed after the hydrothermal liquefaction reactions was already contained in the original lignin-rich feedstock, thus it undergoes only through cracking to form non-condensable gases. A fraction of lactic acid still remains trapped in the residual AP and is not extracted by LLE, but it can be recovered through PVP adsorption at a fairly high efficiency. Observing the production data for EU and US, this extraction method has the potential to produce a large amount of lactic acid by 2030, covering about 40% of the global market. The market value has been estimated in the range 0.55-1.6 \$/kg depending on the purity, therefore the production as biorefinery co-product needs to meet this value to smoothly enter in the market in parallel to the other production technologies.

Glycolic acid

Glycolic acid (or hydroxy acetic acid) is the smallest alpha-hydroxy acid that contains both alcohol and carboxyl groups. It is used in a variety of applications in the cosmetic industry and present as excipient in some topical drug products, due to excellent performance as skin treatment (e.g. chemical peeling). In addition, it can be found as an ingredient in some household cleaning products as well as in the textile industry as a dyeing and tanning agent.^{470,471} It is also used as building block for the preparation of polyglycolic acid (PGA), which is a biodegradable polymer that quickly degrades in the natural environment. However, compared to PLA, PGA is mainly used in biomedical applications and has not been used in a broader range of industrial applications, due to high production costs compared to other biodegradable polymers.⁴⁴⁵ Glycolic acid can be extracted from petroleum or renewable sources but at industrial scale is mainly produced from petrochemical feedstock through a reaction of formaldehyde and carbon monoxide over an acidic catalyst.^{472,473} The market size is about 80 kTA and is expected to grow in the future driven by the demand in cosmetic products and cleaning agents.^{443,474} Observing the potential amount recoverable from the HTL AP in EU and US, also in this case the potential production exceeds the demand, thus opening the ground for larger utilization driven by research of new application. Obviously, the growth and utilization of this compound at larger scale would need a correct economical evaluation in order to keep the production price low and comparable to other extraction technologies.

Techno Economic Analysis: evaluation of LLE integration at industrial scale

After discussing the experimental results obtained on the extraction of compound from the AP through and LLE and PVP adsorption and the market implication, it is important to investigate if the employment of a co-product recovery unit is an economically viable route in the lignin HTL biorefinery. Therefore, a HTL model has been created and hereby the main results will be presented.

The continuous HTL plant techno-economic analysis (TEA) was designed as a potential integration to the first industrial demonstration-scale plant in the world for the production of bioethanol from lignocellulosic biomass. The plant was built by Biochemtex S.p.A. in Crescentino (VC, Italy) with a capacity of 40.000 tonnes per year of produced ethanol, based on PROESA™ technology, with a dry biomass input of about 180.000 tonnes/year and a vast amount of lignin-rich stream (LRS) is available as co-product at the production site in considerable quantities.⁴⁷⁵ The HTL plant was modelled on a capacity of 55 tonnes per hour biomass-water slurry according to about the amount of LRS

which is yearly produced in the ethanol plant. The detailed HTL scheme of the model is presented in Appendix C1. In this configuration, it was considered the use of a base catalytic additive (Na_2CO_3) to improve the depolymerization and Table C1.1 summarizes all the parameters used in the model. The model and the sensitivity analysis were carried out using Microsoft Excel spreadsheets as main tool. In this work, the effect of the integration of a LLE step as potential first path for the extraction of chemicals from the residual aqueous phase will be analyzed and discussed. The main output considered was the minimum biocrude selling price (MBSP) and it was first calculated in absence of an aqueous phase valorization step (Appendix C3), then the economic impact of the recovery of monomers through the implementation of a LLE column was evaluated.

The aqueous phase, that still contains a fair amount of oxygenated compounds (yield in the range 20-30 wt.% db) recovered at the outlet of the HTL section can be recirculated in order to increase the conversion efficiency as reported by other authors. For example, in the continuous pilot plant of Aarhus University⁴⁷⁶, some experiments were conducted on dried distiller grains with water phase recirculation, with or without the addition of an alkali catalyst. After 6th round of recycling, the biocrude yield increased from 39.4 wt.% to 54 wt.% with water phase recirculation without the use of alkali catalyst. With the addition of the alkali K_2CO_3 , the increment was quicker and after the first round of recycling the yield was 60 wt.% compared to the 44.3 wt.% of the continuous baseline experiment⁴²³. As a result of the recirculation, also the composition of the aqueous phase was modified. The total organic content (TOC) was increased after the 1st round of recycling from 36 g/l to 42 g/l and steady increased up to 90 g/l in the 8th round of recycling. The nitrogen content showed the same trend, a steady increase from 6.5 g/l to 26 g/l. The pH of the aqueous phase was stable around 7 during the entire recycling rounds without the use of alkali catalyst. With the addition of K_2CO_3 , the pH increased from 7.6 in the baseline experiment to 10 after 8th recycle⁴²³. After the 3rd recycle, the biocrude yield rose from 34.9 wt.% to 38.4 wt.% and the HHV from 27.29 MJ/kg to 28.4-29.4 MJ/kg.

In this model, the aqueous phase composition was taken from the experimental results reported here, while the recirculation was modelled based on literature data. Figure 66 shows the simplified scheme of the aqueous phase valorization pathway that was integrated in the model. In the process described here, a fraction of the recirculated aqueous phase (AP) of the HTL enters in liquid-liquid extraction column (LLE) where is mixed with a solvent. The flows coming out of the LLE column are two: extract and raffinate. In this model, the raffinate flow, rich in water, is directed to wastewater treatment even though it still contains small amount of WSO dissolved (mostly acids and alcohols), thus other acids recovery downstream processes were not modelled. The extract flow, composed by mainly solvent and phenolic organics dissolved, is directed to a distillation column in which the solvent is recovered by evaporation and recycled to the LLE column inlet. The remaining extracts can be further refined through distillation in order to separate single compounds, but this step is not considered in the model. Regarding the recirculation of the AP, since no experimental results were available, literature data were used as baseline to hypothesize the increment in the TOC and foresee the organic concentration.

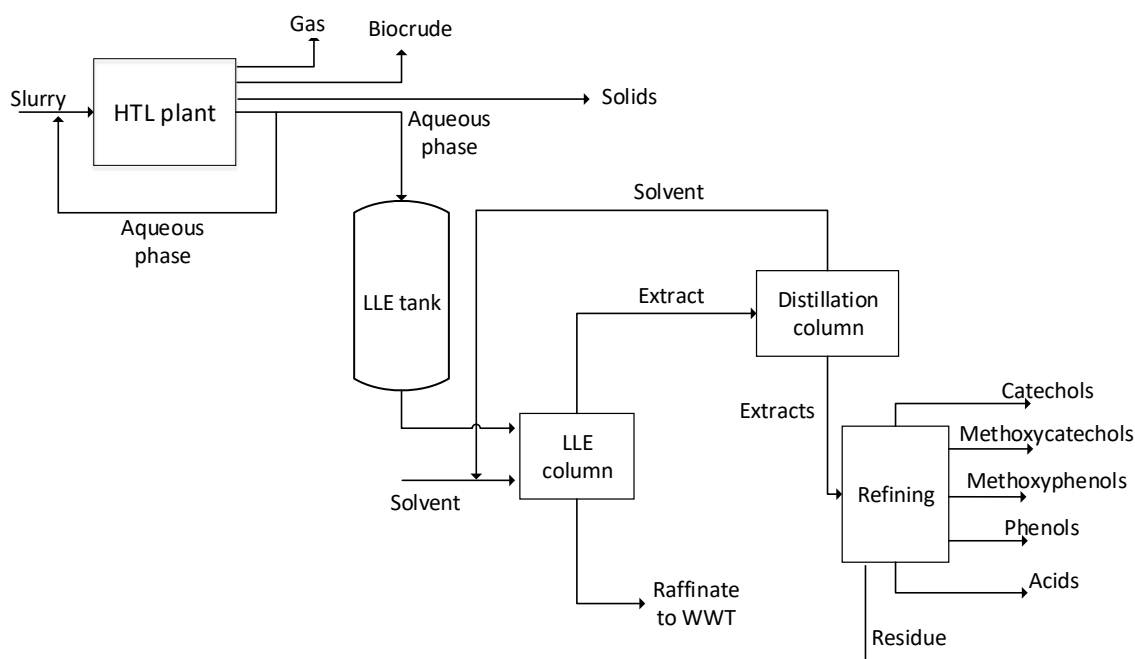


Figure 66: Scheme of the HTL with AP recirculation and LLE integration for the extraction of organic compounds

The operating hours per year were considered equal to the one of the HTL plant. While for the experimental campaign a ratio AP/Solvent was kept at 1, in the industrial model the ratio was considered equal to 5, to be more realistic and reduce the volume of solvent handled. Future works needs to be done in order to correct the model input regarding the extraction results should be corrected. Also, the mass flows of extract and raffinate depends on the solvent used in LLE column. The same experimentally tested organic solvents were considered as model input (Table 18). Regarding the safety, health and environmental score of the four solvents, the DEE should not be considered as industrial viable route even though it has a low boiling temperature.⁴³² In addition, BuAc and MIBK have the higher boiling temperature and higher specific vaporization enthalpy, consequently the recovery from the raffinate aqueous phase cannot be performed by distillation as well as a higher energy demand for the extract recovery. For these reasons, EtAc was selected as the more appropriate solvent for the model but BuAc can be used as well due to similar performance addressed.

Mass balances

In the HTL set-up depicted in Figure 66, the total amount of organic compounds dissolved in the aqueous phase increase constantly due to recirculation up to the equilibrium. Therefore, the carbon content, measured through TOC, of the aqueous phase increases in each round of recycling. Biller et al.⁴²³ reported an increment in the TOC per cycle from 6 g/l up to a maximum TOC of 90 g/l. In lab-scale experiments reported in the previous section the TOC of the AP was about 9 g/l. In order to reach the theoretical maximum TOC of 90 g/l, about 14 rounds of recirculation are needed. The total AP mass flow is 48919 kg/h. In order to obtain a constant TOC in the AP flow through the LLE, it was decided to sample part of the AP recycle flow in a discontinuous way. After a start-up period of 14 recirculation cycles in the HTL, 30% of the aqueous phase is pumped out in a collecting tank, corresponding with a mass flow of 14675 kg/h. For keeping constant the B/W ratio in inlet slurry, reintegration with DI water is necessary when the AP is extracted.

The TOC of the AP with the water integration resulted in 63 g/l, through the equation:

$$TOC_m = \frac{TOC_{AP}(\dot{m}_{recycled} - \dot{m}_{tank})}{\dot{m}_{recycled}}$$

The total residence time of the plant was evaluated considering a total tubes length of 393 m and the average axial velocity of 0.35 m/s, calculated considering different velocities for different fluid densities in the unit zones:

$$\dot{v}_m = \frac{\dot{v}_{reactor} \cdot L_{reactor} + (L_{exchangers} + L_{other tubes}) \cdot \dot{v}_{exchangers}}{L_{tot}}$$

Therefore, the total plant residence time resulted in 21.3 minutes and it was calculated as a sum of different contributions of the plant zones (reactor, heath exchangers and connection tubes):

$$R_t = \frac{L_{reactor}}{\dot{v}_{reactor}} + \frac{L_{exchangers}}{\dot{v}_{exchangers}} + \frac{L_{other tubes}}{\dot{v}_m}$$

In order to maintain a constant TOC in the inlet, the mass flow \dot{m}_{tank} is directed to the LLE tank for a residence time (R_t). The total mass collected in tank for each R_t is 5219 kg:

The period between two AP bleeds was calculated as the time required to return to a TOC of 90 g/l after the reactions. The number of AP round of recirculation was calculated considering that, during the period of bleed, the inlet AP with the slurry flow through the entire length of the plant:

$$n^{\circ} \text{ of recycle rounds} = \frac{TOC_{AP} - TOC_m}{TOC_{increase}} - 1 = 3.5$$

The n° of recycle rounds were approximated to 4 of a total time of 85.3 minutes (t_{BR}). The total AP mass collected in the LLE tank per year is then:

$$m_{tot tank} = \frac{h_{year}}{t_{BR}} \cdot m_{tank} = 14675 \frac{tonne}{year}$$

In order to keep a constant flow in the LLE unit for the same annual operative hours of the HTL plant, the AP inlet mass flow for the LLE was calculated as:

$$\dot{m}_{AP LLE} = \frac{m_{tot tank}}{h_{year}} = 3668.9 \frac{kg}{h}$$

As previously described, solvent extraction can lead to a selective separation of phenols from the remaining acids and alcohols, thus recovering interesting light monomers that can be inserted in the chemical market as commodity chemicals or building block for bio-based materials (e.g. polymers). The compounds targets considered in this analysis (Table 25), are trapped in the organic solvent during the LLE at different percentages and the experimental results was used to populate the model. In order to integrate the downstream separation into the model it was considered the addition of a LLE column followed by a distillation column for solvent recovery. The final refining step showed in Figure 66 and Figure 67, it comprises further purification through distillations step but in this preliminary analysis it was chosen to simplify the calculations using a conservative overall extraction efficiency per compounds of 0.3.

The mass fraction of organic compounds was related to the TOC of the aqueous phase considering the carbon number of the main molecule for each set of compounds. The total mass flow of each components in the AP was calculated in relation to the whole molecular weight and the results are summarized in Figure 67.

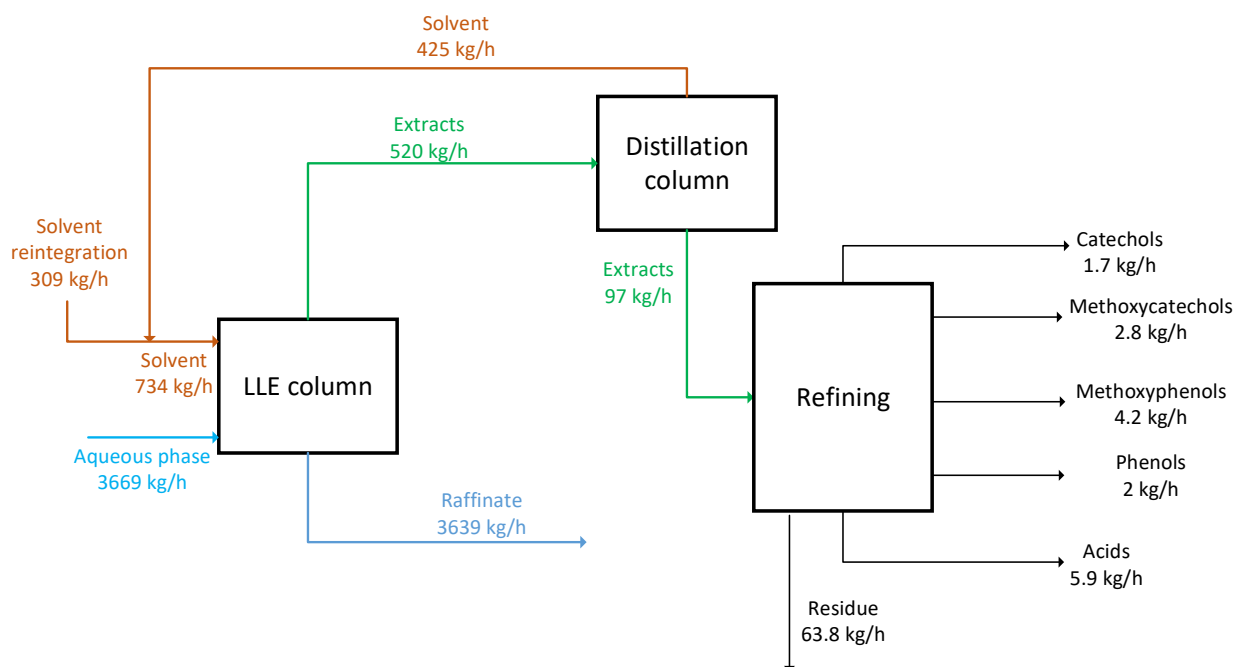


Figure 67. Model mass flows for HTL-LLE integration; AP/solvent ratio of 5:1

Table 25. Experimental data of fraction extracted and calculated mass flow of organic components in raffinate and extract.

| Organic components | Fraction in extract [wt.%] | Extract mass flow [kg/h] | Fraction in raffinate [wt.%] | Raffinate mass flow [kg/h] |
|--------------------|----------------------------|--------------------------|------------------------------|----------------------------|
| Catechols | 54% | 5.7 | 46% | 4.8 |
| Methoxycatechols | 42% | 9.4 | 58% | 12.9 |
| Methoxyphenols | 43% | 13.9 | 57% | 18.4 |
| Phenol | 45% | 6.7 | 55% | 8.2 |
| Acids | 23% | 19.8 | 77% | 66.4 |
| Alcohols | 32% | 35.7 | 68% | 75.8 |
| Total | | 91.1 | | 186.6 |

In the distillation column it was considered that 99% of the inlet solvent is evaporated and recycled to the LLE column. The refining step was considered as composed by several processes in order to obtain the separation and purification of pure components from the total inlet mass flow. Since no more accurate information was found in literature research, for the refining step it was considered an overall extraction efficiency per component of $\eta_{ref} = 0.3$. The mass flows of the chemicals that come out of the refining step are shown in Table 26.

Table 26. Mass flows of the chemicals coming out of the refining step.

| Chemicals | Mass flow [kg/h] |
|------------------|------------------|
| Catechols | 1.7 |
| Methoxycatechols | 2.8 |
| Methoxyphenols | 4.2 |
| Phenol | 2 |
| Acids | 5.9 |
| Alcohols | 10.7 |
| Total | 27.3 |

Energy balances

The LLE column and the distillation column are complex to design in details and it was chosen to identify and calculate only the thermal power required for the evaporation of the solvent in the distillation column was calculated, supposing a larger contribution. Figure 68 shows the electrical power installed for each pump and the thermal power required for the distillation column. The pumps are needed to provide liquids circulation. Centrifugal pumps were selected in this case because the ΔP required are modest and the fluids are at low temperature. The power consumptions were calculated considering an overall efficiency of 0.5. The hydraulic head was approximated equal to 45 m, as suggested in other works⁴⁷⁷. The electrical power required for each pump is shown in Table 27. The circulation pump for the extract coming out of the distillation column was omitted because of the very low mass flow. The electricity consumptions per year per equipment are shown in Table 27. Considering the vaporization enthalpy of the EtAc as 375 kJ/kg and the solvent mass flow rate, the thermal power required for the vaporization was estimated as 70.1 kW.

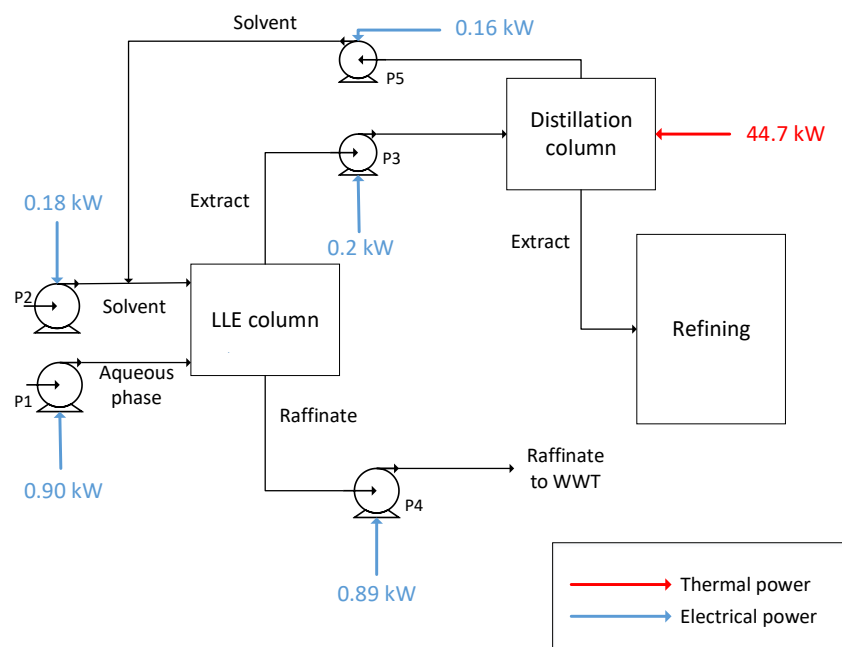


Figure 68. Electrical and thermal power of the LLE section.

Table 27. Electrical power installed and electricity consumption per year for each pump.

| Equipment | Electrical power [kW] | Electricity consumption |
|--------------|-----------------------|-------------------------|
| | | [kWh/year] |
| P1 | 0.90 | 7018.4 |
| P2 | 0.18 | 1403.7 |
| P3 | 0.19 | 1461.5 |
| P4 | 0.89 | 6960.6 |
| P5 | 0.16 | 1274.3 |
| Total | 2.57 | 18118.5 |

Also, the thermal, plant and chemical efficiencies were calculated as 87.5%, 38.7% and 70.9% respectively. While the biocrude mass flow in this configuration was estimated as 5133.3 kg/h with a carbon efficiency as 66.9%.

Also the specific thermal consumption was estimated to be 9.2 kWh_{th}/kg_{biocrude} and the specific electric consumption is 0.25 kWh_{el}/kg_{biocrude}.

Economic analysis

After the mass and energy balances, the estimation of the capital and operating costs of the LLE sections was incorporated in the model. The prices of the pumps were obtained from Knorr et al.⁴⁷⁷ while the LLE and distillation column prices from Funkenbusch et al.⁴⁷⁸. A static mixer was also included for mixing the recycled aqueous phase with clean water reintegrated and the reference price was obtained from Knorr et al.⁴⁷⁷.

The equipment prices, obtained for different years, were converted to Euro and adjusted to the common base year 2018 as well as considering a scale factor depending on the size, according to the equations presented in Appendix C2. Also for the installed equipment costs, adjustments were done following Knorr et al.⁴⁷⁷ as described in Appendix C2 (Figure C2.1). In order to calculate the total capital investment (TCI) of the new plant configuration, the LLE equipment costs were added to the total equipment costs of the baseline HTL model. The additional direct, indirect cost and working capital were calculated by using the value by Knorr et al, reported in Figure C2.2. The resulting additional costs of the LLE unit are shown in Table 28. Therefore, the total capital investment is 76 M€, compared to the previous 42M€ in absence of downstream AP valorization.

In addition, in order to consider the increment in the electricity cost per year, the energy consumption of the LLE circulation pumps was added to the total electricity consumption of HTL baseline model. Also, the thermal energy required by the distillation column was considered for the correction of the annual natural gas cost.

In this plant configuration, the aqueous phase post-LLE (raffinate) was considered as wastewater and no acids recover were considered in the model, resulting in a stream of 28381 tonnes per year. While the total make-up water added to reintegrate the AP mass flow used in the LLE column resulted in 28617 tonnes per year. The unit costs of natural gas, electricity and wastewater treatment were considered unvaried from the base case and the HTL-LLE operating costs are summarized in Table 29.

Table 28. Equipment cost of the LLE integration.

| | |
|----------------------------------|--------------------|
| LLE column + distillation column | 4.744.311 € |
| Solvent pump | 632 € |
| AP pump | 6.944 € |
| Extract pump | 653 € |
| Raffinate pump | 2.275 € |
| Solvent recycle pump | 585 € |
| Total | 4.758.886 € |

Table 29. Operating costs of the HTL plant with LLE integration.

| Operating Cost [€/year] | |
|--------------------------------|---------------------|
| Natural gas | 5.431.786 € |
| Property Insurance | 3.433.917 € |
| Electricity | 669.239 € |
| Sodium carbonate catalyst | 475.113 € |
| Labour cost | 729.000 € |
| Overhead and maintenance | 656.100 € |
| Maintenance capital | 1.545.263 € |
| Water added | 5.151 € |
| Wastewater treatment | 470.470 € |
| Total | 13.416.040 € |

Since only the LLE unit was considered in this model, only the phenolic mixture with the addition of a fraction of acetic acid were considered in the techno-economic analysis to calculate the annual revenue from the sales of each pure compound. Therefore only one compound per class was considered with market price for each substance that was found in literature, as previously showed in Table 23 and Table 24, here converted in €/kg in Table 36. For the 3-methoxycatechol the same value of catechol has been taken in first approximation since no reliable data were found.

Table 30. Prices of the chemicals considered in the economic analysis.

| Chemical | Molecule | Price [€/kg] |
|------------------|---------------------------|---------------------|
| Catechols | 1,2-Benzenediol | 1.81 ³⁸ |
| Methoxycatechols | 3-methoxycatechol | 1.81 |
| Methoxyphenols | 2,6-dimethoxy-,2-methoxy- | 1.80 ²¹ |
| Phenol | Phenol | 1.77 ³⁸ |
| Acids | Acetic acid | 0.63 ⁴⁷⁹ |

Then, the annual mass flow and revenue have been calculated to observe the total annual income due to the introduction of these compounds into the market, as listed in Table 31.

Table 31. Annual mass flow and revenue of the chemicals coming out of the refining step.

| Chemical | Mass flow [kg/y] | Annual revenue [€/y] |
|---------------------------|------------------|----------------------|
| 1,2-Benzenediol | 13228 | 23989 |
| 3-Methoxycatechols | 21917 | 34558 |
| 2,6-dimethoxy-,2-methoxy- | 32506 | 58511 |
| Phenol | 15775 | 27956 |
| Acetic acid | 46405 | 29034 |
| Total | 129831 | 174049 |

The recycle of the AP in HTL reactor has also beneficial effect on the quality and yield of biocrude as other authors suggest⁴⁸⁰. As a consequence, in this analysis, the biocrude yield was considered enhanced by 5 wt.%, thus the annual biocrude production increased from 36822 tonnes per year to 40040 tonnes per year. While the enhanced biocrude quality was considered as an increment in the HHV, from 28 MJ/kg to 29 MJ/kg.

It was also possible to estimate the minimum biocrude revenue per year in order to pay back the investment in 30 years was about 21.6 M€ as calculated from the equations listed in Appendix C3.

Thus, the minimum biocrude selling price per gasoline gallon equivalent was estimated for the HTL configuration including the aqueous phase valorization unit, resulting in 2.44 \$/gge. Therefore, a total reduction of 0.66 \$/gge from the 3.10 \$/gge obtained as HTL baseline without any aqueous phase valorization. As noticeable in Figure 69, the MBSP increment due to LLE was evaluated to be 0.18 \$/gge, however the total O&M expenses resulted decreased mostly due to a great reduction in the amount of wastewater sent to traditional treatment, as well as the slight positive impact of the revenue of the chemicals produced and sold in the market (accountable as about 2% of the total operating costs).

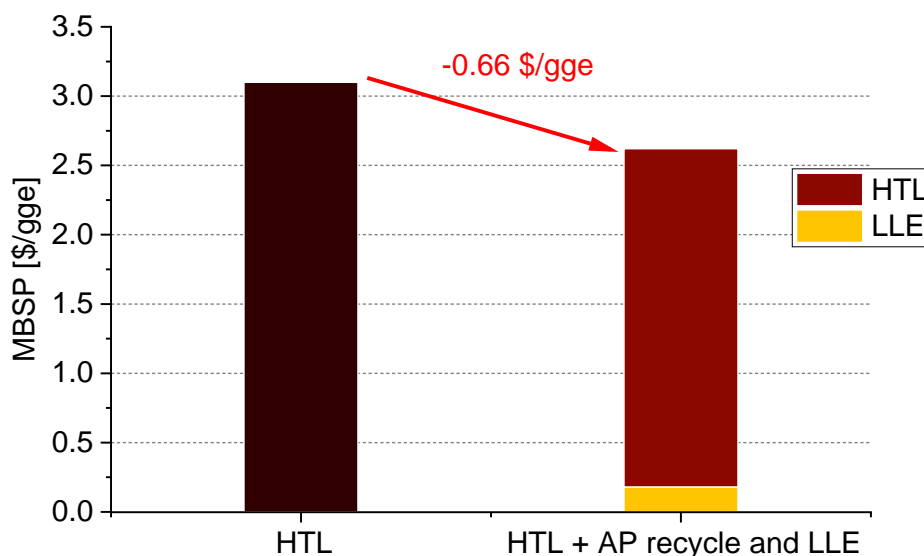


Figure 69. Influence of aqueous phase recycle and LLE integration on MBSP: base case in absence of aqueous phase valorization (left) and with recycle coupled with LLE (right)

To sum up, even though the AP recirculation and compounds extraction through LLE introduces other capital and operating costs as well as technical complexity to the system, there are evident economic advantages on pursuing in this direction. Moreover, the parallel production of biobased chemicals has the potential to cover a large portion of markets that are still predominantly covered by fossil-derived sources, thus helping on the switch towards a greener bio-based circular economy.

In addition, the implementation of another subsequent separation step for the organic acids still contained in the raffinate phase, such as the PVP adsorption previously presented, needs to be evaluated in order to address the economic impact on the system. It is foreseeable a further MBSP reduction due to the large volume of acids that can be extracted. However, the resin costs can also negatively impact the economy and limit the benefits of the production of chemicals. In the future, the model will also be improved to include the distillation columns needed for the pure compound separation and purification.

3.3.4 - Conclusion

In this work, a potential route for the extraction of co-products from the residual aqueous phase derived from hydrothermal liquefaction of lignocellulosic ethanol lignin-rich stream has been proposed. First a complete characterization of the aqueous phase has been carried out to identify the organic composition and the total organic carbon content. After a HTL reaction, about 2 wt.% of organic matter remains trapped in the aqueous phase mostly in form of methanol, carboxylic acids and light-phenolics. The diluted organic matter corresponds to about 12 wt.% of the initial carbon contained in the lignin feedstock, thus representing a high loss in term of overall process efficiency as well as increasing the cost for downstream traditional wastewater treatment. Moreover, the compounds dissolved in the aqueous medium have a high potential in the chemical industry as commodities or building block for bio-based materials. Therefore, a first step of liquid-liquid extraction has been experimentally tested in order to obtain a selective separation of phenolic species over acids and alcohols. Four different water-immiscible solvents (diethyl ether, ethyl acetate, butyl acetate and methyl isobutyl ketone) have been tested. The best performance in term of phenolic selectivity as well as industrial applicability have been obtained with butyl acetate, ethyl acetate and methyl isobutyl ketone. The main difference among ethyl acetate and the other two solvents is the boiling point and thus the downstream recovery procedure for the small fraction dissolved in the raffinate phase. In addition, since the aqueous raffinate phase post-LLE still contains valuable carbon, the adsorption over polymeric resins (PVP) were addressed targeting lactic and glycolic acid. The experimental campaign showed that among the carboxylic acids, 86 wt.% of lactic acid was recovered, followed by acetic acid (76 wt.%), propionic acid (55 wt.%) and glycolic acid (48 wt.%). Increasing the amount of eluent (ethanol) it may possible to improve the percentage of recovery for some acids (such as glycolic), however the downstream separation would be more expansive due to higher quantity of eluent that needs to be thermally separated. Regarding the methanol adsorption-desorption it was hard to obtain a correct evaluation due to repeatability issues and potential evaporation.

Moreover, the impact on the market of the chemicals identified in the lignin HTL aqueous phase, assessing the producibility based on the LLE and PVP-adsorption data experimentally obtained. The estimation considered the future prediction of ethanol biorefinery lignin availability in EU and US. In many cases the predictions show that the amount of extractable compounds will exceed the global market demand, therefore leading the way for future utilization in new applications and market (such as polymers, bio-pesticides or bio-based material in general). In order

to evaluate the impact of the co-products extraction from the aqueous phase a techno-economic model was realized, modifying a baseline HTL model. The base case was considered with no aqueous phase recycle or downstream valorization. The model was modified considering the aqueous phase recycle into the reactor to improve the conversion efficiency and therefore obtains a higher organic concentration in the aqueous phase. The conceptual scheme is done in a way that the aqueous phase exiting the reactor is not sent to a traditional wastewater stream but recirculated until a certain level of organic matter. Based on literature data, it was supposed a TOC of 90 g/l at the 8th recycle, where a certain amount of aqueous phase was extracted to be processed in a downstream liquid-liquid extraction unit. The economic analysis was carried out for the evaluation of the minimum biocrude selling price (MBSP) comparing the results obtained with the aqueous phase valorization unit and the baseline with traditional wastewater treatment. Obviously, the highest positive impact is due to the recycle that reduce the amount and the cost of the wastewater treatment, while the annual revenue obtained by the introduction of chemicals into the market represent a smaller percentage. However, this plant configuration showed a lower minimum biocrude selling price (from 3.10 \$/gge to 2.44 \$/gge), therefore confirming the economic benefits of a recycle, even in presence of another LLE unit for the separation of phenolic compounds. Future investigation needs to be addressed to introduce another recovery step for the acids and alcohols still dissolved in the raffinate phase exiting the LLE, such as the resin adsorption experimentally tested. Moreover, the model can be improved populating the inlet data with experimental results on the AP recycle as well as the actual fraction extracted in LLE when a lower amount of solvent is used such as AP to solvent ratio of 1:5 or 1:10.

3.4 - Process scale up: HTL pilot plant design and commissioning

3.4.1 - Introduction

In the previous paragraph, a HTL model was generated in order to evaluate the impact of co-product extraction already paving the road to the importance of scale-up consideration on experimental research. In this section a scale-up example will be presented showing how an HTL pilot plant has been designed starting from lab-scale experimental data. The objective is to demonstrate the process at larger scale in a continuous operating mode, identifying bottlenecks and technical issues.

Moreover, most of the experiments published in scientific literature refers to batch experiments performed in autoclaves or small tubular reactors heated by hot sand bath. However, these studies suffer from the inherent limitations caused by the small and batch-wise adopted experimental setup. On the contrary, continuous units would lead to more reliable results, as, for example, the separation of reaction products could be carried out gravimetrically, i.e. without the aid of solvents.⁴⁸¹

The HTL continuous process possesses several advantages compared to batch studies. Among these the stable temperature-pressure conditions achievable at steady state, while in batch the pressure is always autogenous, thus removing the reaction transient that can have a very high impact on the reaction control. Therefore, a continuous configuration permits a complete decoupling of pressure and temperature, thus the effect on the process can be analyzed separately. Also, the residence time can be minimized and better controlled in a continuous system due to the fact that the feedstock can be injected into the reactor when the steady state is reached (usually with pure water), instead of having long heating up and cooling down phases. However, several challenges need to be tackled in a continuous scale-up unit, mostly related to the pumpability of the slurry and blockage of material in the plant channels causing pressure spikes, material failures and dangerous accident. Moreover, the HTL conditions with water near-critical state, requires that all the components that can resist at these conditions safely (e.g. valves or filters), therefore increasing exponentially the plant costs.

A recent study from Castello et al.⁴⁸¹ identified and summarizes a number of continuous units built in research centers and universities around the world, showing configurations and general plant data (e.g. reactor concept and design conditions). Most of the example proposed used a plug-flow tubular reactor (PFR) while in few cases continuous-flow stirred-tank reactor (CSTR) were selected as main solution. Generally, the maximum temperature and pressure adopted in the components design is 350°C and 200-250 bar while only few examples have tested supercritical conditions up to 450°C and 350 bar.

Table 32 summarizes a list of HTL continuous units developed in the last decades around the world and here a brief description of the design concepts will be presented. One of the first HTL pilot plants was developed by Elliot and coworkers at Pacific Northwest National Laboratory (PNNL).⁴⁸² The system, designed originally for catalytic hydrothermal gasification (CHG), consists in a 1 liter continuous-flow stirred tank reactor (CSTR) electrically heated and a 1 liter plug-flow reactor (PFR) heated by circulating oil. This double reactor configuration allows to avoid plugging problems by starting the conversion of the biomass slurry before entering the plug-flow reactor. The feeding system consists in two pressurized piston tanks alternately connected with an Isco 500D dual syringe pump that deliver the flow. In order to remove the solid phase produced in the reactor, a separation vessel, that operate at reaction

temperature and pressure, was placed in-line. In this unit, the solids fall to the bottom of the vessel and are removed while liquid phase passes through the filter, which is connected to a dual liquid pressurized collector vessel that might be alternatively filled. The gas phase is continuously vented through a back-pressure regulator (BPR). With this in-line solid separator, the system is able to produce a solid-free bio-oil that could be easily separated from the water phase and also allows the use of a BPR which is very sensitive to the presence of solids. The HTL experiments were performed at 350°C and 20 MPa. Another pilot plant unit was developed at New Mexico State University, Las Cruces (USA), where slurry with 3-5 wt.% of wastewater-grown microalgae *G. sulphuraria* were converted at 325-350°C at 20 MPa.⁴⁸³ The system consists in a stirred feed tank connected to a cylinder filter to remove the large solid inorganic particle of the slurry before entering the high-pressure pump that deliver a flow rate of 9.12-9.3 l/h. The vertical plug-flow reactor, preceded by a preheater, has a tubing diameter that increases from 0.21 cm to 0.51 cm with a theoretical residence time of 3-9 minutes. HTL products pass through a two parallel custom-made cylinder filters that alternatively removed the solids from the liquid and gas phases. The char is collected in two blowdown pots cooled by water, in which the remained gas is separated and vented. Another plant design from University of Illinois at Urbana Champaign was realized for the processing of swine manure.⁴⁸⁴ This configuration includes a 2 liters CSTR, a valve-less rotary high pressure pump to avoid blockage or backflow, and a stirred separation vessel. Unlike other configurations, in this case there is the possibility of the recirculation of the product gas inside of the reactor vessel. The solid content of the slurry was 20 wt.% and an oil yield of 70%, related to total solids input, was reached with 305°C, 10.3 MPa and 80 minutes residence time without recirculation of product gas. The reactor system was successfully operated continuously for up to 16 hours without any problems, but the piston and sleeve of the pump wore out quickly and caused problems after 20 hours. University of Sydney in Australia designed and commissioned a 2 liters tubular reactor heated in a fluidized sand bed.⁴⁸⁵ Two pumps were placed in series: a low-pressure screw pump and a high-pressure triplex pistons pump that delivers a flow rate of 15 – 90 l/h. Another characteristic of this plant is the presence of two coil-in-shell feed/product heat exchanger for the product heat recovery that are fundamental for the development of a commercial plant. In this unit, the product stream is first cooled with water and then depressurized to reduce the pressure in the shell side of the exchanger.

Regarding the lignin conversion in pilot-scale plants, Chalmers University of Technology (Gothenburg) developed a continuous HTL plant for the conversion of the Kraft lignin from pulp and paper into biofuels and aromatic chemicals.⁴⁸⁶ Here, biomass slurry was prepared by mixing 5.5 wt.% of Kraft lignin in a solution of K₂CO₃ in pure water (0.4-2.2 wt.%) and then mixed with phenol (about 4 wt.%) before entering the feed tank. The slurry was then pumped with high pressure diaphragm pump with a flow rate of 2 kg/h and pre-heated to 80°C. A recirculation of the stream was designed to keep the solids suspended before entering the reactor through a high pressure and temperature pump. The recycle-to-feed ratio was always around 10 and allows to achieve a higher heating rate before the reactions over an heterogeneous catalyst in a fixed bed reactor, equipped with an electrical heater. The heterogeneous catalyst tested was made of zirconia pellets (ZrO₂) with a length and a diameter of 3 mm. After the reactor the products are cooled down with water and depressurized with two pressure control valves disposed in parallel that can be switched in case of congestion by solids. The biocrude yield referred to the total mass products was 5% for all the experiments due to the low lignin concentration in the system feed compared to the sum of the mass fraction of phenol and catalyst (K₂CO₃). The biocrude yield calculated on phenol-free products on a dry lignin basis was 70%, the WSO yield (water soluble organics) 8.7-10.8% and char yield 17.2-20.8%. The biocrude results partially deoxygenated from 26% to 15-17% with an HHV that passes from 27 MJ/kg to 32 MJ/kg. Other experiments were conducted to investigate the effect

of sodium homogeneous catalyst instead of potassium one.⁴⁸⁷ In fact, the sodium catalyst has a lower cost and is possible to use the Kraft pulp mill chemical recovery process. A series of experiments with phenol concentration in the slurry at 4 wt.% were performed and the results expresses that the use of sodium homogeneous catalyst doesn't decrease the biocrude yield. The effect of the phenol as capping agent was investigated with some experiments at constant homogenous catalyst concentration and the results showed that 4 wt.% phenol concentration is the optimum choice in order to reduce the viscosity of the produced biocrude. Another interesting approach is the plant design from Iowa State University that developed a supercritical continuous HTL that can reach a maximum operating temperature of 450°C and pressure of 69 MPa.⁴⁸⁸ The system is equipped with a plunger pump that deliver the system pressure. The slurry passes through a preheater set a 133°C and enter the supercritical plug flow reactor. The residence time ranged from 12 to 30 minutes as the temperature changes despite operating the pump at constant speed.

Table 32. Recent continuous HTL pilot plant (CSTR – Continuous stirred tank reactor; PFR – Plug-flow reactor; BPR – Back-pressure regulator).

| Institution | Reactor type | Reactor Volume [l] | Flow Rate | Pressurization system | Pressure Regulation |
|--|--------------|--------------------|----------------|-------------------------------|---------------------|
| PNNL ⁴⁸⁹ | CSTR + PFR | 1 (CSTR) + 1 (PFR) | 1.5 l/h | Dual Isco Syringe Pump | BPR |
| New Mexico State University ⁴⁸³ | PFR | 1 | 9.12 – 9.3 l/h | No information | BPR |
| University of Illinois ⁴⁸⁴ | CSTR | 2 | | Valve-less Rotary piston pump | BPR |
| University of Sydney ⁴⁸⁵ | PFR | 2 | 15 – 90 l/h | Triplex piston pump | BPR |
| Chalmers University of Technology ⁴⁸⁶ | CSTR | 0.5 | 1 kg/h | Diaphragm pump | BPR |
| Iowa State University ⁴⁸⁸ | PFR | 1.5 | | Plunger pump | Pneumatic Valve |
| Aarhus University ⁴⁹⁰ | PFR | 9.5 | 60 kg/h | Piston pump | Hydraulic pistons |

While an innovative solution was proposed by Aarhus University that developed a continuous hydrothermal liquefaction plant with heat recovery and hydraulic oscillation.⁴⁹⁰ The nominal volumetric flow rate of the plant is 60 l/h with two 0.5 l oscillating pistons that increases the flow turbulence reducing the stratification and clogging issues. The system is also composed of a custom-made heat exchanger with heat claps that realized the heat recovery from the “hot” product coming out of the reactor to the “cold” slurry from the high-pressure pump. The slurry then passes through the trim heater, in which the set temperature of 350°C is achieved, before entering the reactor. Both the trim heater and the reactor are equipped with electrical heaters. The feed is delivered by positive displacement high pressure

pump preceded by a progressive cavity pump which recirculates the slurry in the hopper to ensure homogeneity and providing a steady flow for the second pump. The take-off system consists in two 0.5 liters cylinders working in alternation for pressure release with an operation similar to the hydraulic oscillation systems.

Regarding the HTL technology that reached commercial level, only Steeper Energy ApS in collaboration with Aalborg University developed a process for hydrothermal liquefaction and hydrotreating of lignocellulosic biomass, named Hydrofraction™.⁴⁹¹ The process is divided in two stages: 1st HTL and 2nd hydrotreating and fractionation into drop-in fuels. In 2017 Steeper Energy is partnering with Silva Green Fuel, a Danish-Canadian joint venture to construct a 50.6 millions of euro industrial scale demonstration plant in Tofte, Norway. The demonstration plant will use the woody residue of a former pulp mill and is the first step for a future commercial plant of 2000 barrel-per-day (100.000 tonnes per year).⁴⁹² The fundamental characteristics of this process are: HTL can be performed in sub or supercritical condition at 300-350 bar and 390-420°C respectively, the system includes a residual water recirculation and the use of homogeneous catalysts (K_2CO_3 and NaOH). Reaching and keeping the water at superficial state is challenging due to severe stress conditions on materials and equipment. However, at this state the kinetic of the liquefaction reactions are promoted with a diminished water dielectric constant that allows to better dissolve biomass and biocrude molecules that are hydrophobic at ambient conditions.

In this work a 1-2 l/h continuous pilot HTL was designed to convert lignin-rich streams from ethanol biorefineries. The unit that will be described designed and built within the EU H2020 Heat-to-Fuel project (grant agreement number: 764675), following the data obtained in batch experiments presented in the previous paragraphs. The design temperature and pressure are 350°C and 250 bar, therefore with water in subcritical state and the reactor was designed as a compact PFR indirectly heated. Further investigations are needed to improve and optimize the unit functioning as well as testing different feedstock (such as sewage sludge or municipal solid wastes).

3.4.2 - Plant description

Figure 70 shows a simplified scheme of the continuous unit. Feedstock pretreatment is not included, but generally, it consists in milling and in mixing with a specific amount of water and, if needed, with a certain quantity of homogeneous catalyst (e.g. KOH or NaOH as strong bases). The prepared slurry, contained into a stirred tank, is pumped to the working pressure by a high-pressure pump and reaches the reaction temperature directly in an electrically heated plug flow reactor. A water-cooled heat exchanger decreases the products stream's temperature in order to quench any undesirable reaction that could reduce the biocrude yield. The temperature of the stream should not be lowered to ambient temperature because of biocrude's expected increase in viscosity that would compromise the stream's flowability. On the other hand, the after-cooler temperature should not exceed 100 °C to avoid water evaporation once the depressurization to atmospheric pressure is accomplished. In order to keep the fluid at reaction temperature between the reactor and the cooler, heat tapes were wrapped around tubes, valves and filters; similarly, heat tapes set at 80 °C were adopted between the cooler and the depressurization system. Two alternative pressure letdown systems have been implemented: the first consists in a 1:1 dome-loaded backpressure regulating (BPR) valve, while the second is composed by two oleodynamic pistons. When the former system is used, a prior hot pressurized filtration system is adopted in order to avoid clogging of the small passages of the BPR valve; whereas in the latter case, the solid removal step could be bypassed. The solid removal system is composed by two parallel inline filters (up to 100 µm), whose flow in the respective lines is switched by four ball valves, accordingly to the filter pressure

drops. Liquid and gas products are finally collected at ambient pressure in a tank, where the no condensable gases are vented. The data acquisition and control software were internally developed with NI LabView®.

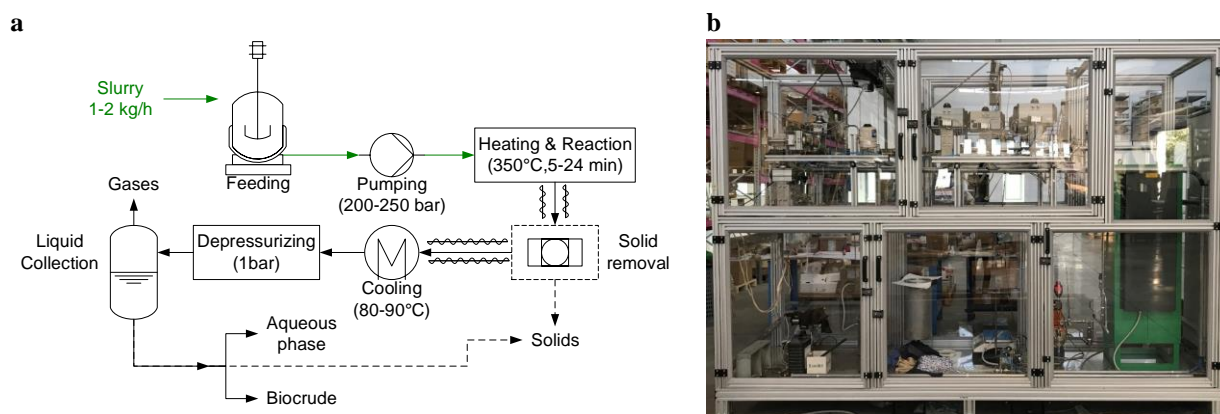


Figure 70. Simplified flow chart (a) and picture of the HTL pilot plant (b)

3.4.3 - Design

Selection of operating parameters

The continuous HTL unit has a lab-scale capacity (1-2 l/h of processed slurry), in order to have the highest flexibility in terms of plant operability. Reaction temperature, residence time and biomass loading were defined after the previous batch experimental campaign, consisting in 350 °C, 5-24 min and 10 wt.% biomass-to-liquid mass ratio. Reaction pressure was autogenous in the batch experiments, here its value was defined by the design process.

Because of the very harsh process conditions, various challenges arose during the selection of the components: the processed fluid is mildly corrosive and therefore the use of stainless steel is needed, the high operation pressure in conjunction with moderately high temperature entails components with special material (especially for gaskets) and high pressure pumps capable of process solid suspensions are needed. As the size of the plant decreases towards small units these problems worsen. In addition, small plants are characterized by very low flow rates and therefore blockage of pipes and valves, due to the settling of the slurry solid particles, can easily occur. For these reasons, the selection of suitable components has been one of the most difficult and time-consuming tasks.

Due to the nature of the HTL process, in the reaction zone of the plant the components are subjected to high pressure and moderately high temperature conditions. The whole system can be considered as a heated pressure vessel and needs to be designed following existing guidelines for pressurized equipment. Moreover, the plant must comply with the current EU regulations for pressurized assemblies, such as the Pressure Equipment Directive (PED) 2014/68/EU.⁴⁹³ Due to the parts volumes and pressure, the PED category indicated was the SEP (sound engineering practice), meaning that there are no specific regulatory requirements for the design or production. Regarding the design of the pilot plant, the worldwide recognized guidelines included in the ASME Boiler and Pressure Vessel Code (BPVC) Section VIII Division 1⁴⁹⁴ were followed. The pressure-temperature ratings of the selected components were verified in accordance with material strength limits listed in 2015 ASME Boiler and Pressure Vessel Code, Section II – Materials.⁴⁹⁵ The valves were verified in accordance to the classes limit proposed in the ASME B16.34.⁴⁹⁶ In accordance with the ASME BPVC Section VIII, the two main parameters to be considered are the maximum allowable working pressure (MAWP) and the maximum allowable working temperature (MAWT). The weakest components were chosen as design point for the maximum operating conditions. The pressure system design followed a sequential

iterative path: first a nominal working pressure had been chosen, then a pressure fluctuation had been considered to obtain the peak pressure (maximum working pressure), in the end the MAWP was calculated as 110% of the maximum working pressure. An appropriate temperature de-rating coefficient has been considered for the tubing (0.82, as given by the manufacturer for AISI 316 stainless steel) and the maximum pressure has been decreased from the nominal 517 bar. Table 33 summarizes the design specifications.

Table 33. HTL continuous unit design specifications

| Parameter | ID | Value | u.m. |
|------------------------------------|--------|-------|------|
| Working Temperature | WT | 350 | °C |
| Max Allowed Working Temperature | MAWT | 370 | °C |
| Design Temperature | DT | 370 | °C |
| Nominal Pressure | NP | 218 | bar |
| Pressure fluctuations after damper | 2%NP | 4.36 | bar |
| Min Working Pressure | WP-min | 214 | bar |
| Max Working Pressure | WP-max | 222 | bar |
| Max Allowable Working Pressure | MAWP | 249 | bar |
| Design Pressure | DP | 249 | bar |
| Operating margin | OM | 14 | bar |

Pump selection

The pressurization step represents one of the critical phases in the whole hydrothermal process because of the handling of suspended solids at high pressure. In general, the use of volumetric pumps is preferred over centrifugal pumps, because the performance of the latter is more sensitive to solid loading. Piston pumps are among the best candidates for HTL application as they are highly reliable in feeding viscous material. Rotary lobe pumps can process slurry with fibrous particles at high temperatures without the need of using check valves, which are the components that are most sensitive to plugging; however, they can't attain high hydraulic head and several pumps must be connected in series in order to reach the required pressure.⁴⁹⁷ In the present plant a single piston pump (Sigma/ 2, Prominent) was installed. The selected pump has a capacity between 1 and 2 l/h and can reach up to 320 bar.

Reactor and cooler design

Firstly, a plug flow reactor with recycle was investigated, as adopted in the CatLiq process.⁴⁹⁸ The advantage of the recycle consists in an increase in the flow velocity inside the reactor and, consequently, limiting the plugging risks. Furthermore, greater diameters can be adopted, making the adoption of heterogeneous catalyst a viable option. However, no commercial pump able to withstand HTL conditions was found. Eventually, a modular plug flow reactor without recycle was designed; the lack of the recycle allows a clear evaluation of the slurry residence time, which can be adjusted by regulating the feed pump's flow rate and/or by modifying the reactor's modules. The final reactor configuration consisted in five sections of ¼" tube coils (total length 30 m) inserted in an electrically heated oven (400x400x1200 mm; maximum power 4.5 kW). The reactor length was determined by considering the heat required to bring the fluid from ambient temperature to the MAWT. Because of the very low flowrate, the flow regime resulted laminar and consequently the Nusselt number was assumed 4.36, under the hypothesis of constant and stable heat flow. The oven was designed considering the total heat dispersion to the ambient. The air inside the oven was

considered at a constant temperature of 400 °C like the case walls' inner surface. The heat released to the ambient was evaluated separately for the oven case's side, top and bottom walls, because different correlations have to be used to determine the Nusselt number; however, the procedure is the same for the three cases: the heat exchanged across metal and insulating walls was equaled to the heat released by external natural convection. Because the insulating panel's outer surface temperature was unknown, an iterative calculation was done. The conductive heat through the metal and insulating walls and the outer natural convective heat are given by:

$$\dot{Q}_{cond} = \frac{A(T_{wall,in} - T_{wall,out})}{R_{metal} + R_{ins}} = \dot{Q}_{conv,out} = h_{conv,out}A(T_{wall,out} - T_{amb}) \quad \text{Eq.3}$$

Where R_{metal} and R_{ins} are, respectively, the thermal conductive resistances of the case side walls and of the insulating panel; they are both defined as their thickness to conductivity ratio. The heat transfer coefficient $h_{conv,out}$ is evaluated with the Nusselt number, that is defined by the traditional correlations⁴⁹⁹ for side, top and bottom walls (Ra and Pr are the Rayleigh and the Prandtl numbers):

$$Nu = \left\{ 0.825 \frac{0.378Ra^{1/6}}{[1 + (0.492/Pr)^{9/16}]^{8/27}} \right\}^2 \quad Nu = 0.15Ra^{1/3} \quad Nu = 0.27Ra^{1/3} \quad \text{Eq.4}$$

The total heat which must be provided by the oven resulted in ~2 kW, however a nominal electric power of 4.5 kW was selected in order to investigate the effect of higher reaction temperatures.

The cooling of the reaction stream was accomplished by adopting a water-cooled tube-in-tube heat exchanger obtained from a combination of bored-through tee fittings and 3/4" outer tube. The inner tube, in which the reacted stream flows, is a 1/4" tube. Similar iterative calculations were adopted for the evaluation of heat exchange area and temperatures, by adopting the ΔT_{ml} method.

Pressure letdown system

The first depressurization system which was selected was a special BPR valve (Equilibar, USA), which is equipped with a flexible diaphragm subjected to the balance of three separate pressures: the fluid inlet and outlet pressure and the pilot set-point pressure, that is applied on its non-wetted side. The valve operates in a 1:1 ratio, so a 300 bar Ar cylinder was used for the regulation of the pilot pressure. Because of the multiple orifices that are present in the membrane, the valve leads to a constant performance with a very wide range of flow rates, but can't be operated with suspended solids and, therefore, a prior filtering must be carried out.

The alternative pressure letdown system consists in the use of two hydraulic pistons designed to work at a nominal pressure of 250 bar. These top pistons are mechanically connected to an external oleodynamic circuit. As the process pistons volume is oversized (0.5 l each), a small fraction of solids in the fluid can be accepted and therefore the filtering step can be avoided.

Safety equipment

Due to the required elevated pressure, it is of the utmost importance to define appropriate safety equipment. The unit is equipped with four redundant “safety systems”, each one consisting in a capacitive pressure transducer (Trafag), a high-pressure relief valve (HPRV) and a rupture disk (RD). These systems are placed before plant’s critical points, where tube plugging is foreseen to be more possible, and have the task of avoiding pressure buildups. A first intervention is done by the logic of the control system, reading the value of pressure acquired by the sensor; if the control system fails to reduce plant pressure the HPRV, which is a spring-loaded valve set to open above the MAWP, will relief the plant pressure. In the worst-case scenario of both control logic and HPRV failing, the RD will burst, ensuring a sudden decrease in the system pressure.

The HPRVs that were selected considering a flow passage area greater than the one required in the following worst-case scenario: all oven thermal power absorbed by the fluid, whose state is completely changed into vapor, leading to a choked flow. The equations for the calculations were obtained by the guidelines provided by the American Institute of Chemical Engineers.⁵⁰⁰ The area in the worst-case scenario was 0.38 mm², therefore, a standard HPRV with ¼” connections was chosen as it provided a flow passage area of 10.2 mm². Given that ¼” tube provides suitable passage area, a bigger ½” size of RDs and discharge line was chosen in order to keep the flow velocity to low levels.

Commissioning of the pressure letdown system

This paragraph reports the results of the testing of the two pressure letdown systems, i.e. the BPR valve and the piston system. Both tests were carried out by using demineralized water. The heaters were not activated during these tests.

Backpressure regulating valve

The aim of the test was to verify the pressure oscillation of the BPR and to identify leakages in the plant. The system pressure was set by adjusting the BPR pilot pressure to 50 and then 100 bar. The piston pump flowrate was set to 1.9 l/h. Average pressure was 102.6 bar, while oscillations are kept within +3 and -1.2 bar. In order to identify possible leakages in the fittings and evaluate the sealing action of the ball valves, both filters lines were isolated, and the flow in the plant was maintained through a bypass line. In this latter test pressure was set to \approx 50 bar. When filter lines were isolated by closing the ball valves, the line pressures (P4 and P5) started to gradually decrease due to leakages in the filters fittings, as reported in Figure 71 and consequently lines maintenance were carried out by tightening the relative fittings.

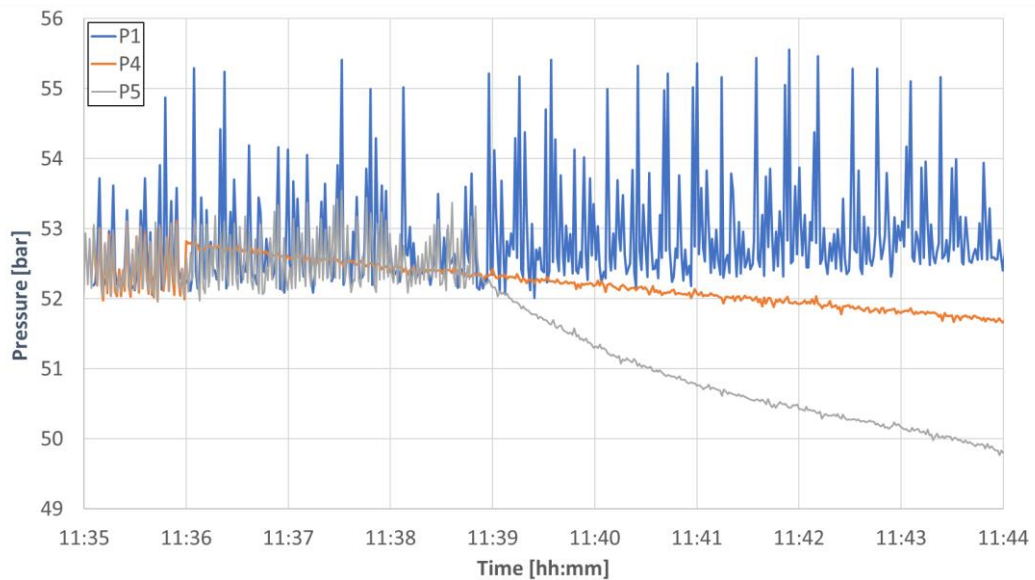


Figure 71. Pressure values showing leakage in the filter's lines during the BRR testing

Piston system

The aim of the test was to verify the functioning of the two pistons: while one piston is being filled, the other is discharging into the outlet tank; as the pistons have only one connection to the process, four pneumatically actuated ball valves were installed for correct operation (two at the inlet and two at the outlet of each piston). In the test the flow was delivered by the pump through the bypass line and the pressure was set to 200 bar. Set pressure was easily reached and maintained until the first piston was filled; when the switch to the other piston occurred, the plant was completely depressurized, as for few seconds the inlet and the outlet valves of the pressure let-down system were both open, connecting the plant to ambient pressure. A new sequence for the opening and closing of the valves was implemented in the control software. However, the problem was only partially solved as a decrease of nearly 70 bar was detected during the switch (Figure 72a). This decrease was due to the fluid expansion in the empty piston after its discharge. This pressure reduction should be absolutely avoided as it can lead to water evaporation if the system when pressure goes below saturation level. To eventually solve the problem, the closure of the outlet valve of the discharging piston was anticipated. In this way, the complete depressurization of the piston volume was avoided, and the pressure decrease after the switch eliminated. However, as reported in Figure 72b, a sudden increase in pressure is detected after each piston switch. This behavior was due to the control of the oleodynamic circuit and was solved by implementing a PID algorithm for the opening of the oil proportional valve (Figure 72c). In this latter configuration, the pressure variations were kept below ± 2 bar (during piston filling) and + 6 bar after the switch.

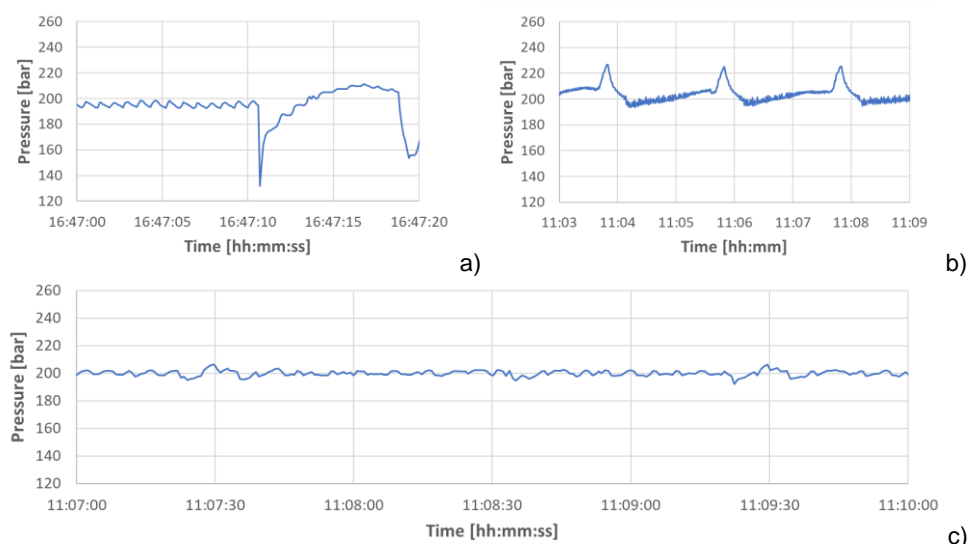


Figure 72. Pressure decrease during piston switch (a); pressure increase after anticipated closure of inlet valve (b) (the switch is occurring every two minutes); pressure fluctuation after PID implementation (c).

3.4.4 - Commissioning with lignin-rich stream as feedstock

After the “cold” commissioning where all the operational parameters as well as the safety and stability of the system have been tested, some preliminary tests with biomass have been carried out. Here a description of a test with lignin-rich stream as feedstock will be presented showing where the system needs further optimization.

Material and methods

The biomass-water slurry was prepared by mixing 5 liters of water (with 0.5 mol/l Na₂CO₃) with 250 g of lignin-rich stream in the stirred tank in order to obtain a biomass-to-water ratio of 5% w/w d.b. The lignin-rich stream (LRS) was treated as described previously in the batch tests experiments (paragraph 3.1.2 - and 3.2.2 -). The reaction conditions are shown in Table 34. It was chosen to use the piston system for back pressure regulation and product discharge. The plant was operated for the start-up period with DI water from a secondary tank. Then, once the LRS-slurry was pumped into the reactor, the test was carried out continuously for almost 2 hours.

Table 34. Reaction conditions for the test with lignin-rich stream.

| Reaction Conditions | Value | Unit |
|--|-------|---------|
| Biomass-to-water ratio | 5 | Wt.% db |
| Reaction Pressure | 200 | bar |
| Reaction Temperature | 350 | °C |
| Na ₂ CO ₃ solution | 0.5 | mol/l |

The lignin used for the test was the same presented in paragraph 3.1.2 - and 3.2.2 -. Na₂CO₃ was added in order to obtain a pumpable slurry. No hot filtration was used and solids, biocrude and aqueous phase were recovered together in collector tank placed after the pressure letdown system.

Results and identification of main issues

Table 35 shows the average, maximum and minimum value of the temperatures during the feeding time. The maximum pressure measured during the test was of 14% compared with the average value.

Table 35. Average, maximum and minimum temperature measured along the system during the whole test.

| Temperatures | T2 [°C] | T3 [°C] | T4 [°C] | T5 [°C] |
|---------------|---------|---------|---------|---------|
| Average value | 318 | 351 | 345 | 69 |
| Maximum value | 341 | 363 | 372 | 100 |
| Minimum value | 291 | 325 | 337 | 50 |

A sample of 1 liter with a pH of 9.1 was recovered at the discharge of the pressure letdown system. In order to facilitate the product recovery method, the base was neutralized by mixing it with 200 ml of 1:1 solution of hydrochloric acid (HCl) and a pH of 3.8 was obtained.

Table 36 summarizes the temperature of different sections during the collection of the sample.

Table 36. Average, maximum and minimum temperature measured along the system during the sample collection.

| Temperatures | T2 [°C] | T3 [°C] | T4 [°C] | T5 [°C] |
|---------------|---------|---------|---------|---------|
| Average value | 321 | 352 | 345 | 67 |
| Maximum value | 342 | 360 | 361 | 100 |
| Minimum value | 305 | 325 | 336 | 50 |

As previously done on batch lab-scale tests, a light and a heavy fraction of the biocrude, named respectively biocrude 1 (BC1) and biocrude 2 (BC2), were recovered with a two-steps solvent extraction method, as showed in Figure 73. The collection procedure was described in previous micro-scale experiments as Procedure 2 (pag. 95). The solvent used for the recovery of the light fraction was diethyl ether (DEE) while the heavy fraction was extracted in acetone (DMK). The products were vacuum filtered over a Whatman glass microfiber filter (1 μ m) in order to separate the aqueous phase from the solid particles. The residual solids and biocrude trapped on the filter were rinsed with DEE for BC1 recovery after vacuum evaporation of DEE. The remaining were further rinsed with DMK in order to recovery BC2. The solid residue (SR) was oven-dried at 105°C overnight as depicted in Figure 68.

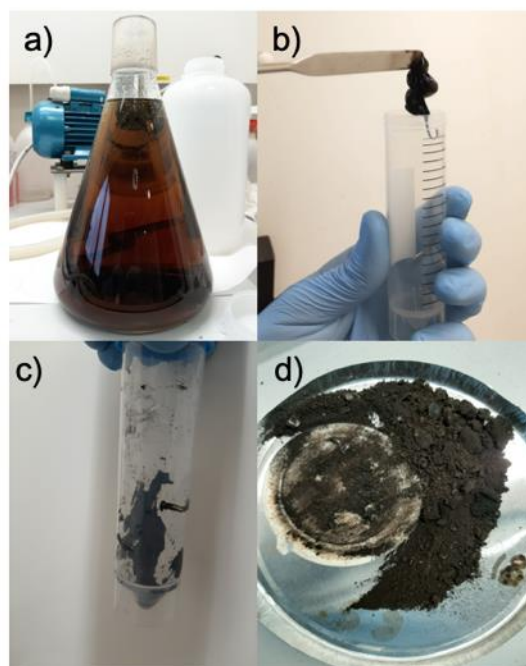
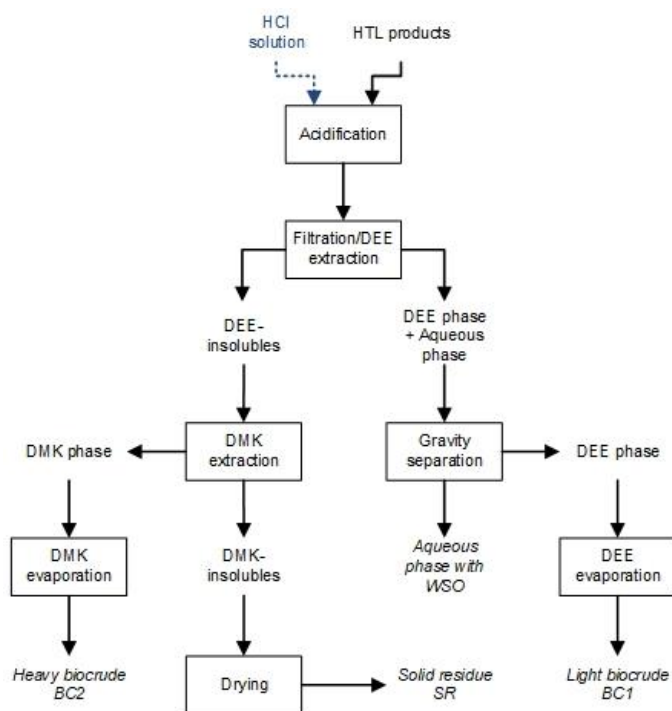


Figure 73. Block diagram of the extraction procedure used for products recovery (left) and pictures of the recovered products (right).

The slurry volumetric flow rate, average velocity and the residence time in the oven during sampling time are summarized in Table 37. The heating rate was approximated using the temperature difference between inlet and outlet of the reactor divided by the residence time. The slurry was kept at reaction temperature through heat tapes placed on the external surface of the connection tubes. The density of the water (at 350°C and 200 bar) is 606.6 kg/m³ and the velocity of the flow was estimated knowing the mass flow rate, the density and the pipe section. In addition, these data were used to estimate the residence time at the reaction conditions.

Table 37. Flow rate, medium velocity and residence time during the feeding.

| Parameter | Value |
|-------------------------------------|-------|
| Volumetric flow rate [l/h] | 1.9 |
| Medium velocity [m/min] | 3.7 |
| Residence time in the oven [min] | 8.2 |
| Residence time in the reactor [min] | 0.4 |
| HR [°C/min] | 42 |

The HTL Biocrudes (BC1 and BC2) and solids yields were calculated measuring the masses obtained after the extraction procedure and knowing the initial dry mass of LRS injected into the reactor, the results are summarized in Table 38. The unrecovered plus water-soluble organics and gases yield was calculated by difference.

Table 38. HTL continuous product yields.

| Products | Yield [wt.%] |
|---------------------|--------------|
| BC1 | 8.9 |
| BC2 | 2.7 |
| Solids | 3.4 |
| Unrecovered+WSO+Gas | 85 |

This preliminary test gave information about the stability of the system over time at severe conditions of high temperature and high pressure. Clearly, observing yields obtained, the optimization of the downstream separation and product recovery step needs to be tackled. Especially, we believe that the 85 wt.% (Unrecovered+WSO+Gas) is mainly composed by unrecovered product that remain trapped in the discharge pipes as well as in the dead zones of the pistons. Mechanical modifications need to be adopted in order to maximize the product recovery and minimize clogging risks.

3.4.5 - Conclusion

A continuous hydrothermal liquefaction unit of 1-2 l/h capacity was designed and built. The whole process design was carried out after a batch experimental campaign, screening several operative points by varying temperature, time and solid load. The pressure equipment selection and design followed ASME guidelines as well as the implementation of safety redundant systems. Pressure tests were carried out on the system observing the behavior of the two installed pressure letdown systems and troubleshooting. No problems were encountered with the BPR valve, whose performance was good, limiting pressure oscillation to + 2.9% and -1.2% with respect to the average pressure (102.6 bar). The matching between the high-pressure pump and the piston system was more challenging as the correct sequence of opening and closing of four ball valves was involved in the operation. Pressure spikes due to the oleodynamic control circuit were eliminated thanks to the implementation of a PID algorithm. Eventually, pressure variations were under $\pm 2\%$ during the filling of the piston and below + 3% after the piston switch (set pressure 200 bar).

A preliminary test with lignin-rich stream as feedstock have been carried out in order to understand potential issues and plan future modifications for the system optimization. The system was able to run for about 2 hours with a 5 wt.% of solid load in form of water slurry. The temperature measured along the reactor and the outlet zones were stable and did not present issues during the operation. The main issue encountered was the downstream product recovery. A large fraction of unrecovered materials remained trapped in the discharge units, even when the temperature was kept at 80-90 °C to improve the flowability. Thus, future mechanical modifications need to be implemented to maximize the product recovery with this type of material.

3.5 - Conclusions

Hydrothermal liquefaction of wet biomass or waste streams has been demonstrated as a potential technology to recover a biocrude that after further upgrading (e.g. hydrotreating) can be introduced in the fuels market. The process is suitable for high water content organic streams due to the fact that water behaves as a solvent when at near-critical state (374°C and 220 bar). In this work, several aspects on the conversion of lignin-rich streams derived from lignocellulosic ethanol biorefinery have been investigated. First an experimental campaign, based on lab-scale micro reactor, has been carried out to address the impact of the operating parameter on the overall conversion in order to optimize the process. It was statistically demonstrated that the most significant parameter on the maximization of the biocrude yield is the reaction temperature. Increasing the reaction temperature, the water is closer to its critical state and thus its dielectric constant drops drastically allowing solubility of non-polar species formed during the thermal cracking. The maximum total biocrude yield (65.7wt.%) was achieved at 300 °C, 10 min, 20% while the maximum yield of the light fraction (41.7wt.%) was achieved at 370 °C, 15 min, 10%. Therefore an higher temperature improves the presence of lighter compounds in the biocrude enhancing its properties for downstream upgrading. These results suggest that the conversion process can be optimized in different ways, depending on the characteristics or on the amount of the biocrude to be obtained. Indeed, the impact of the reaction conditions have been investigated on the regards of the monomers yield formation in both biocrude and aqueous phase evaluating the depolymerization efficacy. Even though temperature was found to be the most influent parameter increasing the LRS depolymerization efficacy at the experimental conditions investigated in this work, the effect of time and B/W was evaluated in order to observe differences in the detected monomeric products yields into BC1 and AP. Regarding residence time, 5 minutes were sufficient for lignin and sugars cleavage in subcritical water, while the increase to 10 minutes eventually promoted substitution and repolymerization reactions, leading to a reduction in methoxyphenols contents while keeping constant the catechols content. Temperature was demonstrated to play a fundamental role in the hydrothermal reaction mechanisms, and an increment from 300 to 370 °C caused an enhanced phenolic monomer content in BC1 and AP, together with a reduction of AP acids content. However, increasing the temperature closer to water critical point (374 °C, 22 MPa) will also increase the CAPEX of a scaled plant, due to higher equipment costs related to materials resistance at these severe operation conditions, however at sufficiently high pH of the liquid medium the corrosion effects on metals will be reduced. For this reason, the use of an alkaline slurry solution is a preferable route at higher temperature ⁴¹⁷ and the impact of KOH on the process was evaluated. the use of KOH as alkaline homogeneous catalyst resulted in an improved overall LRS depolymerization, as observed by the enhanced overall BC1 mass yield and WSO content as well as a reduction in the average molecular weight of the total BC. On the other hand, the presence of KOH did not enhance the formation of phenolic monomers, but the higher yield of methanol in the aqueous solution confirmed the positive effect on lignin structure cleavage. An alternative solution using supercritical CO₂ (sCO₂) in the reaction was tested. sCO₂ behaves as acid catalyst and it showed interesting phenolics-selective properties and comparing acid (sCO₂) to base catalyzed depolymerization (with KOH), similar phenolic yields were generated at low temperature (300 °C). The phenolics fraction produced with sCO₂ was also comparable to the one obtained at 350 °C with and without KOH. Therefore, although the introduction of sCO₂ as acid catalyst into the process had not significant effects on the overall BC yields, it showed an enhanced selectivity on the formation of phenol and methoxyphenols monomers in the products at lower temperature compared to the uncatalyzed control test.

Particular attention has been taken on the regards of the residual aqueous phase valorization. After a comprehensive characterization, identifying the most present phenolic, acidic and alcohol species, a proposed pathway for the extraction of compounds from the aqueous phase has been proposed and experimentally tested. First a liquid-liquid extraction with four different organic solvents have been investigated to select the most performant solvent in term of selectivity towards phenolic compounds. Diethyl ether showed the worst performance in term of partition coefficient, mass fraction extracted and selectivity, while butyl acetate and ethyl acetate showed high extraction and selectivity. High selectivity is desired to reduce the complexity of the overall separation unit, bringing together similar species that can be treated in a singular unit. In fact, the phenolics extracted in the process together with the solvent can be further distilled (recovering the solvent) and crystallized to obtain almost pure compounds for the chemical market. While, since most of the acids and methanol remained still trapped in the aqueous solution. Therefore, adsorption over a polymeric resin (PVP) was tested as a potential approach for the recovery of compounds (especially some acids). The results showed a very high recovery of lactic acid, while glycolic was easily trapped on the PVP surface but the elution in ethanol was not at high efficiency, requiring higher amount of ethanol to maximize the recovery. Other acids extracted were acetic and propionic while methanol was partially trapped on the PVP resin, but the elution results were not reproducible, and this needs further investigation. In order to evaluate the potential application at larger scale of the proposed extraction pathway, a prediction of compounds production has been estimated based on the future biorefinery lignin availability in EU and US. The data obtained showed that in most of the cases the production will exceed the global demand, except for commodity chemicals such as phenol or acetic acid. Therefore, future studies on the applications of these compounds as building blocks for bio-based materials or chemicals in the agriculture pest management (e.g. pesticides from catechol or methoxyphenols) are needed in order to pave the way for a broader switch toward the green economy. In addition, a HTL model has been realized for a techno-economic analysis (TEA), estimating the minimum biocrude selling price (MBSP) of a 55 tonnes per hour biomass-water slurry plant. The TEA was investigated to address the impact of a liquid-liquid extraction unit together with the aqueous phase recycle in the reactor. Even though the LLE column for the compound extraction increases both CAPEX and OPEX, when employed together with aqueous phase recycling the MBSP was reduced from 3.80 \$/gge to 3.04 \$/gge. The most affecting parameter to the MBSP drop was the reduction in the wastewater treatment cost associated with the recycling of the aqueous phase in the HTL reactor, while the annual revenue obtained by selling phenolic monomers into the market has a lower impact. However, the introduction of a LLE units affected the MBSP of only 0.18 \$/gge, resulting in a limited impact on the economy and positive potential benefits in term of production of bio-based chemicals for the growing circular and green economy.

Finally, a real scale-up of the technology has been studied through the design and commissioning of a continuous pilot plant. The micro-scale results were used as baseline for the design of the plant, setting 350°C as maximum temperature and 220 bar as maximum pressure, with a capacity of 1-2 l/h. The pressure equipment selection and design followed ASME guidelines as well as the implementation of safety redundant systems. The main challenge of the HTL technology is the high pressure and high temperature of the reaction zone, therefore particular attention has been taken on the component selections in order to resist at these severe conditions. Moreover, the slurry needs to remain at high pressure during the passage into the reactor in a continuous way. This is the reason why two depressurizing and product discharge solutions were assembled and tested for finding the best performances and avoiding dangerous pressure spikes. Once the preliminary tests were concluded, a first test with LRS slurry was carried out to observe the plant stability when solids is pumped and converted into the system. The promising results paved the way of future

optimizations, especially on the products recovery and biochar filtering at larger scale. In addition, the pilot scale plant will serve as driver to demonstrate the thermochemical conversion applied on other kind of wet feedstocks (e.g. municipal solid wastes or sewage sludge), obtaining information for technical solutions that can be projected to full industrial scales.

4 - Conclusions and future developments

In this work, several aspects on the improvement of thermochemical biorefineries for the conversion of lignocellulosic biomass into precursors for advanced biofuels and bio-derived chemicals have been addressed.

Among potential thermochemical approaches for the deconstruction and conversion of lignocellulosic feedstock into organic liquids, fast pyrolysis (FP or CFP) and hydrothermal liquefaction (HTL) have been widely studied as processes for the valorization of solid dried biomass and wet organic-rich streams respectively. In order to maximize the profits and optimize the conversion pathways several challenges still need to be tackled. Regarding fast pyrolysis biorefineries, catalytic fast pyrolysis (e.g. *ex-situ*) has been demonstrated as one of the best technologies to obtain high yield of bio-oil with reduced level of oxygen and acids that can be further converted into green fuels. In this work a potential upstream treatment through partial upgrading of pyrolysis vapors in a fixed bed catalytic filter has been investigated, demonstrating that the application of heteropolyacids over titania supports in presence of hydrogen led to an increment in the aromatic and alkylated phenols content, reducing the oxygen content and the presence of corrosive acids in the stream. In parallel, char and alkali metals filtration were obtained. This approach can also be used as vapors pretreatment in *ex-situ* CFP to improve the vapors quality for further upgrading. In addition, the fractional condensation of partially upgraded vapors was studied to concentrate fractions of interests with no water content and reduced amount of acids and carbonyls, known to be responsible of bio-oil aging and instability. The organic vapors fractionation can also be implemented for co-products extraction in biorefinery concepts as a first step for roughly concentrate valuable compounds. In this perspective, a study of agrochemical applications of bio-oil fractions was carried out to extract information on the applicability of lignin-derived phenolic mixtures as active ingredients in new insecticides formulations to substitute traditional insecticides such as synthetic pyrethroids or organophosphates. Among many organic molecules contained in bio-oil, alkylphenols (with 3 to 5 carbons in the substituted group) generated during catalytic fast pyrolysis and separated through distillation showed the highest activity towards specific insects. Therefore, a TEA was performed modifying an existing CFP biorefinery model to include a separation stream (comprising fractional condensation and distillation of liquid fractions). The TEA results showed that an increment in the product purity at a reduced yield would lead to an increment in the minimum product selling price (MPSP), while higher production rate with lower purity on the contrary would minimize the production costs. In parallel, a LCA study was carried out to evaluate the energy demand and the GHG emissions of the whole CFP supply chain. The results were compared to traditional insecticides supply chains (pyrethroids and organophosphates). The GHG emissions level was found to be much reduced with mixtures produced in CFP biorefineries compared to traditional processes (mostly fossil-based). A process and model optimization need to be investigated in order to define the optimal operative conditions in term of co-product stream flowrate. In addition, in the perspective of creating a bio-derived insecticidal formulation, a detailed identification of active compounds needs to be addressed through model-compound studies. A fundamental step toward the commercialization is the correct identification of active molecules, especially to be compliant with regulatory frameworks. New pesticides formulations in general need to follow strict rules before entering the market, identifying the active compounds as well as the toxicity to human and non-target animal species, and the impact to the environment. The whole regulation process in both US and EU takes several years and consequently, indirect expenses that will reflect on the final product selling price. However, renewable-based, thermochemically-derived pesticides have the potential to drive a

quicker switch towards a circular and green economy, where plants derived substances are used for agricultural scopes. Even though many decades of studies have drastically improved the CFP technology in term of conversion efficiency and liquid products quality as well as the production of advanced biofuels from CFP oil, commercial applications are still limited at few examples around the world. Therefore, efforts are needed to push the technology spreading and increase the growth and commercialization of CFP plants, together with an enhanced level of renewable fuels in the transportation sector. An interesting approach is represented by the integration of renewable biorefineries into existing petroleum infrastructures through co-processing of liquid bio-intermediates from thermochemical conversion processes and fossil feeds. In this perspective, some studies already showed the possibility of co-processing FP/CFP bio-oil into Fluid catalytic cracker (FCC) with vacuum gas oil (VGO) up to 20 wt.% of renewable fraction in the stream. The main advantage is that, with limited infrastructures modification it is possible to generate fuels with percentages of renewable carbon, thus reducing the environmental impact of the GHG emissions generated during the combustion. At the same time this will lead to higher availability of organic mixtures for co-products manufacturing. The main technological limitation, that inhibits the process optimization and the regulations, is the tracking of the biogenic carbon from the renewable feedstock to the final products. Traditional techniques, such as radiocarbon through AMS analysis, are expensive, time-consuming and carried out in few facilities around the world. Most of all, these methods cannot be implemented in-lines at refineries sites. Therefore, new analytical methods are needed in order to drive the process optimization as well as to be compliant with regulation policies and regional incentives. In this work two different approaches have been proposed as valid candidate to be applied directly online at refinery sites after improvements in precision and flexibility. These methods are the ^{14}C optical analysis or the stable isotopes $^{13}\text{C}/^{12}\text{C}$ analysis. The first has a large potential but enhanced accuracy and reliability are needed while the second has already been demonstrated as a suitable approach, but problems of feedstock flexibility have been observed when renewable source from specific kind of biomass are co-processed (i.e. C4 biomasses).

The other biorefinery presented in this thesis is the HTL of lignin-rich streams (LRS) derived as by-product of lignocellulosic ethanol production. HTL is a suitable process for wet-streams due to the fact that cracking reactions are carried out with water at its near-critical or critical state. Compared to CFP, the HTL presents several technical challenges that still needs to be completely addressed in order to improve the plants economy and conversion efficiency. Few examples of HTL pilot plants successfully demonstrated the conversion of organic-rich wet streams (e.g. algae or sewage sludge) but not many studies investigated the valorization of lignin-rich streams from ethanol biorefineries through hydrothermal depolymerization, especially at larger scale. Lignin constitutes about 15-35 wt.% of the total biomass matter and during the ethanol production is separated from sugars (cellulose and hemicellulose) before the enzymatic hydrolysis and fermentation process. More than 300000 kilotonnes per annum of lignin is expected to be available in US and EU by 2030 due to a foreseeable growth in the ethanol production from lignocellulosic sources. Therefore, there is large interest in converting and valorize this material for the production of biofuels and chemicals precursors. For this reason, in this study the conversion of lignin-rich streams derived from ethanol biorefineries have been addressed through a first batch experimental campaign followed by co-products extraction studies and scale-up. The batch tests, carried out in micro-reactors, were used to investigate the effect of process conditions (temperature, residence time and biomass-to-water ratio) on the yield of the liquid biocrude as well as to investigate the product quality through molecular weight analysis and monomers generation. In addition, since the residual aqueous phase traps part of the light organic fraction generated during the depolymerization, a pathway

for the extraction of co-products precursors have been addressed. The backbone idea is to extract organic monomers through a first selective liquid-liquid extraction (LLE) that separate the phenolic content from the acids and alcohols contained in the aqueous phase in order to concentrate a mixture of valuable compounds that can be recovered after further distillation and purification step. Four different water-immiscible solvents (diethyl ether, ethyl acetate, butyl acetate and methyl isobutyl ketone) have been tested highlighting ethyl acetate and butyl acetate as the most effective and industrial scalable solvents. The raffinate aqueous phase post-LLE still contained acids and alcohols and the adsorption over polymeric resins (PVP) have been investigated as potential solution especially for valuable acids recovery (lactic acid and glycolic acid). The experimental results showed that 86 wt.% of lactic acid was recovered, followed by acetic acid (76 wt.%), propionic acid (55 wt.%) and glycolic acid (48 wt.%). The overall yield data were used to estimate the potential production considering the lining available, especially with future prediction. The data showed that high volumes of bio-based chemicals precursors can be potentially extracted and inserted into the market, in some cases saturating or exceeding the global demand. Therefore, the future large availability of these substances (both phenolics and acids) would open the way for research and development of new bio-based products (such as polymers or agrochemicals) in perspective of a stronger green and circular economy, thus reducing the dependence from fossil sources. In addition, a HTL scale-up model have been realized to evaluate the economic impact of the aqueous phase valorization and co-product extraction. The minimum biocrude selling price (MBSP) have been calculated in absence of residual water valorization, considering traditional wastewater treatment, and compared to the once calculated in presence of aqueous phase recirculation and co-products extraction, including only a LLE unit. The TEA data showed that large economic benefits are achievable, mostly due to reduced costs of wastewater treatment, as well as a low contribution of a LLE installation for co-products extraction. The analysis needs further investigation to include the complete pathway for co-products extraction (e.g. distillation units and resin adsorption) in order to better evaluate the economic feasibility of this application. Moreover, the conversion of LRS have been widely studied in lab-scale tests but not deeply investigated at larger scale, a continuous pilot-scale HTL unit have been designed and commissioned to convert the material at 350°C and 250 bar with a capacity of 1-2 l/h. The first experimental tests were carried out with only water tracking the functioning with two different pressure letdown systems (a back-pressure regulator and a pistons unit). The results showed a good reliability of the back-pressure regulator that can be used when the solid load in the slurry and the biocrude viscosity are limited, reducing risks of clogging. While the piston systems is a preferred solution due to larger passage sections but the matching with the high-pressure pump is more challenging, enhancing risks of positive and negative pressure spikes. However, pressure spikes were eliminated implementing a PID algorithm on the control. A preliminary test with lignin-rich stream was performed underlining potential issues and planning future modifications for the system optimization. The conversion at 350°C and at steady state proceeded for two hours without issues, however the main issues was found in the products recover due to a large portion of biocrude trapped in the cold zones. Future mechanical modifications are needed to optimize the product recovery as well as the introduction of a hot filtration unit to separate the solids generated during the process.

To sum up, several aspects of two thermochemical biorefineries have been addressed in order to improve the overall process efficiencies, investigating the potential application of co-products extraction as well as define pathways for scale-up and commercialization. Fast pyrolysis process applied on lignocellulosic feedstocks has been extensively studied over the years but challenges of biorefinery commercialization are still under evaluation. However, co-

processing of pyrolysis oils in petroleum refineries seems to be the most suitable way to enhance the process commercialization in the mid-term and to quickly introduce renewable carbon in the fuel sector using existing infrastructures. Issues on the renewable carbon evaluation and analysis in final products have been highlighted but it is foreseeable a development of advanced techniques in the field, as proposed in this work. Hydrothermal liquefaction of lignin is still a step behind, especially on scale-up applications, but it has been demonstrated as a viable route for the valorization of lignin co-products derived from lignocellulosic ethanol biorefineries, expanding the products portfolio, from ethanol to aromatic mixtures that can be further upgraded into advanced fuels and chemicals. In addition, co-products and co-products precursors can be extracted from both processes, improving the biorefinery economics as well as introducing bio-based carbon into the chemicals market toward a more sustainable green economy, potentially circular (e.g. agrochemicals).

Appendix A – Analytical methods for catalytic hot gas filtration studies

Appendix A1 – Molecular Beam Mass Spectrometer

The molecular beam mass spectrometer (MBMS) slipstream indicated in Figure 9 and Figure 10 (Chapter 2 -) employed an Extrel Core Mass Spectrometer system for real-time analysis of hot product vapors. The MBMS slipstream product sample undergoes adiabatic expansion through a 250 μm orifice into a vacuum chamber held at ~ 50 mtorr, which rapidly cools the product stream, effectively freezing the chemistry and hindering further reactions. The resulting cooled product gas is then skimmed into a molecular beam to be positively ionized prior to being mass-resolved and analyzed via a quadrupole mass spectrometer. As MBMS separates and identifies compounds based on mass (m/z) and because the system has a resolution of 0.1 amu, full speciation was not achieved, leaving isomers unresolved. Speciation of pyrolysis and CFP products has been conducted on similar systems in previous studies with results from these studies used in this work.⁵⁰¹⁻⁵⁰³ All MBMS data was acquired using the Merlin Automation Data System (version 1.20.1827.0) supplied by Extrel where data was collected over an m/z range of 30-510 in centroid mode with no averaging and a scan time of one second. Ion formation within the mass spectrometer was achieved via electron impact ionization employing a potential of - 20.0 eV. The MBMS system was calibrated using perfluorotributylamine (PFTBA) standard in profile mode to ensure peak widths of respective m/z values were within ± 0.5 amu of the target value. An argon tracer introduced through the pilot-scale pyrolyzer was used throughout all experiments to correct for MBMS signal drift. For data analysis, the MBMS spectral intensity was normalized against argon prior to being background subtracted.

Appendix A2 – Other analytical methods

Gas bag analysis was conducted via GC-FID equipped with a Polyarc® universal carbon detector (Activated Research Company). The Polyarc® employs a catalytic methanation reaction to convert all GC-separated species into methane prior to FID analysis (i.e., normalizes response S3 factors to 1) to provide for a uniform carbon quantification (i.e., carbon number). An HP 6890 GC was employed using a 250 μm sample loop. The column used for separation of compounds was a 60 m x 0.32 mm Agilent J&W GS-GasPro (Catalog #: 113-4362). The GC oven temperature was held at 32°C for 1 min, ramped to 175°C at 25°C/min, held for 2 min and then ramped to 250°C at 25°C/min and held for 6 min. The inlet temperature was 250°C, FID temperature 315°C, and Polyarc® temperature of 293°C. The system employed a helium carrier gas flowrate of 3.3 mL/min without a split ratio. Three calibration standards containing varying concentrations of 17 compounds were used to quantify all compounds detected in the samples. These standards included carbon monoxide, carbon dioxide, methane, acetylene, ethylene, ethane, propylene, propane, 1,3-butadiene, 1-butene, isobutylene, cis-2-butene, trans-2-butene, nbutane, isobutane, n-pentane, and isopentane. Prior to GC-MS analysis, organic samples were diluted 20:1 in acetone and aqueous samples were diluted 1:1 in methanol. A volume of 1 μL was injected onto an Agilent G1530A GC - HP 5973 MS. Gas samples were injected onto the same instrument; 1 mL injections. The column used for separation of compounds was a 30 m x 0.25 mm x 0.25 μm Restek Rtx-50 (50%-phenyl-methylpolysiloxane phase). The GC oven temperature was held at 40°C for 2 min, ramped to

140°C at 7°C/min, then to 290°C at 12°C/min and held for 5 min. The inlet temperature was 250°C, transfer line temperature 300°C, and an employed helium carrier gas flowrate of 1 mL/min with a split ratio of 10:1. A calibration standard containing 20 compounds was used to quantify all compounds detected in the samples. For determining water content of the organic and aqueous samples, Karl Fischer (KF) titration was conducted using aliquots of ~0.1 g, with each aliquot weighed before going into the titration cell. Titration was done with a 701KF Titrimo unit, using CombiTitrant 5 (Merck) titrant. Calibration of titrant was done before S4 any samples were run using 1% water in 1-methoxy-2-propanol standard (Merck). Samples are added directly to anhydrous methanol in the titration cell for KF moisture determination. Alkali metals analysis of organic samples was conducted via ICP-AES. Approximately 0.5 g of each oil was weighed out in triplicate and placed in a Teflon pressure vessel. Ten mL of 72 wt.% nitric acid (reagent grade) was added to each vessel and then sealed. Pressure and temperature were monitored continuously in the “master” vessel. The vessels were heated in a microwave oven from room temperature to 200°C over 15 min and then held at 200°C for 10 min. After cooling to room temperature, the vessels were removed and vented. The samples were diluted to a final volume of 50 mL and transferred to sample containers for ICP-AES analysis. The ICP-AES is equipped with an argon purged optical path to allow analysis of elemental emission lines in the range of 130 nm to 773 nm. All lines were acquired at 1425 W plasma power. Nebulizer flowrate was 2 mL/min sample, 0.8 L/min argon, auxiliary flowrate of 1.2 L/min argon and coolant flowrate of 12 L/min argon. Calibration of the ICP-AES was done by dilution of commercial 1000 ppm standards diluted with nitric acid solution (1 vol conc. nitric acid + 4 vol deionized water). Prior to ICP-AES, BET and TPD analysis, both pre- and post-reaction catalyst materials were calcined in air. The calcination protocol entailed heating in air using a muffle furnace to 550°C at 3°C/min, holding for 4 h, and then passively cooling to ambient temperature. Molybdenum and phosphorus content of the fresh and reacted Mo-HPA/TiO₂ catalyst materials were analyzed via ICP-AES (Huffman Hazen Laboratories, Golden, CO). Aliquots of nominal 0.1 and 0.15 g were weighed into Teflon test tubes and digested with a combination of nitric, perchloric, and hydrofluoric acids. The digested samples were then diluted to a final mass of 200 g and then analyzed by ICP-AES. The instrument was calibrated prior to analysis with S5 commercial standard solutions. Calibration checks were run before the samples and after at least every ten samples to ensure there was no instrumental drift over the course of the analysis. The catalyst surface area was measured via nitrogen physisorption at -196°C using a Quadrasorb SI Instrument (Quantachrome Instruments). Prior to the measurement, samples were degassed at 350°C under vacuum overnight. The surface area was calculated using multi-point Brunauer–Emmett–Teller (BET) from a relative pressure range of $P/P_0 = 0.01-0.06$. Ammonia temperature-programmed desorption (TPD) was used to determine catalyst acidity using a microflow reactor system (Altamira Instruments 390) equipped with a thermal conductivity detector. Catalyst samples (~200 mg) were pretreated by heating in helium to 500°C for 30 min, and then cooled to 120°C in He flow. Next, ammonia adsorption consisted of flowing 10 vol% NH₃/He for 30 min at 120°C, followed by flushing with He. The TPD was performed by heating at 30°C/min from 120-600°C, with a 30 min hold at 600°C. The gas flowrate in all steps was 25 SCCM. A 5 mL sample loop was used to calibrate the thermal conductivity detector (TCD) response for NH₃ and quantify the amount of NH₃ desorbed from the catalysts.

Appendix B – Further details and analysis on HTL lab-scale investigations

Appendix B1 – Biocrude extraction procedures and analytical methods

This appendix provides details on which basis the solvent for the extraction of the light biocrude (BC1) was chosen. The multi-step solvent extraction method was applied by many authors^{349,354,364,400,504–508}. Usually, the first solvent needs to be immiscible in water in order to be easily separated from the aqueous phase. On the other hand, the secondary solvent must dissolve most of the higher molecular weight organic compounds in order to maximize the collections of biocrude. The total yield of biocrude is an over-estimation of the real biocrude obtainable in a scaled-up continuous plant. The maximization of the biocrude yield is necessary on this batch lab-scale bench in order to collect a higher amount of material and facilitate its characterization analysis.

The composition of biocrude obtained from HTL of lignin is known to be mainly composed of aromatic oxygenated compounds (e.g., phenols, methoxyphenols).³⁶⁴ Since these classes of compounds have the peculiarity to be polar, the choice of the solvent has fallen on those with similar polarity. The three selected solvents were diethyl ether (DEE), dichloromethane (DCM) and dimethyl ketone (DMK or acetone). The former two were chosen for dissolving the lighter organic compounds since they are polar and slightly miscible in water; while acetone was selected for the heavier fraction dissolution. DEE and DCM have been used for the biocrude extraction in many works, some examples are reported in references^{349,364,505} and references^{400,506–508} respectively. As extraction solvent for the heavy biocrude, DMK was chosen only on literature guidelines^{354,504,507}, as BC2 is composed of complex high-molecular aromatic oxygenated polymers, which are not possible to be characterized with the same analytical techniques applied on the light biocrude and due to its low toxicity. THF and methanol are other suitable candidates for BC2 extraction.
350,364,392,504,509

The choice of the extraction solvent was assessed in Procedure 1. The comparison of the GC-detectable compounds in the BC1 extracted with DCM and DEE is reported in Table B1.1, while the quantitative comparison by GC-FID is shown in Table B1.2.

The identification and quantification of the different compound classes were carried out in a gas-chromatograph GC-2010 (Shimadzu) equipped with a mass spectrometer GCMS-QP2010 GC 2010 Plus (Shimadzu) and a GC-FID GC 2010 Plus (Shimadzu), both equipped with ZB 5HT Inferno (Zebron) columns (30 m length, internal diameter 0.25 mm, film diameter 0.25 μm). In particular, the GC-MS apparatus was used to investigate the qualitative composition of the sample, comparing the spectrum with a NIST 17 library; GC-FID was used for the quantitative analysis of the selected compounds after a 4-point calibration with pure molecular standards and using o-terphenyl as an internal standard. The analysis was performed with a column flow of 2.02 mL min⁻¹ for GC-MS and 3.17 mL min⁻¹ in GC-FID, with an initial temperature of 40 °C (holding time 10 min), increased to 200 °C (heating rate 8 °C min⁻¹, holding time 10 min) and then to 280 °C (heating rate 10 °C min⁻¹, holding time 30 min).

Table B1.1. Comparison of GC-MS identified compounds between DCM and DEE-solubles in BC1 (experiments carried out at 300 °C-10 min-10% with Procedure 1).

| Compound class | DCM-solubles | DEE-solubles |
|----------------|---------------------------------------|---------------------------------------|
| Acids | - | Acetic acid |
| | - | Propionic acid |
| | - | Isovaleric acid |
| | Cyclopentanone | 2-Cyclopenten-1-one |
| | 2-Cyclopenten-1-one | 2,3-Dimethyl-2-cyclopenten-1-one |
| Ketones | 2-Methyl-2-cyclopenten-1-one | 3-Ethyl-2-hydroxy-2-cyclopenten-1-one |
| | 3-Ethyl-2-hydroxy-2-cyclopenten-1-one | Acetoin |
| Aldehydes | Acetoin | Acetovanillone |
| | Acetosyringone | Acetosyringone |
| | Desaspidinol | Desaspidinol |
| | Vanillin | Vanillin |
| | Syringaldehyde | Syringaldehyde |
| Phenols | Phenol | Phenol |
| | Syringol | Syringol |
| Methoxyphenols | Methoxyeugenol | Methoxyeugenol |
| | Guaiacol | Guaiacol |
| | Creosol | Creosol |
| | 4-Propylguaiacol | 4-Propylguaiacol |
| | 4-Ethylguaiacol | 4-Ethylguaiacol |
| | - | Eugenol |
| - | Isoeugenol | |

Table B1.2. Comparison of GC-FID quantification between DCM and DEE-soluble compounds in BC1 (experiment carried out at 300 °C, 10 min, 10% with Procedure 1).

| Compound class | Concentration ($\mu\text{g mL}^{-1}$) | |
|----------------|---|--------------|
| | DCM-solubles | DEE-solubles |
| Acids | 0.28 | 3.09 |
| Ketones | 0.05 | 0.06 |
| Aldehydes | 0.17 | 0.29 |
| Phenols | 3.49 | 7.28 |
| Methoxyphenols | 4.04 | 7.19 |
| Total | 8.03 | 17.9 |

The GC-MS qualitative analysis shows that by using DEE as extraction solvent it is possible to identify more compounds with respect to DCM. Moreover, the quantification by GC-FID in the DEE sample gives a total value that is more than double than in the sample collected via DCM. However, with the DCM extraction, the yield of BC1 and BC2 was, respectively 33.4% and 32.8wt.% (d.b.), while in the case of DEE they are 12.3 and 36.3wt.% (d.b.).

Dichloromethane is able to extract a higher amount of heavier compounds that are not detectable in GC, leading to a decrease in concentration of the lighter quantifiable organics. After this consideration, DEE was chosen.

Appendix B2 – Further results on the effects of reaction conditions to biocrude yields

This appendix provides details on the effects of temperature, time, biomass-to-water mass ratio and their interactions on BC1, BC2 and total biocrude yield.

Figure B2.1 (a) shows that, as far as the light biocrude yield is concerned, the temperature is the most influencing parameter, followed by time and B/W: an increase in the value of these parameters leads to an increase in the BC1 yield. Figure B2.1 (b) shows the influence of the interaction of the process parameters: only at 350 °C and 5 min the effect of B/W was negligible.

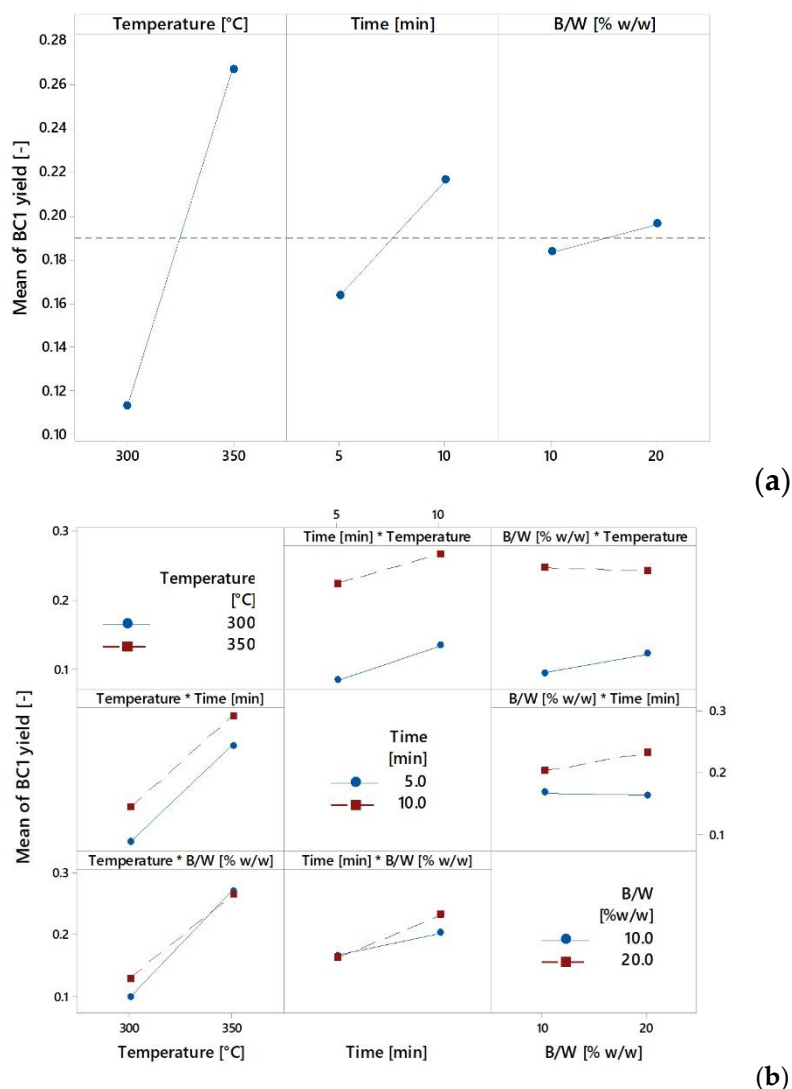


Figure B2.1. Influence of operating parameters on the yield of biocrude 1: main effects plot (a) and interaction effects plot (b).

Similarly, Figure B2.2 reports the influence of the operating parameters and their interactions on the yield of BC2. Again, temperature and time are the most influencing factors, but, in this case, along with their interactions, they negatively affect the yield, except for B/W, when the temperature is 300 °C or the time is 10 min.

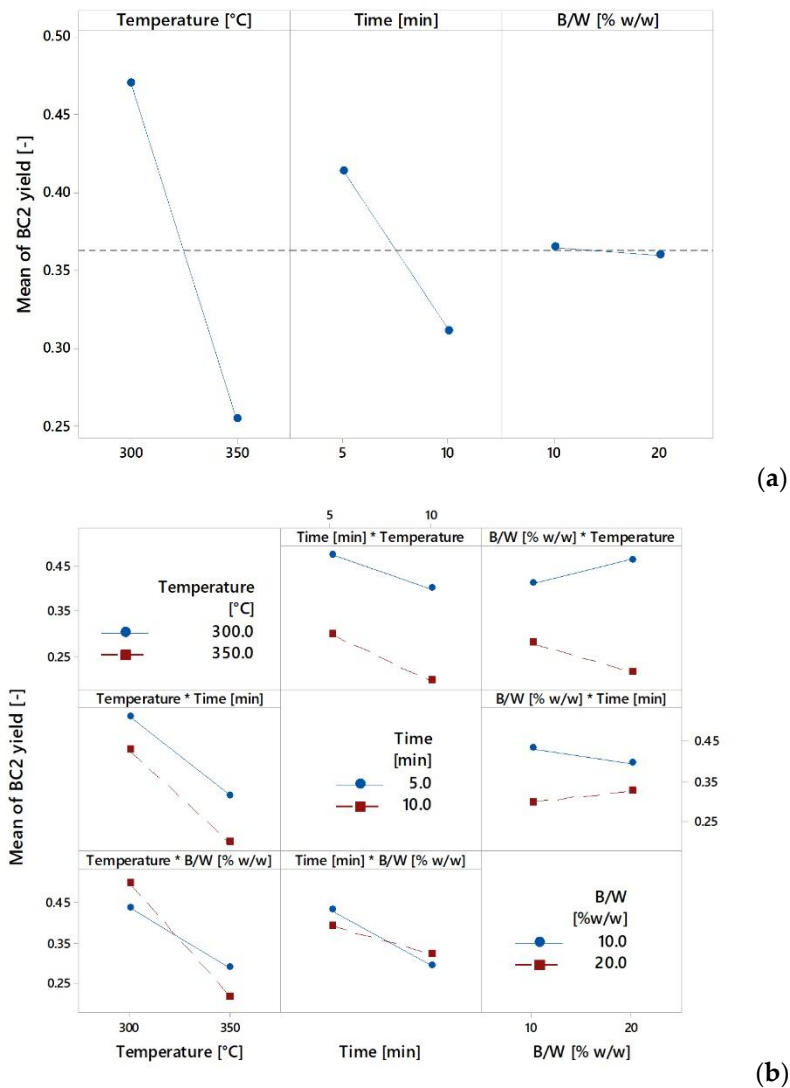
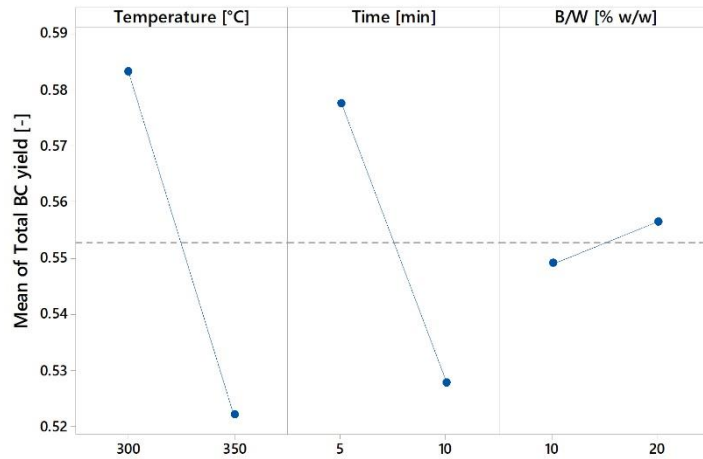
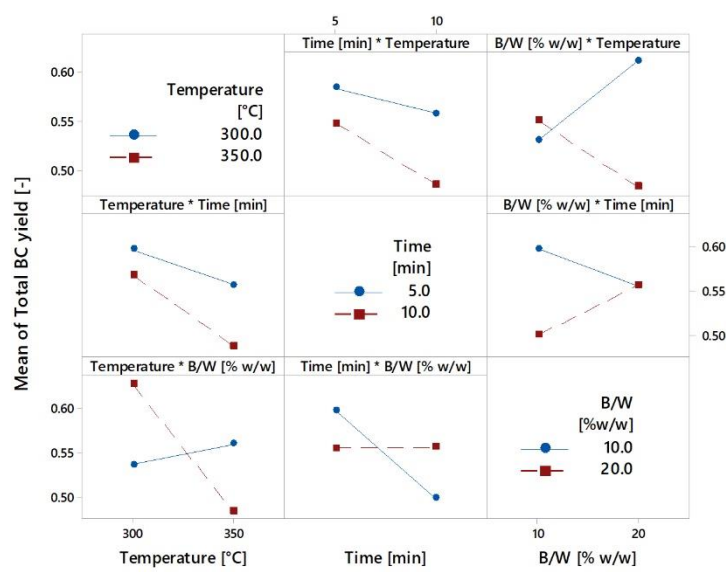


Figure B2.2. Influence of operating parameters on the yield of biocrude 2: main effects plot (a) and interaction effects plot (b).

Concerning total biocrude mass yield (Figure B2.3), an increase in temperature and time leads to a decrease in yield, as for BC2, but B/W imparts an opposite effect, behaving like in the BC1 case. Consequently, the interactions effects are more complex and the total biocrude yield increases with B/W when the temperature is 300 °C or when the residence time is 10 min. It slightly increases with temperature when B/W is 10wt.% and is nearly unaffected by time when B/W is 20wt.%.



(a)



(b)

Figure B2.3. Influence of operating parameters on total biocrude yield: main effects plot (a) and interaction effects plot 2(b).

Appendix B3 – Total organic carbon correction

This appendix provides details on the method adopted for the TOC correction, eliminating the contribution of the DEE dissolved in the aqueous samples collected with Procedure 1.

- The TOC and the carbon content of the HPLC-detected compounds (C_{HPLC}) was determined for the aqueous phase of the experiment whose products were collected with Procedure 2 (350 °C, 10 min, 10%) and thus not contaminated with DEE
- The carbon content of the unknown water-soluble species ($C_{unknown}$) was evaluated by the difference
- By supposing the ratio between $C_{unknown}$ and C_{HPLC} to be constant at different HTL conditions and collection procedures, the carbon content due to DEE in the aqueous phase from experiments whose products were collected with Procedure 1 (C_{DEE}) was evaluated according to equation:

$$C_{DEE} = TOC - C_{HPLC} \left[1 + \left(\frac{C_{unknown}}{C_{HPLC}} \right)_{Proc.2} \right]$$

- The corrected TOC was determined by subtracting C_{DEE}

Appendix B4 – Biocrude elemental analysis

This appendix provides details on the biocrudes' elemental analysis and on the validation of the Channiwala and Parikh equation for the evaluation of the HHV of the BC1 and BC2.

Table B4.1. Elemental composition of light biocrude fraction (wt.%, as received). Absolute standard deviation, where available, is reported in brackets.

| Reaction Condition | Biocrude 1 | | | | |
|---------------------|-------------|-------------|---------------|-------------|----------------|
| | C | H | N | O | Ash |
| 300 °C, 5 min, 10% | 65.6 (0.3) | 7.35 (0.03) | 0.692 (0.028) | 25.9 (n.d.) | 0.501 (n.d.) |
| 300 °C, 5 min, 20% | 61.4 (n.d.) | 7.07 (n.d.) | 0.687 (n.d.) | 30.6 (n.d.) | 0.230 (n.d.) |
| 300 °C, 10 min, 10% | 60.6 (2.5) | 7.20 (0.15) | 1.11 (0.33) | 30.6 (n.d.) | 0.501 (n.d.) |
| 300° C, 10 min, 20% | 62.3 (n.d.) | 7.49 (n.d.) | 0.830 (n.d.) | 29.1 (n.d.) | 0.287 (n.d.) |
| 350 °C, 5 min, 10% | 67.2 (0.6) | 7.15 (0.04) | 0.683 (0.002) | 25.0 (n.d.) | (n.d.) |
| 350 °C, 5 min, 20% | 63.9 (0.2) | 7.40 (0.04) | 0.659 (0.015) | 28.0 (n.d.) | 0.0108 (n.d.) |
| 350 °C, 10 min, 10% | 64.2 (0.4) | 7.51 (0.07) | 0.930 (0.031) | 27.3 (n.d.) | 0.0433 (n.d.) |
| 350 °C, 10 min, 20% | 62.9 (0.1) | 7.25 (0.02) | 0.719 (0.008) | 29.1 (n.d.) | 0.00113 (n.d.) |
| 370 °C, 5 min, 10% | 57.1 (1.0) | 7.29 (0.04) | 0.868 (0.073) | 34.7 (n.d.) | 0.0160 (n.d.) |
| 370 °C, 5 min, 20% | 64.2 (1.2) | 7.51 (0.03) | 0.930 (0.018) | 27.3 (n.d.) | 0.0143 (n.d.) |

Table B4.2. Elemental composition of heavy biocrude fraction (wt.%, as received). Absolute standard deviation, where available, is reported in brackets.

| Reaction Condition | Biocrude 2 | | | | |
|---------------------|-------------|--------------|---------------|-------------|---------------|
| | C | H | N | O | Ash |
| 300 °C, 5 min, 10% | 65.9 (0.6) | 6.77 (0.09) | 0.847 (0.043) | 26.4 (n.d.) | 0.136 (n.d.) |
| 300 °C, 5 min, 20% | 66.7 (0.1) | 6.42 (0.01) | 0.948 (0.013) | 25.6 (n.d.) | 0.146 (n.d.) |
| 300 °C, 10 min, 10% | 67.1 (0.2) | 6.91 (0.02) | 1.13 (0.03) | 24.9 (n.d.) | 0.0760 (n.d.) |
| 300 °C, 10 min, 20% | 67.0 (n.d.) | 6.98 (n.d.) | 0.860 (n.d.) | 25.0 (n.d.) | 0.138 (n.d.) |
| 350 °C, 5 min, 10% | 68.3 (0.4) | 6.51 (0.01) | 1.07 (0.03) | 24.0 (n.d.) | 0.124 (n.d.) |
| 350 °C, 5 min, 20% | 69.2 (0.7) | 6.32 (0.10) | 1.13 (0.03) | 23.2 (n.d.) | 0.122 (n.d.) |
| 350 °C, 10 min, 10% | 68.9 (0.4) | 6.69 (0.06) | 1.110 (0.001) | 23.1 (n.d.) | 0.232 (n.d.) |
| 350 °C, 10 min, 20% | 68.2 (0.3) | 4.23 (0.04) | 1.82 (0.03) | 25.5 (n.d.) | 0.240 (n.d.) |
| 370 °C, 5 min, 10% | 68.0 (0.5) | 6.61 (0.018) | 1.28 (0.02) | 23.7 (n.d.) | 0.457 (n.d.) |
| 370 °C, 5 min, 20% | 67.1 (0.2) | 6.99 (0.15) | 1.278 (0.001) | 24.1 (n.d.) | 0.470 (n.d.) |

Because of the low amount of material produced in each experiment, the higher heating value of the BC1 and BC2 was determined by the Channiwala and Parikh unified correlation ³⁵⁵:

$$\text{HHV} = 0.3491\text{C} + 1.1783\text{H} + 0.1005\text{S} - 0.1034\text{O} - 0.0151\text{N} - 0.0211\text{Ash},$$

where C, H, O, N, S and Ash respectively represents carbon, hydrogen, oxygen, nitrogen, sulphur and ash content of the sample expressed in mass percentages on dry basis. In the present evaluation, the sulphur content-term was neglected as the LRS has a very limited amount of S (0.2wt.%, d.b.). In order to validate equation B2, the HHV of a sample of BC1 and BC2 was measured according to UNI EN 14918 and this value was compared to the Dulong equation ⁵¹⁰, which is a correlation widely used in many studies for HHV calculation of HTL biocrude ^{365,508,511,512}. The results are reported in Table B4.3: it can be depicted that HHV equation leads to a lower relative error, determined according to equation>

$$\text{Relative error} = 100 \cdot (\text{measured value} - \text{calculated value}) / \text{measured value}$$

Table B4.3. Measured and evaluated HHV of BC1 and BC2 samples produced at 350 °C-5 min-20% (Procedure 1) in MJ kg⁻¹.

| Value | Biocrude 1 | Biocrude 2 |
|--------------------------------------|------------|------------|
| Measure | 28.47 | 29.43 |
| Dulong | 27.17 | 28.72 |
| Dulong relative error | 4.5% | 2.4% |
| Channiwala and Parikh | 28.13 | 29.53 |
| Channiwala and Parikh relative error | 1.2% | 0.3% |

The HHV values calculated with A2 correlation for BC1, BC2 as well as the yield-based weight-average total biocrude are reported in Table B4.4 below:

Table B.4.4. Higher heating value of the biocrude samples.

| Reaction condition | Higher heating value (MJ kg ⁻¹) | | |
|---------------------|---|------------|----------------|
| | Biocrude 1 | Biocrude 2 | Total biocrude |
| 300 °C, 5 min, 10% | 28.9 | 28.3 | 28.4 |
| 300 °C, 5 min, 20% | 26.6 | 29.0 | 28.6 |
| 300 °C, 10 min, 10% | 26.5 | 28.2 | 27.8 |
| 300 °C, 10 min, 20% | 27.5 | 29.0 | 28.6 |
| 350 °C, 5 min, 10% | 29.3 | 29.0 | 29.1 |
| 350 °C, 5 min, 20% | 28.1 | 29.5 | 28.9 |
| 350 °C, 10 min, 10% | 28.4 | 29.2 | 28.7 |
| 350 °C, 10 min, 20% | 27.5 | 26.1 | 27.0 |
| 370 °C, 5 min, 10% | 24.9 | 29.1 | 26.2 |
| 370 °C, 5 min, 20% | 28.4 | 29.2 | 28.6 |

Appendix B5 – Biocrude molecular weight

In this appendix the GPC data are listed in terms of weight-average molecular weight (M_w), number-average molecular weight (M_n) and the polydispersity index ($PDI = M_w/M_n$) for BC1 and BC2 samples.

Table B5.1. Weight-average, number-average molar mass (in g mol⁻¹) and a polydispersity index of BC1 and BC2; the absolute standard deviation is reported in brackets.

| Reaction condition | Biocrude 1 | | | Biocrude 2 | | |
|---------------------|------------|----------|-----|------------|----------|-----|
| | M_w | M_n | PDI | M_w | M_n | PDI |
| 300 °C, 5 min, 10% | 412 (2) | 128 (1) | 3.2 | 1332 (30) | 720 (8) | 1.8 |
| 300 °C, 5 min, 20% | 459 (13) | 204 (2) | 2.2 | 1243 (16) | 668 (9) | 1.9 |
| 300 °C, 10 min, 10% | 427 (2) | 101 (1) | 4.3 | 1359 (14) | 694 (6) | 2.0 |
| 300 °C, 10 min, 20% | 473 (13) | 232 (2) | 2.0 | 1217 (13) | 623 (2) | 2.0 |
| 350 °C, 5 min, 10% | 467 (3) | 223 (5) | 2.1 | 1147 (9) | 697 (10) | 1.6 |
| 350 °C, 5 min, 20% | 488 (41) | 265 (76) | 1.9 | 1397 (23) | 714 (10) | 2.0 |
| 350 °C, 10 min, 10% | 457 (2) | 213 (2) | 2.1 | 1030 (15) | 657 (20) | 1.6 |
| 350 °C, 10 min, 20% | 469 (3) | 222 (4) | 2.1 | 1142 (18) | 701 (9) | 1.6 |
| 370 °C, 5 min, 10% | 400 (0) | 105 (1) | 3.8 | 1151 (30) | 714 (8) | 1.6 |
| 370 °C, 5 min, 20% | 391 (2) | 107 (4) | 3.7 | 1029 (4) | 670 (27) | 1.5 |

Appendix B6 – Monomers detection in HTL-derived liquids

Table B6.1 shows the calibration compounds selected for the qualitative and quantitative analysis of BC1 and AP in GC-MS and HPLC.

Table B6.1. Compounds calibrated in GC-MS and HPLC.

| Compound class | GC-MS | HPLC |
|--------------------|---------------------------------------|----------------------------------|
| Sugars | | D-cellobiose |
| | | D(+)-glucose |
| | | D(+)-xylose |
| | | D(+)-galactose |
| | | L(+)-arabinose |
| | | D(+)-mannose |
| Acids | | Xylitol |
| | | Acetic acid |
| | | Propionic acid |
| | Acetic acid | Benzoic acid |
| | Propionic acid | Succinic acid |
| | Benzoic acid | Lactic acid |
| Alcohols | | Glutaric acid |
| | | Glycolic acid |
| | | Methanol |
| Alkylphenols | | Ethanol |
| | | Glycerol |
| | | |
| Aromatics/HC | m-Cresol | |
| | p-Cresol | |
| | o-Cresol | |
| Catechols | Toluene | |
| | 1,2-Benzenediol | 1,2-Benzenediol |
| Dimethoxyphenols | 1,4-Benzenediol | |
| | Phenol, 2,6-dimethoxy- | Phenol, 2,6-dimethoxy- |
| Furanics | HMF | HMF |
| | 2-Acetylfuran | |
| Ketones | Cyclopentanone | |
| | 2-Cyclopenten-1-one | |
| | 2-Cyclopenten-1-one, 2,3-dimethyl- | 1,2-Cyclopentanedione, 3-methyl- |
| | 2-Cyclopenten-1-one, 3-methyl- | |
| | 1,2-Cyclopentanedione, 3-methyl- | |
| Methoxycatechols | 1,4-Benzenediol, 3-methoxy- | 1,4-Benzenediol, 3-methoxy- |
| | Phenol, 2-methoxy- | |
| Methoxyphenols | Phenol, 2-methoxy-4-propyl- | |
| | Phenol, 2-methoxy-4-methyl- | |
| | Phenol, 2-methoxy-4-propenyl- | Phenol, 2-methoxy- |
| | Phenol, 2,6-dimethoxy-4-(2-propenyl)- | |
| | Phenol, 4-ethyl-2-methoxy- | |
| Phenolic Aldehydes | Benzaldehyde, 4-hydroxy-3-methoxy- | |
| | | |

| | | |
|------------------|--|--------|
| | Benzaldehyde, 4-hydroxy-3,5-dimethoxy- | |
| Phenolic Ketones | Ethanone, 1-(3-hydroxy-4-methoxyphenyl)- | |
| | Ethanone, 1-(4-hydroxy-3,5-dimethoxyphenyl)- | |
| Phenol | Phenol | Phenol |

An example of a complete BC1 GC-MS qualitative analysis with absolute and relative peaks area is reported in Table B6.2. The identified compounds are divided in classes to facilitate the data reading.

Table B6.2. Qualitative analysis of a light biocrude sample produced at 350 °C, 10 min, 10 wt.% (procedure 1).

| Compounds | Ret. Time | Peak Area | Peak Area % |
|--|-----------|----------------|-------------|
| Acids | | 2151718 | 2.51 |
| Acetic acid | 1.5 | 813323 | 0.95 |
| Benzoic acid | 18.8 | 605610 | 0.71 |
| Benzoic acid, 4-hydroxy-, | 22.2 | 46651 | 0.05 |
| Benzoic acid, methyl ester | 17.2 | 32652 | 0.04 |
| Butanoic acid | 3.9 | 60503 | 0.07 |
| Butanoic acid, 2-methyl- | 6.3 | 89297 | 0.1 |
| Butanoic acid, 3-methyl- | 5.9 | 125501 | 0.15 |
| p-Coumaric acid | 26.0 | 49121 | 0.06 |
| Propanoic acid | 2.3 | 249107 | 0.29 |
| Propanoic acid, 2-methyl- | 3.1 | 79953 | 0.09 |
| Alcohols | | 161551 | 0.19 |
| 4-Hydroxy-3-methoxyphenylethyl alcohol | 25.3 | 161551 | 0.19 |
| Alkylphenols | | 1194483 | 1.39 |
| Phenol, 2,4-dimethyl- | 18.5 | 28564 | 0.03 |
| Phenol, 2-methyl- | 16.1 | 337350 | 0.39 |
| Phenol, 3-ethyl- | 18.2 | 175917 | 0.21 |
| Phenol, 4-ethyl- | 18.9 | 166345 | 0.19 |
| Phenol, 4-methyl- | 16.7 | 486307 | 0.57 |
| Aromatics/HC | | 714058 | 0.83 |
| Benzene, (1,2-dimethyl-1-propenyl)- | 19.7 | 42199 | 0.05 |
| Benzene, 1,2,4-tripropyl- | 28.8 | 346325 | 0.4 |
| Naphthalene, 2,3-dimethoxy- | 28.9 | 176218 | 0.21 |
| Naphthalene, 2,6-dimethoxy- | 28.9 | 149316 | 0.17 |
| Catechols | | 5477458 | 6.37 |
| 1,2,3-Benzenetriol, 5-methyl- | 24.3 | 187823 | 0.22 |
| 1,2-Benzenediol, 4-ethyl | 22.9 | 371959 | 0.43 |
| 1,2-Benzenediol, 4-methyl- | 21.2 | 625851 | 0.73 |
| 1,3-Benzenediol, 4-propyl- | 24.4 | 371289 | 0.43 |
| 1,4-Benzenediol | 21.0 | 422458 | 0.49 |

| | | | |
|---|------|-----------------|--------------|
| 1,4-Benzenediol, 2,5-dimethyl- | 46.9 | 142710 | 0.16 |
| 1,4-Benzenediol, 2-methyl- | 22.3 | 574502 | 0.67 |
| 1,2-Benzenediol | 19.4 | 2780866 | 3.24 |
| Dimethoxyphenols | | 13437988 | 15.67 |
| 2,3-Dimethoxyphenol | 20.4 | 129738 | 0.15 |
| 3,4-Dimethoxyphenol, 2-methylpropyl ether | 22.2 | 110302 | 0.13 |
| 4-(3-hydroxypropyl)-2,6-dimethoxyphenol | 30.4 | 197007 | 0.23 |
| 4-(4-Hydroxy-3-methoxystyryl)-2,6-dimethoxyphenol | 49.4 | 76189 | 0.09 |
| Phenol, 2,6-dimethoxy- | 22.4 | 9784411 | 11.41 |
| Phenol, 2,6-dimethoxy-4-(1E)-1-propen-1-yl- | 27.4 | 1165517 | 1.36 |
| Phenol, 2,6-dimethoxy-4-(2-propenyl)- | 26.4 | 346115 | 0.4 |
| Phenol, 2,6-dimethoxy-4-methyl- | 22.8 | 47078 | 0.05 |
| Phenol, 3,4-dimethoxy- | 21.9 | 108115 | 0.13 |
| Phenol, 3,4-dimethoxy-, acetate | 22.5 | 1473516 | 1.72 |
| Furanics | | 192004 | 0.22 |
| 3,4-dimethylfuran | 20.5 | 45455 | 0.05 |
| Benzofuran, 2-methyl- | 17.5 | 146549 | 0.17 |
| Ketones | | 1675868 | 1.95 |
| 1,3-Cyclopentanedione, 2-ethyl-2-methyl- | 18.4 | 37007 | 0.04 |
| 2-Cyclohexen-1-one, 6-methyl-3-(1-methylethyl)- | 21.9 | 136547 | 0.16 |
| 2-Cyclopenten-1-one, 2,3-dimethyl- | 29.9 | 450594 | 0.52 |
| 2-Cyclopenten-1-one, 2-methyl- | 9.6 | 544991 | 0.64 |
| 2-Cyclopenten-1-one, 3,4-dimethyl- | 29.4 | 136475 | 0.16 |
| 2-Ethyl-3-methylcyclopent-2-en-1-one | 18.0 | 71029 | 0.08 |
| Cyclohexanone, 2-isopropyl-2,5-dimethyl- | 16.1 | 79909 | 0.09 |
| Cyclopentanone | 4.2 | 33382 | 0.04 |
| Ethanone, 1-(2,3,4-trihydroxyphenyl)- | 24.2 | 57754 | 0.07 |
| p-Hydroxyphenylacetone | 24.0 | 128180 | 0.15 |
| Methoxyaromatics HC | | 3548055 | 4.14 |
| 1,5-Dimethoxy-4-methylnaphthalene | 29.7 | 51569 | 0.06 |
| Benzene, 1,2,3-trimethoxy-5-(1-propenyl)-, (E)- | 29.0 | 171577 | 0.2 |
| Benzene, 1,2,3-trimethoxy-5-methyl- | 25.2 | 1773608 | 2.07 |
| Benzene, 1,2-dimethoxy- | 18.4 | 17150 | 0.02 |
| Benzene, 1,3-dimethoxy-2-(2-propenyloxy)- | 27.9 | 850040 | 0.99 |
| Benzene, 1,3-dimethoxy-5-methyl- | 20.9 | 88082 | 0.1 |
| Benzene, 1,4-dimethoxy-2-methyl- | 20.7 | 152616 | 0.18 |
| Benzene, 4-butyl-1,2-dimethoxy- | 25.6 | 66052 | 0.08 |
| Benzene, methoxy- | 10.3 | 46139 | 0.05 |
| Benzenepropanol, 4-hydroxy-3-methoxy- | 27.1 | 331222 | 0.39 |
| Methoxycatechols | | 7338192 | 8.56 |
| 1,2-Benzenediol, 3-methoxy-5-(2-propen-1-yl)- | 53.6 | 307819 | 0.36 |
| 1,2-Benzenediol, 3-methoxy- | 20.8 | 143951 | 0.17 |
| 1,4-Benzenediol, 2-methoxy- | 20.7 | 6886422 | 8.03 |
| Methoxyphenols | | 16898117 | 19.7 |

| | | | |
|--|------|----------------|--------------|
| Phenol, 4-butyl-2-methoxy- | 25.3 | 923710 | 1.08 |
| (4-Methoxyphenyl)(5-methyl-2-furyl)methane | 30.9 | 59699 | 0.07 |
| Phenol, 2,6-dimethoxy-4-methyl- | 24.0 | 3283984 | 3.83 |
| Phenol, 2-methoxy- | 16.9 | 6154852 | 7.17 |
| Phenol, 2-methoxy-3-methyl- | 19.1 | 136254 | 0.16 |
| Phenol, 2-methoxy-4-propenyl- | 24.1 | 274826 | 0.32 |
| Phenol, 2-methoxy-4-propyl- | 22.7 | 1785865 | 2.08 |
| Phenol, 2-methoxy-5-(2-propenyl)- | 26.2 | 205889 | 0.24 |
| Phenol, 4-ethyl-2-methoxy- | 21.0 | 1860442 | 2.17 |
| Phenol, 4-methoxy-3-methyl- | 23.6 | 301356 | 0.35 |
| Phenol, 2-methoxy-4-methyl- | 19.4 | 1850915 | 2.16 |
| Phenol, 3-methoxy- | 20.1 | 60325 | 0.07 |
| Phenolic Aldehydes | | 2405789 | 2.81 |
| 3,4-Dihydroxy-5-methoxybenzaldehyde | 26.2 | 67849 | 0.08 |
| Benzaldehyde, 3-hydroxy- | 22.6 | 62335 | 0.07 |
| Benzaldehyde, 3-hydroxy-4-methoxy- | 23.2 | 254863 | 0.3 |
| Benzaldehyde, 4-hydroxy-3,5-dimethoxy- | 27.2 | 193350 | 0.23 |
| Homosyringaldehyde | 26.5 | 1827392 | 2.13 |
| Phenolic Ketones | | 3335028 | 3.9 |
| 1-(3-Methoxymethyl-2,4,5,6-tetramethylphenyl)ethanone | 30.5 | 135034 | 0.16 |
| 1,2-Benzenediol, 4-(2-propen-1-yl)- | 25.8 | 148716 | 0.17 |
| 1H-Inden-1-one, 2,3-dihydro- | 21.2 | 111014 | 0.13 |
| 5-Sec-butylpyrogallol | 25.4 | 810996 | 0.95 |
| 2-Butanone, 4-(4-hydroxy-3,5-dimethoxyphenyl)- | 28.7 | 817407 | 0.95 |
| 2H-1-Benzopyran-2-one, 3,4-dihydro-6-methyl- | 27.0 | 53659 | 0.06 |
| 4-Hydroxy-1-indanone | 26.7 | 78536 | 0.09 |
| Ethanone, 1-(2,5-dihydroxyphenyl)- | 24.9 | 126032 | 0.15 |
| Ethanone, 1-(2,6-dihydroxyphenyl)- | 27.2 | 150364 | 0.18 |
| Ethanone, 1-(2-hydroxy-6-methoxyphenyl)- | 22.0 | 35491 | 0.04 |
| Ethanone, 1-(3-hydroxy-4-methoxyphenyl)- | 24.6 | 271930 | 0.32 |
| Ethanone, 1-(3-hydroxyphenyl)- | 23.2 | 256152 | 0.3 |
| Ethanone, 1-(4-hydroxy-3,5-dimethoxyphenyl)- | 28.2 | 339697 | 0.4 |
| Ethanone,1-(2,3-dihydro-5-benzofuryl)-, o-(4-chlorobenzoyl)oxime | 25.8 | 80110 | 0.09 |
| Phenol | | 9748189 | 11.36 |
| Phenol | 13.8 | 9748189 | 11.36 |

Appendix C – Techno-economic analysis of a demo-scale HTL plant

In this Appendix, the HTL model calculation will be summarized, showing the design procedures implied to obtain mass and energy balances as well as the techno-economic analysis (TEA) performed on a full-scale plant. Most of the

work reported here below has been carried out in collaboration with Arturo di Fraia (master students at University of Florence).

Appendix C1 – HTL model

In this model the lignin-rich stream from the ethanol plant is mixed in the dilution conveyor with the aqueous solution coming out of the stirred tank E3, in order to obtain the expected biomass-to-water ratio. Downstream of the conveyor, there is a screw feeder that delivers the feed to the high-pressure pump (HP), that raises the pressure to reaction setpoint. After the pump, the feed enters two shell and tube heat exchangers (HE1 and trim heater in Figure C1.1) that rise the temperature to reaction conditions. Then, the slurry enters the plug-flow reactor and the reaction temperature is kept through indirect heat exchange using a jacketed diathermic oil heat exchanger, externally heated using a natural gas burner. The products coming out of the reactor are cooled down in a shell and tube heat exchanger (HE2) that lowers the slow temperature to 150°C. The diathermic oil, coming out of HE2, is constantly recirculated towards HE1 where the slurry is preheated up to a temperature of about 225°C. After the HE2, the products flow into a hot pressurized filtering system for the removal of the solid phase and then through a water-cooled heat exchanger. After the cooler, the temperature drops below 100°C in order to avoid vapor formation and quench any other undesirable reaction that could reduce the biocrude yield. The temperature of this stream should not be lowered to ambient temperature to avoid increase in biocrude viscosity, that would compromise the stream's flowability. Then, the liquid stream is depressurized through a oligodynamic pistons system which has a similar configuration as the one described in paragraph 3.4. Finally, the whole product mixture enters in a centrifuge that separates the residual aqueous phase, the biocrude and the gas phase.

Figure C1.1 shows the scheme of the HTL plant adopted for modelling the TEA briefly described also in paragraph 3.3.

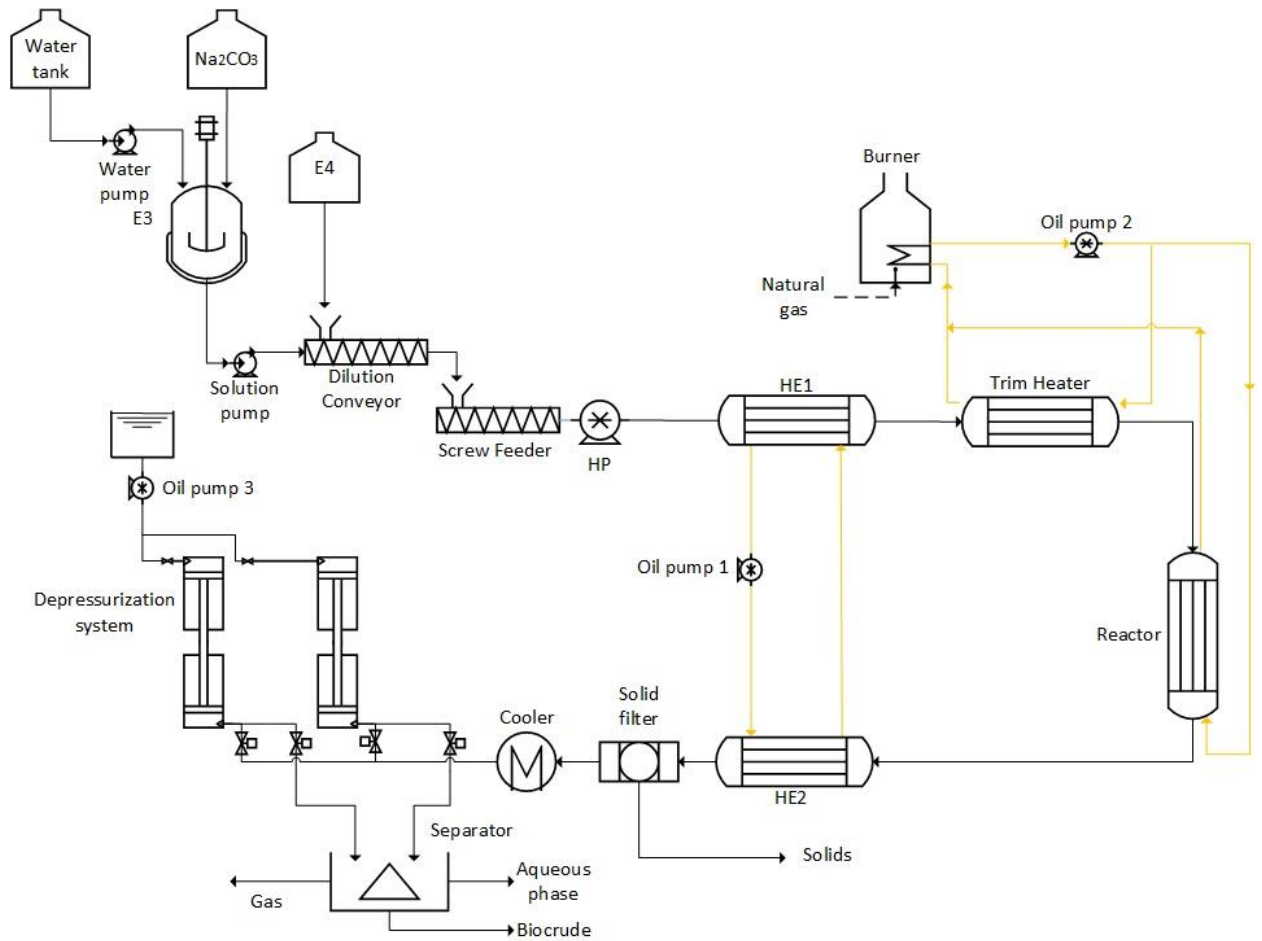


Figure C1.1. Scheme of the continuous HTL plant used for TEA model

Mass balance

The plant was designed to have an operating time of 7800 h/year and, according to the amount of LRS which is yearly produced in the ethanol plant, a capacity of 55 ton/h of biomass-water slurry. No material loss was considered in the plant. The pressure drop was considered concentrated in the stationary and adiabatic equipment. The inlet mass flow rates and process parameters of the plant are shown in Table C1.1. In this model, the B/W ratio was considered of 20 wt.% because in a commercial scale plant the problem of blockage is reduced due to larger tubes and equipment size compared to small scale pilot plants. The products yield Table C1.2 was derived to the results of HTL batch experiments performed at RE-CORD laboratory with the biomass-to-water ratio of 20 wt.% and a residence time of 10 minutes. The biocrude yield was increased of 5% compared to the batch experiments to take into account the effect of homogeneous catalyst in the inlet slurry. The residence time of 10 minutes was selected because it increases the yield of lighter biocrude (BC1), compared to heavier fraction (BC2).

Table C1.1 – List of HTL design parameters used in the model

| Parameter | Value | Unit |
|---|--------------|-------------|
| LRS flowrate | 15583 | kg/h |
| Moisture content | 70 | wt. % |
| Biomass to water ratio | 20 | wt. % db |
| Water | 24518 | kg/h |
| Na₂CO₃ Concentration | 0.05 | mol/L |
| Na₂CO₃ flowrate | 243 | kg/h |
| Slurry flowrate [ton/h] | 55243 | kg/h |
| Pressure | 200 | bar |
| Reaction Temperature | 350 | °C |
| Residence time | 10 | min |

The product yields and the resulting mass flows are resumed in Table C1.2. The mass flows of the plant, derived from the component design, are shown in the block scheme of Figure C1.2.

Table C1.2 Measured products yields of the experiments performed at 350°C, 10 min residence time, 20% B/W.

| Product | Yield (% w/w d.b.) |
|----------------|---------------------------|
| Biocrude | 51.0 |
| Solid residue | 10.5 |
| WSO | 33.0 |
| Gas | 5.5 |
| Stream | Value [kg/h] |
| Biocrude | 4675 |
| Solid residue | 1082 |
| Aqueous Phase | 48918 |
| Gas | 504 |

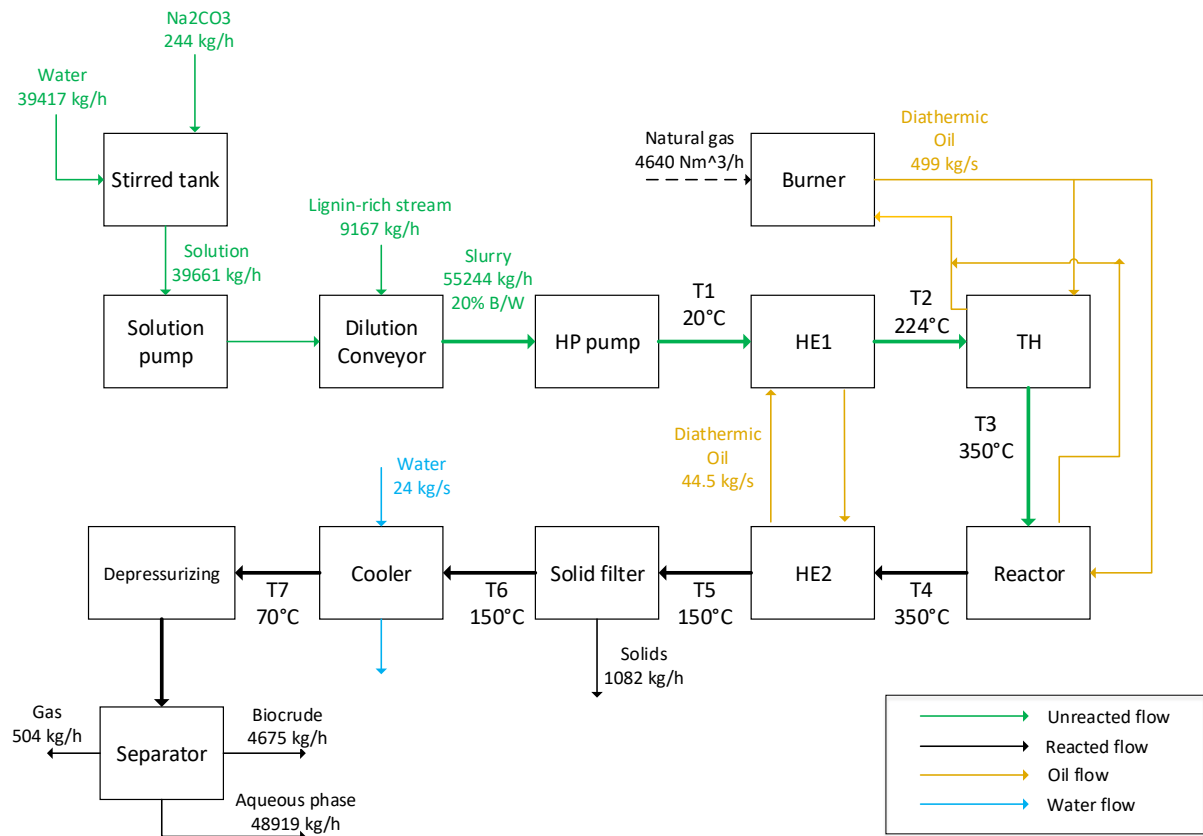


Figure C1.2 Mass flows of the HTL plant.

Table C1.3 shows the biocrude elemental composition that was calculated as the weighted average of the elemental composition of BC1 and BC2 obtained in HTL batch reaction at 350°C, 10 minutes of residence time and 20% dry mass content³⁴⁰.

Table C1.3 Elemental composition of biocrude.

| Parameter | Value |
|----------------|-------|
| C (% w/w) d.b. | 64.84 |
| H (% w/w) d.b. | 6.14 |
| N (% w/w) d.b. | 1.22 |
| O (% w/w) d.b. | 27.78 |

Energy analysis

This section reports the calculations of the required electrical and thermal powers for the components of the plant. The design of the components was performed considering no material loss in the plant. The mass flow considered is shown in Figure .

Reactor

The design of the reactor is fundamental for the optimization of the hydrothermal liquefaction process. Based on the experimental data, the plug-flow reactor configuration has been chosen for the plant because it can be assembled in a

standard heat exchanger configuration, reducing the equipment cost. Due to the corrosive characteristics of the biocrude, the material chosen for tubing and fittings was stainless steel (AISI 316). The tube dimensions, shown in Table , were chosen to withstand the pressure of 250 bar at the temperature of 350°C. The effect of the operating temperature has been considered by means of an appropriate de-rating factor of 0.82⁵¹³. The temperature in the reactor must be maintained to reaction temperature (350°C) throughout its entire length. In order to evaluate the thermal losses, the reactor was modelled as a shell-and-tube heat exchanger in which the slurry flows in the tubes, with the dimensions expressed in Table C1.4, and the diathermic oil in the shell side. The heat exchanger was also considered covered by a 5 cm thick insulation.

Table C1.4 Reactor tubing dimensions.

| Parameter | Value | Unit |
|----------------------------|---------|------|
| Tube OD | 1'' 1/4 | inch |
| Tube wall thickness | 0.156'' | inch |
| Maximum allowable pressure | 337 | bar |

In order to obtain a residence time in the reactor of 10 minutes, the maximum mass flow per tube was limited to 200 $\frac{kg}{h}$ (\dot{m}_{tube}) and the length (L) of 123 m for each tube has been selected. Considering the total mass flow of the plant, the number of tubes required is 275 (N_T). In order to limit the number of tubes per reactor, it was decided to use four reactors in parallel with 80 tubes each. The axial average velocity ($V_{average}$) of the fluid was calculated as:

$$V_{average} = \frac{\dot{m}_{tube}}{\rho_{slurry} \cdot A_i} = 0.21 \frac{m}{s}$$

It was assumed that the slurry temperature is constant through the entire length of the reactor. The thermal power exchanged in the reactor was calculated by considering the heat exchange between the diathermic oil and the slurry and the thermal losses. The heat loss was considered concentrated in the diathermic oil medium that is in contact with the shell side of the heat exchanger.

In order to calculate the average convection coefficient for the oil in the shell side, the design for a baffle shell-and-tube heat exchanger followed ⁵¹⁴. The tube was considered as a triangular configuration of pitch (p) equal to 25.96 mm⁵¹⁵. The pitch parallel to flow and normal to flow were considered equal. The iterative calculation of the convective heat exchange coefficient of the diathermic oil has been initialized with a mass flow of 80 $\frac{kg}{s}$. The inlet temperature of the diathermic oil was considered 380°C and the outlet temperature 355°C. In order to maintain that ΔT , the oil mass flow per reactor was 113.3 $\frac{kg}{s}$.

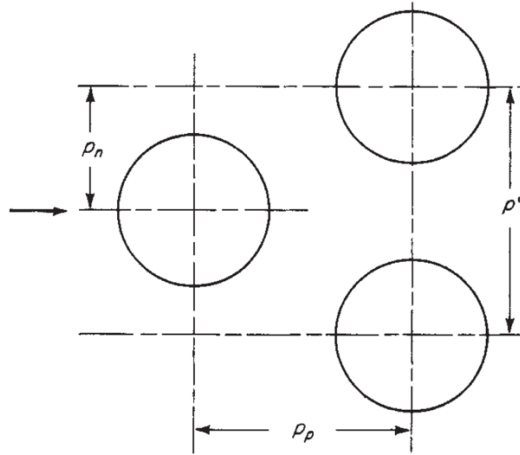


Figure C1.3 Tubes configuration base tubes layout for the heat exchange ⁵¹⁴.

The shell diameter D_s was calculated following the process in ⁵¹⁶:

1. Calculation of the surface occupied by the tubes in triangular pitch configuration (Figure C1.3).
2. Calculation of the shell diameter to contain this area, the result obtained is the outer tube limit (D_{OTL}).
3. Two tube diameters were added to the previous shell diameter in order to obtain the minimum shell diameter $D_{min\ shell}$.
4. For initial design, 2-inch increment was considered.

The shell diameter obtained (D_s) is 0.487 m.

The minimum baffle cut area recommended in ⁵¹⁶ is 40% of the total shell area. The corresponding baffle cut is $l_c = 0.22\ m$.

The number of tubes crossed in one section of flow (N_c) and the fraction of total tube in crossflow (F_c) were calculated as:

$$N_c = \frac{D_s \left[1 - 2 \frac{l_c}{D_s} \right]}{p} = 1.3$$

$$F_c = \frac{1}{\pi} \cdot \left[\pi + 2 \cdot \frac{D_s - 2l_c}{D_{OTL}} \sin \left(\cos^{-1} \frac{D_s - 2l_c}{D_{OTL}} \right) - 2 \cos^{-1} \frac{D_s - 2l_c}{D_{OTL}} \right] = 0.18$$

Also, the number of effective crossflow in each window (N_{cw}) and the crossflow area at or near centerline for one cross-flow section for triangular layout (S_m) were calculated:

$$N_{cw} = \frac{0.8l_c}{p} = 4.39 \text{ Eq. 1}$$

$$S_m = l_s \left[D_s - D_{OTL} + \frac{D_{OTL} - D_0}{2p} \cdot (2p - D_0) \right] = 0.03\ m^2$$

D_0 is the external diameter of the tube. The dynamic viscosity of the diathermic oil is $\mu_{oil} = 0.00038 \frac{kg}{m \cdot s}$ ⁵¹⁷ and the shell side Reynolds number (Re) was evaluated according to Eq.12:

$$Re = \frac{D_0 \dot{m}_{oil}}{\mu_{oil} S_m} = 3.1 \cdot 10^5$$

The resulting ideal convection coefficient (\bar{h}_{id}) for an ideal tube bank was approximated through a correlation, calculating some factors as hereby reported:

$$j = a_1 \cdot \left(\frac{1.33}{\frac{p}{D_0}} \right)^a \cdot Re^{a_2}$$

$$a = \frac{a_3}{1 + 0.14 Re^{a_4}}$$

$$\bar{h}_{id} = j \cdot c_p \frac{\dot{m}_{oil}}{S_m} \cdot \left(\frac{k}{c_p \mu} \right)^{\frac{2}{3}} \cdot \left(\frac{\mu_b}{\mu_s} \right)^{0.14}$$

Then the \bar{h}_{id} was corrected, considering the baffle configuration effect, by the factor J_c derived from the diagram of Figure C1.4 and then reduced of another 50%, in order to consider other effects not analyzed in this preliminary design (baffle configuration and leakage effects, temperature gradient, bundle-bypassing effects). The \bar{h}_{oil} obtained is 1238 W/m²K. The thermal convection resistance was calculated considering the internal surface of the shell is $A_i = 15.3 \text{ m}^2$:

$$R_{conv\ oil} = \frac{1}{\bar{h}_{oil} \cdot A_i} = 0.000058 \frac{K}{W}$$

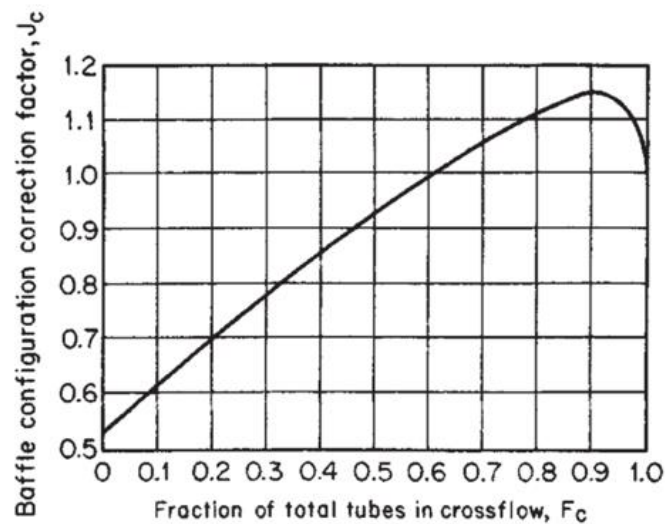


Figure C1.4 Correction factor for baffle-configuration effects ⁵¹⁴.

The thermal conduction resistance of shell and of the thermal insulation were calculated through:

$$R_{cond} = \frac{\ln\left(\frac{r_2}{r_1}\right)}{2\pi L\lambda}$$

The thermal conduction coefficient of the stainless steel is $\lambda = 17 \frac{W}{mK}$ and for thermal insulation was considered $\lambda = 0.022 \frac{W}{mK}$ ⁵¹⁸. The thermal conduction resistances are:

- $R_{cond\ shell} = 0.000003 \frac{K}{W}$
- $R_{cond\ insulation} = 0.08 \frac{K}{W}$

Outside the insulation, the heat loss is mainly due to the natural convection and the Rayleigh number Ra_D was calculated according to:

$$Ra_D = \frac{g \cdot \beta \cdot (T_s - T_\infty) \cdot D^3}{\nu \cdot \alpha} = 4.84 \cdot 10^5$$

In which:

- Surface temperature of the insulation $T_s = 303\ K$
- Air temperature $T_\infty = 293\ K$
- Gravity acceleration $g = 9.81 \frac{m}{s^2}$
- Volumetric coefficient of thermal dilatation of air considered as an ideal gas $\beta = \frac{1}{T_\infty}$
- Cinematic viscosity of air $\nu = 0.0000159 \frac{m^2}{s}$
- Thermal diffusivity of air $\alpha = 0.0000225 \frac{m^2}{s}$
- Diameter of tube-in-tube heat exchanger with insulation $D = D_{oil} + 2 \cdot s_{insulation} = 0.1\ m$

The Nusselt number for long horizontal cylinder of diameter D was calculated using Eq.19:

$$Nu_D = 0.125 \cdot Ra_D^{0.333}$$

From which it was evaluated:

$$\bar{h}_{natural\ convection} = \frac{Nu_D \cdot \lambda}{D} = 6.7 \frac{W}{m^2 K}$$

The thermal conductivity of air is $\lambda = 0.0263 \frac{W}{mK}$ ⁵¹⁹. The thermal resistance for the natural convection was calculated with Eq.16 and the total thermal resistance is:

$$R_{tot} = R_{conv\ oil} + R_{cond\ shell} + R_{cond\ ins} + R_{nat\ conv} = 0.0157 \frac{K}{W}$$

In order to calculate the heat loss by the diathermic oil in the heat exchanger, the average temperature of the diathermic oil was considered 370°C (T_{oil}) and the air temperature outside the tube 20°C (T_∞). The total thermal power dissipated by the oil is:

$$\dot{Q}_L = \frac{T_{feed} - T_\infty}{R_{tot}} = 22.3\ kW$$

The total thermal power dissipated in four reactors is 89.2 kW. The mean convection coefficient of the slurry was calculated considering the slurry properties equal to the water properties (Table C1.5) at reactor temperature (350°C) and pressure (200 bar).

Table C1.5 Water properties at 350°C and 200 bar.

| Properties | Value | Unit |
|------------------------------------|---------|-------|
| Dynamic viscosity (μ) | 0.00007 | kg/ms |
| Thermal conductivity (λ) | 0.4233 | W/mk |
| Specific heat (c_p) | 7825 | J/kgK |

The Reynolds and Prandtl number were evaluated according to:

$$Re = \frac{4 \cdot \dot{m}}{\pi \cdot D \cdot \mu}$$

$$Pr = \frac{c_p \mu}{\lambda}$$

D is the the internal diameter of the feed tube (Table). For the calculations of the Nusselt number (Nu_D) was used the Dittus-Boelter correlation for smooth pipes when flow are heated up ⁵¹⁹:

$$Nu_D = 0.023 \cdot Re^{\frac{4}{5}} \cdot Pr^{0.4} = 125$$

This equation can be applied to turbulent flow when:

- $\frac{L}{D} \gg 10$
- $Re \geq 10000$
- $0.6 \leq Pr \leq 160$

The mean convection coefficient (\bar{h}_{slurry}) for the slurry flow in the inner tube and the corresponding thermal resistance ($R_{conv\ slurry}$) were calculated considering the internal surface of the inner tube is $A = A_i = \pi \cdot R_i \cdot L = 9.2 \text{ m}^2$. Therefore, it was possible to estimate the global heat exchange coefficient:

$$\bar{h}_{slurry} = \frac{Nu_D \cdot \lambda}{d_i} = 2221 \frac{W}{m^2K}$$

$$R_{conv\ slurry} = 0.00005 \frac{K}{W}$$

$$U = \frac{1}{\frac{1}{\bar{h}_{slurry}} + \frac{r_1}{\lambda_{inox}} \cdot \ln \frac{r_2}{r_1} + \frac{d_1}{d_2} \cdot \frac{1}{\bar{h}_{oil}}} = 685.4 \frac{W}{m^2K}$$

The inlet temperature of the diathermic oil was considered 380°C and the outlet temperature 355°C. The logarithmic mean temperature difference is:

$$\Delta T_{ml} = \frac{\Delta T_1 - \Delta T_2}{\ln \frac{\Delta T_1}{\Delta T_2}} = 14.3 \text{ K}$$

The thermal power exchanged by the diathermic oil is:

$$\dot{Q}_{oil} = UA_T \Delta T_{ml} + \dot{Q}_{Ltot} = 7059 \text{ kW}$$

The internal surface of the tubes is $A_T = 738 \text{ m}^2$. The total thermal power required in four reactors is 28.3 MW.

Heat exchangers

The plant configuration includes three shell and tube heat exchangers. HE1 and the trim heater bring the slurry to reaction temperature and HE2 recovers heat from the products coming out of the reactor. In all heat exchangers the slurry flows in the tube side and the diathermic oil in the shell side. Two different diathermic oil lines were considered:

- *Oil line 1.* The products coming out of the reactors are cooled down by the diathermic oil in the HE2 that is, then, recirculated in the HE1.
- *Oil line 2.* The thermal power required in the trim heater and the reactors is provided to diathermic oil by a natural gas burner.

As assumed in the reactor design, the slurry properties were modelled with water thermophysical properties at the average temperatures of the exchangers (Table C1.6). This assumption is an approximation, used also in other works⁵²⁰, that can be justified by the fact that the feed flow is almost entirely composed by water (80% in this analysis).

Table C1.6 Water properties at HE1 and TH temperatures and pressures.

| Parameter | HE1 (100°C; 200 bar) | HE2 (250°C; 200 bar) | TE (280°C; 200 bar) |
|---|-------------------------|-------------------------|------------------------|
| Dynamic viscosity (μ) [kg/m s] | 0.000287 | 0.00011 | 0.000098 |
| Thermal conductivity (λ) [W/mK] | 0.675 | 0.630 | 0.593 |
| Specific heat (c_p) [J/kgK] | 4172 | 4665 | 4967 |
| Density (ρ) [kg/m ³] | 968 | 817 | 772 |

An initial design of the exchangers, modelled as shell-and-tube with six tube passes and three shell passes, was done following this procedure⁵¹⁹:

1. Calculation of the required thermal power (\dot{Q}_T) using the inlet temperature of the fluids and the total mass flow.
2. Initial estimate of the global convection coefficient (U) based of initial consideration about tubes number.
3. Correction of global heat exchange coefficient, considering a fouling factor (F_f) for the feed side.
4. Correction of the ΔT_{ml} with the correction factor F_t based on selected heat exchanger typology.
5. Estimation of the global heat exchange coefficient based on the tubes configuration inside the reactor (number of tubes, tube length).

The process has been repeated until the two estimates are the same to one degree of decimal accuracy.

The required heat transfer rate in the HE2 was calculated by considering the temperatures shown in Figure C1.5:

$$\dot{Q}_{HE2} = \dot{m}_4 \cdot c_{p4} \cdot (T_4 - T_5) = 14.5 \text{ MW}$$

The oil mass flow in the shell is:

$$\dot{m}_{oil1} = \frac{W}{c_p \cdot \Delta T} = 44.5 \frac{\text{kg}}{\text{s}}$$

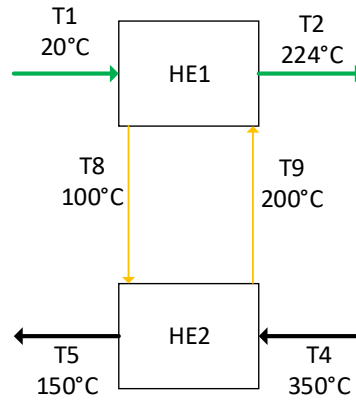


Figure C1.5 Temperatures of diathermic oil and process stream in the two heat exchangers HE1 and HE2.

The average convection coefficient for the slurry flow in the tube was obtained and the convection coefficient for the shell side by following the equation used for the reactor design. The results of the calculations are shown in Table C1.7.

The products in HE2 were approximated to a heavy oil with a fouling factor $F_f = 0.00053 \frac{m^2K}{W}$. The $\Delta T_{ml,cc}$ was calculated for a counter current heat exchanger and then corrected for a shell-and-tube heat exchangers with 6 tube passes and 3 shell passes with the correction factor (F_t) from Figure C1.6⁵¹⁴. The corrected ΔT_{ml} is:

$$\Delta T_{ml} = F_t \cdot \Delta T_{ml,cc} = 72.1^\circ\text{C}$$

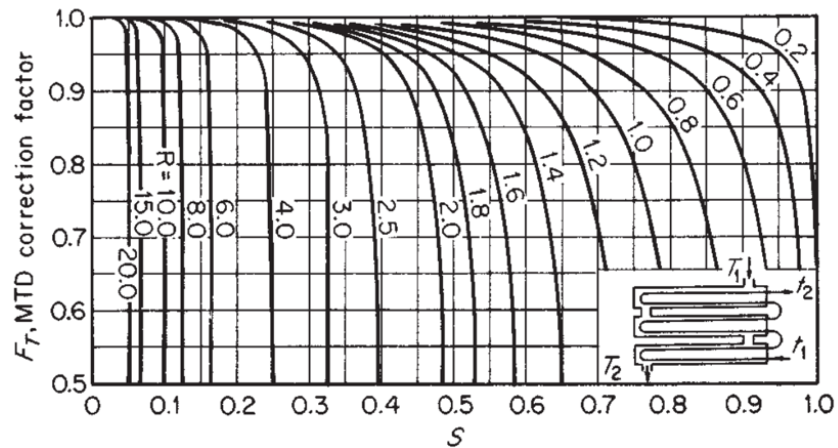


Figure C1.6 Correction factor for a 6 tube passes and 3 shell passes heat exchanger⁵¹⁴.

In the final design, HE2 is composed of 100 tubes, having the same geometrical characteristics as those adopted in the reactors (Table) and the global heat exchange coefficient is:

$$U_{HE2} = \frac{1}{\frac{1}{\bar{h}_{slurry}} + \frac{r_1}{\lambda_{inox}} \cdot \ln \frac{r_2}{r_1} + F_f + \frac{d_1}{d_2 \cdot \bar{h}_{oil}}} = 351.9 \frac{W}{m^2K}$$

The total required surface is:

$$A_{HE2} = \frac{\dot{Q}_{HE2}}{U_{HE2} \cdot \Delta T_{ml}} = 633.9 m^2$$

Assuming a thermal loss of 10% in the oil connection line between the two heat exchangers, the inlet temperature of the diathermic oil in HE1 and the thermal power exchanged are:

$$T_{in\ oil\ HE1} = T_{out\ oil\ HE2} - \frac{Q_{losses}}{c_p \dot{m}_{oil1}} = 235^\circ\text{C}$$

$$\dot{Q}_{HE1} = 13.1\ \text{MW}$$

Based on this assumption, the outlet temperature of the slurry from the heat exchanger was calculated as:

$$T_{out\ HE1} = T_{in\ HE1} + \frac{\dot{Q}_{HE1}}{c_p \cdot \dot{m}_{slurry}} = 224^\circ\text{C}$$

The same equations were used for the design of HE1, the global heat exchange coefficient and logarithmic average temperature are:

$$U_{HE1} = 618.2\ \frac{\text{W}}{\text{m}^2\text{K}}$$

$$\Delta T_{ml} = 64^\circ\text{C}$$

The convection coefficients are shown in Table. The total internal surface area of the tubes required is 346 m². In the final design, HE1 is composed of 85 tubes, having the same geometrical characteristics as those adopted in the reactor (Table C1.4), in a six tube passes and 3 shell passes heat exchanger.

The trim heater brings the slurry to reaction temperature (350°C), the inlet temperature of the slurry was derived from the outlet temperature of the HE1:

$$T_{in\ TH} = 224^\circ\text{C}$$

The required heat transfer rate was calculated with Eq.31 and the process stream temperatures shown in Figure C1.7:

$$\dot{Q}_{TH} = 9.5\ \text{MW}$$

The inlet temperature of the oil is 380°C and the outlet temperature was set at 300°C. The oil mass flow was then calculated:

$$\dot{m}_{oil\ TH} = 47.6\ \frac{\text{kg}}{\text{s}}$$

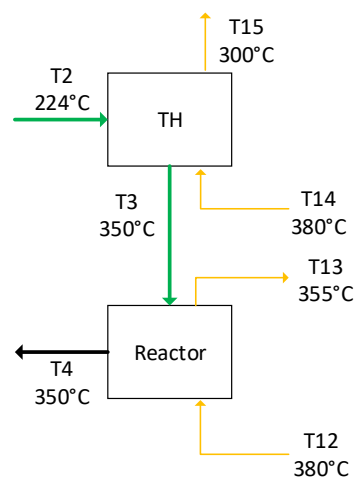


Figure C1.7 Temperature of diathermic oil and process stream in the trim heater and reactors.

The same equations adopted for the design of the other shell and tube heat exchangers were used for the calculation of the global heat exchange coefficient and the logarithmic average temperature, which are:

$$U_{TH} = 397.3 \frac{W}{m^2K}$$

$$\Delta T_{ml,TH} = 46.8^\circ\text{C}$$

The calculated convection coefficients are shown in Table C1.7. The total required internal surface area of tubes required is 512 m². In the final design, TH is composed of 104 tubes in a six tube passes and 3 shell passes heat exchanger.

Table C1.7 Convection coefficients for the tube side and shell side of HE1, HE2 and trim heater.

| Coefficient | HE1 | HE2 | Trim heater |
|---|------------|------------|--------------------|
| Slurry convection coefficient (\bar{h}_{slurry}) [W/m ² K] | 3205.2 | 4455.8 | 4529.1 |
| Oil convection coefficient (\bar{h}_{oil}) [W/m ² K] | 434.8 | 397.8 | 647.6 |

Pumps

The pressurizing step is a critical phase of the HTL process due to the high involved pressures and the particular characteristics of the medium to be pumped, i.e. a viscous fluid with dispersed solid particles. Based on the experiments performed on the cHTL pilot plant RE-CORD, a pneumatic piston pump was considered the most suitable for pumping the biomass-water slurry because it is highly reliable in feeding viscous materials. The power consumption of the pump (HP pump) was calculated with the formula:

$$\dot{W}_{HP\ pump} = \dot{V} \cdot P \cdot \eta_{pump} = 613\ W$$

Where the volumetric flow rate is $\dot{V} = 55244 \frac{kg}{s}$, $P = 20\ MPa$ is the discharge pressure of the pump and $\eta_{pump} = 0.5$ is the overall efficiency⁵²¹.

The water pump and the solution pump are supposed to provide liquids circulation. Centrifugal pumps were selected in this case because the ΔP required are modest and the fluids are at low temperatures and without solids. The efficiencies were calculated with the formula provided in⁵¹⁶, that was derived from multiple vendors data. The hydraulic head was approximated to 45 m, as used in other works⁴⁷⁷. For the oil recirculation in the two oil lines (oil line 1 and 2) two pneumatic piston pumps were selected. The power consumptions were calculated in the same way considering an overall efficiency of 0.5⁵²¹. The power consumption of the dilution conveyor was not calculated but it was scaled from NREL techno-economic analysis⁴⁷⁷.

The back-pressure regulation system was designed as a scale up of the one used in the pilot plant described in Paragraph 3.4 -. The pressure is regulated by an oleo-dynamic circuit connected to the pistons depressurization system and it was designed to keep the pressure at 200 bar in the reaction zone with a lower pressure on the oil side.

Agitator

An anchor agitator was selected in order to create a homogenous solution of Na_2CO_3 and water. The power to drive the impeller (shaft power) was calculated as:

$$\dot{W}_M = N_p N_M^3 D_i^5 \rho_s \text{ Eq. 2}$$

The revolution speed (N_M) was fixed at $70 \frac{\text{rev}}{\text{min}}$, a typical value for anchor impellers⁵²¹. The Reynolds number in the tank and N_p , analogous to a friction factor, was evaluated according to Furukawa et al.⁵²² as:

$$Re = \frac{N_M D_i^2 \rho_{\text{solution}}}{\mu}$$

$$N_p = 94.043 Re^{-0.559}$$

The impeller diameter D_i was calculated through the mixer diameter D_m . The stirred tank volume was fixed at 20 m^3 and a tank height of 4 m. The $\frac{D_i}{D_m} = 0.892$ as proposed by Furukawa et al.⁵²². The solution density and apparent viscosity were considered the same as water because the mass concentration of homogeneous catalyst in water is $\sim 0.5\%$.

Cooling System

Based on the mass flow shown in Figure and the temperature in Figure C1.8, the thermal power for cooling the products was calculated as:

$$Q = \dot{m}_{\text{water}} \cdot c_p \cdot \Delta T_{\text{water}} = 5.1 \text{ MW}$$

The total water mass flow required was then calculated:

$$\dot{m}_{\text{water tot}} = 24.4 \frac{\text{kg}}{\text{s}}$$

The cooler was designed as a shell and tube heat exchanger using the same equation as the others heat exchangers (HE1, HE2 and trim heater). The results of the calculation are shown in Table C1.8.

Table C1.8 Convection coefficients and global heat exchange coefficient for the cooler.

| Coefficient | Cooler |
|---|--------|
| Slurry convection coefficient (\bar{h}_{slurry}) [$\text{W}/\text{m}^2\text{K}$] | 5463.8 |
| Oil convection coefficient (\bar{h}_{water}) [$\text{W}/\text{m}^2\text{K}$] | 1081.3 |
| Global heat exchange coefficient (U) [$\text{W}/\text{m}^2\text{K}$] | 621.8 |
| Surface [m^2] | 132.7 |

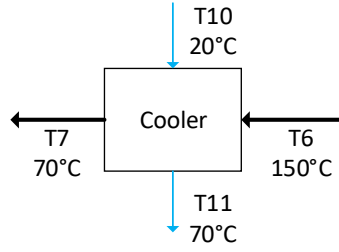


Figure C1.8 Temperature of water and products in the cooling system.

Burner

The thermal power required in the trim heater and in the reactors is provided by a natural gas burner and it was calculated as:

$$\dot{Q}_{out\ burner,net} = \dot{Q}_{TH} + \dot{Q}_{reactors} = 38\ MW$$

The total efficiency of the methane burner can be assumed $\eta_{burner} = 0.8$ and the total thermal power to be provided by the natural gas is:

$$\dot{Q}_{in\ burner} = \frac{\dot{Q}_{out\ burner,net}}{\eta_{burner}} = 47\ MW$$

Considering $h_{year} = 7800 \frac{h}{year}$ of plant operation, the thermal energy per year is:

$$Q_{in\ burner} = \dot{Q}_{in\ burner} \cdot h_{year} = 36.8 \frac{MWh}{year} = 1.33 \cdot 10^9 \frac{MJ}{year}$$

The lower heating value (LHV) of the natural gas is $36.6 \frac{MJ}{Nm^3}$ and the total Nm^3 of natural gas per year are:

$$\dot{V}_{methane} = \frac{Q_{in\ burner}}{LHV_{methane}} = 3.62 \cdot 10^7 \frac{Nm^3}{year}$$

Depressurization System

The depressurization system was considered as a scale up of the pistons system used in the continuous HTL pilot plant previously designed and commissioned. The mass flow of the plant is $15 \frac{kg}{s}$ and the filling time of the cylinder was fixed to 2 minutes. The total volume of products in that time is:

$$V = \dot{V}_{products} \cdot t_{filling} = 1805\ l$$

In order to reduce the cylinders dimensions, the volume of each cylinder was limited to 113 liters by considering 16 pistons that filling up at the same time. In this configuration, the total number of pistons required is 32. The piston stroke is 1.6 meters and the cylinder internal diameter is 0.3 meters.

Energy consumption

The thermal and electrical powers calculated in the previous section for each equipment of the plant are shown in Figure . The electrical power of the separator was obtained from the commercial separator Alfa Laval PX115⁵²³. The installed electrical power of the screw feeder was neglected and the power consumption of the dilution conveyor was derived from NREL techno-economic analysis⁴⁷⁷. The chemical powers in lignin-rich stream, biocrude and solids were evaluated according to:

$$\dot{W}_{chemical} = \dot{m} \cdot HHV$$

In the proposed layout, the following equipment required electric energy: water pump, stirrer, solution pump, dilution conveyor, high pressure pump, oil pump 1 and 2, oil pump of the depressurization system and the separator. The electrical powers required are shown in Table C1.9.

The electric energy consumption of each equipment of the plant was calculated considering $h_{year} = 7800 \frac{h}{year}$ of plant operation:

$$W_e = \dot{W} \cdot h_{year}$$

The electric energy consumption of the oil pump of the depressurization system was calculated considering the commissioning test performed on the continuous HTL plant. The electric motor of the oil pump is activated only during the discharge stroke of one of the pistons of the depressurization system. The total time for filling and discharges the system was considered $t_{tot} = 2.5 \text{ min}$, $t_f = 2 \text{ min}$ for the filling and $t_d = 30 \text{ s}$ for the discharge stroke. The total operating hours of the oil pump was:

$$h_{oil \text{ pump}} = \frac{h_{year}}{t_{tot}} = 1200 \frac{h}{year}$$

The electricity consumption per year of the equipment of the plant is shown in Table C1.9.

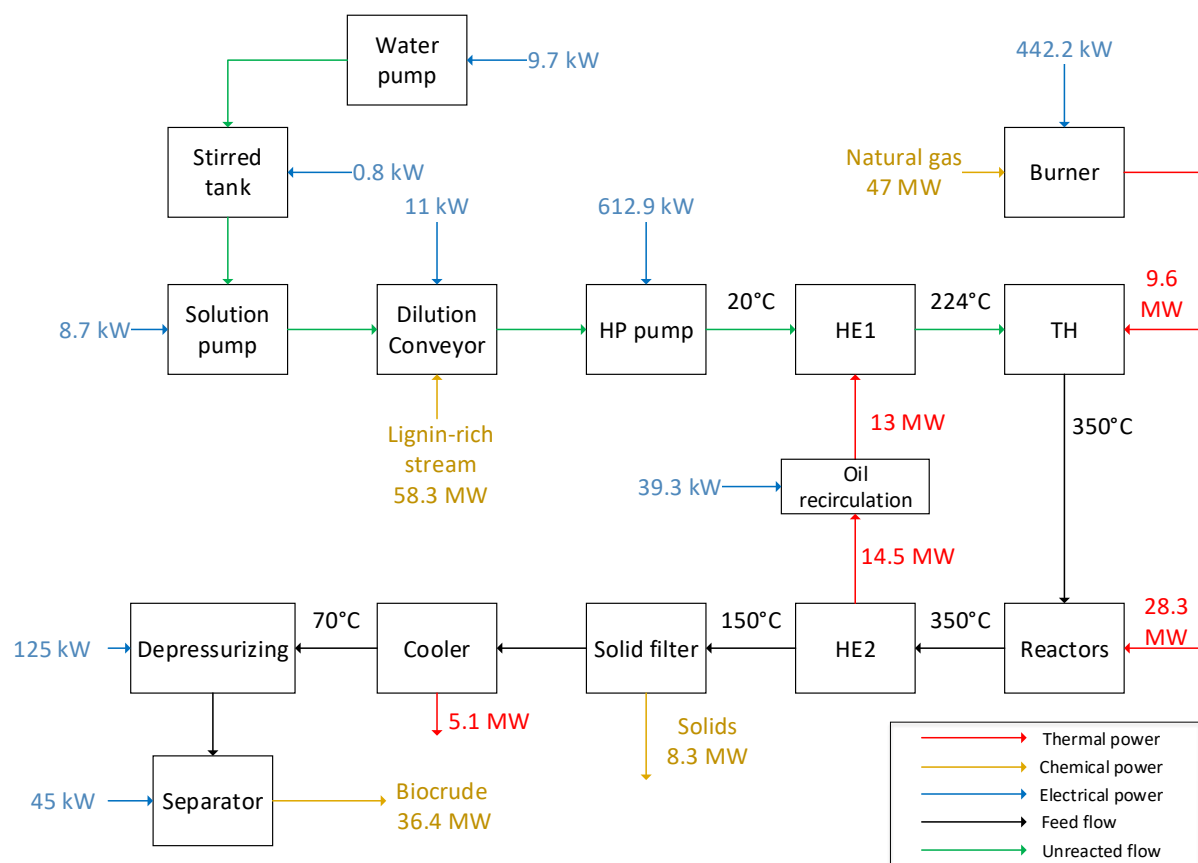


Figure C1.9 Thermal and electrical power for the equipment of the HTL plant.

Table C1.9 Electricity consumption per equipment per year.

| Equipment | Electrical power [kW] | Electricity consumption |
|-------------------|-----------------------|-------------------------|
| | | [MWh/year] |
| Water pump | 9.7 | 74.1 |
| Stirrer | 0.8 | 5.9 |
| Solution pump | 8.7 | 67.6 |
| Dilution conveyor | 4.7 | 36.6 |
| HP pump | 612.9 | 4718 |
| Oil pump 1 | 39.3 | 30.6 |
| Oil pump 2 | 442.2 | 3448.8 |
| Oil pump 3 | 125.1 | 975.7 |
| Separator | 45.0 | 351 |
| Total | 1288.3 | 10048.5 |

The thermal efficiency is the ratio between the chemical power in the biocrude coming out of the plant and the chemical power provided by the natural gas in the burner. The plant efficiency was evaluated and, differently from thermal efficiency, contains in the denominator the chemical power of the inlet feedstock and the electrical power consumption of the plant.

$$\eta_{th} = \frac{\dot{W}_{bc}}{\dot{W}_{ng}} = \frac{\dot{m}_{bc} \cdot HHV_{bc}}{\dot{m}_{ng} \cdot HHV_{ng}} = 77\%$$

$$\eta_{plant} = \frac{\dot{W}_{bc}}{\dot{W}_{ng} + \dot{W}_{el} + \dot{W}_{LRS}} = \frac{\dot{m}_{bc} \cdot HHV_{bc}}{\dot{m}_{ng} \cdot HHV_{ng} + \dot{W}_{el} + \dot{m}_{LRS} \cdot HHV_{LRS}} = 34\%$$

The chemical efficiency was calculated as the ratio between the chemical power of biocrude and the chemical power of the inlet biomass:

$$\eta_{ch} = \frac{\dot{m}_{bc} \cdot HHV_{bc}}{\dot{m}_{LRS} \cdot HHV_{LRS}} = 62.4\%$$

The specific thermal consumption is the ratio between the total thermal energy provided with natural gas per year and the annual biocrude production and it is 10.1 kWh_{th}/kg_{biocrude} for this plant configuration. The specific electric consumption is 0.28 kWh_{el}/kg_{biocrude} calculated as the ratio between the annual electricity consumption and the annual biocrude production.

The carbon efficiency is defined as the ratio between the carbon mass flow in the biocrude coming out of the plant and the carbon mass flow inlet with LRS:

$$\eta_{C\%} = \frac{\dot{m}_{bc} \cdot C\%_{bc}}{\dot{m}_{LRS} \cdot C\%_{LRS}} = 61\%$$

Appendix C2 – HTL TEA data

The cost indexes used in the TEA analysis for updating the equipment values are calculated by the use of this equation:

$$2018 \text{ Costs} = \text{Base Cost} \cdot \frac{2018 \text{ Cost Index}}{\text{Base Cost Index}}$$

While the index values are summarized in Table C2.1

Table C2.1. Cost indexes considered in the economic analysis

| Year | 2011 | 2012 | 2018 |
|------------|-------|-------|-------|
| Cost index | 585.7 | 575.4 | 603.1 |

The model changes in capacity and size of equipment were adjusted using an exponential scaling method accordingly to an exponential scaling calculation.

$$\text{New Cost} = \text{Base Cost} \cdot \left(\frac{\text{New size}}{\text{Base size}} \right)^n$$

The scaling exponent (n) is based on some characteristics of the equipment and they are summarized in Table C2.2 and were adopted from the NREL studies by Knorr et al.⁵²⁴

Table C2.2 Scaling exponents of the equipment prices.⁵²⁴

| Item | Exponent |
|----------------------------------|----------|
| Agitators | 0.5 |
| Compressor, motor driven | 0.6 |
| Heat Exchangers | 0.7 |
| Inline mixers | 0.5 |
| Package quotes/skidded equipment | 0.6 |
| Pressure vessels | 0.7 |
| Pumps | 0.8 |
| Tanks, atmospheric | 0.7 |
| Solids handling equipment | 0.8 |

In order to obtain the installed cost of the equipment, a factored approach was chosen as described using the installation factors listed in Knorr et al.⁵²⁴ and report in Figure C2.1:

$$\text{Installed Cost} = \text{Purchased Equipment Cost} \cdot \text{Installation factor}$$

| Item | Multiplier ^a |
|--|-------------------------|
| Agitators, stainless steel | 1.5 |
| Boiler | 1.8 |
| Compressors, motor driven | 1.6 |
| Heat exchangers, shell and tube, stainless steel | 2.2 |
| Heat exchangers, double pipe, stainless steel | 2.2 |
| Inline mixers | 1.0 |
| Skidded equipment | 1.8 |
| Solids handling equipment (including filters) | 1.7 |
| Pressure vessels, stainless steel | 2.0 |
| Pumps, stainless steel | 2.3 |
| Tanks, field erected stainless steel | 1.5 |

Figure C2.1. Equipment installation factors from Knorr et al.⁵²⁴

A list of the installation factors is shown in Figure C2.1. A complete list of equipment with purchased and installed cost is provided in Table C2.4. The sum of all the equipment installed cost is called inside-battery-limit (ISBL) cost. The ISBL is defined as all equipment and associated components (piping, etc.) that act upon the primary feed stream of a process. The other direct costs were based on the ISBL cost (Figure C2.2). The sum of ISBL cost and other direct costs is the total direct cost (TDC). The indirect costs were expressed in relations of the TDC (Figure C2.2) and the sum of TDC with indirect cost is the fixed capital investment (FCI). The working capital is defined as the difference between current assets and current liability and, in this work, it was based on the FCI.

| Item | Description | Amount |
|--------------------------------|--|--------------------------------|
| Additional Direct Costs | | |
| Warehouse | On-site storage of equipment and supplies | 4% of installed equipment cost |
| Site development | Fencing, curbing, parking lot, roads, drainage, general paving. This allows for minimum site development assuming a clear site with no unusual problems. | 9% of ISBL |
| Additional piping | To connect ISBL equipment to storage and utilities | 4.5% of ISBL |
| Indirect Costs | | |
| Proratable expenses | This includes fringe benefits, burdens, and insurance of the construction contractor | 10% of total direct cost (TDC) |
| Field expenses | Consumables, small tool and equipment rental, field services, temporary construction facilities, and field construction supervision | 10% of TDC |
| Home office and construction | Engineering plus incidentals, purchasing, and construction | 20% of TDC |
| Project contingency | Extra cash on hand for unforeseen issues during construction | 10% of TDC |
| Other costs | Start-up, commissioning costs. Land, rights of way, permits, and fees. Piling, soil compaction, unusual foundations. Sales, use, and other taxes. Freight, insurance in transit, and import duties on equipment. Overtime pay during construction. Field insurance. Project team. Transportation equipment, bulk shipping containers, plant vehicles, etc. | 10% of TDC |

Figure C2.2. Indirect cost and other direct cost descriptions and amounts from Knorr et al.⁵²⁴

The operating costs were divided in fixed and variable. Fixed operating costs include employee salaries, overhead and maintenance, property insurance, maintenance capital. The number of employees was considered equal to the one reported in the PNNL report⁵²⁵, the employee salaries were converted to Euro and scaled to the base year 2018. The overhead and maintenance cost were based on the labor cost, the maintenance capital was based on TCI and the insurance and taxes on the FCI.⁵²⁵ Natural gas, electricity, sodium carbonate, wastewater treatment and make up water were considered as variable costs per year. The natural gas cost, the electricity cost and the wastewater treatment cost per year were estimated as 0.15 €/m³, 0.067 €/kWh and 0.0137 €/kg respectively, as suggested by Lucian et al.⁵²¹ The sodium carbonate cost per year was considered 0.278 €/kg⁵²⁴ and for the water make up 0.18 €/ton. The results of the calculations for the total capital investment (TCI) and the operating costs are shown Table C2.3. While Figure C2.3 shows the costs distribution for the HTL plant, highlighting that about 34% of the TCI is due to the equipment cost and, among these, about 26% is due to the HTL reaction section.

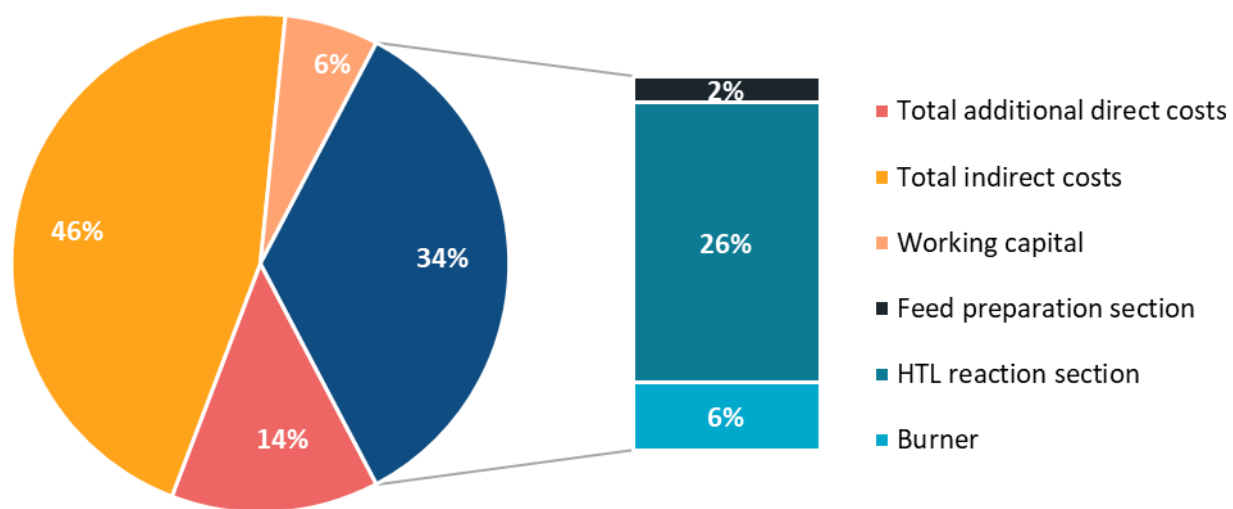


Figure C2.3. Total capital investment cost distribution

Table C2.3 Total capital investment and operating costs for the HTL plant

| Equipment | | Operating Cost | |
|---|---------------------|--------------------------|---------------------|
| Make Up Water pump | 208,857 € | Total Methane Cost/year | 5,431,786 € |
| Na ₂ CO ₃ Sack Feeder | 54,600 € | Property Insurance | 5,068,078 € |
| Na ₂ CO ₃ Solution agitator | 55,815 € | Electricity | 669,239 € |
| Na ₂ CO ₃ Make Up Tank | 117,106 € | Water make-up | 34,320 € |
| Solution Pump | 17,268 € | Homogeneous catalyst | 527,903 € |
| Dilution Conveyor | 64,514 € | Labour Cost | 729,000 € |
| HP pump + Twin Screw Feeder | 947,194 € | Overhead and maintenance | 656,100 € |
| Feed preparation | 1,465,355 € | Maintenance Capital | 2,280,635 € |
| HE1 | 1,229,031 € | Wastewater Treatment | 5,227,447 € |
| Trim Heater | 1,945,683 € | Total | 17,316,017 € |
| Reactor | 3,133,317 € | | |
| HE2 | 2,259,730 € | | |
| Solid Filter | 404,091 € | | |
| Cooler | 100,859 € | | |
| Separator | 968,382 € | | |
| Piston System+pumps | 5,283,208 € | | |
| HTL reaction section | 15,324,301 € | | |
| Burner | 3,686,238 € | | |
| Total ISBL cost | 20,475,894 € | | |
| Additional direct cost | | | |
| Warehouse | 1,489,735 € | | |
| Site development | 3,351,903 € | | |
| Buildings | 1,489,735 € | | |
| Additional piping | 1,675,952 € | | |
| Total additional direct cost | 8,007,325 € | | |
| Total direct cost (TDC) | 45,250,695 € | | |
| Indirect Cost | | | |
| Proratable expenses | 4,525,070 € | | |
| Field expenses | 4,525,070 € | | |
| Home office and construction | 9,050,139 € | | |
| Project contingency | 4,525,070 € | | |
| Other cost | 4,525,070 € | | |
| Total Indirect Cost | 27,150,417 € | | |
| Fixed Capital Investment (FCI) | 72,401,112 € | | |
| Working Capital | 3,620,056 € | | |
| Total Capital Investment (TCI) | 76,021,168 € | | |

Table C2.4. Equipment cost calculations

| Trim heater | HE1 | HP pump and twin-screw | Dilution conveyor | Solution pump | Solution tank | Solution agitator | Sack feeder | Water pump | | | | | | |
|----------------------|----------------------|------------------------|-----------------------|----------------------|-------------------------|-------------------|---------------------|----------------------|------------|-----------------------|--------------------------------|------------------------------|-----------------|------------|
| | Reference price | Year of quote | Scaling variable | Scaling value | Converted scaling value | Scaling exponents | Installation factor | New value | Size ratio | Scaled purchased cost | Purchased cost in project year | Install cost in project year | n° of equipment | Total cost |
| 898.965,00 € | 898.965,00 € | 328.230,00 € | 84.870,00 € | 9.837,00 € | 81.414,00 € | 36.565,20 € | 54.600,00 € | 7.830,00 € | | | | | | |
| 2012 | 2012 | 2011 | 2012 | 2012 | 2012 | 2012 | 2012 | 2012 | | | | | | |
| Duty | Area | Pump Feed | Feed Rate | Pump Feed | Capacity | Diameter | N/A | Pump Feed | | | | | | |
| 6032 ft ² | 6032 ft ² | 190 gpm | 353304 $\frac{lb}{h}$ | 300 gpm | 15000 gal | 8 ft | N/A | 10 gpm | | | | | | |
| 560 m ² | 560 m ² | 43153 $\frac{kg}{h}$ | 160229 $\frac{kg}{h}$ | 68136 $\frac{kg}{h}$ | 56775 L | 2.4 | N/A | 2271 $\frac{kg}{h}$ | | | | | | |
| 0,7 | 0,7 | 0,8 | 0,8 | 0,8 | 0,7 | 0,5 | N/A | 0,8 | | | | | | |
| 2,2 | 2,2 | 2,3 | 1,7 | 2,3 | 1,5 | 1,5 | 1,7 | 2,3 | | | | | | |
| 478 m ² | 455 m ² | 55244 $\frac{kg}{h}$ | 55244 $\frac{kg}{h}$ | 39661 $\frac{kg}{h}$ | 50000 L | 2.3 | N/A | 45833 $\frac{kg}{h}$ | | | | | | |
| 0,91 | 1,62 | 1,28 | 0,34 | 0,67 | 0,24 | 0,94 | N/A | 20,18 | | | | | | |
| 843.781 € | 640.716 € | 399.942 € | 36.207 € | 7.163 € | 74.485 € | 35.501 € | 54.600 € | 86.637 € | | | | | | |
| 884.401 € | 671.560 € | 411.823 € | 37.950 € | 7.508 € | 78.071 € | 37.210 € | 57.228 € | 90.808 € | | | | | | |
| 1.945.683 € | 1.477.433 € | 947.194 € | 64.514 € | 17.268 € | 117.106 € | 55.815 € | 97.288 € | 208.857 € | | | | | | |
| 1 | 1 | 1 | 1 | 1 | 1 | 1 | 1 | 1 | | | | | | |
| 1.945.683 € | 1.477.433 € | 947.194 € | 64.514 € | 17.268 € | 117.106 € | 55.815 € | 97.288 € | 208.857 € | | | | | | |

| Cooling water pump | Cooling tower system | Oil pump 2 | Oil pump 1 | Depressurizati on system | Separator | Cooler | Solid filter | Burner | HE2 | Reactor |
|----------------------|------------------------|------------------------|-----------------------|--------------------------|-----------------------|-----------------------|-----------------------|----------------------|----------------------|----------------------|
| 9.837,00 € | 5.310,00 € | 9.837,00 € | 9.837,00 € | 3.380,00 € | 3.208.500,00 € | 230.040,00 € | 1.179.900,00 € | 1.080.450,00 € | 898.965,00 € | 693.892,80 € |
| 2013 | 2013 | 2012 | 2012 | 2018 | 2011 | 2012 | 2011 | 2012 | 2012 | 2011 |
| Water Flow | Water Flow | Pump Feed | Pump Feed | Volume (2 cylinders) | Separator Feed | Area | Filter feed | Duty | Area | Mass flow |
| 300 gpm | 150 gpm | 300 gpm | 300 gpm | 1 L | 3689 gpm | 13020 ft ² | 3689 gpm | 60 $\frac{MMBtu}{h}$ | 6032 ft ² | 33333 $\frac{lb}{h}$ |
| 68136 $\frac{kg}{h}$ | 34068,0 $\frac{kg}{h}$ | 68136 $\frac{kg}{h}$ | 68136 $\frac{kg}{h}$ | 1 L | 837845 $\frac{kg}{h}$ | 1209 m ² | 837845 $\frac{kg}{h}$ | 17584 kW | 560 m ² | 15117 $\frac{kg}{h}$ |
| 0,6 | 0,6 | 0,8 | 0,8 | 0,7 | 0,7 | 0,7 | 0,6 | 0,6 | 0,7 | 1 |
| 4 | 10 | 2,3 | 2,3 | 2,2 | 2 | 2,2 | 1,7 | 1,8 | 2,2 | 1,2 |
| 88000 $\frac{kg}{h}$ | 88000 $\frac{kg}{h}$ | 1489879 $\frac{kg}{h}$ | 128744 $\frac{kg}{h}$ | 226 L | 55000 $\frac{kg}{h}$ | 78.2 m ² | 55244 $\frac{kg}{h}$ | 3882,3 kW | 264.5 m ² | 15117 $\frac{kg}{h}$ |
| 1.29 | 2.58 | 5.29 | 2.35 | 226 | 0.06 | 0.11 | 0.07 | 2.68 | 1.13 | 0.91 |
| 11.469,02 € | 9.384 € | 37.304 € | 19.490 € | 150.091 € | 470.222 € | 48.975 € | 230.843 € | 1.953.851 € | 979.974 € | 633.941 € |
| 12.021 € | 9.835 € | 39.100 € | 20.428 € | 150.091 € | 484.191 € | 51.332 € | 237.701 € | 2.047.910 € | 1.027.150 € | 652.774 € |
| 48.085 € | 98.355 € | 89.931 € | 46.985 € | 330.200 € | 968.382 € | 112.931 € | 404.091 € | 3.686.238 € | 2.259.730 € | 783.329 € |
| 1 | 1 | 5 | 1 | 16 | 1 | 1 | 1 | 1 | 1 | 4 |
| 48.085 € | 98.355 € | 449.654 € | 46.985 € | 5.283.208 € | 968.382 € | 112.931 € | 404.091 € | 3.686.238 € | 2.259.730 € | 3.133.317 € |

Appendix C3 – Minimum Biocrude Selling Price

The MBSP is defined as the plant gate selling price of the product that makes the net present value of the project equal to zero.⁵²⁵ The base scenario was calculated using a discounted cash flow rate of return analysis with 10% internal rate of return (i) over 30 years plant life (n). A tax rate (t_6) of 37% was considered for the analysis.⁵²¹ The modelled biocrude has a higher heating value of 28 MJ/kg and the total biocrude production per year is $BP = 36465$ tonnes/year. A straight-line depreciation was evaluated over a period of 30 year for the total equipment cost (ISBL). The plant salvage value after 30 year was considered equal to zero so the annual depreciation is:

$$d_k = \frac{ISBL - SV_{30}}{n} = 1.2 \text{ M€}$$

The return of investment (ROI) over the 30 years plant life was calculated as:

$$ROI = \frac{i(1+i)^n}{(1+i)^n - 1} \cdot TCI = 8.1 \text{ M€}$$

The total operating costs (OC) of the plant are 17.2 M€ and the income taxes per year could be calculated as:

$$IT = t_r \cdot (BR - OC - d_k)$$

Then the biocrude revenue per year (BR) was evaluated according to:

$$BR = OC + \frac{ROI}{1 - t_r} - \frac{DC \cdot t_r}{1 - t_r} = 23.9 \text{ M€}$$

The minimum biocrude selling price is:

$$MBSP_{\text{€}} = \frac{BR}{BP} = 0.66 \frac{\text{€}}{\text{kg}} = 2.37 \frac{\text{€}}{\text{gal}}$$

In order to calculate the MBSP in \$ per gasoline gallon equivalent (gge), the gasoline HHV was considered 43.34 MJ/kg and the MBSP per gasoline gallon equivalent is:

$$MBSP_{\text{gge}} = MBSP_{\text{€}} \cdot \frac{HHV_g}{HHV_{bc}} = 3.10 \frac{\$}{\text{gge}}$$

The influence of the TCI and O&M costs on MBSP is shown in Figure C3.1. The estimated MBSP is in good agreement with literature data, where the HTL biocrude has been estimated in similar ranges. Snowden-Swan et al.⁵²⁵ estimated a MBSP of 2.35 \$/gge for HTL of sewage sludge while Watson et al.⁵²⁶ reported a range of 5-16 \$/gge for HTL of algae.

References

- (1) Lindorfer, J.; Lettner, M.; Hesser, F.; Fazeni, K.; Rosenfeld, D.; Annevelink, B.; Mandl, M. *Technical, Economic and Environmental Assessment of Biorefinery Concepts*; 2019.
- (2) Stahel, W. R. The Circular Economy. *Nature* **2016**, *531* (7595), 435–438. <https://doi.org/10.1038/531435a>.
- (3) US EPA, O. Overview for Renewable Fuel Standard.
- (4) US EPA, O. Clean Air Act Text.
- (5) Intergovernmental Panel on Climate Change (IPCC). *Climate Change 2014 Mitigation of Climate Change*; 2014. <https://doi.org/10.1017/cbo9781107415416>.
- (6) Bidy, M. J.; Scarlata, C. J.; Kinchin, C. M. Chemicals from Biomass: A Market Assessment of Bioproducts with near-Term Potential. *NREL Rep.* **2016**, No. March. <https://doi.org/10.2172/1244312>.
- (7) Home - Task 42 <http://task42.ieabioenergy.com/> (accessed Aug 24, 2020).
- (8) Bakker, R.; den Uil, H.; v Ree, R. v. Financieel-Economische Aspecten van Biobrandstofproductie. *WUR Food Biobased Res.* **2010**, No. January 2012.
- (9) de Jong, E.; Stichnothe, H.; Bell, G.; Jørgensen, H. *Bio-Based Chemicals. A 2020 Update*; 2020.
- (10) Dutta, A.; Iisa, M. K.; Talmadge, M.; Mukarakate, C.; Griffin, M. B.; Tan, E. C.; Wilson, N.; Yung, M. M.; Nimlos, M. R.; Schaidle, J. A.; Wang, H.; Thorson, M.; Hartley, D.; Klinger, J.; Cai, H. *Ex Situ Catalytic Fast Pyrolysis of Lignocellulosic Biomass to Hydrocarbon Fuels: 2018 State of Technology and Future Research*; 2018. <https://doi.org/10.2172/1605092>.
- (11) Zeng, J.; Tong, Z.; Wang, L.; Zhu, J. Y.; Ingram, L. Isolation and Structural Characterization of Sugarcane Bagasse Lignin after Dilute Phosphoric Acid plus Steam Explosion Pretreatment and Its Effect on Cellulose Hydrolysis. *Bioresour. Technol.* **2014**, *154*, 274–281. <https://doi.org/10.1016/j.biortech.2013.12.072>.
- (12) Hongzhang, C.; Liying, L. Unpolluted Fractionation of Wheat Straw by Steam Explosion and Ethanol Extraction. *Bioresour. Technol.* **2007**, *98* (3), 666–676. <https://doi.org/10.1016/j.biortech.2006.02.029>.
- (13) Brandt-Talbot, A.; Gschwend, F. J. V.; Fennell, P. S.; Lammens, T. M.; Tan, B.; Weale, J.; Hallett, J. P. An Economically Viable Ionic Liquid for the Fractionation of Lignocellulosic Biomass. *Green Chem.* **2017**, *19* (13), 3078–3102. <https://doi.org/10.1039/c7gc00705a>.
- (14) Tu, W. C.; Hallett, J. P. Recent Advances in the Pretreatment of Lignocellulosic Biomass. *Curr. Opin. Green Sustain. Chem.* **2019**, *20*, 11–17. <https://doi.org/10.1016/j.cogsc.2019.07.004>.
- (15) Dell'Orco, S.; Rizzo, A. M.; Buffi, M.; Chiaramonti, D. Design of a Circulating Fluidized Bed Combustor for Lignin-Rich Residue Derived from Second-Generation Bioethanol Production Plant. *Chem. Eng. Trans.* **2018**, *65*. <https://doi.org/10.3303/CET1865047>.
- (16) Tribot, A.; Amer, G.; Abdou Alio, M.; de Baynast, H.; Delattre, C.; Pons, A.; Mathias, J. D.; Callois, J. M.; Vial, C.; Michaud, P.; Dussap, C. G. Wood-Lignin: Supply, Extraction Processes and Use as Bio-Based Material. *Eur. Polym. J.* **2019**, *112* (January), 228–240. <https://doi.org/10.1016/j.eurpolymj.2019.01.007>.
- (17) Ragauskas, A. J.; Beckham, G. T.; Bidy, M. J.; Chandra, R.; Chen, F.; Davis, M. F.; Davison, B. H.; Dixon, R. A.; Gilna, P.; Keller, M.; Langan, P.; Naskar, A. K.; Saddler, J. N.; Tschaplinski, T. J.; Tuskan, G. A.; Wyman, C. E. Lignin Valorization: Improving Lignin Processing in the Biorefinery. *Science* (80-.). **2014**, *344*. <https://doi.org/10.1126/science.1246843>.
- (18) Azadi, P.; Inderwildi, O. R.; Farnood, R.; King, D. A. Liquid Fuels, Hydrogen and Chemicals from Lignin: A Critical Review. *Renew. Sustain. Energy Rev.* **2013**, *21*, 506–523. <https://doi.org/10.1016/j.rser.2012.12.022>.
- (19) Schuler, J.; Hornung, U.; Kruse, A.; Dahmen, N.; Sauer, J. Hydrothermal Liquefaction of Lignin. *J. Biomater. Nanobiotechnol.* **2017**, *08* (01), 96–108. <https://doi.org/10.4236/jbnb.2017.81007>.
- (20) Alekhina, M.; Ershova, O.; Ebert, A.; Heikkinen, S.; Sixta, H. Softwood Kraft Lignin for Value-Added Applications: Fractionation and Structural Characterization. *Ind. Crops Prod.* **2015**, *66*, 220–228. <https://doi.org/10.1016/j.indcrop.2014.12.021>.
- (21) Varanasi, P.; Singh, P.; Auer, M.; Adams, P. D.; Simmons, B. A.; Singh, S. Survey of Renewable Chemicals Produced from Lignocellulosic Biomass during Ionic Liquid Pretreatment. *Biotechnol. Biofuels* **2013**, *6* (1), 1. <https://doi.org/10.1186/1754-6834-6-14>.
- (22) Holladay, J. E.; White, J. F.; Bozell, J. J.; Johnson, D. Top Value-Added Chemicals from Biomass Volume II — Results of Screening for Potential Candidates from Biorefinery Lignin. Prepared for the U.S. Department of Energy under Contract DE-AC05-76RL01830. **2007**, *II* (October).
- (23) Schutyser, W.; Renders, T.; Van Den Bosch, S.; Koelewijn, S. F.; Beckham, G. T.; Sels, B. F. Chemicals from Lignin: An Interplay of Lignocellulose Fractionation, Depolymerisation, and Upgrading. *Chem. Soc. Rev.* **2018**, *47* (3), 852–908. <https://doi.org/10.1039/c7cs00566k>.
- (24) Ten, E.; Vermerris, W. Recent Developments in Polymers Derived from Industrial Lignin, 2015. <https://doi.org/10.1002/app.42069>.
- (25) Gillet, S.; Aguedo, M.; Petitjean, L.; Morais, A. R. C.; Da Costa Lopes, A. M.; Łukasik, R. M.; Anastas, P. T. Lignin Transformations for High Value Applications: Towards Targeted Modifications Using Green

- Chemistry. *Green Chem.* **2017**, *19* (18), 4200–4233. <https://doi.org/10.1039/c7gc01479a>.
- (26) Graichen, F. H. M.; Grigsby, W. J.; Hill, S. J.; Raymond, L. G.; Sanglard, M.; Smith, D. A.; Thorlby, G. J.; Torr, K. M.; Warnes, J. M. Yes, We Can Make Money out of Lignin and Other Bio-Based Resources. *Ind. Crops Prod.* **2017**, *106*, 74–85. <https://doi.org/10.1016/j.indcrop.2016.10.036>.
- (27) Bridgwater, A. V.; Peacocke, G. V. C. Fast Pyrolysis Processes for Biomass. *Renew. Sustain. energy Rev.* **2000**, *4* (1), 1–73. [https://doi.org/10.1016/S1364-0321\(99\)00007-6](https://doi.org/10.1016/S1364-0321(99)00007-6).
- (28) Mukarakate, C.; Zhang, X.; Stanton, A. R.; Robichaud, D. J.; Ciesielski, P. N.; Malhotra, K.; Donohoe, B. S.; Gjersing, E.; Evans, R. J.; Heroux, D. S.; Richards, R.; Iisa, K.; Nimlos, M. R. Real-Time Monitoring of the Deactivation of HZSM-5 during Upgrading of Pine Pyrolysis Vapors. *Green Chem.* **2014**, *16* (3), 1444–1461. <https://doi.org/10.1039/C3GC42065E>.
- (29) Mukarakate, C.; Mcbrayer, J. D.; Evans, T. J.; Budhi, S.; Robichaud, D. J.; Iisa, K.; Ten Dam, J.; Watson, M. J.; Baldwin, R. M.; Nimlos, M. R. Catalytic Fast Pyrolysis of Biomass: The Reactions of Water and Aromatic Intermediates Produces Phenols. *Green Chem.* **2015**, *17* (8), 4217–4227. <https://doi.org/10.1039/c5gc00805k>.
- (30) Murugappan, K.; Mukarakate, C.; Budhi, S.; Shetty, M.; Nimlos, M. R.; Román-Leshkov, Y. Supported Molybdenum Oxides as Effective Catalysts for the Catalytic Fast Pyrolysis of Lignocellulosic Biomass. *Green Chem.* **2016**, *18* (20), 5548–5557. <https://doi.org/10.1039/c6gc01189f>.
- (31) Iisa, K.; French, R. J.; Orton, K. A.; Dutta, A.; Schaidle, J. A. Production of Low-Oxygen Bio-Oil via Ex Situ Catalytic Fast Pyrolysis and Hydrotreating. *Fuel* **2017**, *207*, 413–422. <https://doi.org/https://doi.org/10.1016/j.fuel.2017.06.098>.
- (32) Bridgwater, A. V. Review of Fast Pyrolysis of Biomass and Product Upgrading. *Biomass and Bioenergy* **2012**, *38*, 68–94. <https://doi.org/10.1016/j.biombioe.2011.01.048>.
- (33) Stefanidis, S. D.; Kalogiannis, K. G.; Lappas, A. A. Co-Processing Bio-Oil in the Refinery for Drop-in Biofuels via Fluid Catalytic Cracking. *Wiley Interdiscip. Rev. Energy Environ.* **2018**, *7* (3), 1–18. <https://doi.org/10.1002/wene.281>.
- (34) Baldwin, R. M.; Feik, C. J. Bio-Oil Stabilization and Upgrading by Hot Gas Filtration. *Energy & Fuels* **2013**, *27* (6), 3224–3238. <https://doi.org/10.1021/ef400177t>.
- (35) Davidson, S. D.; Lopez-Ruiz, J. A.; Zhu, Y.; Cooper, A. R.; Albrecht, K. O.; Dagle, R. A. Strategies to Valorize Hydrothermal Liquefaction-Derived Aqueous Phase into Fuels and Chemicals. *ACS Sustain. Chem. Eng.* **2019**, *accsuschemeng.9b05308*. <https://doi.org/10.1021/accsuschemeng.9b05308>.
- (36) Tomasi Morgano, M.; Leibold, H.; Richter, F.; Seifert, H. Screw Pyrolysis with Integrated Sequential Hot Gas Filtration. *J. Anal. Appl. Pyrolysis* **2015**, *113*, 216–224. <https://doi.org/10.1016/j.jaap.2014.12.019>.
- (37) De Wild, P.; Reith, H.; Heeres, E. *Biomass Pyrolysis for Chemicals*; 2011; Vol. 2. <https://doi.org/10.4155/bfs.10.88>.
- (38) Wilson, A. N.; Dutta, A.; Black, B. A.; Mukarakate, C.; Schaidle, J. A.; Michener, W. E.; Beckham, G. T.; Nimlos, M. R. Valorization of Aqueous Waste Streams from Thermochemical Biorefineries. *Green Chem.* **2019**, Accepted. <https://doi.org/10.1039/c9gc00902g>.
- (39) Wilson, A. N.; Price, M. J.; Mukarakate, C.; Katahira, R.; Gri, M. B.; Dorgan, J. R.; Olstad, J.; Magrini, K. A.; Nimlos, M. R. Integrated Biorefining: Coproduction of Renewable Resol Biopolymer for Aqueous Stream Valorization. **2017**. <https://doi.org/10.1021/accsuschemeng.7b00864>.
- (40) FAO. *The Future of Food and Agriculture – Alternative Pathways to 2050*; 2018.
- (41) How to Feed the World. In *How to Feed the World*; FAO, Ed.; Rome, 12–13 October 2009, 2018; pp 1–250. <https://doi.org/10.5822/978-1-61091-885-5>.
- (42) Eise, J.; Foster, K. *How to Feed the World*; Eise, J., Alan Foster, K., Eds.; Island Press: Washington, DC, 2018. <https://doi.org/10.5822/978-1-61091-885-5>.
- (43) Capel, P. D.; McCarthy, K. A.; Coupe, R. H.; Grey, K. M.; Amenumey, S. E.; Baker, N. T.; Johnson, R. L. Agriculture — A River Runs through It — The Connections between Agriculture and Water Quality. *Circular* **2018**, 1–201. <https://doi.org/10.3133/cir1433>.
- (44) Suqi, L.; Caceres, L.; Schieck, K.; Booker, C. J.; McGarvey, B. M.; Yeung, K. K. C.; Pariente, S.; Briens, C.; Berruti, F.; Scott, I. M. Insecticidal Activity of Bio-Oil from the Pyrolysis of Straw from Brassica Spp. *J. Agric. Food Chem.* **2014**, *62* (16), 3610–3618. <https://doi.org/10.1021/jf500048t>.
- (45) Campisi, T.; Samorì, C.; Torri, C.; Barbera, G.; Foschini, A.; Kiwan, A.; Galletti, P.; Tagliavini, E.; Pasteris, A. Chemical and Ecotoxicological Properties of Three Bio-Oils from Pyrolysis of Biomasses. *Ecotoxicol. Environ. Saf.* **2016**, *132*, 87–93. <https://doi.org/10.1016/j.ecoenv.2016.05.027>.
- (46) Bedmutha, R.; Booker, C. J.; Ferrante, L.; Briens, C.; Berruti, F.; Yeung, K. K. C.; Scott, I.; Conn, K. Insecticidal and Bactericidal Characteristics of the Bio-Oil from the Fast Pyrolysis of Coffee Grounds. *J. Anal. Appl. Pyrolysis* **2011**, *90* (2), 224–231. <https://doi.org/10.1016/j.jaap.2010.12.011>.
- (47) Booker, C. J.; Bedmutha, R.; Vogel, T. Pesticide Properties of Tobacco Bio-Oil. 1–14.
- (48) Hossain, M. M.; Scott, I. M.; McGarvey, B. D.; Conn, K.; Ferrante, L.; Berruti, F.; Briens, C. Toxicity of Lignin, Cellulose and Hemicellulose-Pyrolyzed Bio-Oil Combinations: Estimating Pesticide Resources. *J. Anal. Appl. Pyrolysis* **2013**, *99*, 211–216. <https://doi.org/10.1016/j.jaap.2012.07.008>.

- (49) Hossain, M. M.; Scott, I. M.; McGarvey, B. D.; Conn, K.; Ferrante, L.; Berruti, F.; Briens, C. Insecticidal and Anti-Microbial Activity of Bio-Oil Derived from Fast Pyrolysis of Lignin, Cellulose, and Hemicellulose. *J. Pest Sci.* (2004). **2015**, 88 (1), 171–179. <https://doi.org/10.1007/s10340-014-0568-4>.
- (50) Booker, C. J.; Bedmutha, R.; Vogel, T.; Gloor, A.; Xu, R.; Ferrante, L.; Yeung, K. K. C.; Scott, I. M.; Conn, K. L.; Berruti, F.; Briens, C. Experimental Investigations into the Insecticidal, Fungicidal, and Bactericidal Properties of Pyrolysis Bio-Oil from Tobacco Leaves Using a Fluidized Bed Pilot Plant. *Ind. Eng. Chem. Res.* **2010**, 49 (20), 10074–10079. <https://doi.org/10.1021/ie100329z>.
- (51) Mattos, C.; Veloso, M. C. C.; Romeiro, G. A.; Folly, E. Biocidal Applications Trends of Bio-Oils from Pyrolysis: Characterization of Several Conditions and Biomass, a Review. *J. Anal. Appl. Pyrolysis* **2019**, 139 (December 2018), 1–12. <https://doi.org/10.1016/j.jaap.2018.12.029>.
- (52) Booker, C. J.; Bedmutha, R.; Vogel, T.; Gloor, A.; Xu, R.; Ferrante, L.; Yeung, K. K.; Scott, I. M.; Conn, K. L.; Berruti, F.; Briens, C. Experimental Investigations into the Insecticidal, Fungicidal, and Bactericidal Properties of Pyrolysis Bio-Oil from Tobacco Leaves Using a Fluidized Bed Pilot Plant - Industrial & Engineering Chemistry Research (ACS Publications). **2010**, 10074–10079.
- (53) Saini, R. K.; Hassanali, A. A 4-Alkyl-Substituted Analogue of Guaiacol Shows Greater Repellency to Savannah Tsetse (*Glossina* Spp.). *J. Chem. Ecol.* **2007**, 33 (5), 985–995. <https://doi.org/10.1007/s10886-007-9272-7>.
- (54) Freeman, C. J.; Jones, S. B.; AB Padmaperuma; Santosa, M.; Valkenburg, C.; Shinn, J. *Initial Assessment of U.S. Refineries for Purposes of Potential Bio-Based Oil Insertions*; 2013.
- (55) Karatzos, S.; Mcmillan, J.; Saddler, J. *The Potential and Challenges of “Drop in” Biofuels*; 2014.
- (56) Stephen, J. D.; Mabee, W. E.; Saddler, J. N. Biomass Logistics as a Determinant of Second- Generation Biofuel Facility Scale, Location and Technology Selection James. *Biofuels, Bioprod. Biorefining* **2010**, 4 (5), 503–518. <https://doi.org/10.1002/bbb>.
- (57) BTG-BTL. News - BTG Bioliquids BV <https://www.btg-btl.com/en/company/news/news/article?id=137> (accessed Oct 26, 2020).
- (58) Finnish company buys 4 pyrolysis plants in the Netherlands - Agro & Chemistry <https://www.agro-chemistry.com/news/finnish-company-buys-4-pyrolysis-plants-in-the-netherlands/> (accessed Oct 26, 2020).
- (59) Wang, C.; Li, M.; Fang, Y. Coprocessing of Catalytic-Pyrolysis-Derived Bio-Oil with VGO in a Pilot-Scale FCC Riser. *Ind. Eng. Chem. Res.* **2016**, 55 (12), 3525–3534. <https://doi.org/10.1021/acs.iecr.5b03008>.
- (60) Wang, C.; Venderbosch, R.; Fang, Y. Co-Processing of Crude and Hydrotreated Pyrolysis Liquids and VGO in a Pilot Scale FCC Riser Setup. *Fuel Process. Technol.* **2018**, 181 (July), 157–165. <https://doi.org/10.1016/j.fuproc.2018.09.023>.
- (61) Fogassy, G.; Thegarid, N.; Schuurman, Y.; Mirodatos, C. The Fate of Bio-Carbon in FCC Co-Processing Products. *Green Chem.* **2012**, 14 (5), 1367. <https://doi.org/10.1039/c2gc35152h>.
- (62) Pinho, A. D. R.; De Almeida, M. B. B.; Mendes, F. L.; Ximenes, V. L.; Casavechia, L. C. Co-Processing Raw Bio-Oil and Gasoil in an FCC Unit. *Fuel Process. Technol.* **2015**, 131, 159–166. <https://doi.org/10.1016/j.fuproc.2014.11.008>.
- (63) Pinho, A. de R.; de Almeida, M. B. B.; Mendes, F. L.; Casavechia, L. C.; Talmadge, M. S.; Kinchin, C. M.; Chum, H. L. Fast Pyrolysis Oil from Pinewood Chips Co-Processing with Vacuum Gas Oil in an FCC Unit for Second Generation Fuel Production. *Fuel* **2017**, 188, 462–473. <https://doi.org/10.1016/j.fuel.2016.10.032>.
- (64) Lindfors, C.; Paasikallio, V.; Kuoppala, E.; Reinikainen, M.; Oasmaa, A.; Solantausta, Y. Y. Co-Processing of Dry Bio-Oil, Catalytic Pyrolysis Oil, and Hydrotreated Bio-Oil in a Micro Activity Test Unit. *Energy and Fuels* **2015**, 29 (6), 3707–3714. <https://doi.org/10.1021/acs.energyfuels.5b00339>.
- (65) de Miguel Mercader, F.; Groeneveld, M. J.; Kersten, S. R. A.; Way, N. W. J.; Schaverien, C. J.; Hogendoorn, J. A. Production of Advanced Biofuels: Co-Processing of Upgraded Pyrolysis Oil in Standard Refinery Units. *Appl. Catal. B Environ.* **2010**, 96 (1–2), 57–66. <https://doi.org/10.1016/j.apcatb.2010.01.033>.
- (66) Mukarakate, C.; Orton, K.; Kim, Y.; Dell’orco, S.; Farberow, C. A.; Kim, S.; Watson, M. J.; Baldwin, R. M.; Magrini, K. A. Isotopic Studies for Tracking Biogenic Carbon during Co-Processing of Biomass and Vacuum Gas Oil. *ACS Sustain. Chem. Eng.* **2020**, 8 (7), 2652–2664. <https://doi.org/10.1021/acssuschemeng.9b05762>.
- (67) Corma, A.; Huber, G. W.; Sauvanaud, L.; O’Connor, P. Processing Biomass-Derived Oxygenates in the Oil Refinery: Catalytic Cracking (FCC) Reaction Pathways and Role of Catalyst. *J. Catal.* **2007**, 247 (2), 307–327. <https://doi.org/10.1016/j.jcat.2007.01.023>.
- (68) Toor, S. S.; Rosendahl, L.; Rudolf, A. Hydrothermal Liquefaction of Biomass: A Review of Subcritical Water Technologies. *Energy* **2011**, 36 (5), 2328–2342. <https://doi.org/10.1016/j.energy.2011.03.013>.
- (69) Akhtar, J.; Amin, N. A. S. A Review on Process Conditions for Optimum Bio-Oil Yield in Hydrothermal Liquefaction of Biomass. *Renew. Sustain. Energy Rev.* **2011**, 15 (3), 1615–1624. <https://doi.org/10.1016/j.rser.2010.11.054>.
- (70) Clariant’s new plant in Romania progressing well | Biofuels International Magazine <https://biofuels-news.com/news/clariants-new-plant-in-romania-progressing-well/> (accessed Oct 26, 2020).
- (71) Chudziak, C.; Alberts, G.; Bauen, A. Ramp up of Lignocellulosic Ethanol in Europe to 2030 Final Report.

- 2017, No. December.
- (72) Sannigrahi, P.; Pu, Y.; Ragauskas, A. Cellulosic Biorefineries-Unleashing Lignin Opportunities. *Curr. Opin. Environ. Sustain.* **2010**, *2* (5–6), 383–393. <https://doi.org/10.1016/j.cosust.2010.09.004>.
 - (73) Porzio, G. F.; Prussi, M.; Chiamonti, D.; Pari, L. Modelling Lignocellulosic Bioethanol from Poplar: Estimation of the Level of Process Integration, Yield and Potential for Co-Products. *J. Clean. Prod.* **2012**, *34*, 66–75. <https://doi.org/10.1016/j.jclepro.2012.01.028>.
 - (74) Isaacs, S. H. Ethanol Production by Enzymatic Hydrolysis Parametric: Analysis of a Base-Case Process. **1984**, 65. <https://doi.org/10.2172/6527601>.
 - (75) Fast pyrolysis - Biomass Technology Group BV <https://www.btgworld.com/en/rtd/technologies/fast-pyrolysis> (accessed Aug 21, 2020).
 - (76) Overview - Ensyn - Renewable Fuels and Chemicals from Non-Food Biomass. <http://www.ensyn.com/overview.html> (accessed Aug 21, 2020).
 - (77) Steeper Energy <https://steeperenergy.com/> (accessed Aug 21, 2020).
 - (78) Panisko, E.; Wietsma, T.; Lemmon, T.; Albrecht, K.; Howe, D. Characterization of the Aqueous Fractions from Hydrotreatment and Hydrothermal Liquefaction of Lignocellulosic Feedstocks. *Biomass and Bioenergy* **2015**, *74*, 162–171. <https://doi.org/10.1016/j.biombioe.2015.01.011>.
 - (79) Ciesielski, P. N.; Pecha, M. B.; Bharadwaj, V. S.; Mukarakate, C.; Leong, G. J.; Kappes, B.; Crowley, M. F.; Kim, S.; Foust, T. D.; Nimlos, M. R. Advancing Catalytic Fast Pyrolysis through Integrated Multiscale Modeling and Experimentation: Challenges, Progress, and Perspectives. *Wiley Interdiscip. Rev. Energy Environ.* **2018**, *7* (4), e297. <https://doi.org/10.1002/wene.297>.
 - (80) Krutof, A.; Hawboldt, K. A. Upgrading of Biomass Sourced Pyrolysis Oil Review: Focus on Co-Pyrolysis and Vapour Upgrading during Pyrolysis. *Biomass Convers. Biorefinery* **2018**, *8* (3), 775–787. <https://doi.org/10.1007/s13399-018-0326-6>.
 - (81) Luo, G.; Resende, F. L. P. In-Situ and Ex-Situ Upgrading of Pyrolysis Vapors from Beetle-Killed Trees. *Fuel* **2016**, *166*, 367–375. <https://doi.org/10.1016/j.fuel.2015.10.126>.
 - (82) Mante, O. D.; Dayton, D. C.; Carpenter, J. R.; Wang, K.; Peters, J. E. Pilot-Scale Catalytic Fast Pyrolysis of Loblolly Pine over γ -Al₂O₃ Catalyst. *Fuel* **2018**, *214*, 569–579. <https://doi.org/10.1016/j.fuel.2017.11.073>.
 - (83) Rahman, M. M.; Liu, R.; Cai, J. Catalytic Fast Pyrolysis of Biomass over Zeolites for High Quality Bio-Oil – A Review. *Fuel Process. Technol.* **2018**, *180*, 32–46. <https://doi.org/10.1016/j.fuproc.2018.08.002>.
 - (84) Saraeian, A.; Nolte, M. W.; Shanks, B. H. Deoxygenation of Biomass Pyrolysis Vapors: Improving Clarity on the Fate of Carbon. *Renew. Sustain. Energy Rev.* **2019**, *104*, 262–280. <https://doi.org/10.1016/j.rser.2019.01.037>.
 - (85) Wang, K.; Dayton, D. C.; Peters, J. E.; Mante, O. D. Reactive Catalytic Fast Pyrolysis of Biomass to Produce High-Quality Bio-Crude. *Green Chem.* **2017**, *19* (14), 3243–3251. <https://doi.org/10.1039/C7GC01088E>.
 - (86) Peterson, B.; Engtrakul, C.; Wilson, A. N.; Orco, S. D.; Orton, K. A.; Deutch, S.; Yung, M. M.; Starace, A. K.; Parent, Y.; Chiamonti, D.; Magrini, K. A. Catalytic Hot-Gas Filtration with a Supported Heteropolyacid Catalyst for Preconditioning Biomass Pyrolysis Vapors. *ACS Sustain. Chem. Eng.* **2019**, *7*, 14941–14952. <https://doi.org/10.1021/acssuschemeng.9b03188>.
 - (87) Ruddy, D. A.; Schaidle, J. A.; Ferrell III, J. R.; Wang, J.; Moens, L.; Hensley, J. E. Recent Advances in Heterogeneous Catalysts for Bio-Oil Upgrading via “Ex Situ Catalytic Fast Pyrolysis”: Catalyst Development through the Study of Model Compounds. *Green Chem.* **2014**, *16* (2), 454–490. <https://doi.org/10.1039/C3GC41354C>.
 - (88) Mukarakate, C.; Zhang, X.; Stanton, A. R.; Robichaud, D. J.; Ciesielski, P. N.; Malhotra, K.; Donohoe, B. S.; Gjersing, E.; Evans, R. J.; Heroux, D. S.; Richards, R.; Iisa, K.; Nimlos, M. R. Real-Time Monitoring of the Deactivation of HZSM-5 during Upgrading of Pine Pyrolysis Vapors. *Green Chem.* **2014**, *16* (3), 1444–1461. <https://doi.org/10.1039/c3gc42065e>.
 - (89) Yung, M. M.; Starace, A. K.; Griffin, M. B.; Wells, J. D.; Patalano, R. E.; Smith, K. R.; Schaidle, J. A. Restoring ZSM-5 Performance for Catalytic Fast Pyrolysis of Biomass: Effect of Regeneration Temperature. *Catal. Today* **2019**, *323*, 76–85. <https://doi.org/10.1016/j.cattod.2018.06.025>.
 - (90) Alsou, E.; Helleur, B. Accelerated Aging of Bio-Oil from Fast Pyrolysis of Hardwood. *Energy and Fuels* **2014**, *28* (5), 3224–3235. <https://doi.org/10.1021/ef500399n>.
 - (91) Bridgwater, A. V. Upgrading Biomass Fast Pyrolysis Liquids. *Environ. Prog. Sustain. Energy* **2012**, *31* (2), 261–268. <https://doi.org/10.1002/ep.11635>.
 - (92) Elliott, D. C.; Oasmaa, A.; Preto, F.; Meier, D.; Bridgwater, A. V. Results of the IEA Round Robin on Viscosity and Stability of Fast Pyrolysis Bio-Oils. *Energy & Fuels* **2012**, *26* (6), 3769–3776. <https://doi.org/10.1021/ef300384t>.
 - (93) Huber, G. W.; Iborra, S.; Corma, A. Synthesis of Transportation Fuels from Biomass: Chemistry, Catalysts, and Engineering. *Chem. Rev.* **2006**, *106* (9), 4044–4098. <https://doi.org/10.1021/cr068360d>.
 - (94) Oasmaa, A.; Elliott, D. C.; Korhonen, J. Acidity of Biomass Fast Pyrolysis Bio-Oils. *Energy & Fuels* **2010**, *24* (12), 6548–6554. <https://doi.org/10.1021/ef100935r>.

- (95) Kumar, R.; Enjamuri, N.; Shah, S.; Al-Fatesh, A. S.; Bravo-Suárez, J. J.; Chowdhury, B. Ketonization of Oxygenated Hydrocarbons on Metal Oxide Based Catalysts. *Catal. Today* **2018**, *302*, 16–49. <https://doi.org/10.1016/j.cattod.2017.09.044>.
- (96) Pham, T. N.; Sooknoi, T.; Crossley, S. P.; Resasco, D. E. Ketonization of Carboxylic Acids: Mechanisms, Catalysts, and Implications for Biomass Conversion. *ACS Catal.* **2013**, *3* (11), 2456–2473. <https://doi.org/10.1021/cs400501h>.
- (97) Pacchioni, G. Ketonization of Carboxylic Acids in Biomass Conversion over TiO₂ and ZrO₂ Surfaces: A DFT Perspective. *ACS Catalysis*. American Chemical Society September 5, 2014, pp 2874–2888. <https://doi.org/10.1021/cs500791w>.
- (98) Lu, F.; Jiang, B.; Wang, J.; Huang, Z.; Liao, Z.; Yang, Y.; Zheng, J. Promotional Effect of Ti Doping on the Ketonization of Acetic Acid over a CeO₂ Catalyst. *RSC Adv.* **2017**, *7* (36), 22017–22026. <https://doi.org/10.1039/c7ra00521k>.
- (99) Ruddy, D. A.; Schaidle, J. A.; Ferrell, J. R.; Wang, J.; Moens, L.; Hensley, J. E. Recent Advances in Heterogeneous Catalysts for Bio-Oil Upgrading via “Ex Situ Catalytic Fast Pyrolysis”: Catalyst Development through the Study of Model Compounds. *Green Chemistry*. February 2014, pp 454–490. <https://doi.org/10.1039/c3gc41354c>.
- (100) Chan, W. P.; Veksha, A.; Lei, J.; Oh, W. Da; Dou, X.; Giannis, A.; Lisak, G.; Lim, T. T. A Hot Syngas Purification System Integrated with Downdraft Gasification of Municipal Solid Waste. *Appl. Energy* **2019**, *237*, 227–240. <https://doi.org/10.1016/j.apenergy.2019.01.031>.
- (101) Dutta, A.; Schaidle, J. A.; Humbird, D.; Baddour, F. G.; Sahir, A. Conceptual Process Design and Techno-Economic Assessment of Ex Situ Catalytic Fast Pyrolysis of Biomass: A Fixed Bed Reactor Implementation Scenario for Future Feasibility. *Top. Catal.* **2016**, *59* (1), 2–18. <https://doi.org/10.1007/s11244-015-0500-z>.
- (102) Heidenreich, S. Hot Gas Filtration - A Review. *Fuel*. February 2013, pp 83–94. <https://doi.org/10.1016/j.fuel.2012.07.059>.
- (103) Heidenreich, S.; Foscolo, P. U. New Concepts in Biomass Gasification. *Progress in Energy and Combustion Science*. Elsevier Ltd February 1, 2015, pp 72–95. <https://doi.org/10.1016/j.peccs.2014.06.002>.
- (104) Nacken, M.; Lina, M.; Engelen, K.; Heidenreich, S.; Baron, G. V. Development of a Tar Reforming Catalyst for Integration in a Ceramic Filter Element and Use in Hot Gas Cleaning. *Ind. Eng. Chem. Res.* **2007**, *46* (7), 1945–1951. <https://doi.org/10.1021/ie060887t>.
- (105) Nacken, M.; Ma, L.; Heidenreich, S.; Baron, G. V. Performance of a Catalytically Activated Ceramic Hot Gas Filter for Catalytic Tar Removal from Biomass Gasification Gas. *Appl. Catal. B Environ.* **2009**, *88* (3–4), 292–298. <https://doi.org/10.1016/j.apcatb.2008.11.011>.
- (106) Nacken, M.; Ma, L.; Heidenreich, S.; Verpoort, F.; Baron, G. V. Development of a Catalytic Ceramic Foam for Efficient Tar Reforming of a Catalytic Filter for Hot Gas Cleaning of Biomass-Derived Syngas. *Appl. Catal. B Environ.* **2012**, *125*, 111–119. <https://doi.org/10.1016/j.apcatb.2012.05.027>.
- (107) Johansson, A. C.; Iisa, K.; Sandström, L.; Ben, H.; Pilath, H.; Deutch, S.; Wiinikka, H.; Öhrman, O. G. W. Fractional Condensation of Pyrolysis Vapors Produced from Nordic Feedstocks in Cyclone Pyrolysis. *J. Anal. Appl. Pyrolysis* **2017**, *123*, 244–254. <https://doi.org/10.1016/j.jaap.2016.11.020>.
- (108) Kim, P.; Weaver, S.; Noh, K.; Labbé, N. Characteristics of Bio-Oils Produced by an Intermediate Semipilot Scale Pyrolysis Auger Reactor Equipped with Multistage Condensers. *Energy and Fuels* **2014**, *28* (11), 6966–6973. <https://doi.org/10.1021/ef5016186>.
- (109) Ma, S.; Zhang, L.; Zhu, L.; Zhu, X. Preparation of Multipurpose Bio-Oil from Rice Husk by Pyrolysis and Fractional Condensation. *J. Anal. Appl. Pyrolysis* **2018**, *131*, 113–119. <https://doi.org/10.1016/j.jaap.2018.02.017>.
- (110) Schulzke, T.; Conrad, S.; Westermeyer, J. Fractionation of Flash Pyrolysis Condensates by Staged Condensation. *Biomass and Bioenergy* **2016**, *95*, 287–295. <https://doi.org/10.1016/j.biombioe.2016.05.022>.
- (111) Sui, H.; Yang, H.; Shao, J.; Wang, X.; Li, Y.; Chen, H. Fractional Condensation of Multicomponent Vapors from Pyrolysis of Cotton Stalk. *Energy and Fuels* **2014**, *28* (8), 5095–5102. <https://doi.org/10.1021/ef5006012>.
- (112) Westerhof, R. J. M.; Brilman, D. W. F.; Garcia-Perez, M.; Wang, Z.; Oudenhoven, S. R. G.; Van Swaaij, W. P. M.; Kersten, S. R. A. Fractional Condensation of Biomass Pyrolysis Vapors. *Energy and Fuels* **2011**, *25* (4), 1817–1829. <https://doi.org/10.1021/ef2000322>.
- (113) Westerhof, R. J. M.; Kuipers, N. J. M.; Kersten, S. R. A.; Van Swaaij, W. P. M. Controlling the Water Content of Biomass Fast Pyrolysis Oil. *Ind. Eng. Chem. Res.* **2007**, *46* (26), 9238–9247. <https://doi.org/10.1021/ie070684k>.
- (114) Grossman, A.; Wilfred, V. Lignin-Based Polymers and Nanomaterials. *Current Opinion in Biotechnology*. Elsevier Ltd April 1, 2019, pp 112–120. <https://doi.org/10.1016/j.copbio.2018.10.009>.
- (115) Parsell, T.; Yohe, S.; Degenstein, J.; Jarrell, T.; Klein, I.; Gencer, E.; Hewetson, B.; Hurt, M.; Kim, J. I.; Choudhari, H.; Saha, B.; Meilan, R.; Mosier, N.; Ribeiro, F.; Delgass, W. N.; Chapple, C.; Kenttämaa, H. I.; Agrawal, R.; Abu-Omar, M. M. A Synergistic Biorefinery Based on Catalytic Conversion of Lignin Prior to

- Cellulose Starting from Lignocellulosic Biomass. *Green Chem.* **2015**, *17* (3), 1492–1499. <https://doi.org/10.1039/c4gc01911c>.
- (116) Wang, S. S.; Yang, G. Y. Recent Advances in Polyoxometalate-Catalyzed Reactions. *Chemical Reviews*. American Chemical Society 2015, pp 4893–4962. <https://doi.org/10.1021/cr500390v>.
- (117) Anderson, E.; Crisci, A.; Murugappan, K.; Román-Leshkov, Y. Bifunctional Molybdenum Polyoxometalates for the Combined Hydrodeoxygenation and Alkylation of Lignin-Derived Model Phenolics. *ChemSusChem* **2017**, *10* (10), 2226–2234. <https://doi.org/10.1002/cssc.201700297>.
- (118) Murugappan, K.; Mukarakate, C.; Budhi, S.; Shetty, M.; Nimlos, M. R.; Román-Leshkov, Y. Supported Molybdenum Oxides as Effective Catalysts for the Catalytic Fast Pyrolysis of Lignocellulosic Biomass. *Green Chem.* **2016**, *18* (20), 5548–5557. <https://doi.org/10.1039/c6gc01189f>.
- (119) Zhang, X.; Chen, Q.; Zhang, Q.; Wang, C.; Ma, L.; Xu, Y. Conversion of Pyrolytic Lignin to Aromatic Hydrocarbons by Hydrocracking over Pristine MoO₃ Catalyst. *J. Anal. Appl. Pyrolysis* **2018**, *135*, 60–66. <https://doi.org/10.1016/j.jaap.2018.09.020>.
- (120) Ranga, C.; Lødeng, R.; Alexiadis, V. I.; Rajkhowa, T.; Bjørkan, H.; Chytil, S.; Svenum, I. H.; Walmsley, J.; Detavernier, C.; Poelman, H.; Van Der Voort, P.; Thybaut, J. W. Effect of Composition and Preparation of Supported MoO₃ Catalysts for Anisole Hydrodeoxygenation. *Chem. Eng. J.* **2018**, *335*, 120–132. <https://doi.org/10.1016/j.cej.2017.10.090>.
- (121) Saidi, M.; Samimi, F.; Karimipourfard, D.; Nimmanwudipong, T.; Gates, B. C.; Rahimpour, M. R. Upgrading of Lignin-Derived Bio-Oils by Catalytic Hydrodeoxygenation. *Energy and Environmental Science*. Royal Society of Chemistry 2014, pp 103–129. <https://doi.org/10.1039/c3ee43081b>.
- (122) Shetty, M.; Murugappan, K.; Green, W. H.; Román-Leshkov, Y. Structural Properties and Reactivity Trends of Molybdenum Oxide Catalysts Supported on Zirconia for the Hydrodeoxygenation of Anisole. *ACS Sustain. Chem. Eng.* **2017**, *5* (6), 5293–5301. <https://doi.org/10.1021/acssuschemeng.7b00642>.
- (123) Li, X.; Pang, J.; Zhang, J.; Yin, C.; Zou, W.; Tang, C.; Dong, L. Vapor-Phase Deoxygenation of Lactic Acid to Biopropionic Acid over Dispersant-Enhanced Molybdenum Oxide Catalyst. *Ind. Eng. Chem. Res.* **2019**, *58* (1), 101–109. <https://doi.org/10.1021/acs.iecr.8b04713>.
- (124) Zhao, A.; Masa, J.; Xia, W. Oxygen-Deficient Titania as Alternative Support for Pt Catalysts for the Oxygen Reduction Reaction. *J. Energy Chem.* **2014**, *23* (6), 701–707. [https://doi.org/10.1016/S2095-4956\(14\)60202-3](https://doi.org/10.1016/S2095-4956(14)60202-3).
- (125) Mukarakate, C.; Watson, M. J.; Ten Dam, J.; Baucherel, X.; Budhi, S.; Yung, M. M.; Ben, H.; Iisa, K.; Baldwin, R. M.; Nimlos, M. R. Upgrading Biomass Pyrolysis Vapors over β -Zeolites: Role of Silica-to-Alumina Ratio. *Green Chem.* **2014**, *16* (12), 4891–4905. <https://doi.org/10.1039/c4gc01425a>.
- (126) Evans, R. J.; Milne, T. A. Molecular Characterization of the Pyrolysis of Biomass. 1. Fundamentals. *Energ. Fuel.* **1987**, *1* (2), 123–137. <https://doi.org/10.1021/ef00002a001>.
- (127) Evans, R. J.; Milne, T. A. Molecular Characterization of the Pyrolysis of Biomass. 2. Applications. *Energ. Fuel.* **1987**, *1* (4), 311–319. <https://doi.org/10.1021/ef00004a001>.
- (128) Jarvis, M. W.; Haas, T. J.; Donohoe, B. S.; Daily, J. W.; Gaston, K. R.; Frederick, W. J.; Nimlos, M. R. Elucidation of Biomass Pyrolysis Products Using a Laminar Entrained Flow Reactor and Char Particle Imaging. *Energy and Fuels* **2011**, *25* (1), 324–336. <https://doi.org/10.1021/ef100832d>.
- (129) Atia, H.; Armbruster, U.; Martin, A. Dehydration of Glycerol in Gas Phase Using Heteropolyacid Catalysts as Active Compounds. *J. Catal.* **2008**, *258* (1), 71–82. <https://doi.org/10.1016/j.jcat.2008.05.027>.
- (130) Byrne, C.; Moran, L.; Hermosilla, D.; Merayo, N.; Blanco, Á.; Rhatigan, S.; Hinder, S.; Ganguly, P.; Nolan, M.; Pillai, S. C. Effect of Cu Doping on the Anatase-to-Rutile Phase Transition in TiO₂ Photocatalysts: Theory and Experiments. *Appl. Catal. B Environ.* **2019**, *246*, 266–276. <https://doi.org/10.1016/j.apcatb.2019.01.058>.
- (131) Nair, V.; Vinu, R. Production of Guaiacols via Catalytic Fast Pyrolysis of Alkali Lignin Using Titania, Zirconia and Ceria. *J. Anal. Appl. Pyrolysis* **2016**, *119*, 31–39. <https://doi.org/10.1016/j.jaap.2016.03.020>.
- (132) Black, B. A.; Michener, W. E.; Ramirez, K. J.; Bidy, M. J.; Knott, B. C.; Jarvis, M. W.; Olstad, J.; Mante, O. D.; Dayton, D. C.; Beckham, G. T. Aqueous Stream Characterization from Biomass Fast Pyrolysis and Catalytic Fast Pyrolysis. *ACS Sustain. Chem. Eng.* **2016**, *4* (12), 6815–6827. <https://doi.org/10.1021/acssuschemeng.6b01766>.
- (133) Anderson, E.; Crisci, A.; Murugappan, K.; Román-Leshkov, Y. Bifunctional Molybdenum Polyoxometalates for the Combined Hydrodeoxygenation and Alkylation of Lignin-Derived Model Phenolics. *ChemSusChem* **2017**, *10* (10), 2226–2234. <https://doi.org/10.1002/cssc.201700297>.
- (134) Peterson, B.; Engtrakul, C.; Wilson, A. N.; Dell'Orco, S.; Orton, K. A.; Deutch, S.; Yung, M. M.; Starace, A. K.; Parent, Y.; Chiamonti, D.; Magrini, K. A. Catalytic Hot-Gas Filtration with a Supported Heteropolyacid Catalyst for Preconditioning Biomass Pyrolysis Vapors. *ACS Sustain. Chem. Eng.* **2019**, *7* (17), 14941–14952. <https://doi.org/10.1021/acssuschemeng.9b03188>.
- (135) Bridgwater, A. V. Upgrading Biomass Fast Pyrolysis Liquids. *Environ. Prog. Sustain. Energy* **2012**, *31* (2), 261–268. <https://doi.org/10.1002/ep.11635>.
- (136) Dutta, A.; Schaidle, J. A.; Humbird, D.; Baddour, F. G.; Sahir, A. Conceptual Process Design and Techno-

- Economic Assessment of Ex Situ Catalytic Fast Pyrolysis of Biomass: A Fixed Bed Reactor Implementation Scenario for Future Feasibility. *Top. Catal.* **2016**, *59* (1), 2–18. <https://doi.org/10.1007/s11244-015-0500-z>.
- (137) Papari, S.; Hawboldt, K. A Review on Condensing System for Biomass Pyrolysis Process. *Fuel Processing Technology*. Elsevier B.V. November 1, 2018, pp 1–13. <https://doi.org/10.1016/j.fuproc.2018.08.001>.
- (138) Moens, L.; Black, S. K.; Myers, M. D.; Czernik, S. Study of the Neutralization and Stabilization of a Mixed Hardwood Bio-Oil. *Energ. Fuel.* **2009**, *23*, 2696–2699.
- (139) Diebold, J. P. A Review of the Chemical and Physical Mechanisms of the Storage Stability of Fast Pyrolysis Bio-Oils. *Order A J. Theory Ordered Sets Its Appl.* **2000**, No. January.
- (140) Snell, R. W.; Combs, E.; Shanks, B. H. Aldol Condensations Using Bio-Oil Model Compounds : The Role of Acid – Base Bi-Functionality. **2010**, 1248–1253. <https://doi.org/10.1007/s11244-010-9576-7>.
- (141) Black, S.; Ferrell, J. R. Determination of Carbonyl Groups in Pyrolysis Bio-Oils Using Potentiometric Titration: Review and Comparison of Methods. *Energy and Fuels* **2016**, *30* (2), 1071–1077. <https://doi.org/10.1021/acs.energyfuels.5b02511>.
- (142) Guda, V. K.; Toghiani, H. Catalytic Pyrolysis of Pinewood Using Metal Oxide Catalysts in an Integrated Reactor System. *Biofuels* **2017**, *8* (5), 527–536. <https://doi.org/10.1080/17597269.2016.1231960>.
- (143) Mante, O. D.; Rodriguez, J. A.; Babu, S. P. Selective Defunctionalization by TiO₂ of Monomeric Phenolics from Lignin Pyrolysis into Simple Phenols. *Bioresour. Technol.* **2013**, *148*, 508–516. <https://doi.org/10.1016/j.biortech.2013.09.003>.
- (144) Grossman, A.; Wilfred, V. Lignin-Based Polymers and Nanomaterials. *Curr. Opin. Biotechnol.* **2019**, *56*, 112–120. <https://doi.org/10.1016/j.copbio.2018.10.009>.
- (145) Parsell, T.; Yohe, S.; Degenstein, J.; Jarrell, T.; Klein, I.; Gencer, E.; Hewetson, B.; Hurt, M.; Kim, J. I.; Choudhari, H.; Agrawal, R.; Abu-Omar, M. M. A Synergistic Biorefinery Based on Catalytic Conversion of Lignin Prior to Cellulose Starting from Lignocellulosic Biomass. *Green Chem.* **2015**, *17* (3), 1492–1499. <https://doi.org/10.1039/c4gc01911c>.
- (146) Papari, S.; Hawboldt, K. A Review on Condensing System for Biomass Pyrolysis Process. *Fuel Process. Technol.* **2018**, *180* (July), 1–13. <https://doi.org/10.1016/j.fuproc.2018.08.001>.
- (147) Rover, M. R.; Johnston, P. A.; Whitmer, L. E.; Smith, R. G.; Brown, R. C. The Effect of Pyrolysis Temperature on Recovery of Bio-Oil as Distinctive Stage Fractions. *J. Anal. Appl. Pyrolysis* **2014**, *105*, 262–268. <https://doi.org/10.1016/j.jaap.2013.11.012>.
- (148) Meng, J.; Moore, A.; Tilotta, D.; Kelley, S.; Park, S. Toward Understanding of Bio-Oil Aging: Accelerated Aging of Bio-Oil Fractions. *ACS Sustain. Chem. Eng.* **2014**, *2* (8), 2011–2018. <https://doi.org/10.1021/sc500223e>.
- (149) Ramaswamy, S.; Huang, H. J.; Ramarao, B. V. *Separation and Purification Technologies in Biorefineries*; Wiley, 2013. <https://doi.org/10.1002/9781118493441>.
- (150) Kohli, K.; Prajapati, R.; Sharma, B. K. Bio-Based Chemicals from Renewable Biomass for Integrated Biorefineries. *Energies* **2019**, *12* (2). <https://doi.org/10.3390/en12020233>.
- (151) Iisa, K.; Robichaud, D. J.; Watson, M. J.; Ten Dam, J.; Dutta, A.; Mukarakate, C.; Kim, S.; Nimlos, M. R.; Baldwin, R. M. Improving Biomass Pyrolysis Economics by Integrating Vapor and Liquid Phase Upgrading. *Green Chem.* **2018**, *20* (3), 567–582. <https://doi.org/10.1039/c7gc02947k>.
- (152) Mabrouk, A.; Erdocia, X.; Alriols, M. G.; Labidi, J. Economic Analysis of a Biorefinery Process for Catechol Production from Lignin. *J. Clean. Prod.* **2018**, *198*, 133–142. <https://doi.org/10.1016/j.jclepro.2018.06.294>.
- (153) PricewaterhouseCoopers et al. Sustainable and Optimal Use of Biomass for Energy in the EU beyond 2020. **2017**, No. May 2017, 198.
- (154) De Wild, P.; Reith, H.; Heeres, E. Biomass Pyrolysis for Chemicals. *Biofuels* **2011**, *2* (2), 185–208. <https://doi.org/10.4155/bfs.10.88>.
- (155) Hunter, M. C.; Smith, R. G.; Schipanski, M. E.; Atwood, L. W.; Mortensen, D. A. Agriculture in 2050: Recalibrating Targets for Sustainable Intensification. *Bioscience* **2017**, *67* (4), 386–391. <https://doi.org/10.1093/biosci/bix010>.
- (156) FAOSTAT <http://www.fao.org/faostat/en/#data/RP/visualize> (accessed Aug 18, 2020).
- (157) Aktar, W.; Sengupta, D.; Chowdhury, A. Impact of Pesticides Use in Agriculture: Their Benefits and Hazards. *Interdiscip. Toxicol.* **2009**, *2* (1), 1–12. <https://doi.org/10.2478/v10102-009-0001-7>.
- (158) Hakeem, K. R.; Akhtar, M. S.; Abdullah, S. N. A. *Plant, Soil and Microbes: Volume 1: Implications in Crop Science*; 2016; Vol. 1. <https://doi.org/10.1007/978-3-319-27455-3>.
- (159) Jayaraj, R.; Megha, P.; Sreedev, P. Organochlorine Pesticides, Their Toxic Effects on Living Organisms and Their Fate in the Environment. *Interdiscip. Toxicol.* **2016**, *9* (3–4), 90–100. <https://doi.org/10.1515/intox-2016-0012>.
- (160) Audsley, E.; Stacey, K.; Parsons, D. J.; Williams, A. G. *Estimation of the Greenhouse Gas Emissions from Agricultural Pesticide Manufacture and Use*; Cranfield, Bedford, UK, 2009. <https://doi.org/10.13140/RG.2.1.5095.3122>.
- (161) U.S. EPA. Sources of Greenhouse Gas Emissions | Greenhouse Gas (GHG) Emissions | US EPA. *Greenhouse*

- Gas Emissions*. 2020.
- (162) FAO. Global Database of GHG Emissions Related to Feed Crops: A Life Cycle Inventory. **2017**.
- (163) Gallai, N.; Salles, J. M.; Settele, J.; Vaissière, B. E. Economic Valuation of the Vulnerability of World Agriculture Confronted with Pollinator Decline. *Ecol. Econ.* **2009**, *68* (3), 810–821. <https://doi.org/10.1016/j.ecolecon.2008.06.014>.
- (164) Sánchez-Bayo, F.; Goulson, D.; Pennacchio, F.; Nazzi, F.; Goka, K.; Desneux, N. Are Bee Diseases Linked to Pesticides? - A Brief Review. *Environ. Int.* **2016**, *89–90*, 7–11. <https://doi.org/10.1016/j.envint.2016.01.009>.
- (165) Kulhanek, K.; Steinhauer, N.; Rennich, K.; Caron, D. M.; Sagili, R. R.; Pettis, J. S.; Ellis, J. D.; Wilson, M. E.; Wilkes, J. T.; Tarpy, D. R.; Rose, R.; Lee, K.; Rangel, J.; vanEngelsdorp, D. Encuesta Nacional 2015–2016 Sobre Pérdidas Anuales de Colonias de La Abeja de La Miel Manejada En Los EE.UU. *J. Apic. Res.* **2017**, *56* (4), 328–340. <https://doi.org/10.1080/00218839.2017.1344496>.
- (166) European Commission. *REPORT FROM THE COMMISSION TO THE EUROPEAN PARLIAMENT AND THE COUNCIL, Evaluation of Regulation (EC) No 1107/2009 on the Placing of Plant Protection Products on the Market and of Regulation (EC) No 396/2005 on Maximum Residue Levels of Pesticides*; Brussels, 2020.
- (167) Schedule for Review of Neonicotinoid Pesticides | Protecting Bees and Other Pollinators from Pesticides | US EPA <https://www.epa.gov/pollinator-protection/schedule-review-neonicotinoid-pesticides> (accessed Oct 28, 2020).
- (168) Margus, A.; Piironen, S.; Lehmann, P.; Tikka, S.; Karvanen, J.; Lindström, L. Sublethal Pyrethroid Insecticide Exposure Carries Positive Fitness Effects Over Generations in a Pest Insect. *Sci. Rep.* **2019**, *9* (1), 1–10. <https://doi.org/10.1038/s41598-019-47473-1>.
- (169) Gould, F.; Brown, Z. S.; Kuzma, J. Wicked Evolution: Can We Address the Sociobiological Dilemma of Pesticide Resistance? *Science*. American Association for the Advancement of Science May 18, 2018, pp 728–732. <https://doi.org/10.1126/science.aar3780>.
- (170) WHO. WHO | Highly hazardous pesticides https://www.who.int/ipcs/assessment/public_health/pesticides/en/ (accessed Aug 1, 2020).
- (171) Organization, W. H. Exposure To Highly Hazardous Pesticides : A Major Public Health Concern. *WHO Doc. Prod. Serv.* **2010**.
- (172) Nicolopoulou-Stamati, P.; Maipas, S.; Kotampasi, C.; Stamatis, P.; Hens, L. Chemical Pesticides and Human Health: The Urgent Need for a New Concept in Agriculture. *Front. Public Heal.* **2016**, *4*, 1. <https://doi.org/10.3389/fpubh.2016.00148>.
- (173) Marrone, P. G. Pesticidal Natural Products – Status and Future Potential. *Pest Manag. Sci.* **2019**, *75* (9), 2325–2340. <https://doi.org/10.1002/ps.5433>.
- (174) Pesticides Market Global Opportunities And Strategies To 2023 <https://www.thebusinessresearchcompany.com/report/pesticides-market> (accessed Mar 24, 2020).
- (175) Insecticides Market | Growth, Trends, and Forecast - 2022 <https://www.marketsandmarkets.com/Market-Reports/insecticide-market-142427569.html> (accessed Mar 24, 2020).
- (176) Huang, Y.; Ho, S. H.; Lee, H. C.; Yap, Y. L. Insecticidal Properties of Eugenol, Isoeugenol and Methyleugenol and Their Effects on Nutrition of *Sitophilus Zeamais* Motsch. (Coleoptera: Curculionidae) and *Tribolium Castaneum* (Herbst) (Coleoptera: Tenebrionidae). *J. Stored Prod. Res.* **2002**, *38* (5), 403–412. [https://doi.org/10.1016/S0022-474X\(01\)00042-X](https://doi.org/10.1016/S0022-474X(01)00042-X).
- (177) EPA. United States Environmental Protection Agency | US EPA <https://www.epa.gov/> (accessed Mar 30, 2020).
- (178) Marchand, P. A. Basic and Low-Risk Substances under European Union Pesticide Regulations: A New Choice for Biorational Portfolios of Small and Medium-Sized Enterprises. *J. Plant Prot. Res.* **2017**, *57* (4), 433–440. <https://doi.org/10.1515/jppr-2017-0056>.
- (179) Ngoh, S. P.; Choo, L. E. W.; Pang, F. Y.; Huang, Y.; Kini, M. R.; Ho, S. H. Insecticidal and Repellent Properties of Nine Volatile Constituents of Essential Oils against the American Cockroach, *Periplaneta Americana* (L.). *Pestic. Sci.* **1998**, *54* (3), 261–268. [https://doi.org/10.1002/\(SICI\)1096-9063\(199811\)54:3<261::AID-PS794>3.0.CO;2-C](https://doi.org/10.1002/(SICI)1096-9063(199811)54:3<261::AID-PS794>3.0.CO;2-C).
- (180) Silva, C. G. V.; Zago, H. B.; Júnior, H. J. G. S.; Da Camara, C. A. G.; De Oliveira, J. V.; Barros, R.; Schwartz, M. O. E.; Lucena, M. F. A. Composition and Insecticidal Activity of the Essential Oil of *Croton Grewioides* Baill. against Mexican Bean Weevil (*Zabrotes Subfasciatus* Boheman). *J. Essent. Oil Res.* **2008**, *20* (2), 179–182. <https://doi.org/10.1080/10412905.2008.9699985>.
- (181) Ruddy, D. A.; Schaidle, J. A.; Ferrell, J. R.; Wang, J.; Moens, L.; Hensley, J. E. *Recent Advances in Heterogeneous Catalysts for Bio-Oil Upgrading via “Ex Situ Catalytic Fast Pyrolysis”*: Catalyst Development through the Study of Model Compounds; 2014; Vol. 16. <https://doi.org/10.1039/c3gc41354c>.
- (182) Mukarakate, C.; Mcbrayer, J. D.; Evans, T. J.; Budhi, S.; Robichaud, D. J.; Iisa, K.; Ten Dam, J.; Watson, M. J.; Baldwin, R. M.; Nimlos, M. R. Catalytic Fast Pyrolysis of Biomass: The Reactions of Water and Aromatic Intermediates Produces Phenols. *Green Chem.* **2015**, *17* (8), 4217–4227. <https://doi.org/10.1039/c5gc00805k>.

- (183) Elkasabi, Y.; Mullen, C. A.; Boateng, A. A. Distillation and Isolation of Commodity Chemicals from Bio-Oil Made by Tail-Gas Reactive Pyrolysis. *ACS Sustain. Chem. Eng.* **2014**, *2* (8), 2042–2052. <https://doi.org/10.1021/sc5002879>.
- (184) Olarte, M. V.; Padmaperuma, A. B.; Ferrell, J. R.; Christensen, E. D.; Hallen, R. T.; Lucke, R. B.; Burton, S. D.; Lemmon, T. L.; Swita, M. S.; Fioroni, G.; Elliott, D. C.; Drennan, C. Characterization of Upgraded Fast Pyrolysis Oak Oil Distillate Fractions from Sulfided and Non-Sulfided Catalytic Hydrotreating. *Fuel* **2017**, *202*, 620–630. <https://doi.org/10.1016/j.fuel.2017.03.051>.
- (185) Griffin, M. B.; Iisa, K.; Wang, H.; Dutta, A.; Orton, K. A.; French, R. J.; Santosa, D. M.; Wilson, N.; Christensen, E.; Nash, C.; Van Allsburg, K. M.; Baddour, F. G.; Ruddy, D. A.; Tan, E. C. D.; Cai, H.; Mukarakate, C.; Schaidle, J. A. Driving towards Cost-Competitive Biofuels through Catalytic Fast Pyrolysis by Rethinking Catalyst Selection and Reactor Configuration. *Energy Environ. Sci.* **2018**, *11* (10), 2904–2918. <https://doi.org/10.1039/c8ee01872c>.
- (186) Burrack, H. J.; Asplen, M.; Bahder, L.; Collins, J.; Drummond, F. A.; Guédot, C.; Isaacs, R.; Johnson, D.; Blanton, A.; Lee, J. C.; Loeb, G.; Rodriguez-Saona, C.; Timmeren, S. Van; Walsh, D.; McPhie, D. R. Multistate Comparison of Attractants for Monitoring *Drosophila Suzukii* (Diptera: Drosophilidae) in Blueberries and Caneberries. *Environ. Entomol.* **2015**, *44* (3), 704–712. <https://doi.org/10.1093/ee/nvv022>.
- (187) Cini, A.; Ioriatti, C.; Anfora, G. A Review of the Invasion of *Drosophila Suzukii* in Europe and a Draft Research Agenda for Integrated Pest Management. *Bull. Insectology* **2012**, *65* (1), 149–160.
- (188) Deprá, M.; Poppe, J. L.; Schmitz, H. J.; De Toni, D. C.; Valente, V. L. S. The First Records of the Invasive Pest *Drosophila Suzukii* in the South American Continent. *J. Pest Sci. (2004)*. **2014**, *87* (3), 379–383. <https://doi.org/10.1007/s10340-014-0591-5>.
- (189) Calabria, G.; Máca, J.; Bächli, G.; Serra, L.; Pascual, M. First Records of the Potential Pest Species *Drosophila Suzukii* (Diptera: Drosophilidae) in Europe. *J. Appl. Entomol.* **2012**, *136* (1–2), 139–147. <https://doi.org/10.1111/j.1439-0418.2010.01583.x>.
- (190) Dos Santos, L. A.; Mendes, M. F.; Krüger, A. P.; Blauth, M. L.; Gottschalk, M. S.; Garcia, F. R. M. Global Potential Distribution of *Drosophila Suzukii* (Diptera, Drosophilidae). *PLoS One* **2017**, *12* (3), 1–13. <https://doi.org/10.1371/journal.pone.0174318>.
- (191) Dalton, D. T.; Walton, V. M.; Shearer, P. W.; Walsh, D. B.; Caprile, J.; Isaacs, R. Laboratory Survival of *Drosophila Suzukii* under Simulated Winter Conditions of the Pacific Northwest and Seasonal Field Trapping in Five Primary Regions of Small and Stone Fruit Production in the United States. *Pest Manag. Sci.* **2011**, *67* (11), 1368–1374. <https://doi.org/10.1002/ps.2280>.
- (192) Dutta, A.; Iisa, M. K.; Mukarakate, C.; Griffin, M. B.; Tan, E. C. D.; Schaidle, J. A.; Humbird, D.; Wang, H.; Hartley, D.; Thompson, D.; Cai, H. *Ex Situ Catalytic Fast Pyrolysis of Lignocellulosic Biomass to Hydrocarbon Fuels: 2019 State of Technology and Future Research*; 2020. <https://doi.org/10.2172/1605092>.
- (193) Gmehling, J.; Wittig, R.; Lohmann, J.; Joh, R. A Modified UNIFAC (Dortmund) Model. 4. Revision and Extension. *Ind. Eng. Chem. Res.* **2002**, *41* (6), 1678–1688. <https://doi.org/10.1021/ie0108043>.
- (194) Hanes, R. J.; Carpenter, A. Evaluating Opportunities to Improve Material and Energy Impacts in Commodity Supply Chains. *Environ. Syst. Decis.* **2017**, *37* (1), 6–12. <https://doi.org/10.1007/s10669-016-9622-5>.
- (195) Materials Flows through Industry Supply Chain Modeling Tool | Advanced Manufacturing Research | NREL <https://www.nrel.gov/manufacturing/mfi-modeling-tool.html> (accessed Aug 13, 2020).
- (196) ecoinvent <https://www.ecoinvent.org/> (accessed Oct 26, 2020).
- (197) Oasmaa, A.; Czernik, S. Fuel Oil Quality of Biomass Pyrolysis Oils - State of the Art for the End Users. *Energy and Fuels* **1999**, *13* (4), 914–921. <https://doi.org/10.1021/ef980272b>.
- (198) Zhang, X. S.; Yang, G. X.; Jiang, H.; Liu, W. J.; Ding, H. S. Mass Production of Chemicals from Biomass-Derived Oil by Directly Atmospheric Distillation Coupled with Co-Pyrolysis. *Sci. Rep.* **2013**, *3*, 1–7. <https://doi.org/10.1038/srep01120>.
- (199) Pollard, A. S.; Rover, M. R.; Brown, R. C. Characterization of Bio-Oil Recovered as Stage Fractions with Unique Chemical and Physical Properties. *J. Anal. Appl. Pyrolysis* **2012**, *93*, 129–138. <https://doi.org/10.1016/j.jaap.2011.10.007>.
- (200) Jing, C.; Gou, J.; Han, X.; Wu, Q.; Zhang, C. In Vitro and in Vivo Activities of Eugenol against Tobacco Black Shank Caused by *Phytophthora Nicotianae*. *Pestic. Biochem. Physiol.* **2017**, *142*, 148–154. <https://doi.org/10.1016/j.pestbp.2017.07.001>.
- (201) Albaseer, S. S.; Nageswara Rao, R.; Swamy, Y. V.; Mukkanti, K. An Overview of Sample Preparation and Extraction of Synthetic Pyrethroids from Water, Sediment and Soil. *J. Chromatogr. A* **2010**, *1217* (35), 5537–5554. <https://doi.org/10.1016/j.chroma.2010.06.058>.
- (202) Metcalf, R. L. Insect Resistance to Insecticides. *Pestic. Sci.* **1989**, *26* (4), 333–358. <https://doi.org/10.1002/ps.2780260403>.
- (203) Wouters, W.; Bercken, J. den. Action of Pyrethroids. *Gen. Pharmacol. Vasc. Syst.* **1978**, *9* (6), 387–398. [https://doi.org/https://doi.org/10.1016/0306-3623\(78\)90023-X](https://doi.org/https://doi.org/10.1016/0306-3623(78)90023-X).
- (204) lambda-Cyhalothrin - Commission, EU Pesticides database <https://ec.europa.eu/food/plant/pesticides/eu->

- pesticides-database/public/?event=activesubstance.detail&language=EN&selectedID=1509 (accessed Aug 14, 2020).
- (205) (NPIC), N. P. I. C. Lambda-Cyhalothrin (General Fact Sheet). **2001**, No. 4, 1–6.
- (206) Bates, N.; Campbell, A. Organophosphate Insecticides. *Handb. Poisoning Dogs Cats* **2008**, 199–204. <https://doi.org/10.1002/9780470699010.ch50>.
- (207) Organophosphates - StatPearls - NCBI Bookshelf <https://www.ncbi.nlm.nih.gov/books/NBK499860/> (accessed Aug 14, 2020).
- (208) Mulla, S. I.; Ameen, F.; Talwar, M. P.; Eqani, S. A. M. A. S.; Bharagava, R. N.; Saxena, G.; Tallur, P. N.; Ninnekar, H. Z. Organophosphate Pesticides: Impact on Environment, Toxicity, and Their Degradation. *Bioremediation Ind. Waste Environ. Saf.* **2020**, 265–290. https://doi.org/10.1007/978-981-13-1891-7_13.
- (209) Malathion - EU Pesticides database - European Commission <https://ec.europa.eu/food/plant/pesticides/eu-pesticides-database/public/?event=activesubstance.detail&language=EN&selectedID=1525> (accessed Aug 14, 2020).
- (210) Malathion | Mosquito Control | US EPA <https://www.epa.gov/mosquitocontrol/malathion> (accessed Aug 14, 2020).
- (211) Patel, M.; Oyedun, A. O.; Kumar, A.; Doucette, J. The Development of a Cost Model for Two Supply Chain Network Scenarios for Decentralized Pyrolysis System Scenarios to Produce Bio-Oil. *Biomass and Bioenergy* **2019**, 128 (July), 105287. <https://doi.org/10.1016/j.biombioe.2019.105287>.
- (212) Braimakis, K.; Atsonios, K.; Panopoulos, K. D.; Karellas, S.; Kakaras, E. Economic Evaluation of Decentralized Pyrolysis for the Production of Bio-Oil as an Energy Carrier for Improved Logistics towards a Large Centralized Gasification Plant. *Renew. Sustain. Energy Rev.* **2014**, 35, 57–72. <https://doi.org/10.1016/j.rser.2014.03.052>.
- (213) Muth, D. J.; Langholtz, M. H.; Tan, E. C. D.; Jacobson, J. J.; Schwab, A.; Wu, M. M.; Argo, A.; Brandt, C. C.; Cafferty, K. G.; Chiu, Y. W.; Dutta, A.; Eaton, L. M.; Searcy, E. M. Investigation of Thermochemical Biorefinery Sizing and Environmental Sustainability Impacts for Conventional Supply System and Distributed Pre-Processing Supply System Designs. *Biofuels, Bioprod. Biorefining* **2014**, 8 (4), 545–567. <https://doi.org/10.1002/bbb.1483>.
- (214) EPA. Biopesticides | Pesticides | US EPA <https://www.epa.gov/pesticides/biopesticides> (accessed Mar 18, 2020).
- (215) EPA. What Are Biopesticides ?
- (216) US EPA, O. About Pesticide Registration.
- (217) USDA. *Active Ingredients Eligible for Minimum Risk Pesticide Products*; 2015.
- (218) Frederiks, C.; Wessler, J. H. H. A Comparison of the EU and US Regulatory Frameworks for the Active Substance Registration of Microbial Biological Control Agents. *Pest Manag. Sci.* **2019**, 75 (1), 87–103. <https://doi.org/10.1002/ps.5133>.
- (219) Integrated Pest Management (IPM) | Food Safety https://ec.europa.eu/food/plant/pesticides/sustainable_use_pesticides/ipm_en (accessed May 20, 2020).
- (220) Pesticide evaluations: overview and procedure | European Food Safety <https://www.efsa.europa.eu/en/applications/pesticides> (accessed Oct 26, 2020).
- (221) Alemanno, A.; Gabbi, S. *Foundations of EU Food Law and Policy: Ten Years of the European Food Safety Authority*; 2014. <https://doi.org/10.4324/9781315582887>.
- (222) Hardy, T.; Bopp, S.; Egsmose, M.; Fontier, H.; Mohimont, L.; Steinkellner, H.; Streissl, F. Risk Assessment of Plant Protection Products. *EFSA J.* **2012**, 10 (10), 1–10. <https://doi.org/10.2903/j.efsa.2012.s1010>.
- (223) Bozzini, E. Pesticide Policy and Politics in the European Union: Regulatory Assessment, Implementation and Enforcement. *Pestic. Policy Polit. Eur. Union Regul. Assessment, Implement. Enforc.* **2017**, 1–120. <https://doi.org/10.1007/978-3-319-52736-9>.
- (224) *The European Green Deal*; 2019. <https://doi.org/10.2307/j.ctvd1c6zh.7>.
- (225) EPA. Renewable Fuel Standard Program <https://www.epa.gov/renewable-fuel-standard-program> (accessed Jul 1, 2020).
- (226) California Air Resources Board <https://ww2.arb.ca.gov/> (accessed Jul 1, 2020).
- (227) Airlines For America <https://www.airlines.org/#> (accessed Jul 1, 2020).
- (228) Renewable Energy – Recast to 2030 (RED II) | EU Science Hub <https://ec.europa.eu/jrc/en/jec/renewable-energy-recast-2030-red-ii> (accessed May 18, 2020).
- (229) Dahmen, N.; Lewandowski, I.; Zibek, S.; Weidtmann, A. Integrated Lignocellulosic Value Chains in a Growing Bioeconomy: Status Quo and Perspectives. *GCB Bioenergy* **2019**, 11 (1), 107–117. <https://doi.org/10.1111/gcbb.12586>.
- (230) Liu, C.; Wang, H.; Karim, A. M.; Sun, J.; Wang, Y. Catalytic Fast Pyrolysis of Lignocellulosic Biomass. *Chem. Soc. Rev.* **2014**, 43 (22), 7594–7623. <https://doi.org/10.1039/c3cs60414d>.
- (231) Elliott, D. C. Biofuel from Fast Pyrolysis and Catalytic Hydrodeoxygenation. *Curr. Opin. Chem. Eng.* **2015**, 9, 59–65. <https://doi.org/10.1016/j.coche.2015.08.008>.

- (232) Wildschut, J.; Mahfud, F. H.; Venderbosch, R. H.; Heeres, H. J. Hydrotreatment of Fast Pyrolysis Oil Using Heterogeneous Noble-Metal Catalysts. *Ind. Eng. Chem. Res.* **2009**, *48*, 10324–10334. <https://doi.org/https://doi.org/10.1021/ie9006003>.
- (233) Zacher, A. H.; Olarte, M. V.; Santosa, D. M.; Elliott, D. C.; Jones, S. B. A Review and Perspective of Recent Bio-Oil Hydrotreating Research. *Green Chem.* **2014**, *16* (2), 491–515. <https://doi.org/10.1039/c3gc41382a>.
- (234) Mahadevan, R.; Adhikari, S.; Shakya, R.; Wang, K.; Dayton, D.; Lehrich, M.; Taylor, S. E. Effect of Alkali and Alkaline Earth Metals on In-Situ Catalytic Fast Pyrolysis of Lignocellulosic Biomass: A Microreactor Study. *Energy and Fuels* **2016**, *30* (4), 3045–3056. <https://doi.org/10.1021/acs.energyfuels.5b02984>.
- (235) Patel, A.; Agrawal, B.; Rawal, B. R. Pyrolysis of Biomass for Efficient Extraction of Biofuel. *Energy Sources, Part A Recover. Util. Environ. Eff.* **2020**, *42* (13), 1649–1661. <https://doi.org/10.1080/15567036.2019.1604875>.
- (236) Iisa, K.; French, R. J.; Orton, K. A.; Yung, M. M.; Johnson, D. K.; Ten Dam, J.; Watson, M. J.; Nimlos, M. R. In Situ and Ex Situ Catalytic Pyrolysis of Pine in a Bench-Scale Fluidized Bed Reactor System. *Energy and Fuels* **2016**, *30* (3), 2144–2157. <https://doi.org/10.1021/acs.energyfuels.5b02165>.
- (237) Howe, D.; Westover, T.; Carpenter, D.; Santosa, D.; Emerson, R.; Deutch, S.; Starace, A.; Kutnyakov, I.; Lukins, C. Field-to-Fuel Performance Testing of Lignocellulosic Feedstocks: An Integrated Study of the Fast Pyrolysis-Hydrotreating Pathway. *Energy and Fuels* **2015**, *29* (5), 3188–3197. <https://doi.org/10.1021/acs.energyfuels.5b00304>.
- (238) Black, S.; Ferrell, J. R. Accelerated Aging of Fast Pyrolysis Bio-Oil: A New Method Based on Carbonyl Titration. *RSC Adv.* **2020**, *10* (17), 10046–10054. <https://doi.org/10.1039/d0ra00046a>.
- (239) Freeman, C. J.; Padmaperuma, A. B.; Santosa, M. Initial Assessment of U.S. Refineries for Purposes of Potential Bio-Based Oil Insertions. **2013**, No. April, 35.
- (240) van Dyk, S.; Su, J.; Mcmillan, J. D.; Saddler, J. (John). Potential Synergies of Drop-in Biofuel Production with Further Co-Processing at Oil Refineries. *Biofuels, Bioprod. Biorefining* **2019**, *13* (3), 760–775. <https://doi.org/10.1002/bbb.1974>.
- (241) FACT SHEET: Overview of USDA’s BioPreferred Program | USDA <https://www.usda.gov/media/press-releases/2016/02/18/fact-sheet-overview-usdas-biopreferred-program> (accessed Jul 1, 2020).
- (242) Bioeconomy policy | Bioeconomy - Research & Innovation - European Commission <https://ec.europa.eu/research/bioeconomy/index.cfm?pg=policy&lib=strategy> (accessed Jul 1, 2020).
- (243) Horvat, P.; Kržan, A. Certification of Bioplastics. *Plast. - Innov. value Chain Dev. Sustain. Plast. Cent. Eur.* **2012**.
- (244) Reddy, C. M.; Demello, J. A.; Carmichael, C. A.; Peacock, E. E.; Xu, L.; Arey, J. S. Determination of Biodiesel Blending Percentages Using Natural Abundance Radiocarbon Analysis: Testing the Accuracy of Retail Biodiesel Blends. *Environ. Sci. Technol.* **2008**, *42* (7), 2476–2482. <https://doi.org/10.1021/es071814j>.
- (245) Dijs, I. J.; van der Windt, E.; Kaihola, L.; van der Borg, K. Quantitative Determination by 14c Analysis of the Biological Component in Fuels. *Radiocarbon* **2006**, *48* (3), 315–323. <https://doi.org/10.1017/S0033822200038777>.
- (246) Edler, R. *The Use of Liquid Scintillation Counting Technology for the Determination of Biogenic Materials*; J Eikenberg, M Jäggi, H Beer, H. B., Ed.; Arizona Board of Regents, University of Arizona, 2009.
- (247) Norton, G. A.; Cline, A. M.; Thompson, G. C. Use of Radiocarbon Analyses for Determining Levels of Biodiesel in Fuel Blends - Comparison with ASTM Method D7371 for FAME. *Fuel* **2012**, *96*, 284–290. <https://doi.org/10.1016/j.fuel.2012.01.026>.
- (248) Telloli, C.; Rizzo, A.; Canducci, C.; Bartolomei, P. Determination of Bio Content in Polymers Used in the Packaging of Food Products. *Radiocarbon* **2019**, *00* (00), 1973–1981. <https://doi.org/10.1017/RDC.2019.141>.
- (249) Schimmel, M.; Toop, G.; Alberici, S.; Koper, M. *Determining the Renewability of Co-Processed Fuels, Final Report*; Utrecht, Netherlands, 2018.
- (250) ASTM International. ASTM D6866-20, Standard Test Methods for Determining the Biobased Content of Solid, Liquid, and Gaseous Samples Using Radiocarbon Analysis. West Conshohocken, PA 2020, pp 1–19. <https://doi.org/10.1520/D6866-20>.
- (251) *Regulation of Fuels and Fuel Additives: Changes to Renewable Fuel Standard Program; Final Rule*; 2006; Vol. 71.
- (252) Dell’Orco, S.; Christensen, E. D.; Iisa, K.; Starace, A. K.; Dutta, A.; Talmadge, M. S.; Magrini, K. A.; Mukarakate, C. Online Biogenic Carbon Analysis Enables Refineries to Reduce Carbon Footprint during Coprocessing Biomass- and Petroleum-Derived Liquids. *Anal. Chem.* **2021**. <https://doi.org/10.1021/acs.analchem.0c04108>.
- (253) Deniz Uner. *Advances in Refining Catalysis*; CRC Press, 2017.
- (254) Fogassy, G.; Thegarid, N.; Schuurman, Y.; Mirodatos, C. From Biomass to Bio-Gasoline by FCC Co-Processing: Effect of Feed Composition and Catalyst Structure on Product Quality. *Energy Environ. Sci.* **2011**, *4* (12), 5068–5076. <https://doi.org/10.1039/c1ee02012a>.
- (255) Agblevor, F. A.; Mante, O.; McClung, R.; Oyama, S. T. Co-Processing of Standard Gas Oil and Biocrude Oil

- to Hydrocarbon Fuels. *Biomass and Bioenergy* **2012**, *45*, 130–137. <https://doi.org/10.1016/j.biombioe.2012.05.024>.
- (256) *Fuels Europe - Statistical Report*; 2017. <https://doi.org/10.1080/0034408180130314>.
- (257) New Pilot Plant Demonstrates the Potential to Co-Process Biomass Streams with Petroleum, Department of Energy, USA <https://www.energy.gov/eere/bioenergy/articles/new-pilot-plant-demonstrates-potential-co-process-biomass-streams-petroleum> (accessed Apr 15, 2020).
- (258) Bezergianni, S.; Dimitriadis, A.; Kikhryanin, O.; Kubička, D. Refinery Co-Processing of Renewable Feeds. *Prog. Energy Combust. Sci.* **2018**, *68*, 29–64. <https://doi.org/10.1016/j.pecs.2018.04.002>.
- (259) Chen, Y. M. Recent Advances in FCC Technology. *Powder Technol.* **2006**, *163* (1–2), 2–8. <https://doi.org/10.1016/j.powtec.2006.01.001>.
- (260) Vogt, E. T. C.; Weckhuysen, B. M. Fluid Catalytic Cracking: Recent Developments on the Grand Old Lady of Zeolite Catalysis. *Chem. Soc. Rev.* **2015**, *44* (20), 7342–7370. <https://doi.org/10.1039/c5cs00376h>.
- (261) Fogassy, G.; Thegarid, N.; Toussaint, G.; van Veen, A. C.; Schuurman, Y.; Mirodatos, C. Biomass Derived Feedstock Co-Processing with Vacuum Gas Oil for Second-Generation Fuel Production in FCC Units. *Appl. Catal. B Environ.* **2010**, *96* (3–4), 476–485. <https://doi.org/10.1016/j.apcatb.2010.03.008>.
- (262) Renewable Identification Numbers (RINs) under the Renewable Fuel Standard Program | Renewable Fuel Standard Program | US EPA <https://www.epa.gov/renewable-fuel-standard-program/renewable-identification-numbers-rins-under-renewable-fuel-standard> (accessed Jul 6, 2020).
- (263) Mcphail, L.; Westcott, P.; Lutman, H. USDA - A Report from the Economic Research Service: The Renewable Identification Number System and U. S. Biofuel Mandates. **2011**.
- (264) Mukarakate, C.; Zhang, X.; Stanton, A. R.; Robichaud, D. J.; Ciesielski, P. N.; Malhotra, K.; Donohoe, B. S.; Gjersing, E.; Evans, R. J.; Heroux, D. S.; Richards, R.; Iisa, K.; Nimlos, M. R. Real-Time Monitoring of the Deactivation of HZSM-5 during Upgrading of Pine Pyrolysis Vapors. *Green Chem.* **2014**, *16* (3), 1444–1461. <https://doi.org/10.1039/c3gc42065e>.
- (265) Peterson, B.; Engtrakul, C.; Wilson, A. N.; Dell'Orco, S.; Orton, K. A.; Deutch, S.; Yung, M. M.; Starace, A. K.; Parent, Y.; Chiamonti, D.; Magrini, K. A. Catalytic Hot-Gas Filtration with a Supported Heteropolyacid Catalyst for Preconditioning Biomass Pyrolysis Vapors. *ACS Sustain. Chem. Eng.* **2019**, *7* (17), 14941–14952. <https://doi.org/10.1021/acssuschemeng.9b03188>.
- (266) *ISCC 203-01 Guidance for the Certification of Co-Processing*; 2017.
- (267) Air Resources Board. *Co-Processing of Biogenic Feedstocks in Petroleum Refineries*; 2017.
- (268) Libby, W. F.; Anderson, E. C.; Arnold, J. R. Age Determination by Radiocarbon Content: World-Wide Assay of Natural Radiocarbon. *Science* (80-.). **1949**, *109* (2827), 227–228. <https://doi.org/10.1126/science.109.2827.227>.
- (269) Taylor, R. E. Radiocarbon Dating. In *Chronometric Dating in Archaeology. Advances in Archaeological and Museum Science*; M.J., A., Ed.; Springer: Boston, MA, 1997; Vol. 2. <https://doi.org/10.1126/science.133.3453.621>.
- (270) ASTM D6866 Biogenic Carbon Content Testing <https://www.betalabservices.com/renewable-carbon/astmd6866.html> (accessed May 1, 2020).
- (271) Hajdas, I.; Bonani, G.; Thut, J.; Leone, G.; Pfenninger, R.; Maden, C. A Report on Sample Preparation at the ETH/PSI AMS Facility in Zurich. *Nucl. Instruments Methods Phys. Res. Sect. B Beam Interact. with Mater. Atoms* **2004**, *223–224* (SPEC. ISS.), 267–271. <https://doi.org/10.1016/j.nimb.2004.04.054>.
- (272) Noakes, J.; Norton, G.; Culp, R.; Nigam, M.; Dvoracek, D. A Comparison of Analytical Methods for the Certification of Biobased Products. In *Prace Naukowe GIG. Gornictwo i Srodowisko; Conference: LSC 2005 - Advances in Liquid Scintillation Spectrometry*; Katowice (Poland), 2005.
- (273) Norton, G. A.; Devlin, S. L. Determining the Modern Carbon Content of Biobased Products Using Radiocarbon Analysis. *Bioresour. Technol.* **2006**, *97* (16), 2084–2090. <https://doi.org/10.1016/j.biortech.2005.08.017>.
- (274) Norton, G. A. Interlaboratory Variability of Radiocarbon Results Obtained from Blind AMS Analyses on Several Modern Carbon Samples. *Radiocarbon* **2011**, *53* (3), 551–556. <https://doi.org/10.1017/S0033822200034652>.
- (275) Keck, B. D.; Ognibene, T.; Vogel, J. S. Analytical Validation of Accelerator Mass Spectrometry for Pharmaceutical Development. *Bioanalysis*. **2010**, *2* (3), 469–485. <https://doi.org/doi:10.4155/bio.10.14>.
- (276) Haverly, M. R.; Fenwick, S. R.; Patterson, F. P. K.; Slade, D. A. Biobased Carbon Content Quantification through AMS Radiocarbon Analysis of Liquid Fuels. *Fuel* **2019**, *237*, 1108–1111. <https://doi.org/10.1016/j.fuel.2018.10.081>.
- (277) Culp, R.; Cherkinsky, A.; Ravi Prasad, G. V. Comparison of Radiocarbon Techniques for the Assessment of Biobase Content in Fuels. *Appl. Radiat. Isot.* **2014**, *93*, 106–109. <https://doi.org/10.1016/j.apradiso.2014.01.007>.
- (278) Qureshi, R. M.; Aravena, R.; Fritz, P.; Drimmie, R. The CO₂ Absorption Method as an Alternative to Benzene Synthesis Method for ¹⁴C Dating. *Appl. Geochemistry* **1989**, *4* (6), 625–633. [229](https://doi.org/10.1016/0883-</p>
</div>
<div data-bbox=)

- 2927(89)90072-3.
- (279) Woo, H. J.; Chun, S. K.; Cho, S. Y.; Kim, Y. S.; Kang, D. W.; Kim, E. H. Optimization of Liquid Scintillation Counting Techniques for the Determination of Carbon-14 in Environmental Samples. *J. Radioanal. Nucl. Chem.* **1999**, *239* (3), 649–655. <https://doi.org/10.1007/BF02349085>.
- (280) Bronić, I. K.; Barešić, J.; Horvatinčić, N.; Sironić, A. Determination of Biogenic Component in Liquid Fuels by the ¹⁴C Direct LSC Method by Using Quenching Properties of Modern Liquids for Calibration. *Radiat. Phys. Chem.* **2017**, *137*, 248–253. <https://doi.org/10.1016/j.radphyschem.2016.01.041>.
- (281) Doll, C. G.; Wright, C. W.; Morley, S. M.; Wright, B. W. Analysis of Fuel Using the Direct LSC Method Determination of Bio-Originated Fuel in the Presence of Quenching. *Appl. Radiat. Isot.* **2017**, *122* (November 2016), 215–221. <https://doi.org/10.1016/j.apradiso.2017.01.040>.
- (282) Edler, R.; Kaihola, L. Differentiation between Fossil and Biofuels by Liquid Scintillation Beta Spectrometry - Direct Method1. *Nukleonika* **2010**, *55* (1), 127–131.
- (283) Norton, G. A.; Woodruff, M. X. Simplified Radiocarbon Analysis Procedure for Measuring the Renewable Diesel Concentration in Diesel Fuel Blends. *JAOCs, J. Am. Oil Chem. Soc.* **2012**, *89* (5), 797–803. <https://doi.org/10.1007/s11746-011-1966-x>.
- (284) Krištof, R.; Logar, J. K. Direct LSC Method for Measurements of Biofuels in Fuel. *Talanta* **2013**, *111*, 183–188. <https://doi.org/10.1016/j.talanta.2013.03.009>.
- (285) Krištof, R.; Hirsch, M.; Kožar Logar, J. Implementation of Direct LSC Method for Diesel Samples on the Fuel Market. *Appl. Radiat. Isot.* **2014**, *93*, 101–105. <https://doi.org/10.1016/j.apradiso.2014.04.003>.
- (286) Ognibene, T. J.; Bench, G.; Brown, T. A.; Peaslee, G. F.; Vogel, J. S. A New Accelerator Mass Spectrometry System for ¹⁴C-Quantification of Biochemical Samples. *Int. J. Mass Spectrom.* **2002**, *218* (3), 255–264. [https://doi.org/10.1016/S1387-3806\(02\)00734-0](https://doi.org/10.1016/S1387-3806(02)00734-0).
- (287) Schulze-König, T.; Dueker, S. R.; Giacomo, J.; Suter, M.; Vogel, J. S.; Synal, H. A. BioMICADAS: Compact next Generation AMS System for Pharmaceutical Science. *Nucl. Instruments Methods Phys. Res. Sect. B Beam Interact. with Mater. Atoms* **2010**, *268* (7–8), 891–894. <https://doi.org/10.1016/j.nimb.2009.10.057>.
- (288) Bard, E.; Tuna, T.; Fagault, Y.; Bonvalot, L.; Wacker, L.; Fahrni, S.; Synal, H. A. AixMICADAS, the Accelerator Mass Spectrometer Dedicated to ¹⁴C Recently Installed in Aix-En-Provence, France. *Nucl. Instruments Methods Phys. Res. Sect. B Beam Interact. with Mater. Atoms* **2015**, *361*, 80–86. <https://doi.org/10.1016/j.nimb.2015.01.075>.
- (289) Salehpour, M.; Håkansson, K.; Possnert, G.; Wacker, L.; Synal, H. A. Performance Report for the Low Energy Compact Radiocarbon Accelerator Mass Spectrometer at Uppsala University. *Nucl. Instruments Methods Phys. Res. Sect. B Beam Interact. with Mater. Atoms* **2016**, *371*, 360–364. <https://doi.org/10.1016/j.nimb.2015.10.034>.
- (290) Lee, S. H.; Park, S. H.; Kong, M. J.; Kim, Y. S. A New Compact AMS Facility at the Dongguk University. *Nucl. Instruments Methods Phys. Res. Sect. B Beam Interact. with Mater. Atoms* **2020**, *465* (December 2019), 15–18. <https://doi.org/10.1016/j.nimb.2019.12.027>.
- (291) Peters, K. E.; Moldowan, J. M.; Schoell, M.; Hempkins, W. B. Petroleum Isotopic and Biomarker Composition Related to Source Rock Organic Matter and Depositional Environment. *Org. Geochem.* **1986**, *10* (1–3), 17–27. [https://doi.org/10.1016/0146-6380\(86\)90006-9](https://doi.org/10.1016/0146-6380(86)90006-9).
- (292) Rashmi, D.; Shree, P.; Singh, D. K. Stable Isotope Ratio Analysis in Determining the Geographical Traceability of Indian Wheat. *Food Control* **2017**, *79*, 169–176. <https://doi.org/10.1016/j.foodcont.2017.03.025>.
- (293) Botosoa, E. P.; Caytan, E.; Silvestre, V.; Robins, R. J.; Akoka, S. Unexpected Fractionation in Site-Specific ¹³C Isotopic Distribution Detected by Quantitative ¹³C NMR at Natural Abundance. *J. Am. Chem. Soc.* **2008**, *130* (2), 414–415. <https://doi.org/10.1021/ja0771181>.
- (294) Fleisher, A. J.; Long, D. A.; Liu, Q.; Gameson, L.; Hodges, J. T. Optical Measurement of Radiocarbon below Unity Fraction Modern by Linear Absorption Spectroscopy. *J. Phys. Chem. Lett.* **2017**, *8* (18), 4550–4556. <https://doi.org/10.1021/acs.jpcclett.7b02105>.
- (295) Lancet, M. S.; Winschel, R. A.; Burke, F. P.; Burke, P. Stable Carbon Isotope Analysis Coprocessing Materials. *Fuel* **1993**, *72* (8), 1209–1217.
- (296) dos Santos, V. H. J. M.; Ketzer, J. M. M.; Rodrigues, L. F. Classification of Fuel Blends Using Exploratory Analysis with Combined Data from Infrared Spectroscopy and Stable Isotope Analysis. *Energy and Fuels* **2017**, *31* (1), 523–532. <https://doi.org/10.1021/acs.energyfuels.6b01937>.
- (297) dos Santos, V. H. J. M.; Ramos, A. S.; Pires, J. P.; Engelmann, P. de M.; Lourega, R. V.; Ketzer, J. M. M.; Rodrigues, L. F. Discriminant Analysis of Biodiesel Fuel Blends Based on Combined Data from Fourier Transform Infrared Spectroscopy and Stable Carbon Isotope Analysis. *Chemom. Intell. Lab. Syst.* **2017**, *161* (August 2016), 70–78. <https://doi.org/10.1016/j.chemolab.2016.12.004>.
- (298) Li, Z.; Magrini-Bair, K.; Wang, H.; Maltsev, O. V.; Geeza, T. J.; Mora, C. I.; Lee, J. E. Tracking Renewable Carbon in Bio-Oil/Crude Co-Processing with VGO through ¹³C/¹²C Ratio Analysis. *Fuel* **2020**, *275* (December 2019), 117770. <https://doi.org/10.1016/j.fuel.2020.117770>.

- (299) Monson, R. K.; Edwards, G. E.; Ku, M. S. B. C3-C4 Intermediate Photosynthesis Plants. *Russell J. Bertrand Russell Arch.* **2012**, *34* (9), 563–566.
- (300) Sage, R. F.; Christin, P. A.; Edwards, E. J. The C4 Plant Lineages of Planet Earth. *J. Exp. Bot.* **2011**, *62* (9), 3155–3169. <https://doi.org/10.1093/jxb/err048>.
- (301) Ehleringer, J. R.; Cerling, T. E. C3 and C4 Photosynthesis. *Encycl. Glob. Environ. Chang. earth Syst. Biol. Ecol. Dimens. Glob. Environ. Chang.* **2002**, *2*, 186–190.
- (302) Cerling, T. E.; Wang, Y.; Quade, J. Expansion of C4 Ecosystems as an Indicator of Global Ecological Change in the Late Miocene. *Nature* **1993**, *361* (6410), 344–345. <https://doi.org/10.1038/361344a0>.
- (303) Kohn, M. J. Carbon Isotope Compositions of Terrestrial C3 Plants as Indicators of (Paleo)Ecology and (Paleo)Climate. *Proc. Natl. Acad. Sci. U. S. A.* **2010**, *107* (46), 19691–19695. <https://doi.org/10.1073/pnas.1004933107>.
- (304) O’Leary, M. H. Carbon Isotopes in Photosynthesis: Fractionation Techniques May Reveal New Aspects of Carbon Dynamics in Plants. *Bioscience* **1988**, *38* (5), 328–336.
- (305) Coplen, T. B.; Böhlke, J. K.; De Bièvre, P.; Ding, T.; Holden, N. E.; Hopple, J. A.; Krouse, H. R.; Lamberty, A.; Peiser, H. S.; Révész, K.; Rieder, S. E.; Rosman, K. J. R.; Roth, E.; Taylor, P. D. P.; Vocke, R. D.; Xiao, Y. K. Isotope-Abundance Variations of Selected Elements (IUPAC Technical Report). *Pure Appl. Chem.* **2002**, *74* (10), 1987–2017. <https://doi.org/10.1351/pac200274101987>.
- (306) Geeza, T. J.; Li, Z.; Maltsev, O. V.; Lee, J. E. Cold-Weld Sealing in Argon Atmosphere for High Precision Carbon Isotope Analysis of Co-Processed Bio-Fuels Using a Continuous-Flow Isotope Ratio Mass Spectrometer. *Energy & Fuels* **2020**. <https://doi.org/10.1021/acs.energyfuels.0c02114>.
- (307) Langholtz, M.; Stokes, B.; Eaton, L. 2016 Billion-Ton Report: Advancing Domestic Resources for a Thriving Bioeconomy (Executive Summary). *Ind. Biotechnol.* **2016**, *12* (5), 282–289. <https://doi.org/10.1089/ind.2016.29051.doe>.
- (308) Carpenter, D.; Westover, T. L.; Czernik, S.; Jablonski, W. Biomass Feedstocks for Renewable Fuel Production: A Review of the Impacts of Feedstock and Pretreatment on the Yield and Product Distribution of Fast Pyrolysis Bio-Oils and Vapors. *Green Chemistry.* 2014, pp 384–406. <https://doi.org/10.1039/c3gc41631c>.
- (309) Zare, R. N. Ultrasensitive Radiocarbon Detection Species Choked and Blended. *Nature* **2012**, *482*, 312–313.
- (310) Murnick, D. E. Laser-Based Radiocarbon Detection in the Laboratory: How Soon? *J. Label. Compd. Radiopharm.* **2019**, *62* (11), 768–775. <https://doi.org/10.1002/jlcr.3794>.
- (311) Galli, I.; Bartalini, S.; Borri, S.; Cancio, P.; Mazzotti, D.; De Natale, P.; Giusfredi, G. Molecular Gas Sensing below Parts per Trillion: Radiocarbon-Dioxide Optical Detection. *Phys. Rev. Lett.* **2011**, *107* (27), 1–4. <https://doi.org/10.1103/PhysRevLett.107.270802>.
- (312) Giusfredi, G.; Galli, I.; Mazzotti, D.; Cancio, P.; De Natale, P. Theory of Saturated-Absorption Cavity Ring-down: Radiocarbon Dioxide Detection, a Case Study. *J. Opt. Soc. Am. B* **2015**, *32* (10), 2223. <https://doi.org/10.1364/josab.32.002223>.
- (313) Giusfredi, G.; Bartalini, S.; Borri, S.; Cancio, P.; Galli, I.; Mazzotti, D.; De Natale, P. Saturated-Absorption Cavity Ring-down Spectroscopy. *Phys. Rev. Lett.* **2010**, *104* (11), 1–4. <https://doi.org/10.1103/PhysRevLett.104.110801>.
- (314) Cancio, P.; Bartalini, S.; Borri, S.; Galli, I.; Gagliardi, G.; Giusfredi, G.; Maddaloni, P.; Malara, P.; Mazzotti, D.; De Natale, P. Frequency-Comb-Referenced Mid-IR Sources for next-Generation Environmental Sensors. *Appl. Phys. B Lasers Opt.* **2011**, *102* (2), 255–269. <https://doi.org/10.1007/s00340-010-4216-2>.
- (315) Galli, I.; Bartalini, S.; Barucci, M.; Cancio, P.; Cappelli, F.; Giusfredi, G.; Mazzotti, D.; Akikusa, N.; De Natale, P. Spectroscopic Detection of Radiocarbon Dioxide at Parts-per-Quadrillion Sensitivity. *Optica* **2016**, *3* (4), 385–388. <https://doi.org/10.1364/optica.3.000385>.
- (316) Lehmann, K. K. Theoretical Detection Limit of Saturated Absorption Cavity Ring-down Spectroscopy (SCAR) and Two-Photon Absorption Cavity Ring-down Spectroscopy. *Appl. Phys. B Lasers Opt.* **2014**, *116* (1), 147–155. <https://doi.org/10.1007/s00340-013-5663-3>.
- (317) Sadiq, I.; Friedrichs, G. Saturation Dynamics and Working Limits of Saturated Absorption Cavity Ringdown Spectroscopy. *Phys. Chem. Chem. Phys.* **2016**, *18* (33), 22978–22989. <https://doi.org/10.1039/c6cp01966h>.
- (318) Genoud, G.; Vainio, M.; Phillips, H.; Dean, J.; Merimaa, M. Radiocarbon Dioxide Detection Based on Cavity Ring-down Spectroscopy and a Quantum Cascade Laser. *Opt. Lett.* **2015**, *40* (7), 1342. <https://doi.org/10.1364/ol.40.001342>.
- (319) Galli, I.; Pastor, P. C.; Di Lonardo, G.; Fusina, L.; Giusfredi, G.; Mazzotti, D.; Tamassia, F.; De Natale, P. The ν_3 Band Of $^{14}\text{C}^{16}\text{O}_2$ molecule Measured by Optical-Frequency-Comb-Assisted Cavity Ring-down Spectroscopy. *Mol. Phys.* **2011**, *109* (17–18), 2267–2272. <https://doi.org/10.1080/00268976.2011.614284>.
- (320) McCart, A. D.; Ognibene, T. J.; Bench, G.; Turteltaub, K. W. Quantifying Carbon-14 for Biology Using Cavity Ring-Down Spectroscopy. *Anal. Chem.* **2016**, *88* (17), 8714–8719. <https://doi.org/10.1021/acs.analchem.6b02054>.
- (321) Genoud, G.; Lehmoskoski, J.; Bell, S.; Palonen, V.; Oinonen, M.; Reinikainen, M. Laser Spectroscopy for

- Monitoring of Radiocarbon in Atmospheric Samples. **2019**. <https://doi.org/10.1021/acs.analchem.9b02496>.
- (322) Murnick, D. E.; Dogru, O.; Ilkmen, E. Intracavity Optogalvanic Spectroscopy, A New Ultra-Sensitive Analytical Technique for ^{14}C Analysis. *Anal. Chem.* **2008**, *80* (13), 4820–4824. <https://doi.org/10.1021/ac800751y>.
- (323) Persson, A.; Eilers, G.; Ryderfors, L.; Mukhtar, E.; Possnert, G.; Salehpour, M. Evaluation of Intracavity Optogalvanic Spectroscopy for Radiocarbon Measurements. *Anal. Chem.* **2013**, *85* (14), 6790–6798. <https://doi.org/10.1021/ac400905n>.
- (324) Marino, B. D. V. *Near Surface Leakage Monitoring for the Verification and Accounting of Geologic Carbon Sequestration Using a Field Ready ^{14}C Isotopic Analyzer*; United States, 2014.
- (325) Carson, C. G.; Stute, M.; Ji, Y.; Polle, R.; Reboul, A.; Lackner, K. S. Invalidation of the Intracavity Optogalvanic Method for Radiocarbon Detection. *Radiocarbon* **2016**, *58* (1), 213–225. <https://doi.org/10.1017/RDC.2016.5>.
- (326) Paul, D.; Meijer, H. A. J. Intracavity OptoGalvanic Spectroscopy Not Suitable for Ambient Level Radiocarbon Detection. *Anal. Chem.* **2015**, *87* (17), 9025–9032. <https://doi.org/10.1021/acs.analchem.5b02226>.
- (327) Eilers, G.; Persson, A.; Gustavsson, C.; Ryderfors, L.; Mukhtar, E.; Possnert, G.; Salehpour, M. The Radiocarbon Intracavity Optogalvanic Spectroscopy Setup at Uppsala. *Radiocarbon* **2013**, *55* (2), 237–250. <https://doi.org/10.1017/s0033822200057349>.
- (328) Lewis, G.; Scientific, T. F.; Kingdom, U. Fast On-Line Monitoring of Flare Gases with the Prima PRO Process Mass Spectrometer. **2015**.
- (329) Komulainen, T.; Sourander, M.; Jämsä-Jounela, S. L. An Online Application of Dynamic PLS to a Dearomatization Process. *Comput. Chem. Eng.* **2004**, *28* (12), 2611–2619. <https://doi.org/10.1016/j.compchemeng.2004.07.014>.
- (330) Espinosa, A.; Lambert, D. Use NIR Technology to Optimize Plant Operations. *Hydrocarb. Process.* **1995**, *72* (2), 86. <https://doi.org/10.1108/17473611011026037>.
- (331) Chung, H. Applications of Near-Infrared Spectroscopy in Refineries and Important Issues to Address. *Appl. Spectrosc. Rev.* **2007**, *42* (3), 251–285. <https://doi.org/10.1080/05704920701293778>.
- (332) Czernik, S.; Bridgwater, A. V. Overview of Applications of Biomass Fast Pyrolysis Oil. *Energy and Fuels* **2004**, *18* (2), 590–598. <https://doi.org/10.1021/ef034067u>.
- (333) Sahoo, S.; Seydibeyoğlu, M. Ö.; Mohanty, A. K.; Misra, M. Characterization of Industrial Lignins for Their Utilization in Future Value Added Applications. *Biomass and Bioenergy* **2011**, *35* (10), 4230–4237. <https://doi.org/10.1016/j.biombioe.2011.07.009>.
- (334) Farag, S.; Chaouki, J. Economics Evaluation for On-Site Pyrolysis of Kraft Lignin to Value-Added Chemicals. *Bioresour. Technol.* **2015**, *175*, 254–261. <https://doi.org/10.1016/j.biortech.2014.10.096>.
- (335) Obydenkova, S. V.; Kouris, P. D.; Hensen, E. J. M.; Heeres, H. J.; Boot, M. D. Environmental Economics of Lignin Derived Transport Fuels. *Bioresour. Technol.* **2017**, *243*, 589–599. <https://doi.org/10.1016/j.biortech.2017.06.157>.
- (336) Biermann, C. J. Pulping Fundamentals. In *Handbook of Pulping and Papermaking*; Biermann, C. J., Ed.; 1996; pp 55–100. <https://doi.org/doi.org/10.1016/B978-012097362-0/50007-8>.
- (337) Xu, C.; Arancon, R. A. D.; Labidi, J.; Luque, R. Lignin Depolymerisation Strategies: Towards Valuable Chemicals and Fuels. *Chem. Soc. Rev.* **2014**, *43* (22), 7485–7500. <https://doi.org/10.1039/c4cs00235k>.
- (338) Solimene, R.; Cammarota, A.; Chirone, R.; Leoni, P.; Rossi, N.; Salatino, P. Devolatilization and Fragmentation of Solid Lignin-Rich Residues from Bioethanol Production in Lab-Scale Fluidized Bed Reactors. *Chem. Eng. Trans.* **2016**, *50*, 79–84. <https://doi.org/10.3303/CET1650014>.
- (339) Akiya, N.; Savage, P. E. Roles of Water for Chemical Reactions in High-Temperature Water. *Chem. Rev.* **2002**, *102* (8), 2725–2750. <https://doi.org/10.1021/cr000668w>.
- (340) Miliotti, E.; Dell’Orco, S.; Lotti, G.; Rizzo, A. M.; Rosi, L.; Chiaramonti, D. Lignocellulosic Ethanol Biorefinery: Valorization of Lignin-Rich Stream through Hydrothermal Liquefaction. *Energies* **2019**, *12* (4). <https://doi.org/10.3390/en12040723>.
- (341) Dell’Orco, S.; Miliotti, E.; Lotti, G.; Rizzo, A. M.; Rosi, L.; Chiaramonti, D. Hydrothermal Depolymerization of Biorefinery Lignin-Rich Streams: Influence of Reaction Conditions and Catalytic Additives on the Organic Monomers Yields in Biocrude and Aqueous Phase. *Energies* **2020**, *13* (5), 1241. <https://doi.org/10.3390/en13051241>.
- (342) Rizzo, A. M.; Dell’Orco, S.; Miliotti, E.; Chiaramonti, D. Design, Commissioning And Start-Up of a New Hydrothermal Liquefaction Continuous Pilot Unit. *Chem. Eng. Trans.* **2020**, *80* (February), 367–372. <https://doi.org/10.3303/CET2080062>.
- (343) Cao, L.; Zhang, C.; Chen, H.; Tsang, D. C. W.; Luo, G.; Zhang, S.; Chen, J. Hydrothermal Liquefaction of Agricultural and Forestry Wastes: State-of-the-Art Review and Future Prospects. *Bioresour. Technol.* **2017**, *245* (September), 1184–1193. <https://doi.org/10.1016/j.biortech.2017.08.196>.
- (344) Castello, D.; Pedersen, T.; Rosendahl, L. Continuous Hydrothermal Liquefaction of Biomass: A Critical Review. *Energies* **2018**, *11* (11), 3165. <https://doi.org/10.3390/en11113165>.

- (345) Barbier, J.; Charon, N.; Dupassieux, N.; Loppinet-Serani, A.; Mahé, L.; Ponthus, J.; Courtiade, M.; Ducrozet, A.; Quoineaud, A. A.; Cansell, F. Hydrothermal Conversion of Lignin Compounds. A Detailed Study of Fragmentation and Condensation Reaction Pathways. *Biomass and Bioenergy* **2012**, *46*, 479–491. <https://doi.org/10.1016/j.biombioe.2012.07.011>.
- (346) Wahyudiono; Kanetake, T.; Sasaki, M.; Goto, M. Decomposition of a Lignin Model Compound under Hydrothermal Conditions. *Chem. Eng. Technol.* **2007**, *30* (8), 1113–1122. <https://doi.org/10.1002/ceat.200700066>.
- (347) Zhang, B.; Huang, H.-J.; Ramaswamy, S. Reaction Kinetics of the Hydrothermal Treatment of Lignin. *Appl. Biochem. Biotechnol.* **2008**, *147* (1–3), 119–131. <https://doi.org/10.1007/s12010-007-8070-6>.
- (348) Nguyen, T. D. H.; Maschietti, M.; Ámand, L. E.; Vamling, L.; Olausson, L.; Andersson, S. I.; Theliander, H. The Effect of Temperature on the Catalytic Conversion of Kraft Lignin Using Near-Critical Water. *Bioresour. Technol.* **2014**, *170*, 196–203. <https://doi.org/10.1016/j.biortech.2014.06.051>.
- (349) Pińkowska, H.; Wolak, P.; Złocińska, A. Hydrothermal Decomposition of Alkali Lignin in Sub- and Supercritical Water. *Chem. Eng. J.* **2012**, *187*, 410–414. <https://doi.org/10.1016/j.cej.2012.01.092>.
- (350) Saisu, M.; Sato, T.; Watanabe, M.; Adschiri, T.; Arai, K. Conversion of Lignin with Supercritical Water - Phenol Mixtures. *Energy & Fuels* **2003**, No. 17, 922–928.
- (351) Miliotti, E.; Casini, D.; Lotti, G.; Pennazzi, S.; Rizzo, A. M.; Chiaramonti, D. Hydrothermal Carbonization of Digestate: Characterization of Solid and Liquid Products. In *TC Biomass*; Gas Technology Institute: Chicago, 2017. <https://doi.org/10.13140/RG.2.2.27310.82247>.
- (352) Peterson, A. A.; Vogel, F.; Lachance, R. P.; Fröling, M.; Antal, Jr., M. J.; Tester, J. W. Thermochemical Biofuel Production in Hydrothermal Media: A Review of Sub- and Supercritical Water Technologies. *Energy Environ. Sci.* **2008**, *1* (1), 32–65. <https://doi.org/10.1039/b810100k>.
- (353) Ahmad, Z.; Mahmood, N.; Yuan, Z.; Paleologou, M.; Xu, C. Effects of Process Parameters on Hydrolytic Treatment of Black Liquor for the Production of Low-Molecular-Weight Depolymerized Kraft Lignin. *Molecules* **2018**, *23* (10), 2464. <https://doi.org/10.3390/molecules23102464>.
- (354) Cheng, S.; Wilks, C.; Yuan, Z.; Leitch, M.; Xu, C. (Charles). Hydrothermal Degradation of Alkali Lignin to Bio-Phenolic Compounds in Sub/Supercritical Ethanol and Water–Ethanol Co-Solvent. *Polym. Degrad. Stab.* **2012**, *97* (6), 839–848. <https://doi.org/10.1016/j.polymdegradstab.2012.03.044>.
- (355) Channiwala, S. A.; Parikh, P. P. A Unified Correlation for Estimating HHV of Solid, Liquid and Gaseous Fuels. *Fuel* **2002**, *81* (8), 1051–1063. [https://doi.org/10.1016/S0016-2361\(01\)00131-4](https://doi.org/10.1016/S0016-2361(01)00131-4).
- (356) Sluiter, A.; Ruiz, R.; Scarlata, C.; Sluiter, J.; Templeton, D. *Determination of Extractives in Biomass, Technical Report NREL/TP-510-42619*; Golden, Colorado, 2008. <https://doi.org/NREL/TP-510-42621>.
- (357) Sluiter, A.; Hames, B.; Ruiz, R.; Scarlata, C.; Sluiter, J.; Templeton, D.; Nrel, D. C. *Determination of Structural Carbohydrates and Lignin in Biomass Determination of Structural Carbohydrates and Lignin in Biomass, Technical Report NREL/TP-510-42618*; Golden, Colorado, 2011. <https://doi.org/NREL/TP-510-42618>.
- (358) Sluiter, A.; Hames, B.; Ruiz, R. O.; Scarlata, C.; Sluiter, J.; Templeton, D.; Energy, D. of; Dötsch, A.; Severin, J.; Alt, W.; Galinski, E. a; Kreft, J.-U. *Determination of Ash in Biomass, Technical Report NREL/TP-510-42622*; Golden, Colorado, 2008. <https://doi.org/TP-510-42622>.
- (359) Sluiter, A.; Hames, B.; Ruiz, R.; Scarlata, C.; Sluiter, J.; Templeton, D. *Determination of Sugars, Byproducts, and Degradation Products in Liquid Fraction Process Samples, Technical Report NREL/TP-510-42623*; Golden, Colorado, 2008.
- (360) Jensen, M. M.; Djajadi, D. T.; Torri, C.; Rasmussen, H. B.; Madsen, R. B.; Venturini, E.; Vassura, I.; Becker, J.; Iversen, B. B.; Meyer, A. S.; Jørgensen, H.; Fabbri, D.; Glasius, M. Hydrothermal Liquefaction of Enzymatic Hydrolysis Lignin: Biomass Pretreatment Severity Affects Lignin Valorization. **2018**. <https://doi.org/10.1021/acssuschemeng.7b04338>.
- (361) Kang, S.; Li, X.; Fan, J.; Chang, J. Hydrothermal Conversion of Lignin: A Review. *Renew. Sustain. Energy Rev.* **2013**, *27*, 546–558. <https://doi.org/10.1016/j.rser.2013.07.013>.
- (362) Otromke, M.; White, R. J.; Sauer, J. Hydrothermal Base Catalyzed Depolymerization and Conversion of Technical Lignin – An Introductory Review. *Carbon Resour. Convers.* **2019**, *2* (1), 59–71. <https://doi.org/10.1016/j.crcon.2019.01.002>.
- (363) Toledano, A.; Serrano, L.; Labidi, J. Improving Base Catalyzed Lignin Depolymerization by Avoiding Lignin Repolymerization. *Fuel* **2014**, *116*, 617–624. <https://doi.org/10.1016/j.fuel.2013.08.071>.
- (364) Arturi, K. R.; Strandgaard, M.; Nielsen, R. P.; Sjøgaard, E. G.; Maschietti, M. Hydrothermal Liquefaction of Lignin in Near-Critical Water in a New Batch Reactor: Influence of Phenol and Temperature. *J. Supercrit. Fluids* **2017**, *123*, 28–39. <https://doi.org/10.1016/j.supflu.2016.12.015>.
- (365) Li, Q.; Liu, D.; Hou, X.; Wu, P.; Song, L.; Yan, Z. Hydro-Liquefaction of Microcrystalline Cellulose, Xylan and Industrial Lignin in Different Supercritical Solvents. *Bioresour. Technol.* **2016**, *219*, 281–288. <https://doi.org/10.1016/j.biortech.2016.07.048>.
- (366) Orebom, A.; Verendel, J. J.; Samec, J. S. M. High Yields of Bio Oils from Hydrothermal Processing of Thin

- Black Liquor without the Use of Catalysts or Capping Agents. *ACS Omega* **2018**, *3* (6), 6757–6763. <https://doi.org/10.1021/acsomega.8b00854>.
- (367) Montgomery, D. C. *Design and Analysis of Experiments, 5Ed*; Wiley: New York, 2001.
- (368) Ramirez, J. A.; Brown, R. J.; Rainey, T. J. A Review of Hydrothermal Liquefaction Bio-Crude Properties and Prospects for Upgrading to Transportation Fuels. *Energies* **2015**, *8* (7), 6765–6794. <https://doi.org/10.3390/en8076765>.
- (369) Jiang, W.; Lyu, G.; Wu, S.; Lucia, L. A. Near-Critical Water Hydrothermal Transformation of Industrial Lignins to High Value Phenolics. *J. Anal. Appl. Pyrolysis* **2016**, *120*, 297–303. <https://doi.org/10.1016/j.jaap.2016.05.017>.
- (370) Nazari, L.; Yuan, Z.; Souzanchi, S.; Ray, M. B.; Xu, C. Hydrothermal Liquefaction of Woody Biomass in Hot-Compressed Water: Catalyst Screening and Comprehensive Characterization of Bio-Crude Oils. *Fuel* **2015**, *162*, 74–83. <https://doi.org/10.1016/j.fuel.2015.08.055>.
- (371) Bui, N. Q.; Fongarland, P.; Rataboul, F.; Dartiguelongue, C.; Charon, N.; Vallée, C.; Essayem, N. FTIR as a Simple Tool to Quantify Unconverted Lignin from Chars in Biomass Liquefaction Process: Application to SC Ethanol Liquefaction of Pine Wood. *Fuel Process. Technol.* **2015**, *134*, 378–386. <https://doi.org/10.1016/j.fuproc.2015.02.020>.
- (372) Watanabe, M.; Kanaguri, Y.; Smith, R. L. Hydrothermal Separation of Lignin from Bark of Japanese Cedar. *J. Supercrit. Fluids* **2018**, *133* (September 2017), 696–703. <https://doi.org/10.1016/j.supflu.2017.09.009>.
- (373) Zhao, J.; Xiuwen, W.; Hu, J.; Liu, Q.; Shen, D.; Xiao, R. Thermal Degradation of Softwood Lignin and Hardwood Lignin by TG-FTIR and Py-GC/MS. *Polym. Degrad. Stab.* **2014**, *108*, 133–138. <https://doi.org/10.1016/j.polymdegradstab.2014.06.006>.
- (374) Okuda, K.; Umetsu, M.; Takami, S.; Adschiri, T. Disassembly of Lignin and Chemical Recovery - Rapid Depolymerization of Lignin without Char Formation in Water-Phenol Mixtures. *Fuel Process. Technol.* **2004**, *85* (8–10), 803–813. <https://doi.org/10.1016/j.fuproc.2003.11.027>.
- (375) Yuan, Z.; Cheng, S.; Leitch, M.; Xu, C. C. Hydrolytic Degradation of Alkaline Lignin in Hot-Compressed Water and Ethanol. *Bioresour. Technol.* **2010**, *101* (23), 9308–9313. <https://doi.org/10.1016/j.biortech.2010.06.140>.
- (376) Katahira, R.; Mittal, A.; McKinney, K.; Chen, X.; Tucker, M. P.; Johnson, D. K.; Beckham, G. T. Base-Catalyzed Depolymerization of Biorefinery Lignins. *ACS Sustain. Chem. Eng.* **2016**, *4* (3), 1474–1486. <https://doi.org/10.1021/acssuschemeng.5b01451>.
- (377) Nielsen, J. B.; Jensen, A.; Madsen, L. R.; Larsen, F. H.; Felby, C.; Jensen, A. D. Noncatalytic Direct Liquefaction of Biorefinery Lignin by Ethanol. *Energy and Fuels* **2017**, *31* (7), 7223–7233. <https://doi.org/10.1021/acs.energyfuels.7b00968>.
- (378) Belkheiri, T.; Mattsson, C.; Andersson, S. I.; Olausson, L.; Åmand, L. E.; Theliander, H.; Vamling, L. Effect of PH on Kraft Lignin Depolymerisation in Subcritical Water. *Energy and Fuels* **2016**, *30* (6), 4916–4924. <https://doi.org/10.1021/acs.energyfuels.6b00462>.
- (379) Xu, Y.; Isom, L.; Hanna, M. A. Adding Value to Carbon Dioxide from Ethanol Fermentations. *Bioresour. Technol.* **2010**, *101* (10), 3311–3319. <https://doi.org/10.1016/j.biortech.2010.01.006>.
- (380) McAloon, A.; Taylor, F.; Yee, W.; Regional, E.; Ibsen, K.; Wooley, R.; Biotechnology, N. *Determining the Cost of Producing Ethanol from Corn Starch and Lignocellulosic Feedstocks.*; Golden, Colorado, 2000.
- (381) Restrepo-Valencia, S.; Walter, A. Techno-Economic Assessment of Bio-Energy with Carbon Capture and Storage Systems in a Typical Sugarcane Mill in Brazil. *Energies* **2019**, *12* (6). <https://doi.org/10.3390/en12061129>.
- (382) Patel, R. N.; Bandyopadhyay, S.; Ganesh, A. Extraction of Cardanol and Phenol from Bio-Oils Obtained through Vacuum Pyrolysis of Biomass Using Supercritical Fluid Extraction. *Energy* **2011**, *36* (3), 1535–1542. <https://doi.org/10.1016/J.ENERGY.2011.01.009>.
- (383) Naik, S. N.; Goud, V. V.; Rout, P. K.; Dalai, A. K. Production of First and Second Generation Biofuels: A Comprehensive Review. *Renew. Sustain. Energy Rev.* **2010**, *14* (2), 578–597. <https://doi.org/10.1016/j.rser.2009.10.003>.
- (384) Montesantos, N.; Pedersen, T. H.; Nielsen, R. P.; Rosendahl, L.; Maschietti, M. Supercritical Carbon Dioxide Fractionation of Bio-Crude Produced by Hydrothermal Liquefaction of Pinewood. *J. Supercrit. Fluids* **2019**, *149*, 97–109. <https://doi.org/10.1016/j.supflu.2019.04.001>.
- (385) Montesantos, N.; Pedersen, T. H.; Nielsen, R. P.; Rosendahl, L. A.; Maschietti, M. High-Temperature Extraction of Lignocellulosic Bio-Crude by Supercritical Carbon Dioxide. *Chem. Eng. Trans.* **2019**, *74* (April 2018), 799–804. <https://doi.org/10.3303/CET1974134>.
- (386) Numan-Al-Mobin, A. M.; Kolla, P.; Dixon, D.; Smirnova, A. Effect of Water–Carbon Dioxide Ratio on the Selectivity of Phenolic Compounds Produced from Alkali Lignin in Sub- and Supercritical Fluid Mixtures. *Fuel* **2016**, *185*, 26–33. <https://doi.org/10.1016/j.fuel.2016.07.043>.
- (387) Heng, Y.; Quitain, A. T.; Yusup, S.; Uemura, Y.; Sasaki, M. Optimization of Hydrothermal Liquefaction of Palm Kernel Shell and Consideration of Supercritical Carbon Dioxide Mediation e Ff Ect. *J. Supercrit. Fluids*

- 2018**, *133* (April 2017), 640–646. <https://doi.org/10.1016/j.supflu.2017.06.007>.
- (388) Beckner, M.; Ivey, M. L.; Phister, T. G. Microbial Contamination of Fuel Ethanol Fermentations. *Let. Appl. Microbiol.* **2011**, *53* (4), 387–394. <https://doi.org/10.1111/j.1472-765X.2011.03124.x>.
- (389) Nissen, T. L.; Hamann, C. W.; Kielland-Brandt, M. C.; Nielsen, J.; Villadsen, J. Anaerobic and Aerobic Batch Cultivations of *Saccharomyces Cerevisiae* Mutants Impaired in Glycerol Synthesis. *Yeast* **2000**, *16* (5), 463–474. [https://doi.org/10.1002/\(SICI\)1097-0061\(20000330\)16:5<463::AID-YEA535>3.0.CO;2-3](https://doi.org/10.1002/(SICI)1097-0061(20000330)16:5<463::AID-YEA535>3.0.CO;2-3).
- (390) Wang, C.; Li, H.; Li, M.; Bian, J.; Sun, R. Revealing the Structure and Distribution Changes of Eucalyptus Lignin during the Hydrothermal and Alkaline Pretreatments. *Sci. Rep.* **2017**, *7* (1), 1–10. <https://doi.org/10.1038/s41598-017-00711-w>.
- (391) Bobleter, O. Hydrothermal Degradation of Polymers Derived from Plants. *Prog. Polym. Sci.* **1994**, *19* (5), 797–841. [https://doi.org/10.1016/0079-6700\(94\)90033-7](https://doi.org/10.1016/0079-6700(94)90033-7).
- (392) Sasaki Mitsuru, W.; Motonobu, G. Recovery of Phenolic Compounds through the Decomposition of Lignin in near and Supercritical Water. *Chem. Eng. Process. Process Intensif.* **2008**, *47* (9–10), 1609–1619. <https://doi.org/10.1016/j.cep.2007.09.001>.
- (393) Lawson, J. J. R.; Klein, M. M. T. Influence of Water on Guaiacol Pyrolysis. *Ind. Eng. Chem. Fundam.* **1985**, *24* (2), 203–208. <https://doi.org/10.1021/i100018a012>.
- (394) Miller, J. E.; Evans, L. R.; Mudd, J. E.; Brown, K. A. *Batch Microreactor Studies of Lignin Depolymerization by Bases. 2. Aqueous Solvents*; 2002. <https://doi.org/10.2172/800964>.
- (395) Robak, K.; Balcerek, M. Review of Second Generation Bioethanol Production from Residual Biomass. *Food Technol. Biotechnol.* **2018**, *56* (2), 174–187. <https://doi.org/10.17113/ftb.56.02.18.5428>.
- (396) Möller, M.; Harnisch, F.; Schröder, U. Hydrothermal Liquefaction of Cellulose in Subcritical Water-the Role of Crystallinity on the Cellulose Reactivity. *RSC Adv.* **2013**, *3* (27), 11035–11044. <https://doi.org/10.1039/c3ra41582a>.
- (397) Pedersen, T. H. HydroThermal Liquefaction of Biomass and Model Compounds, Ph.d.-serien for Det Teknisk-Naturvidenskabelige Fakultet, Aalborg Universitet, Aalborg Universitetsforlag, 2015. <https://doi.org/https://doi.org/10.5278/vbn.phd.engsci.00050>.
- (398) Pedersen, T. H.; Rosendahl, L. A. Production of Fuel Range Oxygenates by Supercritical Hydrothermal Liquefaction of Lignocellulosic Model Systems. *Biomass and Bioenergy* **2015**, *83*, 206–215. <https://doi.org/10.1016/j.biombioe.2015.09.014>.
- (399) Aden, A.; Ruth, M.; Ibsen, K.; Jechura, J.; Neeves, K.; Sheehan, J.; Wallace, B.; Montague, L.; Slayton, A.; Lukas, J. *Lignocellulosic Biomass to Ethanol Process Design and Economics Utilizing Co-Current Dilute Acid Prehydrolysis and Enzymatic Hydrolysis for Corn Stover*; Golden, Colorado, 2002.
- (400) Villadsen, S. R.; Dithmer, L.; Forsberg, R.; Becker, J.; Rudolf, A.; Iversen, S. B.; Glasius, M. Development and Application of Chemical Analysis Methods for Investigation of Bio-Oils and Aqueous Phase from Hydrothermal Liquefaction of Biomass. *Energy Fuels* **2012**, *26*, 6988–6998. <https://doi.org/10.1021/ef300954e>.
- (401) Jensen, M. M.; Madsen, R. B.; Becker, J.; Iversen, B. B.; Glasius, M. Products of Hydrothermal Treatment of Lignin and the Importance of Ortho-Directed Repolymerization Reactions. *J. Anal. Appl. Pyrolysis* **2017**, *126* (January), 371–379. <https://doi.org/10.1016/j.jaap.2017.05.009>.
- (402) Biswas, B.; Singh, R.; Kumar, J.; Khan, A. A.; Krishna, B. B.; Bhaskar, T. Slow Pyrolysis of Prot, Alkali and Dealkaline Lignins for Production of Chemicals. *Bioresour. Technol.* **2015**, *213*, 319–326. <https://doi.org/10.1016/j.biortech.2016.01.131>.
- (403) Li, S.; Lundquist, K. A New Method for the Analysis of Phenolic Groups in Lignins by ¹H NMR Spectrometry. *Nordic Pulp and Paper Research Journal*. 1994, pp 191–195. <https://doi.org/10.3183/NPPRJ-1994-09-03-p191-195>.
- (404) Chu, S.; Subrahmanyam, A. V.; Huber, G. W. The Pyrolysis Chemistry of a β -O-4 Type Oligomeric Lignin Model Compound. *Green Chem.* **2013**, *15* (1), 125–136. <https://doi.org/10.1039/c2gc36332a>.
- (405) Ingram, L.; Mohan, D.; Bricka, M.; Steele, P.; Strobel, D.; Crocker, D.; Mitchell, B.; Mohammad, J.; Cantrell, K.; Pittman, C. U. J. Pyrolysis of Wood and Bark in an Auger Reactor: Physical Properties and Chemical Analysis of the Produced Bio-Oils. *Energy & Fuels* **2008**, *22*, 614–625. <https://doi.org/10.1021/ef700335k>.
- (406) Ralph, S.; Ralph, J.; Landucci, L. L. NMR Database of Lignin and Cell Wall Model Compounds. 2009.
- (407) Mullen, C. A.; Strahan, G. D.; Boateng, A. A. Characterization of Various Fast-Pyrolysis Bio-Oils by NMR Spectroscopy. *Energy and Fuels* **2009**, *23* (5), 2707–2718. <https://doi.org/10.1021/ef801048b>.
- (408) Chern, S.; Tu, H.; Materials, A. The Thermochemical Conversion of Lactic Acid in Subcritical and Supercritical Water. *Eng. Technol. Int. J. Chem. Mol. Eng.* **2017**, *11* (1), 98–102.
- (409) Islam, M. N.; Taki, G.; Rana, M.; Park, J. H. Yield of Phenolic Monomers from Lignin Hydrothermolysis in Subcritical Water System. *Ind. Eng. Chem. Res.* **2018**, *57* (14), 4779–4784. <https://doi.org/10.1021/acs.iecr.7b05062>.
- (410) Singh, R.; Prakash, A.; Dhiman, S. K.; Balagurumurthy, B.; Arora, A. K.; Puri, S. K.; Bhaskar, T. Hydrothermal Conversion of Lignin to Substituted Phenols and Aromatic Ethers. *Bioresour. Technol.* **2014**,

- 165 (C), 319–322. <https://doi.org/10.1016/j.biortech.2014.02.076>.
- (411) Wahyudiono; Kanetake, T.; Sasaki, M.; Goto, M. Decomposition of a Lignin Model Compound under Hydrothermal Conditions. *Chem. Eng. Technol.* **2007**, *30* (8), 1113–1122. <https://doi.org/10.1002/ceat.200700066>.
- (412) Jegers, H. E.; Klein, M. T. Primary and Secondary Lignin Pyrolysis Reaction Pathways. *Ind. Eng. Chem. Process Des. Dev.* **1985**, *24* (1), 173–183. <https://doi.org/10.1021/i200028a030>.
- (413) Numan-Al-Mobin, A. M.; Voeller, K.; Bilek, H.; Kozliak, E.; Kubatova, A.; Raynie, D.; Dixon, D.; Smirnova, A. Selective Synthesis of Phenolic Compounds from Alkali Lignin in a Mixture of Sub- and Supercritical Fluids: Catalysis by CO₂. *Energy and Fuels* **2016**, *30* (3), 2137–2143. <https://doi.org/10.1021/acs.energyfuels.5b02136>.
- (414) Tabasinejad, F.; Moore, R. G.; Mehta, S. A.; Van Fraassen, K. C.; Barzin, Y.; Rushing, J. A.; Newsham, K. E. Water Solubility in Supercritical Methane, Nitrogen, and Carbon Dioxide: Measurement and Modeling from 422 to 483 K and Pressures from 3.6 to 134 MPa. *Ind. Eng. Chem. Res.* **2011**, *50* (7), 4029–4041. <https://doi.org/10.1021/ie101218k>.
- (415) Takenouchi, S.; Kennedy, G. C. The Binary System H₂O-CO₂ at High Temperature and Pressures. *Am. J. Sci.* **1964**, *262*, 1055–1074.
- (416) Pipitone, G.; Zoppi, G.; Bocchini, S.; Rizzo, A. M.; Chiaramonti, D.; Pirone, R.; Bensaid, S. Aqueous Phase Reforming of the Residual Waters Derived from Lignin-Rich Hydrothermal Liquefaction: Investigation of Representative Organic Compounds and Actual Biorefinery Streams. *Catal. Today* **2019**, No. July. <https://doi.org/10.1016/j.cattod.2019.09.040>.
- (417) INCO. *Corrosion Resistance of the Austenitic Chromium-Nickel Stainless Steels in Chemical Environments*; New York, USA, 1963.
- (418) Zhu, Y.; Bidy, M. J.; Jones, S. B.; Elliott, D. C.; Schmidt, A. J. Techno-Economic Analysis of Liquid Fuel Production from Woody Biomass via Hydrothermal Liquefaction (HTL) and Upgrading. *Appl. Energy* **2014**, *129*, 384–394. <https://doi.org/10.1016/j.apenergy.2014.03.053>.
- (419) Wang, Y.; Zhang, Y.; Wang, J.; Meng, L. Effects of Volatile Fatty Acid Concentrations on Methane Yield and Methanogenic Bacteria. *Biomass and Bioenergy* **2009**, *33* (5), 848–853. <https://doi.org/10.1016/j.biombioe.2009.01.007>.
- (420) Dewil, R.; Appels, L.; Baeyens, J.; Degre, J. Principles and Potential of the Anaerobic Digestion of Waste-Activated Sludge. **2008**, *34*, 755–781. <https://doi.org/10.1016/j.peccs.2008.06.002>.
- (421) Davidson, S. D.; Lopez-Ruiz, J. A.; Zhu, Y.; Cooper, A. R.; Albrecht, K. O.; Dagle, R. A. Strategies to Valorize the Hydrothermal Liquefaction-Derived Aqueous Phase into Fuels and Chemicals. *ACS Sustain. Chem. Eng.* **2019**. <https://doi.org/10.1021/acssuschemeng.9b05308>.
- (422) Starace, A. K.; Black, B. A.; Lee, D. D.; Palmiotti, E. C.; Orton, K. A.; Michener, W. E.; ten Dam, J.; Watson, M. J.; Beckham, G. T.; Magrini, K. A.; Mukarakate, C. Characterization and Catalytic Upgrading of Aqueous Stream Carbon from Catalytic Fast Pyrolysis of Biomass. *ACS Sustain. Chem. Eng.* **2017**, *acssuschemeng.7b03344*. <https://doi.org/10.1021/acssuschemeng.7b03344>.
- (423) Biller, P.; Madsen, R. B.; Klemmer, M.; Becker, J.; Iversen, B. B.; Glasius, M. Effect of Hydrothermal Liquefaction Aqueous Phase Recycling on Bio-Crude Yields and Composition. *Bioresour. Technol.* **2016**, *220*, 190–199. <https://doi.org/10.1016/j.biortech.2016.08.053>.
- (424) Law, J. D.; Todd, T. A. Liquid-Liquid Extraction Equipment. *Idaho Natl. Lab.* **2015**, 14.
- (425) Robbins, L. A.; Cusack, R. W. Liquid-Liquid Extraction Operations and Equipment. *Perry's Chem. Eng. Handb.* **1997**, 15-1-15–47. <https://doi.org/10.1036/0071511385>.
- (426) Typical Industrial Applications for Separation by Extraction | Koch Modular <https://kochmodular.com/liquid-liquid-extraction/industrial-applications/> (accessed Jun 29, 2020).
- (427) Karp, E. M.; Cywar, R. M.; Manker, L. P.; Saboe, P. O.; Nimlos, C. T.; Salvachúa, D.; Wang, X.; Black, B. A.; Reed, M. L.; Michener, W. E.; Rorrer, N. A.; Beckham, G. T. Post-Fermentation Recovery of Biobased Carboxylic Acids. *ACS Sustain. Chem. Eng.* **2018**, *6* (11), 15273–15283. <https://doi.org/10.1021/acssuschemeng.8b03703>.
- (428) Kawabata, N.; Yoshida, J. L.; Tanigawa, Y. Removal and Recovery of Organic Pollutants from Aquatic Environment. 4. Separation of Carboxylic Acids from Aqueous Solution Using Cross-Linked Poly(4-Vinylpyridine). *Ind. Eng. Chem. Prod. Res. Dev.* **1981**, *20* (2), 386–390. <https://doi.org/10.1021/i300002a030>.
- (429) Black, B. A.; Michener, W. E.; Ramirez, K. J.; Bidy, M. J.; Knott, B. C.; Jarvis, M. W.; Olstad, J.; Mante, O. D.; Dayton, D. C.; Beckham, G. T. Aqueous Stream Characterization from Biomass Fast Pyrolysis and Catalytic Fast Pyrolysis. *ACS Sustain. Chem. Eng.* **2016**, *4* (12), 6815–6827. <https://doi.org/10.1021/acssuschemeng.6b01766>.
- (430) Bader, R. G. Use of Factors for Converting Carbon or Nitrogen to Total Sedimentary Organics. *Science (80-)*. **1954**, *120* (3122), 709 LP – 710. <https://doi.org/10.1126/science.120.3122.709>.
- (431) Iglesias Jiménez, E.; Pérez García, V. Relationships between Organic Carbon and Total Organic Matter in Municipal Solid Wastes and City Refuse Composts. *Bioresour. Technol.* **1992**, *41* (3), 265–272.

- [https://doi.org/10.1016/0960-8524\(92\)90012-M](https://doi.org/10.1016/0960-8524(92)90012-M).
- (432) Prat, D.; Wells, A.; Hayler, J.; Sneddon, H.; McElroy, C. R.; Abou-Shehada, S.; Dunn, P. J. CHEM21 Selection Guide of Classical- and Less Classical-Solvents. *Green Chem.* **2015**, *18* (1), 288–296. <https://doi.org/10.1039/c5gc01008j>.
- (433) Chudziak, C.; Alberts, G.; Bauen, A. *Ramp up of Lignocellulosic Ethanol in Europe to 2030 Final Report*; 2017.
- (434) Koehler, N.; Mccaherty, J.; Wilson, C.; Cooper, G.; Schwarck, R.; Kemmet, N.; Baker, R.; McAfee, E.; Drook, R.; Markham, S.; Sitzmann, C.; Friedberg, J.; Ricketts, M.; Christensen, S.; Boyle, P.; Harder, S.; Keiser, K.; Woodside, C.; Roe, S.; Wilson, C. 2020 Ethanol Industry Outlook. *Renew. fuels Assoc.* **2020**, 40.
- (435) NREL. NREL Leads the Way, Cellulosic Ethanol. *NREL Rep.* **2007**, 1–8.
- (436) Catechol Faces Supply Crunch While Prices Rise | GEP <https://www.gep.com/mind/blog/catechol-faces-supply-crunch-while-prices-rise> (accessed May 5, 2020).
- (437) Acetic acid production capacity globally 2023 | Statista <https://www.statista.com/statistics/1063215/acetic-acid-production-capacity-globally/> (accessed Jul 31, 2020).
- (438) ICIS Pricing - Acetic Acid 2014. **2014**.
- (439) Chemical profile: propionic acid | ICIS <https://www.icis.com/explore/resources/news/2007/10/01/9065938/chemical-profile-propionic-acid/> (accessed Aug 3, 2020).
- (440) Osmundsen, C. M.; Egeblad, K.; Taarning, E. *Trends and Challenges in Catalytic Biomass Conversion*; Elsevier B.V., 2013. <https://doi.org/10.1016/B978-0-444-53878-9.00004-7>.
- (441) Yuan, S. F.; Hsu, T. C.; Wang, C. A.; Jang, M. F.; Kuo, Y. C.; Alper, H. S.; Guo, G. L.; Hwang, W. S. Production of Optically Pure l(+)-Lactic Acid from Waste Plywood Chips Using an Isolated Thermotolerant *Enterococcus Faecalis* SI at a Pilot Scale. *J. Ind. Microbiol. Biotechnol.* **2018**, *45* (11), 961–970. <https://doi.org/10.1007/s10295-018-2078-5>.
- (442) Wee, Y. J.; Kim, J. N.; Ryu, H. W. Biotechnological Production of Lactic Acid and Its Recent Applications. *Food Technol. Biotechnol.* **2006**, *44* (2), 163–172.
- (443) Global Glycolic Acid Market is Expected to Reach USD 203.3 million in 2018: Transparency Market Research <https://www.prnewswire.com/news-releases/global-glycolic-acid-market-is-expected-to-reach-usd-2033-million-in-2018-transparency-market-research-219392381.html> (accessed Jul 31, 2020).
- (444) Producer Price Index by Commodity for Chemicals and Allied Products: Industrial Chemicals. **2020**.
- (445) Jem, K. J.; Tan, B. The Development and Challenges of Poly (Lactic Acid) and Poly (Glycolic Acid). *Adv. Ind. Eng. Polym. Res.* **2020**, *3* (2), 60–70. <https://doi.org/10.1016/j.aiepr.2020.01.002>.
- (446) Rimdusit, S.; Ishida, H. Development of New Class of Electronic Packaging Materials Based on Ternary Systems of Benzoxazine, Epoxy, and Phenolic Resins. *Polymer (Guildf).* **2000**, *41* (22), 7941–7949. [https://doi.org/10.1016/S0032-3861\(00\)00164-6](https://doi.org/10.1016/S0032-3861(00)00164-6).
- (447) Weil, E. D.; Levchik, S. A Review of Current Flame Retardant Systems for Epoxy Resins. *Journal of Fire Sciences.* 2004, pp 25–40. <https://doi.org/10.1177/0734904104038107>.
- (448) Kamke, F. A.; Lee, J. N. Adhesive Penetration in Wood - A Review. *Wood Fiber Sci.* **2007**, *39* (2), 205–220.
- (449) Meng, X. Y.; Ye, L.; Zhang, X. G.; Tang, P. M.; Tang, J. H.; Ji, X.; Li, Z. M. Effects of Expandable Graphite and Ammonium Polyphosphate on the Flame-Retardant and Mechanical Properties of Rigid Polyurethane Foams. *J. Appl. Polym. Sci.* **2009**, *114* (2), 853–863. <https://doi.org/10.1002/app.30485>.
- (450) Fiege, H.; Voges, H.; Hamamoto, T.; Umemura, S.; Iwata, T.; Miki, H.; Fujita, Y.; Buysch, H.; Garbe, D.; Paulus, W. Phenol Derivatives. *Ullman's encyclopedia of industrial chemistry*; 2012; Vol. 26, pp 522–582. <https://doi.org/10.1002/14356007.a19>.
- (451) Catechol | Solvay <https://www.solvay.com/en/brands/catechol> (accessed Aug 5, 2020).
- (452) Ben-Haida, A.; Colquhoun, H. M.; Hodge, P.; Williams, D. J. Synthesis of a Catechol-Based Poly(Ether Ether Ketone) (“o-PEEK”) by Classical Step-Growth Polymerization and by Entropically Driven Ring-Opening Polymerization of Macrocyclic Oligomers. *Macromolecules* **2006**, *39* (19), 6467–6472. <https://doi.org/10.1021/ma060885k>.
- (453) Varadwaj, P. R. Combined Molecular Dynamics and DFT Simulation Study of the Molecular and Polymer Properties of a Catechol-Based Cyclic Oligomer of Polyether Ether Ketone. *Polymers (Basel).* **2020**, *12* (5). <https://doi.org/10.3390/POLYM12051054>.
- (454) Guaiacol - American Chemical Society <https://www.acs.org/content/acs/en/molecule-of-the-week/archive/g/guaiacol.html> (accessed Jul 31, 2020).
- (455) Syringol - American Chemical Society <https://www.acs.org/content/acs/en/molecule-of-the-week/archive/s/syringol.html> (accessed Jul 31, 2020).
- (456) Liu, H.; Lepoittevin, B.; Roddier, C.; Guerineau, V.; Bech, L.; Herry, J. M.; Bellon-Fontaine, M. N.; Roger, P. Facile Synthesis and Promising Antibacterial Properties of a New Guaiacol-Based Polymer. *Polymer (Guildf).* **2011**, *52* (9), 1908–1916. <https://doi.org/10.1016/j.polymer.2011.02.046>.
- (457) Wang, C.; Sun, J.; Liu, X.; Sudo, A.; Endo, T. Synthesis and Copolymerization of Fully Bio-Based

- Benzoxazines from Guaiacol, Furfurylamine and Stearylamine. *Green Chem.* **2012**, *14* (10), 2799–2806. <https://doi.org/10.1039/c2gc35796h>.
- (458) Llevot, A.; Grau, E.; Carlotti, S.; Grelier, S.; Cramail, H. From Lignin-Derived Aromatic Compounds to Novel Biobased Polymers. *Macromol. Rapid Commun.* **2016**, *37* (1), 9–28. <https://doi.org/10.1002/marc.201500474>.
- (459) Koelewijn, S. F.; Van Den Bosch, S.; Renders, T.; Schutyser, W.; Lagrain, B.; Smet, M.; Thomas, J.; Dehaen, W.; Van Puyvelde, P.; Witters, H.; Sels, B. F. Sustainable Bisphenols from Renewable Softwood Lignin Feedstock for Polycarbonates and Cyanate Ester Resins. *Green Chem.* **2017**, *19* (11), 2561–2570. <https://doi.org/10.1039/c7gc00776k>.
- (460) Holmberg, A. L.; Reno, K. H.; Nguyen, N. A.; Wool, R. P.; Epps, T. H. Syringyl Methacrylate, a Hardwood Lignin-Based Monomer for High-Tg Polymeric Materials. *ACS Macro Lett.* **2016**, *5* (5), 574–578. <https://doi.org/10.1021/acsmacrolett.6b00270>.
- (461) Acetic acid | CH₃COOH - PubChem <https://pubchem.ncbi.nlm.nih.gov/compound/Acetic-acid> (accessed Aug 5, 2020).
- (462) Five uses of Acetic Acid - Industry News <https://www.monarchchemicals.co.uk/Information/News-Events/415-Five-uses-of-Acetic-Acid> (accessed Aug 5, 2020).
- (463) Cheung, H.; Tanke, R. S.; Torrence, G. P. Acetic Acid. In *Ullmann's Encyclopedia of Industrial Chemistry*; Wiley-VCH Verlag GmbH & Co. KGaA: Weinheim, Germany, 2000. https://doi.org/10.1002/14356007.a01_045.
- (464) Ouyang, J.; Ma, R.; Zheng, Z.; Cai, C.; Zhang, M.; Jiang, T. Open Fermentative Production of L-Lactic Acid by Bacillus Sp. Strain NL01 Using Lignocellulosic Hydrolyzates as Low-Cost Raw Material. *Bioresour. Technol.* **2013**, *135*, 475–480. <https://doi.org/10.1016/j.biortech.2012.09.096>.
- (465) Abdel-Rahman, M. A.; Sonomoto, K. Opportunities to Overcome the Current Limitations and Challenges for Efficient Microbial Production of Optically Pure Lactic Acid. *J. Biotechnol.* **2016**, *236*, 176–192. <https://doi.org/10.1016/j.jbiotec.2016.08.008>.
- (466) Lasprilla, A. J. R.; Martinez, G. A. R.; Lunelli, B. H.; Jardini, A. L.; Filho, R. M. Poly-Lactic Acid Synthesis for Application in Biomedical Devices - A Review. *Biotechnol. Adv.* **2012**, *30* (1), 321–328. <https://doi.org/10.1016/j.biotechadv.2011.06.019>.
- (467) Komesu, A.; de Oliveira, J. A. R.; Martins, L. H. da S.; Maciel, M. R. W.; Filho, R. M. Lactic Acid Production to Purification: A Review. *BioResources* **2017**, *12* (2), 4364–4383. <https://doi.org/10.15376/biores.12.2.4364-4383>.
- (468) Neureiter, M.; Danner, H.; Madzingaidzo, L.; Miyafuji, H.; Thomasser, C.; Bvochora, J.; Bamusi, S.; Braun, R. Lignocellulose Feedstocks for the Production of Lactic Acid. *Chem. Biochem. Eng. Q.* **2004**, *18* (1), 55–63.
- (469) Sun, X.; Wang, Q.; Zhao, W.; Ma, H.; Sakata, K. Extraction and Purification of Lactic Acid from Fermentation Broth by Esterification and Hydrolysis Method. *Sep. Purif. Technol.* **2006**, *49* (1), 43–48. <https://doi.org/10.1016/j.seppur.2005.08.005>.
- (470) Glycolic acid | HOCH₂COOH - PubChem <https://pubchem.ncbi.nlm.nih.gov/compound/Glycolic-acid#section=Human-Metabolite-Information> (accessed Aug 6, 2020).
- (471) *DuPont™ Glycolic Acid*; 2006.
- (472) Loder, D. J. Process For Manufacture Of Glycolic Acid - United States Patent Office, December 31, 1936.
- (473) Lapporte, S. J.; Orinda, W. G.; Toland, S.; Rafael, C. Glycolic Acid Production - United States Patent Office, August 21, 1972.
- (474) Glycolic Acid Market Size, Share and Industry Research Reports by 2030 | MRFR <https://www.marketresearchfuture.com/reports/glycolic-acid-market-3141> (accessed Aug 6, 2020).
- (475) Mergner, R.; Janssen, R.; Rutz, D.; Bari, I. de; Sissot, F.; Chiaramonti, D.; Giovannini, A.; Pescarolo, S.; Nistri, R. *2^o Generation Bioethanol The World's Largest Demo Plant Ready to Be Transferred All over the World - A Handbook Part II*; David Chiaramonti, Arianna Giovannini, Rainer Janssen, R. M., Ed.; WIP Renewable Energies, Munich, Germany, 2013.
- (476) Zhu, Z.; Rosendahl, L.; Toor, S. S.; Yu, D.; Chen, G. Hydrothermal Liquefaction of Barley Straw to Bio-Crude Oil: Effects of Reaction Temperature and Aqueous Phase Recirculation. *Appl. Energy* **2015**, *137*, 183–192. <https://doi.org/10.1016/j.apenergy.2014.10.005>.
- (477) Knorr, D.; Lukas, J.; Schoen, P.; Technical, N.; Mary, M.; Knorr, D.; Lukas, J.; Schoen, P. Production of Advanced Biofuels via Liquefaction Production of Advanced Biofuels via Liquefaction Hydrothermal Liquefaction Reactor Design. **2013**, No. November.
- (478) Funkenbusch, L. L. T.; Mullins, M. E.; Vamling, L.; Belkhier, T.; Srettiwat, N.; Winjobi, O.; Shonnard, D. R.; Rogers, T. N. Technoeconomic Assessment of Hydrothermal Liquefaction Oil from Lignin with Catalytic Upgrading for Renewable Fuel and Chemical Production. *Wiley Interdiscip. Rev. Energy Environ.* **2019**, *8* (1), 1–12. <https://doi.org/10.1002/wene.319>.
- (479) Aghazadeh, M.; Engelberth, A. S. Techno-Economic Analysis for Incorporating a Liquid-Liquid Extraction System to Remove Acetic Acid into a Proposed Commercial Scale Biorefinery. *Biotechnol. Prog.* **2016**, *32*

- (4), 971–977. <https://doi.org/10.1002/btpr.2325>.
- (480) Biller, P.; Madsen, R. B.; Klemmer, M.; Becker, J.; Iversen, B. B.; Glasius, M. Effect of Hydrothermal Liquefaction Aqueous Phase Recycling on Bio-Crude Yields and Composition. *Bioresour. Technol.* **2016**, *220*, 190–199. <https://doi.org/10.1016/j.biortech.2016.08.053>.
- (481) Castello, D.; Pedersen, T. H. Continuous Hydrothermal Liquefaction of Biomass : A Critical Review. **2018**. <https://doi.org/10.3390/en11113165>.
- (482) Elliott, D. C.; Hart, T. R.; Schmidt, A. J.; Neuenschwander, G. G.; Rotness, L. J.; Olarte, M. V.; Zacher, A. H.; Albrecht, K. O.; Hallen, R. T.; Holladay, J. E. Process Development for Hydrothermal Liquefaction of Algae Feedstocks in a Continuous-Flow Reactor. *ALGAL* **2013**, *2* (4), 445–454. <https://doi.org/10.1016/j.algal.2013.08.005>.
- (483) Cheng, F.; Jarvis, J. M.; Yu, J.; Jena, U.; Nirmalakhandan, N.; Schaub, T. M.; Brewer, C. E. Bio-Crude Oil from Hydrothermal Liquefaction of Wastewater Microalgae in a Pilot-Scale Continuous Flow Reactor. *Bioresour. Technol.* **2019**, *294* (September), 122184. <https://doi.org/10.1016/j.biortech.2019.122184>.
- (484) Ocfemia, K. S.; Zhang, Y.; Funk, T. Hydrothermal Processing of Swine Manure into Oil Using a Continuous Reactor System: Development and Testing. **2006**, *49* (2).
- (485) Jazrawi, C.; Biller, P.; Ross, A. B.; Montoya, A.; Maschmeyer, T.; Haynes, B. S. Pilot Plant Testing of Continuous Hydrothermal Liquefaction of Microalgae. *Algal Res.* **2013**, *2* (3), 268–277. <https://doi.org/10.1016/j.algal.2013.04.006>.
- (486) Nguyen, T. D. H.; Maschietti, M.; Belkheiri, T.; Åmand, L. E.; Theliander, H.; Vamling, L.; Olausson, L.; Andersson, S. I. Catalytic Depolymerisation and Conversion of Kraft Lignin into Liquid Products Using Near-Critical Water. *J. Supercrit. Fluids* **2014**, *86*, 67–75. <https://doi.org/10.1016/j.supflu.2013.11.022>.
- (487) Bernadas, L. H. Hydrothermal Liquefaction of Lignin into Bio-Oil. **2017**.
- (488) Suesse, A. R.; Norton, G. A.; Van Leeuwen, J. Pilot-Scale Continuous-Flow Hydrothermal Liquefaction of Filamentous Fungi. *Energy and Fuels* **2016**, *30* (9), 7379–7386. <https://doi.org/10.1021/acs.energyfuels.6b01229>.
- (489) Elliott, D. C.; Hart, T. R.; Schmidt, A. J.; Neuenschwander, G. G.; Rotness, L. J.; Olarte, M. V.; Zacher, A. H.; Albrecht, K. O.; Hallen, R. T.; Holladay, J. E. Process Development for Hydrothermal Liquefaction of Algae Feedstocks in a Continuous-Flow Reactor. *Algal Res.* **2013**, *2* (4), 445–454. <https://doi.org/10.1016/j.algal.2013.08.005>.
- (490) Anastasakis, K.; Biller, P.; Madsen, R.; Glasius, M.; Johannsen, I. Continuous Hydrothermal Liquefaction of Biomass in a Novel Pilot Plant with Heat Recovery and Hydraulic Oscillation. *Energies* **2018**, *11* (10), 2695. <https://doi.org/10.3390/en11102695>.
- (491) Jensen, C. U. PIUS - Hydrofaction™ Platform with Integrated Upgrading Step, 2018.
- (492) Hydrofaction™ : Advanced Biofuels from Stranded Biomass A Global Leader in Biomass to Transport Fuel. Steeper Energy 2018.
- (493) The European Parliament and the Council of the European Union. Directive 2014/68/EU of the European Parliament and of the Council of 15 May 2014 on the Harmonisation of the Laws of the Member States Relating to the Making Available on the Market of Pressure Equipment. *Off. J. Eur. Union* **2014**, *93* (765), 164–259. https://doi.org/http://eur-lex.europa.eu/pri/en/oj/dat/2003/l_285/l_28520031101en00330037.pdf.
- (494) ASME Boiler and Pressure Vessel Code (BPVC) Section VIII Division 1. Rules for Construction of Pressure Vessels. **2013**.
- (495) ASME Boiler and Pressure Vessel Code, Section II, part D. Materials. **2015**, 2015. <https://doi.org/http://dx.doi.org/10.1016/B978-032303506-4.10361-X>.
- (496) ASME B16.34. Valves — Flanged , Threaded , and Welding End. **2004**.
- (497) Berglin, E. J. . *Review and Assessment of Commercial Vendors / Options for Feeding and Pumping Biomass Slurries for Hydrothermal Liquefaction*; 2012.
- (498) Hammerschmidt, A.; Boukis, N.; Hauer, E.; Galla, U.; Dinjus, E.; Hitzmann, B.; Larsen, T.; Nygaard, S. D. Catalytic Conversion of Waste Biomass by Hydrothermal Treatment. *Fuel* **2011**, *90* (2), 555–562. <https://doi.org/10.1016/j.fuel.2010.10.007>.
- (499) Çengel, Y. *Introduction to Thermodynamics and Heat Transfer*, 2nd ed.; McGraw-Hill: Dubuque IA, 2008.
- (500) Crowl, D. A.; Tipler, S. A. Sizing Pressure-Relief Devices. *Chem. Eng. Prog.* **2013**, *109* (10), 68–76.
- (501) Evans, R. J.; Milne, T. A. Molecular Characterization of the Pyrolysis of Biomass. 1. Fundamentals. *Energ. Fuel.* **1987**, *1* (2), 123–137. <https://doi.org/10.1021/ef00002a001>.
- (502) Evans, R. J.; Milne, T. A. Molecular Characterization of the Pyrolysis of Biomass. 2. Applications. *Energ. Fuel.* **1987**, *1* (4), 311–319. <https://doi.org/10.1021/ef00004a001>.
- (503) Mukarakate, C.; Zhang, X.; Stanton, A. R.; Robichaud, D. J.; Ciesielski, P. N.; Malhotra, K.; Donohoe, B. S.; Gjersing, E.; Evans, R. J.; Heroux, D. S.; Iisa, K.; Nimlos, M. R. Real-Time Monitoring of the Deactivation of HZSM-5 during Upgrading of Pine Pyrolysis Vapors. *Green Chem.* **2014**, *16* (3), 1444–1461. <https://doi.org/10.1039/c3gc42065e>.
- (504) Yang, X.; Lyu, H.; Chen, K.; Zhu, X.; Zhang, S.; Chen, J. Selective Extraction of Bio-Oil from Hydrothermal

- Liquefaction of *Salix Psammophila* by Organic Solvents with Different Polarities through Multistep Extraction Separation. *BioResources* **2014**, 9 (3), 5219–5233.
- (505) Nguyen Lyckeskog, H.; Mattsson, C.; Åmand, L. E.; Olausson, L.; Andersson, S. I.; Vamling, L.; Theliander, H. Storage Stability of Bio-Oils Derived from the Catalytic Conversion of Softwood Kraft Lignin in Subcritical Water. *Energy and Fuels* **2016**, 30 (4), 3097–3106. <https://doi.org/10.1021/acs.energyfuels.6b00087>.
- (506) Grigoras, I. F.; Stroe, R. E.; Sintamarean, I. M.; Rosendahl, L. A. Effect of Biomass Pretreatment on the Product Distribution and Composition Resulting from the Hydrothermal Liquefaction of Short Rotation Coppice Willow. *Bioresour. Technol.* **2017**, 231, 116–123. <https://doi.org/10.1016/j.biortech.2017.01.056>.
- (507) Cheng, S.; D'cruz, I.; Wang, M.; Leitch, M.; Xu, C. (Charles). Highly Efficient Liquefaction of Woody Biomass in Hot-Compressed Alcohol–Water Co-Solvents. *Energy & Fuels* **2010**, 24 (9), 4659–4667. <https://doi.org/10.1021/ef901218w>.
- (508) Duan, P.; Savage, P. E. Hydrothermal Liquefaction of a Microalga with Heterogeneous Catalysts. *Ind. Eng. Chem. Res.* **2011**, 50 (1), 52–61. <https://doi.org/10.1021/ie100758s>.
- (509) Li, C.; Yang, X.; Zhang, Z.; Zhou, D.; Zhang, L.; Zhang, S.; Chen, J. Hydrothermal Liquefaction of Desert Shrub *Salix Psammophila* to High Value-Added Chemicals and Hydrochar with Recycled Processing Water. *BioResources* **2013**, 8 (2009), 2981–2997.
- (510) WA, S.; IH, G. Caloric Value of Coal. In *Chemistry of coal utilization Vol. 1*; Lowry, H., Ed.; Wiley: New York, 1945; p 139.
- (511) Biller, P.; Riley, R.; Ross, A. B. Catalytic Hydrothermal Processing of Microalgae: Decomposition and Upgrading of Lipids. *Bioresour. Technol.* **2011**, 102 (7), 4841–4848. <https://doi.org/10.1016/j.biortech.2010.12.113>.
- (512) Feng, S.; Yuan, Z.; Leitch, M.; Xu, C. C. Hydrothermal Liquefaction of Barks into Bio-Crude – Effects of Species and Ash Content/Composition. *Fuel* **2014**, 116, 214–220. <https://doi.org/10.1016/j.fuel.2013.07.096>.
- (513) Swagelok. Tubing Data. **2017**, 224–239.
- (514) Factors, C.; Data, C.; Transfer, M.; Dynamics, P.; Kinetics, R.; Control, P.; Economics, P.; Equipment, H.; Cooling, E.; Drying, S.; Absorption, G.; Operations, L. E. L.; Operations, G.; Operations, L. E. L.; Operations, S.; Reduction, S.; Enlargement, S.; Processes, A. S.; Reactors, C.; Safety, P.; Resources, E. *Perry 's Chemical Engineers Engineers Handbook*; 1999.
- (515) Karac, S.; Liu, H. Heat Exchangers: Selection, Rating and Thermal Design.
- (516) Branan, C. *Rule of Thumb for Chemical Engineers*.
- (517) DelcoTerm S DbT. DelcoTerm.
- (518) Superwool Blanket Superwool Blanket. Morgan Advanced Matherials 2016, pp 3–5.
- (519) Moran, M. J.; Shapiro, H. N.; Munson, B. R.; Dewitt, D. P.; Wiley, J.; Hepburn, K.; Grossman, H.; Fleming, L. *Introduction to Thermal Systems Engineering: Thermodynamics, Fluid Mechanics and Heat Transfer*.
- (520) Miliotti, E.; Martelli, F.; Carcasci, C.; Chiamonti, D.; Rizzo, A. M. Analysis, Study and Design of a Biomass Hydrothermal Liquefaction Plant. **2013**.
- (521) Lucian, M.; Fiori, L. Hydrothermal Carbonization of Waste Biomass: Process Design, Modeling, Energy Efficiency and Cost Analysis. *Energies* **2017**, 10 (211). <https://doi.org/10.3390/en10020211>.
- (522) Furukawa, H.; Kato, Y.; Inoue, Y.; Kato, T.; Tada, Y.; Hashimoto, S. Correlation of Power Consumption for Several Kinds of Mixing Impellers. *Int. J. Chem. Eng.* **2012**, 2012. <https://doi.org/10.1155/2012/106496>.
- (523) Px 115 & Px 115ex. Alfa Laval.
- (524) Knorr, D.; Lukas, J.; Schoen, P. *Production of Advanced Biofuels via Liquefaction Hydrothermal Liquefaction Reactor Design*; 2013. [https://doi.org/REPORT 30352.00/01](https://doi.org/REPORT%2030352.00/01).
- (525) Snowden-Swan, L. J.; Hallen, R. T.; Zhu, Y.; Hart, T. R.; Bearden, M. D.; Liu, J.; Seiple, T. E.; Albrecht, K. O.; Jones, S. B.; Fox, S. P.; Schmidt, A. J.; Maupin, G. D.; Billing, J. M. Conceptual Biorefinery Design and Research Targeted for 2022: Hydrothermal Liquefaction Processing of Wet Waste to Fuels. **2017**. <https://doi.org/10.3389/fimmu.2012.00346>.
- (526) Watson, J.; Wang, T.; Si, B.; Chen, W. T.; Aierzhati, A.; Zhang, Y. Valorization of Hydrothermal Liquefaction Aqueous Phase: Pathways towards Commercial Viability. *Progress in Energy and Combustion Science*. Elsevier Ltd March 1, 2020, p 100819. <https://doi.org/10.1016/j.peccs.2019.100819>.

